frontiers | Research Topics

Genomic discoveries and pharmaceutical development in urologic tumors

Edited by
Jialin Meng, Yin Sun, Xiaolei Sun, Lei Yin and Huan Yang

Published in
Frontiers in Pharmacology
Frontiers in Oncology

ISSN 1664-8714
ISBN 978-2-8325-5825-6
DOI 10.3389/978-2-8325-5825-6

About Frontiers

Frontiers is more than just an open access publisher of scholarly articles: it is a pioneering approach to the world of academia, radically improving the way scholarly research is managed. The grand vision of Frontiers is a world where all people have an equal opportunity to seek, share and generate knowledge. Frontiers provides immediate and permanent online open access to all its publications, but this alone is not enough to realize our grand goals.

Frontiers journal series

The Frontiers journal series is a multi-tier and interdisciplinary set of open-access, online journals, promising a paradigm shift from the current review, selection and dissemination processes in academic publishing. All Frontiers journals are driven by researchers for researchers; therefore, they constitute a service to the scholarly community. At the same time, the *Frontiers journal series* operates on a revolutionary invention, the tiered publishing system, initially addressing specific communities of scholars, and gradually climbing up to broader public understanding, thus serving the interests of the lay society, too.

Dedication to quality

Each Frontiers article is a landmark of the highest quality, thanks to genuinely collaborative interactions between authors and review editors, who include some of the world's best academicians. Research must be certified by peers before entering a stream of knowledge that may eventually reach the public - and shape society; therefore, Frontiers only applies the most rigorous and unbiased reviews. Frontiers revolutionizes research publishing by freely delivering the most outstanding research, evaluated with no bias from both the academic and social point of view. By applying the most advanced information technologies, Frontiers is catapulting scholarly publishing into a new generation.

What are Frontiers Research Topics?

Frontiers Research Topics are very popular trademarks of the *Frontiers journals series*: they are collections of at least ten articles, all centered on a particular subject. With their unique mix of varied contributions from Original Research to Review Articles, Frontiers Research Topics unify the most influential researchers, the latest key findings and historical advances in a hot research area.

Find out more on how to host your own Frontiers Research Topic or contribute to one as an author by contacting the Frontiers editorial office: frontiersin.org/about/contact

Genomic discoveries and pharmaceutical development in urologic tumors

Topic editors

Jialin Meng — University of Science and Technology of China, China
Yin Sun — University of Rochester Medical Center, United States
Xiaolei Sun — Fudan University, China
Lei Yin — Shanghai Jiaotong University School of Medicine, China
Huan Yang — Huazhong University of Science and Technology, China

Citation

Meng, J., Sun, Y., Sun, X., Yin, L., Yang, H., eds. (2025). *Genomic discoveries and pharmaceutical development in urologic tumors*. Lausanne: Frontiers Media SA. doi: 10.3389/978-2-8325-5825-6

Table of contents

frontiers | Frontiers in Pharmacology

TYPE Editorial
PUBLISHED 09 December 2024
DOI 10.3389/fphar.2024.1508979

OPEN ACCESS

EDITED AND REVIEWED BY
Dianwen Ju,
Fudan University, China

*CORRESPONDENCE
Lei Yin,
yltale@126.com

RECEIVED 10 October 2024
ACCEPTED 15 November 2024
PUBLISHED 09 December 2024

CITATION
Meng J, Yang H and Yin L (2024) Editorial: Genomic discoveries and pharmaceutical development in urologic tumors.
Front. Pharmacol. 15:1508979.
doi: 10.3389/fphar.2024.1508979

Editorial: Genomic discoveries and pharmaceutical development in urologic tumors

Jialin Meng[1,2,3], Huan Yang[4] and Lei Yin[5,6]*

[1]Department of Urology, The First Affiliated Hospital of Anhui Medical University, Hefei, China, [2]Institute of Urology and Anhui Province Key Laboratory of Urological and Andrological Diseases Research and Medical Transformation, Anhui Medical University, Hefei, China, [3]School of Life Sciences, Anhui Medical University, Hefei, China, [4]Department of Urology, Tongji Hospital, Tongji Medical College, Huazhong University of Science and Technology, Wuhan, China, [5]Department of Urology, Ruijin Hospital, Shanghai Jiao Tong University School of Medicine, Shanghai, China, [6]Department of Urology, Shanghai Ninth People's Hospital, Shanghai Jiao Tong University School of Medicine, Shanghai, China

KEYWORDS

urologic tumors, cancer biomarkers, drug screen, drug repurposing, genomic sequence

Editorial on the Research Topic
Genomic discoveries and pharmaceutical development in urologic tumors

The prevalence of urologic tumors is rapidly increasing, leading to severe clinical outcomes. In the United States, approximately 169,360 new cases of urologic tumors are estimated for 2024, with about 32,350 tumor-specific deaths (Siegel et al., 2024). Similarly, China faces a staggering annual estimate of 244,300 new cases, resulting in 113,700 deaths (Han et al., 2024). These alarming statistics underscore the urgent need for advanced therapeutic strategies and personalized treatments to improve survival rates for patients suffering from urologic tumors.

A particularly exciting area of research is genomic sequencing, which facilitates the identification of specific genetic mutations and biomarkers for targeted drug therapies. This includes recognizing molecular subtypes that enable precision clinical therapy (Li et al., 2024; Figiel et al., 2024). For instance, drugs targeting the androgen receptor (AR) pathway, such as abiraterone and enzalutamide, have demonstrated efficacy in treating prostate cancers with relevant genetic alterations (Dai et al., 2023). Additionally, drugs like sunitinib and pazopanib, which inhibit the vascular endothelial growth factor (VEGF) pathway, have significantly improved survival rates in patients with metastatic renal cell carcinoma (George et al., 2019). This Research Topic explores cutting-edge therapies, molecular markers, and mechanisms reshaping the field.

Advanced-stage castration-resistant prostate cancer presents significant challenges in clinical practice, often necessitating combination therapy strategies. Consequently, the search for novel clinical treatments, the exploration of tumor progression signaling pathways, and the identification of prognostic biomarkers are imperative. In this Research Topic, Wei et al. report that apalutamide neoadjuvant therapy enhances resectability in unresectable prostate cancer, facilitating successful surgeries. Zhang et al. recommend cabazitaxel plus prednisone as the most effective first-line treatment for metastatic castration-resistant prostate cancer. Meanwhile, Lampe et al. discuss challenges associated with bi-specific T-cell engagers (BiTEs) therapy for prostate cancer and suggest improvement strategies. In terms of mechanisms, Zhang et al.

review the role of m6A regulators in prostate cancer, particularly in AR signaling pathways and disease progression. Chen et al. demonstrate that combining PTEN restoration with IL-23 inhibition significantly enhances therapeutic outcomes in metastatic prostate cancer. Lin et al. discover that SGLT2 inhibition reduces prostate cancer risk by modulating circulating metabolites, especially uridine levels. Finally, Xia et al. identify anoikis-related gene signatures as potential prognostic markers for prostate cancer bone metastasis.

Urothelial bladder cancer exhibits one of the highest mutation burdens among all cancer types (Cancer Genome Atlas Research, 2014), contributing to variable patient responses to immunotherapy, particularly with the use of *bacillus* Calmette-Guérin for early-stage non-muscle invasive bladder cancer (Morales, 1992). In this Research Topic, Peng et al. find that IL4I1 expression in bladder cancer correlates with better responses to immune checkpoint inhibitors. Zhu et al. show that HER2 positivity in urothelial carcinoma is associated with advanced disease stages and combining disitamab vedotin with PD-1 inhibitors shows promise. Uysal et al. reveal that EGFR, AREG, and EREG amplification predicts poor survival in muscle-invasive bladder cancer. Additionally, Li et al. suggest that rosuvastatin may reduce bladder cancer risk, while other statins appear ineffective.

Furthermore, Geng et al. develop a vasculogenic mimicry gene signature that predicts survival and immune responses in clear cell renal cell carcinoma. Huang et al. identify GJA5 and GJB1 as prognostic markers for renal clear cell carcinoma, with lower expression linked to poorer outcomes. Song et al. show that KHSRP knockdown inhibits the progression of papillary renal cell carcinoma and enhances gemcitabine sensitivity. Qu et al. report a rare case of ossifying renal tumor of infancy, emphasizing the need for careful monitoring due to high Ki-67 expression. Duan et al. explore alternative splicing events associated with clinical features across multiple cancers, offering insights into tumor progression and immune infiltration.

This Research Topic highlights advances in genomic discoveries and therapeutic approaches. While significant progress has been made in understanding the molecular mechanisms and targeted therapies for conditions like advanced-stage castration-resistant prostate cancer and metastatic renal cell carcinoma, challenges remain, particularly regarding resistance to existing therapies and the necessity for personalized treatment options. The studies presented here underscore the importance of integrating novel biomarkers and therapeutic strategies, such as BiTEs and m6A regulators, to enhance patient outcomes. Future research should prioritize several key areas. First, deeper investigations into the interactions between the tumor microenvironment and the immune system are essential for elucidating the mechanisms of immune evasion by tumors, which could pave the way for novel immunotherapies. Furthermore, identifying and validating new therapeutic targets, especially those linked to resistance mechanisms, will be crucial for improving patient prognoses. The integration of genomics, proteomics, and metabolomics data to create more comprehensive personalized treatment strategies could significantly enhance therapeutic outcomes for patients.

In conclusion, while substantial strides have been made in the research and treatment of urologic tumors, ongoing efforts are necessary. Through interdisciplinary collaboration and innovation, integrating new technologies and discoveries, we can significantly improve the prognosis and quality of life for patients with urologic tumors. The vision for the future includes not only better therapeutic strategies but also a more profound understanding of cancer biology, ultimately leading to effective treatments tailored to individual patient needs. We eagerly anticipate the application of these research findings in clinical practice, which could revolutionize treatment options for urologic tumor patients.

Author contributions

JM: Data curation, Formal Analysis, Investigation, Visualization, Writing–original draft. HY: Data curation, Writing–original draft, Methodology, Project administration. LY: Project administration, Conceptualization, Funding acquisition, Supervision, Writing–review and editing.

Funding

The author(s) declare that financial support was received for the research, authorship, and/or publication of this article. This work was supported by grants from the National Natural Science Foundation of China (82203698). The Sailing Program of Shanghai Science and Technology Commission (22YF1425000). Anhui Province Key Project for Clinical Medical Research Translation and Advancement (202204295107020031 and 202204295107020007).

Acknowledgments

We wish to thank all the authors contributing to this Research Topic and all the reviewers and invited editors who have helped to make it solid.

Conflict of interest

The authors declare that the research was conducted in the absence of any commercial or financial relationships that could be construed as a potential conflict of interest.

Generative AI statement

The author(s) declare that no Generative AI was used in the creation of this manuscript.

Publisher's note

References

Cancer Genome Atlas Research, N. (2014). Comprehensive molecular characterization of urothelial bladder carcinoma. *Nature* 507 (7492), 315–322. doi:10.1038/nature12965

Dai, C., Dehm, S. M., and Sharifi, N. (2023). Targeting the androgen signaling Axis in prostate cancer. *J. Clin. Oncol.* 41 (26), 4267–4278. doi:10.1200/JCO.23.00433

Figiel, S., Bates, A., Braun, D. A., Eapen, R., Eckstein, M., Manley, B. J., et al. (2024). Clinical implications of basic research: exploring the transformative potential of spatial 'omics in uro-oncology. *Eur. Urol.* doi:10.1016/j.eururo.2024.08.025

George, S., Rini, B. I., and Hammers, H. J. (2019). Emerging role of combination immunotherapy in the first-line treatment of advanced renal cell carcinoma: a review. *JAMA Oncol.* 5 (3), 411–421. doi:10.1001/jamaoncol.2018.4604

Han, B., Zheng, R., Zeng, H., Wang, S., Sun, K., Chen, R., et al. (2024). Cancer incidence and mortality in China, 2022. *J. Natl. Cancer Cent.* 4 (1), 47–53. doi:10.1016/j.jncc.2024.01.006

Li, R., Linscott, J., Catto, J. W. F., Daneshmand, S., Faltas, B. M., Kamat, A. M., et al. (2024). FGFR inhibition in urothelial carcinoma. *Eur. Urol.* doi:10.1016/j.eururo.2024.09.012

Morales, A. From the 19th to the 21st centuries: BCG in the treatment of superficial bladder cancer. *Eur. Urol*, 1992, 21 2, 6. doi:10.1159/000474913

Siegel, R. L., Giaquinto, A. N., and Jemal, A. (2024). Cancer statistics, 2024. *CA Cancer J. Clin.* 74 (1), 12–49. doi:10.3322/caac.21820

frontiers | Frontiers in Oncology

TYPE Original Research
PUBLISHED 25 September 2023
DOI 10.3389/fonc.2023.1249932

OPEN ACCESS

EDITED BY
Lei Yin,
Shanghai Jiao Tong University, China

REVIEWED BY
Tingshuai Zhai,
Chinese Academy of Medical Sciences and Peking Union Medical College, China
Fei Wu,
Shandong Academy of Sciences, China

*CORRESPONDENCE
Zhiquan Hu
huzhiquan2000@163.com
Hua Xu
xu-hua@whu.edu.cn

†These authors have contributed equally to this work

RECEIVED 12 July 2023
ACCEPTED 17 August 2023
PUBLISHED 25 September 2023

CITATION
Duan C, Zhang Y, Li L, Liu K, Yao X, Wu X, Li B, Mao X, Wu H, Liu H, Zeng J, Li S, Gong Y, Hu Z and Xu H (2023) Identification of alternative splicing associated with clinical features: from pan-cancers to genitourinary tumors. *Front. Oncol.* 13:1249932. doi: 10.3389/fonc.2023.1249932

Identification of alternative splicing associated with clinical features: from pan-cancers to genitourinary tumors

Chen Duan[1†], Yangjun Zhang[2,3†], Lu Li[4], Kai Liu[3], Xiangyang Yao[3], Xiaoliang Wu[1], Bo Li[1], Xiongmin Mao[3], Huahui Wu[3], Haoran Liu[5], Jin Zeng[6], Sheng Li[2], Yan Gong[2], Zhiquan Hu[1*] and Hua Xu[2,3,7*]

[1]Department of Urology, Tongji Hospital, Tongji Medical College, Huazhong University of Science and Technology, Wuhan, Hubei, China, [2]Tumor Precision Diagnosis and Treatment Technology and Translational Medicine, Hubei Engineering Research Center, Zhongnan Hospital of Wuhan University, Wuhan, Hubei, China, [3]Department of Urology, Zhongnan Hospital of Wuhan University, Wuhan, Hubei, China, [4]Department of Radiation Oncology, Sichuan Cancer Hospital and Institute, Sichuan Cancer Center, School of Medicine, University of Electronic Science and Technology of China, Chengdu, Sichuan, China, [5]Department of Urology, Stanford University School of Medicine, Stanford, CA, United States, [6]Department of Urology, The First Affiliated Hospital of Nanchang University, Nanchang, Jiangxi, China, [7]Taikang Center for Life and Medical Sciences, Wuhan University, Wuhan, Hubei, China

Background: Alternative splicing events (ASEs) are vital causes of tumor heterogeneity in genitourinary tumors and many other cancers. However, the clinicopathological relevance of ASEs in cancers has not yet been comprehensively characterized.

Methods: By analyzing splicing data from the TCGA SpliceSeq database and phenotype data for all TCGA samples from the UCSC Xena database, we identified differential clinical feature-related ASEs in 33 tumors. CIBERSORT immune cell infiltration data from the TIMER2.0 database were used for differential clinical feature-related immune cell infiltration analysis. Gene function enrichment analysis was used to analyze the gene function of ASEs related to different clinical features in tumors. To reveal the regulatory mechanisms of ASEs, we integrated race-related ASEs and splicing quantitative trait loci (sQTLs) data in kidney renal clear cell carcinoma (KIRC) to comprehensively assess the impact of SNPs on ASEs. In addition, we predicted regulatory RNA binding proteins in bladder urothelial carcinoma (BLCA) based on the enrichment of motifs around alternative exons for ASEs.

Results: Alternative splicing differences were systematically analyzed between different groups of 58 clinical features in 33 cancers, and 30 clinical features in 24 cancer types were identified to be associated with more than 50 ASEs individually. The types of immune cell infiltration were found to be significantly different between subgroups of primary diagnosis and disease type. After integrating ASEs with sQTLs data, we found that 63 (58.9%) of the race-related ASEs were significantly SNP-correlated ASEs in KIRC. Gene function enrichment analyses showed that metastasis-related ASEs in KIRC mainly enriched Rho GTPase signaling pathways. Among those ASEs associated with metastasis,

alternative splicing of GIT2 and TUBB3 might play key roles in tumor metastasis in KIRC patients. Finally, we identified several RNA binding proteins such as PCBP2, SNRNP70, and HuR, which might contribute to splicing differences between different groups of neoplasm grade in BLCA.

Conclusion: We demonstrated the significant clinical relevance of ASEs in multiple cancer types. Furthermore, we identified and validated alternative splicing of TUBB3 and RNA binding proteins such as PCBP2 as critical regulators in the progression of urogenital cancers.

KEYWORDS

alternative splicing, pan-cancers, tumor heterogeneity, clinical features, genitourinary tumors

Introduction

As the second leading cause of death worldwide, cancer kills several millions of people per year, and this number has been increasing for decades (1, 2). Nowadays, multiple cancer therapies are available and greatly improve patient outcomes, such as surgical procedures, chemoradiotherapy, immunotherapy, targeted therapy, and comprehensive treatment. Although exciting progress has been made in cancer therapy, the extensive heterogeneity and complexity of tumors pose tremendous challenges to the treatment of tumors. This heterogeneity underlies the emergence of resistance to cancer therapies to a great extent. As patients with tumors of the same histological type often respond differently to the same treatment (3), personalized treatment is the future direction, which requires a deeper understanding of tumor heterogeneity and its clinical relevance.

Tumor heterogeneity is now a broad concept that means both the inter-patient heterogeneity resulting from genetic variation or environment factors and the intratumoral heterogeneity manifested as genetically diverse subpopulations or dynamic genetic variations over time of an individual tumor (4). Advances in sequencing technologies and computational methods enable the uncovering of tumor heterogeneity and its clinical relevance (5–7). Van Allen et al. generated a database of gene alterations with clinical implications for cancer patients by using whole exome sequencing and applied it to clinical decision-making (8). By using targeted deep sequencing, Burkhardt et al. revealed age dependency of mutations in Burkitt lymphoma in children and adolescents (9). Drews et al. illuminated the relationship between chromosomal instability and clinical phenotypes in cancers and predicted platinum sensitivity of ovarian cancer by integrating impaired homologous recombination signatures (10). Previous studies also investigated the roles of post-transcriptional mechanisms in tumor heterogeneity. Han et al. identified clinically relevant adenosine-to-inosine RNA editing events (11). Several researchers focused on the methylation of N^6 adenosine (m^6A), and found that the landscape of m^6A regulators was related to cancer progression (12–14). All these studies characterized the profiles of molecular alterations related to clinical characteristics across cancers and guided individualized treatment of cancers. However, the specific mechanisms of how post-transcriptional regulation affect tumor heterogeneity and tumorigenesis still need further study.

Alternative splicing (AS) is a vital cause of tumor heterogeneity. As a common post-transcriptional regulation, AS causes distinct transcript isoforms and protein variants (15). Aberrant AS, which is significantly increased in malignant tissues, reshapes the transcriptome and proteome, influencing signaling pathways related to cellular homeostasis, cell proliferation, and differentiation (16, 17). For instance, the CD44 splice isoform promotes epithelial-mesenchymal transition across cancers (18–21). AS is precisely regulated by RNA-binding proteins (RBPs), especially splicing factors including serine/arginine-rich (SR) proteins and heterogeneous nuclear ribonucleoproteins (hnRNPs) (22). SR proteins and hnRNPs regulate the recruitment and function of spliceosomes, thereby promoting or repressing splicing. Mutation or dysfunction of splicing factors can cause the generation of abnormal isoforms associated with the occurrence and progression of tumors (23). Numerous studies demonstrated that the expression of splicing factors varied in normal tissues and cancers, while altered expression or activity of splicing factors could contribute to cancer progression. The mutation of splicing factor U2AF1 and relative aberrant AS events were identified in multiple cancer types (24), while splicing factor SF3B1 was suggested to be a therapeutic target for breast cancer patients (25). Therefore, clinically relevant aberrant AS events (ASEs) and specific splicing factors can be promising targets for cancer therapy.

To comprehensively reveal the clinically relevant differential ASEs involved in tumorigenesis, progression, and prognosis of multiple cancers, we integrally analyzed mRNA splicing data in 31 human cancers, identified thousands of tumor-specific and survival-associated ASEs, and created a website tool OncoSplicing for the exploration and visualization of clinical relevant ASEs (26, 27). In this study, we analyzed multiple clinical indicator-relevant differential ASEs in 33 human cancers based on the OncoSplicing database and explored changes in splicing factors expression. Furthermore, we identified alternative splicing of GIT2 and

TUBB3 and RNA binding proteins such as PCBP2 as critical regulators in the progression of urogenital cancers. Together, we believe that our work will help to further reveal the relationship between AS and clinicopathological features in cancers, and also to provide more available molecular targets for cancer therapy by regulating clinically relevant AS and splicing factors.

Materials and methods

Data acquisition and pre-processing

Splicing data for all splicing events of 33 tumors were downloaded from the TCGA SpliceSeq database (http://projects.insilico.us.com/TCGASpliceSeq/PSIdownload.jsp), with the parameter percent-samples-with-values (PCT) set to no less than 75%. This contains splicing events belonging to 7 splicing types, including alternative acceptor sites (AA), alternative donor sites (AD), exon skipping (ES), mutually exclusive exons (ME), retained introns (RI), alternate promoter (AP) and alternate terminator (AT).

Phenotype data for all TCGA samples were downloaded in the GDC cohort of each cancer type separately from the UCSC Xena database (https://xenabrowser.net/datapages/). Basic patient information, such as age (full name is "age at initial pathologic diagnosis"), gender, race, and other nonredundant and different clinical features, were manually collected, by which patients were separated into 2 groups for each cancer type. Clinical features with continuous data in each cancer type were grouped by the median cutoff value. For category clinical features, the top 2 groups with the most samples in each cancer type were kept. After integration with splicing data by samples, clinical features in a cancer type were reserved for further analysis only if there were > 20 records per group.

Identification of clinical feature-related alternative splicing event

Differential alternative splicing analysis was performed between 2 groups for each clinical feature. The P value of the significance of the difference was evaluated using the Wilcoxon rank sum test, and the splicing events with the absolute value of the delta PSI greater than 0.1 and the Benjamini-Hochberg (BH) adjusted P value less than 0.05 were considered as clinical feature related ASEs.

Identification of clinical feature-related immune cell infiltration

CIBERSORT immune cell infiltration data were obtained from the TIMER2.0 database (http://timer.cistrome.org/). Differential immune cell infiltration analysis was performed between 2 groups for each clinical feature. The P value of the significance of the difference was evaluated using the Wilcoxon rank sum test, and cell types with the absolute delta proportion greater than 3 percent and the Benjamini-Hochberg (BH) adjusted P value less than 0.05 were considered as significant.

Gene function enrichment analysis

Genes of clinical feature-related ASEs for each interested clinical feature in individual cancer types were submitted to Metascape (http://metascape.org) separately to implement gene function enrichment analysis. The top 10 pathways with significant P values were analyzed and displayed. Plots of survival and differences between 2 groups for ASEs enriched in interesting pathways were performed using the OncoSplicing website (www.oncosplicing.com).

Structure and genomic location of alternative splicing events

The gene structure file was downloaded from the TCGA SpliceSeq database to obtain the genomic position of each exon. According to the exon composition of a splicing event, the genome locations of the whole event and the start-end positions of the alternative exon are determined, and then the range between 250 nt upstream and downstream of the alternative exon was considered the region that most likely influenced the splicing level of a splicing event.

Splicing quantitative trait loci analysis

The splicing quantitative trait loci (sQTLs) data of the renal clear cell carcinoma cohort was downloaded from the CancerSplicingQTL database (http://www.cancersplicingqtl-hust.com/#/). Significant SNPs associated with each splicing event were identified and mapped to the genome locations of the splicing event, and only SNPs in the range between 250 nt upstream and downstream of alternative exon were considered meaningful sQTLs.

Splicing events map to RNA motifs of RBPs

To explore the potential regulator of clinical feature-related splicing events in each cancer type, splicing events were extracted with genome coordination and organized into the format that meets the requirements of rMAPS2 (http://rmaps.cecsresearch.org/) for each splice type separately (28). Splice types with considerable AS events were chosen to perform enrichment analysis of RBP motifs. Clinical feature-related alternative splicing events were separated as up-regulated and down-regulated events by the direction of PSI change. ASEs with delta PSI less than 0.001 and FDR more than 0.9 were set as background control.

Cell culture and stable transfection

Kidney cancer (OS-RC-2 and 786-O) and bladder cancer (T24 and 5637) cells were obtained from the Shanghai Cell Bank Type Culture Collection Committee and maintained in Department of Biological Repositories, Zhongnan Hospital of Wuhan University (Wuhan, China). Cells used in this study underwent STR authentication. Tumor cells were cultured in McCoy's 5A (T24)

and RPMI-1640 (OS-RC-2, 786-O, and 5637) medium containing 10% FBS (Gibco, USA). The lentiviruses carrying small hairpin RNAs (shRNA) targeting TUBB3, PCBP2, and control shRNA were constructed by Tsingke (Beijing, China). The target sequences were as follows: 5'-CAGTATTTATGGCCTCGTCCT-3' (shRNA1-TUBB3), 5'-CATCTCTTCAGGCCTGACAAT-3' (shRNA2-TUBB3), 5'-CCATGATCCATCTGTGTAGTT-3' (shRNA1-PCBP2) and 5'-CCCACTAATGCCATCTTCAAA-3' (shRNA2-PCBP2). Lipo2000 (Invitrogen, 11668030, USA) was used to transfect the lentiviral vectors into tumor cells, and the transfection efficiency was confirmed by qPCR.

qPCR

Total RNAs were extracted from cells by using Trizol reagent (Thermo Fisher Scientific, USA). HiScript III RT SuperMix (Vazyme, R323-01, China) was applied to synthesize cDNA, and ChamQ Universal SYBR qPCR Master Mix (Vazyme, Q711-02/03, China) was used for real-time PCR experiments according to the manufacturer's instructions. qPCR analysis was performed on QuantStudio Flex system (Applied Biosystem, USA). Primers sequences were as follows: TUBB3, 5′-GACTCCC TTGAACAGGGACAG-3′ (forward), 5′-GGCACGTACT TGTGAGAAGA-3′ (reverse); PCBP2, 5′-TCTGCGTGGTCATG TTGGAG-3′ (forward), 5′-TGCATCCAAACCTGCCCAATA-3′ (reverse); GAPDH, 5′-AATGGGCAGCCGTTAGGAAA-3′ (forward), 5′-GCCCAATACGACCAAATCAGAG-3′ (reverse).

Cell viability assay

Tumor cell proliferation was detected by CCK-8 assay. Briefly, cells were inoculated into 96-well plates (2×10^3 cells per well) and cultured in the 5% CO2 incubator at 37°. After mixing with 10 μL CCK-8 reagent (MCE, HY-K0301, USA) for 2 h, absorbance was detected at 450nm with an absorbance reader (Molecular Devices, USA).

Colony formation assay

Approximately 1000 cells were seeded in a 60 mm petri dish with the complete medium. After 2-3 weeks, cells were fixed for 15 min and stained with crystal violet for 10 min. Visible clones were counted by using ImageJ software.

Modified Boyden chamber assay

For tumor cell migration, approximately 5×10^4 cells were suspended in 100 μL serum-free medium and plated in the apical chambers of transwell plates (Corning, USA), and 500 μL complete medium was added in the lower chamber. After 24 h, the migrated cells were fixed and then dyed in crystal violet. The cell number was counted from 6 random fields under an inverted microscope.

Statistics and visualization

Statistical analysis was performed using R software (4.0.1). Data analysis and visualization tools in the R software include R packages such as ggplot2, ComplexHeatmap, limma, survminner, and venn.diagram. One-way or two-way ANOVA was used to analyze the differences in multiple groups, and a P-value < 0.05 was considered statistically significant.

Results

Clinical features in cancers

This study contains 33 TCGA cancers, including Adrenocortical Carcinoma (ACC), Kidney Renal Clear Cell Carcinoma (KIRC), Prostate Adenocarcinoma (PRAD), Bladder Urothelial Carcinoma (BLCA), Kidney Renal Papillary Cell Carcinoma (KIRP), Rectum Adenocarcinoma (READ), Breast Invasive Carcinoma (BRCA), Acute Myeloid Leukemia (LAML), Sarcoma (SARC), Cervical Squamous Cell Carcinoma (CESC), Lower Grade Glioma (LGG), Skin Cutaneous Melanoma (SKCM), Cholangiocarcinoma (CHOL), Liver Hepatocellular Carcinoma (LIHC), Stomach Adenocarcinoma (STAD), Colon Adenocarcinoma (COAD), Lung Adenocarcinoma (LUAD), Testicular Germ Cell Tumors (TGCT), Diffuse Large B-cell Lymphoma (DLBC), Lung Squamous Cell Carcinoma (LUSC), Thyroid Carcinoma (THCA), Esophageal Carcinoma (ESCA), Mesothelioma (MESO), Thymoma (THYM), Glioblastoma Multiforme (GBM), Ovarian Serous Cystadenocarcinoma (OV), Uterine Corpus Endometrial Carcinoma (UCEC), Head and Neck Squamous Cell Carcinoma (HNSC), Pancreatic Adenocarcinoma (PAAD), Uterine Carcinosarcoma (UCS), Kidney Chromophobe (KICH), Pheochromocytoma and Paraganglioma (PCPG), Uveal Melanoma (UVM).

Clinical features were manually collected, by which patients were separated into 2 groups for each cancer type. After organizing and filtering the phenotype data for each tumor, 58 clinical features were retained in 33 tumors, with an average of 7 in each tumor, 15 in ESCA at most, and 3 in OV at least. Clinical features common in more than 10 tumors included age (n = 33 tumors), gender (n = 25), pathologic T (n = 20), race (n = 19), tumor stage (n = 18), pathologic N (n = 16), BMI (n = 12) and clinicopathological features such as the site of resection or biopsy (n = 10). Other important cancer-specific features such as "history of colon polyps" in COAD, "fetoprotein outcome value" in LIHC, and "acute myeloid leukemia calgb cytogenetics risk category" in LAML were also included (Figure 1; Table S1).

Identification of clinical feature-related AS and immune cell infiltration

Differential AS analysis was performed for each clinical feature in each cancer type for the splicing events whose non-null-PSI

(Percent samples with values, PCT) was greater than 75%. The results showed that clinical features such as race (the number of cancers is 17), pathologic T (n = 9), neoplasm histologic grade (n = 7), and disease type (n = 6) were associated with at least 50 ASEs in more than 5 tumors (Figure 2; Table S2). On the other hand, ESCA has the most clinical features (the number of clinical features is 10) that were associated with AS, followed by KIRC, KIRP, and LIHC (n > 5). It is worth noting that there are also obvious differences in AS between different groups of age and gender in some cancer types, such as age in THYM and LIHC, and gender in KIRP and KIRC. The most significant splicing differences exist between different pathological subtypes or clinical diagnoses in the same cancer type, such as embryonal carcinoma and seminoma in TGCT (the number of ASEs is 3,593), adenocarcinomas and squamous cell carcinoma in ESCA (n = 2,097) or CESC (n = 1,344), adenocarcinoma and mucinous adenocarcinoma in UCEC (n = 603) or COAD (n = 166), papillary and non-papillary tumors in BLCA (n = 474). Further analysis showed that these clinical feature-related ASEs were mainly enriched in splice types AP, ES, and AT (Figure S1). These results indicate that significant differences in AS exist between different groups of many clinical features, such as different pathological subtypes, grades of the same tumor type as well as different races.

It is known that AS may influence immune cell infiltration in several facets. Here we further analyzed the immune cell infiltration in different groups of clinical features. We found that "B cell plasma" and "T cell CD4 memory resting" were significantly different between subgroups of primary diagnosis of LGG, and "T cell CD4 memory resting" and "T cell regulatory Tregs" were significantly different between subgroups of ESCA (Figure S2).

FIGURE 1
Statistics of different clinical features in 33 TCGA tumors. Red squares indicate that clinical features in the corresponding tumors were included in the analysis, while grey squares indicate that not included.

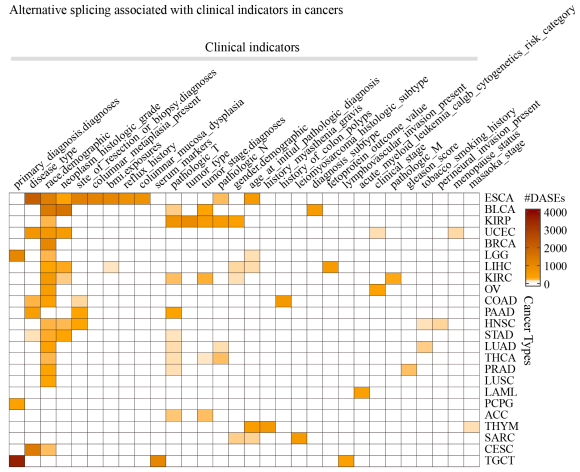

FIGURE 2
The statistics of the number of splicing events associated with clinical features in cancers. Only the 30 clinical features in 24 cancer types that were found associated with more than 50 ASEs were displayed.

Interestingly, there were a lot of ASEs identified between these subgroups of ESCA as well as LGG primary diagnosis (Figure 2). These results indicated that different strategies should be organized to deal with the patients in these different subgroups.

Analysis of race-related AS

Race-related ASEs differ in most tumors (Figure 2). Al Abo et al. analyzed the differences in AS between African/Black Americans (BAs) and White Americans (WAs) in tumors using TCGA SpliceSeq data, but they did not compare the splicing differences between Asian Americans (AAs) and BAs and the roles of SNPs in producing race-related AS (29). Therefore, we further analyzed the differences in AS among different races in several tumors.

The results showed that tumors including BLCA, ESCA, LIHC, STAD, and THCA contain enough AAs for differential AS analysis compared with WAs, while other tumors such as BRCA and KIRC contain enough BAs for differential AS analysis compared with WAs (Figure 3A). We identified more than 1000 race-related ASEs in BRCA, BLCA, and ESCA, and more than 500 race-related ASEs in KIRC and UCEC, among which AP, AT, and ES accounted for the most (Figure 3B). To identify more significant race-related ASEs, considering the difference in the number of tumors involved, we required ASEs to be differential in at least 5 tumors when selecting race-related ASEs between WAs and BAs and selected ASEs between WAs and AAs requiring the presence of differences in at least 3 tumors. Finally, a total of 74 splicing events were identified as differential ASEs between WAs and BAs, another 74 splicing events were identified as significantly different between WAs and AAs, and there were 13 common splicing events in both comparisons (Figure 3C). Most of these common ASEs had the same directions of PSI changes in either comparison of WAs and BAs or comparison of WAs and AAs, except for RPS9_AD_51827 which was upregulated in WAs when compared with BAs while

10.3389/fonc.2023.1249932

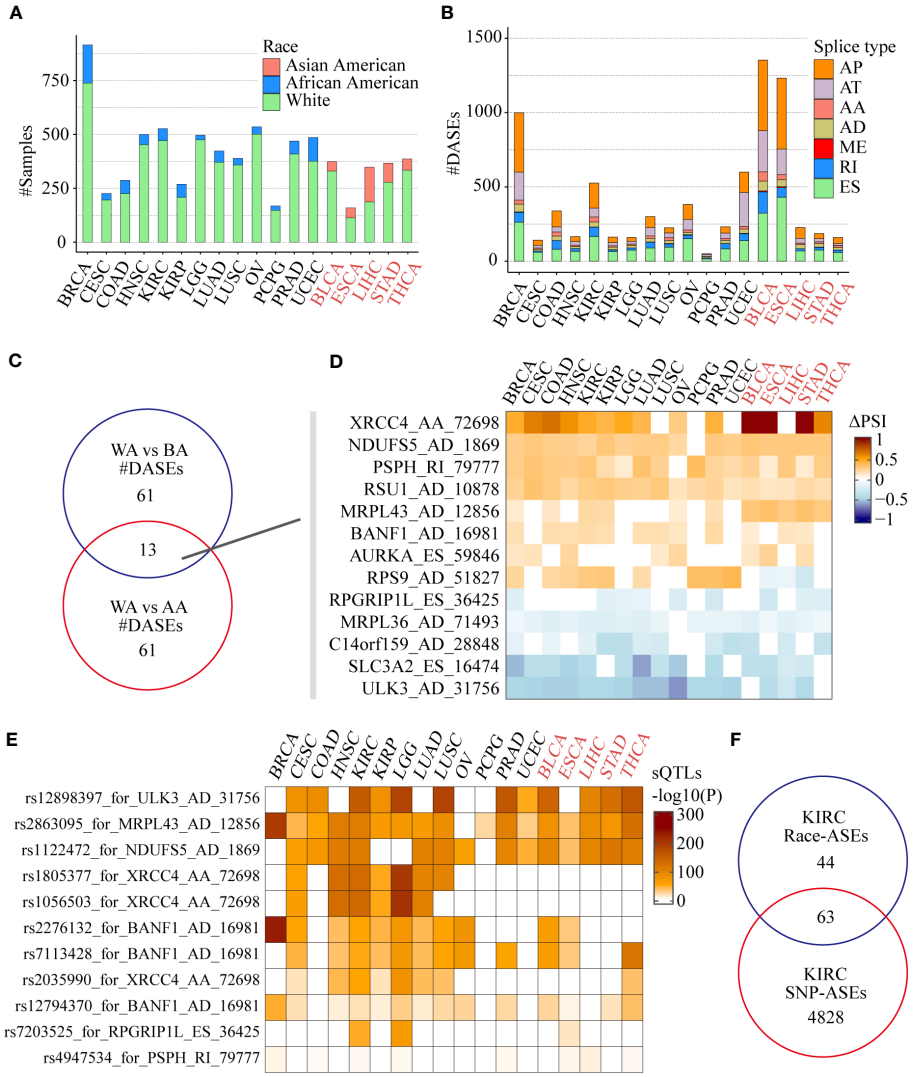

FIGURE 3
Race-related ASEs in the SpliceSeq project. **(A)** The number of samples of different races among the 18 tumors eligible for screening and differential analysis. **(B)** The number of splicing events in different splicing types associated with different races in each tumor. **(C)** Comparison of differential splicing events in the White and the Black, the White and the Asian American populations. **(D)** Splicing changes of the common ASEs of the 2 comparisons in each tumor. **(E)** Effects of SNPs on race-related splicing events and their differences in different tumors or races. **(F)** Comparison of 107 race-related ASEs (|ΔPSI| >0.1, FDR < 0.05) and 4891 SNP-related ASEs in the KIRC cohort (Fisher's exact test P = 8.79e-10).

downregulated in WAs when compared with AAs (Figure 3D). Besides, race-related ASEs between WAs and BAs specifically included ARL6IP4_AA_25028, SLC25A26_ES_65549, PSMG4_RI_75176, and NMRAL1_AD_33740, while race-related ASEs between WAs and AAs specifically included ZDHHC4_ES_78754, TOR1AIP1_AA_9127, POMZP3_ES_80187, and IP6K2_RI_64750 (Table S3).

Among those 13 common race-related ASEs, there were 7 splicing events significantly correlated with nearby SNPs located between upstream and downstream 250 nt of the alternative exon. By using the search function of the CancerSplicingQTL database, it was found that splicing events such as ULK3_AD_31756, NDUFS5_AD_1869, and MRPL43_AD_12856 were significantly correlated with the corresponding SNPs rs12898397, rs2863095, and rs1122472 respectively in most of the analyzed cancers (Figure 3E). However, the relationship of significant correlations between XRCC4_AA_72698 and the corresponding SNPs rs1805377, rs1056503, and rs2035990 were only found in WAs and BAs tumors, which indicates that in addition to genomic factors, environmental factors such as lifestyle and diet may also play a role in tumors frequently occurring in Asian populations.

We further integrated race-related ASEs and sQTLs data in KIRC to comprehensively assess the impact of SNPs on ASEs. Considering the criteria of data filtering shown in the CancerSplicingQTL database: 1) splicing events exist in more than 90% of samples; 2) alternative exon is an independent single exon, the database included 16,225 ASEs (AA, AD, ES, and RI) in KIRC and 4891 ASEs were found significantly SNPs correlated. The data of race-related ASEs (|ΔPSI| >0.1, FDR < 0.05) in the KIRC cohort was screened further according to the above criteria, and 107

ASEs remained. After integrating with sQTLs data, we found that 63 (58.9%) of the race-related ASEs were SNP-significantly correlated ASEs (Fisher's exact test P = 8.79e-10), including CAST_ES_72854, XRCC4_AA_72698 and Al Abo reported ASEs such as NEK3_ES_25994, ULK3_AD_31756, and NDUFS5_AD_1869 (Figure 3F). This data suggested that SNPs might be the main reason for the differences in alternative splicing in KIRC patients of different races.

Clinical features-related AS in ESCA

We found that there were multiple clinical features such as disease type, race, pathological grade, reflux history, and BMI, that were significantly correlated with ASEs in ESCA (Figure 2). Among these clinical features, the pathological disease type was found related to most ASEs, so the relationship between the disease type and other clinical features was investigated using a "waterfall" plot. In ESCA, pathological disease types were mainly divided into adenocarcinoma and squamous cell carcinoma. Fisher's exact test showed that other clinical features were significantly correlated (overlapped) with pathological disease types, especially for race, tumor location, and BMI ($P < 0.05$, Figure 4A). Esophageal cancer in the Asian populations is mostly squamous cell carcinoma that occurs in the middle third of the esophagus, which may be related to an over-heat diet and other living habits (30). While in the White American population esophageal cancer is mostly adenocarcinoma that occurs in the lower third of the esophagus, which might be related to the incidence of gastroesophageal reflux followed by high BMI.

To effectively identify disease type- and race-related ASEs in ESCA, we further analyzed the splicing differences between adenocarcinoma and squamous cell carcinoma in WAs as well as splicing differences between AAs and WAs in squamous cell carcinoma. The results showed that 1,717 instead of 2,097 ASEs were identified after adjustment by race between different disease types and that 39 instead of 1,232 ASEs were identified after adjustment by disease type between different races. Gene function

FIGURE 4
Analysis of AS-related clinical features in ESCA. **(A)** A waterfall plot was performed to display the relative relationships of AS-related clinical features, and the pathological disease type was set as the fundamental control. Fisher's exact test was used to value the significance of the relationships between these clinical features with disease type. **(B)** Bar chart was used to show the results of gene function enrichment analysis of 1,018 genes within 1,717 disease type-related ASEs in the White Americans.

enrichment analysis showed that 1,018 genes within these 1,717 disease-type-related ASEs were mainly enriched to pathways such as actin filament-based process and signaling by Rho GTPases (Figure 4B). Among these 39 race-related differential ASEs, 23 were identified as race-related between WAs and BAs in at least 5 cancer types. These results indicated that disease type might decide the splicing differences in ESCA, and that race might only contribute a few to these differences. Moreover, race-related ASEs can be found more effectively by requiring of existing in several cancer types at the same time.

Function enrichment analysis of clinical feature-related ASEs in cancers

To analyze the gene function of ASEs related to different clinical features in tumors, clinical features with considerable ASEs in cancers were selected to perform gene function enrichment analysis, including "neoplasm histologic grade" in BLCA, "pathologic M" in KIRC, "acute myeloid leukemia calgb cytogenetics risk category" in LAML, "site of resection" in PAAD, "history of colon polyps" in COAD, "fetoprotein outcome value" in LIHC, "tobacco smoking history" in LUAD, and "gender" in KIRP (Figures 5A; S3A). The results showed that the "GO:0016071/mRNA metabolic process" and "GO:0044265/cellular macromolecule catabolic process" were the most 2 significant enrichment pathways of ASEs related to "neoplasm histologic grade" in BLCA. "R–HSA–194315/Signaling by Rho GTPases" and "R–HSA–71291/Metabolism of amino acids and derivatives" were the most 2 pathways of "pathologic M" in KIRC. "R–HSA–9675108/Nervous system development" and "R–HSA–9006934/Signaling by Receptor Tyrosine Kinases" were the most 2 pathways of "site of resection"-related ASEs in PAAD. "R–HSA–9006934/Signaling by Receptor Tyrosine Kinases" and "R–HSA–9012999/RHO GTPase cycle" were the most 2 pathways of "CALGB cytogenetics risk"-related ASEs in LAML (Figure 5A). "GO:0032878/regulation of establishment of cell polarity" and "GO:0000278/mitotic cell cycle" were the most 2 pathways of the "history of colon polyps" in COAD. "WP2882/Nuclear receptors meta–pathway" and "R–HSA–382551/Transport of small molecules" were the 2 pathways of "fetoprotein outcome value" in LIHC. "hsa05168/Herpes simplex virus 1 infection" and "R–HSA–382551/Transport of small molecules" were the most two pathways of "gender" in KIRP. "WP3678/Amplification and expansion of metastatic traits" and "GO:0006664/glycolipid metabolic process" were the most 2 pathways of "tobacco smoking history" in LUAD (Figure S3A).

For example, the pathway "Signaling by Rho GTPases" showed a significant association with pathological metastasis of KIRC. Among genes in this pathway, AS of GIT2 (GIT2_AA_24375), showed a significant increase in metastasis tissues compared with no-metastasis tissues and was negatively associated with progression-free survival of KIRC patients, while AS of TUBB3 (TUBB3_ES_38175) showed a significant decrease in metastasis tissues and was positively associated with progression-free survival of KIRC patients (Figures 5B, C). The pathway "Signaling by Receptor Tyrosine Kinases" showed a significant association with the "CALGB cytogenetics risk" of LAML. AS of ABI2 (ABI1_ES_11042), a key gene in this pathway, showed a significant increase in the poor category compared with the favorable category and was associated with poor overall survival of LAML patients (Figure 5D). The pathway "regulation of establishment or maintenance of cell polarity" also significantly enriched the "history of colon polyps"-related ASEs in COAD. Among genes in this pathway, AS of LLGL2 (LLGL2_AP_43458) showed a significant increase in COAD with a history of colon polyps when compared to COAD patients without (Figure S3B). The pathway "Nuclear receptors meta-pathway" significantly enriched with the "fetoprotein outcome value"-related ASEs in LIHC. Among these, AS of SCP2 (SCP2_ES_3045) and SLC27A5 (SLC27A5_AP_52472) showed a significant difference in LIHC with different fetoprotein levels and were both. associated with LIHC patients' overall survival (Figure S3C, D).

Identification of RBPs to regulate clinical feature-related ASEs

RBPs could be predicted by the enrichment of motifs around alternative exon for ASEs in splice types AA, AD, ES, RI, and ME respectively. We identified clinical feature-related ASEs in several cancer types (Figure 2). However, these clinical feature-related ASEs were in different proportions of splice types, and exon skipping (ES) accounted for the most (Figure S1). To explore the potential regulators of "neoplasm histologic grade"-related ASEs in BLCA and "history of colon polyps"-related ASEs in COAD, exon skipping (ES) events were extracted with genome coordination and organized into the format that meets the requirements of rMAPS2, due to the considerable amounts of AS events. The results showed that ASEs up-regulated in BLCA with high-level neoplasm grade were enriched to several RBPs' motifs, including "poly-T" motifs and polypyrimidine tract (Py-tract) sequence of HuR, CPEB4, TIA1, HNRNPC, PTBP1, RALY and ZC3H14, and motifs of PCBP2 and SNRNP70 (Figures 6A, B). ASEs upregulated in COAD without a history of colon polyps were similarly enriched to RBP motifs of neoplasm grade-related ASEs in BLCA (Figure 6C). Py-tract sequence was often located in the upstream intron of alternative exon and used to attract spliceosome through the recognition of RBPs to the 3' splice site, resulting in the inclusion of alternative exons (31). The inclusion of alternative exons of these Py-tract ASEs indicated that mechanisms suppressing exon inclusion were wiped out in BLCA with high-grade pathology. In addition, PCBP2 and SNRNP70 might also play important roles in affecting AS regulation in these different clinical feature groups.

Validation of clinical feature-related ASEs and predicted RBPs

To validate the gene function of ASEs related to different clinical features, we chose a metastasis-related ASE in KIRC

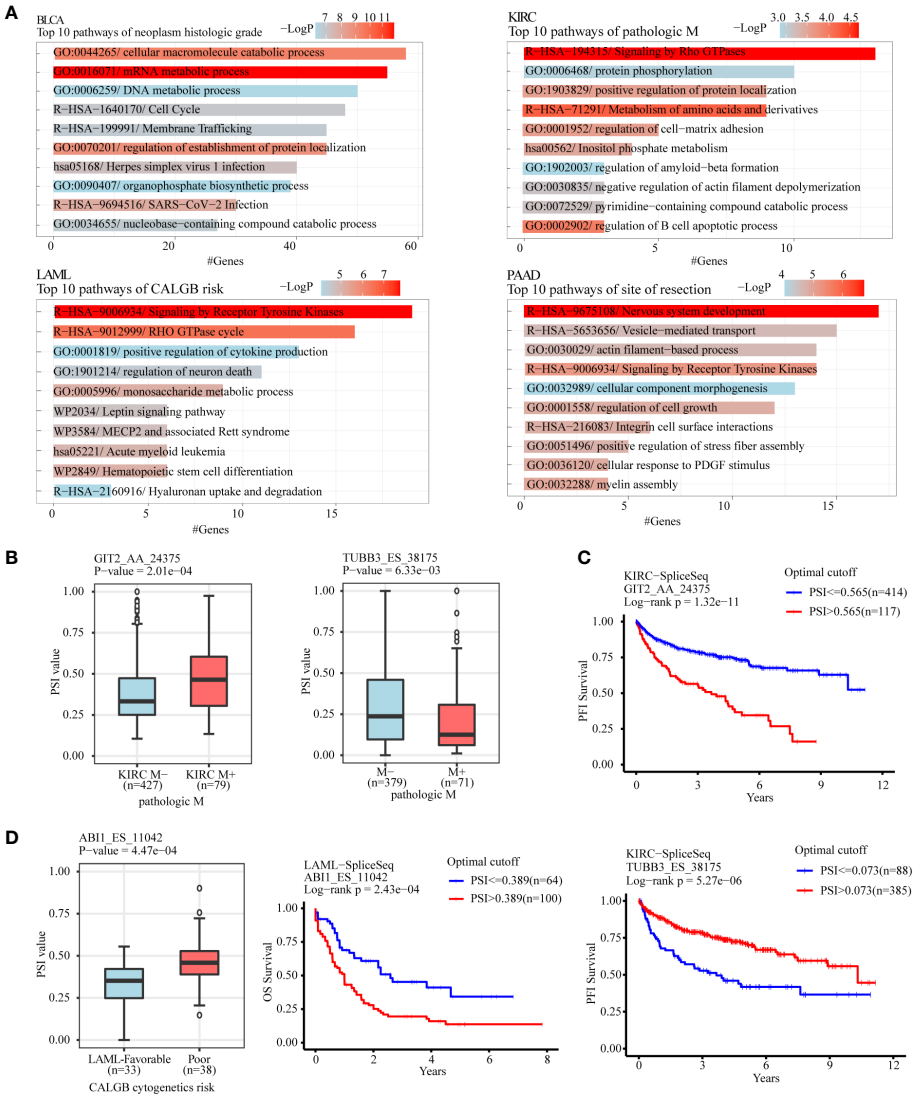

FIGURE 5
Gene function enrichment analysis of clinical feature-related ASEs in cancers. **(A)** Clinical feature-related ASEs in cancers including "neoplasm histologic grade" in BLCA, "pathologic M" in KIRC, "acute myeloid leukemia calgb cytogenetics risk category" in LAML, and "site of resection" in PAAD were selected to perform gene function enrichment analysis. **(B)** GIT2 and TUBB3 were selected as 2 examples of splicing genes belonging to the enriched pathway "Signaling by Rho GTPases" of pathologic metastasis-related ASEs in the KIRC cohort. **(C)** Kaplan-Meier plot showed that AS of GIT2 and TUBB3 was both significantly associated with KIRC patients' progression-free survival. **(D)** ABI1 was selected as an example of splicing genes belonging to the enriched pathway "Signaling by Receptor Tyrosine Kinases" of CALGB cytogenetics risk-related ASEs in the LAML cohort. AS of ABI1 was significantly associated with LAML patients' overall survival.

(TUBB3_ES_38175) as analyzed in Figure 5, and performed experiments to demonstrate the relationship between AS of TUBB3 and metastatic potency of kidney cancer cells. As TUBB3_ES_38175 caused TUBB3 mRNA degradation, we transfected TUBB3 shRNA in OS-RC-2 and 786-O cell lines and verified decreased TUBB3 expression (Figures 7A, B). CCK-8 (Figures 7C, D) and clone formation assays (Figures 7E, F) showed that TUBB3 silencing decreased the proliferation and clonogenic ability in OS-RC-2 and 786-O cells. Importantly, we demonstrated that TUBB3 knock-down significantly weakened the migration ability of OS-RC-2 and 786-O cells (Figures 7G, H), which was consistent with our function enrichment analysis of pathological metastasis-related ASEs in KIRC.

To preliminarily validate the relationship between the above-identified RBPs and associated clinicopathologic features, we explored the role of PCBP2 in the proliferative and migratory ability of bladder cancer cells given the potential regulation of PCBP2 to "neoplasm histologic grade"-related ASEs in BLCA. Human bladder cancer cell lines (T24 and 5637) with PCBP2 stably knocked down were constructed and validated (Figures 8A, B). CCK-8 (Figures 8C, D) and clone formation assays (Figures 8E, F) showed that PCBP2 silencing decreased the proliferation and clonogenic ability in T24 and 5637 cells. Furthermore, we observed that the migration ability was weakened in PCBP2 knock-down T24 and 5637 cells (Figures 8G, H). These results suggested that PCBP2 promoted the malignancy of bladder cancer cells, which was related to the high-grade pathology of BLCA.

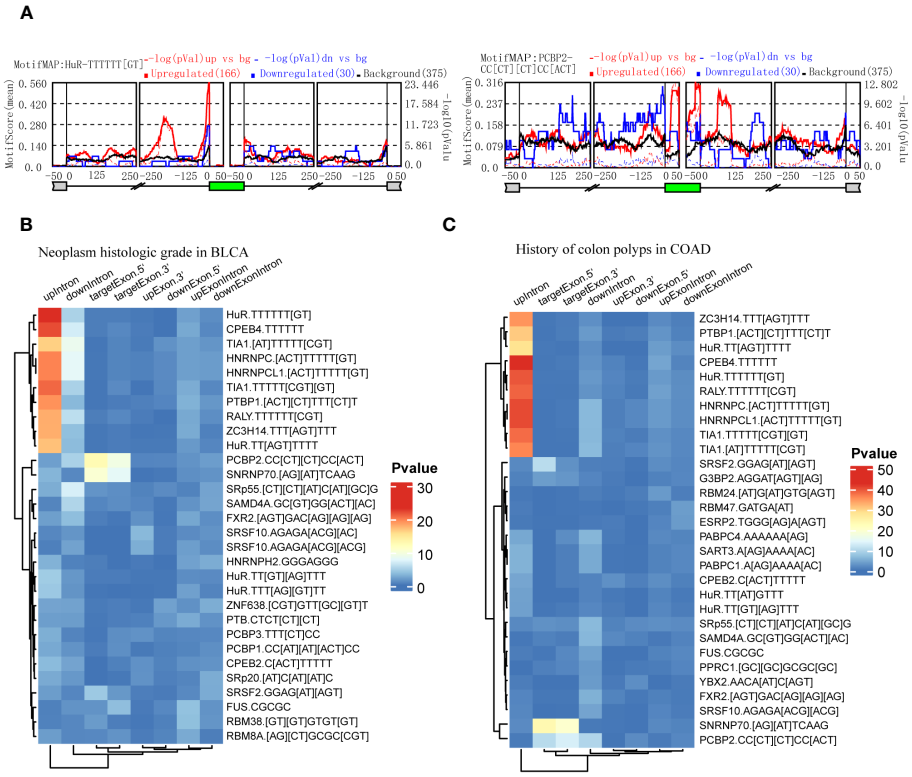

FIGURE 6
Identification of RBPs contributing to the regulation of clinical feature-related ASEs by using rMAPS2. **(A)** HuR and PCBP2 were selected as the 2 most representative RBPs that were enriched to Exon Skipping splicing events in neoplasm histologic grade-related ASEs in BLCA. **(B)** Heatmap showed the most 30 significant enrichments of RBP-motifs to the neoplasm histologic grade-related ASEs in BLCA. **(C)** Heatmap showed the most 30 significant enrichments of RBP-motifs to the colon polyps-related ASEs in COAD.

Discussion

In this study, we systematically analyzed AS differences between different groups of 58 clinical features in 33 cancers, and identified 30 clinical features in 24 cancer types associated with more than 50 ASEs individually. Among these, we found that pathological subtypes might represent the main resource of splicing differences in a cancer type. Race-related ASEs may result from SNPs that vary in different races. Gene function enrichment analyses showed that "pathologic M"-related ASEs in KIRC mainly enriched to "Signaling by Rho GTPases" pathway, "neoplasm histologic grade"-related ASEs in BLCA mainly enriched to "mRNA metabolic process", "CALGB cytogenetics risk category"-related ASEs in LAML mainly enriched to "Signaling by Receptor Tyrosine Kinases". Among those ASEs associated with metastasis, AS of GIT2 and TUBB3 might be 2 represents in KIRC metastasis. While among those ASEs associated with CALGB cytogenetics risk, AS of ABI1 might be an effective representation in LAML. Finally, we identified several RBPs such as PCBP2, SNRNP70, HuR, and TIA1, which might contribute to splicing differences between different groups of neoplasm grade in BLCA. Our work systematically revealed the relationship between AS and clinicopathological features in cancers, providing novel insights for tumor progression and promising molecular targets for cancer therapy by regulating clinically relevant AS and splicing factors.

As aberrant AS has been discovered to be a vital contributor to tumorigenesis and cause of tumor heterogeneity, growing evidence reveals the clinical implications of specific aberrant ASEs in cancers. Among these, most reports focus on the relationship between aberrant ASEs and prognosis and survival in cancer patients. After identification of the overall survival-associated ASEs, prognostic models were developed to predict the survival outcomes of patients with aberrant AS patterns in gastric cancer (32–35), breast cancer (36), CHOL (37), glioblastoma (38), pancreatic cancer (39), LAML (40), UVM (41), HNSC (42), etc. Aberrant AS is also related to chemotherapy resistance. Androgen-receptor splice variant (AR-V7), a transcript generated by the AS mechanism, is responsible for the resistance to enzalutamide and abiraterone in castration-resistant prostate cancer (43). In addition, there are a few studies that reported the relationship between AS and pathological characteristics of tumors. Belluti et al. suggested that different NF-YA isoforms led to different phenotypes of prostate cancers (44). In oral squamous cell carcinoma, TGIF1 splicing variant 8 was reported to be correlated with the pathologic stage (45). In our previous study, we characterized large amounts of different ASEs in 2 pathological subtypes of testicular germ cell tumors (46). However, ASEs related to diverse clinicopathologic characteristics are still rarely systematically profiled in pan-cancers. Herein, the present study included 58 clinicopathologic characteristics of cancers in differential AS analysis and identified

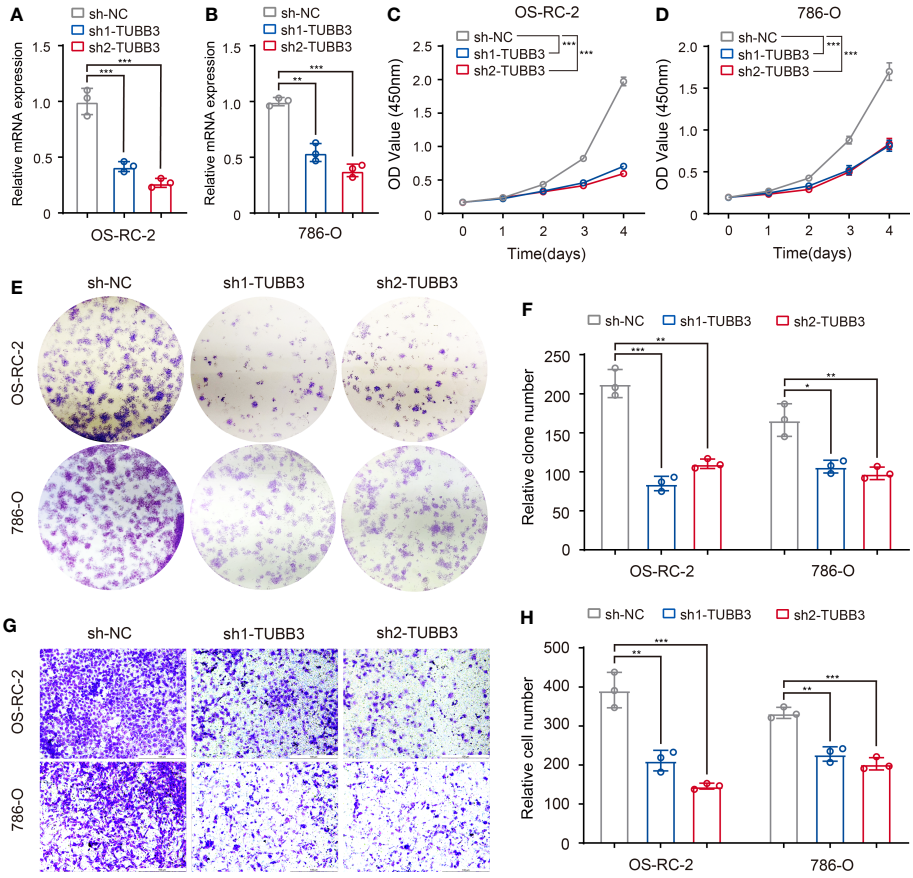

FIGURE 7
Validation of metastasis-related ASEs (TUBB3_ES_38175) in kidney cancer cells. **(A, B)** Expression of TUBB3 mRNA was determined by qPCR in OS-RC-2 and 786-O cells with TUBB3 knockdown. **(C, D)** CCK-8 assays were performed in OS-RC-2 and 786-O cells after sh1-TUBB3, sh2-TUBB3 and sh-NC transfection. **(E, F)** Colony formation assays were performed in OS-RC-2 and 786-O cells after sh1-TUBB3, sh2-TUBB3 and sh-NC transfection. **(G, H)** Modified Boyden chamber assays were applied for migration of OS-RC-2 and 786-O cells after sh1-TUBB3, sh2-TUBB3 and sh-NC transfection. The data are shown as the mean ± SD. One representative plot of n = 3 experiments is shown. *, P < 0.05; **, P < 0.01, ***, P < 0.001, as determined by one-way **(A, B, F, H)** or two-way **(C, D)** ANOVA.

clinically relevant ASEs across multiple cancers. A considerable number of ASEs were found to be associated with clinical features such as race, pathologic T, neoplasm histologic grade and disease type. And profiles of clinically relevant ASEs varied with tumor types. For example, in KIRC, different ASEs were mainly associated with pathological metastasis, and function enrichment analysis showed that these ASEs were enriched in pathway "Signaling by Rho GTPases", which was considered a critical pathway involved in cancer metastasis (47).

Although the relationship between aberrant ASEs and tumor heterogeneity is well characterized, how ASEs contribute to tumor heterogeneity and affect tumorigenesis and tumor progression remains unclear. It is generally accepted that aberrant AS affects the expression patterns of tumor-related genes. Mechanically, aberrant AS may create a premature termination codon (PTC) which can be recognized by the intracellular mRNA quality surveillance system and then trigger the activation of the nonsense-mediated mRNA decay (NMD) pathway (48). For instance, Wollerton et al. revealed that AS of polypyrimidine tract binding protein (PTB) created mRNA isoforms that were destructed during NMD (49). Interestingly, we found that the ASE "TUBB3_ES_38175" was associated with pathological metastasis in KIRC. However, the ASE "TUBB3_ES_38175" generated a TUBB3 mRNA isoform that could be removed by NMD, and was down-regulated in metastatic cancer. This AS event, in turn, increased the expression of TUBB3, which was evidenced to promote the progression of KIRC and also validated by our experiments *in vitro* (50). The ASE "TUBB3_ES_38175" could serve as a marker of tumor heterogeneity in KIRC to evaluate tumor metastasis, guide cancer therapies, and deepen our understanding of the mechanism of cancer progression. Therefore, our result indicated that the occurrence of specific ASEs could exert anti-tumor effects.

Given that AS plays such a critical role in the genesis and development of multiple cancer types, it is urgent to clarify the modulation of AS. As a nuclear process mediated by spliceosome formed by small nuclear ribonucleoproteins (snRNPs), AS is regulated mainly by cis-acting elements and trans-acting RBPs including splicing factors. Through whole-exome and RNA sequencing, the somatic mutation in splicing regulatory cis-

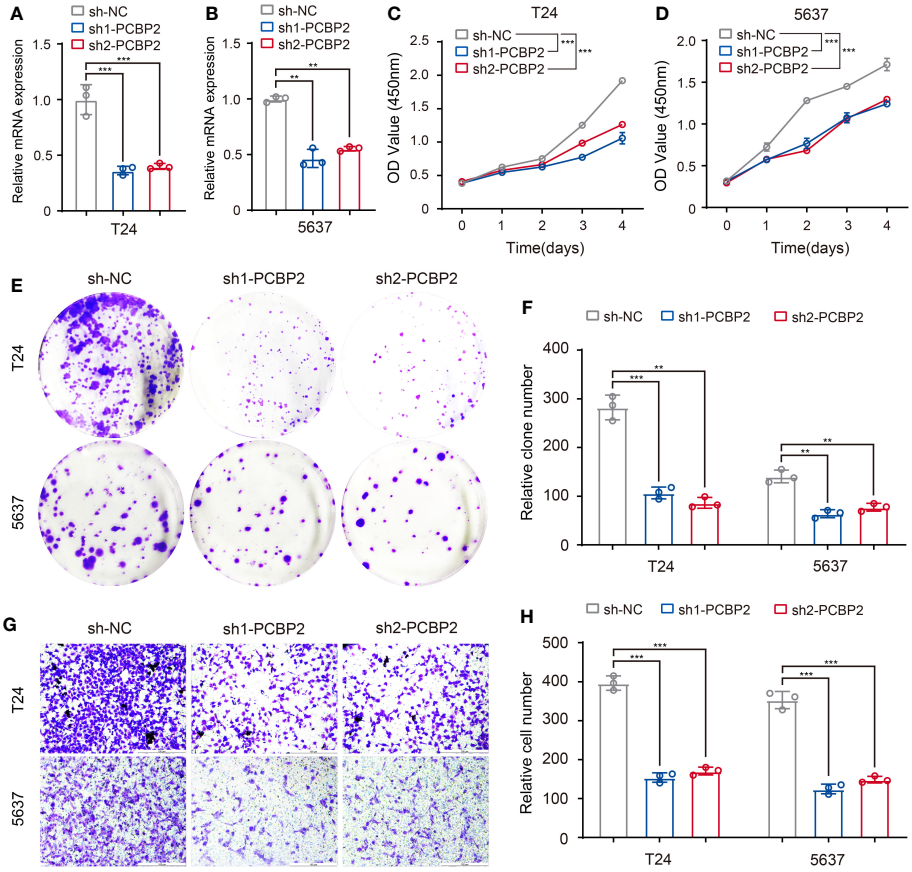

FIGURE 8
Validation of identified RBP (PCBP2) in tumor cells. **(A, B)** Expression of PCBP2 mRNA was determined by qPCR in T24 and 5637 cells with PCBP2 knocked down. **(C, D)** CCK-8 assays were performed in T24 and 5637 cells after sh1-PCBP2, sh2-PCBP2 and sh-NC transfection. **(E, F)** Cell colony formation assays were performed in T24 and 5637 cells after sh1-PCBP2, sh2-PCBP2 and sh-NC transfection. **(G, H)** Transwell assays were applied for migration of T24 and 5637 cells after sh1-PCBP2, sh2-PCBP2 and sh-NC transfection. The data are shown as the mean ± SD. One representative plot of n = 3 experiments is shown. **P < 0.01, ***P < 0.001, as determined by one-way **(A, B, F, H)** or two-way **(C, D)** ANOVA.

elements was shown to affect AS in cancers (51). In the present study, we revealed the relationship between ASEs and nearby SNPs in different races, suggesting that mutations in cis-elements decided race-related ASEs across cancer types. In addition, numerous studies reported that mutations and epigenetic regulation of trans-factors accounted for aberrant ASEs in cancers. Frequent somatic mutations in splicing factors including SF3B1, SRSF2, and U2AF1 were discovered in myeloid malignancies as well as solid tumors (52–59). The expression of splicing factors was also reported to be regulated by DNA methylation and histone modification (60–62). Furthermore, a transcription factors-RBPs-AS triplet analysis was used to interpret aberrant ASEs in cancer (63). Our results identified RBPs including PCBP2 and SNRNP70 responsible for differential ASEs upregulated in BLCA with high-level neoplasm grade. However, the functions and modulations of identified RBPs in cancers need further investigation in experimental and clinical studies.

To sum up, through detailed analysis of the differences in AS among the clinical features of tumors, we found that there are significant correlations between multiple clinical features such as race, disease type, age and gender, and AS. These differences may be affected by SNPs or splicing factors. Although we see associations between clinical features, which somewhat downplays differences in AS among other clinical features, however, this splicing difference plays a role in the differential development of the disease. What kind of effect is not yet achieved, and still needs a lot of further research.

Data availability statement

The original contributions presented in the study are included in the article/Supplementary Material. Further inquiries can be directed to the corresponding authors.

Author contributions

Conceptualization, CD, YZ, ZH, and HX; methodology, validation, CD and YZ; data collection and analyzing, LL, KL, XY, SL, and YG; writing, CD, YZ, YG, and HX; data curation, XW, BL, XM, and HW; project administration, JZ, HL, ZH, and HX. All

authors contributed to the article and approved the submitted version.

Funding

The authors declare that no financial support was received for the research, authorship, and/or publication of this article.

Conflict of interest

The authors declare that the research was conducted in the absence of any commercial or financial relationships that could be construed as a potential conflict of interest.

Publisher's note

Supplementary material

The Supplementary Material for this article can be found online at: https://www.frontiersin.org/articles/10.3389/fonc.2023.1249932/full#supplementary-material

SUPPLEMENTARY FIGURE 1
The statistics of the number of splicing events in different splicing types associated with clinical features in cancers. Only the 30 clinical features in 24 cancer types that were associated with more than 50 ASEs were displayed.

SUPPLEMENTARY FIGURE 2
The statistics of the significance of differences in immune cell infiltration between 2 groups of clinical features in cancers. TCGA-CIBERSORT project data was used to perform differential analysis. Only the 14 immune cells and 23 clinical features in 21 cancer types with a delta proportion of more than 3 percent and BH adjust P value of less than 0.05 were kept and displayed.

SUPPLEMENTARY FIGURE 3
Gene function enrichment analysis of clinical feature-related ASEs in cancers. **(A)** Clinical feature-related ASEs in cancers including "history of colon polyps" in COAD, "fetoprotein outcome value" in LIHC, "tobacco smoking history" in LUAD, and "gender" in KIRP were selected to perform gene function enrichment analysis. **(B)** LLGL2 and ECT2 were selected as an example of splicing genes respectively belonging to the enriched pathways "regulation of establishment or maintenance of cell polarity" and "mitotic cell cycle" of colon polyps-related ASEs in the COAD cohort. **(C)** SLC27A5 and SCP2 were selected as 2 examples of splicing genes belonging to the enriched pathway "Nuclear receptors meta-pathway" of fetoprotein outcome value-related ASEs in the LIHC cohort. **(D)** Kaplan-Meier plots showed that AS of SLC27A5 and SCP2 was significantly associated with LIHC patients' overall survival.

References

1. Bray F, Ren JS, Masuyer E, Ferlay J. Global estimates of cancer prevalence for 27 sites in the adult population in 2008. *Int J Cancer.* (2013) 132(5):1133–45. doi: 10.1002/ijc.27711

2. Collaborators GBDCRF. The global burden of cancer attributable to risk factors, 2010-19: a systematic analysis for the Global Burden of Disease Study 2019. *Lancet* (2022) 400(10352):563–91. doi: 10.1016/S0140-6736(22)01438-6

3. Robin X, Creixell P, Radetskaya O, Santini CC, Longden J, Linding R. Personalized network-based treatments in oncology. *Clin Pharmacol Ther* (2013) 94 (6):646–50. doi: 10.1038/clpt.2013.171

4. Dagogo-Jack I, Shaw AT. Tumour heterogeneity and resistance to cancer therapies. *Nat Rev Clin Oncol* (2018) 15(2):81–94. doi: 10.1038/nrclinonc.2017.166

5. Creixell P, Reimand J, Haider S, Wu G, Shibata T, Vazquez M, et al. Pathway and network analysis of cancer genomes. *Nat Methods* (2015) 12(7):615–21. doi: 10.1038/nmeth.3440

6. Li H, Courtois ET, Sengupta D, Tan Y, Chen KH, Goh JJL, et al. Reference component analysis of single-cell transcriptomes elucidates cellular heterogeneity in human colorectal tumors. *Nat Genet* (2017) 49(5):708–18. doi: 10.1038/ng.3818

7. Mobadersany P, Yousefi S, Amgad M, Gutman DA, Barnholtz-Sloan JS, Velazquez Vega JE, et al. Predicting cancer outcomes from histology and genomics using convolutional networks. *Proc Natl Acad Sci U S A.* (2018) 115(13):E2970–E9. doi: 10.1073/pnas.1717139115

8. Van Allen EM, Wagle N, Stojanov P, Perrin DL, Cibulskis K, Marlow S, et al. Whole-exome sequencing and clinical interpretation of formalin-fixed, paraffin-embedded tumor samples to guide precision cancer medicine. *Nat Med* (2014) 20 (6):682–8. doi: 10.1038/nm.3559

9. Burkhardt B, Michgehl U, Rohde J, Erdmann T, Berning P, Reutter K, et al. Clinical relevance of molecular characteristics in Burkitt lymphoma differs according to age. *Nat Commun* (2022) 13(1):3881. doi: 10.1038/s41467-022-31355-8

10. Drews RM, Hernando B, Tarabichi M, Haase K, Lesluyes T, Smith PS, et al. A pan-cancer compendium of chromosomal instability. *Nature* (2022) 606(7916):976–83. doi: 10.1038/s41586-022-04789-9

11. Han L, Diao L, Yu S, Xu X, Li J, Zhang R, et al. The genomic landscape and clinical relevance of A-to-I RNA editing in human cancers. *Cancer Cell* (2015) 28 (4):515–28. doi: 10.1016/j.ccell.2015.08.013

12. Li Y, Xiao J, Bai J, Tian Y, Qu Y, Chen X, et al. Molecular characterization and clinical relevance of m(6)A regulators across 33 cancer types. *Mol Cancer.* (2019) 18 (1):137. doi: 10.1186/s12943-019-1066-3

13. Xu K, Cai Y, Zhang M, Zou H, Chang Z, Li D, et al. Pan-cancer characterization of expression and clinical relevance of m(6)A-related tissue-elevated long non-coding RNAs. *Mol Cancer.* (2021) 20(1):31. doi: 10.1186/s12943-021-01324-8

14. Zhang C, Zhang Z, Zhang Z, Luo Y, Wu P, Zhang G, et al. The landscape of m(6) A regulators in small cell lung cancer: molecular characteristics, immuno-oncology features, and clinical relevance. *Mol Cancer.* (2021) 20(1):122. doi: 10.1186/s12943-021-01408-5

15. Bonnal SC, Lopez-Oreja I, Valcarcel J. Roles and mechanisms of alternative splicing in cancer - implications for care. *Nat Rev Clin Oncol* (2020) 17(8):457–74. doi: 10.1038/s41571-020-0350-x

16. Dvinge H, Kim E, Abdel-Wahab O, Bradley RK. RNA splicing factors as oncoproteins and tumour suppressors. *Nat Rev Cancer.* (2016) 16(7):413–30. doi: 10.1038/nrc.2016.51

17. Oltean S, Bates DO. Hallmarks of alternative splicing in cancer. *Oncogene* (2014) 33(46):5311–8. doi: 10.1038/onc.2013.533

18. Miwa T, Nagata T, Kojima H, Sekine S, Okumura T. Isoform switch of CD44 induces different chemotactic and tumorigenic ability in gallbladder cancer. *Int J Oncol* (2017) 51(3):771–80. doi: 10.3892/ijo.2017.4063

19. Bhattacharya R, Mitra T, Ray Chaudhuri S, Roy SS. Mesenchymal splice isoform of CD44 (CD44s) promotes EMT/invasion and imparts stem-like properties to ovarian cancer cells. *J Cell Biochem* (2018) 119(4):3373–83. doi: 10.1002/jcb.26504

20. Brown RL, Reinke LM, Damerow MS, Perez D, Chodosh LA, Yang J, et al. CD44 splice isoform switching in human and mouse epithelium is essential for epithelial-mesenchymal transition and breast cancer progression. *J Clin Invest.* (2011) 121 (3):1064–74. doi: 10.1172/JCI44540

21. Sakuma K, Sasaki E, Kimura K, Komori K, Shimizu Y, Yatabe Y, et al. HNRNPLL, a newly identified colorectal cancer metastasis suppressor, modulates alternative splicing of CD44 during epithelial-mesenchymal transition. *Gut* (2018) 67 (6):1103–11. doi: 10.1136/gutjnl-2016-312927

22. Busch A, Hertel KJ. Evolution of SR protein and hnRNP splicing regulatory factors. *Wiley Interdiscip Rev RNA.* (2012) 3(1):1–12. doi: 10.1002/wrna.100

23. Dvinge H, Guenthoer J, Porter PL, Bradley RK. RNA components of the spliceosome regulate tissue- and cancer-specific alternative splicing. *Genome Res* (2019) 29(10):1591–604. doi: 10.1101/gr.246678.118

24. Brooks AN, Choi PS, de Waal L, Sharifnia T, Imielinski M, Saksena G, et al. A pan-cancer analysis of transcriptome changes associated with somatic mutations in U2AF1 reveals commonly altered splicing events. *PloS One* (2014) 9(1):e87361. doi: 10.1371/journal.pone.0087361

25. Maguire SL, Leonidou A, Wai P, Marchio C, Ng CK, Sapino A, et al. SF3B1 mutations constitute a novel therapeutic target in breast cancer. *J Pathol* (2015) 235 (4):571–80. doi: 10.1002/path.4483

26. Zhang Y, Yan L, Zeng J, Zhou H, Liu H, Yu G, et al. Pan-cancer analysis of clinical relevance of alternative splicing events in 31 human cancers. *Oncogene* (2019) 38(40):6678–95. doi: 10.1038/s41388-019-0910-7

27. Zhang Y, Yao X, Zhou H, Wu X, Tian J, Zeng J, et al. OncoSplicing: an updated database for clinically relevant alternative splicing in 33 human cancers. *Nucleic Acids Res* (2022) 50(D1):D1340–D7. doi: 10.1093/nar/gkab851

28. Hwang JY, Jung S, Kook TL, Rouchka EC, Bok J, Park JW. rMAPS2: an update of the RNA map analysis and plotting server for alternative splicing regulation. *Nucleic Acids Res* (2020) 48(W1):W300–W6. doi: 10.1093/nar/gkaa237

29. Al Abo M, Hyslop T, Qin X, Owzar K, George DJ, Patierno SR, et al. Differential alternative RNA splicing and transcription events between tumors from African American and White patients in The Cancer Genome Atlas. *Genomics* (2021) 113 (3):1234–46. doi: 10.1016/j.ygeno.2021.02.020

30. Sung H, Ferlay J, Siegel RL, Laversanne M, Soerjomataram I, Jemal A, et al. Global cancer statistics 2020: GLOBOCAN estimates of incidence and mortality worldwide for 36 cancers in 185 countries. *CA Cancer J Clin* (2021) 71(3):209–49. doi: 10.3322/caac.21660

31. Wilkinson ME, Charenton C, Nagai K. RNA splicing by the spliceosome. *Annu Rev Biochem* (2020) 89:359–88. doi: 10.1146/annurev-biochem-091719-064225

32. Jun Y, Suh YS, Park S, Lee J, Kim JI, Lee S, et al. Comprehensive analysis of alternative splicing in gastric cancer identifies epithelial-mesenchymal transition subtypes associated with survival. *Cancer Res* (2022) 82(4):543–55. doi: 10.1158/0008-5472.CAN-21-2117

33. Lin C, Yu B, Zhang M, Chen Y, Li L, Zhao D. Systematic analyses of the differentially expressed alternative splicing events in gastric cancer and its clinical significance. *Front Genet* (2020) 11:522831. doi: 10.3389/fgene.2020.522831

34. Liu C, Hu C, Li Z, Feng J, Huang J, Yang B, et al. Systematic profiling of alternative splicing in Helicobacter pylori-negative gastric cancer and their clinical significance. *Cancer Cell Int* (2020) 20:279. doi: 10.1186/s12935-020-01368-8

35. Lin P, He RQ, Ma FC, Liang L, He Y, Yang H, et al. Systematic analysis of survival-associated alternative splicing signatures in gastrointestinal pan-adenocarcinomas. *EBioMedicine* (2018) 34:46–60. doi: 10.1016/j.ebiom.2018.07.040

36. Du JX, Liu YL, Zhu GQ, Luo YH, Chen C, Cai CZ, et al. Profiles of alternative splicing landscape in breast cancer and their clinical significance: an integrative analysis based on large-sequencing data. *Ann Transl Med* (2021) 9(1):58. doi: 10.21037/atm-20-7203

37. Lin Z, Gong J, Zhong G, Hu J, Cai D, Zhao L, et al. Identification of mutator-derived alternative splicing signatures of genomic instability for improving the clinical outcome of cholangiocarcinoma. *Front Oncol* (2021) 11:666847. doi: 10.3389/fonc.2021.666847

38. Li Y, Guo D. Genome-wide profiling of alternative splicing in glioblastoma and their clinical value. *BMC Cancer.* (2021) 21(1):958. doi: 10.1186/s12885-021-08681-z

39. Xu L, Pan J, Ding Y, Pan H. Survival-associated alternative splicing events and prognostic signatures in pancreatic cancer. *Front Genet* (2020) 11:522383. doi: 10.3389/fgene.2020.522383

40. Zhang N, Zhang P, Chen Y, Lou S, Zeng H, Deng J. Clusterization in acute myeloid leukemia based on prognostic alternative splicing signature to reveal the clinical characteristics in the bone marrow microenvironment. *Cell Biosci* (2020) 10:118. doi: 10.1186/s13578-020-00481-5

41. Zhou W, Fei P, Li J. Identification of Prognostic alternative splicing signatures and their clinical significance in uveal melanoma. *Exp Eye Res* (2021) 209:108666. doi: 10.1016/j.exer.2021.108666

42. Jiang J, Niu L, Zhang MX, Wang H, Xie JQ, Sun GP. A novel nomogram combining alternative splicing events and clinical factors for prognosis prediction in head and neck squamous cell carcinoma. *J Oncol* (2022) 2022:4552445. doi: 10.1155/2022/4552445

43. Antonarakis ES, Lu C, Wang H, Luber B, Nakazawa M, Roeser JC, et al. AR-V7 and resistance to enzalutamide and abiraterone in prostate cancer. *N Engl J Med* (2014) 371(11):1028–38. doi: 10.1056/NEJMoa1315815

44. Belluti S, Semeghini V, Rigillo G, Ronzio M, Benati D, Torricelli F, et al. Alternative splicing of NF-YA promotes prostate cancer aggressiveness and represents a new molecular marker for clinical stratification of patients. *J Exp Clin Cancer Res* (2021) 40(1):362. doi: 10.1186/s13046-021-02166-4

45. Liborio TN, Ferreira EN, Aquino Xavier FC, Carraro DM, Kowalski LP, Soares FA, et al. TGIF1 splicing variant 8 is overexpressed in oral squamous cell carcinoma and is related to pathologic and clinical behavior. *Oral Surg Oral Med Oral Pathol Oral Radiol* (2013) 116(5):614–25. doi: 10.1016/j.oooo.2013.07.014

46. Yao X, Zhou H, Duan C, Wu X, Li B, Liu H, et al. Comprehensive characteristics of pathological subtypes in testicular germ cell tumor: Gene expression, mutation and alternative splicing. *Front Immunol* (2022) 13:1096494. doi: 10.3389/fimmu.2022.1096494

47. Zeng RJ, Zheng CW, Chen WX, Xu LY, Li EM. Rho GTPases in cancer radiotherapy and metastasis. *Cancer Metastasis Rev* (2020) 39(4):1245–62. doi: 10.1007/s10555-020-09923-5

48. Popp MW, Maquat LE. Organizing principles of mammalian nonsense-mediated mRNA decay. *Annu Rev Genet* (2013) 47:139–65. doi: 10.1146/annurev-genet-111212-133424

49. Wollerton MC, Gooding C, Wagner EJ, Garcia-Blanco MA, Smith CWJ. Autoregulation of polypyrimidine tract binding protein by alternative splicing leading to nonsense-mediated decay. *Mol Cell* (2004) 13:91–100. doi: 10.1016/s1097-2765(03)00502-1

50. Sekino Y, Han X, Babasaki T, Miyamoto S, Kitano H, Kobayashi G, et al. TUBB3 is associated with high-grade histology, poor prognosis, p53 expression, and cancer stem cell markers in clear cell renal cell carcinoma. *Oncology* (2020) 98(10):689–98. doi: 10.1159/000506775

51. Jung H, Lee D, Lee J, Park D, Kim YJ, Park WY, et al. Intron retention is a widespread mechanism of tumor-suppressor inactivation. *Nat Genet* (2015) 47 (11):1242–8. doi: 10.1038/ng.3414

52. Yoshida K, Sanada M, Shiraishi Y, Nowak D, Nagata Y, Yamamoto R, et al. Frequent pathway mutations of splicing machinery in myelodysplasia. *Nature* (2011) 478(7367):64–9. doi: 10.1038/nature10496

53. Darman RB, Seiler M, Agrawal AA, Lim KH, Peng S, Aird D, et al. Cancer-associated SF3B1 hotspot mutations induce cryptic 3' Splice site selection through use of a different branch point. *Cell Rep* (2015) 13(5):1033–45. doi: 10.1016/j.celrep.2015.09.053

54. DeBoever C, Ghia EM, Shepard PJ, Rassenti L, Barrett CL, Jepsen K, et al. Transcriptome sequencing reveals potential mechanism of cryptic 3' splice site selection in SF3B1-mutated cancers. *PloS Comput Biol* (2015) 11(3):e1004105. doi: 10.1371/journal.pcbi.1004105

55. Kim E, Ilagan JO, Liang Y, Daubner GM, Lee SC, Ramakrishnan A, et al. SRSF2 mutations contribute to myelodysplasia by mutant-specific effects on exon recognition. *Cancer Cell* (2015) 27(5):617–30. doi: 10.1016/j.ccell.2015.04.006

56. Zhang J, Lieu YK, Ali AM, Penson A, Reggio KS, Rabadan R, et al. Disease-associated mutation in SRSF2 misregulates splicing by altering RNA-binding affinities. *Proc Natl Acad Sci U S A.* (2015) 112(34):E4726–34. doi: 10.1073/pnas.1514105112

57. Okeyo-Owuor T, White BS, Chatrikhi R, Mohan DR, Kim S, Griffith M, et al. U2AF1 mutations alter sequence specificity of pre-mRNA binding and splicing. *Leukemia* (2015) 29(4):909–17. doi: 10.1038/leu.2014.303

58. Stephens PJ, Tarpey PS, Davies H, Van Loo P, Greenman C, Wedge DC, et al. The landscape of cancer genes and mutational processes in breast cancer. *Nature* (2012) 486(7403):400–4. doi: 10.1038/nature11017

59. Biankin AV, Waddell N, Kassahn KS, Gingras MC, Muthuswamy LB, Johns AL, et al. Pancreatic cancer genomes reveal aberrations in axon guidance pathway genes. *Nature* (2012) 491(7424):399–405. doi: 10.1038/nature11547

60. Cheng M, Zhan X, Xu Y, Wang S, Zhang H, Fang L, et al. DNA methylation of RNA-binding protein for multiple splicing 2 functions as diagnosis biomarker in gastric cancer pathogenesis and its potential clinical significance. *Bioengineered* (2022) 13 (2):4347–60. doi: 10.1080/21655979.2022.2032965

61. Luco RF, Pan Q, Tominaga K, Blencowe BJ, Pereira-Smith OM, Misteli T. Regulation of alternative splicing by histone modifications. *Science* (2010) 327 (5968):996–1000. doi: 10.1126/science.1184208

62. Luco RF, Allo M, Schor IE, Kornblihtt AR, Misteli T. Epigenetics in alternative pre-mRNA splicing. *Cell* (2011) 144(1):16–26. doi: 10.1016/j.cell.2010.11.056

63. He M, Hu F. TF-RBP-AS triplet analysis reveals the mechanisms of aberrant alternative splicing events in kidney cancer: implications for their possible clinical use as prognostic and therapeutic biomarkers. *Int J Mol Sci* (2021) 22(16):8789. doi: 10.3390/ijms22168789

frontiers | Frontiers in Pharmacology

TYPE Brief Research Report
PUBLISHED 19 October 2023
DOI 10.3389/fphar.2023.1284899

OPEN ACCESS

EDITED BY
Lei Yin,
Shanghai Jiao Tong University, China

REVIEWED BY
Chunguang Yang,
Huazhong University of Science and Technology, China
Junfei Gu,
The Second Hospital of Hebei Medical University, China

*CORRESPONDENCE
Yongbao Wei,
weiyb@fjmu.edu.cn
Lili Chen,
qzliy2006@fjmu.edu.cn
Qingguo Zhu,
zqg_1969@126.com

RECEIVED 29 August 2023
ACCEPTED 10 October 2023
PUBLISHED 19 October 2023

CITATION
Wei Y, Zhang R, Zhong D, Chen Z, Chen G, Yang M, Lin L, Li T, Ye L, Chen L and Zhu Q (2023), Androgen deprivation therapy plus apalutamide as neoadjuvant therapy prior radical prostatectomy for patients with unresectable prostate cancer.
Front. Pharmacol. 14:1284899.
doi: 10.3389/fphar.2023.1284899

Androgen deprivation therapy plus apalutamide as neoadjuvant therapy prior radical prostatectomy for patients with unresectable prostate cancer

Yongbao Wei[1,2]*, Ruochen Zhang[1,2], Dewen Zhong[3], Zhensheng Chen[4], Gen Chen[5], Minggen Yang[6], Le Lin[1,2], Tao Li[1,2], Liefu Ye[1,2], Lili Chen[1,7]* and Qingguo Zhu[1,2]*

[1]Shengli Clinical Medical College of Fujian Medical University, Fuzhou, China, [2]Department of Urology, Fujian Provincial Hospital, Fuzhou, China, [3]Department of Urology, Longyan First Affiliated Hospital of Fujian Medical University, Longyan, Fujian, China, [4]Department of Urology, Fuding Hospital Affiliated to Fujian University of Traditional Chinese Medicine, Ningde, Fujian, China, [5]Department of Urology, Gutian County Hospital, Ningde, China, [6]Department of Urology, Zhangzhou Affiliated Hospital of Fujian Medical University, Zhangzhou, China, [7]The School of Nursing, Fujian Medical University, Fuzhou, China

Whether neoadjuvant therapy confers a survival benefit in advanced prostate cancer (PCa) remains uncertain. The primary endpoints of previous retrospective and phase II clinical studies that used neoadjuvant therapy, including androgen deprivation therapy combined with new-generation androgen receptor signaling inhibitors or chemotherapy, were pathological downstaging, progression-free survival, prostate-specific antigen relief, and local symptom improvement. To the best of our knowledge, no studies have explored the efficacy and safety of neoadjuvant therapy in improving the surgical resection rate in cases of unresectable primary tumors of PCa. We first designed this retrospective study to evaluate the potential value of apalutamide as neoadjuvant therapy in improving the resectability rate of radical prostatectomy (RP). We initially reported 7 patients with unresectable primary lesions who underwent neoadjuvant apalutamide treatment for a median of 4 months, and all of them successfully underwent RP treatment. Our study supported apalutamide as neoadjuvant therapy, which helped improve RP's success rate and did not significantly increase perioperative complications, and the neoadjuvant therapy was controllable. Our findings' clinical value and benefit for survival still need further clinical research to confirm.

KEYWORDS

prostate cancer, androgen deprivation therapy, apalutamide, neoadjuvant therapy, radical prostatectomy

Introduction

The main goals of neoadjuvant therapy for prostate cancer (PCa) based on androgen deprivation therapy (ADT) are to reduce tumor size, reduce the rate of positive surgical margins, and achieve pathological remission, but no benefit has been observed in terms of cancer-related death (Ge et al., 2022; Wang et al., 2022). Thus, neoadjuvant therapy has not

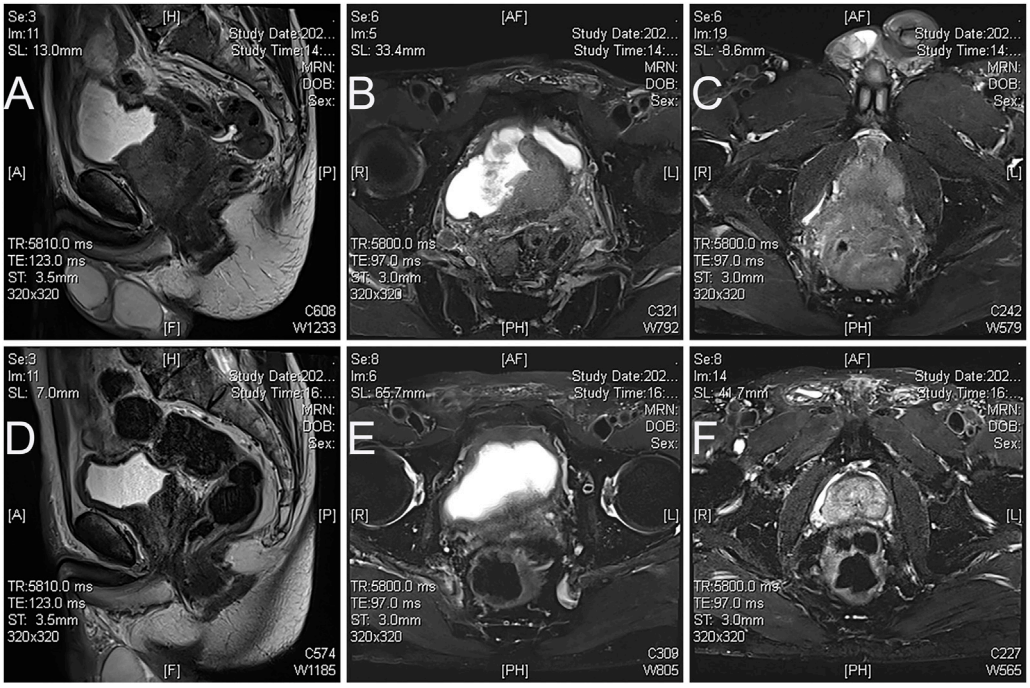

FIGURE 1
Magnetic resonance images of apalutamide before and 3 months post neoadjuvant treatment in case 2. **(A)**, sagittal view, (**B,C**), axial view T2 imaging showed that prostate cancer broke through the prostate capsule and invaded the rectum, bladder neck, and seminal vesicles before neoadjuvant treatment; **(A)**, sagittal view, **(B,C)**, axial view T2 imaging showed that prostate cancer retracted significantly after neoadjuvant therapy **(D)**, the boundary between the prostate and rectum seemed more straightforward, with no apparent tumor involvement in the bladder neck, but lesions invaded seminal vesicle still exists **(E,F)**.

been recommended as the primary treatment option for patients with progressive PCa (Ge et al., 2022; Wang et al., 2022). In the past 20 years, the emergence of new-generation androgen receptor signaling inhibitors (ARSI), such as abiraterone, apalutamide, enzalutamide, and darolutamide, has increased interest in the neoadjuvant treatment of PCa (Devos et al., 2021). Recently, some phase II studies of apalutamide as neoadjuvant therapy, mainly for newly diagnosed patients with medium and high-risk PCa, including a single-arm phase II NEAR trial (Lee et al., 2022; Yang et al., 2022) and a placebo-controlled phase II study (Devos et al., 2023), both their primary endpoints were pathological response rate and safety. Another phase II study explored the effect of apalutamide as neoadjuvant therapy on perioperative complications and found that it did not significantly increase the occurrence of significant complications of grade 3 and above; however, it might increase the risk of thrombosis in patients with RP and lymph node dissection (Ilario et al., 2023).

There is no phase III clinical study data to prove the value of survival benefit in neoadjuvant therapy for progressive PCa. Several phase II clinical studies of ARSI and chemotherapy as neoadjuvant therapy, including docetaxel (Zhuang et al., 2023) or cabazitaxel (Fleshner et al., 2023), main focus is on pathological response rate, pathological downstaging rate, prostate-specific antigen (PSA) benefit, progression-free survival (PFS) and complications. There is no report on the efficacy and safety of neoadjuvant therapy for unresectable progressive PCa. We designed this retrospective study to evaluate the potential value of apalutamide as neoadjuvant therapy in improving the resectability rate of the prostate.

Methods

We included PCa patients diagnosed and treated by the Fujian Prostate Disease Diagnosis and Treatment Alliance (including 45 medical centers) from January 2021 to August 2023. Patients were screened according to the following inclusion and exclusion criteria. The inclusion criteria were as followings: (a) the patient was diagnosed with advanced prostate acinar adenocarcinoma (T4N0-1M0-1); (b) their physical status score were 0 according to Eastern Cooperative Oncology Group (ECOG) (Anker et al., 2016); (c) the patient had completed the multi-parameter magnetic resonance imaging (MRI) plain scan and enhanced examination for prostate before the prostate biopsy (Figure 1), and evaluated by 2 PCa surgeons from Fujian Provincial Hospital as unresectable PCa with progressive primary prostate lesions (defined as PCa with local progression and mainly invading the rectum, bladder and surrounding tissues, and the primary prostate lesions and seminal vesicles could not be removed without avoiding cystectomy or rectal injury; each surgeon had completed 100 or more PCa laparoscopic or robotic surgeries in the past 2 years); (d) patients had undergone at least 3 months of ADT combined with apalutamide 240 mg once daily as neoadjuvant therapy; (e) prostate MRI was re-evaluated after neoadjuvant treatment to evaluate whether the prostate resectable; (f) critical data such as imaging and PSA re-examination were available and the patients were willing to participate this study. Exclusion criteria were as follows: (a) patients with poor physical status (ECOG ≥1); (b) the evaluation of the prostate by MRI or 99mTc-prostate-specific membrane

TABLE 1 Clinicopathological details for this case series.

Cases[a]	Age (years)	BMI (kg/m^2)	Initial PSA (ng/mL)	Needle biopsy Gleason score	cTNM stage	Previous treatments	Pre-surgery PSA (ng/mL)	Duration of surgery (minutes)	Intraoperative blood loss (mL)	Radical prostatectomy Gleason score	ypTNM	Post-surgery PSA (ng/mL)	Post-surgery treatments	PSA (ng/mL) at last follow-up	Follow-up (months)	Surgical complications and grading	\Medication treatment-related adverse events
1	65	23.8	34.23	4 + 4 = 8	T4N1M0	Apalutamide (3 months)	<0.01	190	50	pathological complete response	T0N0M0	<0.01	Apalutamide	<0.01	18	Incontinence for 1 month, Grade 1	Hypertension Grade 1
2	67	26.2	88.49	5 + 5 = 10	T4N1M0	Apalutamide (3 months)	0.78	240	80	5 + 4 = 9	T3bN0M0	<0.01	Apalutamide	<0.01	11	Incontinence for 2 weeks, Grade I	Decreased appetite Grade I; Rash, Grade II; (recovery after reduction)
3	67	21.7	17.34	4 + 5 = 9	T4N0M0	Apalutamide (3 months)	<0.01	230	50	4 + 4 = 8	T2N0M0	<0.01	Apalutamide	<0.01	10	Incontinence for 1 month, Grade I	Fatigue, Grade I
4	81	22.4	271.58	5 + 4 = 9	T4N1M1b	Apalutamide (12 months)	4.09	140	50	4 + 3 = 7	T3bN0M1b	1.32	Apalutamide; Abiraterone plus Olaparib	7.93	20	Incontinence for 3 weeks, Grade I	Rash Grade II (recovery after reduction)
5	66	25.6	41.81	5 + 4 = 9	T4N1M1a	Apalutamide (6 months)	1.34	300	120	4 + 3 = 9	T3aN1M1a	0.10	Apalutamide	<0.01	9	Incontinence for 1 month, Grade II	Pruritus, Grade I
6	74	26.3	70.12	4 + 4 = 8	T4N0M0	Apalutamide (4 months)	<0.01	150	100	3 + 4 = 7	T2N0M0	<0.01	Apalutamide	<0.01	25	Incontinence for 2 weeks, Grade I	Anaemia, Grade I; Hypertriglyceridemia, Grade I
7	67	23.5	147.85	5 + 5 = 10	T4N1M1b	Apalutamide (4 months)	0.09	200	60	4 + 4 = 8	T2N0M1b	<0.01	Apalutamide	<0.01	13	Incontinence for 3 weeks, Grade I	Not observed

[a]Androgen deprivation therapy is the baseline treatment for these patients; BMI, body mass index, weight (in kg)/height‡2 (in m‡2); cTNM, clinical TNM; TNM, according to Union for International Cancer Control TNM, classification of malignant tumours, 8thedition; ypTNM = TNM, staging after neoadjuvant therapy; PSA, prostate-specific antigen.

10.3389/fphar.2023.1284899

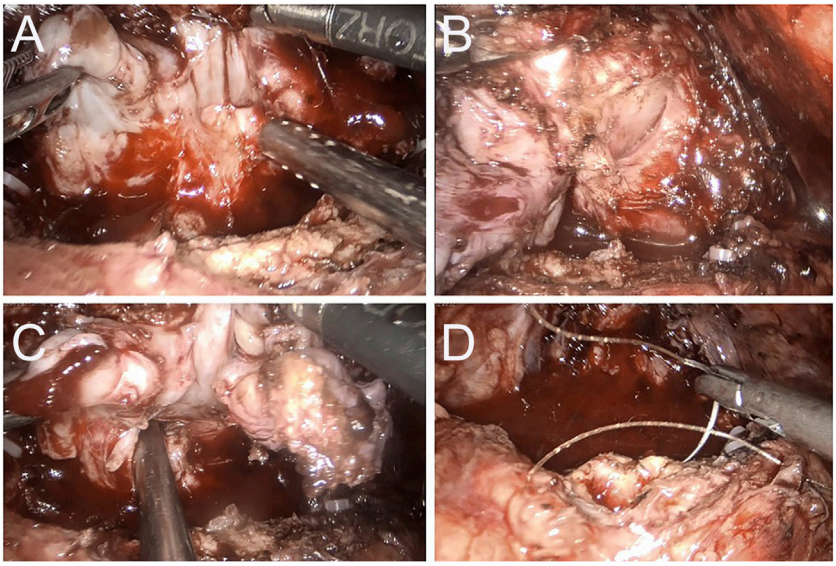

FIGURE 2
Case 2 Intraoperative image of 3 months after apalutamide neoadjuvant therapy. **(A)** The seminal vesicles on both sides are still evident, but apparent adhesions to the rectum are observed; **(B)** a clear separation between the right lobe of the prostate and the rectum; **(C)** the adhesion band with the rectum at the angle of the left seminal vesicles; **(D)** no apparent tumor invasion on the bladder neck and prostate is completely removed.

antigen Computed Tomography (PSMA CT) (Zhang et al., 2022) after neoadjuvant treatment suggested no tumor activity in the prostate; (c) patients with more than 5 bone metastatic foci or combined with visceral metastase (not an oligometastasis) (Wenzel et al., 2023); (d) patients who were not suitable for surgery or who had limited benefit from surgical treatment evaluated by consultation from PCa multidisciplinary team (MDT). The primary endpoint of our study was the number of patients with resectable surgery after neoadjuvant apalutamide therapy. The secondary endpoints were the number of tumor stage remission, the number of pathological remission, and the number of PSA relief (defined as PSA less than 0.10 ng/mL from the start of apalutamide treatment to half a year after surgery), as well as perioperative complications and drug side effects of neoadjuvant treatment.

Results

We finally included 7 patients (Table 1). Their median age was 67 years old (range 65–81 years old), with a median Body mass index of 23.8 kg/m^2 (range 21.7–26.3 kg/m^2). Their median initial PSA was 70.12 ng/mL (range 17.34–271.58 ng/mL), and their median needle biopsy Gleason score was 9 points (range 8–10 points). Their newly diagnosed stage was cT4N0-1M0-1b. Their median ADT plus apalutamide treatment duration was 4 months (range 3–12 months). Preoperative PSA was less than 0.01–4.09 ng/mL. After neoadjuvant treatment, these patients were all re-evaluated as prostate resectable, and all underwent RP or cytoreductive proctectomy (Figure 2), with standard or extended lymph node dissection simultaneously. Their median operative time was 200 min (range 140–300 min), and the median intraoperative blood loss was 60 mL (range 50–120 mL). All patients showed improved lower urinary tract symptoms and downgraded Gleason score after radical prostatectomy, with 1 case achieving pathological complete remission. A decrease in PSA was observed at 1.5 months after surgery, and 5 cases had PSA relief. The median follow-up time was 13 months (range 9–25 months). By the end of the follow-up, 6 cases had sustained PSA relief, and 1 case had PSA decline and then increase, which may be related to the progression of metastatic lesions. No symptom progression was observed in all patients. Neoadjuvant therapy did not significantly increase perioperative complications; no grade 3 or above complications were found (Dindo et al., 2004). Urinary incontinence over 2 months was not observed. No new adverse reactions from neoadjuvant therapy were observed, and the side effects were tolerable.

Discussion

To date, we first reported the potential value of neoadjuvant therapy for unresectable progressive PCa and neoadjuvant therapy did not significantly increase perioperative complications, and the safety was tolerable.

In recent years, some phase II studies of apalutamide as neoadjuvant therapy were performed, mainly for newly diagnosed high-risk PCa patients, with primary endpoints as pathological remission and safety. A single-arm phase II study (NEAR trial) investigating neoadjuvant apalutamide monotherapy and RP in newly diagnosed intermediate- and high-risk PCa patients, cancer burden reduction and PSA relief were obtained without any pathologic complete response (Lee et al., 2022). Neoadjuvant apalutamide treatment was tolerable and did not have a clinically significant negative impact on the patient's overall health status and quality of life scores, with the main side effects of fatigue and sexual dysfunction (Yang et al., 2022). This study was consistent with the secondary findings of our study, but we did not assess sexual

dysfunction because these patients had little need for sex before neoadjuvant therapy. In another randomized, placebo-controlled phase II neoadjuvant trial of neoadjuvant degarelix plus apalutamide compared with degarelix before RP for 12 weeks in patients with high-risk PCa, degarelix plus apalutamide significantly improveed pathological response (including minimal residual disease and residual cancer burden at final pathology) (Devos et al., 2023). From another prospective single-center phase II trial of patients with high-risk PCa, ADT plus abiraterone with or without apalutamide were given as neoadjuvant therapy and no significant difference in complications within 30 days were observed between the two arms, but 4.9% of thromboembolic events occurred in the arm of neoadjuvant triple therapy (Ilario et al., 2023). None of these studies addressed the effect of apalutamide on prostate resectability in patients with progressive PCa. In our limited cases, in addition to finding that neoadjuvant therapy helped improve prostate resectability, pathological downstaging, and PSA relief were also observed. Regarding complications, we did not perform triple neoadjuvant therapy or observe that apalutamide increased perioperative complications, and no thrombotic events were observed.

Although whether ADT combined with ARSI as neoadjuvant therapy can bring survival benefits is worthy of further research, it is relatively sure that ADT alone before RP is not recommended, especially for patients with intermediate- and low-risk PCa, as ADT can cause side effects such as weight gain and mood changes, and increases the risk of cardiovascular disease, diabetes, and osteoporosis, guidelines also strongly recommend that men who choose surgery should not undergo ADT (MacLennan et al., 2023). However, a systematic review suggested a survival benefit with ADT as a neoadjuvant approach in high-risk PCa patients (Cartes et al., 2023). For metastatic PCa (mPCa), the current mainstream view is that local treatment is not recommended (Cornford et al., 2021). However, accumulating retrospective studies have found that for selective metastatic PCa, local treatment such as RP would improve symptoms, PFS and PSA benefits, and even survival benefits (Rajwa et al., 2023). Therefore, how to select appropriate progressive PCa patients for neoadjuvant therapy and then give RP is worthy of attention. A study found that the overall mortality of mPCa benefited from local treatment, and patients with less aggressive tumors and good general health appeared to benefit more (Loppenberg et al., 2017). In our study, 4 cases were localized PCa, and 3 were mPCa. These 3 patients we included were oligometastasis and in good physical condition. After neoadjuvant therapy, RP or cytoreductive prostatectomy brought symptom improvement, PSA relief, and pathological response. However, whether this kind of benefit would bring PFS and survival benefits deserves further observation.

Evaluating which patients are suitable for RP after neoadjuvant therapy is also worth exploring. Recently, it was found that the response of prostate-specific membrane antigen (PSMA) positron emission tomography (PET)/CT to primary PCa lesions after neoadjuvant therapy could predict the pathological response, which might be helpful for the selection of patients to perform RP. In a phase II clinical trial of high-risk PCa patients receiving ADT plus docetaxel or ADT plus abiraterone as neoadjuvant therapy, with a median follow-up time of 30 months, the study found that [68 Ga] PSMA PET/CT was an ideal tool for monitoring response to neoadjuvant therapy (Chen et al., 2023). After apalutamide treatment, we selected patients who underwent MRI or PSMA CT to determine that the prostate still had active cancer lesions and then underwent RP. Another study predicted the clinical parameters and molecular biomarkers after PCa neoadjuvant chemohormonal therapy to evaluate the pathological response to neoadjuvant therapy; they found a lower preoperative PSA level was an independent predictor of good pathological response (Fan et al., 2023). The preoperative PSA levels of the patients included in our study were all low. Only one case with mPCa had a preoperative PSA level exceeding 4 ng/mL. Longer-term PSA relief postoperatively suggested that these patients may have potential survival benefits from neoadjuvant therapy; however, whether these short-term benefits could be translated into long-term survival benefits and how safe this neoadjuvant therapy was still worthy of further exploration.

How to choose follow-up therapy after neoadjuvant therapy with RP is also an uncertain issue (Devos et al., 2021). An advanced PCa consensus conference may complement the knowledge gap in advanced PCa and help the MDT discuss treatment options (Gillessen et al., 2022). It is worth noting that most of the patients selected for neoadjuvant therapy are high-risk or very high-risk PCa, multi-modal active treatment is still required after RP to improve the clinical outcomes of these patients (Devos et al., 2021; Sugino et al., 2023). Although all 7 patients in our study achieved postoperative downstaging and extremely low PSA, most were high-risk or very high-risk PCa, and active continuous multimodal treatment after surgery was also applied.

As an exploratory retrospective study with a small sample size, this study has some limitations specific to retrospective studies. In the future, case-control studies with a large sample size are needed to evaluate this study's conclusions further. It was important to note that the patients we selected had unresectable PCa. The definition of unresectable PCa was subjective, and whether it was resectable had a close relationship with the surgeon's surgical skills. However, our cases were all evaluated by MRI, which objectively confirmed that PCa had progressed and invaded the rectum, bladder, or surrounding tissues. In addition, our case was based on two experienced surgeons who had undergone more than 100 PCa cases, suggesting these two surgeons were already qualified in RP. After a median of 4 months of neoadjuvant therapy with apalutamide, these patients underwent MRI re-examinations, the prostate was resectable was re-evaluated, and the potential benefits of RP through MDT were also discussed to maintain as much as possible the safety of RP and the reduction of surgical complications. Furthermore, although our study had a median follow-up time of 13 months (range 9–25 months), this follow-up time was far from enough to observe patients with PCa to determine whether apalutamide as a neoadjuvant treatment brought benefit in progression-free survival, overall survival, or its long-term side effects. However, for the purpose of our research, neoadjuvant treatment with apalutamide could help transform these selective PCa patients from unresectable primary lesions to resectable primary lesions. This was the paramount significance of this preliminary study.

Conclusion

To the best of our knowledge, we have performed the first preliminary assessment of unresectable progressive prostate cancer; those after neoadjuvant apalutamide therapy were converted to resectable prostate cancer, with no significant increase in perioperative complications and a tolerable safety of the neoadjuvant therapy. Our study provides a new opportunity for RP therapy in progressive prostate cancer. Further clinical studies still need to confirm whether this treatment brings survival benefits to patients.

Data availability statement

The original contributions presented in the study are included in the article/Supplementary Material, further inquiries can be directed to the corresponding authors.

Ethics statement

The studies involving humans were approved by the ethics committee of Fujian Provincial Hospital. The studies were conducted in accordance with the local legislation and institutional requirements. The participants provided their written informed consent to participate in this study. Written informed consent was obtained from the individual(s) for the publication of any potentially identifiable images or data included in this article.

Author contributions

YW: Conceptualization, Funding acquisition, Writing–review and editing. RZ: Data curation, Formal Analysis, Investigation, Methodology, Writing–review and editing. DZ: Data curation, Formal Analysis, Resources, Writing–review and editing. ZC: Data curation, Methodology, Writing–review and editing. GC: Formal Analysis, Methodology, Writing–review and editing. MY: Data curation, Investigation, Writing–review and editing. LL: Formal Analysis, Methodology, Writing–review and editing. TL: Data curation, Formal Analysis, Writing–review and editing. LY: Investigation, Methodology, Writing–review and editing. LC: Conceptualization, Data curation, Formal Analysis, Writing–review and editing. QZ: Data curation, Supervision, Writing–review and editing.

Funding

The author(s) declare financial support was received for the research, authorship, and/or publication of this article. This study was supported by the Natural Science Foundation of Fujian Province (2021J01359, YW; and 2022J01408, TL) and China Urological Oncology Research Fund (#027) (YW).

Acknowledgments

We are grateful to all the patients who contributed to this study.

Conflict of interest

The authors declare that the research was conducted in the absence of any commercial or financial relationships that could be construed as a potential conflict of interest.

Publisher's note

References

Anker, C. J., Grossmann, K. F., Atkins, M. B., Suneja, G., Tarhini, A. A., and Kirkwood, J. M. (2016). Avoiding severe toxicity from combined braf inhibitor and radiation treatment: consensus guidelines from the eastern cooperative oncology group (ecog). *Int. J. Radiat. Oncol. Biol. Phys.* 95, 632–646. doi:10.1016/j.ijrobp.2016.01.038

Cartes, R., Karim, M. U., Tisseverasinghe, S., Tolba, M., Bahoric, B., Anidjar, M., et al. (2023). Neoadjuvant versus concurrent androgen deprivation therapy in localized prostate cancer treated with radiotherapy: a systematic review of the literature. *Cancers (Basel)*, 15. doi:10.3390/cancers15133363

Chen, M., Fu, Y., Peng, S., Zang, S., Ai, S., Zhuang, J., et al. (2023). The association between [(68)ga]psma pet/ct response and biochemical progression in patients with high-risk prostate cancer receiving neoadjuvant therapy. *J. Nucl. Med.* doi:10.2967/jnumed.122.265368

Cornford, P., van den Bergh, R., Briers, E., Van den Broeck, T., Cumberbatch, M. G., De Santis, M., et al. (2021). Eau-eanm-estro-esur-siog guidelines on prostate cancer. Part ii-2020 update: treatment of relapsing and metastatic prostate cancer. *Eur. Urol.* 79, 263–282. doi:10.1016/j.eururo.2020.09.046

Devos, G., Devlies, W., De Meerleer, G., Baldewijns, M., Gevaert, T., Moris, L., et al. (2021). Neoadjuvant hormonal therapy before radical prostatectomy in high-risk prostate cancer. *Nat. Rev. Urol.* 18, 739–762. doi:10.1038/s41585-021-00514-9

Devos, G., Tosco, L., Baldewijns, M., Gevaert, T., Goffin, K., Petit, V., et al. (2023). Arneo: a randomized phase ii trial of neoadjuvant degarelix with or without apalutamide prior to radical prostatectomy for high-risk prostate cancer. *Eur. Urol.* 83, 508–518. doi:10.1016/j.eururo.2022.09.009

Dindo, D., Demartines, N., and Clavien, P. A. (2004). Classification of surgical complications: a new proposal with evaluation in a cohort of 6336 patients and results of a survey. *Ann. Surg.* 240, 205–213. doi:10.1097/01.sla.0000133083.54934.ae

Fan, J., Liang, H., Gu, Y., Jiang, Z., Jiang, F., Wang, Y., et al. (2023). Predictive factors associated with differential pathologic response to neoadjuvant chemohormonal therapy in high-risk localized prostate cancer. *Urol. Oncol.* 41, 351–354. doi:10.1016/j.urolonc.2023.05.006

Fleshner, N. E., Sayyid, R. K., Hansen, A. R., Chin, J., Fernandes, R., Winquist, E., et al. (2023). Neoadjuvant cabazitaxel plus abiraterone/leuprolide acetate in high-risk prostate cancer patients: acdc-rp phase ii trial. *Clin. Cancer Res.* doi:10.1158/1078-0432.CCR-23-0731

Ge, Q., Xu, H., Yue, D., Fan, Z., Chen, Z., Xu, J., et al. (2022). Neoadjuvant chemohormonal therapy in prostate cancer before radical prostatectomy: a systematic review and meta-analysis. *Front. Oncol.* 12, 906370. doi:10.3389/fonc.2022.906370

Gillessen, S., Armstrong, A., Attard, G., Beer, T. M., Beltran, H., Bjartell, A., et al. (2022). Management of patients with advanced prostate cancer: report from the advanced prostate cancer consensus conference 2021. *Eur. Urol.* 82, 115–141. doi:10.1016/j.eururo.2022.04.002

Ilario, E. N., Bastos, D. A., Guglielmetti, G. B., Murta, C. B., Cardili, L., Cordeiro, M. D., et al. (2023). Perioperative morbidity of radical prostatectomy after intensive neoadjuvant androgen blockade in men with high-risk prostate cancer: results of phase ii trial compared to a control group. *Clin. Genitourin. Cancer* 21, 43–54. doi:10.1016/j.clgc.2022.10.009

Lee, L. S., Sim, A., Ong, C. W., Yang, X., Ng, C., Liu, W., et al. (2022). Near trial: a single-arm phase ii trial of neoadjuvant apalutamide monotherapy and radical prostatectomy in intermediate- and high-risk prostate cancer. *Prostate Cancer Prostatic Dis.* 25, 741–748. doi:10.1038/s41391-022-00496-8

Loppenberg, B., Dalela, D., Karabon, P., Sood, A., Sammon, J. D., Meyer, C. P., et al. (2017). The impact of local treatment on overall survival in patients with metastatic prostate cancer on diagnosis: a national cancer data base analysis. *Eur. Urol.* 72, 14–19. doi:10.1016/j.eururo.2016.04.031

MacLennan, S., Azevedo, N., Duncan, E., Dunsmore, J., Fullwood, L., Lumen, N., et al. (2023). Mapping european association of urology guideline practice across europe: an audit of androgen deprivation therapy use before prostate cancer surgery in 6598 cases in 187 hospitals across 31 european countries. *Eur. Urol.* 83, 393–401. doi:10.1016/j.eururo.2022.12.031

Rajwa, P., Zattoni, F., Maggi, M., Marra, G., Kroyer, P., Shariat, S. F., et al. (2023). Cytoreductive radical prostatectomy for metastatic hormone-sensitive prostate cancer-evidence from recent prospective reports. *Eur. Urol. Focus* 9, 637–641. doi:10.1016/j.euf.2023.01.011

Sugino, F., Nakane, K., Kawase, M., Ueda, S., Tomioka, M., Takeuchi, Y., et al. (2023). Biochemical recurrence after chemohormonal therapy followed by robot-assisted radical prostatectomy in very-high-risk prostate cancer patients. *J. Robot. Surg.* doi:10.1007/s11701-023-01670-3

Wang, X., Zhang, J., and Han, B. (2022). Neoadjuvant hormonal therapy for prostate cancer: morphologic features and predictive parameters of therapy response. *Adv. Anat. Pathol.* 29, 252–258. doi:10.1097/PAP.0000000000000347

Wenzel, M., Garcia, C. C., Hoeh, B., Jorias, C., Humke, C., Koll, F., et al. (2023). Real-world evidence of outcomes of oligometastatic hormone-sensitive prostate cancer patients treated with metastasis-directed therapy. *Prostate* 83, 1365–1372. doi:10.1002/pros.24599

Yang, X., Allen, J. C., Aslim, E. J., Tay, K. J., Yuen, S., Kanesvaran, R., et al. (2022). Patient-reported outcomes of a phase ii neoadjuvant apalutamide (arn-509) and radical prostatectomy in treatment of intermediate-to high-risk prostate cancer (near) trial. *Int. J. Urol.* 29, 1322–1330. doi:10.1111/iju.14994

Zhang, Y., Lin, Z., Li, T., Wei, Y., Yu, M., Ye, L., et al. (2022). Head-to-head comparison of (99m)tc-psma and (99m)tc-mdp spect/ct in diagnosing prostate cancer bone metastasis: a prospective, comparative imaging trial. *Sci. Rep.* 12, 15993. doi:10.1038/s41598-022-20280-x

Zhuang, J., Wang, Y., Zhang, S., Fu, Y., Huang, H., Lyu, X., et al. (2023). Androgen deprivation therapy plus abiraterone or docetaxel as neoadjuvant therapy for very-high-risk prostate cancer: a pooled analysis of two phase ii trials. *Front. Pharmacol.* 14, 1217303. doi:10.3389/fphar.2023.1217303

frontiers | Frontiers in Oncology

TYPE Case Report
PUBLISHED 12 December 2023
DOI 10.3389/fonc.2023.1301328

OPEN ACCESS

EDITED BY
Huan Yang,
Huazhong University of Science and Technology, China

REVIEWED BY
Liangfeng Tang,
Fudan University, China
Tong Chen,
Nanjing Medical University, China
Fei Wang,
Department of Urology, Hainan General Hospital, Affiliated Hainan Hospital of Hainan Medical University, Haikou, China

*CORRESPONDENCE
Guoqiang Du
doctordgq@sina.com

RECEIVED 27 September 2023
ACCEPTED 24 November 2023
PUBLISHED 12 December 2023

CITATION
Qu Y, Du G, Guo F, Wu R and Liu W (2023) Ossifying renal tumor of infancy: a case report.
Front. Oncol. 13:1301328.
doi: 10.3389/fonc.2023.1301328

Ossifying renal tumor of infancy: a case report

Yu Qu, Guoqiang Du*, Feng Guo, Rongde Wu and Wei Liu

Department of Pediatric Surgery, Shandong Provincial Hospital Affiliated to Shandong First Medical University, Jinan, China

Ossifying renal tumor of infancy (ORTI) is an extremely rare benign renal solid tumor with typical clinical and pathological features. Most cases are diagnosed in infants that are less than 12 months of age and is more common in males. The first symptom in most patients is painless gross hematuria. Microscopically, the tumor has three main components: an osteoid core, osteoblast-like cells, and spindle cells. We reported a case of a 21-day-old patient diagnosed with ORTI who underwent partial nephrectomy and had good follow-up. The unique features of this case are the strong expression of Wilms Tumor-1 (WT-1) and a high Ki-67 index in the hot spot area. ORTI is considered to have a favorable prognosis. Due to the rarity of WT-1 positivity and high Ki-67 index, we should be highly aware that this patient needs to be followed closely. In addition, we reviewed the available literature on ORTI, with the aim of summarizing the diagnostic and therapeutic experience. The diagnosis needs to be given cautiously on the basis of clinical symptoms, imaging, and pathologic examination. Depending on the location and extent of the tumor, surgery can be performed by partial nephrectomy or nephrectomy to avoid overtreatment.

KEYWORDS

ossifying renal tumor of infancy, diagnosis, pathology, prognosis, partial nephrectomy

1 Introduction

Ossifying renal tumor of infancy (ORTI) is an extremely rare benign renal solid tumor. Most cases are diagnosed in infants that are less than 12 months of age and is more common in males (1). By reviewing the English literature on PubMed, only 25 cases of ORTI have been reported to date since first reported by Chatten and colleagues in 1980 (2). Patients tend to present to the hospital with painless gross hematuria, rarely as an abdominal mass. This typical clinical feature and imaging data may aid in the diagnosis, and pathologic information is key for making a definitive diagnosis. This tumor is a benign lesion, and almost all reported patients have remained well postoperatively, without recurrence or metastasis. ORTI should be distinguished from other renal solid tumors in clinical practice. In this study, we report a case of ORTI and review the literature, with the aim of summarizing its diagnostic experience, improving the diagnostic rate, and avoiding unnecessary treatment.

2 Case presentation

A 21-day-old infant was found to have painless gross hematuria lasting 8 h after birth, which did not improve after symptomatic treatment, such as anti-inflammatory and hemostatic treatment. Routine urinalysis revealed an erythrocyte count up to 2,691 per microliter and 349.8 per high power field. Urologic ultrasound showed a hypoechoic mass in the middle and lower part of the left renal collecting system, measuring approximately 2.2×1.1×1.1 cm (Figure 1C). Enhanced computed tomography (CT) was then performed, which showed abnormal enhancement with localized calcification in the left renal pelvis (Figures 1D–F). Magnetic resonance imaging (MRI) results showed abnormal signal foci in the left renal pelvic region (Figures 1A, B). All of these signs provided evidence to suspect a neoplastic lesion. Therefore, ultrasound-guided renal puncture was performed. The puncture was performed by specialized staff of the department of interventional ultrasound, under ultrasound monitoring throughout the entire process. After local anesthesia, two strips of tissue from the left renal mass were punctured with a type 18G biopsy needle under ultrasound guidance. The exfoliated cells from the punctured tissue were detected and the remaining tissue was sent for pathological examination. The patient had no signs of bleeding on ultrasound and was given a local dressing. Exfoliative cytology showed that one cell type was seen, which was scattered and distributed in small clusters, with a consistent cytosol size, rounded and off-set nuclei, 2–3 nucleoli, and abundant cytoplasm, considered as tumor cells. Puncture pathology showed small patches of spindle cells with no mitotic image, favoring a benign lesion (Figure 2).

After several diagnostic procedures, the renal pelvic mass was resected and a final histologic diagnosis of ORTI was made. Intraoperatively, the renal pelvis was significantly dilated, with a tortuous ureteropelvic junction, and a slight narrowing of the local ureter. Freeing the renal clitoral vessels on the surface of the renal pelvis, the renal pelvis was incised transversely between two branch vessels along the middle and lower pole of the left kidney (Figure 3A). A cauliflower-like lump was seen (Figure 3B). Upon exploration, the tumor was seen to emanate from the left lower renal calyx. The tumor was enucleated along the border of the tumor by approximately 5 mm to ensure a negative tumor margin. A localized collapse at the lower pole of the kidney was seen; the renal cortex was incised from there and the residual mass was stripped and removed (Figures 3C, D). The renal cortex and renal pelvis were sutured, and the renal pelvic outflow tract was checked for patency. The intraoperative frozen pathology result was ORTI. Consequently, the affected kidney was preserved. A double J-tube, model F3, with a length of 120 mm, was placed inside the ureter.

The final pathology revealed ossifying renal tumor of infancy (Figure 4). Immunohistochemical results showed the following: Vimentin (+), Wilms Tumor-1(WT-1) (+), Cyclin D1 (+, partial), CK (-), EMA (-), INI-1 (+), Brg1 (+), Actin (-), Desmin (-), PAX8 (-), CD34 (-), S100 (-), Myogenin (-), MyoD1 (-), and STAT6 (-). Moreover, osteoblast-like cells were positive for STAB2. Approximately 60% of the cells were positive for Ki-67. The patient only had partial nephrectomy, and no other radiation or chemotherapy was given. The patient underwent urologic ultrasound, with no significant findings during postoperative retaining of the double J-tube. The double J-tube was removed at 68 days postoperatively. Up to now, the child has been followed up for 9 months, and no tumor recurrence or metastasis has been detected. The latest re-examined ultrasound results showed that the left kidney size was 5.7×3.7×3.2 cm, renal parenchyma thickness was 1.1 cm, and the collecting system was slightly separated and approximately 0.6 cm wide.

3 Discussion

ORTI is an extremely rare type of renal tumor in infants and young children; it is a benign tumor with a good prognosis. There are only 25 published cases in the literature. There are no statistics

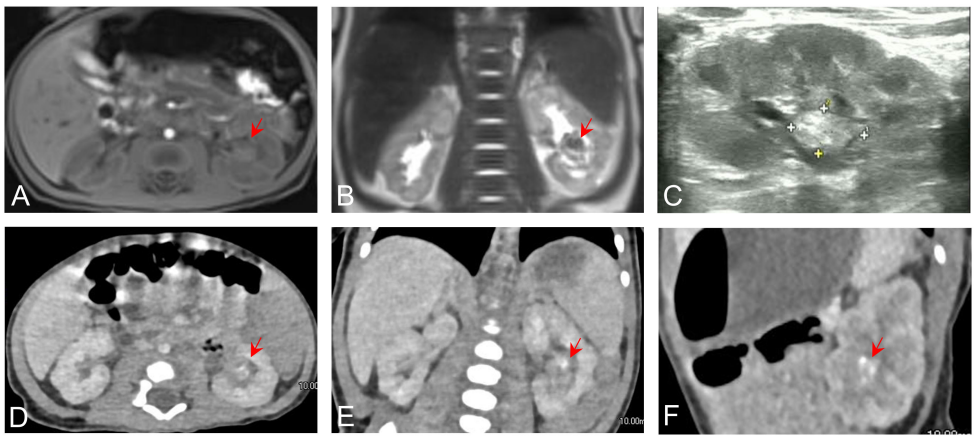

FIGURE 1
Axial **(A)** and coronal **(B)** preoperative MRI images showing abnormal signal foci in the renal pelvic region. **(C)** Ultrasound showing calcification in the left renal pelvis. Axial **(D)**, coronal **(E)**, and sagittal **(F)** contrast-enhanced CT images showing abnormal enhancement in the left renal pelvis.

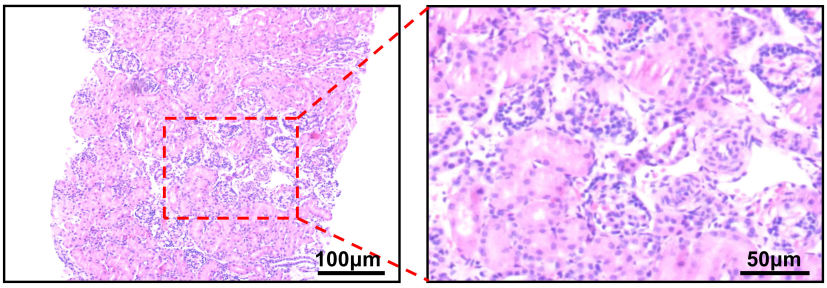

FIGURE 2
Puncture pathology showing the presence of small patches of spindle-shaped cells with interstitial vitreous degeneration and no mitotic image.

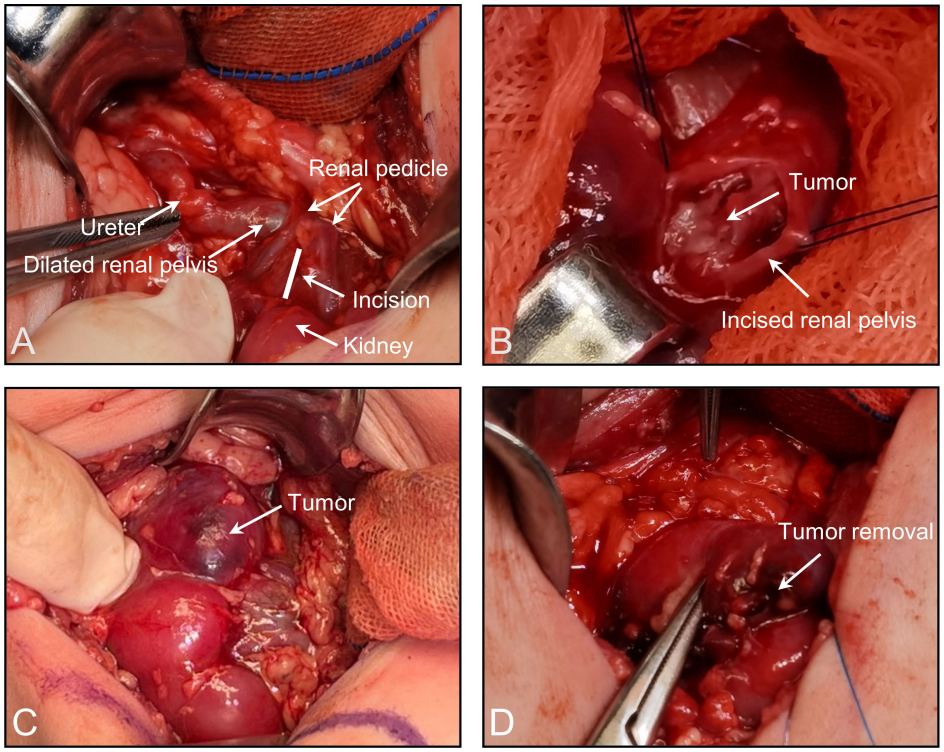

FIGURE 3
(A) The renal pelvis was incised transversely between two branch vessels along the middle and lower pole of the left kidney. **(B)** A cauliflower-like lump was seen. **(C)** Partially collapsed lower pole of the left kidney. **(D)** Stripping and removal of the mass after incising the renal cortex.

on the prevalence or incidence of ORTI in single centers or regions. In the previously reported cases, the age at diagnosis ranged from 6 days to 30 months, and most were diagnosed before the first year of life. It predominantly occurred in males. The most common clinical symptom was gross hematuria, and only two of the previous cases presented with a palpable abdominal mass on exam as the main symptom (1). On imaging, most cases showed a mass in the renal pelvis and calyces with clear borders, often with calcification (1). It is often accompanied by calcification and shows no or moderate enhancement on CT. Calcification may not be evident because of the patient's young age or the small diameter of the tumor (3). Low T2 signal in MRI is a characteristic of this tumor (3, 4).

Microscopically, the tumor has three main components: an osteoid core, osteoblast-like cells, and spindle cells. The central part of the tumor was an osteoid core, which is the typical morphological feature of this tumor, and the proportion and maturity of the osteoid core increased with age (5). Focal osteoblast-like cells were seen between the osteoid core, which were polygonal with large nuclei and abundant cytoplasm. The osteoid core was surrounded by spindle cells with ovoid or spindle-shaped nuclei, fine chromatin, and sparse cytoplasm. The immunohistochemical staining of spindle cells was positive for Vimentin and WT-1, positive for SMA, and negative for EMA and CK in the literature. The osteoblast-like cells were positive for Vimentin, SATB2, EMA,

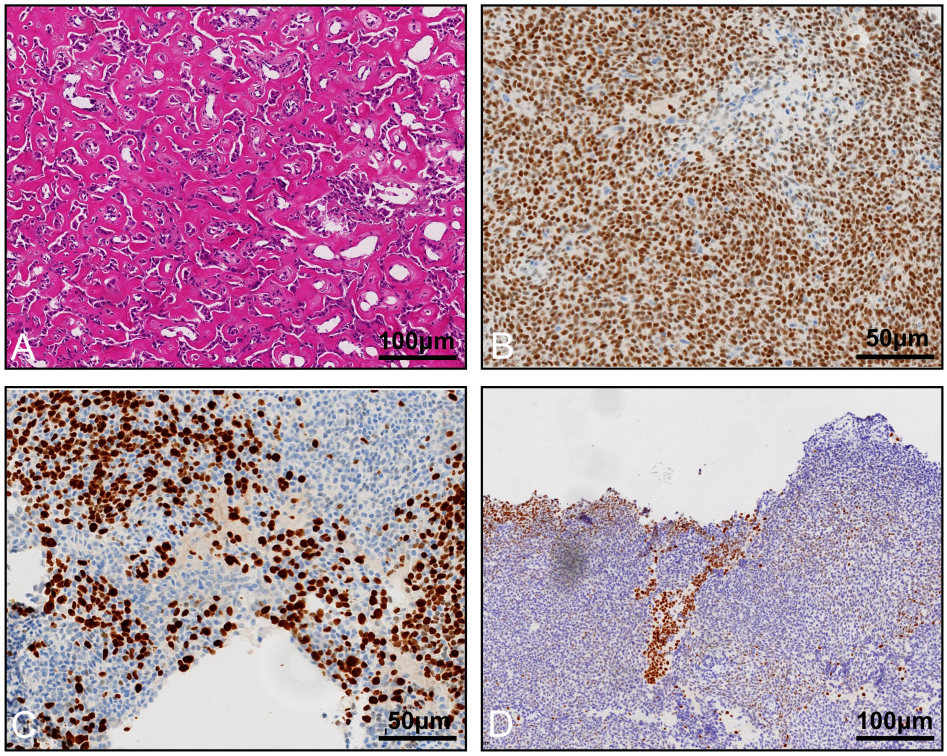

FIGURE 4
Histological appearance and immunohistochemistry staining of the tumor. **(A)** Osteoblast-like cells in an osteoid core, HE staining. Immunohistochemistry staining reveals that the tumor cells are positive for WT-1 **(B)**, Ki-67 **(C)**, and STAB2 **(D)**.

and CK. Both cellular components were positive for Vimentin and INI1 and did not express CD99, Desmin, Myogenin, MYOD1, or CD34. The immunohistochemical results in this case fully support the diagnosis of ORTI.

At present, the histologic origin of ORTI is not well defined. The earliest researchers recognized that it originated from the urethral epithelium (2). Some studies have suggested that ORTI is a subtype of congenital mesangial nephroma (CMN) (6). It has also been suggested that the transformation from spindle cells to osteoblast-like cells suggests that the osteoblast-like cells are derived from intralobular nephrogenic rests (ILNR). Some authors hypothesize that ORTI may arise from hyperplastic ILNR because of the similarity between nephrogenic rests (NR) and the spindle cells in ORTI, and that Wilms tumor (WT) and ORTI may share a common pathogenic pathway (7). Some scholars believed that that the tumor may be a stage in the process of WT formation that tends toward benign differentiation (8). ORTI should also be differentiated from several diseases. Tumors can be polypoid or staghorn-like, extending into the collecting system, even leading to hydronephrosis or dilatation of the renal pelvis and calyces (9). It can be misdiagnosed as a staghorn stone on CT. CMN is common in infants below 6 months of age, and microscopically, consists mainly of a spindle cell component similar to that found in ORTI. The absence of an osteoid core and osteoblast-like cellular components in the tumor, as well as the detection of the ETV6-NTRK3 fusion gene, can differentiate from ORTI. NR have mesenchymal tissue; however, no bone-like tissue or osteoblast-like cells are present to differentiate them. WT is the most common malignant tumor of the kidney. The average age of a child with nephroblastoma is approximately 3 years old. Histology consisted of an undifferentiated embryo, with epithelial and mesenchymal components. Immunohistochemistry of WT showed positive WT-1, yet ORTI is uncommon. Vaillancourt and colleagues reported the first case of an ossifying renal tumor of infancy, positive for WT-1 immunohistochemistry staining, in 2017 (10). In addition, this patient also showed a high expression of Ki-67, which implied that tumor cells are more active in proliferation and are more aggressive. Whether the detection of this feature affects the prognosis of the patient needs to be verified over a longer follow-up period. In recent years, the chromosomal karyotype of ORTI has been reported in the literature with clonal trisomy 4 (11), which is considered to be characteristic of this tumor and differentiates it from other renal tumors in infants and children.

Partial nephrectomy or nephrectomy was seen as the main treatment modality in previously reported cases, and chemotherapy in the minority. Previous cases were well followed up, and no cases of metastasis and relapse have been detected yet, which shows the favorable prognosis for patients with ORTI. One of the patients with the longest follow-up of 23 years showed no progression (12), confirming its benign nature. When the tumor is of appropriate size and location, nephron sparing surgery can provide adequate treatment outcomes and protect as much renal function as possible. Considering that the pathologic findings in this patient showed a low probability of invasiveness, we recommended that

the patient undergo urologic ultrasound every 3 months postoperatively and enhanced CT of the urinary system at 1 year postoperatively.

4 Conclusion

We reported a case of ORTI positive for WT-1 and with a high Ki-67 index. ORTI is extremely rare in clinical practice, diagnosed by its typical clinical symptoms and specific microscopic features. Surgery can be performed by partial nephrectomy or nephrectomy, depending on the location and extent of the tumor, and the prognosis is favorable. Due to the rarity of WT-1 positivity and the high Ki-67 index in this case, regular follow-up is required.

Data availability statement

The original contributions presented in the study are included in the article/supplementary material. Further inquiries can be directed to the corresponding author.

Ethics statement

The studies involving humans were approved by Biomedical Research Ethic Committee of Shandong Provincial Hospital. The studies were conducted in accordance with the local legislation and institutional requirements. Written informed consent for participation in this study was provided by the participants' legal guardians/next of kin. Written informed consent was obtained from the individual(s), and minor(s)' legal guardian/next of kin, for the publication of any potentially identifiable images or data included in this article.

Author contributions

YQ: Conceptualization, Data curation, Formal Analysis, Investigation, Methodology, Project administration, Resources, Software, Validation, Visualization, Writing – original draft, Writing – review & editing. GD: Conceptualization, Data curation, Formal Analysis, Investigation, Methodology, Project administration, Resources, Software, Validation, Visualization, Writing – original draft, Writing – review & editing. FG: Conceptualization, Data curation, Formal Analysis, Investigation, Methodology, Project administration, Resources, Software, Validation, Writing – original draft, Writing – review & editing. RW: Formal Analysis, Funding acquisition, Investigation, Methodology, Project administration, Resources, Software, Supervision, Validation, Visualization, Writing – original draft, Writing – review & editing. WL: Formal Analysis, Funding acquisition, Investigation, Methodology, Project administration, Resources, Software, Supervision, Validation, Visualization, Writing – original draft, Writing – review & editing.

Funding

The author(s) declare financial support was received for the research, authorship, and/or publication of this article. This work was supported by grants from the Youth Science Foundation of Shandong First Medical University (202201-066), the Science and Technology Development Plan Project of Shandong Province, China (2018GSF118209), and the Shandong Provincial Natural Science Foundation (ZR2017MH091, ZR2022MH095, ZR2023MH030).

Conflict of interest

The authors declare that the research was conducted in the absence of any commercial or financial relationships that could be construed as a potential conflict of interest.

Publisher's note

References

1. Guan W, Yan Y, He W, Qiao M, Liu Y, Wang Y, et al. Ossifying renal tumor of infancy (ORIT): The clinicopathological and cytogenetic feature of two cases and literature review. *Pathol Res Pract* (2016) 212(11):1004–9. doi: 10.1016/j.prp.2016.08.008

2. Chatten J, Cromie WJ, Duckett JW. Ossifying tumor of infantile kidney: report of two cases. *Cancer* (1980) 45(3):609–12. doi: 10.1002/1097-0142(19800201)45:3<609::AID-CNCR2820450330>3.0.CO;2-0

3. Lee SH, Choi YH, Kim WS, Cheon JE, Moon KC. Ossifying renal tumor of infancy: findings at ultrasound, CT and MRI. *Pediatr Radiol* (2014) 44(5):625–8. doi: 10.1007/s00247-013-2855-2

4. Schelling J, Schröder A, Stein R, Rösch WH. Ossifying renal tumor of infancy. *J Pediatr Urol* (2007) 3(3):258–61. doi: 10.1016/j.jpurol.2006.05.009

5. Hajiran A, Jessop M, Werner Z, Crigger C, Barnard J, Vos J, et al. Ossifying renal tumor of infancy: laparoscopic treatment and literature review. *Case Rep Urol* (2018) 2018:1935657. doi: 10.1155/2018/1935657

6. Middlebrook PF, Jimenez CL, Schillinger JF. Ossifying renal tumor of infancy: a case report. *J Urol* (1992) 147(5):1337–9. doi: 10.1016/S0022-5347(17)37558-4

7. Sotelo-Avila C, Beckwith JB, Johnson JE. Ossifying renal tumor of infancy: a clinicopathologic study of nine cases. *Pediatr Pathol Lab Med* (1995) 15(5):745–62. doi: 10.3109/15513819509027010

8. Gadd S, Huff V, Huang CC, Ruteshouser EC, Dome JS, Grundy PE, et al. Clinically relevant subsets identified by gene expression patterns support a revised ontogenic model of Wilms tumor: a Children's Oncology Group Study. *Neoplasia* (2012) 14(8):742–56. doi: 10.1593/neo.12714

9. Vazquez JL, Barnewolt CE, Shamberger RC, Chung T, Perez-Atayde AR. Ossifying renal tumor of infancy presenting as a palpable abdominal mass. *Pediatr Radiol* (1998) 28(6):454–7. doi: 10.1007/s002470050381

10. Vaillancourt B, Oligny L, Déry J, Franc-Guimond J, Soglio DB. Ossifying renal tumor of infancy: report of a case with positive WT1 immunohistochemistry and high mitotic index and review of the literature. *Pediatr Dev Pathol* (2017) 20(6):511–6. doi: 10.1177/1093526617693105

11. Liu J, Guzman MA, Pawel BR, Pezanowski DM, Patel DM, Roth JA, et al. Clonal trisomy 4 cells detected in the ossifying renal tumor of infancy: study of 3 cases. *Mod Pathol* (2013) 26(2):275–81. doi: 10.1038/modpathol.2012.120

12. Ito J, Shinohara N, Koyanagi T, Hanioka K. Ossifying renal tumor of infancy: the first Japanese case with long-term follow-up. *Pathol Int* (1998) 48(2):151–9. doi: 10.1111/j.1440-1827.1998.tb03885.x

frontiers | Frontiers in Pharmacology

TYPE Original Research
PUBLISHED 20 December 2023
DOI 10.3389/fphar.2023.1333507

OPEN ACCESS

EDITED BY
Lei Yin,
Shanghai Jiao Tong University, China

REVIEWED BY
Hao Wu,
Zhejiang University, China
Yang Liu,
Guangzhou Medical University, China

*CORRESPONDENCE
Bosen You,
youbosen@hrbmu.edu.cn
Xuedong Li,
h06370@hrbmu.edu.cn
Enyang Zhao,
lspzey@sina.com

†These authors have contributed equally to this work

RECEIVED 05 November 2023
ACCEPTED 07 December 2023
PUBLISHED 20 December 2023

CITATION
Geng B, Liu W, Wang J, Zhang W, Li Z, Zhang N, Hou W, Zhao E, Li X and You B (2023), The categorizations of vasculogenic mimicry in clear cell renal cell carcinoma unveil inherent connections with clinical and immune features.
Front. Pharmacol. 14:1333507.
doi: 10.3389/fphar.2023.1333507

The categorizations of vasculogenic mimicry in clear cell renal cell carcinoma unveil inherent connections with clinical and immune features

Bo Geng†, Weiyang Liu†, Jinpeng Wang†, Wei Zhang, Zhuolun Li, Nan Zhang, Wenbin Hou, Enyang Zhao*, Xuedong Li* and Bosen You*

Department of Urology, The Second Affiliated Hospital of Harbin Medical University, Harbin, China

Background: Clear cell renal cell carcinoma (ccRCC) stands as the prevailing variant kidney cancer in humans. Unfortunately, patients with disseminated RCC at diagnosis often have a diminished prognosis. Rapid tumor growth necessitates efficient blood supply for oxygen and nutrients, involving the circulation of blood from vessels to tumor tissues, facilitating tumor cell entry into the extracellular matrix. Vasculogenic mimicry (VM) significantly contributes to tumor growth and metastasis. Within this investigation, we identified vasculogenic mimicry-related genes (VMRGs) by analyzing data from 607 cases of kidney renal clear cell carcinoma (KIRC) in The Cancer Genome Atlas (TCGA) and the Gene Expression Omnibus (GEO) database (https://www.ncbi.nlm.nih.gov/geo/). These findings offer insights into ccRCC progression and metastasis.

Method: We identified VMRGs-related subtypes using consistent clustering methods. The signature of the VMRGs was created using univariate Cox regression and LASSO Cox regression analyses. To evaluate differences in immune cell infiltration, we employed ssGSEA. Afterwards, we created an innovative risk assessment model, known as the VM index, along with a nomogram to forecast the prognosis of ccRCC. Additionally, we verified the expression of an important gene related to VM, peroxiredoxin 2 (PRDX2), in tissue samples. Furthermore, we assessed the sensitivity to drugs in various groups by utilizing the pRRophetic R package.

Results: Significant predictors of survival rates in both high- and low-risk groups of KIRC patients were identified as VMRGs. The independent prognostic factors for RCC were confirmed by both univariate and multivariate Cox regression analyses, validating VMRG risk signatures. Differences were observed in drug sensitivity, immune checkpoint expression, and responses to immune therapy between patients classified into high- and low-VMRG-risk groups. Our nomograms consistently demonstrated precise predictive capabilities. Finally, we experimentally verified PRDX2 expression levels and their impact on prognosis.

Conclusion: The signature predicts patient prognosis and therapy response, laying the groundwork for future clinical strategies in treating ccRCC patients.

KEYWORDS

ccRCC, vasculogenic mimicry, molecular subtypes, tumor immune microenvironment, drug susceptibility

Highlights

- Using the TCGA database and GEO database, a prognostic and immunotherapy effectiveness prediction model were developed for patients with ccRCC.
- The distinctive signature holds the potential to function as a valuable instrument to appraise and forecasting the overall survival rate in ccRCC.
- These four genetic factors could enhance the process of clinical decision-making and optimize the individualized treatment for individuals afflicted with ccRCC.

Introduction

ccRCC is the predominant form of RCC, accounting for the highest occurrence rate (Cotta et al., 2023). It is characterized by increased hypoxia and the upregulation of angiogenesis-related genes (Hsieh et al., 2017; Linehan and Ricketts, 2019). ccRCC represents a solid tumor with extensive vascularization (Aziz et al., 2013). ccRCC has been treated with anti-angiogenic tyrosine kinase inhibitors (TKIs) like sunitinib (Méjean et al., 2018) and pazopanib (Motzer et al., 2013). However, despite the significant improvement in clinical outcomes compared to a placebo, the results have fallen short of expectations. This raises the question of the possibility of an alternative origin for blood and nutrient provisioning. Although there are theories such as epithelial–mesenchymal transition or the development of cancer stem cells, the requirement for blood and nutrient provision remains crucial in order to support the rapid expansion and, ultimately, the significant size of ccRCCs (Singh and Settleman, 2010; Fendler et al., 2020).

VM is depicted as a novel mode of tumor perfusion (Treps et al., 2021). Unlike traditional tumor angiogenesis, VM entails the formation of channels composed of cancer cells (Hendrix et al., 2016; Delgado-Bellido et al., 2017; Xiang et al., 2018). An increasing amount of evidence suggests that TKIs, like sunitinib, could potentially enhance VM formation. This underscores the potent stimulus that compels tumors to actively pursue nutrient supply, even in the face of angiogenesis inhibition (Zhang et al., 2014; Ribatti et al., 2019). Our prior research on VM in ccRCC also furnishes supporting evidence of its role in fostering tumor growth (You et al., 2021; Liu et al., 2022). Hence, VM plays a crucial role in ccRCC progression.

Traditionally, clinical and pathological patient characteristics have been utilized to assess the risk of ccRCC recurrence and predict disease progression (Graham et al., 2018). In recent years, substantial efforts have been dedicated to identifying molecular biomarkers capable of accurately predicting outcomes in ccRCC patients (Cotta et al., 2023). In pursuit of this goal, numerous studies have devised intricate multigene expression profiles (Frew and Moch, 2015). These profiles, whether utilized independently or in conjunction with the conventional stratification system, have demonstrated their capacity to improve the precision of ccRCC prognosis (Rydzanicz et al., 2013; Frew and Moch, 2015; Wang et al., 2022; Zhang et al., 2022). Nevertheless, the collective insights derived from molecular and clinicopathological parameters still do not provide precise prognostications for patient outcomes. Research aimed at discovering novel biomarkers and molecular techniques is essential for advancing ccRCC prognosis and personalizing medical interventions, including exploring specific VM subclusters and their associations with immune characteristics and prognosis.

In this study, we systematically classified ccRCC into distinct VM phenotypes and observed significant differences in prognosis among these subtypes. Additionally, we identified that the high-scoring group exhibited greater potential for immune escape. Furthermore, our constructed prognostic model demonstrated strong predictive capability. Moreover, through experimental validation, we verified PRDX2 expression's influence on prognosis and its connection to VM.

Materials and methods

Data collection

The study was carried out according to the workflow shown in Figure 1. The VMRGs sets (43 genes) were collected from earlier literature research (Luo et al., 2020; Fu et al., 2021; Treps et al., 2021; Wei et al., 2021; Zheng et al., 2021). Data from the TCGA database were downloaded on 25 June 2022 for ccRCC RNA sequencing and clinical characterization (https://portal.gdc.cancer.gov/repository), a dataset of 541 tumor samples and 72 normal tissue samples was included in the study (Liu et al., 2018). Perl (version Strawberry-Perl-5.30.1; https://www.perl.org) was used to extract the RNA-seq data in fragment per kilobase million (FPKM) format. For identical analysis with the E-MTAB-1980 and the GEO data (GSE29609), FPKM values were converted into transcripts per kilobase million (TPM). Following the merging of TCGA and GEO data, we employed the 'sva' R package to rectify batch effects, and all data were analyzed using R (version 4.1.3).

The analysis of consensus clustering for VMRGs GSVA and ssGSEA

To determine the ideal number of subtypes, we performed consensus clustering analysis. Using the 'GGalluvial' R package, we analyzed subtypes, overall survival status (OS), and risk scores. Pathway differences between these subtypes were examined through gene set variation analysis (GSVA). Afterwards, we evaluated the infiltration of immune cells across the categories using ssGSEA analysis.

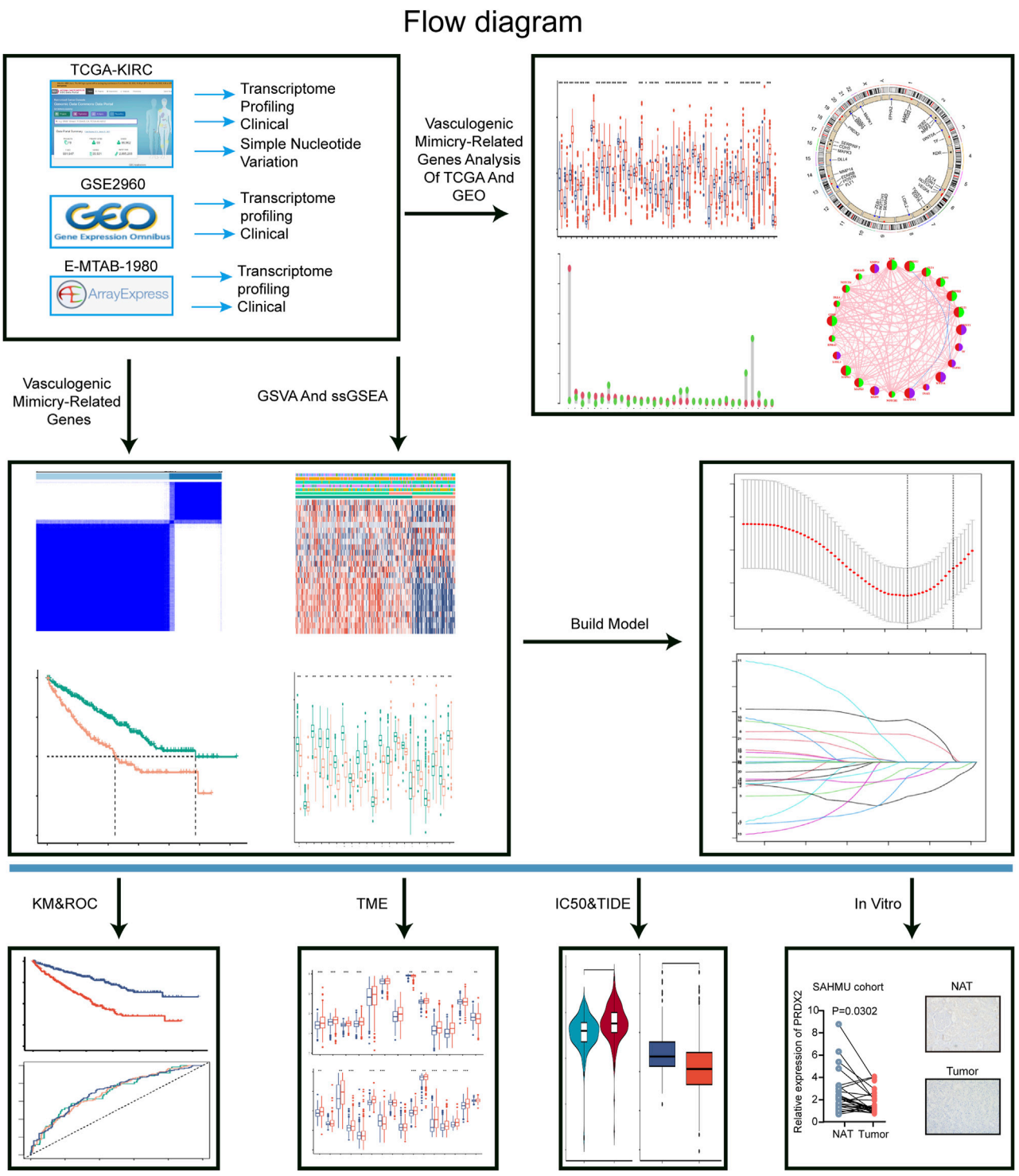

FIGURE 1
The workflow chart of the whole analysis in this study.

The construction of a signature based on VMRGs

Initially, we identified predictive VMRGs in the training group by applying a threshold ($p < 0.05$). Then, we utilized LASSO analysis to minimize estimation variance. Afterwards, a predictive signature was identified using multivariate Cox regression analysis. For every ccRCC, we computed a risk score by summing up the products of the gene's expression value and its corresponding regression coefficient, as per the formula Risk score = $\sum N = A, B.$ n (Coefficient of gene N × Expression value of gene N). Using the median risk score as the threshold, the training cohort was split into groups classified as high-

risk and low-risk. For the purpose of assessing the predictive ability of the signature, we created log-rank survival curves and time-dependent receiver operating characteristic (ROC) curves. We also tested the signature's stability and reliability using similar methods in the E-MTAB-1980 cohorts. The analyses were performed using the R packages 'glmnet,' 'survival,' and 'survminer'.

Evaluation of the forecasting capability of risk indicators

The VMRGs signature's predictive performance was evaluated using Kaplan-Meier (KM) and Receiver Operating Characteristic (ROC) curve analyses with the assistance of the 'survival' and 'survminer' R packages. The evaluation of concordance was performed by utilizing the concordance index (C-index). In addition, we performed univariate and multivariate Cox regression analyses to assess the predictive significance of the risk scores. Additionally, we investigated the clustering capability of risk scores using principal component analysis (PCA) and t-SNE (t-distributed stochastic neighbor embedding) analysis. Furthermore, we conducted a comparison between the VMRGs signature and various clinical attributes, including sex, age, and tumor category.

An illustration of a prognostic nomogram

We evaluated the predictive ability for 1-, 3-, and 5-year OS by employing ROC curves to compute AUC values using time-dependent receiver operating characteristic curves. This analysis took into account risk score, clinical stage, gender, age, and tumor grade. We then constructed a quantitative risk signature for predicting OS rates by creating a nomogram that incorporated the risk score along with other clinical variables. Subsequently, we calibrated the aforementioned nomogram to demonstrate its prognostic value.

Tumor immune microenvironment characterization with risk score

By employing ssGSEA analysis, the assessment of immune cell infiltration was conducted across different categorizations. The assessment of 47 immunoregulatory checkpoint genes in both cohorts was conducted as the ultimate measure. The Xu et al. website provided gene sets associated with cancer and immune response. The website (http//biocc.hrbmu.edu.cn/TIP/) (Xu et al., 2018) provides additional information. Enrichment scores were precisely computed using the GSVA algorithm to compare gene features related to cancer immune cycles and immunotherapy between two subgroups. p-value below 0.05 (Hänzelmann et al., 2013) was considered statistically significant, indicating a significant difference. (Hänzelmann et al., 2013).

Preprocessing of epigenetic mutation data

The calculation of tumor mutation burden (TMB) involves tallying the number of somatic, coding, base substitution, and insertion-deletion mutations per megabase of the genetic material. Analysis of non-synonymous mutations identifies genetic alterations, whereas those below 5% are classified as code-shifting. TMB was considered high if it exceeded 3. To mitigate statistical prejudice, we eliminated ccRCC individuals who lacked clinical information, gene expression data, or TMB metrics. We employed the 'maftools' R package to quantify somatic point mutations in each sample. Somatic changes in ccRCC driver genes were detected in samples exhibiting either low or high-risk scores.

Significance of the VMRGS in drug sensitivity

The TIDE (Tumor Immune Dysfunction and Rejection) method was utilized to anticipate variations in the responsiveness to immunotherapy among the groups categorized as high-risk and low-risk. To evaluate VMRGS and determine IC50 values for commonly employed chemotherapeutics in ccRCC treatment, the 'pRRophetic' R package was employed (Geeleher et al., 2014).

GeneMANIA

Gene MANIA (http//genemania.org) anticipates genes with similar functions among hub genes and forms a network of protein-protein interactions (PPI) connecting them (Xu et al., 2020). Genes that are functionally similar and genes that are hub genes can also be predicted by it (Franz et al., 2018). The aim of this investigation was to examine functionally comparable genes within hub genes and assess their functional enrichment.

Cell culture and transfection

The 786-O cell line, which originated from human renal cell carcinoma (RCC), was obtained from the Cell Bank of the Chinese Academy of Sciences. Cells were cultured in RPMI 1640 medium (Gibco, United States) supplemented with 10% fetal bovine serum (FBS) (Gibco, United States) and maintained in an incubator at 37°C with 5% CO2. TRAM2 siRNA and its corresponding si-control were purchased from GenePharma (Shanghai, China). Lipofectamine 3000 reagent (Invitrogen, California, United States of America) was used for cell transfection following the manufacturer's instructions. After 48 h of transfection, cells were used for protein quantification. The following sequences were employed for targeting PRDX2: 5′-GCCUGGCAGUGACACGAUUAATT-3' (si-PRDX2-1); 5′-GUGAAGCUGUCGGACUACAAATT-3' (si-PRDX2-2); 5′-CAGACGCUUGUCUGAGGAUUATT-3' (si-PRDX2-3).

Sample collection

From 2022 to 2023, all contributors were from the Second Affiliated Hospital of Harbin Medical University, and their specimens were preserved at a temperature of −80°C. Authorization for this investigation was obtained through the

approval of the ethics committee at the Second Affiliated Hospital of Harbin Medical University.

Western blotting analysis

To achieve cell lysis, a cell lysis buffer (Beyotime, China) supplemented with a protease inhibitor cocktail (Seven, China) was used on ice. Afterwards, the cells were collected using cell scrapers from BIOFIL, a company based in China. The Pierce BCA Protein Assay Kit (Beyotime, United States of America) was utilized for protein quantification, with measurements conducted at a wavelength of 562 nm (MD VersaMax, United States of America). Protein samples were applied onto SDS-PAGE gels with varying concentrations, ranging from 7.5% to 12.5%.Following electrophoresis, the proteins underwent transfer onto PVDF membranes (Merck Millipore, United States of America) utilizing an electrophoretic transfer apparatus (Tanon, China). After blocking, The PVDF membranes were subjected to primary antibody incubation for an excess of 12 h at a temperature of 4°C. Afterwards, the protein bands were made visible using chemiluminescence (Tanon) following a 1-h incubation with secondary antibodies under ambient conditions.

Immunohistochemical staining

IHC staining was conducted following a previously established protocol (Wu et al., 2020). Sections of ccRCC tissue embedded in paraffin were treated with anti-PRDX-2 (1:100, Protein-tech) and observed using a microscope (Leica DM2500P, Germany).

Matrigel tube formation assay

The *in vitro* assessment of cellular vasculogenic mimicry (VM) capacity was conducted using a Matrigel tube formation assay. In each well of a 96-well plate, 80 μL of Matrigel (at a concentration of 10 mg/mL) was evenly spread and permitted to solidify at 37°C for 1 h. Subsequently, suspended cells (1×10^5) were introduced into the culture medium containing varying concentrations of substances within the 96-well plates that had solidified Matrigel. The plates were then incubated in an environment maintained at 37°C with 5% CO2 for a duration of 24 h.

Extraction of RNA and qRT-PCR

The cells were used to isolate Total RNA with Trizol reagent (Invitrogen, United States of America). Then, cDNA synthesis was performed using the HiScript® III All-in-one RT SuperMix, which is a suitable option for qPCR applications (Vazyme, China). Following that, mRNA quantification was carried out using qRT-PCR assays on the StepOne Plus Real-Time PCR system from Applied Biosystems in the United States. The alterations in mRNA expression were computed utilizing the $2^{-\Delta\Delta CT}$ technique, while normalizing to β-actin. The PCR primers were specifically synthesized by TSINGKE Biological Technology (located in Nanjing, China) and their details can be found in Supplementary Table S2.

Statistical analysis

The R programming language was utilized for all statistical computations. Two-sample testing was conducted using the Wilcoxon method. The 'ggplot2′ and 'Rtsne' packages in R were used to perform PCA and t-SNE analyses, respectively. For comparing two independent groups, a *t*-test was applied.

Results

Distinctive expression patterns and genetic modifications in VMRGs

Figure 1 illustrates the overall methodology employed in this study. The compilation of VMRGs, consisting of 43 genes, was derived from prior literature research. The expression profiles of these regulators displayed noteworthy disparities between normal tissues and ccRCC tissues (Figure 2A). Our findings indicate that a majority of genes associated with VM exhibited elevated expression levels in ccRCC. These genes encompass TF, MMP9, VEGFA, LOXL2, DLL4, FLT1, EDN1, NRP2, POSTN, NOTCH4, TGFB1, EGFR, MMP14, KDR, CDH5, FLT4, TWIST1, TFPI, SERPINF1, EDNRB, SNAI1, ZEB1, ZEB2, NOTCH1, MAPK3, EPHA2, and MAPK1. Conversely, SEMA4D, PRDX2, PTGS2, WNT5A, and LAMC2 genes were found to have diminished expression levels (Figure 2B).

The co-expression network analysis confirmed a robust correlation among the co-expression patterns of these genes (Figure 2C). Furthermore, we conducted a copy number variation frequency analysis within the VMRGs. These findings indicate a significant gene dysregulation, with many genes experiencing dysfunction in terms of copy number alterations and deletions. (Figures 2D,E).

By employing univariate Cox analysis, we discovered 23 genes linked to prognosis ($p < 0.05$) within the VMRGs (Figure 2F). Prognostic network maps of VMRGs unveiled ZEB1, FLT1, EDNRB, EDN1, FLT4, PRDX2, KDR, SEMA4D, NOTCH4, DLL4, CDH5, EPHA2, MAPK1, MAPK3, and NOTCH1 as protective factors in ccRCC. Conversely, TWIST1, MMP14, WNT5A, POSTN, LOXL2, MMP9, SERPINF1, and TGFB1 were identified as risk factors (Figure 2G). Prognostic significance of VMRGs in ccRCC patients from the TCGA dataset and GEO (GSE29609) collection was assessed using Kaplan-Meier (KM) and Cox analyses (Supplementary Figure S1). In summary, VM exhibits significant differences in ccRCC and exerts a notably important impact on prognosis.

Description of phenotypes associated with VM

For this research, we utilized a coherence grid of subcategories to categorize all ccRCC individuals into two main categories, referred

10.3389/fphar.2023.1333507

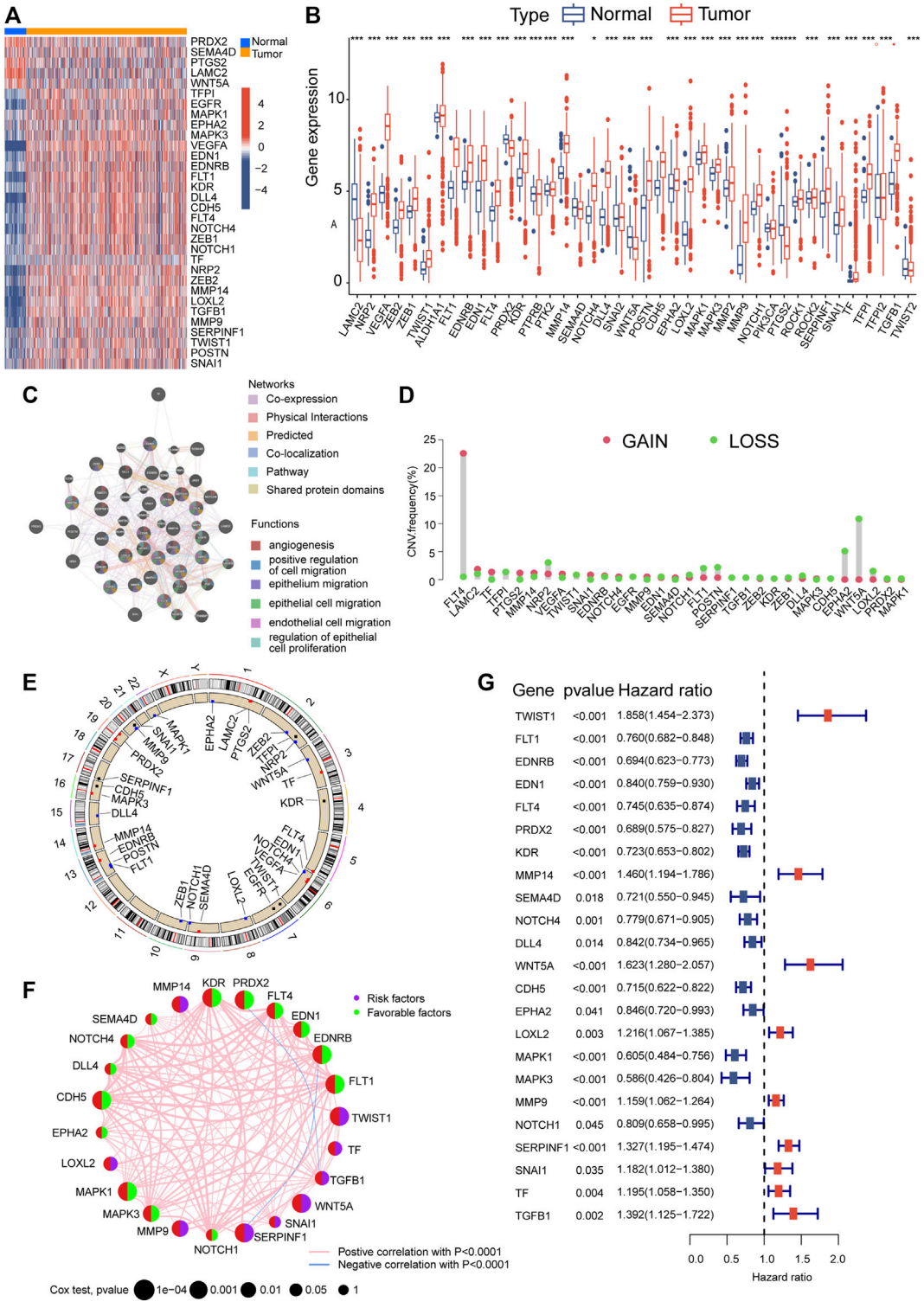

FIGURE 2
Alterations in gene expression and genetic variations in ccRCC. The TCGA heatmap **(A)** and box plot **(B)** demonstrate that 33 out of the 43 genes associated with VM exhibit noticeably different expression patterns between normal and ccRCC samples. **(C)** GeneMANIA analysis of differentially expressed genes and their co-expressed genes. **(D)** VM regulator CNV values for ccRCC specimens. **(E)** A map of the chromosomal location of CNV alterations in VM regulators. **(F)** Prognostic network depicting VMRGs. **(G)** Forest plot of OS derived from univariate Cox analysis. Significance levels: *$p < 0.05$, **$p < 0.01$, ***$p < 0.001$.

10.3389/fphar.2023.1333507

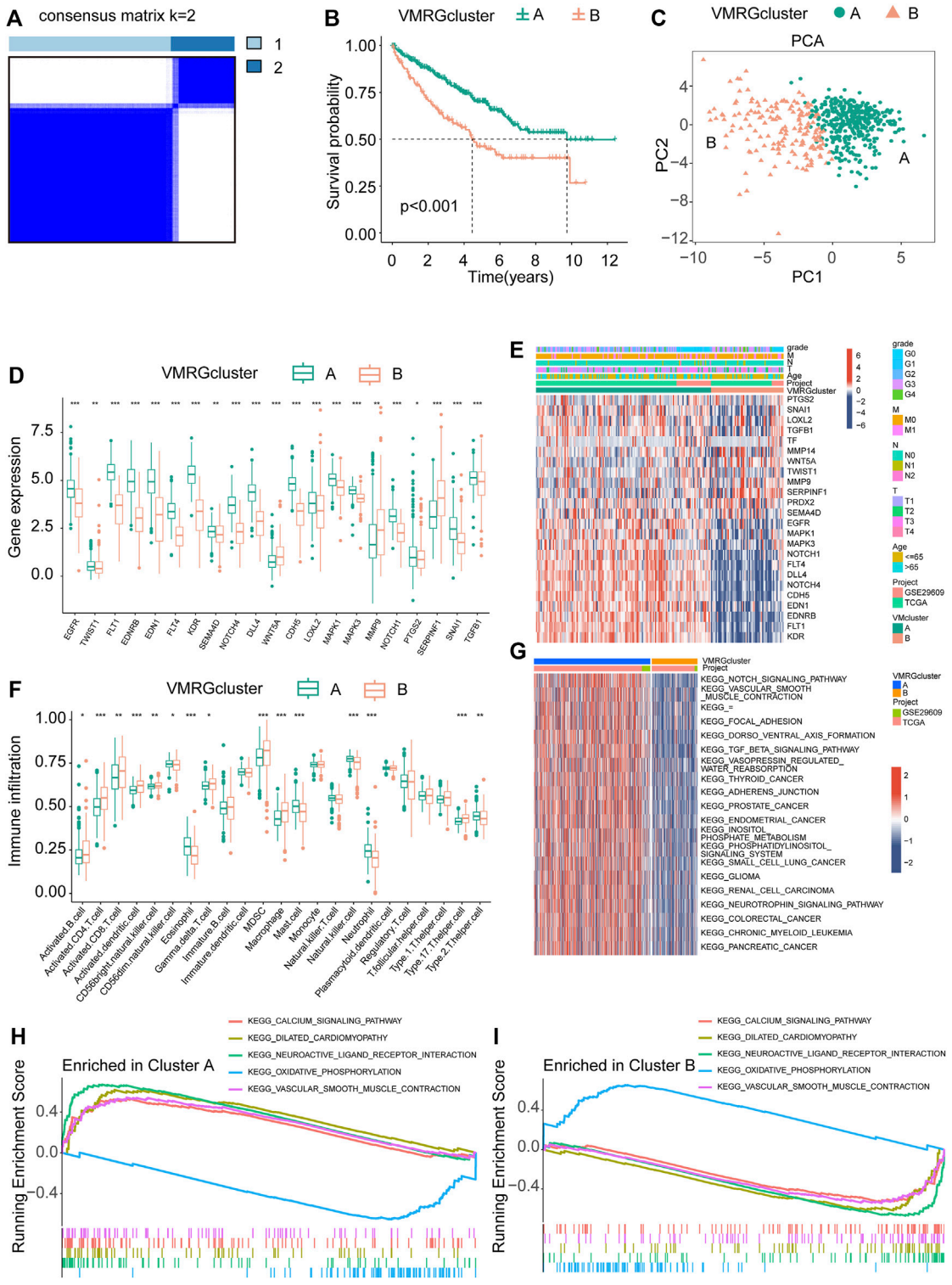

FIGURE 3
Analysis of signature clusters. **(A, B)** A comparison of the K-M survival curves of the two clusters and the concordance matrix. **(C)** Two clusters were analyzed using PCA. **(D)** The difference between clusters A and B in terms of VMRGs. **(E)** A sophisticated heatmap uncovers clinical associations among the two clusters. **(F)** Conducting differential analyses on two clusters of immune cells and fractions. **(G)** GSVA heatmaps showed the differences in pathways between the clusters. **(H, I)** The GSEA analysis uncovers the signaling pathway connecting the two clusters. Significance levels: $*p < 0.05$, $**p < 0.01$, $***p < 0.001$.

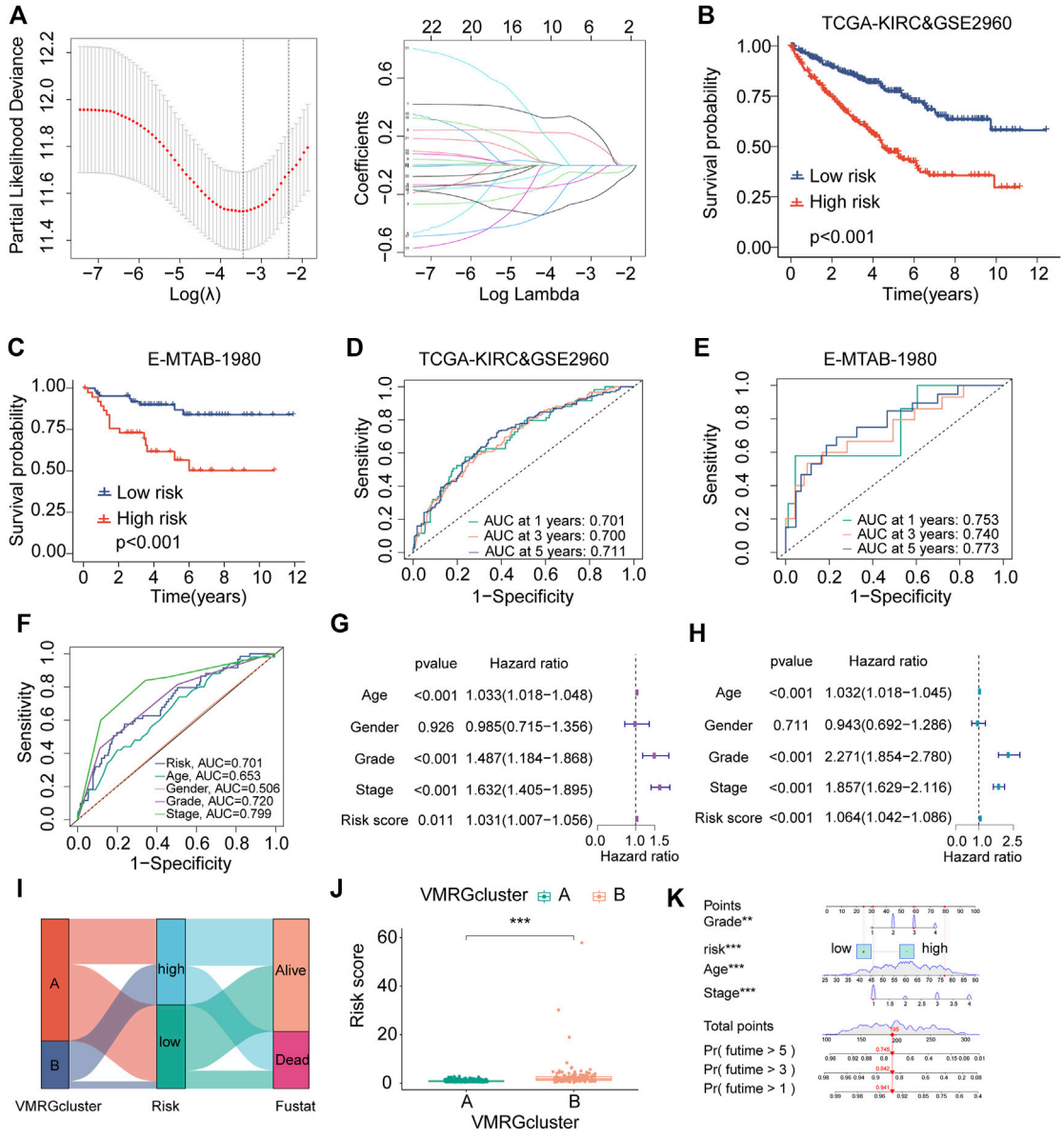

FIGURE 4
The establishment and validation of risk signatures linked to VM. **(A)** The merged dataset revealed four genes associated with VM that are most closely associated with OS using Lasso Cox analysis. **(B, C)** The Kaplan–Meier analysis of combined dataset and E-MTAB-1980 assess the prognostic importance of the risk model. The constructed model in the combined datasets **(D)** and E-MTAB-1980 **(E)** displays a time-dependent ROC curve. **(F)** ROC curves for risk score, age, gender, grade stage, and classification in the merged datasets. **(G, H)** Multivariate and univariate Cox regression findings in the combined dataset. **(I)** A prognostic model is depicted in a Ggalluvial plot. **(J)** Boxplots representing VM clusters illustrate disparities in risk scores. **(K)** A nomogram amalgamating the risk score of risk scores and clinical variables across the datasets, encompassing age, gender, and stage. Significance levels: $*p < 0.05$, $**p < 0.01$, $***p < 0.001$.

to as cluster A and cluster B (Figure 3A). The KM curve, which represents subsequent survival analysis, demonstrated a more positive outlook for ccRCC patients in cluster A compared to cluster B (Figure 3B). By utilizing principal component analysis on the expression profiles of VMRGs, we successfully segregated the data into cluster A and cluster B (Figure 3C). Significantly, we noticed contrasting expression patterns of VMRGs in the two gene clusters, with heightened expression in gene cluster A and diminished expression in gene cluster B (Figure 3D). In order to offer extensive understanding, we combined information from TCGA and GEO (GSE29609) groups, creating a heatmap based on clusters that displays the distribution of age and clinical stage among ccRCC patients (Figure 3E). We utilized the ssGSEA method to appraise the fractions of 23 distinct immune cell types within the two ccRCC clusters. Remarkably, 15 immunocyte types exhibited notable variances between these ccRCC clusters, as depicted in the figure (Figure 3F). Concurrently, GSEA revealed significant distinctions in the top 20 pathways between clusters A and B. Key pathways included NOTCH SIGNALING, AXON GUIDANCE, DORSO VENTRAL AXIS FORMATION,

VASOPRESSIN REGULATED WATER REABSORPTION, and various cancer-related pathways (Figure 3G). Additionally, GSEA enrichment analysis intimated that cluster A was significantly augmented in the CALCIUM signaling pathway and VASCULAR SMOOTH MUSCLE CONTRACTION pathway, while the cluster B primarily exhibited enrichment in OXIDATIVE PHOSPHORYLATION pathways (Figure Figure3 H, I). These observations underscore a strong correlation between VM, neurological and vascular function, and tumor development. These results highlight the strong correlation between defined ccRCC clusters based on VMRGs and both prognosis and the immune status of ccRCC patients.

Developing and validating risk models

With the aid of the LASSO regression analysis, four genes were identified as optimal candidates for the model (Figure 4A), which are listed in Supplementary Table S1. Using Kaplan-Meier analysis, it was ascertained that a substantial correlation existed between high-risk scores and adverse outcomes in the merged cohorts (Figure 4B). This finding was corroborated by the E-MTAB-1980 dataset (Figure 4C). Further, survival status, risk score, and risk gene expression distributions were compared between the Merged and E-MTAB-1980 datasets (Supplementary Figure S2A, B).

The prediction model's effectiveness was assessed using time-dependent ROC curves. The AUCs of the combined dataset at 1, 3, and 5-year intervals were 0.701, 0.700, and 0.711, respectively (Figure 4D). At 1, 3, and 5-year intervals, the time-dependent ROC curves of the E-MTAB-1980 dataset produce area values of 0.753, 0.750, and 0.777, respectively (Figure 4E). ROC curves comparing risk scores with other clinical characteristics (Figure 4F) demonstrated the model's high predictability.

Risk scores were discerned as significant independent prognostic factors in the assessment of prognostic accuracy through univariate and multivariate Cox regression analyses (Figures 4G,H). The Sankey diagram was used to show the construction of the prognostic model, while the box plots were used to show the risk scores among VM clusters based on how the model was developed. (Figures 4I,J).

A nomogram was created using VMRGs to predict the 1, 3, and 5-year OS in ccRCC patients. This nomogram includes stage, age, grade, and risk score (Figure 4K). The calibration curve demonstrated a close alignment between the observed and predicted outcomes (Supplementary Figure S2C). ROC analyses demonstrated the nomogram's higher sensitivity as a method for predicting the survival time of ccRCC patients after 1, 3, and 5 years (Supplementary Figure S2D). In summary, the results of this study demonstrate the prognostic accuracy of the proposed model in predicting the outcomes of patients with ccRCC in the future.

Clinical appraisal of risk model

In order to clarify the connection between the model and clinical traits in the validation group, we utilized Wilcoxon signed-rank tests to examine the correlation between risk groups and pertinent factors. The findings from our study suggest that the risk scores obtained from the model did not show any significant connections with the age of the patients ($p > 0.05$) (Supplementary Figure S3A) and the N stage ($p > 0.05$) (Supplementary Figure S3E). Significant associations with risk were observed for Gender ($p < 0.05$) (Supplementary Figure S3B), tumor grade ($p < 0.05$) (Supplementary Figure S3C), T stage ($p < 0.05$) (Supplementary Figure S3D), and M stage ($p < 0.05$) (Supplementary Figure S3F). The results indicate that the risk model we created is mainly associated with the spread of ccRCC.

Differences in the immune cell infiltration

A Spearman correlation analysis was performed, which showed a noteworthy positive correlation between risk scores and both macrophage M0 and regulatory T cells (Tregs) (Figures 5A,B). In contrast, there was an inverse relationship between Macrophages M1 and risk scores (Figure 5C). Furthermore, notable disparities were observed in the ratios of immune cells and the scores associated with immune functions among the two groups (Figures 5D,E). As a result, a study was conducted to analyze differences in tumor immune pathway functions between the high-risk and low-risk categories (Figure 5F). The results showed heightened activity in specific stages of the process, like Neutrophil attracting (step 4), Eosinophil attracting (step 4), and Basophil attracting (step 4) in the high-risk category, whereas Monocyte attracting (step 4) displayed decreased activity. Significant variations in immune and ESTIMATE scores were evident between the high-risk and low-risk groups, as shown in Supplementary Figure S4A. Furthermore, the group at high risk exhibited an increased expression of PD-1 and CTLA4, which serve as potential targets for checkpoint immunotherapy (Supplementary Figure S4B). The variances in immune reactions among the two categories could be incorporated into antitumor immunotherapy for ccRCC (Figure 5G).

The pRRophetic algorithm was utilized to evaluate the correlation between risk scores and the sensitivity of three frequently prescribed medications (Sunitinib, Rapamycin, and Sorafenib) by determining the half-maximal inhibitory concentration (IC50) in ccRCC. The findings indicated that individuals classified as high-risk displayed greater responsiveness to Sorafenib (Figure 5H), while those classified as low-risk exhibited increased sensitivity to Sunitinib and Rapamycin (Figures 5I, J). The results indicate possible connections between VM, the immune environment, evasion of the immune system, and variations in prognosis among ccRCC patients in the two risk categories.

Tumor mutational burden analysis

The group at high risk had a record of the top 10 genes that underwent frequent mutations, which included VHL, PBRM1, TTN, SETD2, BAP1, MTOR, MUC16, DNAH9, KDM5C, and DST (Figure 6A). In contrast, the low-risk group also exhibited these genes as part of the top 10 most commonly mutated ones (Figure 6B). Their interactions are depicted in Figures 6C, D. The examination showed that ccRCC patients at high risk had a greater tumor mutation load (TMB) linked to reduced OS (Figures 6E, F). The results align with previous findings derived from Kaplan-Meier survival plots for both the high-risk and low-risk categories.

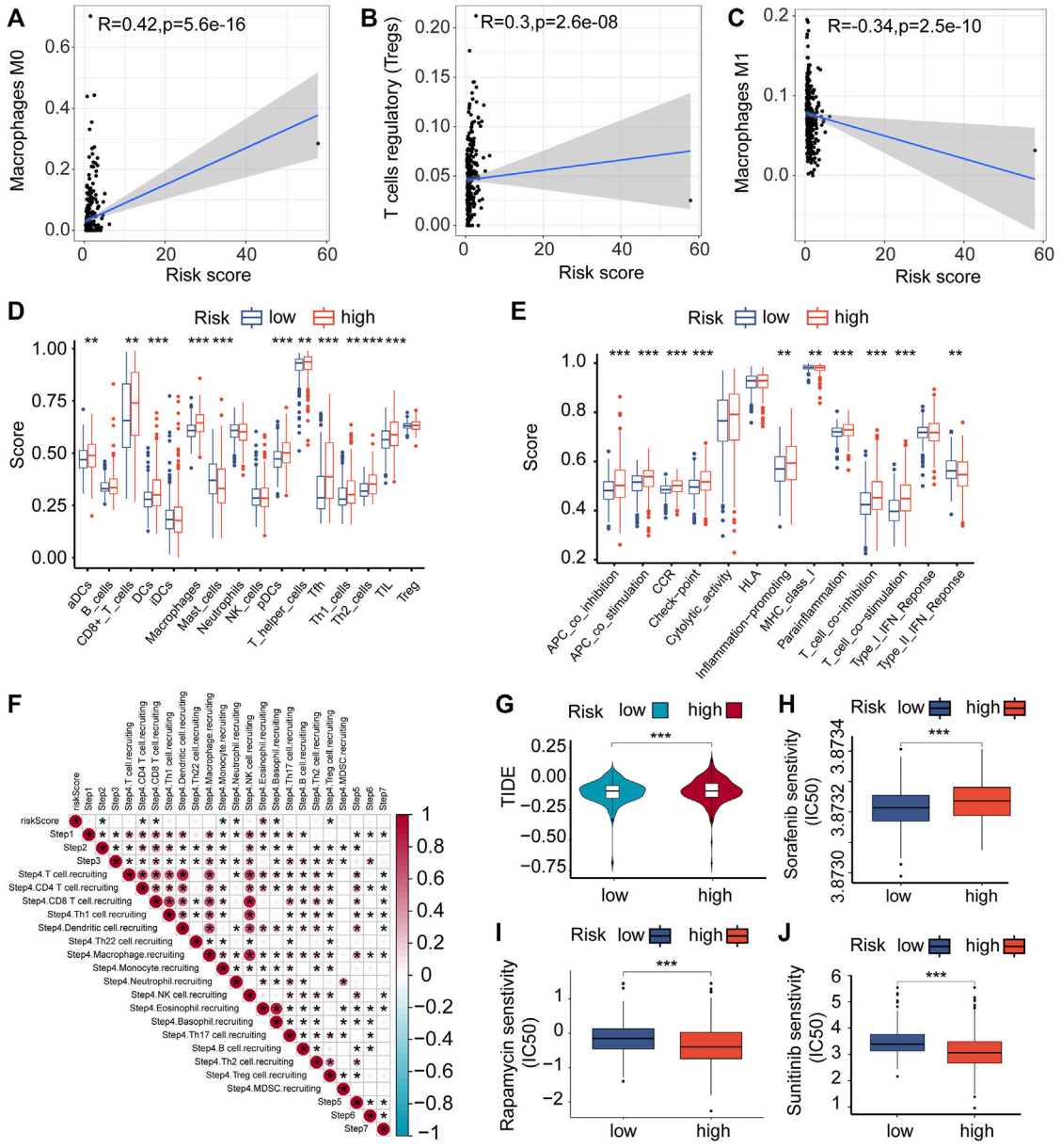

FIGURE 5
Immune cells infiltrating tumors and chemotherapy. **(A–C)** The relationship between the risk score of VMRGS and the infiltration of immune cells in ccRCC. **(D–E)** ssGSEA scores for infiltration of immune cells **(D)** and the functionality of the immune system **(E)**. **(F)** The interrelation amid the stages of the tumor-immune cycle and the scores indicating risk. **(G)** TIDE scores with low and high risk. Comparing the IC50 levels of Sorafenib **(H)**, Sunitinib **(I)**, and Rapamycin **(J)** in two different prognostic risk groups. Significance levels: $*p < 0.05$, $**p < 0.01$, $***p < 0.001$.

Evaluation of signature gene expression levels and functions

In the cohort studies conducted at The Second Affiliated Hospital of Harbin Medical University (SAHMU), It was noted that the expression level of PRDX2 mRNA exhibited a substantial increase in ccRCC tissues. When compared to normal adjacent tissues (NAT) (n = 14 for normal, n = 14 for ccRCC) (Figure 7A). Immunohistochemistry staining (Figure 7D) and Western blot analyses (Figure 7B) confirmed the reduced expression of PRDX2 in paired ccRCC tissue samples. In both the E-MTAB-1980 cohort (Figure 7C) and the SAHMU cohort (Figure 7E), the Kaplan-Meier survival curves indicated that a decreased PRDX2 expression level in ccRCC patients correlated with unfavorable OS. To summarize, our results offer corroborating proof for the reduced PRDX2 expression in ccRCC, emphasizing its negative correlation with the prognostic results of ccRCC individuals.

Additionally, we corroborated the influence of PRDX2 on the formation of VM. Following the knockdown of PRDX2 (Supplementary Figure S4A), there was a marked decrease in VM formation (Supplementary Figure S4B). This suggests that PRDX2 actively encourages the development of VM.

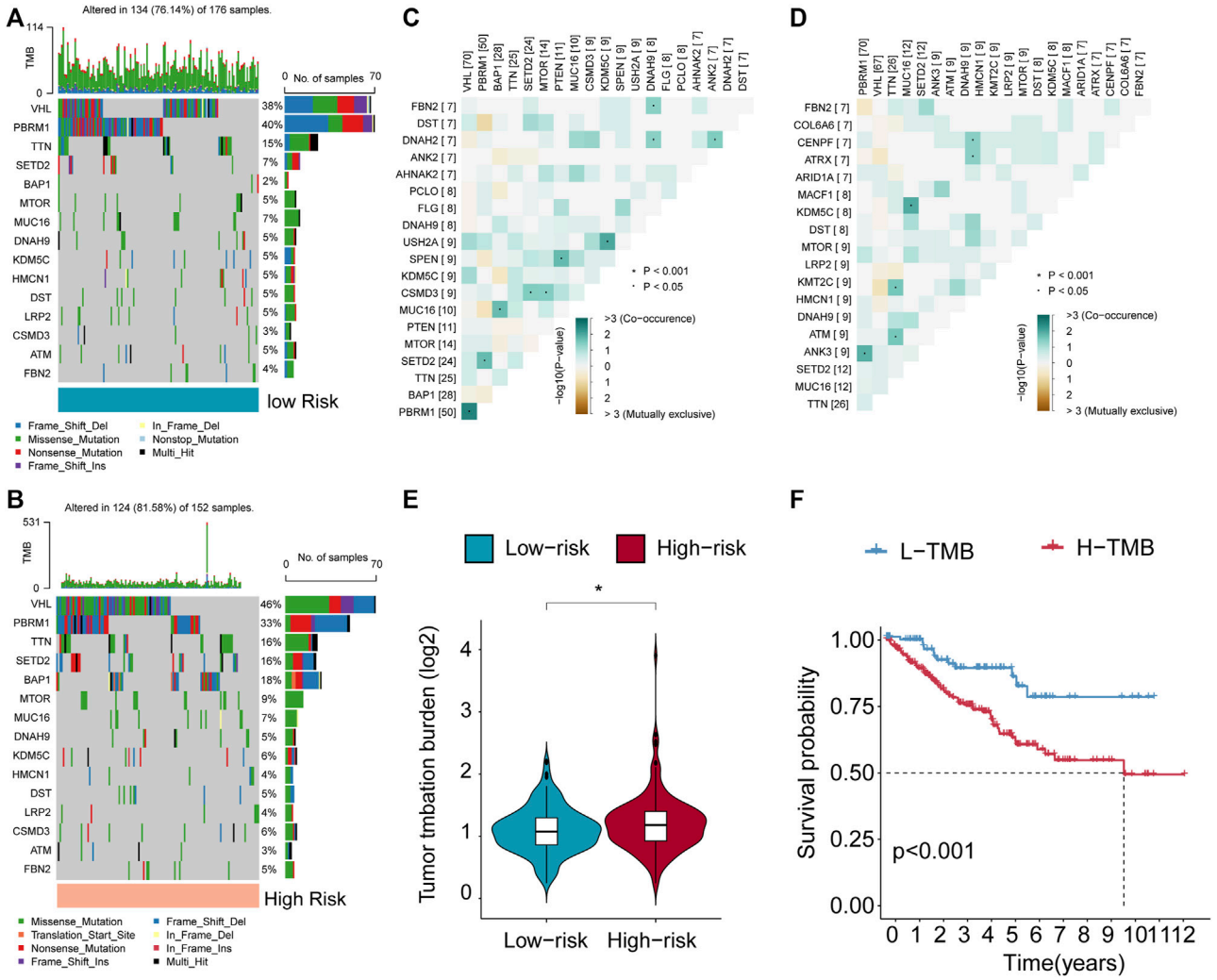

FIGURE 6
Features of VMRGS in tumor somatic mutations. **(A, B)** The Tumor Mutation Burden (TMB) differs among patients in the low- and high-risk score subcategories. **(C, D)** The interplay among the 20 most commonly mutated genes in high- and low-risk subgroups. **(E)** Violin plot illustrating TMB differences in ccRCC patients between the two risk groups. **(F)** Survival curves for patients categorized by both TMB were generated using the Kaplan-Meier method. Significance levels: $*p < 0.05$, $**p < 0.01$, $***p < 0.001$.

Disscusion

A large proportion of RCC occur as ccRCCs in humans. Due to substantial advancements in the clinical management of ccRCC, a comprehensive understanding of various prognostic factors such as tumor grade, tumor stage, and tumor size has been achieved. Additionally, alterations in genes and molecules are observed in ccRCC (Linehan et al., 2016). Several biological processes may be impacted, and certain among them are intricately linked to a patient's prognosis for ccRCC., such as autophagy (Napolitano et al., 2020), ferroptosis (Miess et al., 2018) and redox (Qi-Dong et al., 2020).

ccRCC has been revolutionized by immunotherapies that target co-inhibitory immune checkpoints, resulting in the emergence of immune-checkpoint inhibitors (Rathmell et al., 2022). Nonetheless, after a brief but effective treatment regimen, some patients experience unresponsiveness or secondary drug resistance, subsequently leading to disease progression (Jenkins et al., 2018; Schoenfeld and Hellmann et al., 2020). Since no widely accepted signature exists for predicting immunotherapy sensitivity in ccRCC, A dependable bioindicator for forecasting the susceptibility to immunotherapeutic agents needs to be ascertained.

VM, a phenomenon that promotes an augmentation in blood supply, Plays an indispensable role in the formation of solid neoplasms. It is imperative to form new blood vessels when the tumor diameter exceeds 2 mm to maintain adequate oxygenation. Failure to do so may result in ischemia and hypoxia, leading to necrosis of the tumor (Folkman, 1971; Zhang et al., 2022).

Given the limited efficacy of anti-angiogenic therapies in suppressing tumor development, it is imperative to explore innovative strategies for combating tumor angiogenesis that focus on targeting alternative mechanisms employed by tumor cells,

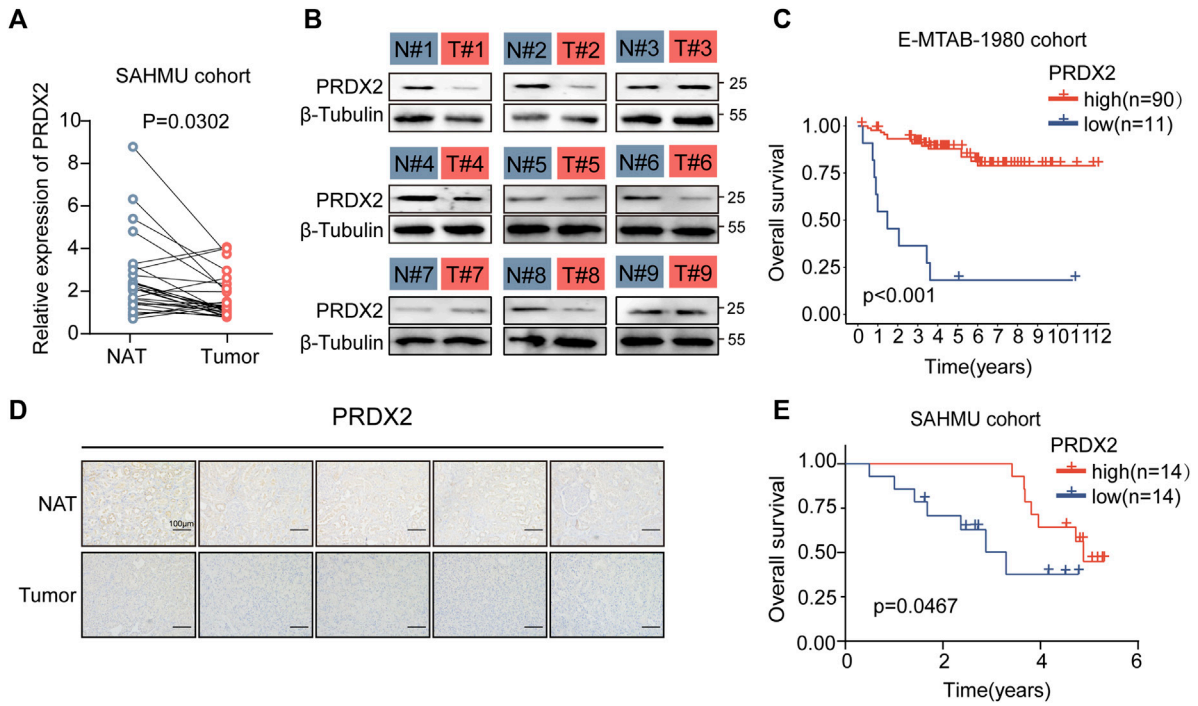

FIGURE 7
Low expression of PRDX2 in tumors is associated with poor prognosis. **(A)** Evaluation of PRDX2 mRNA levels in tumors (T) and corresponding normal adjacent tissues (NAT) within the SAHMU cohort (RT-qPCR data). **(B)** Western blot analysis depicting PRDX2 protein expression in nine pairs of human ccRCC tumors. **(C)** Survival curve (overall survival) based on distinct PRDX2 protein levels in the two ccRCC subtypes within the E-MTAB-1980 cohort. **(D)** Immunohistochemical images illustrating PRDX2 expression in tumors and corresponding normal adjacent tissues. Scale bar, 100 μm. **(E)** Survival curve (overall survival) based on different PRDX2 protein levels in the two ccRCC subtypes within the SAHMU cohort. Significance levels: $*p < 0.05$, $**p < 0.01$, $***p < 0.001$.

specifically trans-differentiation, which enables them to assume a pseudo-vascular phenotype and promote VM (Delgado-Bellido et al., 2017).

Angiogenesis significantly influences ccRCC development. The procedure includes a intricate web of signaling cascades comprising of elements such as pVHL, HIF-1α, VEGF, PDGF, and mTOR (Nicol et al., 1997; Dorević et al., 2009; Dimova et al., 2014; Kornakiewicz et al., 2014). Currently, approved targeted therapy agents for progressed ccRCC include bevacizumab, a monoclonal antibody that blocks VEGF-A from binding to its receptor. Furthermore, there are TKIs such as sorafenib, sunitinib, pazopanib, and axitinib, which predominantly hinder the VEGF receptor. Furthermore, mTOR complex inhibitors like temsirolimus and everolimus are also used. It is worth noting that immunocompromised patients face an increased risk of ccRCC, tumors often contain abundant lymphocytes, and occasional spontaneous tumor regressions have been reported (McDermott and Rini, 2007; Di Lorenzo et al., 2010; Mickley et al., 2015; Cecere et al., 2016; Di Lorenzo et al., 2016). The field of immunotherapy for ccRCC has witnessed a noteworthy progression with the deployment of agents that aim to regulate immune suppression induced by tumors. Particularly, the utilization of nivolumab, which targets PD-1, and ipilimumab, which targets CTLA-4, has exhibited encouraging outcomes.

Through an extensive examination of available literature, a total of 43 VMRGs were initially acquired in this investigation. Subsequently, individuals with ccRCC were randomly allocated to either the training or test group. Following the implementation of univariate Cox regression to detect 20 prognostic indicators for DE-VMRG, LASSO Cox regression was employed to identify four distinct VMRG signatures. Patients with high-risk scores had a more unfavorable prognosis in the KM survival analysis, in contrast to patients with low-risk ccRCC. The newly discovered signature demonstrated strong prognostic potential. Moreover, individuals diagnosed with ccRCC demonstrated consistent outcomes across various risk categories based on an evaluation of the area under the curve (AUC). Hence, evaluating the levels of VMRG expression can function as an indicator of death risk in ccRCC individuals, by utilizing the expression levels of four VMRGs. Altered expressions of MMPs and their inhibitors, TIMPs, have been observed in various tumor tissues. In particular, MMP14 exhibited significantly greater levels of expression in clear cell and papillary RCCs when compared to non-cancerous tissue, which generally had low MMP levels.

Many of the genes in the risk signature have a significant impact on the control of cancer due to their crucial functions. Through lncRNA-TANAR, the Androgen receptor modulates

TWIST1 nonsense-mediated decay in ccRCC to induce VM. Targeting the AR/TANAR/TWIST1 signaling pathways with a novel anti-angiogenesis treatment shows promise in halting the advancement of ccRCC (You et al., 2021). Cancer researchers have established that KDR is an important clinical biomarker and a key drug target in numerous solid tumors. Our signature, however, shows that KDR plays a protective role, which is unexpected. Further investigation is necessary for this observation, especially considering the positive outcomes achieved by different inhibitors of VEGF receptors in improving the prognosis of ccRCC.

Peroxiredoxin 2 (PRDX2) is a member of the peroxiredoxin family and protects cells from oxidative stress by scavenging ROS and H2O2 (De Franceschi et al., 2011). It has been shown that PRDX2 can suppress or enhance tumorigenesis depending on context, cells, and cancer type, etiology, and stage (Lei et al., 2016; Nicolussi et al., 2017). Proliferation and migration are promoted by melanoma PRDX2 expression, which is also linked to EMT and β-catenin signaling (Furuta et al., 2006). Meanwhile, PRDX2 overexpression correlates with cancer progression in several malignancies, including colon, prostate, cervix, and lung (Lomnytska et al., 2011; Xu et al., 2017). As a result of excessive levels of oxidative molecules, a knockdown of peroxiredoxin-2 reduced VEGFR-2 activation in colorectal cancer and caused VM formation (Zhang et al., 2015a). According to the findings from real-time quantitative PCR and immunohistochemistry, it was observed that PRDX2 expression in normal renal cells was considerably higher in comparison to ccRCC cell lines.

Additionally, in our study, we conducted validation of the impact of PRDX2 on VM formation in ccRCC, which is similar to its effect in colorectal cancer (Zhang et al., 2015b), demonstrating a promotion effect. In our previous studies, we observed a positive correlation between VM and poor prognosis in renal cancer (Liu et al., 2022). However, it is noteworthy that PRDX2 exhibits a negative correlation with adverse outcomes in ccRCC. Consequently, whether VM exerts a favorable influence on renal cancer prognosis through alternative pathways or if PRDX2 affects ccRCC prognosis via mechanisms distinct from VM remains unclear. We intend to further explore these mechanisms in our subsequent research endeavors.

The development and utilization of immune-checkpoint inhibitors that target CTLA4, PD-1, and PD-L1 have had a transformative impact on the field of cancer therapy, as acknowledged by the 2018 Nobel Prize in Medicine and Physiology (Braun et al., 2021; Kraehenbuehl et al., 2022), This has introduced a novel immunotherapy strategy with promising potential for treating cancer. Based on the positive outcomes from the randomized phase III trial CheckMate-025 (CM-025), the FDA has granted approval for the use of nivolumab (anti-PD-1) in the management of ccRCC. In prior studies, nivolumab exhibited enhanced OS when compared to everolimus, an mTOR inhibitor, in patients with previously treated ccRCC (Cancer Genome Atlas Research Network, 2013; Miao et al., 2018; Braun et al., 2020).

The study revealed that the group at high risk exhibited elevated levels of expression for the majority of checkpoint indicators, particularly PD-1. These results have important implications for identifying ccRCC patients likely to benefit from ICI therapy.

Additionally, we substantiated the reduced PRDX2 expression within ccRCC tissues through an in-depth examination of both patient mRNA and protein expression profiles. Furthermore, we corroborated its adverse correlation with patient prognosis.

Conclusion

The identified and validated four-VMRG signature may function as a valuable biomarker for ccRCC, offering a potential strategy for treatment. This research may enable us to predict prognosis and formulate efficient chemotherapy and immunotherapy for ccRCC patients.

Data availability statement

Publicly available datasets were analyzed in this study. This data can be found here: The datasets used in this article were derived from the TCGA database (https://portal.gdc.cancer.gov/), the GEO database (https://www.ncbi.nlm.nih.gov/geo/), the accession number is GSE29609) and the EMBL-EBI database (https://www.ebi.ac.uk/biostudies/arrayexpress/studies/, the accession number involves E-MTAB-1980).

Ethics statement

The studies involving humans were approved by the Medical Ethics Committee of the Second Affiliated Hospital of Harbin Medical University. The studies were conducted in accordance with the local legislation and institutional requirements. The human samples used in this study were acquired from primarily isolated as part of your previous study for which ethical approval was obtained. Written informed consent for participation was not required from the participants or the participants' legal guardians/next of kin in accordance with the national legislation and institutional requirements.

Author contributions

BG: Writing–original draft, Writing–review and editing. WL: Writing–original draft, Writing–review and editing. JW: Conceptualization, Writing–original draft, Writing–review and editing. WZ: Investigation, Software, Writing–original draft, Writing–review and editing. ZL: Methodology, Project administration, Writing–original draft. NZ: Conceptualization, Formal Analysis, Writing–original draft. WH: Data curation, Writing–original draft. EZ: Formal Analysis, Funding acquisition, Writing–original draft. XL: Supervision, Visualization, Writing–original draft, Writing–review and editing, Resources. BY: Supervision, Visualization, Writing–original draft, Writing–review and editing, Validation.

Funding

The author(s) declare financial support was received for the research, authorship, and/or publication of this article. The study received funding from the Scientific Research Project of Heilongjiang Provincial Health and Family Planning Commission (2017-070) and the First-Class Discipline First-Class Specialist Construction Project (100123) at the Second Affiliated Hospital of Harbin Medical University.

Conflict of interest

The authors declare that the research was conducted in the absence of any commercial or financial relationships that could be construed as a potential conflict of interest.

Publisher's note

Supplementary material

The Supplementary Material for this article can be found online at: https://www.frontiersin.org/articles/10.3389/fphar.2023.1333507/full#supplementary-material

References

Aziz, S. A., Sznol, J., Adeniran, A., Colberg, J. W., Camp, R. L., and Kluger, H. M. (2013). Vascularity of primary and metastatic renal cell carcinoma specimens. *J. Transl. Med.* 11, 15. doi:10.1186/1479-5876-11-15

Braun, D. A., Bakouny, Z., Hirsch, L., Flippot, R., Van Allen, E. M., Wu, C. J., et al. (2021). Beyond conventional immune-checkpoint inhibition - novel immunotherapies for renal cell carcinoma. *Nat. Rev. Clin. Oncol.* 18 (4), 199–214. doi:10.1038/s41571-020-00455-z

Braun, D. A., Hou, Y., Bakouny, Z., Ficial, M., Sant' Angelo, M., Forman, J., et al. (2020). Interplay of somatic alterations and immune infiltration modulates response to PD-1 blockade in advanced clear cell renal cell carcinoma. *Nat. Med.* 26 (6), 909–918. doi:10.1038/s41591-020-0839-y

Cancer Genome Atlas Research Network (2013). Comprehensive molecular characterization of clear cell renal cell carcinoma. *Nature* 499 (7456), 43–49. doi:10.1038/nature12222

Cecere, S. C., Rossetti, S., Cavaliere, C., Della Pepa, C., Di Napoli, M., Crispo, A., et al. (2016). Corrigendum: pazopanib in metastatic renal cancer: a "Real-World" experience at national cancer institute "fondazione G. Pascale". *Front. Pharmacol.* 7, 468. doi:10.3389/fphar.2016.00468

Cotta, B. H., Choueiri, T. K., Cieslik, M., Ghatalia, P., Mehra, R., Morgan, T. M., et al. (2023). Current landscape of genomic biomarkers in clear cell renal cell carcinoma. *Eur. Urol.* 84 (2), 166–175. doi:10.1016/j.eururo.2023.04.003

De Franceschi, L., Bertoldi, M., De Falco, L., Santos Franco, S., Ronzoni, L., Turrini, F., et al. (2011). Oxidative stress modulates heme synthesis and induces peroxiredoxin-2 as a novel cytoprotective response in beta-thalassemic erythropoiesis. *Haematologica* 96 (11), 1595–1604. doi:10.3324/haematol.2011.043612

Delgado-Bellido, D., Serrano-Saenz, S., Fernández-Cortés, M., and Oliver, F. J. (2017). Vasculogenic mimicry signaling revisited: focus on non-vascular VE-cadherin. *Mol. Cancer* 16 (1), 65. doi:10.1186/s12943-017-0631-x

Di Lorenzo, G., Buonerba, C., Federico, P., Rescigno, P., Milella, M., Ortega, C., et al. (2010). Third-line sorafenib after sequential therapy with sunitinib and mTOR inhibitors in metastatic renal cell carcinoma. *Eur. Urol.* 58 (6), 906–911. doi:10.1016/j.eururo.2010.09.008

Di Lorenzo, G., De Placido, S., Pagliuca, M., Ferro, M., Lucarelli, G., Rossetti, S., et al. (2016). The evolving role of monoclonal antibodies in the treatment of patients with advanced renal cell carcinoma: a systematic review. *Expert Opin. Biol. Ther.* 16 (11), 1387–1401. doi:10.1080/14712598.2016.1216964

Dimova, I., Popivanov, G., and Djonov, V. (2014). Angiogenesis in cancer - general pathways and their therapeutic implications. *J. B.U.ON Official J. Balkan Union Oncol.* 19 (1), 15–21.

Dorević, G., Matusan-Ilijas, K., Babarović, E., Hadzisejdić, I., Grahovac, M., Grahovac, B., et al. (2009). Hypoxia inducible factor-1alpha correlates with vascular endothelial growth factor A and C indicating worse prognosis in clear cell renal cell carcinoma. *J. Exp. Clin. Cancer Res. CR* 28, 40. doi:10.1186/1756-9966-28-40

Fendler, A., Bauer, D., Busch, J., Jung, K., Wulf-Goldenberg, A., Kunz, S., et al. (2020). Inhibiting WNT and NOTCH in renal cancer stem cells and the implications for human patients. *Nat. Commun.* 11 (1), 929. doi:10.1038/s41467-020-14700-7

Folkman, J. (1971). Tumor angiogenesis: therapeutic implications. *N. Engl. J. Med.* 285 (21), 1182–1186. doi:10.1056/NEJM197111182852108

Franz, M., Rodriguez, H., Lopes, C., Zuberi, K., Montojo, J., Bader, G. D., et al. (2018). GeneMANIA update 2018. *Nucleic Acids Res.* 46 (W1), W60-W64–W64. doi:10.1093/nar/gky311

Frew, I. J., and Moch, H. (2015). A clearer view of the molecular complexity of clear cell renal cell carcinoma. *Annu. Rev. Pathology* 10, 263–289. doi:10.1146/annurev-pathol-012414-040306

Fu, R., Du, W., Ding, Z., Wang, Y., Li, Y., Zhu, J., et al. (2021). HIF-1α promoted vasculogenic mimicry formation in lung adenocarcinoma through NRP1 upregulation in the hypoxic tumor microenvironment. *Cell Death Dis.* 12 (4), 394. doi:10.1038/s41419-021-03682-z

Furuta, J., Nobeyama, Y., Umebayashi, Y., Otsuka, F., Kikuchi, K., and Ushijima, T. (2006). Silencing of Peroxiredoxin 2 and aberrant methylation of 33 CpG islands in putative promoter regions in human malignant melanomas. *Cancer Res.* 66 (12), 6080–6086. doi:10.1158/0008-5472.CAN-06-0157

Geeleher, P., Cox, N., and Huang, R. S. (2014). pRRophetic: an R package for prediction of clinical chemotherapeutic response from tumor gene expression levels. *PloS One* 9 (9), e107468. doi:10.1371/journal.pone.0107468

Graham, J., Dudani, S., and Heng, D. Y. C. (2018). Prognostication in kidney cancer: recent advances and future directions. *J. Clin. Oncol. Official J. Am. Soc. Clin. Oncol.* 36, 3567–3573. doi:10.1200/JCO.2018.79.0147

Hänzelmann, S., Castelo, R., and Guinney, J. (2013). GSVA: gene set variation analysis for microarray and RNA-seq data. *BMC Bioinforma.* 14, 7. doi:10.1186/1471-2105-14-7

Hendrix, M. J. C., Seftor, E. A., Seftor, R. E. B., Chao, J. T., Chien, D. S., and Chu, Y. W. (2016). Tumor cell vascular mimicry: novel targeting opportunity in melanoma. *Pharmacol. Ther.* 159, 83–92. doi:10.1016/j.pharmthera.2016.01.006

Hsieh, J. J., Purdue, M. P., Signoretti, S., Swanton, C., Albiges, L., Schmidinger, M., et al. (2017). Renal cell carcinoma. *Nat. Rev. Dis. Prim.* 3, 17009. doi:10.1038/nrdp.2017.9

Jenkins, R. W., Barbie, D. A., and Flaherty, K. T. (2018). Mechanisms of resistance to immune checkpoint inhibitors. *Br. J. Cancer* 118 (1), 9–16. doi:10.1038/bjc.2017.434

Kornakiewicz, A., Solarek, W., Bielecka, Z. F., Lian, F., Szczylik, C., and Czarnecka, A. M. (2014). Mammalian target of Rapamycin inhibitors resistance mechanisms in clear cell renal cell carcinoma. *Curr. Signal Transduct. Ther.* 8 (3), 210–218. doi:10.2174/1574362409666140206222746

Kraehenbuehl, L., Weng, C. H., Eghbali, S., Wolchok, J. D., and Merghoub, T. (2022). Enhancing immunotherapy in cancer by targeting emerging immunomodulatory pathways. *Nat. Rev. Clin. Oncol.* 19 (1), 37–50. doi:10.1038/s41571-021-00552-7

Lei, X. G., Zhu, J. H., Cheng, W. H., Bao, Y., Ho, Y. S., Reddi, A. R., et al. (2016). Paradoxical roles of antioxidant enzymes: basic mechanisms and Health implications. *Physiol. Rev.* 96 (1), 307–364. doi:10.1152/physrev.00010.2014

Linehan, W. M., and Ricketts, C. J. (2019). The Cancer Genome Atlas of renal cell carcinoma: findings and clinical implications. *Nat. Rev. Urol.* 16 (9), 539–552. doi:10.1038/s41585-019-0211-5

Linehan, W. M., Spellman, P. T., Ricketts, C. J., Creighton, C. J., Fei, S. S., et al. (2016). Comprehensive molecular characterization of papillary renal-cell carcinoma. *N. Engl. J. Med.* 374 (2), 135–145. doi:10.1056/NEJMoa1505917

Liu, J., Lichtenberg, T., Hoadley, K. A., Poisson, L. M., Lazar, A. J., Cherniack, A. D., et al. (2018). An integrated TCGA pan-cancer clinical data resource to drive high-quality survival outcome analytics. *Cell* 173 (2), 400–416.e11. doi:10.1016/j.cell.2018.02.052

Liu, Q., Zhao, E., Geng, B., Gao, S., Yu, H., He, X., et al. (2022). Tumor-associated macrophage-derived exosomes transmitting miR-193a-5p promote the progression of

renal cell carcinoma via TIMP2-dependent vasculogenic mimicry. *Cell Death Dis.* 13 (4), 382. doi:10.1038/s41419-022-04814-9

Lomnytska, M. I., Becker, S., Bodin, I., Olsson, A., Hellman, K., Hellström, A. C., et al. (2011). Differential expression of ANXA6, HSP27, PRDX2, NCF2, and TPM4 during uterine cervix carcinogenesis: diagnostic and prognostic value. *Br. J. Cancer* 104 (1), 110–119. doi:10.1038/sj.bjc.6605992

Luo, Q., Wang, J., Zhao, W., Peng, Z., Liu, X., Li, B., et al. (2020). Vasculogenic mimicry in carcinogenesis and clinical applications. *J. Hematol. Oncol.* 13 (1), 19. doi:10.1186/s13045-020-00858-6

McDermott, D. F., and Rini, B. I. (2007). Immunotherapy for metastatic renal cell carcinoma. *BJU Int.* 99 (5 Pt B), 1282–1288. doi:10.1111/j.1464-410X.2007.06818.x

Méjean, A., Ravaud, A., Thezenas, S., Colas, S., Beauval, J. B., Bensalah, K., et al. (2018). Sunitinib alone or after nephrectomy in metastatic renal-cell carcinoma. *N. Engl. J. Med.* 379 (5), 417–427. doi:10.1056/NEJMoa1803675

Miao, D., Margolis, C. A., Gao, W., Voss, M. H., Li, W., Martini, D. J., et al. (2018). Genomic correlates of response to immune checkpoint therapies in clear cell renal cell carcinoma. *Sci. (New York, N.Y.)* 359 (6377), 801–806. doi:10.1126/science.aan5951

Mickley, A., Kovaleva, O., Kzhyshkowska, J., and Gratchev, A. (2015). Molecular and immunologic markers of kidney cancer-potential applications in predictive, preventive and personalized medicine. *EPMA J.* 6, 20. doi:10.1186/s13167-015-0042-2

Miess, H., Dankworth, B., Gouw, A. M., Rosenfeldt, M., Schmitz, W., Jiang, M., et al. (2018). The glutathione redox system is essential to prevent ferroptosis caused by impaired lipid metabolism in clear cell renal cell carcinoma. *Oncogene* 37 (40), 5435–5450. doi:10.1038/s41388-018-0315-z

Motzer, R. J., Hutson, T. E., Cella, D., Reeves, J., Hawkins, R., Guo, J., et al. (2013). Pazopanib versus sunitinib in metastatic renal-cell carcinoma. *N. Engl. J. Med.* 369 (8), 722–731. doi:10.1056/NEJMoa1303989

Napolitano, G., Di Malta, C., Esposito, A., de Araujo, M. E. G., Pece, S., Bertalot, G., et al. (2020). A substrate-specific mTORC1 pathway underlies Birt-Hogg-Dubé syndrome. *Nature* 585 (7826), 597–602. doi:10.1038/s41586-020-2444-0

Nicol, D., Hii, S. I., Walsh, M., Teh, B., Thompson, L., Kennett, C., et al. (1997). Vascular endothelial growth factor expression is increased in renal cell carcinoma. *J. Urology* 157 (4), 1482–1486. doi:10.1016/s0022-5347(01)65028-6

Nicolussi, A., D'Inzeo, S., Capalbo, C., Giannini, G., and Coppa, A. (2017). The role of peroxiredoxins in cancer. *Mol. Clin. Oncol.* 6 (2), 139–153. doi:10.3892/mco.2017.1129

Qi-Dong, X., Yang, X., Lu, J. L., Liu, C. Q., Sun, J. X., Li, C., et al. (2020). Development and validation of a nine-redox-related Long noncoding RNA signature in renal clear cell carcinoma. *Oxidative Med. Cell. Longev.* 2020, 6634247. doi:10.1155/2020/6634247

Rathmell, W. K., Rumble, R. B., Van Veldhuizen, P. J., Al-Ahmadie, H., Emamekhoo, H., Hauke, R. J., et al. (2022). Management of metastatic clear cell renal cell carcinoma: ASCO guideline. *J. Clin. Oncol. Official J. Am. Soc. Clin. Oncol.* 40 (25), 2957–2995. doi:10.1200/JCO.22.00868

Ribatti, D., Annese, T., Ruggieri, S., Tamma, R., and Crivellato, E. (2019). Limitations of anti-angiogenic treatment of tumors. *Transl. Oncol.* 12 (7), 981–986. doi:10.1016/j.tranon.2019.04.022

Rydzanicz, M., Wrzesiński, T., Bluyssen, H. A. R., and Wesoły, J. (2013). Genomics and epigenomics of clear cell renal cell carcinoma: recent developments and potential applications. *Cancer Lett.* 341 (2), 111–126. doi:10.1016/j.canlet.2013.08.006

Schoenfeld, A. J., and Hellmann, M. D. (2020). Acquired resistance to immune checkpoint inhibitors. *Cancer Cell* 37 (4), 443–455. doi:10.1016/j.ccell.2020.03.017

Singh, A., and Settleman, J. (2010). EMT, cancer stem cells and drug resistance: an emerging axis of evil in the war on cancer. *Oncogene* 29 (34), 4741–4751. doi:10.1038/onc.2010.215

Treps, L., Faure, S., and Clere, N. (2021). Vasculogenic mimicry, a complex and devious process favoring tumorigenesis - interest in making it a therapeutic target. *Pharmacol. Ther.* 223, 107805. doi:10.1016/j.pharmthera.2021.107805

Wang, J., Zhang, W., Hou, W., Zhao, E., and Li, X. (2022). Molecular characterization, tumor microenvironment association, and drug susceptibility of DNA methylation-driven genes in renal cell carcinoma. *Front. Cell Dev. Biol.* 10, 837919. doi:10.3389/fcell.2022.837919

Wei, X., Chen, Y., Jiang, X., Peng, M., Liu, Y., Mo, Y., et al. (2021). Mechanisms of vasculogenic mimicry in hypoxic tumor microenvironments. *Mol. Cancer* 20 (1), 7. doi:10.1186/s12943-020-01288-1

Wu, P., Geng, B., Chen, Q., Zhao, E., Liu, J., Sun, C., et al. (2020). Tumor cell-derived TGFβ1 attenuates antitumor immune activity of T cells via regulation of PD-1 mRNA. *Cancer Immunol. Res.* 8 (12), 1470–1484. doi:10.1158/2326-6066.CIR-20-0113

Xiang, T., Lin, Y. X., Ma, W., Zhang, H. J., Chen, K. M., He, G. P., et al. (2018). Vasculogenic mimicry formation in EBV-associated epithelial malignancies. *Nat. Commun.* 9 (1), 5009. doi:10.1038/s41467-018-07308-5

Xu, J., Zhang, S., Wang, R., Wu, X., Zeng, L., and Fu, Z. (2017). Knockdown of PRDX2 sensitizes colon cancer cells to 5-FU by suppressing the PI3K/AKT signaling pathway. *Biosci. Rep.* 37 (3). doi:10.1042/BSR20160447

Xu, L., Deng, C., Pang, B., Zhang, X., Liu, W., Liao, G., et al. (2018). TIP: a web server for resolving tumor immunophenotype profiling. *Cancer Res.* 78 (23), 6575–6580. doi:10.1158/0008-5472.CAN-18-0689

Xu, M., Li, Y., Li, W., Zhao, Q., Zhang, Q., Le, K., et al. (2020). Immune and stroma related genes in breast cancer: a comprehensive analysis of tumor microenvironment based on the cancer Genome Atlas (TCGA) database. *Front. Med. (Lausanne)* 7, 64. doi:10.3389/fmed.2020.00064

You, B., Sun, Y., Luo, J., Wang, K., Liu, Q., Fang, R., et al. (2021). Androgen receptor promotes renal cell carcinoma (RCC) vasculogenic mimicry (VM) via altering TWIST1 nonsense-mediated decay through lncRNA-TANAR. *Oncogene* 40 (9), 1674–1689. doi:10.1038/s41388-020-01616-1

Zhang, D., Zhao, X., Ma, Y., Ji, R., Gu, Q., et al. (2014). Twist1 expression induced by sunitinib accelerates tumor cell vasculogenic mimicry by increasing the population of CD133+ cells in triple-negative breast cancer. *Mol. Cancer* 13, 207. doi:10.1186/1476-4598-13-207

Zhang, S., Fu, Z., Wei, J., Guo, J., Liu, M., and Du, K. (2015a). Peroxiredoxin 2 is involved in vasculogenic mimicry formation by targeting VEGFR2 activation in colorectal cancer. *Med. Oncol.* 32 (1), 414. doi:10.1007/s12032-014-0414-9

Zhang, S., Fu, Z., Wei, J., Guo, J., Liu, M., and Du, K. (2015b). Peroxiredoxin 2 is involved in vasculogenic mimicry formation by targeting VEGFR2 activation in colorectal cancer. *Med. Oncol. N. Lond. Engl.* 32 (1), 414. doi:10.1007/s12032-014-0414-9

Zhang, W., Liu, Z., Wang, J., Geng, B., Hou, W., Zhao, E., et al. (2022). The clinical significance, immune infiltration, and tumor mutational burden of angiogenesis-associated lncRNAs in kidney renal clear cell carcinoma. *Front. Immunol.* 13, 934387. doi:10.3389/fimmu.2022.934387

Zheng, N., Zhang, S., Wu, W., Zhang, N., and Wang, J. (2021). Regulatory mechanisms and therapeutic targeting of vasculogenic mimicry in hepatocellular carcinoma. *Pharmacol. Res.* 166, 105507. doi:10.1016/j.phrs.2021.105507

frontiers | Frontiers in Pharmacology

TYPE Original Research
PUBLISHED 22 February 2024
DOI 10.3389/fphar.2024.1355081

OPEN ACCESS

EDITED BY
Lei Yin,
Shanghai Jiao Tong University, China

REVIEWED BY
Wang Yidi,
First Affiliated Hospital of Zhengzhou University, China
Zhang Yifan,
Tongji University, China

*CORRESPONDENCE
Sentai Ding,
dingsentai@126.com

†These authors have contributed equally to this work and share first authorship

RECEIVED 13 December 2023
ACCEPTED 07 February 2024
PUBLISHED 22 February 2024

CITATION
Zhu K, Chang Y, Zhao D, Guo A, Cao J, Wu C, Guan Y and Ding S (2024), Expression of HER2 in high-grade urothelial carcinoma based on Chinese expert consensus and the clinical effects of disitamab vedotin-tislelizumab combination therapy in the treatment of advanced patients.
Front. Pharmacol. 15:1355081.
doi: 10.3389/fphar.2024.1355081

Expression of HER2 in high-grade urothelial carcinoma based on Chinese expert consensus and the clinical effects of disitamab vedotin-tislelizumab combination therapy in the treatment of advanced patients

Kejia Zhu[1,2,3,4†], Yao Chang[1,5†], Delong Zhao[1], Andong Guo[1], Jishuang Cao[6], Chenrui Wu[6], Yong Guan[1,2,3] and Sentai Ding[1,4,6*]

[1]Department of Urology, Shandong Provincial Hospital Affiliated to Shandong First Medical University, Jinan, Shandong, China, [2]Medical Integration and Practice Center, Cheeloo College of Medicine, Shandong University, Jinan, Shandong, China, [3]Department of Urology, Liaocheng People's Hospital, Liaocheng, Shandong, China, [4]Engineering Laboratory of Urinary Organ and Functional Reconstruction of Shandong Province, Shandong Provincial Hospital Affiliated to Shandong First Medical University, Jinan, Shandong, China, [5]Department of Urology, Central Hospital Affiliated to Shandong First Medical University, Jinan, Shandong, China, [6]Department of Urology, Shandong Provincial Hospital, Cheeloo College of Medicine, Shandong University, Jinan, China

Background: A vast number of researchers have discovered high levels of human epidermal growth factor receptor-2 (HER2) expression in urothelial carcinoma (UC), but they do not use a uniform scoring system. Based on the 2021 edition of clinical pathological expert consensus on HER-2 testing in UC in China, we investigated the expression level and clinical significance of HER2 in high-grade UC. Furthermore, we looked at the prognosis of patients with locally advanced/metastatic UC after combining HER2 targeting antibody-drug conjugates (ADC) medication disitamab vedotin (DV) with programmed cell death protein 1 (PD-1) inhibitor tislelizumab.

Patients and methods: From 2019 to 2022, we collected paraffin specimens of UC from the Department of Urology at the Provincial Hospital Affiliated to Shandong First Medical University. HER2 expression-related factors were investigated. Patients with advanced UC who have failed systemic chemotherapy at least once and had received immune checkpoint inhibitor (ICI) medication during second-line treatment were selected and treated with DV in combination with tislelizumab. We assessed the therapy's efficacy and safety.

Results: 185 patients with high-grade UC were included in this investigation. 127 patients (68.7%) were HER2 positive (IHC 2+/3+) according to the 2021 Clinical pathological expert consensus on HER2 testing in UC in China. The clinical stage of UC differed statistically significantly between the HER2-and HER2+ groups (p = 0.019). Sixteen advanced UC patients were treated with DV and tislelizumab for a median of 14 months. The disease control rate was 87.5%, while the objective response rate (ORR) was 62.5%. The ORR of HER2+ individuals was higher than that of HER2-individuals (70.0% vs. 50.0%). The median

progression-free survival or overall survival was not reached. In this study, the incidence of treatment-related adverse events was 68.8% (11/16), with all of them being grade 1 or 2 adverse reactions.

Conclusion: HER2 protein expressed at a high percentage in UC, and 68.7% patients expressed HER2 positive (IHC 2+/3+). HER2+ expression is positively correlated with higher clinical stage of UC. HER2 targeted ADC drug disitamab vedotin combining with PD-1 inhibitor tislelizumab has shown efficacy, safety and controllable adverse reactions in the treatment of advanced UC.

KEYWORDS

urothelial carcinoma, high-grade, HER2, antibody-drug conjugate, clinical significance, prognosis, pathology

1 Introduction

The urothelial carcinoma (UC) is one of the most prevalent cancers worldwide, with primary locations including the bladder, ureter, and renal pelvis. According to the Global Cancer Statistics in 2020, there were 573,278 new cases of bladder cancer globally and 85,649 in China (Sung et al., 2021). UC can be classified into low-grade UC and high-grade UC. High-grade UC is often associated with stromal invasion and has a poor prognosis. Locally advanced or metastatic (la/mUC) cases account for approximately 5%–11% of all UC cases (Hepp et al., 2021; He et al., 2023). Patients with la/mUC face a bleak prognosis, as the 5-year survival rate ranges from a mere 4.6%–34%. Therefore, there is an urgent need for an improved non-surgical treatment approach.

Currently, adjuvant therapy for advanced UC includes chemotherapy, immunotherapy, and targeted therapy. Chemotherapy is the recommended first-line treatment, while immunotherapy (particularly programmed cell death protein 1 (PD-1)/programmed cell death-ligand 1 (PD-L1) inhibitors) is a second-line option. Enfortumab vedotin antibody-drug conjugates (ADC) after prior platinum chemotherapy and checkpoint inhibitor immunotherapy (ICI) have demonstrated significant survival benefits in la/mUC patients compared to chemotherapy (Rosenberg et al., 2019; Chang et al., 2021). The efficacy and safety of the combination therapy comprising enfortumab vedotin and pembrolizumab as a first-line treatment in cisplatin-ineligible patients with la/mUC were also confirmed (Hoimes et al., 2023).

In recent years, an additional ADC targeting the human epidermal growth factor receptor 2 (HER2, also known as ERBB2) has been developed and implemented in clinical practice. It has been established that HER2 plays a crucial role in the pathogenesis and progression of various malignant tumors, including urothelial carcinoma. Consequently, it is imperative to elucidate the expression of HER2 protein in urothelial carcinoma and its clinicopathological correlation to facilitate the clinical application of anti-HER2 targeted therapy for this disease (Olt et al., 1990; Press et al., 1990; Mendelsohn and Baselga, 2003). Currently, the existing detection methods for HER2 expression primarily rely on breast cancer evaluation standards that lack a standardized scoring system; thus further validation is warranted. Notably, several HER2-targeted ADCs have been approved in recent years, such as trastuzumab emtansine and trastuzumab deruxtecan. Additionally, a novel HER2-targeted ADC named disitamab vedotin (DV) was granted approval by the National Medical Products Administration in January 2022. However, more comprehensive clinical data are required to evaluate the efficacy of this medication.

In this article, we detected the expression of HER2 based on a 2021 edition of Clinical pathological expert consensus on HER-2 testing in UC in China. Besides, we analyzed its clinicopathological relationship with high-grade UC and explored the efficacy of HER2 targeted ADC drug disitamab vedotin, also known as RC48. As well as the efficacy of DV and PD-1 inhibitor tislelizumab combination therapy.

2 Patients and methods

2.1 Clinical patients

All clinical cases of high-grade UC with pathological diagnosis from 2019 to 2022 were included in this study, conducted at the Department of Urology and Pathology, Shandong Provincial Hospital Affiliated to Shandong First Medical University. The pathological diagnosis was based on the 2016 edition of the World Health Organization's diagnostic criteria for urological pathology and genetics. UC specimens were obtained through various surgical procedures including transurethral resection of bladder tumor, partial cystectomy, radical cystectomy, segmental ureterectomy, or total ureteropelvic resection.

For evaluating the efficacy of DV-tislelizumab combination therapy, patients treated between 2020 and 2022 were included in our analysis. The inclusion criteria consisted of: 1) age ≥18 years; histological or cytological confirmation of la/mUC with at least one measurable tumor lesion; 2) Eastern Cooperative Oncology Group (ECOG) performance status ≤1; 3) previous failure with systemic chemotherapy allowed; and 4) prior treatment with PD-1/PD-L1 inhibitors permitted. Exclusion criteria encompassed: 1) insufficient availability of critical clinical data; 2) inability to detect HER2 expression or lack of pathological sections; 3) presence of concurrent malignancies; and finally; 4) history of tyrosine kinase inhibitor therapy.

2.2 Experiment design

The collected high-grade UC specimens were fixed within 1 h after isolation. Prior to fixation, the specimen was incised at intervals

of 0.5–1 cm, and gauze or filter paper was inserted between the tissues for optimal fixation. In cases where the tumor tissue was fragmented, packing fixation was employed. A solution of 10% formalin, with a volume ten times that of the specimen, was utilized for fixation, with biopsy specimens being fixed for a duration ranging from 6 to 24 h. For larger specimens, fixation extended from 12 to 48 h. Subsequently, the paraffin-embedded specimens were subjected to HER2 immunohistochemistry (IHC) analysis following the scoring criteria outlined in accordance with the Clinical Pathological Expert Consensus on HER2 Testing in UC in China (2021 edition): no staining or <10% of invasive cancer cells exhibiting incomplete and weakly stained membranes (scored as 0); ≥10% of invasive cancer cells displaying incomplete and weakly stained membranes (scored as 1+); ≥10% of invasive cancer cells showing weak-moderate full membrane staining or <10% of invasive cancer cells demonstrating strong staining of intact cell membrane (scored as 2+); ≥10% of invasive cancer cells exhibiting strong staining of intact cell membrane (scored as 3+) (HERExpert Committee on Urothelial Carcinoma of Chinese Society of Clinical Oncology, 2021). Additionally, patient demographics including gender and age along with clinical parameters such as maximum tumor size, smoking history, primary sites, histopathological diagnosis, clinical stage classification, muscle invasion status, regional lymph node metastasis presence as well as some laboratory results were also recorded.

Locally-advanced/metastatic UC patients meeting the inclusion criteria were enrolled in this study to receive combination therapy with DV-tislelizumab. The treatment regimen consisted of DV administered at a dose of 2.0 mg/kg every 2 weeks, in combination with tislelizumab, a PD-1 inhibitor, administered at a dose of 200 mg every 3 weeks. Treatment was continued until patients discontinued due to disease progression (PD), intolerable side effects (SE), death, or withdrawal of informed consent. The patients underwent baseline physical examinations. Efficacy assessments were conducted every 4 treatment cycles, following the 1.1 version of the Solid Tumor Response Evaluation Standard and the International Standard for Common Terminology of Adverse Events (RECIST) (Eisenhauer et al., 2009). Short-term evaluation included objective response rate (ORR) and disease control rate (DCR) determination. Median progression-free survival (PFS) and overall survival (OS) served as long-term evaluation endpoints. During treatment, patients were monitored biweekly for blood routine tests (RT), biochemical parameters, liver functions, thyroid functions, stool and urine RT. Side effects were evaluated according to Common Terminology Criteria for Adverse Events (CTCAE) 5.0. Grade 1 or 2 side effects were managed based on symptoms, while grade 3 or higher side effects led to discontinuation from the study protocol. Informed consent was obtained from all participants, and ethical approval was granted by our institution's ethics committee.

2.3 Statistical analysis

Chi-square test was applied to analyze the characteristics of different primary sites, and relationship between HER2 and UC muscle invasion, clinical stage, regional lymph node metastasis, smoke history, primary sites and gender. ANOVA test was used to analyze the difference among three primary sites. *t*-test and Mann-Whitney test were used to analyze the differences between $HER2^{+/-}$groups. Logistic analysis was used for the correlation between HER2 and some blood indicators analysis. $p < 0.05$ was set as statistically significant. All analyses were performed using SPSS version 27.0 software.

3 Results

3.1 Clinical patients baseline

In our study, a total of 185 patients with high-grade UC were included, comprising 139 males and 46 females, with a median age of 68 years (range: 41–93). Among them, bladder was the primary site for UC in 127 cases (68.7%), followed by ureter in 36 cases (19.5%) and renal pelvis in 22 cases (11.9%) (Table 1). According to the diagnostic criteria outlined in the World Health Organization's (WHO) latest edition from 2016, muscle invasive UC was observed in 103 cases (primary site: bladder-54; ureter-31; renal pelvis-18), while non-muscle invasive UC was found in 82 cases (primary site: bladder-73; ureter-5; renal pelvis-4) (Figure 1).

Among the patients with primary tumor located in the bladder ($n = 127$), transurethral resection of bladder tumor was performed on 61 patients with a HER2 positive rate of 80.3%. Radical cystectomy was conducted on 50 patients with a HER2 positive rate of 46.0%, partial cystectomy on 14 patients with a HER2 positive rate of 64.3%, and no surgical treatment or bladder instillation but only immunotherapy using PD-1 inhibitor was administered to 2 patients who had a HER2 positive rate of 50.0%; For 36 patients with a primary tumor located in the ureter, radical nephroureterectomy was performed on 26 patients (HER2 positive rate: 50.0%), while segmental ureterectomy was performed on 10 patients (HER2 positive rate: 70.0%). Among the cohort of 22 patients with primary tumors located in the renal pelvis, a total of 19 patients underwent radical nephroureterectomy combined with partial cystectomy (with a HER2 positive rate of 57.9%). For the remaining 3 patients who did not undergo surgical intervention, PD-1 inhibitor immunotherapy was administered instead (with a HER2 positive rate of 33.3%).

3.2 Expression of HER2 in UC

Among the 185 high-grade UC tissues, HER2 protein expression was observed in 159 cases (86.0%) (Figures 2A–D). Of these, 32 cases (17.3%) showed HER2 1+ expression, while 110 cases (59.5%) exhibited HER2 2+ expression and only 17 cases (7.6%) displayed HER2 3+ expression. 127 of the analyzed samples were high-grade bladder tumor tissues, with a majority of them showing HER2 protein expression in 115 cases (90.6%), 21 (16.5%) expressed HER2 1+, 79 (62.2%) expressed HER2 2+ and 16 (12.6%) expressed HER2 3+; Additionally, 36 cases were high-grade ureteral tumor tissues, and among them 25 cases (69.4%) expressed HER2 protein. Of these, 5 cases (13.9%) had HER2 score of 1+, 19 cases (52.8%) had

TABLE 1 Baseline clinicopathological features of the analyzed cohort [n, n (%)].

	Bladder	Ureteral	Renal pelvis	*P*
N	127	36	22	
Gender				
Male	113	20	6	<0.001
Female	14	16	16	
Age/years (Median)	61	70	68	0.386
Range	41–93	52–85	55–87	
Tumor size/cm				0.807
≥2	95	27	18	
<2	32	9	4	
Muscle invasion				<0.001
MIUC	54	31	18	
NMIUC	73	5	4	
pN				0.038
N1	8	4	5	
N0	119	32	17	
Stage				0.001
I	72	14	4	
II	22	10	3	
III	24	6	8	
IV	9	6	7	

N, number; WHO, world health organization; pN, primary lymph node stage; MIBC, muscle invasive urothelial cancer; NMIBC, non-muscle invasive urothelial cancer.

HER2 score of 2+ and only 1 case (2.8%) had HER2 3+. Among the 22 high-grade renal pelvis tumor tissues, HER2 protein was expressed in 19 cases (86.4%), with 6 cases (27.3%) showing HER2 1+ expression and 13 cases (59.1%) exhibiting HER2 2+ expression (Figure 2E).

3.3 Factors correlated with HER2+ in UC patients

The HER2 positive rate (IHC 2+ and 3+) in 185 high-grade UC patients was found to be 68.65% (127/185). We conducted an analysis to identify potential factors associated with HER2 positivity. Notably, clinical stage exhibited a statistically significant correlation with HER2 positivity in UC (p = 0.019). However, no significant associations were observed between HER2 positivity and gender (p = 0.345), age (p = 0.289), tumor size (p = 0.107), smoking status (p = 0.175), muscle invasion (p = 0.133), regional lymph node metastasis (p = 0.143) or primary site of the tumor (p = 0.066) as shown in Table 2. Furthermore, we investigated whether any blood indicators could predict the expression of HER2+. Logistic regression analysis revealed that none of the blood indicators examined showed predictive value for HER2+ expression (Figure 3).

3.4 The efficacy of DV on the treatment of HER2+ UC patients

Sixteen patients with locally-advanced/metastatic UC, who had failed first-line treatment, were enrolled in this study. They received DV 240 mg every 2 weeks in combination with PD-1 inhibitors tislelizumab 200 mg every 3 weeks. The cohort consisted of an equal distribution of male and female patients, with a median age of 66 (range: 51–81) years old. Metastatic sites included the liver (n = 3), lung (n = 2), and bone (n = 3). Table 3; Figure 2F present the baseline characteristics of these patients.

After a median follow-up duration of 14 (1.0–19.0) months, we presented the treatment cycle and prognosis of each patient in Figure 4. According to RECIST 1.1 criteria, one patient achieved complete response (CR), while nine patients showed partial response (PR). Four patients exhibited stable disease (SD), and two patients experienced progressive disease (PD) as shown in Figures 4A, B. The ORR was found to be 62.5%, with tumor size reduction observed in twelve out of sixteen patients compared to baseline measurements, indicating a decrease rate of 75% as depicted in Figure 4E. The DCR was determined to be 87.5%. Among the ten HER2-positive patients expressing HER2 at level 2+, the ORR reached up to 70%. For six HER2-negative patients expressing HER2 at level 1+, the ORR was recorded as being at a rate of

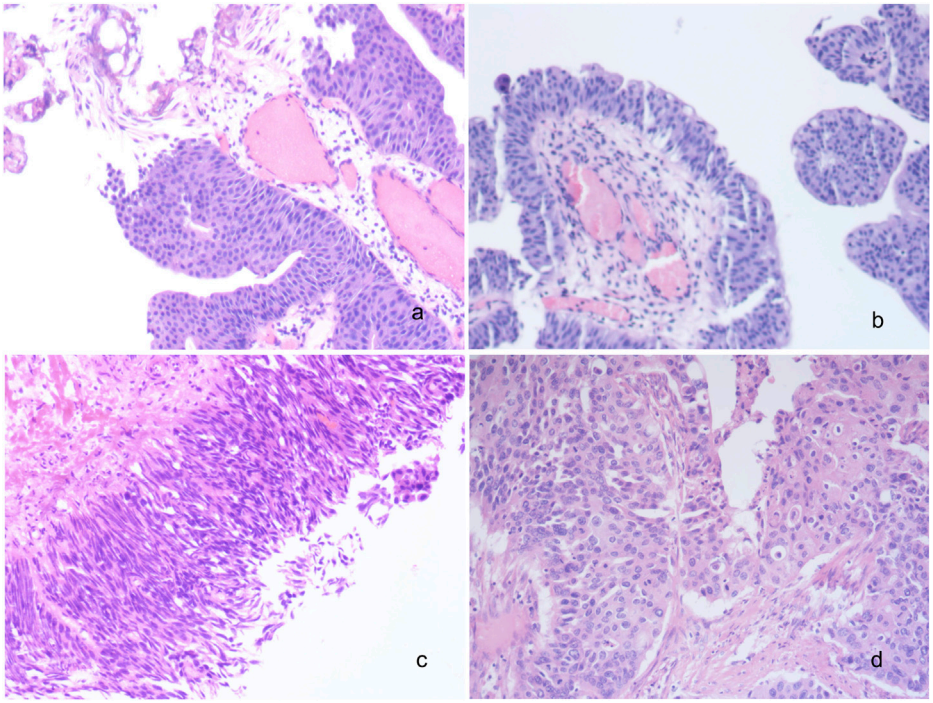

FIGURE 1
Histomorphological spectrum of UC. **(A)** Low grade non-invasive urothelial bladder carcinoma; **(B)** Low grade invasive urothelial bladder carcinoma; **(C)** High grade non-invasive urothelial bladder carcinoma; **(D)** High grade invasive urothelial bladder carcinoma; ×200. UC, urothelial carcinoma.

50%. Median progression-free survival or overall survival has not been reached yet, as illustrated in Figures 4C, D.

3.5 Side effects

Eleven patients reported side effects following DV treatment, with the most frequently observed being hypaesthesia (5/16), alopecia (4/16), leukopenia (4/16), debilitation (4/16), and digestive tract symptoms such as nausea and anorexia (4/16) (Figure 4F). These adverse events were all classified as grade 1 or 2, with no occurrences of grade 3 or higher. Symptomatic treatment was administered to all patients.

4 Discussion

Urothelial carcinoma is the third most common cancer with HER2 overexpression, following breast and stomach cancer. Recent clinical trials have demonstrated the efficacy of HER2 targeted therapy in urothelial carcinoma. However, there is variability in the reported rates of HER2 positivity. A European study found that 4%–20% of urothelial carcinoma patients exhibited HER2 expression (Bellmunt et al., 2015). Cheetham and Petrylak (2016) reported a range of 5%–89% for bladder UCs overexpressing HER2 protein. In Chinese bladder UC patients, the expression of HER2 differs from other countries and also varies among provinces. Studies conducted in Beijing showed a HER2 positive rate ranging from 36.1% to 44% in UCs (Fan et al., 2022; Zhou et al., 2023). In our study conducted in Shandong Province, China, we observed that 159 out of 185 cases (86%) of high-grade UC expressed HER2 protein, with 127 cases exhibiting positive staining (IHC score 2+ and 3+), accounting for 68.6%. Furthermore, we found variations in HER2 expression among different primary sites within high-grade UCs; bladder UCs had a higher rate of positivity (74.8%) compared to ureters (55.6%) or renal pelvises (59.1%). The majority of cases exhibited moderate levels of HER2 expression at an IHC score of 2+ (110/185; 59%), while only a small percentage showed strong staining at an IHC score of 3+ (17/185; 9%). This was significantly lower than those with weak staining at an IHC score of 1+ (32/185; 17%) or moderate staining at an IHC score of 2+. Wide ranges of HER2+ reappearances have been observed in several studies, which can be attributed to suboptimal staining processes and the lack of standardized criteria specific for UC (Scherrer et al., 2022). The frequency of HER2 protein overexpression is influenced by multiple factors, including ERBB2 mutation and amplification. In muscle invasive bladder cancer, the expression rate of HERR2 amplified or single nucleotide variation (SNV) was found to be less than 20% (Kiss et al., 2017). Samples with ERBB2 amplification exhibited higher mRNA and protein expression levels. However, gene amplification alone does not solely drive high HER2 expression in bladder cancer; SNVs occur prior to ERBB2 amplification. SNVs occurring in the extracellular region of ERBB2 appear to result in lower protein expression detection. The practicality and high sensitivity of IHC-based HER2 detection still remain significant.

The detection of HER2 expression in urothelial carcinoma is not currently incorporated into routine clinical practice, thus the understanding of HER2 expression in urothelial carcinoma remains unclear. Despite the known overexpression of HER2 in

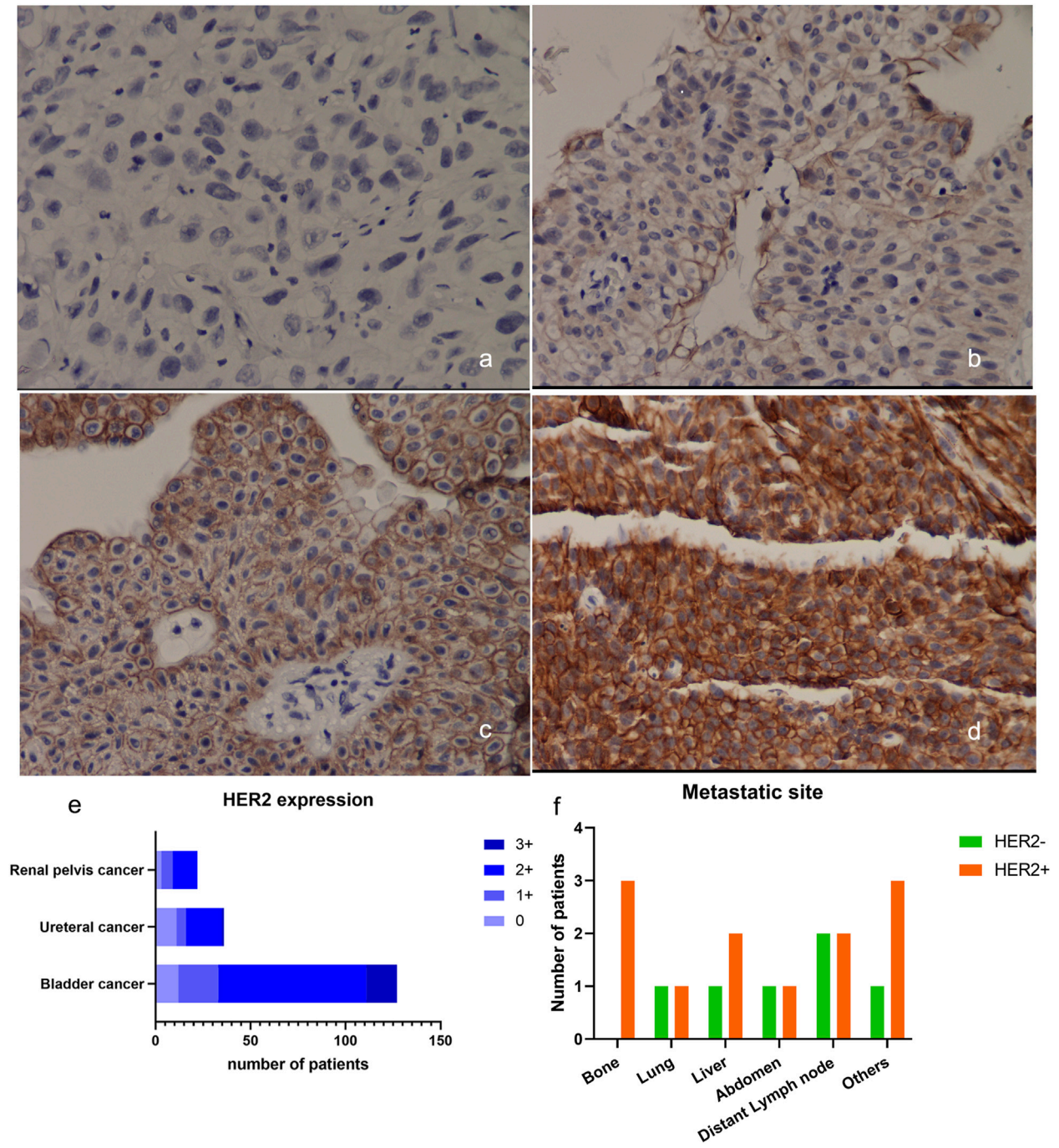

FIGURE 2
Expression of HER2 in UC. **(A–D)** Example of HER2 expression in urothelial bladder carcinoma. **(A)** HER2 IHC scored 0+; **(B)** HER2 IHC scored 1+; **(C)** HER2 IHC scored 2+; **(D)** HER2 IHC scored 3+, ×200; **(E)** Expression of HER2 in UC from different primary sites; **(F)** The metastatic sites of patients included in the DV treatment therapy at baseline. HER2, human epidermal growth factor receptor 2; IHC, immunohistochemistry.

various tumors, there are still conflicting data regarding its role as a carcinogenic driver or prognostic marker for urothelial carcinoma (Krüger et al., 2002; Bellmunt et al., 2015), Notably, treatment with ADC targeted HER2 has significantly improved survival rates for patients with HER2+ breast cancer and gastric cancer. Previous studies on the detection criteria for urothelial cancer HER2 mostly referred to breast cancer or gastric cancer, resulting in substantial variations among research findings. In 2021, China released the Expert Consensus on Clinical Pathology of Human Epidermal Growth Factor Receptor 2 Detection in Urinary Cancer which highlighted key differences between detection criteria for urothelial cancer and breast cancer. For urothelial cancer, scoring is defined as follows: 0 indicates non-staining or <10% incomplete and weak staining of infiltrating cancer cell membranes; 1+ denotes ≥10% incomplete and weak staining; 2+ signifies ≥10% weak to moderate staining of intact cell membrane or <10% strongly

TABLE 2 Relationship between HER2+ and some clinicopathological features of UC [n, n (%)].

	HER2+	HER2-	*P*
N(%)	127 (68.65%)	58 (31.35%)	
Gender			0.345
Male	98	41	
Female	29	17	
Age (years)	68 (41–93)	67 (43–85)	0.289
Tumor diameter (cm)	2.6 (0–10)	3.0 (0.8–8.5)	0.107
Smoke			0.175
Yes	50	29	
No	77	29	
Muscle invasive			0.133
Yes	66	37	
No	61	21	
pN			0.143
N1	9	8	
N0	118	50	
Stage			0.019
I	64	26	
II	24	11	
III	30	8	
IV	91	13	
Primary site			0.066
Bladder	94	33	
Ureter	20	16	
Renal pelvis	13	9	

HER2, human epidermal growth factor receptor 2.

stained intact cell membrane; and finally, 3+ represents ≥10% strong staining of intact cell membranes.

A higher percentage of HER2+ expression is observed in high-grade UC. Bai et al. (2022) conducted immunohistochemical staining to evaluate HER2 expression in 108 patients with bladder UC who underwent radical cystectomy. They discovered that 57.4% of patients exhibited HER2 overexpression, which was significantly correlated with elevated tumor grade ($p = 0.006$) and staging ($p < 0.001$) (Bai et al., 2022). A meta-analysis by Zhao et al. (2015) also revealed a positive association between HER2 expression and high tumor grade. Similarly, Krüger et al. (2002) found that HER2 overexpression was more frequently detected in the high-grade cancer group compared to the low-grade cancer group among 138 bladder cancer cases. It should be noted that within the high-grade category, there are histological types associated with both better and poorer prognosis. Additionally, areas of high-grade UC specimens often exhibit negative tissue for HER2, indicating significant heterogeneity within UC, particularly in poorly differentiated tumors with a higher grade; thus suggesting that differences in HER2 overexpression may be linked to tumor heterogeneity.

According to our study, a significant difference was observed in the percentage of HER2+ among different clinical stages of UC ($p = 0.019$) (Table 2). This finding is consistent with another research study, which demonstrated a strong association between elevated levels of HER2 and the stage of UC at both mRNA and protein levels ($p < 0.001$) (Hussein et al., 2021). It is worth noting that HER2 overexpression is considered an early event in urothelial tumor development and rarely occurs during subsequent tumor progression. Therefore, there may be limited correlation with depth of myometrial invasion or lymph node metastasis (Goodman and Osunkoya, 2016). According to our current knowledge, there is limited literature discussing the association between blood indicators and HER2 expression in UC. However, relevant studies have been conducted in breast cancer. Specifically, red cell distribution width (RDW), RDW to platelet ratio (RPR), and platelet cell distribution width (PDW) have shown correlations with HER-2 expression in breast cancer tissues (Takeuchi et al., 2019).

Disitamab vedotin served as a second-line therapy for patients with locally-advanced or metastatic UC expressing HER2. In a phase II study involving 43 HER2-positive UC patients, the ORR was determined to be 51.2% after a follow-up period of 20.3 months, while the median PFS and OS were found to be 6.9 months and 13.9 months, respectively (Sheng et al., 2021a). Another clinical study reported an ORR of 46.9% and a median PFS of 4.3 months, with a median OS of 14.8 months (Sheng et al., 2021b). Apart from DV, there are several other HER2 ADCs that have also been applied in UC. Trastuzumab emtansine (TDM1), an ADC comprising the anti-HER2 antibody rastuzumab, has received FDA approval for treating HER2-positive bladder cancer patients who have previously undergone paclitaxel/rastuzumab therapy. In the phase II KAMELEON study (NCT02999672), patients with advanced urothelial bladder cancer positive for HER2 were included (de Vries et al., 2023). Following a median follow-up duration of 7.39 months (4.11–10.02) and a median exposure duration of 7.14 weeks for the metastatic UBC cohort, an overall response rate (90% CI) of 38.5% (16.57%–64.52%) to TDM1 was achieved. In total, 84.6% (11/13) of patients in the UC cohort experienced ≥1 adverse event, all considered treatment-related. Trastuzumab deruxtecan (DS-8201a) is another HER2 ADC compound composed of a spliceable linker connecting trastuzumab and an exatecan derivative acting as a topoisomerase I inhibitor. Notably, DS-8201a exhibits a higher drug-antibody ratio compared to TDM1, enabling its efficacy even in tumors with low HER2 expression. The ORR of DS-8201a was reported as 25% (4/16) in a phase I dose-escalation and dose-expansion study (Banerji et al., 2019). Considering the remarkable efficacy of disitamab vedotin, DV received approval from the National Medical Products Administration in January 2022. The extracellular domain of RC48 is a humanized anti-HER2 antibody that conjugates with microtubule protein inhibitors (MMAE) through a cleavable linker. MMAE released via enzymatic hydrolysis exhibits high membrane permeability and exerts therapeutic effects on tumor cells exhibiting low or no expression of HER2 (Padua et al., 2022). Accordingly, an ongoing follow-up study (NCT04073602) investigating RC48-ADC in patients with low HER2 expression enrolled a total of nineteen participants, revealing an ORR of 26.3%, median PFS of 5.5 months, and median OS of 16.4 months (Xu et al., 2022a). Our findings align closely with those observed in our study.

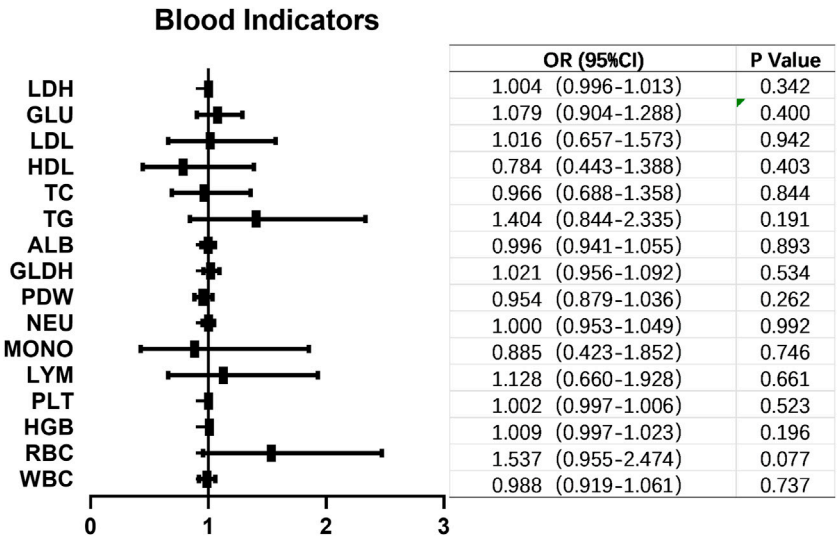

FIGURE 3
Blood indicators that might correlated with HER2+ in UC. No blood indicators showed correlation with HER2+ expression in UC. OR, odds ratio; CI, confidence interval; LDH, lactatedehydrogenase; GLU, glucose; LDL, low density lipoprotein; HDL, high density lipoprotein; TC, total cholesterol; TG, triglyceride; ALB, albumin; GLDH, glutamic dehydrogenase; PDW, platelet distribution width; NEU, neutrophil; MONO, monocyte; LYM, lymphocyte; PLT, platelet; HGB, hemoglobin; WBC, white blood cell.

TABLE 3 Baseline status of patients receiving targeted treatment with disitamab vedotin.

	Gender	Age	HER2	Primary site	TNM stage	Metastasis
1	Male	51	2+	Bladder	T3N1M1b	Liver
2	Male	70	2+	Renal pelvis	T3N2M1	Bone
3	Female	76	1+	Bladder	T4aN1M0	None
4	Male	55	2+	Renal pelvis	T3N1N1	Lung, Bone
5	Male	63	2+	Bladder	T4bN0M0	None
6	Female	65	2+	Renal pelvis	T3N2M1	Supraclavicular lymph Node
7	Male	81	1+	Bladder	T4aN0M1	Lung
8	Female	65	1+	Bladder, Ureter	T2bN0M1	Inguinal lymph node
9	Female	66	2+	Ureter	TxN2M1	Abdomen, Liver
10	Female	66	2+	Renal pelvis	T3N2M1	Bone
11	Male	58	2+	Ureter	T3N2M0	None
12	Female	72	1+	Ureter	T3N0M1	Abdomen
13	Female	66	1+	Ureter	T3N1M1	Cervical lymph node
14	Female	56	1+	Renal pelvis	T2bN0M1	Liver
15	Male	66	2+	Bladder	T4aN3M1a	Distant lymph node
16	Male	78	2+	Bladder	T2bN0M0	None

ICIs targeting PD-1 have demonstrated promising results in the treatment of bladder cancer, particularly in cases of metastatic UC that have progressed after chemotherapy. Recent studies have reported on the combination therapy of PD-1 and HER2 targeting ADCs. In a breast cancer model study, the combination of disitamab vedotin and PD-1 antibody exhibited remarkable efficacy in mice, surpassing the effects observed with either disitamab vedotin or PD-1 antibody alone. Furthermore, this combined treatment facilitated the formation of immunological memory, providing protection against tumor rechallenge (Huang et al., 2022). The observed infiltration of immune cells in mouse tumors following disitamab vedotin therapy suggests the potential for synergistic therapeutic effects by combining an

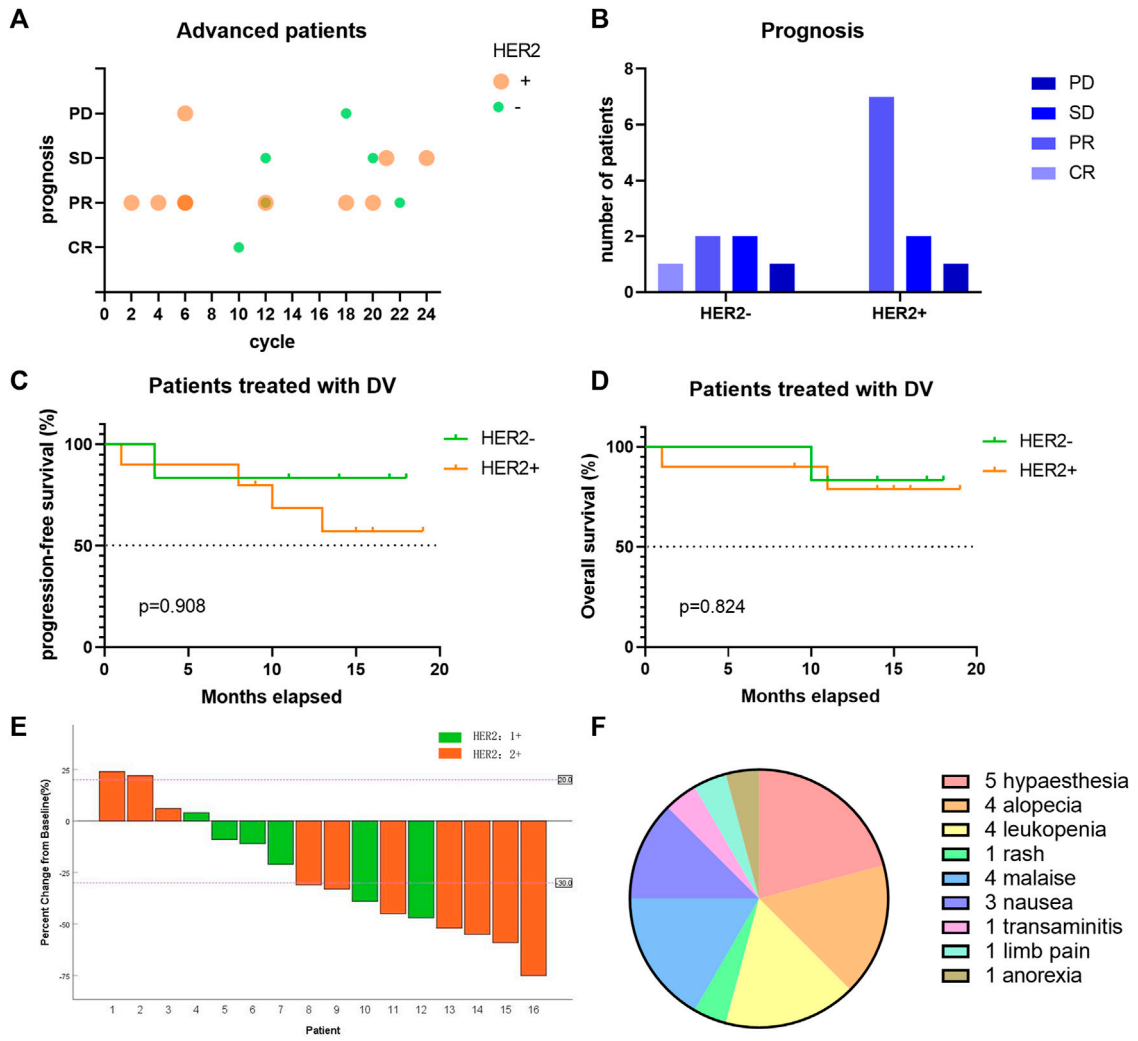

FIGURE 4
The efficacy of DV on the treatment of locally-advanced/metastatic UC patients. **(A)** Each bubble represents one patient, with different treatment cycle, HER2 expression and different prognosis. Bubbles with darker color reflected more than one patient. **(B)** The short-term prognosis of advanced UC patients divided by HER2 expression. **(C–D)** The long-term prognosis of advanced UC patients divided by HER2 expression. **(E)** Changes of patients' tumor size compared to baseline. **(F)** Side effects of DV treatment in locally-advanced/metastatic UC. DV, disitamab vedotin; CR, complete response; PR, partial response; SD, stable disease; PD, progression disease.

immune checkpoint inhibitor (PD-1 inhibitor). Clinical data also supports this, with a report on the combination of RC48 and pembrolizumab in advanced UC (Xu et al., 2022b). The patient achieved CR and long-term PFS (>12 months). In a phase Ib/II study (RC48-C014), preliminary results demonstrated promising synergistic efficacy of RC48 in combination with toripalimab for advanced UC patients (Zhou et al., 2022a). The recommended dosage was RC48-ADC 2 mg/kg + toripalimab 3 mg/kg administered every 2 weeks. After a median follow-up of 8.0 months for 36 patients, the confirmed ORR was 76.7%. The median PFS at that time was 9.2 months, while the median OS had not been reached (Sheng et al., 2022). Another clinical study conducted in Fujian Province, China enrolled nine locally advanced or metastatic UC patients who were treated with DV combined with tislelizumab/toripalimab. After a median follow-up of 12 months, the ORR was found to be 88.9% (Wei et al., 2023). Additionally, ongoing clinical trials are investigating vedotin-tislelizumab as neoadjuvant treatment for HER2-positive locally advanced bladder urothelial carcinoma patients (Wen et al., 2024; Wen et al., 2022). In our study, the addition of DV was implemented following the failure of tislelizumab monotherapy. Notably, positive PD-L1 expression was observed in 20% of cases, while the efficacy of PD-1 alone exhibited limitations (Ma et al., 2023). Encouragingly, a clinical trial (RC48-C014) demonstrated that combining RC48-ADC with toripalimab yielded promising efficacy (ORR of 75% in all patients) for individuals with metastatic urothelial carcinoma (Zhou et al., 2022b), surpassing the outcomes achieved by DV monotherapy. Consequently, we opted for combination therapy involving disitamab vedotin and tislelizumab. In our study involving sixteen locally-advanced/metastatic UC patients, after a median follow-up of 14 months, the ORR among HER2+ patients was observed to be 70%, whereas it was found to be 50% among HER2-patients. Overall, the ORR reached up to 62.5% across all sixteen patients studied. These findings highlight the efficacy of RC48 not only in HER2+ but also in HER2- UC patients.

The RC48 exhibited manageable adverse effects in patients with UC. In our study, 68.8% (11/16) of the patients reported side effects, all of which were classified as grade 1 or 2. The most frequently reported side effects included hypaesthesia, hair loss, and leukopenia. In other studies on UC, patients experienced grade 1 or 2 side effects such as loss of appetite, rash, and fatigue (Wei et al., 2023), as well as grade 3 side effects including hypoesthesia and neutropenia (Sheng et al., 2021a). Other reported grade 3 side effects comprised anemia, hypoalbuminemia, urinary tract infection, and autoimmune encephalitis (Chen et al., 2023). All these side effects were effectively managed through appropriate treatments.

There are several limitations in our study. Firstly, the duration of follow-up was insufficient to obtain data on PFS or OS. In this paper, we solely investigated HER2 expression in UC based on the 2021 edition of the clinical pathological expert consensus on HER2 testing in UC in China. The association between HER2 positivity and long-term prognosis in UC patients remains unknown. Secondly, advanced patients received a combination therapy of DV and PD-1 inhibitors rather than DV alone, as our aim was to achieve improved patient outcomes. Further research is warranted to gain a better understanding of the long-term efficacy of DV monotherapy in UC patients. Although preclinical studies have shown promising results with RC48 used alongside PD-1/L1 inhibitors, additional evidence is required from clinical practice.

5 Conclusion

HER2 is a promising therapeutic target for UC, and its expression level holds critical significance in treatment response. Currently, HER2-targeting ADCs have demonstrated remarkable efficacy in select clinical trials (Zhou et al., 2023). However, the existing evaluation criteria for HER2 are inadequate for UC, leading to substantial discrepancies among research findings. Therefore, the establishment of a standardized scoring system is imperative to accurately identify individuals suitable for anti-HER2 ADC therapy and holds significant clinical implications. In this study, we adopted a novel Chinese standard to assess the expression rate of HER2 in high-grade UC patients with the aim of promoting uniformity in evaluating HER2 expression across UC studies. Our results indicate widespread protein expression of HER2 in urothelial carcinoma and reveal its close association with advanced stages of high-grade urothelial carcinoma. Targeting HER2 presents a potential therapeutic pathway for tumor management in UC patients. Combination therapy involving DV inhibitors and PD-1 blockade demonstrates both efficacy and acceptable side effects when treating advanced UC patients with either positive or negative HER2 status.

Data availability statement

The original contributions presented in the study are included in the article/Supplementary material, further inquiries can be directed to the corresponding author.

Ethics statement

The studies involving humans were approved by the ethics committee of Shandong Provincial Hospital Affiliated to Shandong First Medical University. The studies were conducted in accordance with the local legislation and institutional requirements. The participants provided their written informed consent to participate in this study.

Author contributions

KZ: Data curation, Funding acquisition, Software, Writing–original draft, Writing–review and editing. YC: Data curation, Investigation, Methodology, Writing–original draft. DZ: Data curation, Investigation, Writing–original draft. AG: Data curation, Writing–original draft. JC: Methodology, Writing–original draft. CW: Data curation, Writing–original draft. YG: Data curation, Formal Analysis, Software, Writing–review and editing. SD: Conceptualization, Project administration, Supervision, Writing–review and editing.

Funding

The author(s) declare financial support was received for the research, authorship, and/or publication of this article. This work was supported by the Shandong Provincial Natural Science Foundation (Grant No. ZR2021QH313, ZR202306200045, and ZR2023LZL005); and the Academic Promotion Programme by Shandong First Medical University (Grant No. 2020LI001).

Acknowledgments

The authors thank the study patients for their participation and trust.

Conflict of interest

The authors declare that the research was conducted in the absence of any commercial or financial relationships that could be construed as a potential conflict of interest.

Publisher's note

References

Bai, X., He, W., Yin, H., Li, X., Zhou, X., Wei, Z., et al. (2022). Prognostic significance of HER2 status evaluation using immunohistochemistry in patients with urothelial carcinoma of the bladder: a retrospective single-center experience. *Exp. Ther. Med.* 24 (5), 704. doi:10.3892/etm.2022.11640

Banerji, U., van Herpen, C. M. L., Saura, C., Thistlethwaite, F., Lord, S., Moreno, V., et al. (2019). Trastuzumab duocarmazine in locally advanced and metastatic solid tumours and HER2-expressing breast cancer: a phase 1 dose-escalation and dose-expansion study. *Lancet Oncol.* 20 (8), 1124–1135. doi:10.1016/S1470-2045(19)30328-6

Bellmunt, J., Werner, L., Bamias, A., Fay, A. P., Park, R. S., Riester, M., et al. (2015). HER2 as a target in invasive urothelial carcinoma. *Cancer Med.* 4 (6), 844–852. doi:10.1002/cam4.432

Chang, E., Weinstock, C., Zhang, L., Charlab, R., Dorff, S. E., Gong, Y., et al. (2021). FDA approval summary: enfortumab vedotin for locally advanced or metastatic urothelial carcinoma. *Clin. Cancer Res.* 27 (4), 922–927. doi:10.1158/1078-0432.CCR-20-2275

Cheetham, P. J., and Petrylak, D. P. (2016). New agents for the treatment of advanced bladder cancer. *Oncol. Willist. Park* 30 (6), 571–588.

Chen, M., Yao, K., Cao, M., Liu, H., Xue, C., Qin, T., et al. (2023). HER2-targeting antibody-drug conjugate RC48 alone or in combination with immunotherapy for locally advanced or metastatic urothelial carcinoma: a multicenter, real-world study. *Cancer Immunol. Immunother.* 72 (7), 2309–2318. doi:10.1007/s00262-023-03419-1

de Vries, E. G. E., Ruschoff, J., Lolkema, M., Tabernero, J., Gianni, L., Voest, E., et al. (2023). Phase II study (KAMELEON) of single-agent T-DM1 in patients with HER2-positive advanced urothelial bladder cancer or pancreatic cancer/cholangiocarcinoma. *Cancer Med.* 12 (11), 12071–12083. doi:10.1002/cam4.5893

Eisenhauer, E. A., Therasse, P., Bogaerts, J., Schwartz, L. H., Sargent, D., Ford, R., et al. (2009). New response evaluation criteria in solid tumours: revised RECIST guideline (version 1.1). *Eur. J. Cancer* 45 (2), 228–247. doi:10.1016/j.ejca.2008.10.026

Fan, Y., Li, Q., Shen, Q., Liu, Z., Zhang, Z., Hu, S., et al. (2022). Head-to-Head comparison of the expression differences of NECTIN-4, TROP-2, and HER2 in urothelial carcinoma and its histologic variants. *Front. Oncol.* 12, 858865. doi:10.3389/fonc.2022.858865

Goodman, A. L., and Osunkoya, A. O. (2016). Human epidermal growth factor receptor 2 expression in micropapillary urothelial carcinoma of the bladder: an analysis of 27 cases. *Hum. Pathol.* 57, 160–164. doi:10.1016/j.humpath.2016.07.014

He, W., Chen, C., Lin, T., Xu, Q., Ye, C., Du, J., et al. (2023). Epidemiology, treatments, and related biomarkers of locally advanced or metastatic urothelial carcinoma in Chinese population: a scoping review. *Cancer Med.* 12 (14), 15384–15403. doi:10.1002/cam4.6112

Hepp, Z., Shah, S. N., Smoyer, K., and Vadagam, P. (2021). Epidemiology and treatment patterns for locally advanced or metastatic urothelial carcinoma: a systematic literature review and gap analysis. *J. Manag. Care Spec. Pharm.* 27 (2), 240–255. doi:10.18553/jmcp.2020.20285

HERExpert Committee on Urothelial Carcinoma of Chinese Society of Clinical Oncology (2021). Clinical pathological expert consensus on HER-2 testing in urothelial carcinoma in China. *Zhonghua Zhong Liu Za Zhi* 43 (10), 1001–1006. doi:10.3760/cma.j.cn112152-20210809-00597

Hoimes, C. J., Flaig, T. W., Milowsky, M. I., Friedlander, T. W., Bilen, M. A., Gupta, S., et al. (2023). Enfortumab vedotin plus pembrolizumab in previously untreated advanced urothelial cancer. *J. Clin. Oncol.* 41 (1), 22–31. doi:10.1200/JCO.22.01643

Huang, L., Wang, R., Xie, K., Zhang, J., Tao, F., Pi, C., et al. (2022). A HER2 target antibody drug conjugate combined with anti-PD-(L)1 treatment eliminates hHER2+ tumors in hPD-1 transgenic mouse model and contributes immune memory formation. *Breast Cancer Res. Treat.* 191 (1), 51–61. doi:10.1007/s10549-021-06384-4

Hussein, S., Fathi, A., Abouhashem, N. S., Amer, S., Hemeda, M., and Mosaad, H. (2021). SATB-1 and Her2 as predictive molecular and immunohistochemical markers for urothelial cell carcinoma of the bladder. *Cancer Biomark.* 30 (2), 249–259. doi:10.3233/CBM-200072

Kiss, B., Wyatt, A. W., Douglas, J., Skuginna, V., Mo, F., Anderson, S., et al. (2017). Her2 alterations in muscle-invasive bladder cancer: patient selection beyond protein expression for targeted therapy. *Sci. Rep.* 7, 42713. doi:10.1038/srep42713

Krüger, S., Weitsch, G., Büttner, H., Matthiensen, A., Böhmer, T., Marquardt, T., et al. (2002). HER2 overexpression in muscle-invasive urothelial carcinoma of the bladder: prognostic implications. *Int. J. cancer* 102 (5), 514–518. doi:10.1002/ijc.10731

Ma, Y. T., Hua, F., Zhong, X. M., Xue, Y. J., Li, J., Nie, Y. C., et al. (2023). Clinicopathological characteristics, molecular landscape, and biomarker landscape for predicting the efficacy of PD-1/PD-L1 inhibitors in Chinese population with mismatch repair deficient urothelial carcinoma: a real-world study. *Front. Immunol.* 14, 1269097. doi:10.3389/fimmu.2023.1269097

Mendelsohn, J., and Baselga, J. (2003). Status of epidermal growth factor receptor antagonists in the biology and treatment of cancer. *J. Clin. Oncol.* 21 (14), 2787–2799. doi:10.1200/JCO.2003.01.504

Olt, G., Berchuck, A., and Bast, R. C., Jr (1990). The role of tumor markers in gynecologic oncology. *Obstet. Gynecol. Surv.* 45 (9), 570–577. doi:10.1097/00006254-199009000-00002

Padua, T. C., Moschini, M., Martini, A., Pederzoli, F., Nocera, L., Marandino, L., et al. (2022). Efficacy and toxicity of antibody-drug conjugates in the treatment of metastatic urothelial cancer: a scoping review. *Urol. Oncol.* 40 (10), 413–423. doi:10.1016/j.urolonc.2022.07.006

Press, M. F., Jones, L. A., Godolphin, W., Edwards, C. L., and Slamon, D. J. (1990). HER-2/neu oncogene amplification and expression in breast and ovarian cancers. *Prog. Clin. Biol. Res.* 354A, 209–221.

Rosenberg, J. E., O'Donnell, P. H., Balar, A. V., McGregor, B. A., Heath, E. I., Yu, E. Y., et al. (2019). Pivotal trial of enfortumab vedotin in urothelial carcinoma after platinum and anti-programmed death 1/programmed death ligand 1 therapy. *J. Clin. Oncol.* 37 (29), 2592–2600. doi:10.1200/JCO.19.01140

Scherrer, E., Kang, A., Bloudek, L. M., and Koshkin, V. S. (2022). HER2 expression in urothelial carcinoma, a systematic literature review. *Front. Oncol.* 12, 1011885. doi:10.3389/fonc.2022.1011885

Sheng, X., He, Z., Han, W., Zhou, A.-P., Luo, H., Shi, Y., et al. (2021b). An open-label, single-arm, multicenter, phase II study of RC48-ADC to evaluate the efficacy and safety of subjects with HER2 overexpressing locally advanced or metastatic urothelial cancer (RC48-C009). 39(15_Suppl. l):4584. doi:10.1200/jco.2021.39.15_suppl.4584

Sheng, X., Yan, X., Wang, L., Shi, Y., Yao, X., Luo, H., et al. (2021a). Open-label, multicenter, phase II study of RC48-ADC, a HER2-targeting antibody-drug conjugate, in patients with locally advanced or metastatic urothelial carcinoma. *Clin. Cancer Res.* 27 (1), 43–51. doi:10.1158/1078-0432.CCR-20-2488

Sheng, X., Zhou, L., He, Z., Guo, H., Yan, X., Li, S., et al. (2022). Preliminary results of a phase Ib/II combination study of RC48-ADC, a novel humanized anti-HER2 antibody-drug conjugate (ADC) with toripalimab, a humanized IgG4 mAb against programmed death-1 (PD-1) in patients with locally advanced or metastatic urothelial carcinoma. 40(16_Suppl. l):4518. doi:10.1200/jco.2022.40.16_suppl.4518

Sung, H., Ferlay, J., Siegel, R. L., Laversanne, M., Soerjomataram, I., Jemal, A., et al. (2021). Global cancer Statistics 2020: GLOBOCAN estimates of incidence and mortality worldwide for 36 cancers in 185 countries. *CA a cancer J. Clin.* 71 (3), 209–249. doi:10.3322/caac.21660

Takeuchi, H., Abe, M., Takumi, Y., Hashimoto, T., Miyawaki, M., Okamoto, T., et al. (2019). Elevated red cell distribution width to platelet count ratio predicts poor prognosis in patients with breast cancer. *Sci. Rep.* 9 (1), 3033. doi:10.1038/s41598-019-40024-8

Wei, Y., Zhang, R., Yu, C., Hong, Z., Lin, L., Li, T., et al. (2023). Disitamab vedotin in combination with immune checkpoint inhibitors for locally and locally advanced bladder urothelial carcinoma: a two-center's real-world study. *Front. Pharmacol.* 14, 1230395. doi:10.3389/fphar.2023.1230395

Wen, F., Lin, T., Tan, P., Zheng, X., Liu, J., Zhang, P., et al. (2022). 135O A multi-center phase Ib/II study of RC48-ADC combined with tislelizumab as neoadjuvant treatment in patients with HER2 positive locally advanced MIBC. *Ann. Oncol.* 33, S1485. doi:10.1016/j.annonc.2022.10.170

Wen, F., Lin, T., Zhang, P., and Shen, Y. (2024). RC48-ADC combined with tislelizumab as neoadjuvant treatment in patients with HER2-positive locally advanced muscle-invasive urothelial bladder cancer: a multi-center phase Ib/II study (HOPE-03). *Front. Oncol.* 13, 1233196. doi:10.3389/fonc.2023.1233196

Xu, H., Sheng, X., Zhou, L., Yan, X., Li, S., Chi, Z., et al. (2022a). A phase II study of RC48-ADC in HER2-negative patients with locally advanced or metastatic urothelial carcinoma. *J. Clin. Oncol.* 40 (16_Suppl. l), 4519. doi:10.1200/jco.2022.40.16_suppl.4519

Xu, Z., Ma, J., Chen, T., and Yang, Y. (2022b). Case report: the remarkable response of pembrolizumab combined with RC48 in the third-line treatment of metastatic urothelial carcinoma. *Front. Immunol.* 13, 978266. doi:10.3389/fimmu.2022.978266

Zhao, J., Xu, W., Zhang, Z., Song, R., Zeng, S., Sun, Y., et al. (2015). Prognostic role of HER2 expression in bladder cancer: a systematic review and meta-analysis. *Int. urology Nephrol.* 47 (1), 87–94. doi:10.1007/s11255-014-0866-z

Zhou, L., Shao, Z., Liu, Y., Yan, X., Li, J., Wu, X., et al. (2023). HER2 expression associated with clinical characteristics and prognosis of urothelial carcinoma in a Chinese population. *Oncologist* 28 (8), e617–e624. doi:10.1093/oncolo/oyad070

Zhou, L., Xu, H., Li, S., Yan, X., Li, J., Wu, X., et al. (2022a). Study RC48-C014: preliminary results of RC48-ADC combined with toripalimab in patients with locally advanced or metastatic urothelial carcinoma. 40(6_Suppl. l):515. doi:10.1200/jco.2022.40.6_suppl.515

Zhou, L., Xu, H., Li, S., Yan, X., Li, J., Wu, X., et al. (2022b). Study RC48-C014: preliminary results of RC48-ADC combined with toripalimab in patients with locally advanced or metastatic urothelial carcinoma. *J. Clin. Oncol.* 40 (6_Suppl. l), 515. doi:10.1200/jco.2022.40.6_suppl.515

frontiers | Frontiers in Oncology

TYPE Original Research
PUBLISHED 22 February 2024
DOI 10.3389/fonc.2024.1354049

OPEN ACCESS

EDITED BY
Huan Yang,
Huazhong University of Science and Technology, China

REVIEWED BY
Jianqiu Kong,
Sun Yat-sen Memorial Hospital, China
Wei Xi,
Fudan University, China

*CORRESPONDENCE
Gangli Gu
ggl0126@126.com
Zhao Liu
zhao.liu@sdu.edu.cn

†These authors have contributed equally to this work and share first authorship

RECEIVED 11 December 2023
ACCEPTED 31 January 2024
PUBLISHED 22 February 2024

CITATION
Huang Y, Guo W, Zeng Y, Wang X, Fan B, Zhang Y, Yan L, Gu G and Liu Z (2024) Identification and validation of a gap junction protein related signature for predicting the prognosis of renal clear cell carcinoma. *Front. Oncol.* 14:1354049. doi: 10.3389/fonc.2024.1354049

Identification and validation of a gap junction protein related signature for predicting the prognosis of renal clear cell carcinoma

Yongsheng Huang[1†], Wenyi Guo[2†], Yuan Zeng[1], Xinrong Wang[3], Bohao Fan[1], Ying Zhang[4], Lei Yan[1], Gangli Gu[1*] and Zhao Liu[1*]

[1]Department of Urology, Qilu Hospital, Cheeloo College of Medicine, Shandong University, Jinan, China, [2]Department of Pancreatic Surgery, General Surgery, Qilu Hospital, Cheeloo College of Medicine, Shandong University, Jinan, China, [3]Department of Anatomy and Neurobiology, Shandong Provincial Key Laboratory of Mental Disorders, School of Basic Medical Sciences and Qilu Hospital, Cheeloo College of Medicine, Shandong University, Jinan, China, [4]Department of Surgery, Qihe County Traditional Chinese Medicine Hospital, Dezhou, China

Background: Gap junction proteins (GJPs) are a class of channel proteins that are closely related to cell communication and tumor development. The objective of this study was to screen out GJPs related prognostic signatures (GRPS) associated with clear cell renal cell carcinoma (ccRCC).

Materials and Methods: GJPs microarray data for ccRCC patients were obtained from The Gene Expression Omnibus (GEO) database, along with RNA sequencing data for tumor and paired normal tissues from The Cancer Genome Atlas (TCGA) database. In the TCGA database, least absolute shrinkage and selection Operator (LASSO) and Cox regression models were used to identify GJPs with independent prognostic effects as GRPS in ccRCC patients. According to the GRPS expression and regression coefficient from the multivariate Cox regression model, the risk score (RS) of each ccRCC patient was calculated, to construct the RS prognostic model to predict survival. Overall survival (OS) and progression-free survival (PFS) analyses; gene pan-cancer analysis; single gene survival analysis; gene joint effect analysis; functional enrichment analysis; tumor microenvironment (TME) analysis; tumor mutational burden (TMB) analysis; and drug sensitivity analysis were used to explore the biological function, mechanism of action and clinical significance of GRPS in ccRCC. Further verification of the genetic signature was performed with data from the GEO database. Finally, the cytofunctional experiments were used to verify the biological significance of GRPS associated GJPs in ccRCC cell lines.

Results: GJA5 and GJB1, which are GRPS markers of ccRCC patients, were identified through LASSO and Cox regression models. Low expression of GJA5 and GJB1 is associated with poor patient prognosis. Patients with high-RS had significantly shorter OS and PFS than patients with low-RS ($p< 0.001$). The risk of death for individuals with high-RS was 1.695 times greater than that for those with low-RS (HR = 1.695, 95%CI= 1.439-1.996, $p< 0.001$). Receiver Operating Characteristic (ROC) curve showed the great predictive power of the RS prognostic model for the survival rate of patients. The area under curve (AUC)

values for predicting 1-year, 3-year and 5-year survival rates were 0.740, 0.781 and 0.771, respectively. The clinical column chart was also reliable for predicting the survival rate of patients, with AUC values of 0.859, 0.846 and 0.796 for predicting 1-year, 3-year and 5-year survival, respectively. The GRPS was associated with immune cell infiltration, the TME, the TMB, and sensitivity to chemotherapy drugs. Further *in vitro* experiments showed that knockdown of GJA5 or GJB1 could promote the proliferation, migration and epithelial-mesenchymal transition (EMT) and inhibit apoptosis of ccRCC cells.

Conclusion: GJA5 and GJB1 could be potential biological markers for predicting survival in patients with ccRCC.

KEYWORDS

gap junction protein, clear cell renal cell carcinoma, biomarkers, prognostic model, cellular verification

1 Introduction

Among all types of cancer, renal cancer is the 16th most common cancer, accounting for approximately 1.8% of cancer-related deaths (1). Clear cell renal cell carcinoma (ccRCC) is the most common histological type of cancer and represents 75% of all cases (2, 3). More than 50% of renal cancer cases are detected through health examination (4). At the time of initial diagnosis, approximately 30% of patients have already developed distant metastasis (5–7). The 5-year survival rate for patients with ccRCC varies depending on the stage of the disease. The survival rate ranges from 20% to 95% for patients in the early, middle, and advanced stages, while for patients with metastatic ccRCC, the survival rate is only between 0% and 10% (8, 9). Early diagnosis plays a crucial role in improving overall survival (OS) and progression-free survival (PFS) in ccRCC patients. Therefore, it is clinically important to explore valuable prognostic indicators that can be used for personalized prognosis assessment and treatment planning, to ultimately improve the overall prognosis of patients.

Gap junction proteins (GJPs) are a family of hexamer-structured channel proteins that facilitate molecular and ion exchange between neighboring cells, thereby regulating various biological processes (10–12). The functional diversity of GJPs is attributed to variations in the molecular weight of the constituent proteins that form the gap junction channels (13). These proteins are involved in multiple biological processes, such as apoptosis, proliferation, immune response, and digestion (14, 15). Presently, 35 genetic diseases in humans are known to result from mutations in 11 different GJPs (16, 17). In addition, the obstruction of gap junction channels diminishes communication between immune cells and reduces the permeability of chemotherapy drugs. These findings suggest that GJPs potentially play a crucial role in cancer development and treatment, as well as in maintaining intercellular signal transmission and the stability of the tumor microenvironment (TME). To our knowledge, no reports have explored the clinical significance of GJPs in ccRCC, necessitating further investigation. This study identified a GJP-related prognostic signatures (GRPS) in ccRCC. Subsequently, an in-depth analysis was conducted to explore the clinical value of the GRPS in assessing ccRCC prognosis, as well as its influence on the tumor mutational burden (TMB) and the tumor microenvironment (TME). Furthermore, additional cytological experiments validated the analysis results, providing evidence that the GRPS may serve as a novel biomarker for predicting the survival prognosis of ccRCC patients.

2 Materials and methods

2.1 Bioinformatics analysis

The RNA sequencing data, clinical trait data, pan-cancer data and simple nucleotide variation data of ccRCC were obtained from The Cancer Genome Atlas (TCGA) database (https://portal.gdc.cancer.gov/); Microarray data (GSE29609, GSE95425, GSE73731) were retrieved from Gene Expression Omnibus (GEO) database (https://www.ncbi.nlm.nih.gov/geo/). This study constructed and validated the GRPS for ccRCC prognosis using various statistical methods. The detailed workflow of this analysis is depicted in Figure 1. The general clinical information of the ccRCC patients in the TCGA database can be found in Supplementary Table 1.

2.1.1 Identification of GRPS in ccRCC

A total of 21 GJPs were observed to be expressed in ccRCC. This study combines the survival information of ccRCC patients in the TCGA database (including survival status and survival time) with the gene expression data of GJP to generate a total sample (total sample, TS) for data analysis. Subsequently, a sequence of univariate

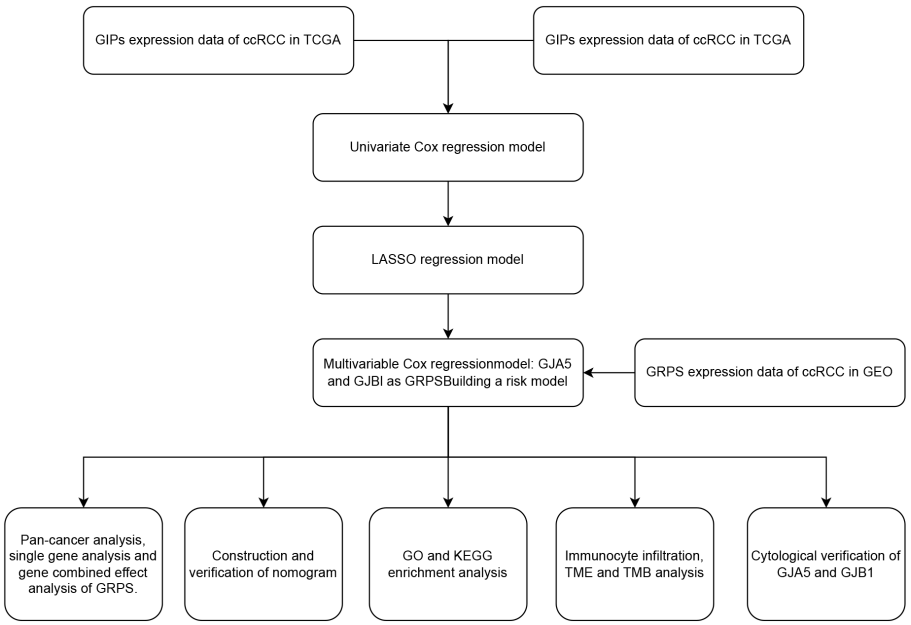

FIGURE 1
Workflow chart.

Cox regression models ($p< 0.001$, KMP = 1 for filtration criteria), LASSO regression models, and multivariate Cox regression models was constructed for TS.

2.1.2 Analysis of the combined effects of GJA5 and GJB1 on single gene and dual genes

Pan-cancer data for 33 tumors were obtained from the TCGA database. The differential expression of GJA5 and GJB1 in 33 cancers was examined via pan-cancer analysis. The difference analysis data of GRPS in ccRCC tumor tissue and normal tissue were obtained from TCGA database and GEO database (GSE73731 and GSE95425). Single-and dual-gene combined survival (Kaplan-Meier, [KM]) analyses were used to determine the significance of GJA5 and GJB1 in survival and prognosis of patients with ccRCC.

2.1.3 Construction and validation of the prognostic risk score model

To further explore the prognostic significance of the GRPS in ccRCC, a computation was performed based on the coefficients derived from the multivariate Cox regression model, along with the corresponding gene expression levels. Subsequently, an risk scores (RS) prognostic model was constructed utilizing the RS values. The RS formula employed in the RS model was as follows:

$$Risk\ \ score\ \ =\ \ \sum(Coefficient\ of\ gene * expression\ of\ gene)\ .$$

The high-RS group and low-RS group were divided according to the median RS. The RS prognostic model was developed and validated. The 70% of the samples randomly selected from the TS were assigned to the training dataset, while the remaining 30% of the samples and the GSE29609 dataset were used as the testing set (18), to confirm the generalizability of the GRPS. KM analysis, ROC curve analysis, and comparisons of clinical traits (including age, sex, grade, stage, and metastasis) between risk groups were also performed to assess the clinical significance of the GRPS.

2.1.4 Construction of a clinical nomogram

This study developed a clinical nomogram incorporating patient clinicopathologic characteristics, risk groupings, and GJA5 and GJB1 expressions. Furthermore, calibration curve, ROC curve, and Decision Curve Analysis (DCA) analyses were performed to assess the clinical availability of the nomogram.

2.1.5 Enrichment analysis

The biological function and underlying mechanisms of GRPS were investigated through gene enrichment analysis. Genes with statistical significance in the risk grouping (selected using the R package "Limma" with the criteria of $p< 0.05$, logFC = 1, and FDR< 1) were subjected to GO and KEGG enrichment analysis.

2.1.6 Analysis of immune cell infiltration, TME and TMB

Alterations in the TME and the infiltration of immune cells have garnered significant attention in the field of cancer therapy. The mechanism triggering immune escape was investigated by examining the TME and immune cell infiltration in risk groups.

After the calculation of the levels of 22 immune cells and the abundance of TME-related molecules in patients with ccRCC, the differences in the levels of immune cells and the abundance of TME-related molecules between risk groups were analyzed, and $p< 0.05$ was considered statistically significant. TMB refers to the number of gene mutation sites that occur in tumor tissues and includes somatic gene coding errors, base substitutions, insertions

or deletions (19). The TMB values of patients in the TS cohort were calculated based on simple nucleotide variation data from ccRCC patients in the TCGA database. The estimated TMB was calculated as the ratio of the total mutation frequency to the length of human exons (20). Finally, the TMB values of the 'high-RS and low-RS groups were compared for any significant difference.

2.1.7 Drug sensitivity analysis

The GDSC2 dataset used for drug sensitivity analysis was derived from the GDSC database (https://www.cancerrxgene.org). We calculated the susceptibility of ccRCC patients to 198 chemotherapeutic agents from the TCGA database. To provide accurate individualized treatment plans for patients, we used $p< 0.001$ as the filtering standard to analyze the difference in the sensitivity of patients with advanced ccRCC to targeted drugs according to risk group, which is helpful for providing medication guidance for different groups of patients with ccRCC.

2.1.8 Statistical analysis

The analysis of the data and the generation of graphs were carried out with R language (version 4.2.1). The LASSO regression model, univariate and multivariate Cox regression models were constructed through the "glmnet" package; The "survival, survminer" package was used to perform KM analysis of the combined effect of a single gene and dual genes. The "timeROC" package was used to perform ROC curve analysis; The clinical nomogram was developed through the "survival", "regplot" and "rms" packages; The "ggDCA" package was used for DCA analysis; GO enrichment analysis was carried out through the package "clusterProfiler, org.Hs.eg.db, enrichplot, ggplot2"; The "clusterProfiler, org.Hs.eg.db, enrichplot, ggplot2, circlize, RColorBrewer, ComplexHeatmap" package was used for KEGG enrichment analysis. We calculated the proportions of 22 immune cells in ccRCC tissue using the CIBERSORT algorithm and evaluated the abundance of related molecules in the TME using the R package "estimate". The oncoPredict package was used to calculate a sensitivity score for ccRCC patients to chemotherapy drugs. The chi-square test was used to analyze the difference in clinicopathological information between the training set and the testing set. Unless otherwise stated in this paper, $p< 0.05$ was considered to indicate statistically significant.

2.2 Cell function experiment

2.2.1 Cell culture and transfection

The HK2 and A498 cells were cultured in Dulbecco's modified eagle medium (DMEM) supplemented with 10% fetal bovine serum (FBS) at 37°C in a 5% CO2 incubator; the 786-O cells were cultured in Roswell Park Memorial Institute-1640 (RPMI-1640) supplemented with 10% FBS at 37°C in a 5% CO2 incubator. Cells in logarithmic phase were chosen for functional experiments. Interference of GJA5 was performed using small interfering RNA (si-GJA5-NC; si-GJA5-1, si-GJA5-2, and si-GJA5-3) sequences synthesized by RiboBio Biotechnology (Guangzhou, China). The sequences used were as follows: si-GJA5-1 (AGGCTGATTTCCGGTGTGA), si-GJA5-2 (CATGGCTATCATAGTGACA), si-GJA5-3 (AATCCCTTC AGCAATAATA). Interference of GJB1 was performed using small interfering RNA (si-GJB1-NC; si-GJB1-1, si-GJB1-2, and si-GJB1-3) sequences synthesized by RiboBio Biotechnology (Guangzhou, China). The sequences used were as follows: si-GJB1-1 (GCTGCAACAGCGTTTGCTA), si-GJB1-2 (TGTTCCG GCTGTTGTTTGA), si-GJB1-3 (CGTGAACCGGCATTCTACT). Transfection was performed using Lipofectamine 3000 (Invitrogen, Shanghai, China). The relevant experiments were conducted 48 hours post transfection.

2.2.2 The quantitative reverse transcription-polymerase chain reaction

Total RNA was extracted from HK2, A498, and 786O cells using TRIzol Reagent (Servicebio, Wuhan, China). The quality of the extracted RNA was assessed by measuring the OD ratio (A260/A280) using a Nano-400A spectrophotometer (Allsheng, Hangzhou, China). Subsequently, total RNA was transcribed into complementary DNA (cDNA) using the HiScript II Q RT SuperMix Kit (Vazyme). Amplified products were then detected using SYBR Green (Vazyme, Nanjing, China). β-actin was selected as the endogenous references. The specific primers used were GJA5: 5′-GAACACAGACAGGCAGAGGAT-3′ (F), 5′-GGAAGCTCAAT CGCCCATC-3′ (R); GJB1: 5′-CCTGCACAGACATGAGACCA-3′ (F), 5′-AGAGCCATACTCGGCCAATG-3′ (R); and β-actin: 5′-CCTAGAAGCATTTGCGGT -3′ (F), 5′- GAGCTACGAGCTGCC TGACG-3′ (R).

2.2.3 5-Ethynyl-2-deoxyuridine assay

An EdU Kit (Beyotime, Shanghai, China) was used to detect cell proliferation. Then, the A498 and 786O cells were incubated with EdU solution, fixed with 4% paraformaldehyde and infiltrated with Triton X-100 solution (Solarbio, Beijing, China). Then, the cells were stained with 4',6-diamidino-2-phenylindole (DAPI; Beyotime, Shanghai, China). Ultimately, the EdU-positive cells (EdU+ DAPI-stained cells) were counted under a fluorescence microscope.

2.2.4 Wound healing assay

The cells were seeded in 6-well plates. The confluent cell cultures were then scratched using a sterile tip. The wound healing process was monitored at different time points, and images of the scratches were captured using an inverted microscope after 12 hours.

2.2.5 Transwell assay

Cell migration was assessed using the transwell assay. In this assay, we seeded 1.5×10^4 cells into the upper chamber and cultured them in a serum-free medium, while the lower chamber was supplemented with DMEM or RPMI-1640 containing 10% FBS as a chemoattractant. After 24 hours of incubation, the cells that had migrated through the pores of the transwell membrane were fixed with 4% methanol. Subsequently, the sections were stained with

crystal violet, images were captured and cell counts were performed using an inverted microscope.

2.2.6 Western blot

Total protein was extracted using radioimmunoprecipitation assay (RIPA) lysis buffer (Servicebio, Wuhan, China) supplemented with phenylmethylsulfonyl fluoride (Beyotime, Shanghai, China) at a ratio of 50:1. The protein concentration was determined using the bicinchoninic acid (BCA) assay (Solarbio, Beijing, China). Subsequently, the samples were mixed with loading buffer and boiled for 10 minutes to denature the proteins before further analysis. Subsequently, 20 μg of protein was loaded into each lane and separated by sodium dodecyl sulfate-polyacrylamide gel electrophoresis (SDS-PAGE) with an 8-15% acrylamide gradient gel. The separated proteins were then transferred onto polyvinylidene fluoride (PVDF) membranes. To prevent nonspecific binding, the membranes were blocked with 5% nonfat dry milk in Tris-buffered saline supplemented with 0.1% Tween 20 (TBST) for a period of 2 hours. Primary antibodies against GJA5 (1:1,000; ABclonal, Wuhan, China), GJB1 (1:1000; ABclonal, Wuhan, China), GADPH (1:10,000; Proteintech, Wuhan, China), E-cad (1:1000; ABclonal, Wuhan, China), N-cad (1:1000; ABclonal, Wuhan, China), VIM (1:1000; ABclonal, Wuhan, China), Bax (1:1000; ABclonal, Wuhan, China), and Bcl-2 (1:1000; ABclonal, Wuhan, China) were incubated with the membrane overnight at 4°C. After the membranes were washed with TBST for 10 minutes, they were incubated with secondary antibodies (1:5000; Proteintech, Wuhan, China) for 2 hours, after which the membranes were washed 3 times with TBST. Finally, electrochemiluminescence (ECL, Thermo, China) was applied to visualize the results.

2.2.7 Flow cytometric analysis

Apoptosis was detected with an annexin V apoptosis kit (Vazyme, Jiangsu, China). Fluorescence-activated cell sorting (FACS) was performed on a BD Accuri® C6 Plus [Becton, Dickinson, and Co. (BD) Biosciences, Franklin Lakes, NJ, USA] and analyzed by FlowJo software (https://www.flowjo.com/). Briefly, 1×10^6 cells were collected and resuspended after adding 100 μL of binding buffer. Next, 100 μL of binding buffer containing 4 μL of annexin V-FIFC and 4 μL of propidium iodide (PI) staining solution were added. Finally, 400 μL of binding buffer was added to the culture tube, which was subsequently analyzed after 10 to 15 minutes using flow cytometry.

2.2.8 Statistical analysis

All the statistical analyses were conducted using GraphPad Prism 8.0 software. Significance was determined using Student's t-test or one-way analysis of variance (ANOVA), as appropriate. Each experiment was performed in triplicate, and $p< 0.05$ was considered to indicate statistical significance.

3 Results

3.1 Bioinformatics analysis results

3.1.1 Identification of GRPS in the TCGA database

Firstly, a univariate Cox regression model for TS was constructed in this study, yielding five OS-related GJPs (OR-GJPs) that were most significantly related to the patients' OS. To prevent data overfitting, a LASSO regression model for OR-GJPs was constructed (Figures 2A, B). Ultimately, a multivariate Cox regression model was constructed based on the outcomes of the LSAAO regression analysis. This model identified two genes (Gene GJA5 and Gene GJB1) with independent prognostic impacts on ccRCC (Table 1), which were identified as GRPS genes for subsequent data examination, clinical validation, and cellular functional experiments. The univariate Cox regression analysis for all 21 GJPs and the corresponding KM survival analysis for 5 GJPs with differential survival significance can be found in Supplementary Table 2 and Supplementary Figure 1.

3.1.2 Pan-cancer analysis, single gene analysis and combined effect analysis of GJA5 and GJB1

The Pan-cancer analysis revealed that GJA5 exhibited the highest expression level in ccRCC, whereas GJB1 was the 12th

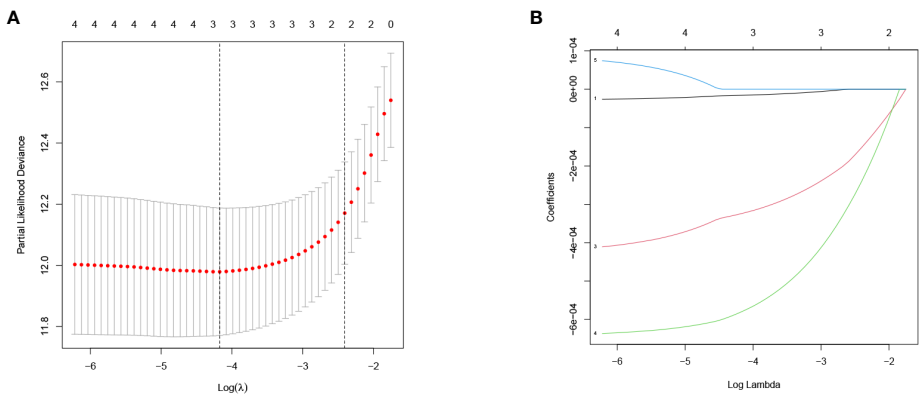

FIGURE 2
LASSO regression model of OR-GJPs: **(A)** Coefficient distribution diagram. **(B)** Parameter change diagram.

TABLE 1 Univariate and multivariate Cox regression models of GRPS.

	Univariate Cox regression model			Multivariate Cox regression model			
	HR	95% CI	*p*	coef	HR	95% CI	*p*
GJA5	0.9995	0.9993~0.9996	**<0.001**	-0.0005	0.9995	0.9993~0.9997	**<0.001**
GJB1	0.9992	0.9989~0.9994	**<0.001**	-0.0004	0.9996	0.9993~0.9999	**0.014**

The results with bold font indicate statistical significance ($p < 0.05$).

highest in terms of expression in ccRCC (Supplementary Figures 2A, B). Notably, GJA5 and GJB1 were differentially expressed between tumor tissues and matched normal tissues in 15 distinct cancers (Supplementary Figures 2C, D), including breast invasive carcinoma, renal chromophobe cell carcinoma, renal clear cell carcinoma, renal papillary cell carcinoma, endometrial carcinoma, thyroid carcinoma, prostate cancer, hepatocellular carcinoma, and lung squamous cell carcinoma. These findings suggested that GJA5 and GJB1 might play crucial roles in the development and progression of urological tumors, as well as a variety of human malignant tumors. These findings warrant further in-depth investigation. Employing the TS dataset, a comprehensive analysis was conducted to examine the differences in gene expression between GJA5 and GJB1 in tumor tissues and normal tissues. The findings demonstrated that both GJA5 and GJB1 exhibited decreased expression in tumor tissues and elevated expression in normal tissues ($p< 0.001$) (Figures 3A, B). These findings suggested that the expression of GJA5 and GJB1 was repressed during the occurrence of ccRCC, a phenomenon that was consistent with that observed in additional independent cohorts (GSE73731, GSE95425) (Figures 3C, D). Finally, this study further validated the differential expression of GJA5 and GJB1 in ccRCC using the oncopression database (http://www.oncopression.com/downloads.html) (Supplementary Figure 3. The results showed that the expression of GJA5 and GJB1 in normal tissue of ccRCC was significantly higher than that in tumoral tissue. Ultimately, the prognostic significance of GJA5 and GJB1 was further assessed. In the TS dataset, KM analysis revealed a significant correlation between low expression of GJA5 and GJB1 and a shorter OS ($p< 0.05$) (Figures 3E, F). Patients exhibiting concurrent low expression of GJA5 and GJB1 had the shortest OS, while those with high expression of GJA5 and GJB1 had a prolonged OS (Figure 3G). Given the results of the differential expression analysis, we speculated that GJA5 and GJB1 act as tumor suppressors in ccRCC.

3.1.3 Establishment of the RS prognostic model and validation by using clinical characteristics

The RS for each patient was calculated using the following formula:

$$Risk\ score = GJA5 \times (-0.0003) + GJB1 \times (-0.0005)$$

The OS and PFS of patients in the high-RS subgroup were markedly inferior to those in the low-RS subgroup ($p< 0.001$) (Figures 4A, B). A prognostic model for RS was developed, encompassing hazard curves, survival scatter plots, and heatmaps of GJA5 and GJB1 expression. The model revealed that patients in the high-RS subgroup exhibited shorter survival, greater mortality, and decreased GJA5 and GJB1 expression (Figure 4C). The ROC curve demonstrated that the RS prognostic model exhibited a potent ability to predict patient survival rates (the AUC for predicting 1-year, 2-year, and 3-year survival rates were 0.740, 0.781, and 0.771, respectively). In comparison with other clinical traits, the RS model exhibited strong credibility in predicting patient survival rates (Figures 4D, E). Finally, the differences in clinical characteristics between the high-RS and low-RS subgroups were verified. The findings indicated that, in the high-RS subgroup, ccRCC patients exhibited a greater malignancy grade and a greater probability of tumor metastasis, with a greater proportion of male patients than female patients (Table 2).

3.1.4 Validation of the RS prognostic model

Combined with the GSE29609 dataset, a training set and a testing set of TSs were constructed to assess the prognostic significance of the GRPS in ccRCC. The chi-square test revealed no significant differences in the clinicopathological traits between the training and testing sets (Table 3), indicating that the study's grouping was random and reasonable. In both the training and testing sets, patients in the high-RS subgroup exhibited significantly poorer OS and PFS than did those in the low-RS subgroup (Figures 5A, B, E, F). Subsequently, the RS prognostic model was constructed on the training cohort and validated using ROC curve analysis (Figures 5C, D). These results align with those for TS, demonstrating that the RS prognostic model in the training cohort was also reliable at predicting the patient survival status (the AUC for predicting 1-year, 3-year, and 5-year survival rates were 0.750, 0.778 and 0.775, respectively). Finally, comparable outcomes were obtained in the testing cohort (Figure 5G). The AUC of the RS prognostic model in the testing cohort for predicting 1-year, 3-year, and 5-year survival was 0.708, 0.696, and 0.741, respectively (Figure 5H).

3.1.5 Construction and validation of clinical nomograms

To further explore the relationship between the RS prognostic model and clinical characteristics, univariate and multivariate stepwise Cox analysis were performed. The results showed that risk score, age, and tumor stage were closely associated with survival time and clinical outcomes of ccRCC patients, and could serve as independent prognostic factors (Table 4). The risk of death for

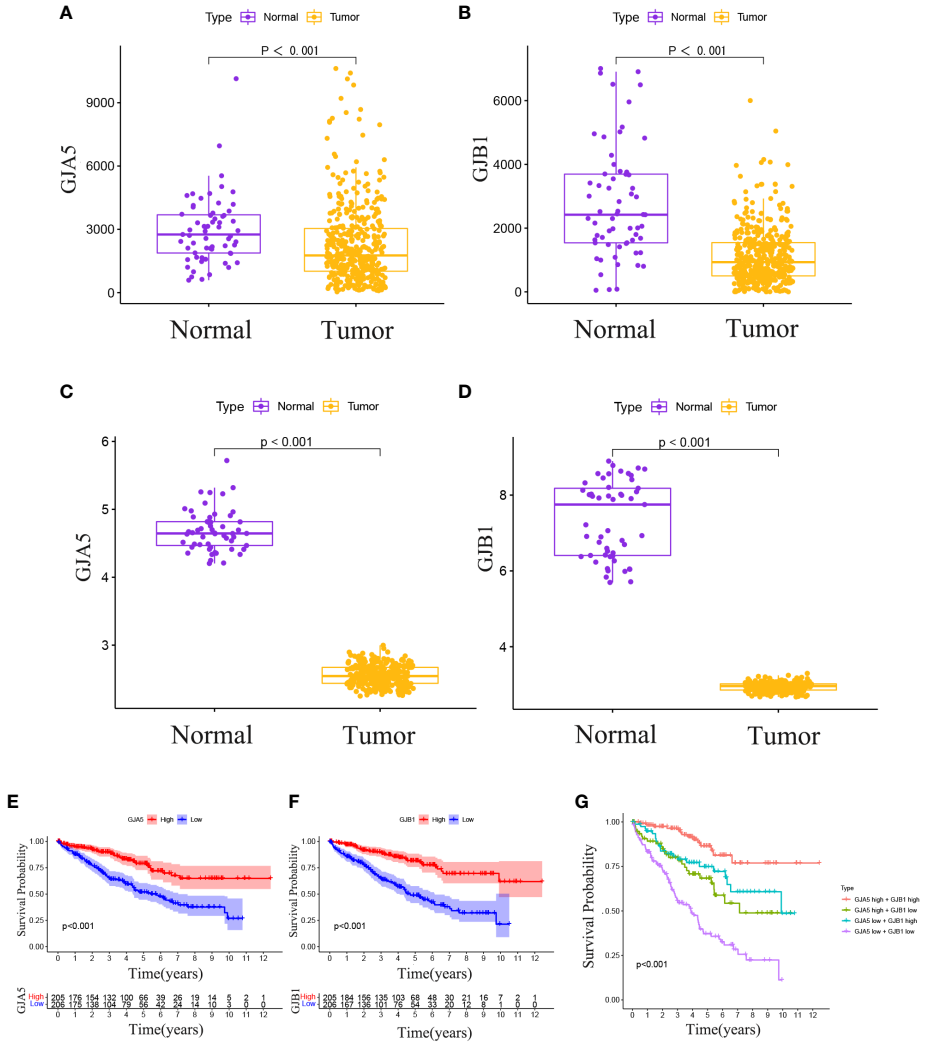

FIGURE 3
(A) In the TCGA database, differential expression of GJA5 in tumor tissues and paired normal tissues. **(B)** In the TCGA database, differential expression of GJB1 in tumor tissues and paired normal tissues. **(C)** Differential expression of GJA5 in ccRCC in the GEO database. **(D)** Differential expression of GJB1 in ccRCC in the GEO database. **(E)** KM analysis of GJA5 in ccRCC in the TCGA database. **(F)** KM analysis of GJB1 in ccRCC in the TCGA database. **(G)** Analysis of the combined effect of GJA5 and GJB1 in ccRCC in the TCGA database.

individuals with high-RS was 1.695 times greater than that for those with low-RS (HR = 1.695, 95%CI = 1.439-1.996, $p< 0.001$).

A nomogram incorporating clinicopathological traits (tumor grade, tumor stage), the gene expression pattern of the GRPS, and risk grouping was constructed to assist clinicians in making initial predictions of OS in ccRCC patients (Figure 6A). The clinical nomogram was subsequently validated. The calibration curves demonstrated good agreement between the predicted probabilities generated by the nomogram and the actual observed OS values at 1, 2, and 3 years (Figure 6B). The results of the ROC curve and DCA analyses revealed that the nomogram exhibited excellent reliability in predicting the survival rate of ccRCC patients (the AUC of the nomogram for predicting the survival rate of patients at 1, 3 and 5 years was 0.876, 0.853 and 0.816, respectively) (Figure 6C).

3.1.6 GO and KEGG enrichment analysis

Among the total differential expressed 899 genes, 540 genes were highly expressed in the high-RS subgroup, while the other 359 genes exhibited high expression in the low-RS subgroup (Supplementary Figure 4). To determine the biological functions and pathways active in the high-RS subgroup, further exploration was conducted. The results of GO enrichment analysis (Figure 7A) revealed that Biological Processes such as “negative regulation of proteolysis”, Cellular Component such as “collagen-containing extracellular matrix”, and Molecular Function such as “enzyme inhibitor activity” were enriched in the high-RS population. Additionally, KEGG enrichment analysis indicated that “neuroactive ligand-receptor interaction”, “cAMP signaling

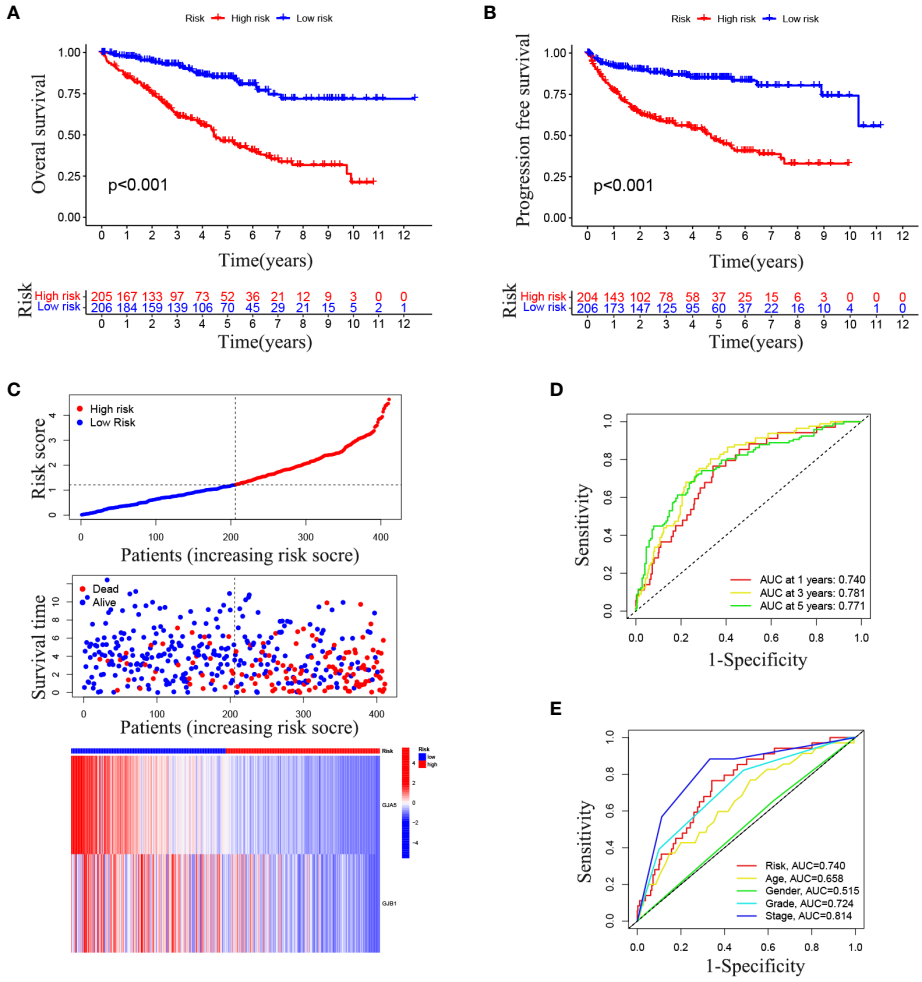

FIGURE 4
(A) OS analysis between the high-RS score group and low-RS score group. **(B)** PFS analysis between the high-RS score group and low-RS score group. **(C)** RS prognosis model for TS (including the RS curve, survival time and survival status of patients, and GRPS gene expression). **(D, E)** ROC curve of the RS prognosis model of TS.

pathway", "cytokine-cytokine receptor interaction", "adrenergic signaling pathway in cardiomyocytes", "GnRH secretion", and "TGF-beta signaling pathway" were enriched in high-RS population (Figure 7B).

3.1.7 Immunocyte infiltration, TME and TMB analysis

Differences in 22 immune cell types and TMB in the RS group were investigated. Patients in high-RS subgroup presented with higher TMB than that in low-RS subgroup (Figure 8A). Compared to those in the low-RS subgroup, the TME in the high-RS subgroup exhibited greater immune cell infiltration and a lower stromal cell content (Figures 8B, C). As for TME-related molecular abundance, statistically significant differences were detected for naive B cells ($p< 0.05$), T cell follicular helper cells ($p< 0.001$), regulatory T cells ($p< 0.05$), M0 macrophages ($p< 0.05$), stationary dendritic cells ($p< 0.01$), stationary mast cells ($p< 0.01$), immune cell content ($p< 0.05$) and stromal cell content ($p< 0.001$)(Figure 8D). These findings offer a new perspective for exploring the mechanism of individualized immunotherapy in ccRCC patients and the role of GJPs in the occurrence and development of ccRCC. And low expression of GJA5 and GJB1 might be associated with an imbalance in immune homeostasis and compromised responses to immunotherapy in ccRCC patients.

3.1.8 Drug sensitivity analysis

Drug sensitivity analysis of commonly used chemotherapeutic drugs for ccRCC was conducted based on the RS grouping (Figures 9A-E). Among the several chemotherapy drugs used to treat advanced ccRCC, erlotinib ($p< 0.001$), axitinib ($p = 0.0029$), afatinib ($p< 0.001$), rapamycin ($p< 0.001$), and sorafenib ($p< 0.001$) were found to be significantly different among the risk groups. Notably, axitinib exhibited lower sensitivity in the low-RS subgroup, while afatinib, erlotinib, rapamycin, and sorafenib had lower sensitivity in the high-RS subgroup. These findings offer new

10.3389/fonc.2024.1354049

TABLE 2 Differential analysis of clinicopathological parameters between the high-RS subgroup and the low-RS subgroup.

Variable	Sum	High-RS	Low-RS	Chi-square value	*P*
Survival state					
Survival	259(66.24%)	93(47.69%)	166(84.69%)	58.203	< 0.001
Death	132(33.76%)	102(52.31%)	30(15.31%)		
Age					
≤65	258(65.98%)	122(62.56%)	136(69.39%)	1.735	0.188
>65	133(34.02%)	73(37.44%)	60(30.61%)		
Gender					
Female	142(36.32%)	54(27.69%)	88(44.9%)	11.779	< 0.001
Male	249(63.68%)	141(72.31%)	108(55.1%)		
Tumor grade					
G1-2	142(36.32%)	54(27.69%)	88(44.9%)	18.568	< 0.001
G3-4	249(63.68%)	141(72.31%)	108(55.1%)		
Neoplasm staging					
Stage I-II	184(47.06%)	70(35.9%)	114(58.16%)	40.380	< 0.001
Stage III-IV	207(52.94%)	125(64.1%)	82(41.84%)		

insights into individualized targeted drug therapy for patients with advanced ccRCC.

3.2 Cytological experimental verification of GJA5 and GJB1 results

3.2.1 Results of GJA5 and GJB1 expression in renal cell lines

Furthermore, the expression of GJA5 and GJB1 at the protein level was detected via Western blot analysis, and the expression of GJA5 and GJB1 at the RNA level was detected via qRT-PCR. qRT-PCR revealed that the mRNA levels of GJA5 and GJB1 in renal tumor cells (A498 and 786-O) were lower than those in noncancerous renal cells (HK2) (Figure 10A) and this pattern was confirmed at the protein level (Figure 10B). Moreover, according to the qRT-PCR and Western blot detection results, at both the RNA and protein expression levels, GJB1 was expressed at higher levels in A498 cells, while GJA5 was expressed at higher levels in 786-O cells. Therefore, functional experiments were conducted to knock down GJB1 in the A498 cell line and GJA5 in the 786-O cell line.

TABLE 3 Analysis of differences in clinical traits between training set and testing set n (n%).

Variable	Sum	Training	Testing	Chi-square value	*P*
Survival state					
Survival	281(65.50%)	175(63.64%)	106(68.83%)	0.960	0.327
Death	148(34.50%)	100(36.36%)	48(31.17%)		
Age					
≤65	279(65.03%)	184(66.91%)	95(61.69%)	0.965	0.326
>65	150(34.97%)	91(33.09%)	59(38.31%)		
Tumor grade					
G1-2	197(45.92%)	125(45.45%)	72(46.75%)	0.025	0.875
G3-4	232(54.08%)	150(54.55%)	82(53.25%)		
Neoplasm staging					
Stage I-II	250(58.28%)	165(60.00%)	85(55.19%)	0.750	0.386
Stage III-IV	179(41.72%)	69(44.81%)	110(40.00%)		

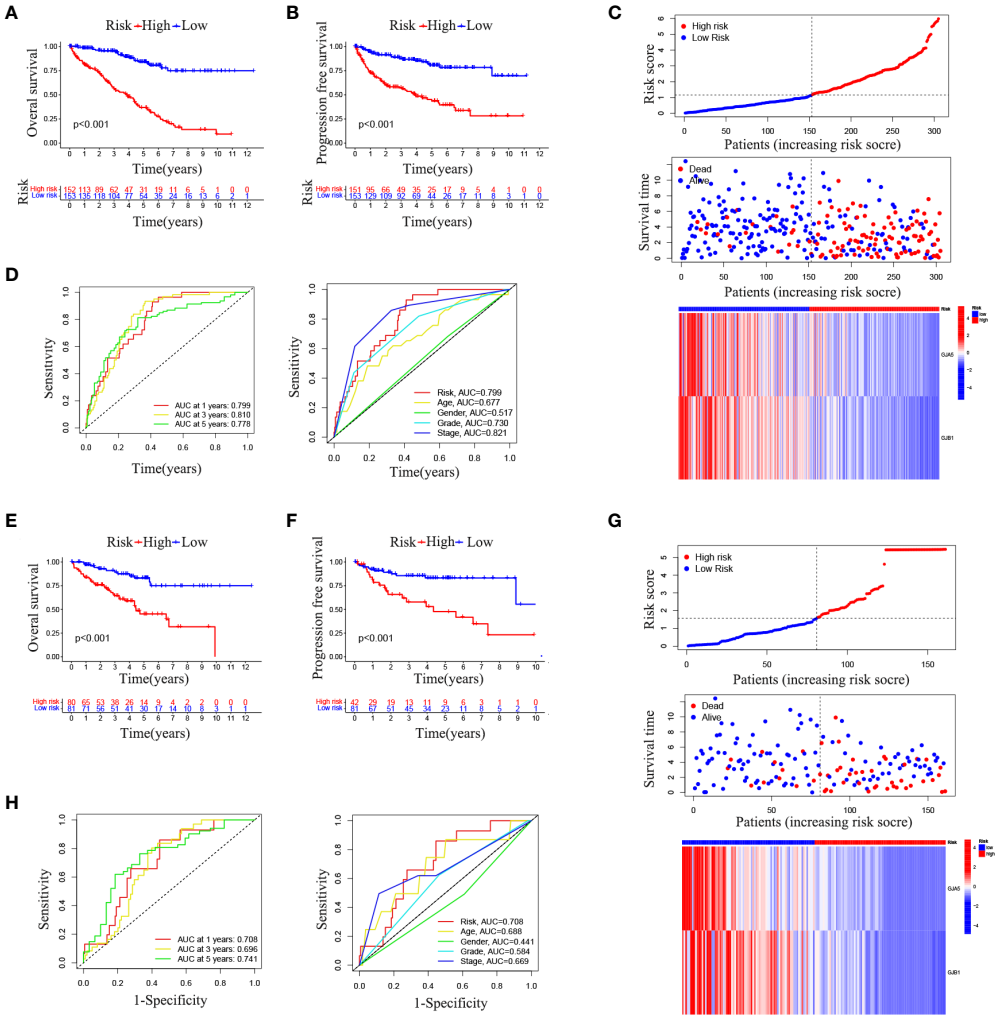

FIGURE 5
(A) OS analysis results in the training set. **(B)** PFS analysis results in the training set. **(C)** RS prognostic model in the training set. **(D)** ROC curve analysis of the RS prognostic model in the training set. **(E)** OS analysis results in the testing set. **(F)** PFS analysis results of testing set. **(G)** RS prognostic model of testing set. **(H)** ROC curve analysis of the RS Prognostic model in the testing Set.

3.2.2 Construction of GJA5 and GJB1 knockdown cell lines

Furthermore, to investigate the effects of GJA5 and GJB1 interference on the cytological behavior of ccRCC cells, at least three independent cell experiments were conducted (Figures 10C, D). The expression of GJA5 in the 786-O cell line and GJB1 in the A498 cell line were specifically targeted and knocked down by chemically synthesized siRNA. Western blot analysis revealed that si-GJA5-2, si-GJA5-3, si-GJB1-1 and si-GJB1-2 had relatively high knockdown efficiencies. Therefore, the above four kinds of siRNAs were selected for subsequent cell behavioral experiments.

TABLE 4 Univariate and multivariate stepwise Cox regression analysis of RS and clinical characteristics in ccRCC.

	Univariate Cox regression		Multivariable Cox regression	
	p-value	Hazard ratio	*p*-value	Hazard ratio
Age	< **0.001**	1.032(1.017-1.047)	< **0.001**	1.036(1.018-1.053)
Gender	0.935	0.986(0.692-1.403)	0.994	1.001(0.695-1.444)
Grade	< **0.001**	2.204(1.752-2.773)	0.162	1.203(0.929-1.558)
Stage	< **0.001**	1.845(1.591-2.140)	< **0.001**	1.574(1.327-1.867)
Risk score	< **0.001**	1.944(1.685-2.244)	< **0.001**	1.695(1.439-1.996)

The results with bold font indicate statistical significance ($p < 0.05$).

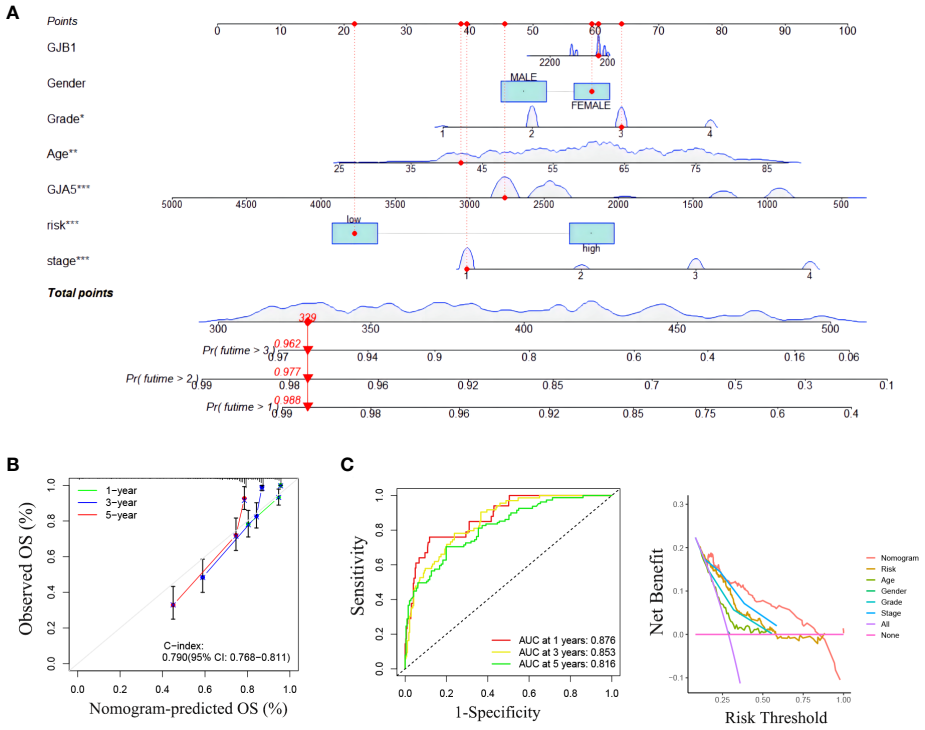

FIGURE 6
(A) Clinical nomogram. **(B)** The calibration curve for predicting 1-year, 3-year and 5-year survival rates with a nomograph. **(C)** ROC curve and DCA curve of the nomogram.

3.2.3 Low expression of GJA5 and GJB1 promote the proliferation, migration and EMT and inhibit apoptosis of ccRCC cells

CCK-8 and EdU assays demonstrated that cell viability was sharply increased in the si-GJA5 and si-GJB1 groups (Figures 11A, B). Similarly, transwell and wound healing assays demonstrated that cell migration increased significantly after GJA5 and GJB1 were knocked down (Figures 11C, D). Western blot analysis revealed that after GJA5 or GJB1 knockdown, the expression of E-cad and Bax in ccRCC cells decreased, while the expression of N-cad, VIM and Bcl-2 increased (Figures 12A, B). Flow cytometry showed that knockdown of GJA5 or GJB1 inhibited cells apoptosis (Figure 12C). Collectively, these results indicate that GJA5 and GJB1 may inhibit ccRCC development.

4 Discussion

Gap junctions are intercellular channel clusters formed on the plasma membrane by the connexin family of proteins expressed by GJPs (21, 22), which allows the diffusion of ions or small molecules and the transmission of electrical signals (23, 24). As important

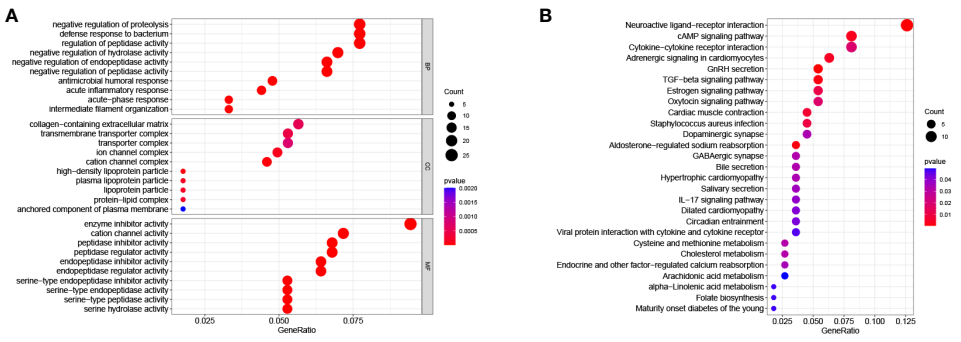

FIGURE 7
(A) GO enrichment analysis. **(B)** KEGG enrichment analysis.

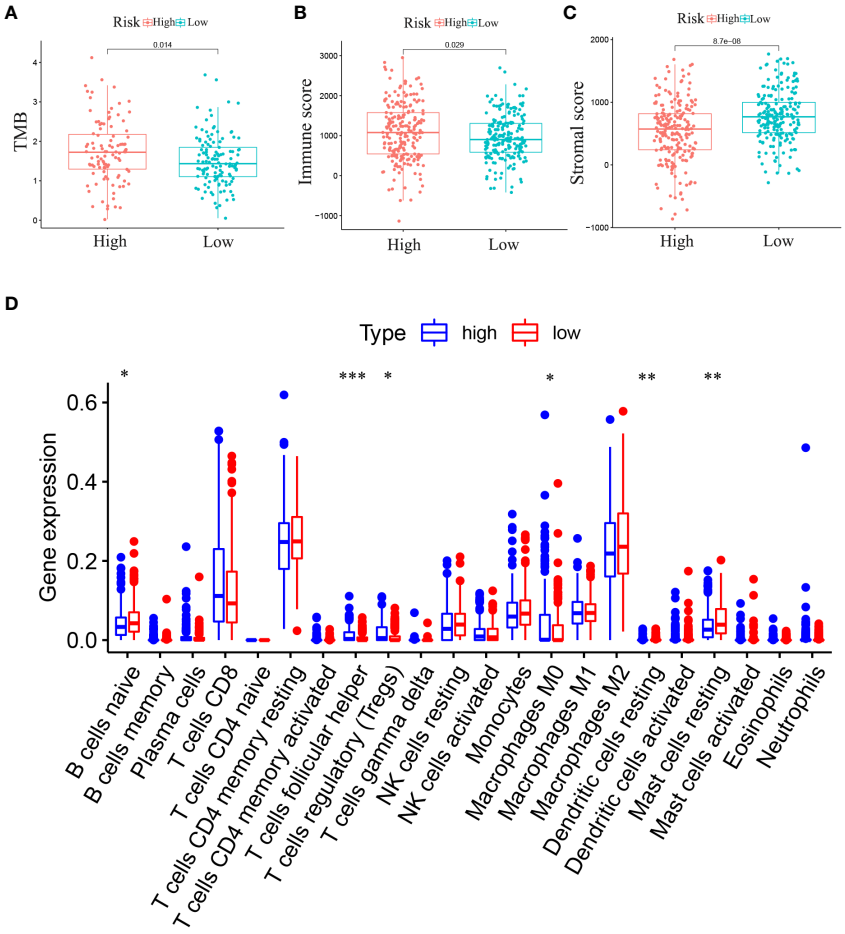

FIGURE 8
(A) Analysis of the difference in TMB between high-RS and low-RS groups. **(B)** Analysis of the Difference in Immune Score between high-RS and low-RS Groups. **(C)** Analysis of the Difference in Stromal Score between high-RS and low-RS Groups. **(D)** Differential expression of immune cells between high-RS and low-RS groups (Immune cell content in the low-RS group is represented in red, and that in the high-RS group is represented in blue. (*p< 0.05, **p< 0.01, ***p< 0.001).

channels of intercellular communication, gap junction proteins provide a basis for the cooperative work and functional integrity of various systems and organs in organisms (25, 26). Genetic or acquired changes in connexin proteins are closely related to cancer (27). Abnormal GJP expression is related to the recurrence and metastasis of cancer and to increase patient mortality. This difference may be due to the loss of channel function, which leads to a decrease in tumor inhibition ability (usually called tumor dormancy) (28, 29), and this inhibition ability depends on the function of gap junction coupling among cells (30). Moreover, when the gap junction channel is damaged, the permeability and sensitivity to chemotherapy drugs are reduced (31, 32). For example, defects in GJA1 function mediate the resistance of breast cancer to tamoxifen (33). Destruction of GJB1 plays a role in promoting the occurrence and development of ovarian cancer and is not conducive to the action of chemical drugs (34). Mutations and loss of function of the GJA5 gene are closely related to the occurrence of isolated ventricular fibrillation in humans (35). Therefore, GJPs are crucial to the steady state of the human body. However, the role of GJPs in ccRCC is unclear. In our study, we comprehensively analyzed the biological function, pathway, clinical significance and prognostic value of GJPs in patients with ccRCC, which filled the gap in the study of GJPs in ccRCC.

In addition, the occurrence and development of cancer are always accompanied by changes in the tumor microenvironment and the triggering of immune escape mechanisms (36, 37). When gap junctions are blocked, humoral and CD8+ T-cell immune responses are inhibited or even eliminated (38). It has been proven that there are many gap junction channels between immune cells, such as GJA5 in T and B lymphocytes (39), and GJB1 in mast cells (40), and that communication between cardiac cells is promoted by cardiac macrophages through gap junctions (41). Therefore, the stability of GJP function is crucial for the immune system to function. However, the role of GJPs in ccRCC remains unclear. We analyzed the clinical significance and biological function of GJPs in ccRCC through a public database system. Furthermore, we developed the GRPS, a novel tumor-related prognostic feature. Low expression levels of GJA5 and GJB1 predict poor prognosis in ccRCC patients, and could be used as independent prognostic markers and drug therapeutic targets for ccRCC. Additionally, GJA5 and GJB1 were

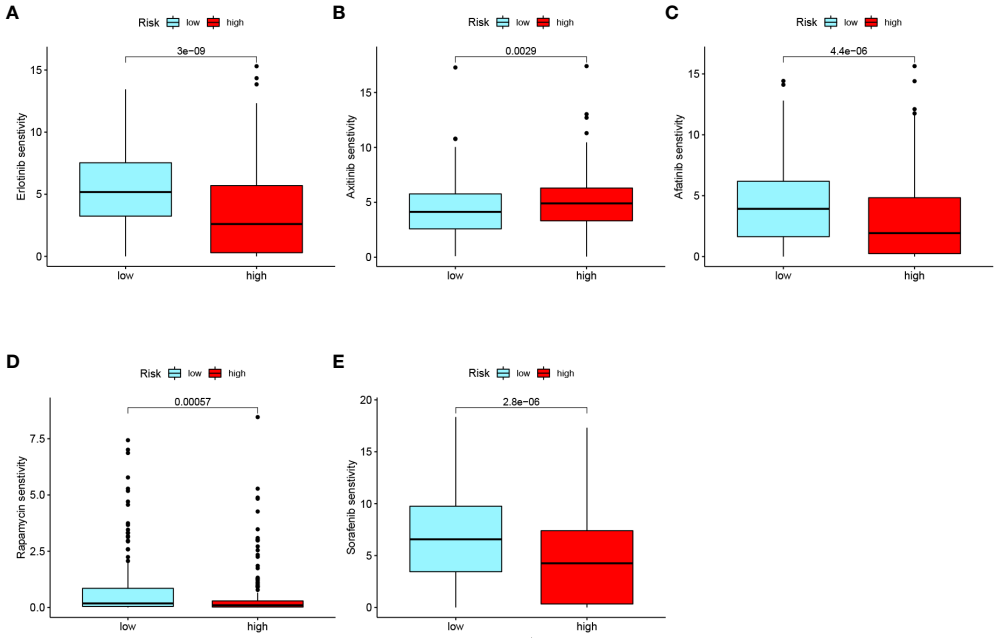

FIGURE 9
Drug sensitivity analysis of common chemotherapeutic drugs in ccRCC risk groups: **(A)** Erlotinib. **(B)** Axitinib. **(C)** Afatinib. **(D)** Rapamycin. **(E)** Sorafenib.

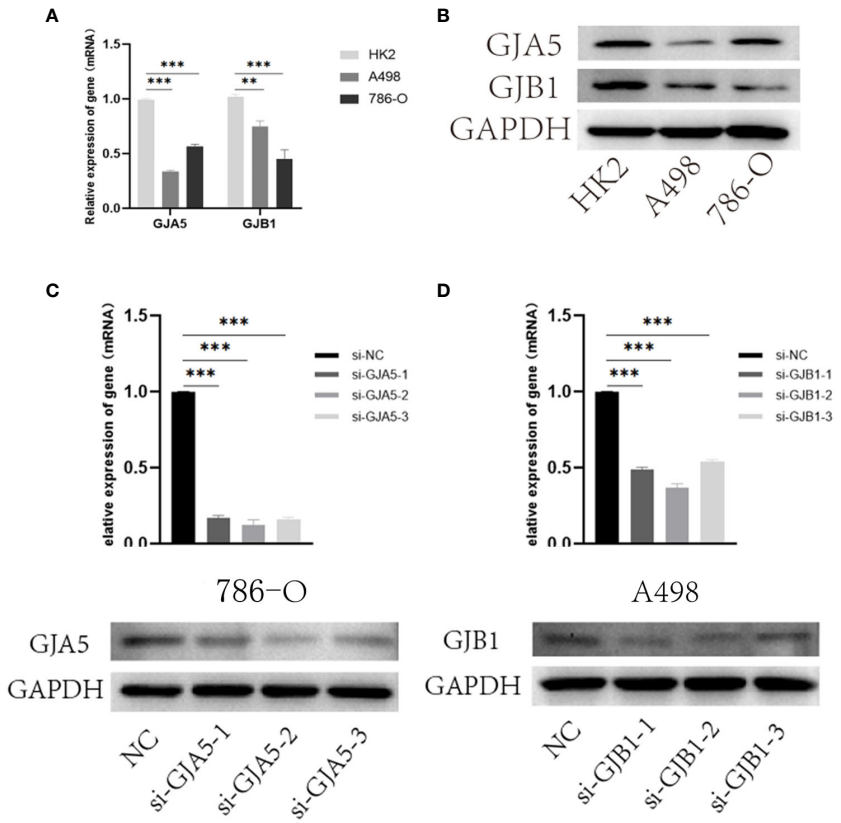

FIGURE 10
(A) qRT-PCR results of GJA5 and GJB1 expression at the RNA level. **(B)** Western blot results of GJA5 and GJB1 expression at protein level. **(C)** qRT-PCR and Western blot results of GJA5 in 786-O cells after transfection with three small interfering RNAs. **(D)** qRT-PCR and Western blot results of GJB1 in A498 cells after transfection with three small interfering RNAs. (*p< 0.05, **p< 0.01, ***p< 0.001).

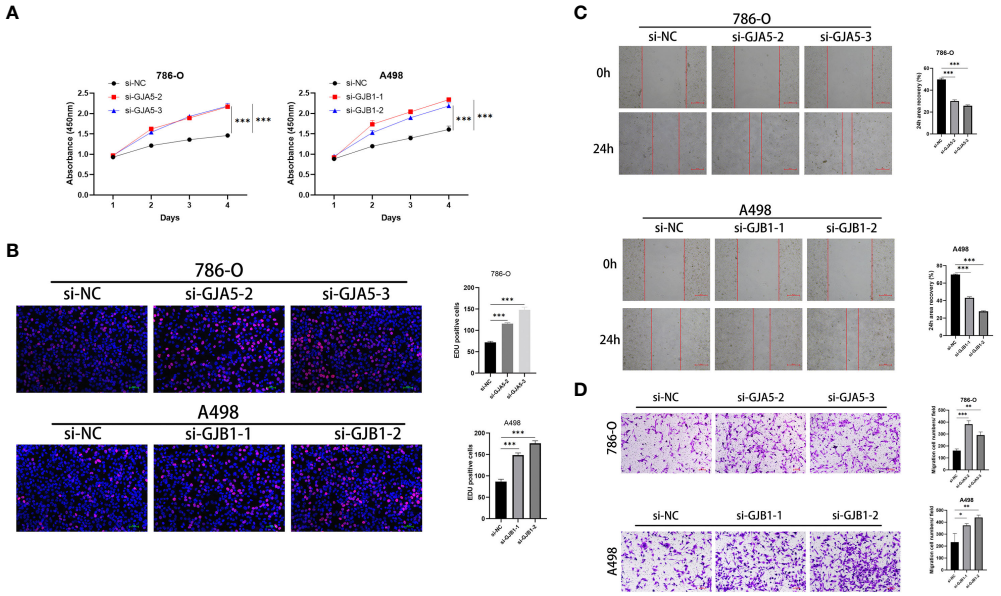

FIGURE 11
(A) The CCK8 experiment results of GJA5 and GJB1 knockdown on the cell proliferation in 786-O cells and A498 cells, respectively. **(B)** The EdU experiment results of GJA5 and GJB1 knockdown on the cell proliferation in 786-O cells and A498 cells, respectively (Error bar = 50 μm). **(C)** The cell scratch test results of GJA5 and GJB1 knockdown on the cell migration in 786-O cells and A498 cells, respectively (Error bar = 500 μm). **(D)** The Transwell experiment results of GJA5 and GJB1 knockdown on the cell migration potential in 786-O cells and A498 cells, respectively (Error bar = 100 μm). (*$p < 0.05$, **$p < 0.001$, ***$p < 0.01$).

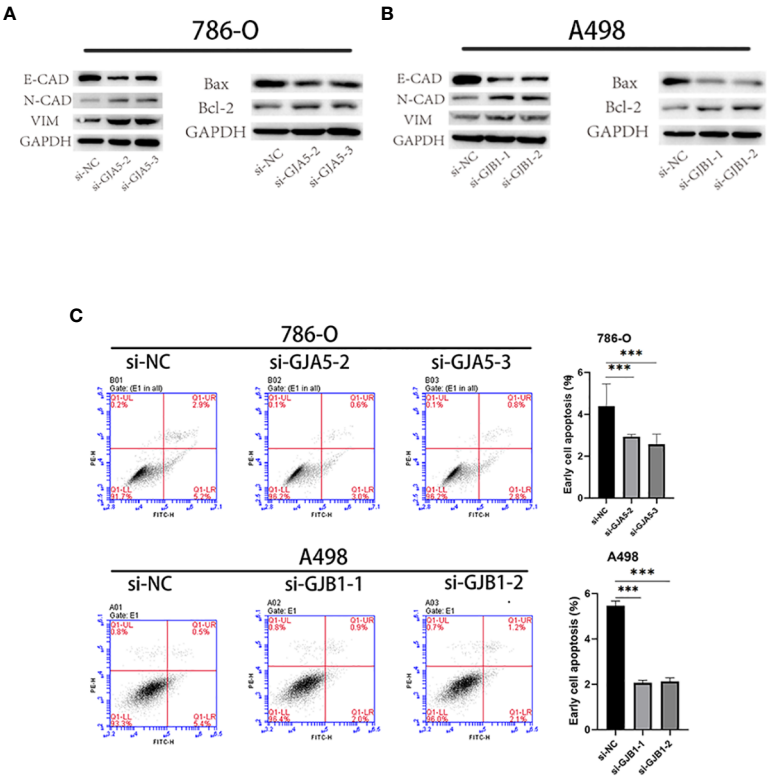

FIGURE 12
(A) After knocking down GJA5, the protein expression of E-cad, N-cad, VIM, Bax, and Bcl-2 was detected in the 786-O cell line. **(B)** After knocking down GJB1, the protein expression of E-cad, N-cad, VIM, Bax, and Bcl-2 was detected in the A-498 cell line. **(C)** Flow cytometry analysis of cell apoptosis after knockdown of GJA5 and GJB1 genes in 786-O and A498 cells, respectively. (*$p < 0.05$, **$p < 0.001$, ***$p < 0.01$).

verified by cellular functional experiments, and the results showed that GJA5 and GJB1 could be used as prognostic markers for ccRCC.

In this study, LASSO and Cox regression models were developed for 21 GJPs to identify genes with independent prognostic effects, and the relationships between GRPS and tumor grade, tumor stage and survival status of patients were further explored. The results showed that GJA5 and GJB1 have independent prognostic value in ccRCC. The RS was subsequently calculated for each patient, and an RS prognostic model was constructed. Analysis of the ROC curve confirmed that the prediction model developed in this study is reliable, indicating its potential application in clinical practice for predicting the prognosis of patients with ccRCC.

Moreover, a clinical nomogram that incorporates the GPRS score, patient clinical characteristics, and the RS was developed. ROC curve and DCA analyses demonstrated that the nomogram is highly sensitive for predicting the survival status of patients (AUC values for 1-, 3-, and 5-year were 0.876, 0.853 and 0.816, respectively). To assess the generalizability of the RS prognostic model, this study combined it with external datasets, and the results were positive. Further investigations revealed correlations between the GRPS and immune cell infiltration, the TME, and the TMB. Drug sensitivity analysis indicated that the high-RS subgroup was more sensitive to afatinib, erlotinib, rapamycin, and sorafenib, while the low-RS subgroup exhibited greater sensitivity to axitinib, which is conducive to the development of individualized chemotherapy regimens for patients with advanced ccRCC.

This study has certain limitations. Firstly, the dataset examined in this analysis was merely derived from the public (TCGA and GEO) database, and has a limited sample size. The findings still need to be further confirmed by a multi-database and multi-center study. Secondly, although our constructed model obtained promising results, further clinical experiments are necessary to validate and assess the efficacy of our model.

In conclusion, this study established a more economical and personalized prognostic model that is easy to apply and could provide clinicians with new ideas for the prognosis and treatment of ccRCC patients.

Data availability statement

Publicly available datasets were analyzed in this study. This data can be found here: TCGA database (https://portal.gdc.cancer.gov/) and GEO database (https://www.ncbi.nlm.nih.gov/geo/), Microarray data (GSE29609, GSE95425, GSE73731).

Author contributions

YH: Conceptualization, Data curation, Software, Visualization, Writing – original draft. WG: Formal analysis, Validation, Visualization, Writing – original draft. YuZ: Conceptualization, Investigation, Software, Writing – review & editing. XW: Conceptualization, Writing – review & editing. BF: Conceptualization, Writing – review & editing. YiZ: Conceptualization, Writing – review & editing. LY: Project administration, Supervision, Writing – review & editing. ZL: Funding acquisition, Methodology, Software, Supervision, Writing – review & editing. GG: Conceptualization, Funding acquisition, Investigation, Resources, Writing – review & editing.

Funding

The author(s) declare financial support was received for the research, authorship, and/or publication of this article. This study was financially supported by the Natural Science Foundation of Shandong Province (no. ZR2020QH068 and no. ZR2021MH049).

Conflict of interest

The authors declare that the research was conducted in the absence of any commercial or financial relationships that could be construed as a potential conflict of interest.

Publisher's note

Supplementary material

The Supplementary Material for this article can be found online at: https://www.frontiersin.org/articles/10.3389/fonc.2024.1354049/full#supplementary-material

SUPPLEMENTARY TABLE 1
General clinical data of ccRCC patients involved in data analysis in this study.

SUPPLEMENTARY TABLE 2
Univariate Cox regression results for gap junction protein gene.

SUPPLEMENTARY FIGURE 1
The Kaplan-Meier survival analysis for 5 GJPs with differential survival significance: **(A)** GJA1 **(B)** GJA4 **(C)** GJA5 **(D)** GJB1 **(E)** GJC1.

SUPPLEMENTARY FIGURE 2
GJA5 and GJB1 expression and differential expression in pan-cancer: **(A)** Expression of GJA5 in pan-cancer **(B)** Expression of GJB1 in pan-cancer **(C)** Differential expression of GJA5 between normal and tumoral tissues in pan-cancer **(D)** Differential expression of GJB1 between normal and tumoral tissues in pan-cancer.

SUPPLEMENTARY FIGURE 3
In the oncopression database, the differential expression of GJA5 and GJB1 in ccRCC tumor tissue and normal tissue: **(A)** Differential expression of GJA5 between normal and tumoral kidney tissues in the Oncopression database **(B)** Differential expression of GJB1 between normal and tumoral kidney tissues in the Oncopression database.

SUPPLEMENTARY FIGURE 4
Visualization of differentially expressed genes ($P< 0.05$, logFC = 1, FDR< 1) in risk groups: **(A)** Heatmap **(B)** Volcano plot.

References

1. Sung H, Ferlay J, Siegel RL, Laversanne M, Soerjomataram I, Jemal A, et al. Global cancer statistics 2020: GLOBOCAN estimates of incidence and mortality worldwide for 36 cancers in 185 countries. *CA Cancer J Clin*. (2021) 71:209–49. doi: 10.3322/caac.21660

2. Turajlic S, Swanton C, Boshoff C. Kidney cancer: The next decade. *J Exp Med*. (2018) 215:2477–9. doi: 10.1084/jem.20181617

3. Wu Y, Zhang S, Chen C, Pang J. Dysregulation and implications of N6-methyladenosine modification in renal cell carcinoma. *Curr Urol*. (2023) 17:45–51. doi: 10.1097/CU9.0000000000000135

4. Harrison H, Thompson RE, Lin Z, Rossi SH, Stewart GD, Griffin SJ, et al. Risk prediction models for kidney cancer: A systematic review. *Eur Urol Focus*. (2021) 7:1380–90. doi: 10.1016/j.euf.2020.06.024

5. Motzer RJ, Bukowski RM, Figlin RA, Hutson TE, Michaelson MD, Kim ST, et al. Prognostic nomogram for sunitinib in patients with metastatic renal cell carcinoma. *Cancer*. (2008) 113:1552–8. doi: 10.1002/cncr.23776

6. Han W, Fan B, Huang Y, Wang X, Zhang Z, Gu G, et al. Construction and validation of a prognostic model of RNA binding proteins in clear cell renal carcinoma. *BMC Nephrol*. (2022) 23:172. doi: 10.1186/s12882-022-02801-y

7. Teishima J, Murata D, Inoue S, Hayashi T, Mita K, Hasegawa Y, et al. Prediction of early progression of metastatic renal cell carcinoma treated with first-line tyrosine kinase inhibitor. *Curr Urol*. (2021) 15:187–92. doi: 10.1097/CU9.0000000000000042

8. Linehan WM, Schmidt LS, Crooks DR, Wei D, Srinivasan R, Lang M, et al. The metabolic basis of kidney cancer. *Cancer Discovery*. (2019) 9:1006–21. doi: 10.1158/2159-8290.Cd-18-1354

9. Inoue T. Invited commentary: When and how to initiate systemic therapy in treating favorable risk metastatic renal cell carcinoma. *Curr Urol*. (2021) 15:185–6. doi: 10.1097/CU9.0000000000000052

10. Brissette JL, Kumar NM, Gilula NB, Hall JE, Dotto GP. Switch in gap junction protein expression is associated with selective changes in junctional permeability during keratinocyte differentiation. *Proc Natl Acad Sci U.S.A*. (1994) 91:6453–7. doi: 10.1073/pnas.91.14.6453

11. Willecke K, Eiberger J, Degen J, Eckardt D, Romualdi A, Güldenagel M, et al. Structural and functional diversity of connexin genes in the mouse and human genome. *Biol Chem*. (2002) 383:725–37. doi: 10.1515/bc.2002.076

12. Nielsen MS, Axelsen LN, Sorgen PL, Verma V, Delmar M, Holstein-Rathlou NH. Gap junctions. *Compr Physiol*. (2012) 2:1981–2035. doi: 10.1002/cphy.c110051

13. Harris AL. Emerging issues of connexin channels: biophysics fills the gap. *Q Rev Biophys*. (2001) 34:325–472. doi: 10.1017/s0033583501003705

14. Saez JC, Berthoud VM, Branes MC, Martinez AD, Beyer EC. Plasma membrane channels formed by connexins: their regulation and functions. *Physiol Rev*. (2003) 83:1359–400. doi: 10.1152/physrev.00007.2003

15. Maeda S, Tsukihara T. Structure of the gap junction channel and its implications for its biological functions. *Cell Mol Life Sci*. (2011) 68:1115–29. doi: 10.1007/s00018-010-0551-z

16. Peracchia C. Gap junction channelopathies and calmodulinopathies. Do disease-causing calmodulin mutants affect direct cell-cell communication? *Int J Mol Sci*. (2021) 22:17. doi: 10.3390/ijms22179169

17. Laird DW. The gap junction proteome and its relationship to disease. *Trends Cell Biol*. (2010) 20:92–101. doi: 10.1016/j.tcb.2009.11.001

18. Liu Q, Wang Y, Gao H, Sun F, Wang X, Zhang H, et al. An individualized prognostic signature for clinically predicting the survival of patients with bladder cancer. *Front Genet*. (2022) 13:837301. doi: 10.3389/fgene.2022.837301

19. Addeo A, Friedlaender A, Banna GL, Weiss GJ. TMB or not TMB as a biomarker: That is the question. *Crit Rev Oncol Hematol*. (2021) 163:103374. doi: 10.1016/j.critrevonc.2021.103374

20. Bravaccini S, Bronte G, Ulivi P. TMB in NSCLC: A broken dream? *Int J Mol Sci*. (2021) 22:12. doi: 10.3390/ijms22126536

21. Dhein S, Salameh A. Remodeling of cardiac gap junctional cell-cell coupling. *Cells*. (2021) 10:9. doi: 10.3390/cells10092422

22. Kumar NM, Gilula NB. The gap junction communication channel. *Cell*. (1996) 84:381–8. doi: 10.1016/s0092-8674(00)81282-9

23. Martínez AD, Acuña R, Figueroa V, Maripillan J, Nicholson B. Gap-junction channels dysfunction in deafness and hearing loss. *Antioxid Redox Signal*. (2009) 11:309–22. doi: 10.1089/ars.2008.2138

24. Simon AM, Goodenough DA. Diverse functions of vertebrate gap junctions. *Trends Cell Biol*. (1998) 8:477–83. doi: 10.1016/s0962-8924(98)01372-5

25. Dhein S. Gap junction channels in the cardiovascular system: pharmacological and physiological modulation. *Trends Pharmacol Sci*. (1998) 19:229–41. doi: 10.1016/s0165-6147(98)01192-4

26. Grek CL, Rhett JM, Bruce JS, Ghatnekar GS, Yeh ES. Connexin 43, breast cancer tumor suppressor: Missed connections? *Cancer Lett*. (2016) 374:117–26. doi: 10.1016/j.canlet.2016.02.008

27. Totland MZ, Rasmussen NL, Knudsen LM, Leithe E. Regulation of gap junction intercellular communication by connexin ubiquitination: physiological and pathophysiological implications. *Cell Mol Life Sci*. (2020) 77:4–573-591. doi: 10.1007/s00018-019-03285-0

28. Sinha G, Ferrer AI, Moore CA, Naaldijk Y, Rameshwar P. Gap junctions and breast cancer dormancy. *Trends Cancer*. (2020) 6:348–57. doi: 10.1016/j.trecan.2020.01.013

29. King TJ, Lampe PD. The gap junction protein connexin32 is a mouse lung tumor suppressor. *Cancer Res*. (2004) 64:7191–6. doi: 10.1158/0008-5472.Can-04-0624

30. Krutovskikh VA, Troyanovsky SM, Piccoli C, Tsuda H, Asamoto M, Yamasaki H. Differential effect of subcellular localization of communication impairing gap junction protein connexin43 on tumor cell growth in *vivo*. *Oncogene*. (2000) 19:505–13. doi: 10.1038/sj.onc.1203340

31. Bonacquisti EE, Nguyen J. Connexin 43 (Cx43) in cancer: Implications for therapeutic approaches via gap junctions. *Cancer Lett*. (2019) 442:439–44. doi: 10.1016/j.canlet.2018.10.043

32. Chen Q, Boire A, Jin X, Valiente M, Er EE, Lopez-Soto A, et al. Carcinoma-astrocyte gap junctions promote brain metastasis by cGAMP transfer. *Nature*. (2016) 533:493–8. doi: 10.1038/nature18268

33. Wu DP, Zhou Y, Hou LX, Zhu XX, Yi W, Yang SM, et al. Cx43 deficiency confers EMT-mediated tamoxifen resistance to breast cancer via c-Src/PI3K/Akt pathway. *Int J Biol Sci*. (2021) 17:2380–98. doi: 10.7150/ijbs.55453

34. Yang J, Fan Y, Xie B, Yang D. A combination of RNA-seq analysis and use of TCGA database for determining the molecular mechanism and identifying potential drugs for GJB1 in ovarian cancer. *Onco Targets Ther*. (2021) 14:2623–33. doi: 10.2147/ott.S303589

35. Gollob MH, Jones DL, Krahn AD, Danis L, Gong XQ, Shao Q, et al. Somatic mutations in the connexin 40 gene (GJA5) in atrial fibrillation. *N Engl J Med*. (2006) 354:2677–88. doi: 10.1056/NEJMoa052800

36. Efimova I, Catanzaro E, van der Meeren L, Turubanova VD, Hammad H, Mishchenko TA, et al. Vaccination with early ferroptotic cancer cells induces efficient antitumor immunity. *J Immunother Cancer*. (2020) 8:2. doi: 10.1136/jitc-2020-001369

37. Li B, Severson E, Pignon JC, Zhao H, Li T, Novak J, et al. Comprehensive analyses of tumor immunity: implications for cancer immunotherapy. *Genome Biol*. (2016) 17:1–174. doi: 10.1186/s13059-016-1028-7

38. Wang J, Li P, Yu Y, Fu Y, Jiang H, Lu M, et al. Pulmonary surfactant-biomimetic nanoparticles potentiate heterosubtypic influenza immunity. *Science*. (2020) 367:6480. doi: 10.1126/science.aau0810

39. Oviedo-Orta E, Hoy T, Evans WH. Intercellular communication in the immune system: differential expression of connexin40 and 43, and perturbation of gap junction channel functions in peripheral blood and tonsil human lymphocyte subpopulations. *Immunology*. (2000) 99:578–90. doi: 10.1046/j.1365-2567.2000.00991.x

40. Vliagoftis H, Hutson AM, Mahmudi-Azer S, Kim H, Rumsaeng V, Oh CK, et al. Mast cells express connexins on their cytoplasmic membrane. *J Allergy Clin Immunol*. (1999) 103:656–62. doi: 10.1016/s0091-6749(99)70239-3

41. Sugita J, Fujiu K, Nakayama Y, Matsubara T, Matsuda J, Oshima T, et al. Cardiac macrophages prevent sudden death during heart stress. *Nat Commun*. (2021) 12:1910. doi: 10.1038/s41467-021-22178-0

frontiers | Frontiers in Oncology

TYPE Systematic Review
PUBLISHED 15 April 2024
DOI 10.3389/fonc.2024.1378993

OPEN ACCESS

EDITED BY
Lei Yin,
Shanghai Jiao Tong University, China

REVIEWED BY
Jagpreet Singh Nanda,
Cedars Sinai Medical Center, United States
Yupeng Wu,
First Affiliated Hospital of Fujian Medical University, China

*CORRESPONDENCE
Yinfeng Ma
yinfeng_ma@163.com

†These authors share first authorship

RECEIVED 30 January 2024
ACCEPTED 02 April 2024
PUBLISHED 15 April 2024

CITATION
Zhang D, Weng H, Zhu Z, Gong W and Ma Y (2024) Evaluating first-line therapeutic strategies for metastatic castration-resistant prostate cancer: a comprehensive network meta-analysis and systematic review. *Front. Oncol.* 14:1378993. doi: 10.3389/fonc.2024.1378993

Evaluating first-line therapeutic strategies for metastatic castration-resistant prostate cancer: a comprehensive network meta-analysis and systematic review

Duojie Zhang[1†], Haimin Weng[1†], Zhangji Zhu[1], Weilun Gong[1] and Yinfeng Ma[2*]

[1]The Second Clinical Medical College of Zhejiang Chinese Medical University, Hangzhou, Zhejiang, China, [2]Department of Urology, The Second Affiliated Hospital of Zhejiang Chinese Medicine University, Hangzhou, Zhejiang, China

Objective: This study aimed to evaluate the relative efficacy and safety of first-line treatment options for metastatic castration-resistant prostate cancer (mCRPC).

Methods: We systematically searched electronic databases, including PubMed and Web of Science, for studies published from their inception to April 3rd, 2023. Inclusion criteria were: 1) Completed Phase III or IV randomized controlled trials (RCTs) registered on ClinicalTrials.gov; 2) Patients with a confirmed diagnosis of mCRPC who had not previously received chemotherapy or novel endocrine therapies. We conducted a network meta-analysis using R software (version 3.4.0). Network graphs and risk of bias graphs were generated using Stata 14.0 and RevMan 5.4, respectively. The primary outcome was overall survival (OS), and the secondary outcome was the incidence of severe adverse events (SAEs).

Results: Seven RCTs encompassing 6,641 patients were included. The network meta-analysis revealed that both docetaxel+prednisone (DP) and cabazitaxel +prednisone (CP) significantly improved OS compared to abiraterone. Compared to placebo, DP showed comparable results to both cabazitaxel 20 mg/m^2 +prednisone (C20P) and cabazitaxel 25 mg/m^2+prednisone (C25P) in terms of OS. For SAEs, both DP and C20P were superior to C25P, with no statistical difference between C20P and DP. The probability ranking plots indicated that C25P ranked highest for OS, while DP ranked highest for SAEs.

Conclusions: Based on our network meta-analysis, we recommend cabazitaxel 20 mg/m^2+prednisone (C20P) as the primary choice for first-line management of mCRPC, followed by DP. Enzalutamide and abiraterone are suggested as subsequent options. Radium-223 may be considered for patients presenting with bone metastases.

Systematic review registration: https://www.crd.york.ac.uk/prospero/, identifier CRD42023443943.

KEYWORDS

castration resistant prostate cancer, first-line treatment, chemotherapy, antihormone therapy, network meta-analysis

Introduction

Prostate cancer (PC), the most prevalent malignancy in the male genitourinary system, has recently emerged as the second most common cancer globally (1). The world age-standardized incidence rate is 37.5 per 100,000, with higher prevalence in regions with a high Human Development Index, such as Europe and North America. Many PC patients undergo Androgen Deprivation Therapy (ADT) post-laparoscopic or robotic surgery, showing promising efficacy in the initial and intermediate stages. However, due to various mechanisms such as androgen receptor amplification, mutation, PI3K pathway, or NF-κB pathway aberrations, tumors often develop resistance to ADT, progressing to mCRPC within 18-24 months, frequently accompanied by distant metastases (2). This phase is marked by a dismal prognosis and escalated treatment costs (3). Current therapeutic approaches include second-generation antiandrogens (e.g., abiraterone, enzalutamide, apalutamide), chemotherapy (docetaxel, cabazitaxel), and radionuclide therapy (Radium-223, 177Lu-PSMA) (4, 5). Abiraterone, a CYP17 inhibitor, diminishes androgen levels by inhibiting a crucial enzyme in androgen synthesis. Enzalutamide and apalutamide, as androgen receptor antagonists, prevent androgen from binding to its receptor. Clinical trials have demonstrated the effectiveness of abiraterone and enzalutamide in extending progression-free survival (PFS) and overall survival (OS) in mCRPC patients (6, 7).

Despite this, the absence of direct comparative trials for first-line treatments leaves a gap in knowledge regarding the optimal balance of efficacy and safety. This study aims to fill this void by comparing the effectiveness and safety of first-line mCRPC treatments as reported in randomized clinical trials (RCTs), thereby guiding clinical decision-making.

Methods

Eligibility criteria

The inclusion criteria for trials were as follows: 1) Phase III or IV randomized controlled trials (RCTs); 2) Participants diagnosed with metastatic castration-resistant prostate cancer (mCRPC); 3) No history of cytotoxic therapy or androgen receptor inhibitor therapy; 4) Interventions including abiraterone acetate, enzalutamide, apalutamide, docetaxel, cabazitaxel, or Radium-223; 5) Outcomes measuring overall survival (OS) and severe adverse events (SAEs). Exclusion criteria comprised: 1) Studies with incomplete data; 2) Non-English language publications; 3) Trials terminated prematurely for various reasons.

Following initial study selection, a preliminary network graph was produced. In cases where key studies were missing, additional relevant studies were identified and included after thorough discussion, ensuring the completeness of the network graph. The study protocol was registered with PROSPERO (Registration number: CRD42023443943). Our approach to study selection and inclusion aligned with the Preferred Reporting Items for Systematic Reviews and Meta-Analyses (PRISMA) guidelines (8).

Data sources and extraction

We conducted a comprehensive search of electronic databases, including PubMed and Web of Science, for studies published from their inception through April 3rd, 2023. The search included: 1) Completed Phase III or IV randomized controlled trials (RCTs) registered with ClinicalTrials.gov; 2) Patient cohorts with a confirmed diagnosis of metastatic castration-resistant prostate cancer (mCRPC) who had not previously received chemotherapy or novel endocrine therapies. The literature search employed the following terms, used as title/abstract keywords or MeSH terms: 'castration-resistant prostate cancer', 'abiraterone', 'enzalutamide', 'docetaxel', 'Radium-223', 'cabazitaxel'.

Data extraction was independently conducted by two reviewers (ZD and WH), following a thorough assessment of all potential abstracts and titles for eligibility. In instances of disagreement or insufficient information, a third reviewer (MY) was consulted to examine the full text for eligibility. Extracted information included patient characteristics (median age, treatment descriptions, and doses) and sites of metastatic disease.

The analysis focused on median overall survival (OS) as the efficacy criterion, while toxicity criteria included the incidence of Grade 3-5 toxicities as per the National Cancer Institute Common Toxicity Criteria, along with the incidence of serious adverse events.

Risk of bias assessment

Methodological quality of the included studies was assessed independently by two investigators, utilizing the Cochrane Handbook for Systematic Reviews of Interventions. Each trial was evaluated on the following criteria and assigned a risk of bias rating as low, medium, or high: random sequence generation, allocation concealment, blinding of participants and personnel, blinding of outcome assessment, completeness of outcome data, selective reporting, and presence of any other biases. A trial was deemed to have an overall low risk of bias if all domains were rated as low risk, and high risk if any domain was assessed as high risk. Discrepancies in assessment were resolved through discussion between the two investigators, or by consulting a third investigator for an adjudicated decision.

Statistical analysis

The network meta-analysis was performed using a Bayesian framework model, employing R software (version 4.3.0) with the gemtc package (9). For the outcomes, overall survival (OS) was estimated using pooled hazard ratios (HRs) with 95% confidence intervals (CIs), and severe adverse events (SAEs) were analyzed

using odds ratios (ORs) with 95% CIs. Both fixed-effects and random-effects models were fitted, with the latter accounting for heterogeneity between studies. The results presented in this study are based on the fixed-effects model.

Results

Study selection and network geometry

Initial database screening yielded 4,273 references from PubMed and 3,751 from Web of Science (Figure 1). This was narrowed down to 835 potentially relevant trials after initial screening. Upon detailed examination, 7 studies fulfilling the inclusion criteria were selected for analysis. A network graph depicting treatment comparisons is illustrated in Figure 2.

The most frequently studied treatment was abiraterone acetate + prednisone (4 trials). To complete the network graph, a phase IV second-line treatment RCT comparing cabazitaxel 25mg/m$^{\wedge 2}$ and abiraterone acetate was included after discussion.

Characteristics of included trials

The analysis included seven multicenter RCTs, predominantly phase III first-line treatments, with the exception of one phase IV second-line treatment RCT included for network completeness (10–16). These trials spanned 2015 to 2020, involving a total of 6,411 participants. Median sample size per treatment arm was 396 (range, 126-872) patients; median age was 70.6 years (range, 68-71.6 years); median overall survival (OS) was 30.15 months (range, 11-39.1 months). Eligibility criteria primarily required newly diagnosed prostate adenocarcinoma with radiographic evidence of metastasis and adequate performance status, excluding or restricting prior chemotherapy and hormone therapy in the metastatic setting. To ensure network completeness, the CARD trial was additionally included. Baseline characteristics of the 7 studies are detailed in Table 1.

Risk of bias

The Cochrane Collaboration tool was employed for quality assessment of the included trials. Bias risk was evaluated across six domains mentioned in the selection criteria. Five of the seven studies demonstrated adequate randomization. The remaining studies lacked specific details on sequence generation methods. Allocation concealment was reported in five trials, with two trials employing open-label designs. Attrition and reporting biases were assessed and managed effectively in the included studies. A summary of the risk-of-bias assessment for each trial is presented in Figure 3.

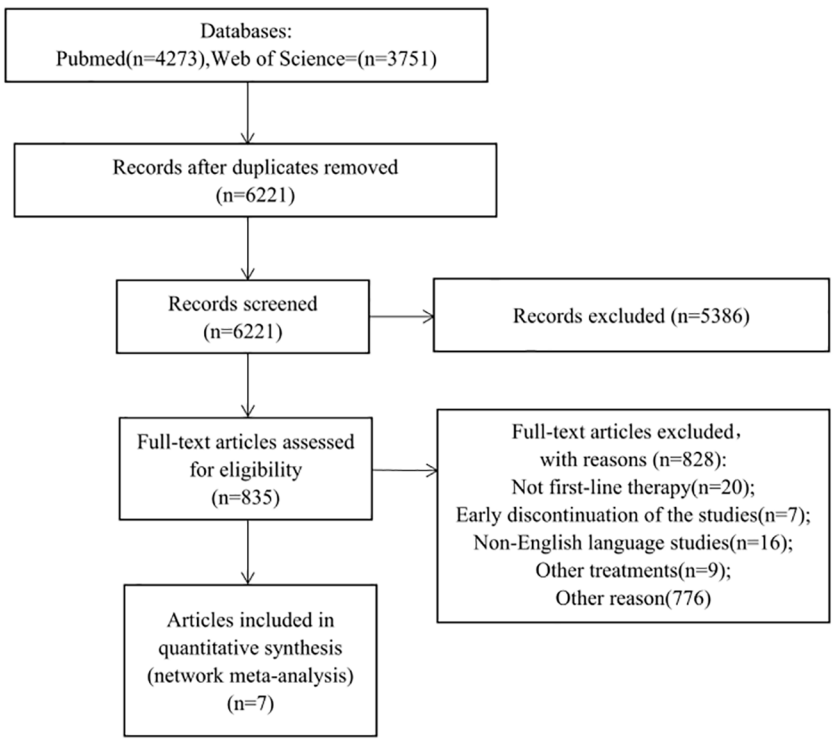

FIGURE 1
Study fow chart. This network meta-analysis incorporated 6 phase III and 1 phase IV randomized controlled trials (RCTs), enrolling a total of 6,411 patients with metastatic castration-resistant prostate cancer (mCRPC). Eight treatment modalities were analyzed: placebo/prednisone, abiraterone acetate + prednisone, enzalutamide, cabazitaxel 20/25mg/m$^{\wedge 2}$, docetaxel, Radium-223 + abiraterone acetate + prednisone, and apalutamide + abiraterone acetate + prednisolone.

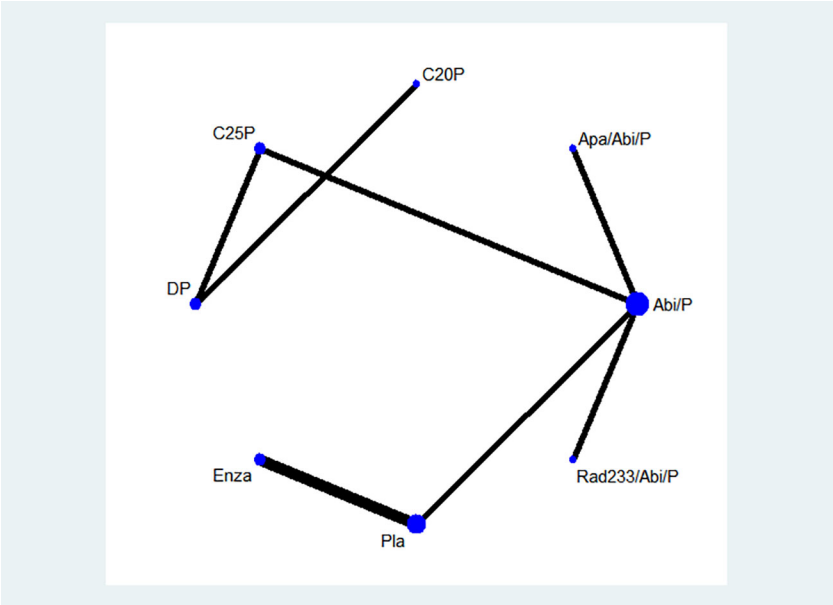

FIGURE 2
A network graph depicting treatment comparisons is illustrated.DP-docetaxel+prednisone. C25P-cabazitaxel 25 mg/m^2+prednisone, C20P-cabazitaxel 20 mg/m^2+prednisone, Apa/abi/p-apalutamide + abiraterone acetate + prednisolone, Abi/p-abiraterone acetate + prednisone, Rad233/abi/p-Radium-223 + abiraterone acetate + prednisone, Pla-placebo, Enza-enzalutamide.

Syntheses of results

Network meta-analyses incorporated all eight treatments, evaluating both effectiveness (OS) and safety (SAEs) outcomes (Figure 4).

Effectiveness outcomes

Treatments showing significant OS improvement over placebo included: docetaxel (HR, 0.53; 95% CI, 0.36-0.79), abiraterone acetate (HR, 0.81; 95% CI, 0.70-0.94), enzalutamide (HR, 0.70; 95% CI, 0.61-0.82), cabazitaxel 20 mg/m^2 (HR, 0.53; 95% CI, 0.35-0.84), and cabazitaxel 25 mg/m^2 (HR, 0.52; 95% CI, 0.36-0.75). Docetaxel also demonstrated superior OS improvement compared to abiraterone and Radium-223 + abiraterone, and was comparable with enzalutamide, cabazitaxel, and apalutamide (Figure 4). Treatment ranking probabilities indicated cabazitaxel 25 mg/m^2 as the most likely best treatment for OS (45% probability).

Safety outcomes

Regarding SAEs, treatments ranked from safest to least safe were: docetaxel, cabazitaxel 20mg/m^2, cabazitaxel 25mg/m^2, abiraterone, Radium-223 combined with abiraterone, enzalutamide, and apalutamide combined with abiraterone. There were no significant differences between docetaxel, cabazitaxel 20/25 mg/m^2, and placebo in terms of SAEs.

Heterogeneity

The heterogeneity of our findings (I^2) was less than 30%, which indicated that our findings were homogeneous. Therefore, we did not conduct subgroup analysis to identify the source of heterogeneity. Comprehensive results can be found in Supplementary Figure 3.

Grade assessment

Out of 7 RCTs, 4 of them were categorized as low risk of bias. Due to the lack of sufficient blinding methods, 3 RCTs were revealed to have high risk of bias. Based on grading the evidence in Table 2, 3 low risk of bias articles were included and produced high certainty of evidence. Based on the grading analysis, it is revealed that all 3 studies not only have low risk of bias but are also not serious in terms of inconsistency, indirectness, and imprecision. All these criteria increase the certainty level and can guide clinicians and policymakers for future events or discussions. Comprehensive results can be found in Table 2.

Discussion

This network meta-analysis systematically evaluated first-line treatments for metastatic castration-resistant prostate cancer (mCRPC) as delineated in existing Phase III and IV randomized controlled trials (RCTs). A notable majority of these treatments had

10.3389/fonc.2024.1378993

TABLE 1 Detailed description of baseline characteristics of 7 studies.

Trail	Study name, Registration	Patients enrolled	Treatment arms	Patients included for analysis	Median age(y)	Median OS(m)	No. of countries or areas
Charles J Ryan 2015	COU-AA-302	1088	Abiraterone Acetate + Prednisone	546	70.5	34.7	11 (Australia, Belgium, Canada, et al.)
	NCT00887198		Placebo+Prednisone	542	70.1	30.3	
Yohann Loriot 2015	PREVAIL	1717	Enzalutamide	872	71.3	32.4	23 (Australia, Austria, Belgium, et al.)
	NCT01212991		Placebo	845	71.2	30.2	
Stéphane Oudard 2017	FIRSTANA	1168	Cabazitaxel 20 mg/m^2	389	68.0	24.5	25 (Australia, Belarus, Brazil, et al.)
	NCT01308567		Docetaxel	391	69.0	24.3	
			Cabazitaxel 25 mg/m^2	388	68.5	25.2	
			Docetaxel	391	69.0	24.3	
Matthew Smith 2019	ERA 223	806	Radium-223 Dichloride + Abiraterone Acetate + Prednisone	401	70.9	30.1	19 (Australia, Belgium, Brazil, et al.)
	NCT02043678		Placebo+Abiraterone Acetate + Prednisone	405	71.4	34.8	
Karim Fizazi 2020	CARD	255	Cabazitaxel 25 mg/m^2	129	69.7	13.6	13 (Austria, Belgium, Czechia, et al.)
	NCT02485691		Abiraterone Acetate or Enzalutamide	126	69.7	11.0	
Fred Saad 2021	ACIS	982	Apalutamide + Abiraterone Acetate + Prednisolone	492	71.4	36.2	17 (Argentina, Australia, Belgium, et al.)
	NCT02257736		Placebo+ Abiraterone Acetate + Prednisolone	490	70.7	33.7	
Yeong-Shiau Pu 2022	9785-CL-0232	395	Enzalutamide	202	71.6	39.1	Asian
	NCT02294461		Placebo	193	71.0	27.1	

not previously been directly compared in face-to-face trials. Our comprehensive analysis revealed that chemotherapy regimens, specifically docetaxel and cabazitaxel, demonstrated superior efficacy and safety compared to second-generation anti-hormonal therapies, including abiraterone, enzalutamide, and apalutamide, in the first-line management of mCRPC.

The findings of this network meta-analysis provide new insights into the first-line treatment of metastatic castration-resistant prostate cancer (mCRPC). Current guidelines from the American Urological Association (AUA) recommend abiraterone and enzalutamide as grade A treatments, and docetaxel as a grade B treatment for mCRPC (17). Similarly, the Apccc expert consensus endorses abiraterone and enzalutamide as primary treatments (18). These recommendations contrast with our results, prompting an exploration of potential reasons for these discrepancies. Several factors may contribute to this variation:

AR-V7 Presence: AR-V7, a variant of the androgen receptor (AR) lacking the ligand-binding domain, is frequently observed in mCRPC patients, with about a 30% mutation rate. Antonarakis (19) demonstrated a significant correlation between AR-Vs in circulating tumor cells and clinical outcomes in CRPC patients receiving new AR-targeted therapies. Studies indicate that AR-V7 positivity is associated with resistance and poor efficacy in patients treated with enzalutamide and abiraterone (20). Conversely, AR-V7 status does not significantly affect responses to paclitaxel-based therapies like docetaxel or cabazitaxel (21).

PTEN Deficiency: The tumor suppressor gene PTEN, frequently lost or mutated in cancers, regulates the PI3K–AKT–mTOR signaling pathway. In mCRPC, PTEN gene deletion occurs in 40-60% of cases (22–24). Studies have shown that PTEN deficiency negatively impacts the effectiveness of abiraterone, but does not affect the antitumor activity of docetaxel (25, 26).

DDR Gene Mutations: The impact of DDR (DNA damage response) gene mutations on second-generation hormone therapy and paclitaxel-based therapy remains unclear. Some studies suggest that DDR gene mutations attenuate the efficacy of second-generation hormone therapies, but their impact on the efficacy of cabazitaxel is less certain (27, 28).

Tumor Neuroendocrine Differentiation (NED): NED in mCRPC is a significant factor in treatment response. Hormone

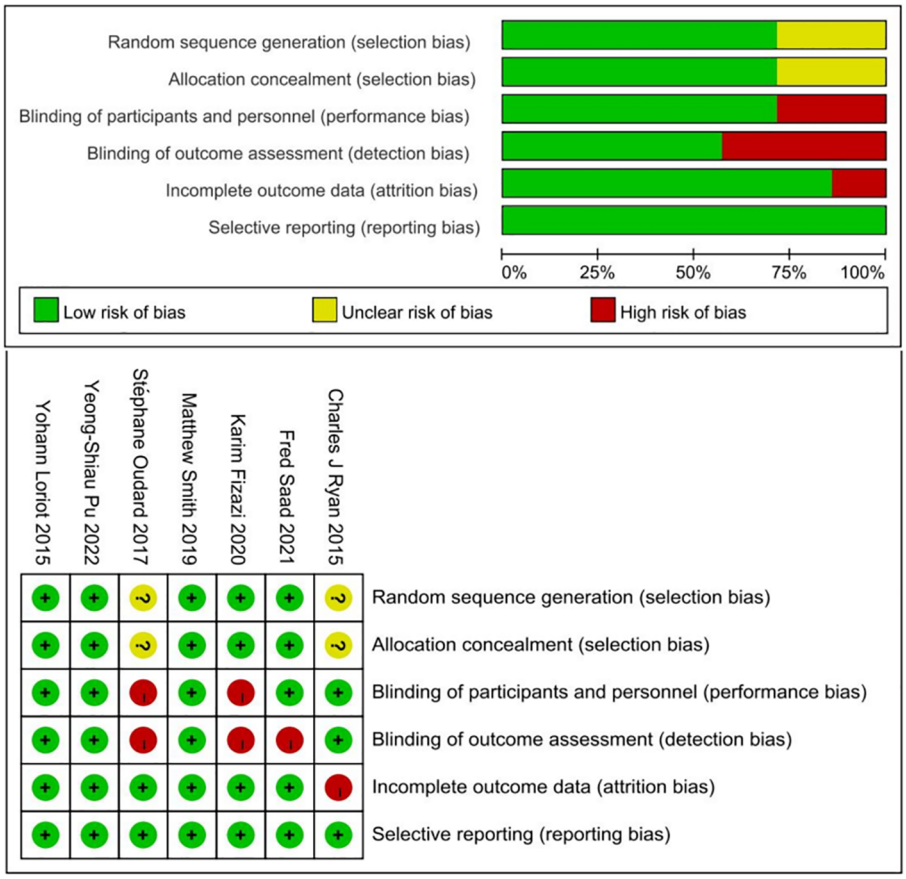

FIGURE 3
Risk of bias of selected studies.

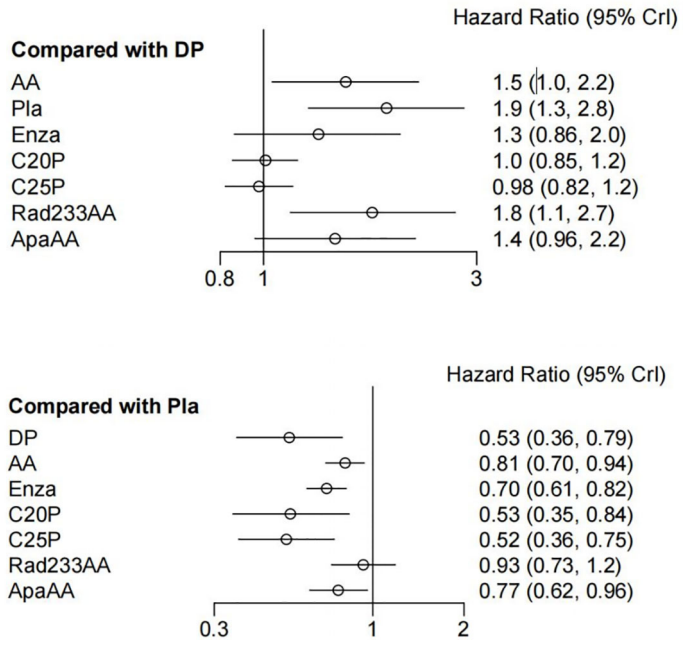

FIGURE 4
Summary of effectiveness (OS) and safety (SAE) assessments of eight treatments.

TABLE 2 Grading the evidence with GRADEpro Guideline Development Tool.

Certainty assessment							№ of patients		Effect	Certainty	Importance
№ of studies	Study design	Risk of bias	Inconsistency	Indirectness	Imprecision	Other considerations	Intervention	Control	Relative (95% CI)		
DP vs C20P(OS)											
1	randomised trials	serious	not serious	not serious	not serious	none	391 participants	389 participants	**HR 0.99** (0.84 to 1.20) [DP vs C20P(OS)]	⨁⨁⨁◯ Moderate	CRITICAL
DP vs C25P(OS)											
1	randomised trials	not serious	not serious	serious	not serious	none	391 participants	388 participants	**HR 1.00** (0.86 to 1.20) [DP vs C25P(OS)]	⨁⨁⨁◯ Moderate	CRITICAL
C25P vs Abi/P(OS)											
1	randomised trials	serious	not serious	serious	not serious	none	129 participants	126 participants	**HR 0.64** (0.46 to 0.89) [C25P vs Abi/P(OS)]	⨁⨁◯◯ Low	CRITICAL
Abi/P vs Apa/Abi/P(OS)											
1	randomised trials	serious	not serious	not serious	not serious	none	492 participants	490 participants	**HR 1.10** (0.89 to 1.20) [Abi/P vs Apa/Abi/P(OS)]	⨁⨁⨁◯ Moderate	CRITICAL
Abi/P vs Rad233/Abi/P(OS)											
1	randomised trials	not serious	not serious	not serious	not serious	none	405 participants	401 participants	**HR 0.87** (0.72 to 1.10) [Abi/P vs Rad233/Abi/P(OS)]	⨁⨁⨁⨁ High	CRITICAL
Abi/P vs Pla(OS)											

(Continued)

10.3389/fonc.2024.1378993

TABLE 2 Continued

№ of studies	Study design	Certainty assessment					№ of patients		Effect	Certainty		Importance
		Risk of bias	Inconsistency	Indirectness	Imprecision	Other considerations	Intervention	Control	Relative (95% CI)			
Abi/P vs Pla(OS)												
1	randomised trials	not serious	not serious	not serious	not serious	none	546 participants	542 participants	**HR 0.81** (0.70 to 0.94) [Abi/P vs Pla(OS)]	⨁⨁⨁⨁ High		CRITICAL
Enza vs Pla(OS)												
2	randomised trials	not serious	not serious	not serious	not serious	none	872 participants	845 participants	**HR 0.70** (0.61 to 0.82) [Enza vs Pla(OS)]	⨁⨁⨁⨁ High		CRITICAL

CI, confidence interval; HR, hazard ratio; OR, odds ratio.

therapy is generally less effective in patients with NED. A study found greater OS benefit with a Docetaxel+Prednisone (DP) - Abiraterone Acetate (AA) treatment sequence in patients with elevated NED, compared to an AA-DP sequence (29).In light of these findings, our analysis suggests that the choice of first-line treatment for mCRPC should consider molecular and genetic tumor characteristics to optimize patient outcomes.

The objective of this network meta-analysis was to elucidate the efficacy of cabazitaxel 20 mg/m$^{\wedge 2}$ (C20P) and cabazitaxel 25 mg/m$^{\wedge 2}$ (C25P) over docetaxel+prednisone (DP) in chemotherapy- or hormone therapy-naive patients with metastatic castration-resistant prostate cancer (mCRPC), focusing on overall survival (OS). Our recommendation favors C20P, as it shows comparable OS to C25P but exhibits superior safety in terms of severe adverse events (SAEs), suggesting enhanced tolerability at the lower dose.

The choice of optimal treatment for mCRPC remains a subject of debate. Recently, some scholars have also performed network meta-analysis for first-line treatment of mCRPC (30). Unlike our analysis, this analysis included all period RCTs to form a network and was therefore more exploratory. Our analysis includes Phase III and IV RCTs, and focuses on the high level of evidence to guide clinical application. This analysis included 29 RCTs, involving 12,706 patients and investigating 16 interventions. According to the OS results of this analysis, in addition to docetaxel and cabazitaxel-based chemotherapy regimens, chemotherapy combined with targeted therapy (capivasertib or cabozantinib) and chemotherapy combined with PD-1 (ipilimumab) showed significant effects. Cabozantinib is a tyrosine kinase inhibitor that targets multiple genes, including MET, VEGFR1/2/3, ROS1, RET, AXL, NTRK, and KIT, and is currently used to treat renal cancer (31). Capivasertib is an AKT inhibitor with potential efficacy in patients with PIK3CA, AKT1, and or PTEN mutations. These therapeutic strategies of targeted therapy combined with chemotherapy are providing a new direction for mCRPC.

Different levels of genetic mutations are often found in malignant tumors, which can cause poor response to castration therapy or chemotherapy. Therefore, the use of monotherapy in cancer therapy has limitations, and monotherapy specifically inhibits a therapeutic target and triggers compensatory mechanisms or other signal transduction bypasses, which require the assistance of other drugs to improve efficacy. Researchers are increasingly interested in using combinations of low-dose anti-cancer agents with different modes of action rather than administering single agents at high doses. Combinations of anticancer drugs with different mechanisms of action may show synergistic effects in inhibiting the growth of prostate cancer cells and inducing apoptosis. In response to the aberrant activation of PI3K and NF-κB pathways in the late stage of docetaxel chemotherapy in mCRPC, drugs that can inhibit the transduction of this signaling pathway are required.

In order to achieve precise treatment of mCRPC, genetic testing of patients with mCRPC is required. For patients who have undergone surgical treatment, tumor specimens can be sampled and tested. For inoperable patients, prostate biopsy may be used for testing. Both approaches can be applied to most scenarios. In addition, circulating tumor cells (CTC) can be used to detect

novel mutations. CTCs are tumor cells disseminated from primary and/or metastatic tumor sites that circulate in the vasculature with potential for distant seeding. Studies have shown that CTC detection has been performed in mCRPC patients by a useful platform to detect the presence or absence of AR-V7 mutations (32). A multicentric study replicated these findings using an open-source Automated CTC Classification Enumeration and PhenoTyping software for the prognostication of mCRPC patients (33). In addition to CTC, mCRPC can also be genetically classified by detecting circulating nucleic acids, extracellular vesicles. After that targeted or immune treatment regimens can be used for different types mutations to achieve precise treatment of mCRPC.

According to our analysis, cabazitaxel or docetaxel is preferable over abiraterone or enzalutamide for initial chemotherapy or hormone therapy in mCRPC patients who have not undergone genetic testing. Moreover, there is considerable potential for advancement in prostate cancer treatment. The efficacy of many therapeutics is closely linked to tumor genetic mutations, indicating a need for further research in this area.

Limitations

Our study is not without limitations. Firstly, due to exclusion criteria, we were unable to include emerging treatments such as targeted therapies (olaparib, ipatasertib), vaccine therapies (sipuleucel-T), and radiation therapy (177Lu-PSMA-617). Secondly, the inclusion of a second-line treatment RCT for mCRPC (CARD) was necessary to complete the network graph, which may have introduced bias. It is hoped that future analyses will incorporate more Phase III RCTs focused on first-line mCRPC treatments. Thirdly, the field of prostate cancer treatment is yet to fully embrace precision therapy, and many studies lack genetic data. Therefore, a subgroup analysis of genetic factors in the included patients was not feasible.

Conclusions

We recommend cabazitaxel 20 mg/m^2 as the primary option for first-line treatment of mCRPC. Genetic testing for mCRPC patients is also advised to tailor treatment choices based on mutation profiles. Given the limitations of our network meta-analysis, the need for more comprehensive, high-quality studies for further evaluation is evident.

Data availability statement

The raw data supporting the conclusions of this article will be made available by the authors, without undue reservation.

Author contributions

DZ: Writing – original draft, Investigation, Data curation, Conceptualization. HW: Writing – original draft, Investigation, Data curation, Conceptualization. ZZ: Writing – original draft, Data curation, Conceptualization. WG: Writing – original draft, Data curation, Conceptualization. YM: Writing – review & editing, Supervision, Project administration, Investigation, Funding acquisition, Writing – original draft, Data curation, Conceptualization.

Funding

The author(s) declare financial support was received for the research, authorship, and/or publication of this article. This study was funded by Project of Zhejiang Provincial Scientific Research Fund for Traditional Chinese Medicine (China). (2022ZB154).

Conflict of interest

The authors declare that the research was conducted in the absence of any commercial or financial relationships that could be construed as a potential conflict of interest.

Publisher's note

Supplementary material

The Supplementary Material for this article can be found online at: https://www.frontiersin.org/articles/10.3389/fonc.2024.1378993/full#supplementary-material

References

1. Sweeney C, Bracarda S, Sternberg CN, Chi KN, Olmos D, Sandhu S, et al. Ipatasertib plus abiraterone and prednisolone in metastatic castration-resistant prostate cancer (IPATential150): a multicentre, randomised, double-blind, phase 3 trial. *Lancet*. (2021) 398:131–42. doi: 10.1016/s0140-6736(21)00580-8

2. Chen J, Wu Z, Ding W, Xiao C, Zhang Y, Gao S, et al. SREBP1 siRNA enhance the docetaxel effect based on a bone-cancer dual-targeting biomimetic nanosystem against bone metastatic castration-resistant prostate cancer. *Theranostics*. (2020) 10:1619–32. doi: 10.7150/thno.40489

3. Chandrasekar T, Yang JC, Gao AC, Evans CP. Mechanisms of resistance in castration-resistant prostate cancer (CRPC). *Transl Androl Urol*. (2015) 4:365–80. doi: 10.3978/j.issn.2223-4683.2015.05.02

4. Hoxhaj G, Manning BD. The PI3K-AKT network at the interface of oncogenic signalling and cancer metabolism. *Nat Rev Cancer*. (2020) 20:74–88. doi: 10.1038/s41568-019-0216-7

5. Desai K, McManus JM, Sharifi N. Hormonal therapy for prostate cancer. *Endocr Rev*. (2021) 42:354–73. doi: 10.1210/endrev/bnab002

6. Mori K, Mostafaei H, Sari Motlagh R, Pradere B, Quhal F, Laukhtina E, et al. Systemic therapies for metastatic hormone-sensitive prostate cancer: network meta-analysis. *BJU Int*. (2022) 129:423–33. doi: 10.1111/bju.15507

7. Hernandez I, Cohen M. Linking cell-surface GRP78 to cancer: From basic research to clinical value of GRP78 antibodies. *Cancer Lett*. (2022) 524:1–14. doi: 10.1016/j.canlet.2021.10.004

8. Hutton B, Salanti G, Caldwell DM, Chaimani A, Schmid CH, Cameron C, et al. The PRISMA extension statement for reporting of systematic reviews incorporating network meta-analyses of health care interventions: checklist and explanations. *Ann Intern Med*. (2015) 162:777–84. doi: 10.7326/M14-2385

9. van Valkenhoef G, Dias S, Ades AE, Welton NJ. Automated generation of node-splitting models for assessment of inconsistency in network meta-analysis. *Res Synth Methods*. (2016) 7(1):80–93. doi: 10.1002/jrsm.1167

10. Ryan CJ, Smith MR, Fizazi K, Saad F, Mulders PF, Sternberg CN, et al. Abiraterone acetate plus prednisone versus placebo plus prednisone in chemotherapy-naive men with metastatic castration-resistant prostate cancer (COU-AA-302): final overall survival analysis of a randomised, double-blind, placebo-controlled phase 3 study. *Lancet Oncol*. (2015) 16:152–60. doi: 10.1016/S1470-2045(14)71205-7

11. Loriot Y, Miller K, Sternberg CN, Fizazi K, De Bono JS, Chowdhury S, et al. Effect of enzalutamide on health-related quality of life, pain, and skeletal-related events in asymptomatic and minimally symptomatic, chemotherapy-naive patients with metastatic castration-resistant prostate cancer (PREVAIL): results from a randomised, phase 3 trial. *Lancet Oncol*. (2015) 16:509–21. doi: 10.1016/S1470-2045(15)70113-0

12. Oudard S, Fizazi K, Sengelov L, Daugaard G, Saad F, Hansen S, et al. Cabazitaxel versus docetaxel as first-line therapy for patients with metastatic castration-resistant prostate cancer: A randomized phase III trial-FIRSTANA. *J Clin Oncol*. (2017) 35:3189–97. doi: 10.1200/JCO.2016.72.1068

13. Smith M, Parker C, Saad F, Miller K, Tombal B, Ng QS, et al. Addition of radium-223 to abiraterone acetate and prednisone or prednisolone in patients with castration-resistant prostate cancer and bone metastases (ERA 223): a randomised, double-blind, placebo-controlled, phase 3 trial. *Lancet Oncol*. (2019) 20:408–19. doi: 10.1016/S1470-2045(18)30860-X

14. Fizazi K, Kramer G, Eymard JC, Sternberg CN, de Bono J, Castellano D, et al. Quality of life in patients with metastatic prostate cancer following treatment with cabazitaxel versus abiraterone or enzalutamide (CARD): an analysis of a randomised, multicentre, open-label, phase 4 study. *Lancet Oncol*. (2020) 21:1513–25. doi: 10.1016/S1470-2045(20)30449-6

15. Saad F, Efstathiou E, Attard G, Flaig TW, Franke F, Goodman OB Jr, et al. Apalutamide plus abiraterone acetate and prednisone versus placebo plus abiraterone and prednisone in metastatic, castration-resistant prostate cancer (ACIS): a randomised, placebo-controlled, double-blind, multinational, phase 3 study. *Lancet Oncol*. (2021) 22:1541–59. doi: 10.1016/S1470-2045(21)00402-2

16. Pu YS, Ahn H, Han W, Huang SP, Wu HC, Ma L, et al. Enzalutamide in chemotherapy-naive metastatic castration-resistant prostate cancer: an asian multiregional, randomized study. *Adv Ther*. (2022) 39:2641–56. doi: 10.1007/s12325-022-02140-2

17. Lowrance W, Dreicer R, Jarrard DF, Scarpato KR, Kim SK, Kirkby E, et al. Updates to advanced prostate cancer: AUA/SUO guideline (2023). *J Urol*. (2023) 209:1082–90. doi: 10.1097/JU.0000000000003452

18. Gillessen S, Bossi A, Davis ID, de Bono J, Fizazi K, James ND, et al. Management of patients with advanced prostate cancer-metastatic and/or castration-resistant prostate cancer: Report of the Advanced Prostate Cancer Consensus Conference (APCCC) 2022. *Eur J Cancer*. (2023) 185:178–215. doi: 10.1016/j.ejca.2023.02.018

19. Antonarakis ES, Armstrong AJ, Dehm SM, Luo J. Androgen receptor variant-driven prostate cancer: clinical implications and therapeutic targeting. *Prostate Cancer Prostatic Dis*. (2016) 19:231–41. doi: 10.1038/pcan.2016.17

20. Antonarakis ES, Lu C, Luber B, Wang H, Chen Y, Zhu Y, et al. Clinical significance of androgen receptor splice variant-7 mRNA detection in circulating tumor cells of men with metastatic castration-resistant prostate cancer treated with first- and second-line abiraterone and enzalutamide. *J Clin Oncol*. (2017) 35:2149–56. doi: 10.1200/jco.2016.70.1961

21. Isebia KT, Mostert B, Belderbos BPS, Buck SAJ, Helmijr JCA, Kraan J, et al. CABA-V7: a prospective biomarker selected trial of cabazitaxel treatment in AR-V7 positive prostate cancer patients. *Eur J Cancer*. (2022) 177:33–44. doi: 10.1016/j.ejca.2022.09.032

22. Christine A, Park MK, Song SJ, Song MS. The equilibrium of tumor suppression: DUBs as active regulators of PTEN. *Exp Mol Med*. (2022) 54:1814–21. doi: 10.1038/s12276-022-00887-w

23. Herberts C, Murtha AJ, Fu S, Wang G, Schonlau E, Xue H, et al. Activating AKT1 and PIK3CA mutations in metastatic castration-resistant prostate cancer. *Eur Urol*. (2020) 78:834–44. doi: 10.1016/j.eururo.2020.04.058

24. Chakraborty G, Nandakumar S, Hirani R, Nguyen B, Stopsack KH, Kreitzer C, et al. The impact of PIK3R1 mutations and insulin-PI3K-glycolytic pathway regulation in prostate cancer. *Clin Cancer Res*. (2022) 28:3603–17. doi: 10.1158/1078-0432.CCR-21-4272

25. Ferraldeschi R, Nava Rodrigues D, Riisnaes R, Miranda S, Figueiredo I, Rescigno P, et al. PTEN protein loss and clinical outcome from castration-resistant prostate cancer treated with abiraterone acetate. *Eur Urol*. (2015) 67:795–802. doi: 10.1016/j.eururo.2014.10.027

26. Rescigno P, Lorente D, Dolling D, Ferraldeschi R, Rodrigues DN, Riisnaes R, et al. Docetaxel treatment in PTEN- and ERG-aberrant metastatic prostate cancers. *Eur Urol Oncol*. (2018) 1:71–7. doi: 10.1016/j.euo.2018.02.006

27. Annala M, Struss WJ, Warner EW, Beja K, Vandekerkhove G, Wong A, et al. Treatment outcomes and tumor loss of heterozygosity in germline DNA repair-deficient prostate cancer. *Eur Urol*. (2017) 72:34–42. doi: 10.1016/j.eururo.2017.02.023

28. Castro E, Romero-Laorden N, Del Pozo A, Lozano R, Medina A, Puente J, et al. PROREPAIR-B: A prospective cohort study of the impact of germline DNA repair mutations on the outcomes of patients with metastatic castration-resistant prostate cancer. *J Clin Oncol*. (2019) 37:490–503. doi: 10.1200/jco.18.00358

29. Fan L, Yang Y, Chi C, Ma X, Wang R, Gong Y, et al. Neuroendocrine differentiation markers guide treatment sequence selection in metastatic castration-resistant prostate cancer. *Prostate*. (2019) 79:567–73. doi: 10.1002/pros.23762

30. Liu Y, Deng X, Wen Z, Huang J, Wang C, Chen C, et al. Comparing efficacy of first-line treatment of metastatic castration resistant prostate cancer: a network meta-analysis of randomized controlled trials. *Front Pharmacol*. (2023) 14:1290990. doi: 10.3389/fphar.2023.1290990

31. Krawczyk K, Śladowska K, Holko P, Kawalec P. Comparative safety of tyrosine kinase inhibitors in the treatment of metastatic renal cell carcinoma: a systematic review and network meta-analysis. *Front Pharmacol*. (2023) 14:1223929. doi: 10.3389/fphar.2023.1223929

32. Scher H, Armstrong A, Schonhoft J, Gill A, Zhao JL, Barnett E, et al. Development and validation of circulating tumour cell enumeration (Epic Sciences) as a prognostic biomarker in men with metastatic castration-resistant prostate cancer. *Eur J Cancer*. (2021) 150:83–94. doi: 10.1016/j.ejca.2021.02.042

33. Oeyen S, Liégeois V, De Laere B, Buys A, Strijbos M, Dirix P, et al. Automated enumeration and phenotypic characterization of CTCs and tdEVs in patients with metastatic castration resistant prostate cancer. *Prostate Cancer prostatic Dis*. (2021) 24:499–506. doi: 10.1038/s41391-020-00304-1

frontiers | Frontiers in Oncology

TYPE Original Research
PUBLISHED 28 May 2024
DOI 10.3389/fonc.2024.1370303

OPEN ACCESS

EDITED BY
Lei Yin,
Shanghai Jiaotong University School of Medicine, China

REVIEWED BY
Guglielmo Mantica,
San Martino Hospital (IRCCS), Italy
Xiaotian Tan,
Chinese Academy of Sciences (CAS), China

*CORRESPONDENCE
Katja Nitschke
Katja.Nitschke@medma.uni-heidelberg.de

RECEIVED 25 January 2024
ACCEPTED 09 May 2024
PUBLISHED 28 May 2024

CITATION
Uysal D, Thaqi B, Fierek A, Jurgowski D, Popovic ZV, Siegel F, Michel MS, Nuhn P, Worst TS, Erben P and Nitschke K (2024) Prognostic significance of EGFR, AREG and EREG amplification and gene expression in muscle invasive bladder cancer. *Front. Oncol.* 14:1370303. doi: 10.3389/fonc.2024.1370303

Prognostic significance of EGFR, AREG and EREG amplification and gene expression in muscle invasive bladder cancer

Daniel Uysal[1], Blerta Thaqi[1], Alexander Fierek[1], David Jurgowski[1], Zoran V. Popovic[2], Fabian Siegel[3], Maurice Stephan Michel[1], Philipp Nuhn[4], Thomas Stefan Worst[1], Philipp Erben[1] and Katja Nitschke[1]*

[1]Urologic Research Center, Department of Urology and Urosurgery, Medical Faculty Mannheim, University of Heidelberg, Mannheim, Germany, [2]Institute of Pathology, Medical Faculty Mannheim, University of Heidelberg, Mannheim, Germany, [3]Department of Biomedical Informatics at the Center for Preventive Medicine and Digital Health, Medical Faculty of Mannheim, University of Heidelberg, Mannheim, Germany, [4]Department of Urology, Universitätsklinikum Schleswig-Holstein (UKSH), Kiel, Germany

Introduction: Muscle invasive bladder cancer (MIBC) remains a prevalent cancer with limited therapeutic options, obviating the need for innovative therapies. The epidermal growth factor receptor (*EGFR*) is a linchpin in tumor progression and presents a potential therapeutic target in MIBC. Additionally, the *EGFR* ligands *AREG* and *EREG* have shown associations with response to anti-EGFR therapy and improved progression-free survival in colorectal carcinoma.

Materials and methods: We investigated the prognostic significance of *EGFR*, *AREG*, and *EREG* in MIBC. Gene expression and copy number analyses were performed via qRT-PCR on tissue samples from 100 patients with MIBC who underwent radical cystectomy at the University Hospital Mannheim (MA; median age 72, interquartile range [IQR] 64–78 years, 25% female). Results were validated in 361 patients from the 2017 TCGA MIBC cohort (median age 69, IQR 60–77 years, 27% female), in the Chungbuk and MDACC cohort. Gene expressions were correlated with clinicopathologic parameters using the Mann-Whitney test, Kruskal-Wallis- test and Spearman correlation. For overall survival (OS), cancer-specific survival (CSS) and disease-free survival (DFS) gene expression was analyzed with Kaplan-Meier and Cox-proportional hazard models.

Results: Significant gene expression differences in *EGFR*, *AREG*, and *EREG* could be detected in all cohorts. In the TCGA cohort, *EGFR* expression was significantly elevated in patients with EGFR amplification and KRAS wildtype. High *AREG* expression independently predicted longer OS (HR = 0.35, CI 0.19 - 0.63, p = 0.0004) and CSS (HR = 0.42, CI 0.18 – 0.95, p = 0.0378) in the MA cohort. In the TCGA cohort, high *EGFR*, *AREG*, and *EREG* expression correlated with shorter OS (*AREG*: HR = 1.57, CI 1.12 – 2.20, p = 0.0090) and DFS (*EGFR*: HR = 1.91, CI 1.31 – 2.8, p = 0.0008). *EGFR* amplification was also associated with reduced DFS.

Discussion: High *EGFR* and *EREG* indicate worse survival in patients with MIBC. The prognostic role of AREG should further be investigated in large, prospective

series. Divergent survival outcomes between the four cohorts should be interpreted cautiously, considering differences in analysis methods and demographics. Further *in vitro* investigations are necessary to elucidate the functional mechanisms underlying the associations observed in this study.

KEYWORDS

EGFR, AREG, EREG, bladder cancer, gene expression, survival

1 Introduction

In 2023, bladder cancer (BC) was expected to account for an estimated 82,290 new cases and 16,710 cancer-related deaths in the United States, making it the 4th most common and the 8th most deadly malignancy in men in the US (1). In Europe, BC is the 5th most common cancer with an incidence of more than 200,000 new cases per year (2). While 70% of BC are localized to the mucosa and submucosal tissues and thus classified as non-muscle invasive bladder cancer (NMIBC), 30% invade into the musculature (muscle invasive bladder cancer, MIBC). While the 5-year overall survival (OS) rate for NMIBC is 81%, this drops to 48% when the disease progresses to MIBC (3). Approximately 50% of patients with MIBC develop metastases and have a 5-year survival rate of about 5% (4). Radical cystectomy (RC) with pelvic lymphadenectomy, urinary diversion and in selected cases neoadjuvant chemotherapy, remains the treatment of choice for localized MIBC. In the past decade, treatment in the metastasized setting has evolved from platinum-based chemotherapy regimens to immune checkpoint inhibitors to now include antibody-drug conjugates such as Enfortumab-Vedotin and pan-FGFR inhibitors like Erdafitinib. While these new therapies have the potential to revolutionize the treatment of metastatic MIBC, not all patients will respond and ultimately resistances will arise. Thus, new additional biomarkers and molecular targets in MIBC are still urgently needed. The tyrosine kinase receptor epidermal growth factor receptor (*EGFR*) has been proposed as a potential target in BC, due to its routine therapeutic inhibition in metastatic colorectal carcinoma (mCRC) and non-small cell lung cancer (NSCLC) (5, 6). Immunohistochemistry (IHC) studies in BC showed a comparatively low EGFR expression in normal urothelium and up to 74% protein overexpression in BC, further highlighting the potential role of EGFR as a target in MIBC (7). So far, clinical trials targeting *EGFR* in BC could not convincingly show a benefit for *EGFR*-directed therapy, except for a small group of patients (8, 9). Preclinical studies by Rebouissou et al. support the hypothesis, that a subset of patients with BC will likely respond to *EGFR*-directed therapy (10). Based on these observations, Goodspeed et al. developed a gene signature from *EGFR*-inhibited mCRC data, that could predict the response of BC cell lines to *EGFR* inhibition (11). This signature included, Amphiregulin (*AREG*) and Epiregulin (*EREG*), two of the seven potential *EGFR* ligands, whose predictive role for *EGFR* inhibition and progression-free survival (PFS) has further been confirmed in mCRC (12–15). Based on these promising preclinical and clinical data, we investigated clinicopathologic and survival associations of *EGFR*, *AREG* and *EREG* gene expression and copy number alterations on OS, disease-free survival (DFS) and cancer-specific survival (CSS) in a cohort of patients with MIBC after RC from Mannheim, and on OS and DFS in a second cohort of patients with MIBC from the The Cancer Genome Atlas (TCGA) project (16). Furthermore, OS and CSS were further analyzed in patients with MIBC from the Chungbuk National University Hospital (17) and the MD Anderson Cancer Center (MDACC) MIBC cohort (18).

2 Materials and methods

2.1 Patients and methods

Four independent cohorts were included in this study. The first cohort consisted of patients with MIBC who underwent RC at the Department of Urology and Urosurgery at the University Medical Center Mannheim (MA) between 2008 and 2014. Patients with either no histologic evidence of residual malignancy after RC, NMIBC, non-urothelial histologic subtype, distant metastases at the time of RC or missing detection of the reference gene Calmodulin 2 (*Calm2*) were excluded from further analysis. Figure 1 shows the different stages of analysis with respective exclusion criteria of the MA cohort. Formalin-fixed paraffin-embedded (FFPE) tissue specimens and clinical data were collected in a retrospective study design which had been approved by the local ethics committee before the study (2015–549N-MA). All participants provided written informed consent. All procedures in this study were carried out in accordance with the 1964 declaration of Helsinki and its later amendments or comparable ethical standards. The other three cohort included patients with MIBC from the TCGA cell 2017 study by Robertson et al. (16), from the Chungbuk National University Hospital study by Kim et al. (17) and from an MDACC cohort by Choi et al. (18).

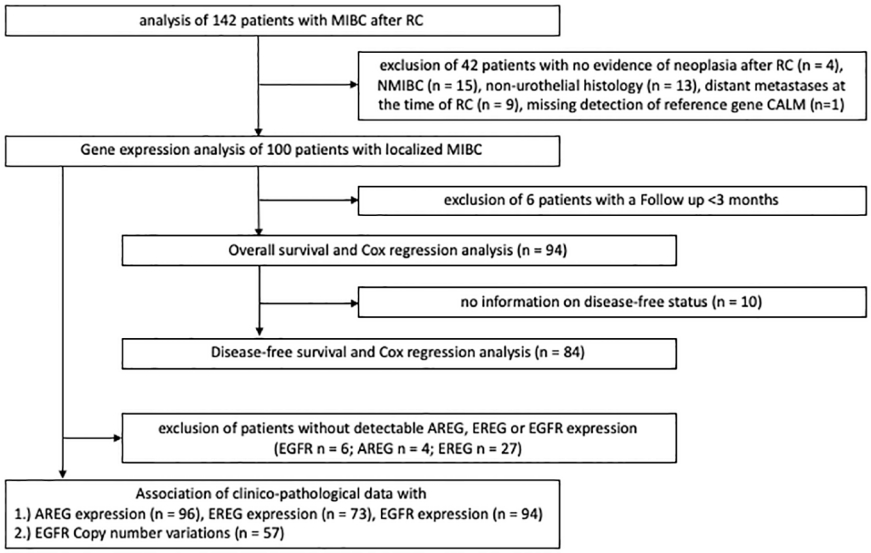

FIGURE 1
REMARK flow diagram of the exclusion criteria of the Mannheim cohort.

2.2 RNA extraction, cDNA synthesis and quantitative PCR analyses of the gene expressions and copy number alterations in patient samples from the MA cohort

All pathology specimens from the MA cohort were evaluated by the Institute of Pathology of the Medical Faculty Mannheim, University of Heidelberg. Tumor bearing FFPE tissue samples were stained with hematoxylin and eosin, examined by a board-certified uro-pathologist (ZVP) and graded according to the TNM classification (2017) and the WHO 2010/2016 classification of genitourinary tumors. RNA extraction was performed with the magnetic-based XTRAKT FFPE kit (Stratifyer, Cologne, Germany) according to the manufacturer's instructions. For the quantitative real-time polymerase chain reaction (qRT-PCR), RNA was reversely transcribed into cDNA with Sequence-specific reverse primers (reference gene *Calm2* and target genes *EGFR*, *AREG* and *EREG*), Superscript III reverse transcriptase (Thermo Fisher Scientific, Waltham, MA, USA) and supporting reagents were incubated at 55°C for 120 min with a subsequent enzyme deactivation step at 70°C for 15 min. cDNA was amplified through 40 cycles at 95°C for 3s and 60°C for 30s on a StepOnePlus qRT-PCR cycler (Applied Biosystems, Waltham, MA, USA). *Calm2* was used as a reference gene for normalization and gene expression determined using the 40-(ΔCt)-method (19). Supplementary Table S1 shows the primers and probes used in this study. Copy number alterations (CNA) in the MA cohort were measured using qPCR with TaqMan Assays according to the manufacturers' instructions (Supplementary Table S2). Predicted CNA values ≥3 were classified as amplification events.

2.3 *In silico* validation of findings

Findings were validated in patients with MIBC from the TCGA, the Chungbuk and the MDACC cohort (16–18). Figure 2 shows patient exclusion criteria at different stages of the analysis of the TCGA cohort. All TCGA data were downloaded from public repositories and have been produced in earlier analyses. CNA and gene expression data were downloaded from the Xenabrowser (https://xenabrowser.net) (20). Clinical data were downloaded from cBioPortal (https://www.cbioportal.org) (21, 22). Briefly, CNA data were generated using Affymetrix SNP6.0 arrays and mRNA gene expression data obtained through RNA Sequencing on an Illumina HiSeq. Data underwent further bioinformatic processing. CNA data were curated with the GISTIC2.0 algorithm and gene expression data quantified and normalized using RNA-Seq by Expectation Maximization (RSEM) and expressed as $\log_2$. CNA data ranged from -2 to 2, with the following nomenclature applied: -2: 2 copy del; -1: 1 copy del; 0: no change, 1: amplification, 2: high amplification. For the purposes of this study a GISTIC2.0 value of 2, or high amplification defined EGFR amplification. All other gene-level events (-2 to 1) were defined as non-amplification. Supplementary Figure S1 shows patient exclusion criteria for the Chungbuk and the MDACC cohorts. Similar exclusion criteria were applied as in the MA and TCGA cohort. Clinical and genomic data for the two cohorts were obtained from the Gene Expression Omnibus database (Chungbuk: GSE13507; MDACC: GSE48276) and were included as Supplementary Material. Gene expression in the Chungbuk cohort was measured using Illumina Human-6 BeadChip microarrays on RC specimens (17). Gene expression in the MDACC cohort was measured using FFPE TUR-B tissue samples on an Illumina HumanHT-12 WG-DASL V4.0 R2 expression beadchip (18).

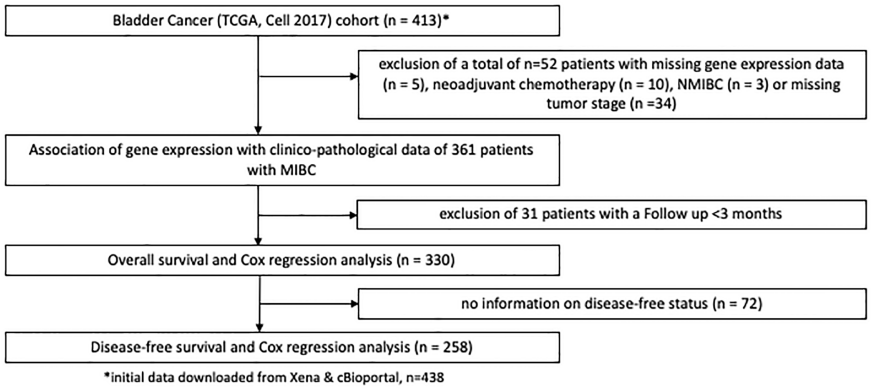

FIGURE 2
REMARK flow diagram of the exclusion criteria of the second study cohort based on the TCGA cell 2017 MIBC cohort.

2.4 Statistical analyses

Statistical analyses were performed using JMP16 (SAS, Cary, North Carolina, USA) and GraphPad Prism 9.0 (GraphPad Software Inc., La Jolla, California, USA). All p values were calculated for two sided tests with $p \leq 0.05$ regarded as statistically significant. Statistical analyses of numeric continuous variables following a non-normal distribution were performed with non-parametric tests (Mann-Whitney-Test, Kruskal-Wallis test). Spearman coefficient analysis was performed to assess gene correlations. Survival analyses were performed using the Kaplan-Meier method and differences between subgroups were tested for significance with the log-rank test. Cut-off values for high and low gene expression groups were provided by using the partition test, with each group representing at least 20% of the total cohort. Uni- und multivariable analyses were performed using Cox-proportional hazard regression models, accepting a cut-off value of $p < 0.2$ to include relevant clinical or pathologic variables into the multivariable analyses, that would have been missed with a more restrictive p value of ≤ 0.05.

3 Results

3.1 Patient demographics

After exclusion of 42 patients (from initially 142 patients) 100 patients with histologically confirmed urothelial MIBC (median age: 72, range: 64 – 78, 25% female patients, 72% locally advanced carcinomas (T3/4)) remained for the subsequent analyses in the MA cohort. In the TCGA MIBC cohort 361 patients could be evaluated after exclusion criteria were applied (median age: 69, range:60 – 77, 27% female patients, 68% T3/4 tumors). Furthermore, 55 patients with MIBC from the Chungbuk cohort (median age 66, IQR 60–73 years, 20% female) and 38 patients from the MDACC MIBC cohort (median age 68, IQR 60–72 years, 16% female) were analyzed after exclusion criteria (Supplementary Figure S1).

Demographic and clinicopathologic data of these cohorts are shown in Table 1. Baseline characteristics between the four cohorts were comparable except for a slightly higher percentage of patients with lymph node metastases (N+) in the TCGA cohort. At a median follow-up (f/u) of 39.5 months (range 3 – 180 months, n = 94) 60 patients in the MA cohort died during the f/u period. Of those 60 patients, 31 (52%) died of MIBC. Median f/u among surviving patients was 120 (72.5 – 142) months. In the TCGA cohort median f/u for surviving patients was 24.8 (14.8 – 53.4) months. Median f/u in the original Chungbuk cohort was 37 (1–137) months (17) and in the MDACC cohort median f/u was 45.2 (4 – 180) months.

3.2 Gene expression analysis

Overall, *EGFR* showed the highest gene expression across all four cohorts (MA: *EGFR* median CT value 37.54 (range 36.94 - 38.25), median CT value *AREG* 29.45 (range 27.99 – 30.39), median CT value *EREG* 29.80 (range 28.25 – 31.56); TCGA: *EGFR* 9.26 (range 7.94 – 10.45), *AREG* 7.04 (range 5.37 – 9.17), *EREG* 4.98 (range 2.78 – 8.09); Chungbuk: *EGFR* median value 8.18 (range 7.88 – 8.180), *AREG* median 7.01 (range 6.95 – 7.06), *EREG* median value 7.28 (range 7.15 – 7.39); MDACC: *EGFR* median value 12.99 (range 12.47 – 13.47), *AREG* median value 5.32 (range 5.17 – 5.42), *EREG* median value 7.97 (range 7.14 – 9.09), Figure 3). Comparing the median gene expression between *EGFR*, *AREG* and *EREG* revealed significant differences between the three genes across all cohorts ($p < 0.0001$ for all cohorts, Figure 3). *AREG* and *EREG* were inversely related between the two cohorts, with a higher *AREG* expression in the TCGA cohort, while AREG showed a lower expression compared to EREG in the other three cohorts. Although high amplification (AMP), compared to low or no amplifications (NOT) of *EGFR* in the TCGA cohort, resulted in a higher gene expression in all three genes, only *EGFR* reached a statistically significant difference (*EGFR*: AMP 13.38 (range 12.08 – 14.66) vs. NOT 9.11 (range 7.89 – 10.21); $p < 0.0001$, Supplementary Figure S2A). Among the 57 patients from the MA cohort with available CNA information on *EGFR* only marginal, non-significant differences in gene expression between the two groups could be observed (AMP vs. Not, Supplementary Figure S2B). Assessing the correlation between the three genes revealed a moderately positive correlation between *AREG* and

10.3389/fonc.2024.1370303

TABLE 1 Demographics of patients in the Mannheim (MA), the TCGA, the Chungbuk, and the MDACC cohort.

Characteristic	MA cohort (n = 100) n (%)	TCGA cohort (n = 361) n (%)	Chungbuk cohort (n=55) n (%)	MDACC cohort (n=38) n (%)
Age (years)*	72 (64 - 78)	69 (60- 77)	66 (60 – 73)	68 (60 – 72)
Gender				
Male	75 (75%)	264 (73%)	44 (80%)	32 (84%)
Female	25 (25%)	97 (27%)	11 (20%)	6 (16%)
Pathological T-stage				
T2	28 (28%)	117 (32%)	29 (53%)	10 (26%)
T3	55 (55%)	188 (52%)	18 (33%)	21 (55%)
T4	17 (17%)	56 (16%)	8 (15%)	7 (18%)
Lymph node metastases				
negative	73 (76%)	216 (64%)	45 (83%)	17 (45%)
positive	23 (24%)	122 (36%)	9 (17%)	21 (55%)
NA	4	23	1	

* median (range); NA, not available.

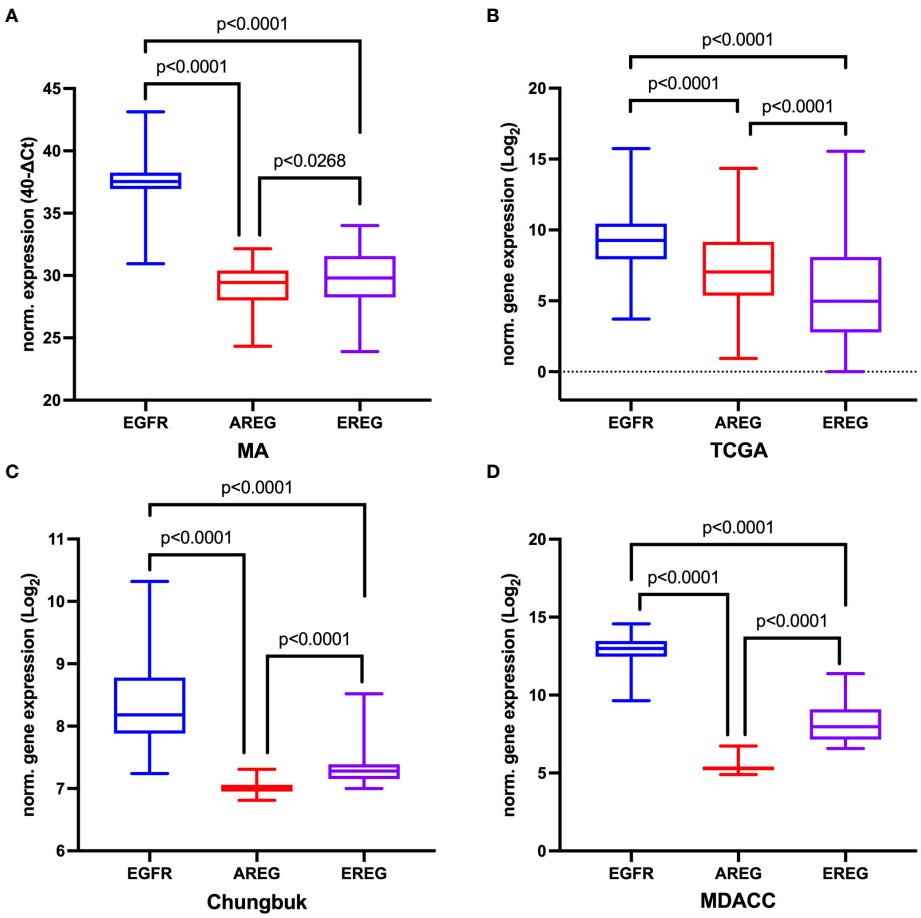

FIGURE 3
Comparison of normalized gene expression of *EGFR, AREG* and *EREG* **(A)** in the Mannheim cohort, **(B)** in the TCGA cell 2017 MIBC cohort, **(C)** in the Chungbuk cohort, and **(D)** in the MDACC cohort. The p value from the Kruskal-Wallis test between all three genes was p<0.0001. For comparisons between two genes the Mann-Whitney-Test was used.

EREG in the MA cohort (Spearman ρ = 0.4960, p < 0.0001) and a highly positive correlation in the TCGA cohort (Spearman ρ = 0.7333, p < 0.0001). *EGFR* and both of its ligands were weakly correlated across both cohorts (Supplementary Figure S3). In the other cohorts, *AREG* and *EREG* were only weakly correlated (Chungbuk: Spearman ρ = 0.0091, p = 0.9472; MDACC: Spearman ρ = 0.0594, p = 0.7231). In the MDACC cohort, *EGFR* and *EREG* showed a weak positive correlation (Spearman ρ = 0.3457, p = 0.0335) (Supplementary Table S3).

3.3 Association with clinicopathologic data

In the TCGA cohort, T3/4 was correlated with a statistically significant increase in *EGFR* and *EREG* expression (*EGFR* p = 0.0176, *EREG* p = 0.0136, Figure 4A). However, this association could not be confirmed in the other three cohorts. Patients from the MA cohort with the presence of lymphovascular invasion (LVI) had a significantly lower *AREG* expression compared to patients without LVI (*AREG* 6.87 (range 5.37 – 8.69) vs. 7.78 (range 4.57 – 9.76); p = 0.0221, Figure 4B). Exploratory analysis of patients with a basal molecular subtype revealed a significantly higher gene expression for *EGFR* and both its ligands in patients with the basal molecular subtype (p < 0.0001 for each gene, Figure 4C). An exploratory analysis of the gene expression according to *KRAS* mutation status in the TCGA cohort showed a statistically significant higher expression of *EGFR* in patients with *KRAS* wildtype (vs. *KRAS* mutation; *EGFR* 9.35 (range 8.13 – 10.48) vs. 7.66 (range 6.59 – 8.53), p = 0.0002, Figure 4D). Further associations of the gene expressions with the investigated clinicopathologic characteristics are reported in Supplementary Tables S4, S5. In the Chungbuk cohort, N+ was associated with a significantly higher median *EGFR* expression (*EGFR* 8.37 (range 8.17 – 9.04) vs. 8.02 (range 7.24 – 10.32), p = 0.0485). In the MDACC cohort, female patients had a significantly higher *EGFR* expression (p = 0.0039) and patients with a basal molecular subtype had a significantly higher *EGFR* (p = 0.0053) and *EREG* expression (p = 0.0061).

3.4 Survival analyses

To evaluate the prognostic impact of *EGFR*, *AREG* and *EREG* expression on OS and CSS in the Chungbuk and MDACC, as well as OS, CSS and DFS in the MA cohort, and OS and DFS in the TCGA cohort, Kaplan-Meier analyses and cox proportional hazard ratios (HR) were used Figures 5, 6. In the MA cohort, a high *AREG* expression was associated with a longer OS (n = 94, median survival (high vs. low) 85 vs. 14 months, p < 0.0001, Figure 5B) and CSS (n = 84, median survival (high vs low) undefined (since the probability of survival exceeds 50% at the most distant time point measured) vs. 21 months, p = 0.0011, Figure 5E). Like *AREG*, a high *EREG* expression was associated with improved OS (n = 94, median survival (high vs. low) 76 vs. 20 months, p = 0.0488, Figure 5C) and improved CSS (n = 84, median survival (high vs. low) undefined vs. 30 months, p = 0.0242, Figure 5E). No statistically significant data for DFS were observed in the MA cohort (data not shown). In the TCGA cohort, a high *EGFR*, *AREG* and *EREG*

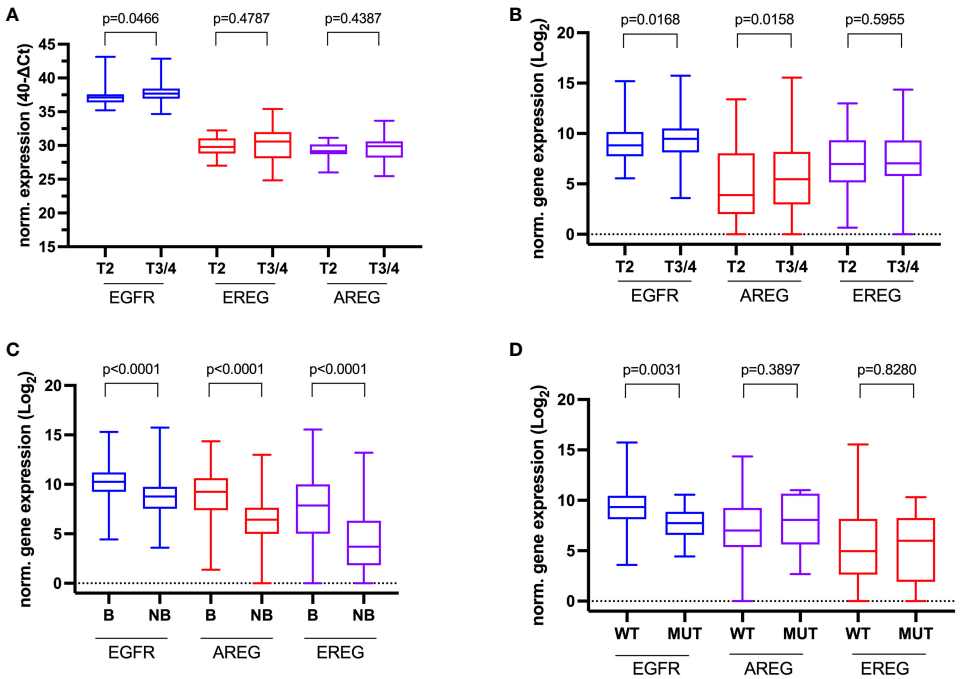

FIGURE 4
Association of clinicopathologic data with normalized gene expression. **(A)** Tumor stage in the Mannheim cohort, **(B)** Tumor stage in the TCGA cell 2017 MIBC cohort, **(C)** Molecular subtype (Basal **(B)** vs. Non-basal (NB) in the TCGA cell 2017 MIBC cohort, and **(D)** KRAS-Mutation status (wildtype (WT) vs. mutated (MUT) in the TCGA cell 2017 MIBC cohort.

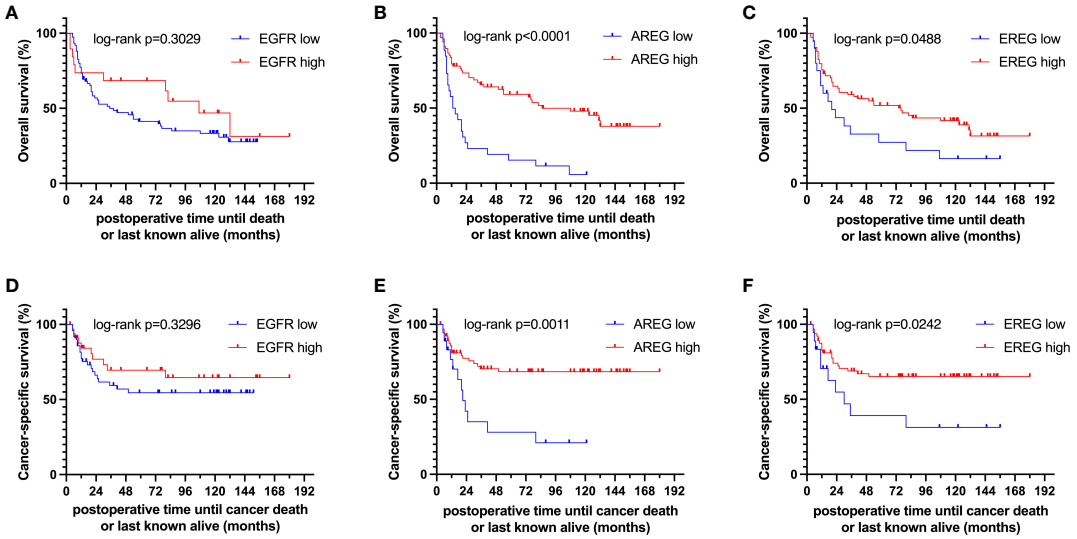

FIGURE 5
Kaplan-Meier curves of **(A–C)** overall survival (OS) and **(D–F)** cancer-specific survival (CSS) of *EGFR, AREG* and *EREG* in patients with MIBC from the Mannheim cohort.

geneexpression was associated with shorter OS for all three genes (n = 330, *EGFR*: median survival (high vs. low) 27 vs. 87 months, p = 0.0003; *AREG*: median survival (high vs. low) 33 vs. 87 months, p = 0.0084, *EREG*, median survival (high vs. low) 33 vs. 59 months, p = 0.0376, Figures 6A–C). The association of worse survival with a high gene expression was maintained on DFS for all three genes but only reached statistical significance for *EGFR* (*EGFR*: n = 258, median survival (high vs. low) 28 vs. 81 months, p = 0.0007, Figures 6D, E). In the Chungbuk cohort, a high *EGFR* expression was associated with worse OS (*EGFR*: n = 54, median survival (high vs. low) 10 vs. 66 months, p = 0.0008; Supplementary Figure S4A). Due to the small sample size in the MDACC MIBC cohort (n=38), the observed survival effects could not be adequately evaluated. Univariable analysis of the MA cohort revealed locally advanced T stage (T3/4) and N+ to be associated with shorter OS, while a high *AREG* expression (HR = 0.30, CI 0.18 – 0.52, p < 0.0001) was associated with longer OS (Table 2). A high *EREG* expression (HR = 0.57 CI 0.32 – 1.01, p=0.0538) was similarly associated with a trend for improved OS, but no statistical significance could be reached (Table 2). On multivariable analysis of OS in the MA cohort, advanced T stages and N+ were associated with a worse outcome, while *AREG* (HR = 0.35, CI 0.19 - 0.63, p = 0.0004) maintained its association with improved survival (Table 2). Regarding CSS in the MA cohort, univariable analysis showed T3/4 and N+ to be

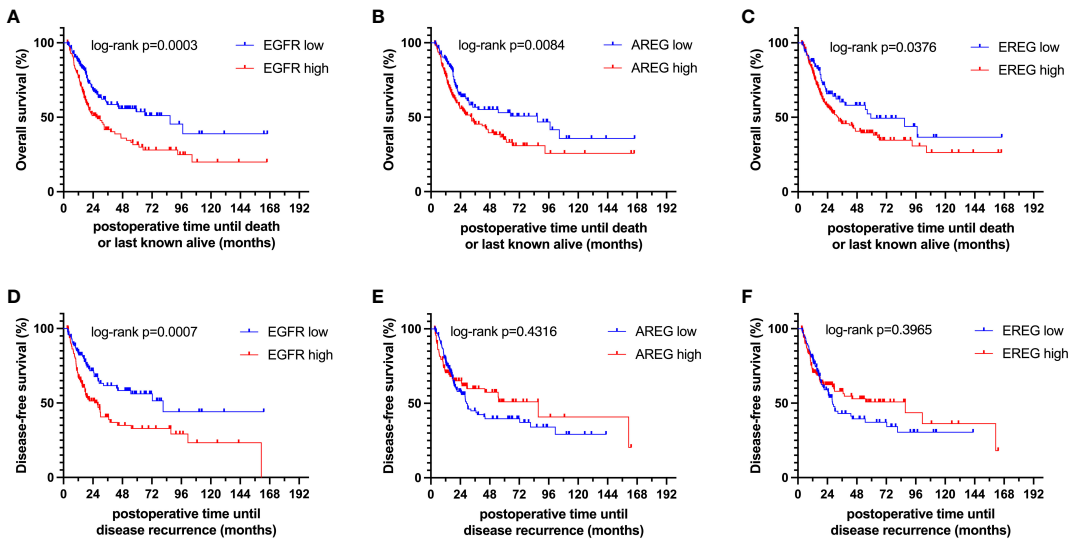

FIGURE 6
Kaplan-Meier curves of **(A–C)** overall survival (OS) and **(D–F)** disease-free survival (DFS) of *EGFR, AREG* and *EREG* in patients with MIBC from the TCGA cell 2017 MIBC cohort.

TABLE 2 Uni- and multivariable cox regression analyses of gene expression and clinicopathological parameters regarding overall survival (OS) in patients with MIBC after radical cystectomy (RC) in the MA cohort.

Parameter	Univariable analysis		Multivariable analysis	
	P value	HR (95% CI)	P value	HR (95% CI)
Gender (female vs. male)	0.4606	1.24 (0.69 – 2.19)	–	–
Age (≥70 years vs. <70 years)	0.1489	1.48 (0.87 – 2.53)	0.0753	1.65 (0.95 – 2.88)
T stage (T3/4 vs. T2)	**0.0013**	2.93 (1.52 – 5.66)	**0.0065**	2.62 (1.31 – 5.25)
N stage (positive vs. negative)	**0.0051**	2.26 (1.28 – 3.99)	**0.0086**	2.27 (1.23 – 4.2)
EGFR copy number (AMP vs. NONAMP)	0.8689	0.94 (0.48 – 1.86)	–	–
EGFR expression (high vs. low)	0.3088	0.70 (0.36 – 1.39)		
AREG expression (high vs. low)	**<0.0001**	0.30 (0.18 – 0.52)	**0.0004**	0.35 (0.19 - 0.63)
EREG expression (high vs. low)	0.0538	0.57 (0.32 – 1.01)	0.7350	0.90 (0.48 – 1.67)

Significant p-values are highlighted in bold.

associated with shorter CSS while a high *AREG* (HR = 0.32, CI 0.15 – 0.66, p=0.0021) and *EREG* (HR = 0.43, CI 0.20 - 0.92, p=0.0296) expression correlated with improved CSS (Table 3). In the multivariable analysis, the *AREG* expression (HR = 0.42, CI 0.18 - 0.95, p = 0.0378) remained as the only significant predictor of better CSS (Table 3). In the univariable analysis of the TCGA cohort, age, T3/4, N+ and high *EGFR*, *AREG* and *EREG* gene expression (EGFR: HR = 1.81, CI 1.30 – 2.52, p = 0.0004; AREG: HR = 1.57, CI 1.12 – 2.20, p = 0.0090; EREG: HR = 1.48, CI 1.02 – 2.15, p = 0.0389) were significant prognostic factors for shorter OS (Table 4). Except for *EREG* this negative survival association was maintained for all of the variables included in the multivariable model (Table 4). Univariable analysis of DFS in the TCGA cohort showed worse DFS with T3/4, N+, *EGFR* amplification (HR = 2.49, CI 1.26 – 4.95, p = 0.0389) and

TABLE 3 Uni- and multivariable cox regression analyses of different parameters regarding cancer-specific survival (CSS) in patients with MIBC after RC in the MA cohort.

Parameter	Univariable analysis		Multivariable analysis	
	P value	HR (95% CI)	P value	HR (95% CI)
Gender (male vs. female)	0.4900	0.76 (0.35 – 1.65)		
Age (<70 years vs. ≥70 years)	0.9890	0.10 (0.49 – 2.03)		
T stage (T3/4 vs. T2)	**0.0195**	3.14 (1.20 – 8.21)	0.3258	1.34 (0.75 – 2.41)
N stage (positive vs. negative)	**0.0069**	2.85 (1.33 – 6.10)	0.2248	0.60 (0.26 – 1.37)
EGFR copy number (AMP vs. NONAMP)	0.2517	0.53 (0.18 – 1.57)		
EGFR expression (high vs. low)	0.33353	0.69 (0.33 - 1.47)		
AREG expression (high vs. low)	**0.0021**	0.32 (0.15 – 0.66)	**0.0378**	0.42 (0.18 - 0.95)
EREG expression (high vs. low)	**0.0296**	0.43 (0.20 - 0.92)	0.3993	1.41 (0.64 – 3.11)

Significant p-values are highlighted in bold.

TABLE 4 Uni- and multivariable cox regression analyses of different parameters regarding OS in patients of the TCGA cohort.

Parameter	Univariable analysis		Multivariable analysis	
	P value	HR (95% CI)	P value	HR (95% CI)
Gender (male vs. female)	0.3833	0.85 (0.60 – 1.22)		
Age (≥70 years vs. <70 years)	**0.0068**	1.57 (1.13 – 2.16)	**0.0052**	1.63 (1.16 – 2.29)
T stage (T3/4 vs. T2)	**0.0002**	2.12 (1.43 – 3.15)	**0.0168**	1.71 (1.10 – 2.65)
N stage (positive vs. negative)	**<0.0001**	2.25 (1.54 – 3.30)	**<0.0001**	2.04 (1.45 – 2.89)
EGFR copy number (AMP vs. NONAMP)	0.2378	1.50 (0.76 – 2.96)		
EGFR expression (high vs. low)	**0.0004**	1.81 (1.30 – 2.52)	**0.0150**	1.57 (1.09 – 2.26)
AREG expression (high vs. low)	**0.0090**	1.57 (1.12 – 2.20)	**0.0286**	1.60 (1.05 – 2.43)
EREG expression (high vs. low)	**0.0389**	1.48 (1.02 – 2.15)	0.8535	1.04 (0.66 – 1.66)

Significant p-values are highlighted in bold.

a high *EGFR* expression (HR = 1.91, CI 1.31 – 2.80, p = 0.0008, Table 5). While the association of *EGFR* amplification with a shorter DFS could not withstand in the multivariable analysis, T3/4, N+ and a high *EGFR* gene expression (HR = 1.73, CI 1.14 – 2.62, p = 0.0094) remained significant independent factors for a worse DFS (Table 5). In the Chungbuk cohort, a higher *AREG* expression was associated with a trend towards better OS (HR = 0.45, CI 0.19 – 1.08, p = 0.0735) on univariable analysis and a significant predictor of better OS (HR = 0.31, CI 0.11 – 0.87, p = 0.0257) in the multivariable OS analysis (Supplementary Table S6).

4 Discussion

In this study, the gene expression of *EGFR*, *AREG* and *EREG* in patients with MIBC, the association of gene expression with clinicopathologic variables of known prognostic impact in MIBC and the correlation of *EGFR*, *AREG* and *EREG* gene expression with survival and progression were investigated.

It was found that high *AREG* expression independently influenced the prediction of significantly longer OS and CSS in the MA (no significant survival associations for DFS) and longer OS

TABLE 5 Uni- and multivariable cox regression analyses of different parameters regarding DFS in patients with MIBC after RC in the TCGA cohort.

Parameter	Univariable analysis		Multivariable analysis	
	P value	HR (95% CI)	P value	HR (95% CI)
Gender (male vs. female)	0.5637	0.89 (0.60 – 1.33)		
Age (≥70 years vs. <70 years)	0.2828	1.22 (0.85 – 1.77)		
T stage (T3/4 vs. T2)	**<0.0001**	2.52 (1.61 – 3.92)	**0.0039**	2.08 (1.27 – 3.43)
N stage (positive vs. negative)	**<0.0001**	2.15 (1.54 – 3.02)	**0.0008**	1.95 (1.32 – 2.87)
EGFR copy number (AMP vs. NONAMP)	**0.0090**	2.49 (1.26 – 4.95)	0.1186	1.88 (0.85 – 4.14)
EGFR expression (high vs. low)	**0.0008**	1.91 (1.31 – 2.80)	**0.0094**	1.73 (1.14 – 2.62)
AREG expression (high vs. low)	0.4322	0.86 (0.58 – 1.26)		
EREG expression (high vs. low)	0.3972	0.85 (0.59 – 1.23)		

Significant p-values are highlighted in bold.

in the Chungbuk cohort. In the TCGA cohort, a high *EGFR*, *AREG* and *EREG* expression were associated with worse OS and DFS. While this association was maintained for *EGFR* and *EREG* in the Chungbuk cohort, a high *EGFR* expression shifted from worse to better CSS prognosis in the Chungbuk cohort. The contradictory nature of these survival results in the three cohorts can partly be attributed to differences in analysis methods (qRT-PCR in the MA cohort, RNA-Seq in the TCGA cohort and microarray gene expression profiling in the Chungbuk cohort) and demographic baseline characteristics. We chose qRT-PCR in favor of IHC to analyze the gene expression, because the former method is free of inter-rater variability and proposed to be a more sensitive and unbiased method (23, 24). Additionally, patients' treatments may further influence differences in gene expression profiles between individual cohorts. We compared the median gene expression of *EGFR*, *AREG* and *EREG* in patients with and without adjuvant chemotherapy in the MA cohort using the Mann-Whitney-Test, but could not find any statistically significant differences between both groups (data not shown).

Our observation that a high *AREG* expression was independently associated with better OS and CSS in the MA cohort is supported by data from Khambata-Ford et al., who found high expression levels of *AREG* and *EREG* on GeneChips and qRT-PCR to be associated with a significantly prolonged PFS under Cetuximab monotherapy (12). Correlation analysis further revealed *AREG* and *EREG* expression to be moderately (MA) and highly (TCGA) correlated with each other, which is in line with findings by Khambata-Ford et al. from mCRC and mostly attributable to colocalization of *AREG* and *EREG* on chromosome 4q13.3 (25). The observed weak correlation between *EGFR* and the two ligands could be explained by the ligand-receptor interaction, with EREG known to bind weaker to EGFR than other ligands but eliciting a stronger and prolonged EGFR activation (26, 27)

Biologically, elevated *AREG* and *EREG* expression have been postulated to stimulate an autocrine loop through EGFR leading Khambata-Ford et al. to hypothesize that these ligands are surrogate markers for an activated EGFR pathway, and potentially a positive feedback loop with EGFR (12). This hypothesis would be supported by our results of worse OS and DFS with a high expression of *AREG*, *EREG* and *EGFR* in the TCGA cohort.

As expected, *EGFR* gene expression was higher than that of its ligands in both cohorts and *EGFR* amplification events were associated with an increase in the expression of all three genes, while only *EGFR* was significantly differently expressed in the TCGA cohort. These findings correspond to the fact that, similar to CRC, activating mutations of *EGFR* in MIBC are rare, and *EGFR* expression is mainly regulated via *EGFR* amplification (12, 14).

Correlation with clinicopathologic data revealed advanced T stages T3/4 (TCGA: *EGFR* and *EREG*) and LVI (MA: *AREG*) to be the only variables associated with significant differences in gene expression. Further mechanistic studies are needed to ascertain if gene expression of *EGFR* and *EREG*/*AREG* truly drives local tumor growth, metastasis, and invasion or whether the observed differences are merely a bystander effect of the increased neoplastic microenvironment activity.

Interestingly, *EGFR*, although not statistically significant, was associated with better OS and CSS in the MA cohort, which corresponds to findings from mCRC showing no association of mRNA expression levels of *EGFR* and other *EGFR*-ligands (except for AREG and EREG) with disease control under Cetuximab (12).

Although a multitude of urinary and blood-based biomarkers exist to detect, monitor and control treatment response in NMIBC, survival prognosis for MIBC after RC is largely based on conventional imaging (CT and MRI scans). Since the gain of EGFR function is an established genomic event in the progression to MIBC, increased EGFR gene expression or amplification from FFPE tissue at the time of RC could be used as an additional marker for tumor aggressiveness besides histopathology and potentially serve as a biomarker (28). Smalley et al. used mass spectrometry to identify potential biomarkers on microparticles in the urine of patients with BC. They were able to show that 5 of the 8 detected proteins were associated with the EGFR pathway (29, 30). Other growth factors, such as the vascular endothelial growth factor A, which is part of the Oncuria® multiplex immunoassay (31), and the fibroblast growth factor 3 (FGFR3), which is part of the FDA-approved Uromonitor test® (32), are currently used in the context of urinary biomarker assays in clinical practice for NMIBC (33). While the above-mentioned markers were derived from urine, there is a clinical application for biomarkers evaluated by qRT-PCR of FFPE tissue samples, since FGFR3 mutations and FGFR2/3 gene fusions, which are currently used to guide the use of the pan-FGFR-inhibitor Erdafitinib for metastatic BC, are assessed using qRT-PCR of FFPE tissue samples (34).

Limitations of this study include its retrospective nature, varying gene expression detection and normalization methods between the MA and the TCGA cohort. Comparisons to other trials are limited through our endpoint selection of OS, CSS and DFS contrary to PFS and treatment response to anti-EGFR therapy. However, to our knowledge this is the first trial to date to assess clinicopathologic and survival associations of *AREG* and *EREG* in patients with MIBC.

Ultimately, the different findings between the MA and TCGA cohorts will need to be further investigated, as differences in used methodology, the existence of splice variants and differences in cohorts are potential biases to a validation. Further *in vitro* studies are needed to examine the nature of the EGFR-AREG/EREG relationship at a molecular level in MIBC.

AREG and EREG are promising prognostic markers in MIBC. Validation in the TCGA and Chungbuk cohort shows diverging survival results. Further *in vitro* studies at the molecular level are needed to explore the nature of the EGFR-AREG/EREG interaction and its potential impact on BC cancer biology and survival.

Data availability statement

The datasets presented in this study can be found in online repositories. The names of the repository/repositories and accession number(s) can be found in the article/Supplementary Material.

Ethics statement

The studies involving humans were approved by review board 2 of the University of Heidelberg under the number 2015- 549N-MA. The studies were conducted in accordance with the local legislation and institutional requirements. The participants provided their written informed consent to participate in this study.

Author contributions

DU: Conceptualization, Data curation, Formal analysis, Investigation, Methodology, Visualization, Writing – original draft, Writing – review & editing. BT: Data curation, Writing – review & editing. AF: Data curation, Writing – review & editing. DJ: Data curation, Writing – review & editing. ZP: Data curation, Writing – review & editing. FS: Formal analysis, Writing – review & editing. MM: Writing – review & editing. PN: Writing – review & editing. TW: Writing – review & editing. PE: Conceptualization, Supervision, Writing – review & editing. KN: Conceptualization, Data curation, Formal analysis, Investigation, Writing – original draft, Writing – review & editing.

Funding

The author(s) declare financial support was received for the research, authorship, and/or publication of this article. Except for institutional funding for the Urologic Research Laboratory no additional funding for this project was received.

Acknowledgments

We would like to thank all the patients who participated in this study. Additionally, we would like to thank and to acknowledge Annette Steidler for her technical and intellectual assistance in conducting the experiments.

Conflict of interest

The authors declare that the research was conducted in the absence of any commercial or financial relationships that could be construed as a potential conflict of interest.

Publisher's note

Supplementary material

The Supplementary Material for this article can be found online at: https://www.frontiersin.org/articles/10.3389/fonc.2024.1370303/full#supplementary-material

References

1. Siegel RL, Miller KD, Wagle NS, Jemal A. Cancer statistics, 2023. *CA Cancer J Clin*. (2023) 73:17–48. doi: 10.3322/caac.21763

2. Sung H, Ferlay J, Siegel RL, Laversanne M, Soerjomataram I, Jemal A, et al. Global cancer statistics 2020: GLOBOCAN estimates of incidence and mortality worldwide for 36 cancers in 185 countries. *CA Cancer J Clin*. (2021) 71:209–49. doi: 10.3322/caac.21660

3. Miller KD, Siegel RL, Lin CC, Mariotto AB, Kramer JL, Rowland JH, et al. Cancer treatment and survivorship statistics, 2016. *CA Cancer J Clin*. (2016) 66:271–89. doi: 10.3322/caac.21349

4. Stein JP, Lieskovsky G, Cote R, Groshen S, Feng AC, Boyd S, et al. Radical cystectomy in the treatment of invasive bladder cancer: long-term results in 1,054 patients. *J Clin Oncol*. (2001) 19:666–75. doi: 10.1200/JCO.2001.19.3.666

5. Arnold D, Lueza B, Douillard JY, Peeters M, Lenz HJ, Venook A, et al. Prognostic and predictive value of primary tumor side in patients with RAS wild-type metastatic colorectal cancer treated with chemotherapy and EGFR directed antibodies in six randomized trials. *Ann Oncol*. (2017) 28:1713–29. doi: 10.1093/annonc/mdx175

6. Ramalingam SS, Vansteenkiste J, Planchard D, Cho BC, Gray JE, Ohe Y, et al. Overall survival with osimertinib in untreated, EGFR-mutated advanced NSCLC. *N Engl J Med*. (2020) 382:41–50. doi: 10.1056/NEJMoa1913662

7. Chaux A, Cohen JS, Schultz L, Albadine R, Jadallah S, Murphy KM, et al. High epidermal growth factor receptor immunohistochemical expression in urothelial carcinoma of the bladder is not associated with EGFR mutations in exons 19 and 21: a study using formalin-fixed, paraffin-embedded archival tissues. *Hum Pathol*. (2012) 43:1590–5. doi: 10.1016/j.humpath.2011.11.016

8. Hussain M, Daignault S, Agarwal N, Grivas PD, Siefker-Radtke AO, Puzanov I, et al. A randomized phase 2 trial of gemcitabine/cisplatin with or without cetuximab in patients with advanced urothelial carcinoma. *Cancer*. (2014) 120:2684–93. doi: 10.1002/cncr.28767

9. Wulfing C, Machiels JP, Richel DJ, Grimm MO, Treiber U, De Groot MR, et al. A single-arm, multicenter, open-label phase 2 study of lapatinib as the second-line treatment of patients with locally advanced or metastatic transitional cell carcinoma. *Cancer*. (2009) 115:2881–90. doi: 10.1002/cncr.24337

10. Rebouissou S, Bernard-Pierrot I, de Reynies A, Lepage ML, Krucker C, Chapeaublanc E, et al. EGFR as a potential therapeutic target for a subset of muscle-invasive bladder cancers presenting a basal-like phenotype. *Sci Transl Med*. (2014) 6:244ra91. doi: 10.1126/scitranslmed.3008970

11. Goodspeed A, Jean A, Theodorescu D, Costello JC. A gene expression signature predicts bladder cancer cell line sensitivity to EGFR inhibition. *Bladder Cancer*. (2018) 4:269–82. doi: 10.3233/BLC-170161

12. Khambata-Ford S, Garrett CR, Meropol NJ, Basik M, Harbison CT, Wu S, et al. Expression of epiregulin and amphiregulin and K-ras mutation status predict disease control in metastatic colorectal cancer patients treated with cetuximab. *J Clin Oncol*. (2007) 25:3230–7. doi: 10.1200/JCO.2006.10.5437

13. Seligmann JF, Elliott F, Richman SD, Jacobs B, Hemmings G, Brown S, et al. Combined epiregulin and amphiregulin expression levels as a predictive biomarker for panitumumab therapy benefit or lack of benefit in patients with RAS wild-type advanced colorectal cancer. *JAMA Oncol*. (2016) 2:633–42. doi: 10.1001/jamaoncol.2015.6065

14. Jacobs B, De Roock W, Piessevaux H, Van Oirbeek R, Biesmans B, De Schutter J, et al. Amphiregulin and epiregulin mRNA expression in primary tumors predicts outcome in metastatic colorectal cancer treated with cetuximab. *J Clin Oncol*. (2009) 27:5068–74. doi: 10.1200/JCO.2008.21.3744

15. Erben P, Wezel F, Wirtz R, Martini T, Stein D, Weis CA, et al. Role of the human ErbB family receptors in urothelial carcinoma of the bladder: mRNA expression status and prognostic relevance. *Aktuelle Urol*. (2017) 48:356–62. doi: 10.1055/s-0043–110403

16. Robertson AG, Kim J, Al-Ahmadie H, Bellmunt J, Guo G, Cherniack AD, et al. Comprehensive molecular characterization of muscle-invasive bladder cancer. *Cell*. (2017) 171:540–56. doi: 10.1016/j.cell.2017.09.007

17. Kim WJ, Kim EJ, Kim SK, Kim YJ, Ha YS, Jeong P, et al. Predictive value of progression-related gene classifier in primary non-muscle invasive bladder cancer. *Mol Cancer*. (2010) 9:3. doi: 10.1186/1476–4598-9–3

18. Choi W, Porten S, Kim S, Willis D, Plimack ER, Hoffman-Censits J, et al. Identification of distinct basal and luminal subtypes of muscle-invasive bladder cancer with different sensitivities to frontline chemotherapy. *Cancer Cell*. (2014) 25:152–65. doi: 10.1016/j.ccr.2014.01.009

19. Breyer J, Otto W, Wirtz RM, Wullich B, Keck B, Erben P, et al. ERBB2 Expression as Potential Risk-Stratification for Early Cystectomy in Patients with pT1 Bladder Cancer and Concomitant Carcinoma in *situ*. *Urol Int*. (2017) 98:282–9. doi: 10.1159/000453670

20. Goldman MJ, Craft B, Hastie M, Repecka K, McDade F, Kamath A, et al. Visualizing and interpreting cancer genomics data via the Xena platform. *Nat Biotechnol*. (2020) 38:675–8. doi: 10.1038/s41587–020-0546–8

21. Cerami E, Gao J, Dogrusoz U, Gross BE, Sumer SO, Aksoy BA, et al. The cBio cancer genomics portal: an open platform for exploring multidimensional cancer genomics data. *Cancer Discovery*. (2012) 2:401–4. doi: 10.1158/2159–8290.CD-12–0095

22. Gao J, Aksoy BA, Dogrusoz U, Dresdner G, Gross B, Sumer SO, et al. Integrative analysis of complex cancer genomics and clinical profiles using the cBioPortal. *Sci Signal*. (2013) 6:pl1. doi: 10.1126/scisignal.2004088

23. Eckstein M, Wirtz RM, Pfannstil C, Wach S, Stoehr R, Breyer J, et al. A multicenter round robin test of PD-L1 expression assessment in urothelial bladder cancer by immunohistochemistry and RT-qPCR with emphasis on prognosis prediction after radical cystectomy. *Oncotarget*. (2018) 9:15001–14. doi: 10.18632/oncotarget.24531

24. Tyekucheva S, Martin NE, Stack EC, Wei W, Vathipadiekal V, Waldron L, et al. Comparing platforms for messenger RNA expression profiling of archival formalin-fixed, paraffin-embedded tissues. *J Mol Diagn*. (2015) 17:374–81. doi: 10.1016/j.jmoldx.2015.02.002

25. Conti M, Hsieh M, Park JY, Su YQ. Role of the epidermal growth factor network in ovarian follicles. *Mol Endocrinol*. (2006) 20:715–23. doi: 10.1210/me.2005–0185

26. Shelly M, Pinkas-Kramarski R, Guarino BC, Waterman H, Wang LM, Lyass L, et al. Epiregulin is a potent pan-ErbB ligand that preferentially activates heterodimeric receptor complexes. *J Biol Chem*. (1998) 273:10496–505. doi: 10.1074/jbc.273.17.10496

27. Freed DM, Bessman NJ, Kiyatkin A, Salazar-Cavazos E, Byrne PO, Moore JO, et al. EGFR ligands differentially stabilize receptor dimers to specify signaling kinetics. *Cell*. (2017) 171:683–95. doi: 10.1016/j.cell.2017.09.017

28. Batista R, Vinagre N, Meireles S, Vinagre J, Prazeres H, Leao R, et al. Biomarkers for bladder cancer diagnosis and surveillance: A comprehensive review. *Diagnostics (Basel)*. (2020) 10:1–19. doi: 10.3390/diagnostics10010039

29. Smalley DM, Sheman NE, Nelson K, Theodorescu D. Isolation and identification of potential urinary microparticle biomarkers of bladder cancer. *J Proteome Res*. (2008) 7:2088–96. doi: 10.1021/pr700775x

30. Oliveira MC, Caires HR, Oliveira MJ, Fraga A, Vasconcelos MH, Ribeiro R. Urinary biomarkers in bladder cancer: where do we stand and potential role of extracellular vesicles. *Cancers (Basel)*. (2020) 12:1–30. doi: 10.3390/cancers12061400

31. Hirasawa Y, Pagano I, Chen R, Sun Y, Dai Y, Gupta A, et al. Diagnostic performance of Oncuria, a urinalysis test for bladder cancer. *J Transl Med*. (2021) 19:141. doi: 10.1186/s12967–021-02796–4

32. Sieverink CA, Batista RPM, Prazeres HJM, Vinagre J, Sampaio C, Leao RR, et al. Clinical validation of a urine test (Uromonitor-V2((R))) for the surveillance of non-muscle-invasive bladder cancer patients. *Diagnostics (Basel)*. (2020) 10:1–11. doi: 10.3390/diagnostics10100745

33. Malinaric R, Mantica G, Lo Monaco L, Mariano F, Leonardi R, Simonato A, et al. The role of novel bladder cancer diagnostic and surveillance biomarkers-what should a urologist really know? *Int J Environ Res Public Health*. (2022) 19:1–20. doi: 10.3390/ijerph19159648

34. Loriot Y, Necchi A, Park SH, Garcia-Donas J, Huddart R, Burgess E, et al. Erdafitinib in locally advanced or metastatic urothelial carcinoma. *N Engl J Med*. (2019) 381:338–48. doi: 10.1056/NEJMoa1817323

frontiers | Frontiers in Pharmacology

TYPE Review
PUBLISHED 30 May 2024
DOI 10.3389/fphar.2024.1399802

OPEN ACCESS

EDITED BY
Huan Yang,
Huazhong University of Science and Technology, China

REVIEWED BY
Jagpreet Singh Nanda,
Cedars Sinai Medical Center, United States
Yupeng Wu,
First Affiliated Hospital of Fujian Medical University, China

*CORRESPONDENCE
Aaron R. Hansen,
aaron.r.hansen@health.qld.gov.au

RECEIVED 12 March 2024
ACCEPTED 13 May 2024
PUBLISHED 30 May 2024

CITATION
Lampe H, Tam L and Hansen AR (2024), Bi-specific T-cell engagers (BiTEs) in prostate cancer and strategies to enhance development: hope for a BiTE-r future.
Front. Pharmacol. 15:1399802.
doi: 10.3389/fphar.2024.1399802

Bi-specific T-cell engagers (BiTEs) in prostate cancer and strategies to enhance development: hope for a BiTE-r future

Harriet Lampe, Laura Tam and Aaron R. Hansen*

Department of Medical Oncology, Division of Cancer Care Services, Princess Alexandra Hospital, Metro South Health Service, Queensland Health, Brisbane, QLD, Australia

Metastatic castrate resistant prostate cancer (mCRPC) continues to have poor survival rates due to limited treatment options. Bi-specific T cell engagers (BiTEs) are a promising class of novel immunotherapies with demonstrated success in haematological malignancies and melanoma. BiTEs developed for tumour associated antigens in prostate cancer have entered clinical testing. These trials have been hampered by high rates of treatment related adverse events, minimal or transient anti-tumour efficacy and generation of high titres of anti-drug antibodies. This paper aims to analyse the challenges faced by the different BiTE therapy constructs and the mCRPC tumour microenvironment that result in therapeutic resistance and identify possible strategies to overcome these issues.

KEYWORDS

prostate cancer, metastatic castrate resistant prostate cancer, novel immunotherapies, bi-specific T-cell engager therapy, T-cell engager therapy, bi-specific antibody therapy, BiTE

1 Introduction

Globally, prostate cancer is the second most common cancer diagnosed amongst men and accounts for the fifth most common cause of malignancy-related deaths (Sung et al., 2021). Androgen deprivation therapy (ADT) has long remained the backbone of treatment of locally advanced or metastatic prostate cancer. The past 2 decades have seen multiple advancements in prostate cancer treatment, with demonstration of improved overall survival in metastatic castrate sensitive prostate cancer (mCSPC) with the introduction of androgen receptor signal inhibitor (ARSi) therapy, docetaxel chemotherapy and external radiation therapy, and in metastatic castrate resistant prostate cancer (mCRPC) with ARSis, a broader range of chemotherapy agents, and Radium-223 radionucleotide treatment (Petrylak et al., 2004; de Bono et al., 2011; Parker et al., 2013; Beer et al., 2014; James et al., 2016; Fizazi et al., 2017; Kyriakopoulos et al., 2018; Armstrong et al., 2019; Chi et al., 2019; Fizazi et al., 2022; Smith et al., 2022). The PSMA-targeted Lutetium-177 radionucleotide therapy has also shown survival benefit in mCRPC patients in the post-chemotherapy setting (Sartor et al., 2021). Additionally, for approximately 20% of men with mCRPC who harbour a homologous recombination defect (HRD), poly-ADP-ribose-polymerase (PARP) inhibitors such as olaparib and rucaparib have demonstrated better survival outcomes and are approved therapies in many countries (Hussain et al., 2020; Fizazi et al., 2023). Despite these significant advancements, overall survival rates amongst those with mCRPC remains low at only 34% at 5 years, thereby necessitating a need to

develop better therapeutic options (SEER Explorer, 2023). BiTEs may represent a drug class that has the potential to improve clinical outcomes for prostate cancer patients and provide them with hope for a "brighter" future.

1.1 Immunotherapies in prostate cancer

Immune checkpoint inhibitors (ICI) have revolutionised the management of a plethora of malignancies in the past decade (Robert, 2020). However, while their use in mCRPC has shown a marginal benefit in a small proportion of prostate cancer patients with mismatch repair (MMR) deficiency mutations, their use in the majority of mCRPC patients has been limited with a number of negative trials including KEYNOTE-641 and the KEYLYNK-010 trial (Kwon et al., 2014; Robinson et al., 2015; Kazandjian et al., 2016; Beer et al., 2017; Hansen et al., 2018; Antonarakis et al., 2019; Sharma et al., 2019). Earlier research in cancer vaccines have shown some success in the prostate cancer landscape. Sipuleucal-T, a dendritic cell-based vaccine which acts via a recombinant protein of granulocyte macrophage colony stimulating factor (GM-CSF) and prostatic acid phosphatase (PAP) to facilitate maturation of PAP-expressing antigen presentation cells, with subsequent T cell activation and PAP-expressing prostate cell killing, was approved by the US Food and Drug Administration (FDA) in 2010 for minimally symptomatic mCRPC. Although it demonstrated an overall survival (OS) benefit, particularly in a sub-population with reduced metastatic burden, and has acted as an important proof of concept for immunotherapies outside of ICIs in prostate cancer treatment, sipuleucal-T has failed to be incorporated into routine treatment for mCRPC due to doubts about limited clinical benefit (Kantoff et al., 2010). These modest results have driven research into other facets of immunotherapy such as T-cell engager (TCE) therapies, which aim to directly crosslink T-cells with tumour associated antigens (TAAs), thus driving localised cancer cell specific cytotoxicity, cytokine release, and downstream activation of a B-cell polyclonal humoral response (Zhou et al., 2021). TCE therapies include chimeric antigen-receptor-modified (CAR) T cells, in which patients' own T-cells are genetically engineered *ex vivo* to express a chimeric T-cell receptor targeted at the desired TAA, and bi-specific T-cell engagers (BiTEs), antibody-based molecules offering a promising "off the shelf" option for achieving cross-linking of cancer and T-cells, which we shall examine in further detail.

1.2 BiTE therapies in cancer

BiTEs are monoclonal antibody (mAb) based molecules comprised of at least two conjoined antibody components which have respective specificity for a TAA of choice, and for an immune cell component, typically the conserved portion of the T-cell receptor, CD3, connected by a flexible linker moiety (Riethmüller, 2012). The mechanism of action of BiTEs involves activation of cytotoxic T-cells independent of the co-stimulation pathway, resulting in robust killing of cancer cells which has been demonstrated *in vitro* to have efficacy 100–10,000 fold greater than that of mAbs (Wolf et al., 2005).

BiTEs can be produced through chemical cross-linking of two antibody fragments, or via fusion of two different monoclonal antibody producing cell lines (so called "quadromas") with subsequent purification of the desired protein outcome (Schaefer et al., 2011). Initial inefficiencies in BiTE production concerning high proportions of incorrect heterodimer products have been addressed with multiple strategies to improve correct heterodimerisation. These have included heavy chain "knobs in holes" alterations (Xu et al., 2015), "crossover" of light and heavy chain combinations within one Fab arm of a bispecific IgG antibody to reliably produce a single desired heterodimer (CrossMabs; (Klein et al., 2019)), and dual affinity re-targeting proteins (DARTs), which favour stable dimerization due to exchange of variable heavy and light chains between two scFv components (Johnson et al., 2010). While the original BiTE molecules comprised two single chain variable fragments (scFv) from two different mAbs connected by a flexible peptide linker, further drug development research has generated an array of structural variations conferring benefits of more efficient production, increased half-life and improved target binding (Suurs et al., 2019). Blinatumomab, an anti-CD3-CD19 BiTE, was the first in its class to be approved by the FDA in 2014 for the treatment of Philadelphia chromosome negative relapsed or refractory B-cell acute lymphoblastic leukaemia (Kantarjian et al., 2017). In solid tumours, tebentafusp, which targets gp100 and CD3, has demonstrated improved survival outcomes for patients with uveal melanoma (Nathan et al., 2021). While there are no other approved solid tumour BiTEs to date, work is currently underway in a variety of cancer histologies to further their development.

1.3 BiTEs in prostate cancer

The use of BiTE therapies in prostate cancer has been trialled in several studies using different structures and TAA targets (See Table 1 for a complete list of finalised and ongoing trials). The first trial of a BiTE therapy in prostate cancer involved pasotuxizumab, an anti-CD3 and anti-prostate specific membrane antigen (PSMA) construct, administered either via subcutaneous injection or continuous intravenous infusion which produced a 54.9% reduction in PSA in the highest dose cohort, but was associated with 81% rate of Grade 3 or 4 treatment related adverse events (tr-AEs; (Hummel et al., 2021)). The trial was terminated in favour of acapatamab, an anti-CD3, anti-PSMA molecule with an IgG crystallisable fragment (Fc) to extend serum half-life. Unfortunately, while the PSA response of a 50% reduction (PSA50) was 34.3%, the rate of grade 3/4 tr-AEs was >50% and consequently acapatamab was not planned for further development (Ben et al., 2020). Subsequent studies have assessed alternative TAAs, including prostate stem cell antigen (PSCA), human kallikrein 2 (KLK2), delta-like protein 3 (DLL-3) and six transmembrane epithelial antigen of prostate 1 (STEAP-1). These studies have also explored a variety of alternative BiTE structures—addition of HLE or immune-interacting domains, incorporation of more complete antibody structures and differences in linker molecules. However, to date the vast majority have failed to move past Phase 1 clinical trials,

TABLE 1 Summary of clinical trials evaluating BiTE therapies in prostate cancer to date.

Drug	Phase	Structure	Population	Route and dose	Treatment related adverse events	Anti-drug antibodies	Anti-tumour efficacy	Trial outcome	Clinical trial
Pasotuxizumab (AMG 212, BAY2010112)	1	Anti-CD3 and anti-PSMA (sequences not specified) (Lutterbuese et al., 2011)	N = 47 mCRPC refractory to ≥1 taxane regimen and abiraterone or enzalutamide, on continuous ADT, ECOG 0–2	2 arms: Daily s.c. injection, 21 days cycles, dose cohorts ranging from 0.5 μg to 172 μg. Or c.i.v. infusion, 6 weeks cycles with 1 week break, dose cohorts of 20, 40 and 80 μg/day cohorts	100% experienced AEs any grade (majority CRS and fatigue). 81% Grade 3–4 (44% lymphopaenia, 44% infections)	Detected in 100% of s.c. arm, nil change with dexamethasone pre-medication. 93% were neutralising. ADAs associated with reduced drug serum concentration however limited data available. Titres did not correlated with AEs or drug dose received	Pre-clinical: EC50 3.4–6.7 ng/mL in PSMA human cell culture	Prematurely terminated—in favour of AMG 160. MTD not established	NCT01723475
						0% in c.i.v.arm. (Hweixian et al., 2023)	Regression of prostate cancer xenografts in mice post s.c. injection (Friedrich et al., 2012)		
							Clinical: S.c. arm −24.7% PSA decline. C.i.v. arm −22.0, −37.7% and −54.9% in 20, 40 and 80 μg/day dosing cohorts (Hummel et al., 2021)		
Acapatamab (AMG 160) ± pembrolizumab	1	Anti-CD3 and anti-PSMA and IgG Fc active fragment (HLE) (Sequences not specified) (Deegen et al., 2021)	N = 43 (monotherapy AMG 160). mCRPC refractory to 1–2 taxane regimens and abiraterone or enzalutamide, on continuous ADT, ECOG 0–1	i.v. dose ranges 0.003–0.9 mg fortnightly	95.3% any grade. >50% Grade 3–4. 31.3% Grade 3 CRS.	Neutralizing ADAs were detected, limited data available	Pre-clinical: EC50 6–42 pmol/L at 42 h in PSMA PC cell lines	Completed without public release of final results. Preliminary data released	NCT03792841
							Clinical: PSA50 in 34.3%		
							PR in 13.3%, SD in 53.3% (Ben et al., 2020; Deegen et al., 2021)		
Acapatamab ± (AMG 404 or enzalutamide or abiraterone) or AMG 404	1	As for AMG 160	N = 65 mCRPC with continuous ADT.	I.v. dosing of acapatamab (Subudhi et al., 2021)	Not reported	Not reported	Not reported	Terminated for business decision, nil further information released	NCT04631601
Solitomab (AMG 110, MT 110)	1	Anti-CD3 and anti-EpCAM (Sequences not specified)	N = 65 (3 with mCRPC). Locally advanced, recurrent or metastatic solid tumours known to express EpCAM.	c.i.v. dosing, protocol not specified	95% Grade ≥3	Not assessed	One unconfirmed PR (Kebenko et al., 2018)	Completed	NCT00635596
APVO414 (ES414, MOR209)	1	Anti-CD3 and anti-PSMA and passive IgG Fc region (HLE) (ADAPTIR®) (Sequences not specified) (Hernandez-Hoyos et al., 2016)	N = 18. CRPC, refractory to abiraterone or enzalutamide, ECOG 0–1, NEPC excluded	2 arms: Weekly i.v. dosing and c.i.v	Not reported	58% of weekly i.v. dosing cohort developed ADAs with very high titres which reduced drug exposure	Not reported	Completed without public release of final results	NCT02262910
						50% of c.i.v. cohort developed ADAs of lower titres. (Author Anynomus, 2017)			

(Continued on following page)

10.3389/fphar.2024.1399802

TABLE 1 (*Continued*) Summary of clinical trials evaluating BiTE therapies in prostate cancer to date.

Drug	Phase	Structure	Population	Route and dose	Treatment related adverse events	Anti-drug antibodies	Anti-tumour efficacy	Trial outcome	Clinical trial
HPN424	1/2a	Anti-CD3 and anti-PSMA and anti-albumin (HLE) (TriTAC®) (Sequences not specified)	N = 110 mCRPC, received ≥2 prior systemic therapies, ongoing ADT	Weekly i.v. dose ranging 1.3–300 ng/kg with step—up dosing regimen	40% Grade ≥3 (18% AST elevation, 11% anaemia, 11% ALT elevation). 63% CRS any grade, 4% CRS Grade ≥3	Not assessed	21% any PSA reduction. 2 PSA30 and 3 PSA50 responses. 1 radiologic PR. (Bono et al., 2021)	Active, no longer recruiting. Challenging safety profile precluding further research. (Author Anynomus, 2022)	NCT03577028
JNJ-63898081 (JNJ-081)	1	Anti-CD3 and anti-PSMA and IgG4 Fc chain (HLE) (Sequences not specified) (DuoBody®)	N = 40 mCRPC or mRCC, refractory to ≥1 prior line of therapy, ECOG 0–1	3 arms: i.v. weekly dose ranging 0.1–3.0 μg/kg, s.c. weekly dose ranging 3–30 μg/kg, or s.c. escalation protocol with target doses ranging 30–60 μg/kg	43.6% Grade ≥3. CRS any grade 66.7%. 84.6% any grade injection/infusion reaction	63% in s.c. groups, 16.7% in i.v. group. In s.c. dosing, ADA associated with decreased drug exposure. 1 case of reversal of PSA30 in setting of developing ADAs	Transient PSA reduction in s.c. dosing >30 μg/kg. 2 subjects achieved PSA50 reduction. Cytokine release was more variable and overall reduced when compared with i.v. dosing. (Lim et al., 2022)	Completed	NCT03926013
CCW702	1	Anti-CD3 (UCHT1 construct) and anti-PSMA DUPA molecule) with triazole linker (Lee et al., 2021)	N = 22 mCRPC refractory to at least one novel androgen receptor targeted therapy, ECOG 0–1 (Markowski et al., 2021)	Daily s.c., dosing not specified	Not reported	Not reported	Not reported	Terminated early 2023 for business decision, nil further information publicly available	NCT04077021
CC-1	1	Anti-CD3 and anti-PSMA (10B3, proprietary) and IgG1 Fc (IgGsc format) (HLE). (Zekri et al., 2021)	N = 66, CRPC refractory to ≥3 lines of therapy, ECOG 0–2	c.i.v., target dose 826 μg	88% CRS (all Grade 1–2) despite prophylactic tocilizumab. 46% hypertension any grade	Not assessed	All except 1 subject had PSA reduction, not quantified (Hackenbruch et al., 2023)	Recruiting, due primary completion December 2024	NCT04104607
CC-1	1	Anti-CD3 (UCHT1 construct) and anti-PSMA (10B3 construct, proprietary) and IgG1 Fc (IgGsc format) (HLE). (Zekri et al., 2021)	N = 56 (Estimated), CRPC with biochemical recurrence post ≥1 line therapy, with low risk of rapid disease progression	3 hours i.v. infusion target dose ranging 78–600 μg with step-up dosing. (Hackenbruch et al., 2023)	Pending	Pending	Pending	Recruiting, due primary completion December 2024	NCT05646550
GEM3PSCA	1	Anti-CD3 and anti-PSCA (Sequences not specified)	N = 23, PSCA positive cancer (Renal, prostate, NSCLC) refractory to standard treatments, ECOG 0–2	1 week c.i.v. dosing (Clinicaltrials, 2019)	Not reported	Not reported	Not reported	Terminated for business decision, nil further information publicly available	NCT03927573
JNJ-78278343	1	Anti-CD3 and anti-KLK2 and effectorless IgG Fc (Shang et al., 2014)	N = 165 (Estimated) mCRPC, refractory to at least either 1 line chemotherapy or novel androgen receptor targeted therapy, ECOG 0–1	s.c. ingection, s.c. infusion, or i.v. infusion, dosing not specified. (Author Anynomus, 2021)	Not reported	Not reported	Not reported	Recruiting, due primary completion November 2024	NCT04898634
JNJ-70218902 (JNJ-902)	1	Anti-CD3 and anti-TMEFF2	N = 82 mCRPC refractory to at least either 1 line chemotherapy or novel androgen receptor targeted therapy, ECOG 0–1	Not specified	45% fatigue, 44% anorexia, 37% injection related reaction, 33% anaemia, lower back pain 25%, arthralgia 22%	Reported as "uncommon" but not specified	PSA50 reduction in 8 subjects. PR in 5 subjects. (Calvo et al., 2022)	Active, no longer recruiting. Preliminary data released	NCT04397276

(Continued on following page)

10.3389/fphar.2024.1399802

TABLE 1 (*Continued*) Summary of clinical trials evaluating BiTE therapies in prostate cancer to date.

Drug	Phase	Structure	Population	Route and dose	Treatment related adverse events	Anti-drug antibodies	Anti-tumour efficacy	Trial outcome	Clinical trial
Tarlatamab (AMG 757, BI 764532)	1b	Anti-CD3 and anti-DLL3 and IgG1 Fc (HLE) (sequences not specified)	N = 41 *De novo* or treatment emergent NEPC refractory to ≥1 systemic therapy, ECOG 0–2 (Aggarwal et al., 2021)	i.v. route, dosing not specified	Pending	Pending	Pending	Active, no longer recruiting	NCT04702737
LAVA-1207	1	Anti-PSMA and anti- Vδ2 (of Vγ9Vδ2T cells) (Gammabody® construct) (Sequences not specified)	N = 66 (Estimated) mCRPC, refractory to ≥1 taxane chemotherapy regimen and novel androgen-receptor targeting therapy, ECOG 0–1	i.v. fortnightly, dose ranging 1.5–40 μg	Nil Grade ≥3 to date	Not reported	SD in 3 of 8 subjects to date (8 weeks therapy) (Mehra et al., 2023)	Recruiting	NCT05369000
AMG 340 (TNB-585)	1	High affinity anti-PSMA and low affinity anti-CD3 and Fc domain (HLE) (Sequences not specified) (Buelow et al., 2021)	N = 100 (estimated) mCRPC refractory to ≥2 systemic therapies, ECOG 0–2	3 weekly i.v. infusion	Pending	Pending	Reduced cytokine release but equivalent anti-tumour activity against PC cell lines *in vitro* compared with higher affinity anti-CD3 constructs	Active, no longer recruiting	NCT04740034
Xaluritamig (AMG 509) ± enzalutamide or abiraterone	1	Anti-CD3 and anti-STEAP-1 and efffectorless IgG1 Fc domain (HLE) (Sequences not specified) (Nolan-Stevaux et al., 2023)	N = 97 mCRPC refractory to ≥1 systemic therapy (>80% had received previous taxane based chemotherapy regimen), ECOG 0–1	Weekly or fortnightly i.v. target dose ranging 0.001–2.0 mg, with step-up dosing and dexamethasone pre-medication	72% any grade CRS, 69% Grade 1–2 CRS, 45% fatigue, 32% pyrexia. 55% Grade ≥3 AEs (anaemia 13%, myalgia 12%, fatigue 11%)	54% treatment emergent ADAs, 51% were neutralising, 45% reduced drug exposure >25%. However, ADAs not associated with PSA50 response at 12 weeks therapy, or with AEs	24% PR, 48% SD, 19% PD. 49% PSA50 reduction, 28% PSA90 reduction for all doses. (Kelly et al., 2023)	Recruiting. MTD identified = 1.5 mg i.v. weekly with 3 tier step-up dosing	NCT04221542
REGN4336 ± cemiplimab	1/2a	Anti-CD3 and anti-PSMA, limited details available on structure	N = TBC mCRPC refractory or intolerant to ≥2 lines systemic therapy and ADT	Weekly or 3 weekly s.c. injection, dosing not specified ± 3 weekly i.v. cemiplimab. (Kelly et al., 2022)	Pending	Pending	Pending	Recruiting	NCT05125016

Abbreviations: CD3, Cluster of differentiation 3, marker of T cells; PSMA, Prostate specific membrane antigen; mCRPC, Metastatic castrate resistant prostate cancer; ADT, Androgen deprivation therapy; ECOG, Eastern Cooperative Oncology Group Performance Status Scale; C.i.v., Continuous intravenous infusion; MTD, maximum tolerated dose; Fc, Crystallisable fragment; HLE, Half-life extended; PSCA, prostate stem cell antigen; KLK, human kallikrein; DLL3, Delta-like protein 3; NEPC, Neuroendocrine prostate cancer; STEAP-1, Six transmembrane epithelial antigen of prostate.

10.3389/fphar.2024.1399802

displaying various combinations of prohibitive side effect profiles, limited anti-tumour efficacy and a high rate of anti-drug antibodies, amongst other issues (Simão et al., 2023). Given the increasing interest in BiTE therapies in prostate cancer, we will explore some of the factors impacting both safety and efficacy associated with this class of drugs.

2 Discussion

2.1 Structural alterations to extend half-life

The original BiTE molecules were comprised of two single chain variable fragments (scFv) from two different mAbs connected by a flexible peptide linker (Ahmad et al., 2012). The small size of these molecules resulted in a short half-life with poor serum stability and rapid renal clearance, which necessitated administration via continuous intravenous infusion. This issue was subsequently addressed with the development of half-life extended (HLE) BiTE variants, which incorporated structures to increase molecular size and stability, enabling BiTEs to be formulated as intermittent infusions or subcutaneous injections, and consequently improving efficacy, convenience and cost of administration schedules. One method involved bonding together of two BiTEs to create a tetravalent "tandem diabody" (TandAbs; (Kipriyanov et al., 1999)). Alternative methods included addition of antibody heavy chain elements, either as part of a IgG-based structure, or as an isolated Fc domain to enable binding to the neonatal Fc receptor in recipient serum and thus reduce the rate of clearance (Brinkmann and Kontermann, 2017). Inclusion of an Fc region confers the ability to bind to the neonatal Fc receptor on innate immune cells, enhancing immune cell engagement. Other HLE strategies have included addition of an albumin receptor to improve serum stability, or molecular modification of heavy chains to increase half-life, such as with the XmAb technology (Zhukovsky et al., 2007). Overall, these customisations have created a myriad of BiTE structural variations which have facilitated administration via intermittent intravenous or subcutaneous routes, and also offer additional functional benefits.

2.2 Excessive adverse events and immunogenicity

2.2.1 Class specific adverse events

The main adverse events of special interest with BiTEs are cytokine release syndrome (CRS) and immune effector cell-associated neurotoxicity syndrome (ICANS). CRS is a systemic inflammatory response syndrome that can produce symptoms ranging from fever to shock with multi-organ failure caused by high levels of cytokine release, particularly IFN-γ, IL-1 and IL-6 (Morris et al., 2022). CRS most commonly occurs hours to short days after the initial dose of TCE therapy, with some evidence showing reduced incidence and severity following pre-medication with dexamethasone and step-up dosing regimens (Shimabukuro-Vornhagen et al., 2018). Severe CRS can be treated with tocilizumab, an anti-IL-6 receptor mAb, without affecting therapeutic activity (Kauer et al., 2020). The occurrence of any-grade CRS in the studies on BiTE therapies in mCRPC to date ranges from 5% with JNJ-902% to 88% with CC-1, although it should be noted that there were no reports of associated mortality even with higher rates of CRS (Calvo et al., 2022; Heitmann et al., 2022).

ICANS pathophysiology remains uncertain, but patients often present with confusion, tremor or dizziness and can progress to seizures or irreversible encephalopathy over a course of days post treatment. Treatment consists of aggressive supportive therapy and corticosteroids. Tocilizumab is unable to cross the blood-brain barrier and has limited clinical utility in management. ICANS occurs infrequently with BiTE therapies in general and appears to be rarer in solid tumour BiTE studies (Siegler and Kenderian, 2020). There have been no formal diagnoses of ICANS in the studies of prostate cancer-targeted BiTEs to date, although seizures, a possible sign of ICANS, was reported in a single patient receiving HPN-424 (Bono et al., 2021).

CRS initially presented a clinical challenge to progression of BiTE therapies in solid tumours. However, with increased exposure to and recognition of the constellation of CRS in clinical settings, the improved availability of tocilizumab, and the growing evidence that even with high grade CRS, survival remains extremely high, this trAE should not be a major factor limiting use of BiTE therapies moving forward. Focus should instead be placed on reducing immunogenicity of the BiTE structure to curb hyperactive cytokine release where possible. Brandt et al. have proposed the "kill switch" mechanism for BiTE therapy similar to that adopted in experimental CAR T-cell therapies (Brandt et al., 2020). These mechanisms rely on the incorporation of an inducible self-destruct process into the original therapy which, when activated, results in the rapid removal of the treatment from the system. In CAR T-cell therapies, this has involved induction of the caspase-9 T-cell apoptosis pathway, or induction of T-cell transcription of viral components subsequently leading to T-cell apoptosis. While purely theoretical, inclusion of a cleavage site within the linker portion of a BiTE therapy could achieve similar effects.

2.2.2 On-target off-tumour effects

A challenge in the adaptation of BiTEs from haematological to solid tumours has been the difficulty in finding solid organ TAAs which are highly specific to the desired tumour cell population, as many solid organ TAAs are also present at low levels in normal tissue. In this instance, BiTE activity poses a risk of so-called "on-target off-tumour" effects resulting from damage to these non-malignant tissues. These can be catastrophic, as demonstrated in trials of catumaxomab, an early example of a solid organ BiTE directed against epithelial cell adhesion molecule (EpCAM) and CD3 for EpCAM-positive advanced solid organ cancers causing malignant ascites, with one patient experiencing fatal acute fulminant liver failure (Linke et al., 2010).

PSMA, the most commonly targeted TAA in prostate cancer BiTE therapies to date, while being highly expressed in prostate cancer, also has high levels of expression within intestinal, liver, salivary glandular cells and proximal kidney tubules (Silver et al., 1997). There has been evidence of PSMA targeting leading to significant on-target off-tumour effects, for example, with the BiTE HPN424, which caused Grade 3–4 AST elevations in 18%

patients, and ALT elevations in 11% (Bono et al., 2021). Although on-target off-tumour AEs appear to be relatively infrequent in trials of BiTEs targeting PSMA, research into more specific TAAs remains warranted to alleviate the risk of these outcomes.

2.2.3 Alternative TAAs

Multiple alternative TAAs are under investigation as therapeutic targets in prostate cancer. One potential target proposed has been STEAP-1, which has some expression in lung tissue but otherwise has limited expression outside of the brain which is considered inaccessible to BiTE molecules (Xu et al., 2022). STEAP-1 has been targeted in a Phase 1 clinical trial using an agent called xaluritamig. Although 72% of patients experienced CRS, the vast majority (69%) were Grade 1–2 (Kelly et al., 2023). Another target being used in clinical trials is TMEFF2 which has expression limited to intestinal tissues, the male reproductive tissues and brain. JNJ-70218902 was designed to target TMEFF2 and entered phase I testing but limited available data exists regarding its efficacy and toxicity profile (Calvo et al., 2022). Kallikrein related peptidase-2 (KLK2) is a highly specific TAA with expression restricted to prostate tissue only and is the putative tumour target for JNJ-78278343. Both efficacy and safety data is still being awaited at this stage (Shang et al., 2014).

The current trials of BiTEs in prostate cancer treatment as described in Table 1 are all targeted at membrane bound extracellular proteins which can be readily accessed by nearby immune effector cells. However, these extracellular proteins represent only a fraction of potential tumour specific targets. Intracellular protein fragments expressed extracellularly bound to human leukocyte antigen (HLA) major histocompatibility complexes (MHC) through antigen presentation to immune cells offer a much more extensive suite of potential therapeutic targets not otherwise accessible to antibody based therapies (Trenevska et al., 2017). BiTEs designed to target these peptide-HLA complexes have been termed immune mobilising monoclonal T-cell receptors against cancer (ImmTACs). Tebentafusp, an approved BiTE therapy for uveal melanoma, is the first in class ImmTAC, designed to target a peptide-HLA combination of gp100:HLA-A*02:01 along with the CD3 component of the T-cell receptor (TCR, Nathan et al., 2021). Disadvantages of this therapy include restriction of eligibility of patients to those with matched HLA typing, challenges of identifying peptide:HLA combinations which are highly conserved across cancer cells and patient populations, and possibility of tumour evasion through downregulation of HLA cell surface expression (Trenevska et al., 2017; Maruta et al., 2019). Nevertheless, the development of ImmTACS represents a breakthrough in BiTE development, and further research into intracellular prostate cancer TAAs may reveal novel therapeutic targets with reduced on-target off-tumour effects.

2.2.4 Increasing specificity of localisation of BiTE activation to tumour tissue

In addition to targeting more tumour-specific TAAs, another approach to improve the localisation of BiTE activation to tumour tissue involves the incorporation of moieties targeting two different TAAs into a single BiTE construct. This has been explored pre-clinically in solid tumour cell lines with AMG-305, a dual targeted BiTE directed against P-cadherin and mesothelin which showed attenuated activity against cells expressing only one of these targets (Pham et al., 2023). Targeting of two separate TAAs may also offer a possible means of reducing immune escape through the common route of downregulated expression of a targeted TAA. However, once again, in the absence of TAAs which are more tightly limited to prostate cancer expression, these therapies continue to pose the risk of unwanted on-target off-tumour effects.

Another possible strategy to localise BiTE activation to tumour tissue is the incorporation of structural elements which prevent activity of the BiTE outside of conditions specific to the tumour microenvironment. One possible approach is masking of BiTE binding sites with structures designed to be cleaved away by tumour-resident proteases, hence restricting activity to tumour deposits (Geiger et al., 2020). Panchal et al. described generation of an EGFR-CD3 BiTE where the heavy and light variable chains of the anti-CD3 portion were separated by a linker degradable only by the tumour specific matrix metalloproteinase 9 (MMP9), permitting anti-CD3 activity only after MMP9 facilitated rearrangement of the molecule (Panchal et al., 2020). Another approach is addition of a second TAA target within a T-cell engager structure with the aim of improving tumour tissue specific cytotoxicity. A variation on this concept is the construction of "hemibodies," two "half" antibodies each containing a different antigen binding scFv fragment fused to either a variable light or variable heavy chain of a CD3 antibody, designed to recombine to form a functional BiTE only in the presence of both TAAs. The proof-of-concept hemibody was targeted against HLA-A2 and CD45, and showed apoptosis restricted to dual positive tumour cells in animal models (Banaszek et al., 2019). To date these experiments have all been pre-clinical, and none have been targeted towards prostate cancer, however these results could be transferable to other BiTE structures in future (Panchal et al., 2020).

2.2.5 Immunogenicity and antidrug antibodies

Drug related immunogenicity, or the response of a patient's immune system to a drug, occurs via recognition of drug components as "non-self," and is a key factor influencing the efficacy and adverse effects of BiTEs (Jawa et al., 2020). Protein sequences within the drug or drug excipients as part of the drug formulation are taken up by patients' antigen presenting cells (APCs), with subsequent breakdown and expression of short protein epitopes on HLA surface molecules. T helper cell recognition of these epitopes as "non-self" will stimulate an immune response including a B cell humoral response with production of anti-drug antibodies (ADAs). ADAs can be broadly split into "neutralizing" antibodies which obstruct binding sites, and "non-neutralizing," which bind epitopes which do not directly interfere with the drug's action. ADAs have critical effects on a drug's efficacy, pharmacokinetics, and adverse events through a wide array of mechanisms, including blocking or changing affinity of binding sites, prolongation or potentiation of drug clearance, aggregation of drug-antibody complexes and effects from inflammatory cytokine production (van Brummelen et al., 2016). Further complicating factors influencing the extent of immunogenicity to a drug include the route of administration, dose regimen, product storage, product purity, and the patient's own immune system factors such as the presence of pre-existing cross-reacting ADAs and skew towards immunoregulatory or

inflammatory immune responses. The desired alternative response is recognition of these epitopes as "self" by the immune system, with subsequent induction of immune tolerance via activation of T regulatory cells (Tregs).

The complex interactions between these therapies and the immune system are a fundamental part of the nature of T cell therapies. ADA quantification and their resultant physiological effects form the backbone of a multifaceted immune response assessment recommended by both the FDA and EMA for drug immunogenicity (Administration USFaD, 2010; Agency, 2017). It should be noted that current detection methods for ADAs are imperfect. A range of assays can be used to detect ADAs, with a wide variability in sensitivity and specificity. Furthermore, assays usually only detect one subclass of Fc immunoglobulin receptors, predominantly IgG, and may not detect drug-bound antibody, leading to under-reporting of ADAs (van Brummelen et al., 2016). Nevertheless, ADA analysis remains the most accurate method of assessing immunogenicity. Notably, these assessments are primarily conducted *in* or *ex vivo* in human clinical studies, given the limitations to mimick a nautral human immune response in animal or human cell lines.

Where data has been released for quantification of ADAs in clinical trials of BiTEs for prostate cancer, ADAs were frequently present in >50% subjects (See Table 1). This is an extremely high incidence compared to other biologic therapies on the market (van Brummelen et al., 2016). When compared with intravenous administration, subcutaneous dosing is associated with a high rate of neutralising antibodies, which has been ascribed to sequential antigen presentation from both APCs residing in the skin and then lymph node-resident APCs. These two "waves" of antigen presentation increase the formation of ADAs (Jarvi and Balu-Iyer, 2021). For instance, during testing of pasotuxizumab, induced ADAs were recorded in 100% subjects receiving s.c. dosing, with 93% of these being neutralizing, but none in those receiving the continuous i.v. dosing (Hweixian et al., 2023).

Further assessment of ADA subclasses and effects in BiTE therapies for mCRPC has been limited to studies in pasotuxizumab and xaluritamig (Hweixian et al., 2023; Kelly et al., 2023). Within this limited sample, it has been demonstrated that treatment emergent neutralizing ADAs can have either adverse (e.g., pasotuxizumab) or neutral (e.g., xaluritmag) clinical effects. (Hweixian et al., 2023; Kelly et al., 2023). For xaluritamag, 54% of subjects developed treatment emergent ADAs for an i.v. formulation, with 45% of subjects developing neutralising antibodies causing reduction in drug exposure by more than 25%. However, these ADAs were not associated with difference in PSA50 response at 12 weeks (Kelly et al., 2023). Conversely, non-neutralising ADAs can lead to formation of serum antibody complexes which are subsequently removed by the host immune system, which theoretically could affect drug efficacy despite their "benign" status, although this was not observed in the above two trials. Despite historical data in other fields showing an association between ADAs and certain AEs, the presence or titre of ADAs does not appear to correlate with the rate or severity of AEs in either population. Importantly, all ADAs, regardless of neutralising status, can dramatically alter pharmacokinetics of the drug by sustaining or expediting drug clearance, with likely construct specific effects on efficacy (Kelly et al., 2023). Unfortunately, a deeper analysis is limited by the restricted published data from clinical trials about ADAs and their effect on drug pharmacokinetics or pharmacodynamics.

The causes of the high rates of ADA formation in response to BiTE therapies are incompletely understood but derives at least partially from particularly immunogenic sequences within the drug's structure, including effector Fv domains, Fc region, half-life extending domains, or peptide linkers. A number of methods can be used to determine the immunogenicity of these sequences, including screening of drug protein structure for known T helper or T regulatory binding epitopes; culturing of antigen presenting cells with *ex vivo* peripheral red blood cells with sequencing of epitopes expressed by APCs; or analysis of the binding sequences of extracted ADAs from trial subjects to match to a complementary epitope from the drug; with the latter detailed by Hweixian et al. for pasotuxizumab (van Brummelen et al., 2016; Hweixian et al., 2023). However, the protein sequences of the drug or ADAs detected have not been made available to the public domain for the majority of BiTEs trialled for prostate cancer so far. Release of this existing information, and wider testing of ADAs in ongoing and future trials would provide invaluable information in helping better understand the interplay between BiTEs and the humoral immune system. It could help to differentiate the concentrations or affinities at which ADAs become clinically significant, and to select drug components with less problematic immune responses. With this information, immune engineering of therapeutic protein structures could enable adjustments to homology to mask or remove immunogenic sequences, or addition of T regulatory epitopes promoting immune tolerance (van Brummelen et al., 2016).

Other factors known to contribute to immunogenicity include drug excipients, which can be comprised of contaminant proteins accidently purified with the therapeutic protein during production, or other components of the drug formulation such as trace heavy metals. Subcutaneous administration has been associated with increased ADAs over an i.v. route for previous biologics, as has re-exposure following a treatment free interval (Agency, 2017). Half-life extending domains, such as an Fc region, may also add to non-humoral immunogenicity through engagement of the immune system via the Fc receptor on APCs, neutrophils and NK cells. Although HLE molecules are attractive for the possibility they offer of a more convenient administration schedule, the added immunogenicity they seem to generate poses challenges, particularly to subcutaneous administration. Finally, there are patient specific factors at play, such as levels of pre-existing ADAs, and different HLA haplotypes influencing the particular epitopes that may produce a patient response (van Brummelen et al., 2016). Once again, limited testing or release of data concerning ADA quantity and sequences, and their association with patient HLA typing and drug excipients, prevents retrospective analysis of how to avoid highly immunogenic structures in the future. Greater transparency and dissemination of available data will assist in further targeted development of this class of agents.

2.3 Limited anti-cancer effect

Unfortunately, the majority of completed clinical trials of BiTEs against prostate cancer have demonstrated limited or inconsistent

anti-tumour effects to date. There is a recurrent pattern of small percentages of study groups achieving PSA50, or radiologic partial response (PR) in clinical trials examining the use of HPN424, JNJ-081 and JNJ-902 (Bono et al., 2021; Calvo et al., 2022; Lim et al., 2022). Pasotuxizumab displayed slightly more promising results with a 19% PSA50 response and two long term PSA50 responders, however this trial was prematurely terminated in favour of acapatamab, which in turn delivered a PSA50 response in 34.3% of subjects (Ben et al., 2020; Hummel et al., 2021). However, the trial using acapatamab was also discontinued in the setting of a high incidence of trAEs. Xaluritamig has recently demonstrated the greatest anti-tumour efficacy in the field, with 49% of patients demonstrating a PSA50 response and 28% of patients also achieving a PSA90 reduction (Kelly et al., 2023).

Despite these promising results, when compared with haematological malignancies, immunotherapies in prostate cancer face multiple barriers to effectiveness, including intra- and inter-tumoral genotypic heterogeneity, and downregulation of TAA expression over time, leading to treatment escape or failure (Middelburg et al., 2021; Ge et al., 2022). They must also contend with a complex solid tumour microenvironment (TME), of which prostate cancer's TME presents specific challenges.

2.3.1 Immunosuppressive "cold" tumour microenvironment

The disappointing response of prostate cancer to ICIs has been predominantly attributed to its multifactorial "cold" or immunosuppressive tumour microenvironment (TME) in comparison to other common malignancies such as melanoma or lung. Metastatic CRPC TMEs are characterised by a dense stroma with relatively high proportions of cancer-associated fibroblasts (CAFs) and myeloid derived suppressor cells (MDSCs) which presents a physical barrier to anti-cancer therapies and results in low numbers of tumour infiltrating lymphocytes (TILs) and innate immune cells. Even within the limited TIL population there is a tendency towards an immunosuppressive phenotype, with a preponderance of Th2 and T regulatory (Treg) lymphocytes over Th1 counterparts, skewing against activation of $CD8^+$ cytotoxic T cells and natural killer (NK) cells (Krueger et al., 2019). There is a similar overabundance of M2 anti-inflammatory macrophages instead of their inflammatory M1 counterparts. Metastatic CRPC TMEs are further masked from the immune system by a low tumour mutational burden with consequent reduced neoantigen expression as well as local overexpression of costimulatory molecules such as PD-1 and CTLA-4, which act as "self" markers, leading over time to an "exhausted" local immune cell phenotype (Gannon et al., 2009).

This immunosuppressive TME is theorised to limit the efficacy of the "bystander" effect of immunotherapies, in which successful cell dependent cytotoxicity creates a local environment of pro-inflammatory cytokines and subsequent upregulation of neoantigens and differentiation of inflammatory immune cell phenotypes, prompting cytotoxicity towards adjacent tumour cells (Ross et al., 2017). Notably, ADT, the cornerstone of prostate cancer treatment, is suspected to contribute to the immunosuppressive TME through increases in intratumoural Tregs, MDSCs and M2 macrophages, reduced markers of interaction between tumour cells and de-regulation of intratumoural Tregs (Pu et al., 2016; Qin et al., 2022). The immunosuppressive TME of prostate cancer is observed to become more extreme with progression to mCRPC, with bony metastases representing the most severe example of this phenotype (Jiao et al., 2019). Synchronous metastatic deposits of CRPC display significant genetic heterogeneity, further predisposing to immune escape and treatment resistance (Sun, 2021).

BiTEs were initially expected to provide a radical solution to many of the problems presented by "cold" TMEs, by localising T cell activation directly to malignant cells. Unfortunately, this has not eventuated, with BiTE therapies demonstrating limited anti-tumour activity in prostate cancer in studies to date. It is possible that the immunosuppressive TME limits the bystander effect of BiTEs to some extent, as it does for ICIs. It should also be noted that the recipients of these BiTEs comprise a heavily pre-treated and castrate-resistant group. In light of the mCRPC TME being highly immunosuppressive post ADT, ARSi and chemotherapy, it can be speculated that BiTEs may show greater efficacy in a less heavily pre-treated patient population, akin to the benefit seen in a similar sub-population with the sipuleucal-T vaccine.

2.3.2 Mitigating the mCRPC TME

There are a multitude of theories as to how to alter the TME pathophysiology to improve the action of BiTEs, predominantly based on improving either systemic or intratumoural immune effector cell populations and activity. A logical option is to trial a combination of immunotherapy with BiTE therapy, to simultaneously aim to reverse TIL anergy, prevent BiTE mediated upregulation of TIL PD-1 expression and tumour and stromal PD-L1 expression (Jiang et al., 2019; Belmontes et al., 2021). This strategy has been tested in prostate cancer BiTE trials (See Table 1), with combinations of anti-PSMA BiTEs with PD-1 inhibitors, namely, acapatamab and pembrolizumab, and REGN4336 and cemiplimab, but results from these combinations are not available (Ben et al., 2020; Kelly et al., 2022). Outside of prostate cancer, there has been great interest in this combination with multiple clinical trials underway (Belmontes et al., 2021). In solid tumours, preliminary phase 1 clinical trial data for a CEA and CD3 targeting BiTE showed increased disease response when paired with atezolizumab in the absence of increased toxicity (Tabernero et al., 2017). Alternative structural variations on the synergy of BiTEs and ICIs includes bifunctional checkpoint-inhibitory T-cell engagers (CiTEs), comprised of a BiTE crosslinked with a PD-L1 inhibitor to provide localised combination therapy and attempt to avoid systemic effects of ICIs (Herrmann et al., 2018).

An alternative experimental approach involves shifting focus to disruption of the stroma of the TME to permit increased TIL migration and improve BiTE intra-tumoural access. Brunker et al. developed a bi-specific antibody designed to crosslink the fibroblast activation protein (FAP) and the death receptor 5 (DR5), triggering the extrinsic apoptotic pathway for tumour cells, with successful cytotoxicity in FAP positive tumour stroma (Brünker et al., 2016). Another example of successful pre-clinical alteration of the structure of the TME has been the use of an oncolytic virus expressing a FAP-CD3 BiTE which successfully increased intra-tumoral accumulation of T cells and decreased FAP concentration, indicating fibroblast apoptosis *in vivo* testing (de Sostoa et al., 2019). The extracellular matrix could also be directly targeted with enzymes such as hyaluronidase to literally open a path for tumour infiltration

by T cells (Eikenes et al., 2005). Yet further studies have targeted function and trafficking of MDSCs to reduce their immunosuppressive local effects (Middelburg et al., 2021). However, these approaches remain pre-clinical and have not been targeted to prostate cancer to date.

2.3.3 Alternative immune cell targets

Rather than focusing on CD3 positive T-cells, some potential therapeutics instead aim to target alternative immune effector cell populations such as the pro-inflammatory natural killer (NK) cells. NK cells have been targeted via bi- and tri-specific NK-cell engagers (BiKEs and TriKEs) in clinical trials for haematological malignancies with promising results (Rothe et al., 2015; Vallera et al., 2016). γδ T-cells present a unique target in prostate cancer. Although they are relatively sparse in comparison to the more common αβ T-cells, they are particularly concentrated in prostate cancer tumours when compared with other solid organ tumours (Tosolini et al., 2017). Activation of intra-tumoral γδ T-cells could potentially kickstart immune cell activation within the prostate TME, and a clinical trial of LAVA-1207, a γδ T-cell-directed BiTE, is currently underway (Mehra et al., 2023).

2.3.4 Increased binding efficacy

A potential strategy for overcoming limited anti-tumour activity of current BiTEs would be to increase the binding affinity of the TAA or CD3 targeted structural components. Multiple antibody components targeting the same TAAs could be added to increase valency and target binding, as exemplified by the TandMab structure. Alternatively, reverse protein engineering could be utilised to design increased affinity of complementarity determining regions within the variable chains directed towards the relevant TAA. For example, Zekri et al. (2021) developed a proprietary PSMA binder, 10B3, which demonstrated increased reactivity against prostate cancer cells *in vitro* compared with a pre-existing J591 PSMA antibody. This improvement was attributed to alternative binding sites to PSMA recognised by the 10B3 molecule. However, it should be noted that protein engineering generally leads to deviation from native antibody structure and consequently higher risk of immunogenicity. Ultimately, while the expression of BiTE targets for prostate cancer remains non-specific to malignant tissue, attempts to increase TAA binding affinity risk increased rates of on-target off-tumour effects.

3 Conclusion

Metastatic CRPC is a prevalent disease which remains a challenging clinical entity to effectively treat, with limited response to the ICIs which have become cornerstones of treatment for multiple other cancers. Novel TCE therapy, particularly BiTE therapy, has been a promising area of immunotherapy development in the past decade with particular interest in their use in prostate cancer. Unfortunately, early investigations of various prostate cancer specific BiTE therapies have been limited by high incidences of intolerable adverse events and insufficient anti-tumour activity. Nevertheless, progress has been made in addressing these shortcomings through identifying a range of possible TAAs to exploit, extending the drug half-life allowing for more convenient administration schedules, and managing class specific AEs. Moreover, there is extensive research into multiple strategies as to how to overcome the challenges presented by the prostate cancer TME, the immunogenicity of BiTE constructs and focused targeting of BiTEs to tumour cells. With these developments and the possibilities of identification of more specific TAAs, improved affinity of BiTEs to TAAs, greater modelling and testing for immunogenicity, and modulation or mitigation of the anti-inflammatory mCRPC TME, it is reasonable to hope that BiTEs may provide a therapeutic benefit in the future for those afflicted with mCRPC.

Author contributions

HL: Writing–original draft, Writing–review and editing. LT: Supervision, Writing–review and editing. AH: Conceptualization, Supervision, Writing–review and editing.

Funding

The author(s) declare that no financial support was received for the research, authorship, and/or publication of this article.

Acknowledgments

The authors would like to acknowledge the contributions of Gina Velli, of the Princess Alexandra Hospital Library and Knowledge Centre, who assisted with the initial literature search for this review.

Conflict of interest

The authors declare that the research was conducted in the absence of any commercial or financial relationships that could be construed as a potential conflict of interest.

Publisher's note

References

Administration USFaD (2010) *Immunogenicity testing of therapeutic protein products - developing and validating assays for anti-drug antibody detection - guidelines for Industry*.

Agency, E. M. (2017) *Guideline on immunogenicity assessment of biotechnology-derived therapeutic proteins*.

Aggarwal, R. R., Aparicio, A., Heidenreich, A., Sandhu, S. K., Zhang, Y., Salvati, M., et al. (2021). Phase 1b study of AMG 757, a half-life extended bispecific T-cell engager (HLE BiTEimmune-oncology therapy) targeting DLL3, in *de novo* or treatment emergent neuroendocrine prostate cancer (NEPC). *J. Clin. Oncol.* 39 (15), TPS5100. doi:10.1200/jco.2021.39.15_suppl.tps5100

Ahmad, Z. A., Yeap, S. K., Ali, A. M., Ho, W. Y., Alitheen, N. B., and Hamid, M. (2012). scFv antibody: principles and clinical application. *Clin. Dev. Immunol.* 2012, 980250. doi:10.1155/2012/980250

Antonarakis, E. S., Shaukat, F., Isaacsson Velho, P., Kaur, H., Shenderov, E., Pardoll, D. M., et al. (2019). Clinical features and therapeutic outcomes in men with advanced prostate cancer and DNA mismatch repair gene mutations. *Eur. Urol.* 75 (3), 378–382. doi:10.1016/j.eururo.2018.10.009

Armstrong, A. J., Szmulewitz, R. Z., Petrylak, D. P., Holzbeierlein, J., Villers, A., Azad, A., et al. (2019). ARCHES: a randomized, phase III study of androgen deprivation therapy with enzalutamide or placebo in men with metastatic hormone-sensitive prostate cancer. *J. Clin. Oncol.* 37 (32), 2974–2986. doi:10.1200/JCO.19.00799

Author Anynomus (2017) *Aptevo therapeutics and MorphoSys end joint development and - commercialization agreement for mor209/es414*. Aptevo Therapeutics Inc. [press release].

Author Anynomus (2021). A study of JNJ-78278343, a T-cell-redirecting agent targeting human kallikrein 2 (KLK2), for advanced prostate cancer. Available at: https://clinicaltrials.gov/study/NCT04898634?tab=history.

Author Anynomus (2022) *Harpoon therapeutics reports fourth quarter and full year 2021 financial results and provides corporate update<harpoon-therapeutics-reports-fourth-quarter-and.pdf&gt*. Harpoon Therapeutics. [press release].

Banaszek, A., Bumm, T. G. P., Nowotny, B., Geis, M., Jacob, K., Wölfl, M., et al. (2019). On-target restoration of a split T cell-engaging antibody for precision immunotherapy. *Nat. Commun.* 10 (1), 5387. doi:10.1038/s41467-019-13196-0

Beer, T. M., Armstrong, A. J., Rathkopf, D. E., Loriot, Y., Sternberg, C. N., Higano, C. S., et al. (2014). Enzalutamide in metastatic prostate cancer before chemotherapy. *N. Engl. J. Med.* 371 (5), 424–433. doi:10.1056/NEJMoa1405095

Beer, T. M., Kwon, E. D., Drake, C. G., Fizazi, K., Logothetis, C., Gravis, G., et al. (2017). Randomized, double-blind, phase III trial of ipilimumab versus placebo in asymptomatic or minimally symptomatic patients with metastatic chemotherapy-naive castration-resistant prostate cancer. *J. Clin. Oncol.* 35 (1), 40–47. doi:10.1200/JCO.2016.69.1584

Belmontes, B., Sawant, D. V., Zhong, W., Tan, H., Kaul, A., Aeffner, F., et al. (2021). Immunotherapy combinations overcome resistance to bispecific T cell engager treatment in T cell-cold solid tumors. *Sci. Transl. Med.* 13 (608), eabd1524. doi:10.1126/scitranslmed.abd1524

Ben, T., Horvath, L., Rettig, M., Fizazi, K., Lolkema, M. P., Dorff, T. B., et al. (2020). Phase I study of AMG 160, a half-life extended bispecific T-cell engager (HLE BiTE immune therapy) targeting prostate-specific membrane antigen, in patients with metastatic castration-resistant prostate cancer (mCRPC). *J. Clin. Oncol.* 38 (15), TPS5590. doi:10.1200/jco.2020.38.15_suppl.tps5590

Bono, J. S. D., Fong, L., Beer, T. M., Gao, X., Geynisman, D. M., Hab, I. I. I., et al. (2021). Results of an ongoing phase 1/2a dose escalation study of HPN424, a tri-specific half-life extended PSMA-targeting T-cell engager, in patients with metastatic castration-resistant prostate cancer (mCRPC). *J. Clin. Oncol.* 39 (15_Suppl. l), 5013. doi:10.1200/jco.2021.39.15_suppl.5013

Brandt, L. J. B., Barnkob, M. B., Michaels, Y. S., Heiselberg, J., and Barington, T. (2020). Emerging approaches for regulation and control of CAR T cells: a mini review. *Front. Immunol.* 11, 326. doi:10.3389/fimmu.2020.00326

Brinkmann, U., and Kontermann, R. E. (2017). The making of bispecific antibodies. *MAbs* 9 (2), 182–212. doi:10.1080/19420862.2016.1268307

Brünker, P., Wartha, K., Friess, T., Grau-Richards, S., Waldhauer, I., Koller, C. F., et al. (2016). RG7386, a novel tetravalent FAP-DR5 antibody, effectively triggers FAP-dependent, avidity-driven DR5 hyperclustering and tumor cell apoptosis. *Mol. Cancer Ther.* 15 (5), 946–957. doi:10.1158/1535-7163.MCT-15-0647

Buelow, B., Dalvi, P., Dang, K., Patel, A., Johal, K., Pham, D., et al. (2021). TNB585.001: a multicenter, phase 1, open-label, dose-escalation and expansion study of tnb-585, a bispecific T-cell engager targeting PSMA in subjects with metastatic castrate resistant prostate cancer. *J. Clin. Oncol.* 39 (15), TPS5092. doi:10.1200/jco.2021.39.15_suppl.tps5092

Calvo, E., Doger de Spéville, B., Carles Galceran, J., Peer, A., Sarid, D. L., Eigl, B. J., et al. (2022). 1367P JNJ-70218902 (JNJ-902), a TMEFF2 x CD3 bispecific antibody, in prostate cancer: initial results from a phase I dose escalation study. *Ann. Oncol.* 33, S1166. doi:10.1016/j.annonc.2022.07.1499

Chi, K. N., Agarwal, N., Bjartell, A., Chung, B. H., Pereira de Santana Gomes, A. J., Given, R., et al. (2019). Apalutamide for metastatic, castration-sensitive prostate cancer. *N. Engl. J. Med.* 381 (1), 13–24. doi:10.1056/NEJMoa1903307

Clinicaltrials (2019). "Study with bispecific antibody engaging T-cells," in *Patients with progressive cancer diseases with positive PSCA marker*. Available at: https://clinicaltrials.gov/study/NCT03927573?tab=history.

de Bono, J. S., Logothetis, C. J., Molina, A., Fizazi, K., North, S., Chu, L., et al. (2011). Abiraterone and increased survival in metastatic prostate cancer. *N. Engl. J. Med.* 364 (21), 1995–2005. doi:10.1056/NEJMoa1014618

Deegen, P., Thomas, O., Nolan-Stevaux, O., Li, S., Wahl, J., Bogner, P., et al. (2021). The PSMA-targeting half-life extended BiTE therapy AMG 160 has potent antitumor activity in preclinical models of metastatic castration-resistant prostate cancer. *Clin. CANCER Res.* 27 (10), 2928–2937. doi:10.1158/1078-0432.CCR-20-3725

de Sostoa, J., Fajardo, C. A., Moreno, R., Ramos, M. D., Farrera-Sal, M., and Alemany, R. (2019). Targeting the tumor stroma with an oncolytic adenovirus secreting a fibroblast activation protein-targeted bispecific T-cell engager. *J. Immunother. Cancer* 7 (1), 19. doi:10.1186/s40425-019-0505-4

Eikenes, L., Tari, M., Tufto, I., Bruland, O. S., and de Lange Davies, C. (2005). Hyaluronidase induces a transcapillary pressure gradient and improves the distribution and uptake of liposomal doxorubicin (Caelyx) in human osteosarcoma xenografts. *Br. J. Cancer* 93 (1), 81–88. doi:10.1038/sj.bjc.6602626

Fizazi, K., Foulon, S., Carles, J., Roubaud, G., McDermott, R., Fléchon, A., et al. (2022). Abiraterone plus prednisone added to androgen deprivation therapy and docetaxel in *de novo* metastatic castration-sensitive prostate cancer (PEACE-1): a multicentre, open-label, randomised, phase 3 study with a 2 × 2 factorial design. *Lancet* 399 (10336), 1695–1707. doi:10.1016/S0140-6736(22)00367-1

Fizazi, K., Piulats, J. M., Reaume, M. N., Ostler, P., McDermott, R., Gingerich, J. R., et al. (2023). Rucaparib or physician's choice in metastatic prostate cancer. *N. Engl. J. Med.* 388 (8), 719–732. doi:10.1056/NEJMoa2214676

Fizazi, K., Tran, N., Fein, L., Matsubara, N., Rodriguez-Antolin, A., Alekseev, B. Y., et al. (2017). Abiraterone plus prednisone in metastatic, castration-sensitive prostate cancer. *N. Engl. J. Med.* 377 (4), 352–360. doi:10.1056/NEJMoa1704174

Friedrich, M., Raum, T., Lutterbuese, R., Voelkel, M., Deegen, P., Rau, D., et al. (2012). Regression of human prostate cancer xenografts in mice by AMG 212/bay2010112, a novel PSMA/CD3-Bispecific BiTE antibody cross-reactive with non-human primate antigens. *Mol. CANCER Ther.* 11 (12), 2664–2673. doi:10.1158/1535-7163.MCT-12-0042

Gannon, P. O., Poisson, A. O., Delvoye, N., Lapointe, R., Mes-Masson, A. M., and Saad, F. (2009). Characterization of the intra-prostatic immune cell infiltration in androgen-deprived prostate cancer patients. *J. Immunol. Methods* 348 (1-2), 9–17. doi:10.1016/j.jim.2009.06.004

Ge, R., Wang, Z., and Cheng, L. (2022). Tumor microenvironment heterogeneity an important mediator of prostate cancer progression and therapeutic resistance. *npj Precis. Oncol.* 6 (1), 31. doi:10.1038/s41698-022-00272-w

Geiger, M., Stubenrauch, K. G., Sam, J., Richter, W. F., Jordan, G., Eckmann, J., et al. (2020). Protease-activation using anti-idiotypic masks enables tumor specificity of a folate receptor 1-T cell bispecific antibody. *Nat. Commun.* 11 (1), 3196. doi:10.1038/s41467-020-16838-w

Hackenbruch, C., Heitmann, J. S., Walz, J. S., Federmann, B., Pflügler, M., Hadaschik, B. A., et al. (2023). ProSperA: phase I study to evaluate safety, tolerability and preliminary efficacy of a bispecific PSMAxCD3 antibody in men with biochemical recurrence of prostate cancer. *J. Clin. Oncol.* 41 (16_Suppl. l), TPS5114–TPS. doi:10.1200/jco.2023.41.16_suppl.tps5114

Hansen, A. R., Massard, C., Ott, P. A., Haas, N. B., Lopez, J. S., Ejadi, S., et al. (2018). Pembrolizumab for advanced prostate adenocarcinoma: findings of the KEYNOTE-028 study. *Ann. Oncol.* 29 (8), 1807–1813. doi:10.1093/annonc/mdy232

Heitmann, J. S., Walz, J. S., Pflügler, M., Marconato, M., Tegeler, C. M., Reusch, J., et al. (2022). Abstract CT141: CC-1, a bispecific PSMAxCD3 antibody for treatment of prostate carcinoma: results of the ongoing phase I dose escalation trial. *Cancer Res.* 82 (12), CT141. doi:10.1158/1538-7445.am2022-ct141

Hernandez-Hoyos, G., Sewell, T., Bader, R., Bannink, J., Chenault, R. A., Daugherty, M., et al. (2016). MOR209/ES414, a novel bispecific antibody targeting PSMA for the treatment of metastatic castration-resistant prostate cancer. *Mol. Cancer Ther.* 15 (9), 2155–2165. doi:10.1158/1535-7163.MCT-15-0242

Herrmann, M., Krupka, C., Deiser, K., Brauchle, B., Marcinek, A., Ogrinc Wagner, A., et al. (2018). Bifunctional PD-1 × αCD3 × αCD33 fusion protein reverses adaptive immune escape in acute myeloid leukemia. *Blood* 132 (23), 2484–2494. doi:10.1182/blood-2018-05-849802

Hummel, H.-D., Kufer, P., Grüllich, C., Seggewiss-Bernhardt, R., Deschler-Baier, B., Chatterjee, M., et al. (2021). Pasotuxizumab, a BiTE® immune therapy for castration-resistant prostate cancer: phase I, dose-escalation study findings. *Immunotherapy* 13 (2), 125–141. doi:10.2217/imt-2020-0256

Hussain, M., Mateo, J., Fizazi, K., Saad, F., Shore, N., Sandhu, S., et al. (2020). Survival with olaparib in metastatic castration-resistant prostate cancer. *N. Engl. J. Med.* 383 (24), 2345–2357. doi:10.1056/NEJMoa2022485

Hweixian, L. P., Kelly, H., Nathaniel, T., Bin, W., Christian, B., Christian, W., et al. (2023). Characterization and root cause analysis of immunogenicity to pasotuxizumab (AMG 212), a prostate-specific membrane antigen-targeting bispecific T-cell engager therapy. *Front. Immunol.* 14, 1261070. doi:10.3389/fimmu.2023.1261070

James, N. D., Sydes, M. R., Clarke, N. W., Mason, M. D., Dearnaley, D. P., Spears, M. R., et al. (2016). Addition of docetaxel, zoledronic acid, or both to first-line long-term hormone therapy in prostate cancer (STAMPEDE): survival results from an adaptive, multiarm, multistage, platform randomised controlled trial. *Lancet* 387 (10024), 1163–1177. doi:10.1016/S0140-6736(15)01037-5

Jarvi, N. L., and Balu-Iyer, S. V. (2021). Immunogenicity challenges associated with subcutaneous delivery of therapeutic proteins. *BioDrugs* 35 (2), 125–146. doi:10.1007/s40259-020-00465-4

Jawa, V., Terry, F., Gokemeijer, J., Mitra-Kaushik, S., Roberts, B. J., Tourdot, S., et al. (2020). T-cell dependent immunogenicity of protein therapeutics pre-clinical assessment and mitigation–updated consensus and review 2020. *Front. Immunol.* 11, 1301. doi:10.3389/fimmu.2020.01301

Jiang, X., Wang, J., Deng, X., Xiong, F., Ge, J., Xiang, B., et al. (2019). Role of the tumor microenvironment in PD-L1/PD-1-mediated tumor immune escape. *Mol. Cancer* 18 (1), 10. doi:10.1186/s12943-018-0928-4

Jiao, S., Subudhi, S. K., Aparicio, A., Ge, Z., Guan, B., Miura, Y., et al. (2019). Differences in tumor microenvironment dictate T helper lineage polarization and response to immune checkpoint therapy. *Cell* 179 (5), 1177–1190. doi:10.1016/j.cell.2019.10.029

Johnson, S., Burke, S., Huang, L., Gorlatov, S., Li, H., Wang, W., et al. (2010). Effector cell recruitment with novel Fv-based dual-affinity re-targeting protein leads to potent tumor cytolysis and *in vivo* B-cell depletion. *J. Mol. Biol.* 399 (3), 436–449. doi:10.1016/j.jmb.2010.04.001

Kantarjian, H., Stein, A., Gokbuget, N., Fielding, A. K., Schuh, A. C., Ribera, J. M., et al. (2017). Blinatumomab versus chemotherapy for advanced acute lymphoblastic leukemia. *N. Engl. J. Med.* 376 (9), 836–847. doi:10.1056/NEJMoa1609783

Kantoff, P. W., Higano, C. S., Shore, N. D., Berger, E. R., Small, E. J., Penson, D. F., et al. (2010). Sipuleucel-T immunotherapy for castration-resistant prostate cancer. *N. Engl. J. Med.* 363 (5), 411–422. doi:10.1056/NEJMoa1001294

Kauer, J., Horner, S., Osburg, L., Muller, S., Marklin, M., Heitmann, J. S., et al. (2020). Tocilizumab, but not dexamethasone, prevents CRS without affecting antitumor activity of bispecific antibodies. *J. Immunother. Cancer* 8 (1), e000621. doi:10.1136/jitc-2020-000621

Kazandjian, D., Suzman, D. L., Blumenthal, G., Mushti, S., He, K., Libeg, M., et al. (2016). FDA approval summary: nivolumab for the treatment of metastatic non-small cell lung cancer with progression on or after platinum-based chemotherapy. *Oncologist* 21 (5), 634–642. doi:10.1634/theoncologist.2015-0507

Kebenko, M., Goebeler, M. E., Wolf, M., Hasenburg, A., Seggewiss-Bernhardt, R., Ritter, B., et al. (2018). A multicenter phase 1 study of solitomab (MT110, AMG 110), a bispecific EpCAM/CD3 T-cell engager (BiTE®) antibody construct, in patients with refractory solid tumors. *Oncoimmunology* 7 (8), e1450710. doi:10.1080/2162402X.2018.1450710

Kelly, W. K., Danila, D. C., Lin, C. C., Lee, J. L., Matsubara, N., Ward, P. J., et al. (2023). Xaluritamig, a STEAP1 x CD3 XmAb 2+1 immune therapy for metastatic castration-resistant prostate cancer: results from dose exploration in a first-in-human study. *Cancer Discov.* OF1-OF14. doi:10.1158/2159-8290.CD-23-0964

Kelly, W. K., Thanigaimani, P., Sun, F., Seebach, F. A., Lowy, I., Sandigursky, S., et al. (2022). A phase 1/2 study of REGN4336, a PSMAxCD3 bispecific antibody, alone and in combination with cemiplimab in patients with metastatic castration-resistant prostate cancer. *J. Clin. Oncol.* 40 (16_Suppl. l), TPS5105–TPS. doi:10.1200/jco.2022.40.16_suppl.tps5105

Kipriyanov, S. M., Moldenhauer, G., Schuhmacher, J., Cochlovius, B., Von der Lieth, C. W., Matys, E. R., et al. (1999). Bispecific tandem diabody for tumor therapy with improved antigen binding and pharmacokinetics. *J. Mol. Biol.* 293 (1), 41–56. doi:10.1006/jmbi.1999.3156

Klein, C., Schaefer, W., Regula, J. T., Dumontet, C., Brinkmann, U., Bacac, M., et al. (2019). Engineering therapeutic bispecific antibodies using CrossMab technology. *Methods.* 154, 21–31. doi:10.1016/j.ymeth.2018.11.008

Krueger, T. E., Thorek, D. L. J., Meeker, A. K., Isaacs, J. T., and Brennen, W. N. (2019). Tumor-infiltrating mesenchymal stem cells: drivers of the immunosuppressive tumor microenvironment in prostate cancer? *Prostate* 79 (3), 320–330. doi:10.1002/pros.23738

Kwon, E. D., Drake, C. G., Scher, H. I., Fizazi, K., Bossi, A., van den Eertwegh, A. J. M., et al. (2014). Ipilimumab versus placebo after radiotherapy in patients with metastatic castration-resistant prostate cancer that had progressed after docetaxel chemotherapy (CA184-043): a multicentre, randomised, double-blind, phase 3 trial. *Lancet Oncol.* 15 (7), 700–712. doi:10.1016/S1470-2045(14)70189-5

Kyriakopoulos, C. E., Chen, Y. H., Carducci, M. A., Liu, G., Jarrard, D. F., Hahn, N. M., et al. (2018). Chemohormonal therapy in metastatic hormone-sensitive prostate cancer: long-term survival analysis of the randomized phase III E3805 CHAARTED trial. *J. Clin. Oncol.* 36 (11), 1080–1087. doi:10.1200/JCO.2017.75.3657

Lee, S. C., Ma, J. S. Y., Kim, M. S., Laborda, E., Choi, S. H., Hampton, E. N., et al. (2021). A PSMA-targeted bispecific antibody for prostate cancer driven by a small-molecule targeting ligand. *Sci. Adv.* 7 (33), eabi8193. doi:10.1126/sciadv.abi8193

Lim, E. A., Schweizer, M. T., Chi, K. N., Aggarwal, R. R., Agarwal, N., Gulley, J. L., et al. (2022). Safety and preliminary clinical activity of JNJ-63898081 (JNJ-081), a PSMA and CD3 bispecific antibody, for the treatment of metastatic castrate-resistant prostate cancer (mCRPC). *J. Clin. Oncol.* 40 (6_Suppl. l), 279. doi:10.1200/jco.2022.40.6_suppl.279

Linke, R., Klein, A., and Seimetz, D. (2010). Catumaxomab: clinical development and future directions. *MAbs* 2 (2), 129–136. doi:10.4161/mabs.2.2.11221

Lutterbuese, R., Friedrich, M., Kischel, R., Rau, D., Hoffmann, P., Ebert, E., et al. (2011). Abstract 4561: preclinical characterization of MT112/BAY 2010112, a novel PSMA/CD3-bispecific BiTE antibody for the treatment of prostate cancer. *Cancer Res.* 71 (8), 4561. doi:10.1158/1538-7445.am2011-4561

Markowski, M. C., Kilari, D., Eisenberger, M. A., McKay, R. R., Dreicer, R., Trikha, M., et al. (2021). Phase I study of CCW702, a bispecific small molecule-antibody conjugate targeting PSMA and CD3 in patients with metastatic castration-resistant prostate cancer (mCRPC). *J. Clin. Oncol.* 39 (15_Suppl. l), TPS5094–TPS. doi:10.1200/jco.2021.39.15_suppl.tps5094

Maruta, M., Ochi, T., Tanimoto, K., Asai, H., Saitou, T., Fujiwara, H., et al. (2019). Direct comparison of target-reactivity and cross-reactivity induced by CAR- and BiTE-redirected T cells for the development of antibody-based T-cell therapy. *Sci. Rep.* 9 (1), 13293. doi:10.1038/s41598-019-49834-2

Mehra, N., Robbrecht, D., Voortman, J., Parren, P. W., Macia, S., Veeneman, J., et al. (2023). Early dose escalation of LAVA-1207, a novel bispecific gamma-delta T-cell engager (Gammabody), in patients with metastatic castration-resistant prostate cancer (mCRPC). *J. Clin. Oncol.* 41 (6_Suppl. l), 153. doi:10.1200/jco.2023.41.6_suppl.153

Middelburg, J., Kemper, K., Engelberts, P., Labrijn, A. F., Schuurman, J., and van Hall, T. (2021). Overcoming challenges for CD3-bispecific antibody therapy in solid tumors. *Cancers (Basel)* 13 (2), 287. doi:10.3390/cancers13020287

Morris, E. C., Neelapu, S. S., Giavridis, T., and Sadelain, M. (2022). Cytokine release syndrome and associated neurotoxicity in cancer immunotherapy. *Nat. Rev. Immunol.* 22 (2), 85–96. doi:10.1038/s41577-021-00547-6

Nathan, P., Hassel, J. C., Rutkowski, P., Baurain, J. F., Butler, M. O., Schlaak, M., et al. (2021). Overall survival benefit with tebentafusp in metastatic uveal melanoma. *N. Engl. J. Med.* 385 (13), 1196–1206. doi:10.1056/NEJMoa2103485

Nolan-Stevaux, O., Li, C., Liang, L., Zhan, J., Estrada, J., Osgood, T., et al. (2023). AMG 509 (xaluritamig), an anti-STEAP1 XmAb 2+1 T-cell redirecting immune therapy with avidity-dependent activity against prostate cancer. *Cancer Discov.* 14, 90–103. doi:10.1158/2159-8290.CD-23-0984

Panchal, A., Seto, P., Wall, R., Hillier, B. J., Zhu, Y., Krakow, J., et al. (2020). COBRA™: a highly potent conditionally active T cell engager engineered for the treatment of solid tumors. *MAbs* 12 (1), 1792130. doi:10.1080/19420862.2020.1792130

Parker, C., Nilsson, S., Heinrich, D., Helle, S. I., O'Sullivan, J. M., Fosså, S. D., et al. (2013). Alpha emitter radium-223 and survival in metastatic prostate cancer. *N. Engl. J. Med.* 369 (3), 213–223. doi:10.1056/NEJMoa1213755

Petrylak, D. P., Tangen, C. M., Hussain, M. H. A., Lara, P. N., Jones, J. A., Taplin, M. E., et al. (2004). Docetaxel and estramustine compared with mitoxantrone and prednisone for advanced refractory prostate cancer. *N. Engl. J. Med.* 351 (15), 1513–1520. doi:10.1056/NEJMoa041318

Pham, E., Lutterbuese, P., Deegen, P., Mariano, N., Matthes, K., Wahl, J., et al. (2023). Abstract ND06: AMG 305, a dual targeting BiTE®molecule with selective activity for solid tumors that co-express CDH3 and MSLN. *Cancer Res.* 83 (7_Suppl. ment), ND06–ND. doi:10.1158/1538-7445.am2023-nd06

Pu, Y., Xu, M., Liang, Y., Yang, K., Guo, Y., Yang, X., et al. (2016). Androgen receptor antagonists compromise T cell response against prostate cancer leading to early tumor relapse. *Sci. Transl. Med.* 8 (333), 333ra47–ra47. doi:10.1126/scitranslmed.aad5659

Qin, C., Wang, J., Du, Y., and Xu, T. (2022). Immunosuppressive environment in response to androgen deprivation treatment in prostate cancer. *Front. Endocrinol.* 13, 1055826. doi:10.3389/fendo.2022.1055826

Riethmüller, G. (2012). Symmetry breaking: bispecific antibodies, the beginnings, and 50 years on. *Cancer Immun.* 12, 12.

Robert, C. (2020). A decade of immune-checkpoint inhibitors in cancer therapy. *Nat. Commun.* 11 (1), 3801. doi:10.1038/s41467-020-17670-y

Robinson, D., Van Allen, E. M., Wu, Y. M., Schultz, N., Lonigro, R. J., Mosquera, J. M., et al. (2015). Integrative clinical genomics of advanced prostate cancer. *Cell* 162 (2), 454. doi:10.1016/j.cell.2015.06.053

Ross, S. L., Sherman, M., McElroy, P. L., Lofgren, J. A., Moody, G., Baeuerle, P. A., et al. (2017). Bispecific T cell engager (BiTE®) antibody constructs can mediate bystander tumor cell killing. *PLoS One* 12 (8), e0183390. doi:10.1371/journal.pone.0183390

Rothe, A., Sasse, S., Topp, M. S., Eichenauer, D. A., Hummel, H., Reiners, K. S., et al. (2015). A phase 1 study of the bispecific anti-CD30/CD16A antibody construct AFM13 in patients with relapsed or refractory Hodgkin lymphoma. *Blood* 125 (26), 4024–4031. doi:10.1182/blood-2014-12-614636

Sartor, O., de Bono, J., Chi, K. N., Fizazi, K., Herrmann, K., Rahbar, K., et al. (2021). Lutetium-177–PSMA-617 for metastatic castration-resistant prostate cancer. *N. Engl. J. Med.* 385 (12), 1091–1103. doi:10.1056/NEJMoa2107322

Schaefer, W., Regula, J. T., Bähner, M., Schanzer, J., Croasdale, R., Dürr, H., et al. (2011). Immunoglobulin domain crossover as a generic approach for the production of bispecific IgG antibodies. *Proc. Natl. Acad. Sci. U. S. A.* 108 (27), 11187–11192. doi:10.1073/pnas.1019002108

SEER Explorer (2023) *An interactive website for SEER cancer statistics: surveillance Research Program*. National Cancer Institute. [updated 16/11/2023. SEER Incidence Data, November 2022 Submission (1975-2020), SEER 22 registries (excluding Illinois and Massachusetts) Available at: https://seer.cancer.gov/statistics-network/explorer/.

Shang, Z., Niu, Y., Cai, Q., Chen, J., Tian, J., Yeh, S., et al. (2014). Human kallikrein 2 (KLK2) promotes prostate cancer cell growth via function as a modulator to promote the ARA70-enhanced androgen receptor transactivation. *Tumor Biol.* 35, 1881–1890. doi:10.1007/s13277-013-1253-6

Sharma, P., Pachynski, R. K., Narayan, V., Flechon, A., Gravis, G., Galsky, M. D., et al. (2019). Initial results from a phase II study of nivolumab (NIVO) plus ipilimumab (IPI) for the treatment of metastatic castration-resistant prostate cancer (mCRPC; CheckMate 650). *J. Clin. Oncol.* 37 (7_Suppl. l), 142. doi:10.1200/jco.2019.37.7_suppl.142

Shimabukuro-Vornhagen, A., Gödel, P., Subklewe, M., Stemmler, H. J., Schlößer, H. A., Schlaak, M., et al. (2018). Cytokine release syndrome. *J. Immunother. Cancer* 6 (1), 56. doi:10.1186/s40425-018-0343-9

Siegler, E. L., and Kenderian, S. S. (2020). Neurotoxicity and cytokine release syndrome after chimeric antigen receptor T cell therapy: insights into mechanisms and novel therapies. *Front. Immunol.* 11, 1973. doi:10.3389/fimmu.2020.01973

Silver, D. A., Pellicer, I., Fair, W. R., Heston, W. D., and Cordon-Cardo, C. (1997). Prostate-specific membrane antigen expression in normal and malignant human tissues. *Clin. Cancer Res.* 3 (1), 81–85.

Simão, D. C., Zarrabi, K. K., Mendes, J. L., Luz, R., Garcia, J. A., Kelly, W. K., et al. (2023). Bispecific T-cell engagers therapies in solid tumors: focusing on prostate cancer. *Cancers* 15 (5), 1412. doi:10.3390/cancers15051412

Smith, M. R., Hussain, M., Saad, F., Fizazi, K., Sternberg, C. N., Crawford, E. D., et al. (2022). Darolutamide and survival in metastatic, hormone-sensitive prostate cancer. *N. Engl. J. Med.* 386 (12), 1132–1142. doi:10.1056/NEJMoa2119115

Subudhi, S. K., Siddiqui, B. A., Maly, J. J., Nandagopal, L., Lam, E. T., Whang, Y. E., et al. (2021). Safety and efficacy of AMG 160, a half-life extended BiTE immune therapy targeting prostate-specific membrane antigen (PSMA), and other therapies for metastatic castration-resistant prostate cancer (mCRPC). *J. Clin. Oncol.* 39 (15), TPS5088. doi:10.1200/jco.2021.39.15_suppl.tps5088

Sun, B. L. (2021). Immunotherapy in treatment of metastatic prostate cancer: an approach to circumvent immunosuppressive tumor microenvironment. *Prostate* 81 (15), 1125–1134. doi:10.1002/pros.24213

Sung, H., Ferlay, J., Siegel, R. L., Laversanne, M., Soerjomataram, I., Jemal, A., et al. (2021). Global cancer statistics 2020: GLOBOCAN estimates of incidence and mortality worldwide for 36 cancers in 185 countries. *CA Cancer J. Clin.* 71 (3), 209–249. doi:10.3322/caac.21660

Suurs, F. V., Lub-de Hooge, M. N., de Vries, E. G. E., and de Groot, D. J. A. (2019). A review of bispecific antibodies and antibody constructs in oncology and clinical challenges. *Pharmacol. Ther.* 201, 103–119. doi:10.1016/j.pharmthera.2019.04.006

Tabernero, J., Melero, I., Ros, W., Argiles, G., Marabelle, A., Rodriguez-Ruiz, M. E., et al. (2017). Phase Ia and Ib studies of the novel carcinoembryonic antigen (CEA) T-cell bispecific (CEA CD3 TCB) antibody as a single agent and in combination with atezolizumab: preliminary efficacy and safety in patients with metastatic colorectal cancer (mCRC). *J. Clin. Oncol.* 35 (15_Suppl. l), 3002. doi:10.1200/jco.2017.35.15_suppl.3002

Tosolini, M., Pont, F., Poupot, M., Vergez, F., Nicolau-Travers, M. L., Vermijlen, D., et al. (2017). Assessment of tumor-infiltrating TCRVγ9Vδ2 γδ lymphocyte abundance by deconvolution of human cancers microarrays. *Oncoimmunology* 6 (3), e1284723. doi:10.1080/2162402X.2017.1284723

Trenevska, I., Li, D., and Banham, A. H. (2017). Therapeutic antibodies against intracellular tumor antigens. *Front. Immunol.* 8, 1001. doi:10.3389/fimmu.2017.01001

Vallera, D. A., Felices, M., McElmurry, R., McCullar, V., Zhou, X., Schmohl, J. U., et al. (2016). IL15 trispecific killer engagers (TriKE) make natural killer cells specific to CD33+ targets while also inducing persistence, *in vivo* expansion, and enhanced function. *Clin. Cancer Res.* 22 (14), 3440–3450. doi:10.1158/1078-0432.CCR-15-2710

van Brummelen, E. M., Ros, W., Wolbink, G., Beijnen, J. H., and Schellens, J. H. (2016). Antidrug antibody formation in oncology: clinical relevance and challenges. *Oncologist* 21 (10), 1260–1268. doi:10.1634/theoncologist.2016-0061

Wolf, E., Hofmeister, R., Kufer, P., Schlereth, B., and Baeuerle, P. A. (2005). BiTEs: bispecific antibody constructs with unique anti-tumor activity. *Drug Discov. Today* 10 (18), 1237–1244. doi:10.1016/S1359-6446(05)03554-3

Xu, M., Evans, L., Bizzaro, C. L., Quaglia, F., Verrillo, C. E., Li, L., et al. (2022). STEAP1-4 (Six-Transmembrane epithelial antigen of the prostate 1-4) and their clinical implications for prostate cancer. *Cancers (Basel)* 14 (16), 4034. doi:10.3390/cancers14164034

Xu, Y., Lee, J., Tran, C., Heibeck, T. H., Wang, W. D., Yang, J., et al. (2015). Production of bispecific antibodies in "knobs-into-holes" using a cell-free expression system. *MAbs* 7 (1), 231–242. doi:10.4161/19420862.2015.989013

Zekri, L., Vogt, F., Osburg, L., Müller, S., Kauer, J., Manz, T., et al. (2021). An IgG-based bispecific antibody for improved dual targeting in PSMA-positive cancer. *EMBO Mol. Med.* 13 (2), e11902. doi:10.15252/emmm.201911902

Zhou, S., Liu, M., Ren, F., Meng, X., and Yu, J. (2021). The landscape of bispecific T cell engager in cancer treatment. *Biomark. Res.* 9 (1), 38. doi:10.1186/s40364-021-00294-9

Zhukovsky, E., Chu, S., Bernett, M., Karki, S., Dang, W., Hammond, P., et al. (2007). XmAb Fc engineered anti-CD19 monoclonal antibodies with enhanced *in vitro* efficacy against multiple lymphoma cell lines. *J. Clin. Oncol.* 25 (18_Suppl. l), 3021. doi:10.1200/jco.2007.25.18_suppl.3021

frontiers | Frontiers in Pharmacology

TYPE Original Research
PUBLISHED 30 May 2024
DOI 10.3389/fphar.2024.1365683

OPEN ACCESS

EDITED BY
Lei Yin,
Shanghai Jiaotong University School of Medicine, China

REVIEWED BY
Keyi Wang,
Fudan University, China
Houliang Zhang,
Tongji University, China

*CORRESPONDENCE
Shenglin Gao,
gaoshenglin12135@njmu.edu.cn
Xiaokai Shi,
shixiaokai@njmu.edu.cn
Li Zuo,
zuoli@njmu.edu.cn

†These authors have contributed equally to this work

RECEIVED 04 January 2024
ACCEPTED 09 May 2024
PUBLISHED 30 May 2024

CITATION
Peng X, Liu C, Zhang L, Chen Y, Mao L, Gao S, Shi X and Zuo L (2024), IL4I1: a novel molecular biomarker represents an inflamed tumor microenvironment and precisely predicts the molecular subtype and immunotherapy response of bladder cancer.
Front. Pharmacol. 15:1365683.
doi: 10.3389/fphar.2024.1365683

IL4I1: a novel molecular biomarker represents an inflamed tumor microenvironment and precisely predicts the molecular subtype and immunotherapy response of bladder cancer

Xiangrong Peng[1,2†], Chuan Liu[1,2†], Li Zhang[1,2†], Yin Chen[1,2], Lixin Mao[1,2], Shenglin Gao[1,2,3*], Xiaokai Shi[1,2*] and Li Zuo[1,2*]

[1]Department of Urology, ChangZhou No.2 people's Hospital, Nanjing Medical University, Changzhou, Jiangsu, China, [2]Laboratory of Urology, ChangZhou Medical Center, Nanjing Medical University, Changzhou, Jiangsu, China, [3]Department of Urology, Gonghe County Hospital of Traditional Chinese Medicine, Hainan Tibetan Autonomous Prefecture, Qinghai, China

Introduction: IL4I1, also known as Interleukin-4-induced gene 1, is an enzyme that can modulate the immune system by acting as a L-amino acid oxidase. Nevertheless, a precise understanding of the correlation of IL4I1 with immunological features and immunotherapy efficacy in bladder cancer (BLCA) remains incomplete.

Methods: We analyzed RNA sequencing data from the Cancer Genome Atlas (TCGA) to investigate the immune function and prognostic importance of IL4I1 across different cancer types. We further examined the TCGA-BLCA cohort for correlations between IL4I1 and various immunological characteristics of tumor microenvironment (TME), such as cancer immune cycle, immune cell infiltration, immune checkpoint expression and T cell inflamed score. Validation was conducted using two independent cohort, GSE48075 and E-MTAB-4321. Finally, RNA sequencing data from the IMvigor210 cohort and immunohistochemistry assays were employed to validate the predictive value of IL4I1 for the TME and immunotherapy efficacy.

Results: In our findings, a positive correlation was observed between IL4I1 expression and immunomodulators expression, immune cell infiltration, the cancer immune cycle, and T cell inflamed score in BLCA, suggesting a significant link to the inflamed TME. In addition, studies have shown that IL4I1 elevated levels of individuals tend to be more performance for basal subtype and exhibit enhanced response rates to diverse treatment modalities, specifically immunotherapy. Clinical data from the IMvigor 210 cohort confirmed a higher rate of response to immunotherapy and better survival benefits in patients with high IL4I1 expression.

Discussion: To summarize, our research showed that elevated IL4I1 levels are indicative of an inflamed TME, the basal subtype, and a more favorable response to various treatment methods, especially immune checkpoint blockade therapy in BLCA.

KEYWORDS

bladder cancer, inflamed tumor microenvironment, IL4I1, immunotherapy, molecular subtype

Introduction

Bladder cancer (BLCA) is among the prevalent urological cancers globally. By 2023, BLCA ranked seventh in incidence among all malignant tumors and fourth in incidence among men globally (Siegel et al., 2023). Surgical removal is the primary approach for initial instances of BLCA, and the outlook for advanced metastatic BLCA remains unfavorable despite the utilization of neoadjuvant and adjuvant chemotherapy (Witjes et al., 2021). In the past few years, immunotherapy, particularly immune checkpoint blockade (ICB) treatment involving anti-PD-1/PD-L1, has provided hopeful survival advantages for individuals with advanced BLCA, and has greatly enhanced the treatment condition for those with advanced BLCA (Necchi et al., 2017; Powles et al., 2018). Nevertheless, due to the presence of either primary or secondary resistance mechanisms, the ICB proves to be effective for only a minority of patients (Rosenberg et al., 2016; Sharma et al., 2017). This suggests that there are variations in the immune status of each host during cancer development. The effective application of ICB therapy heavily relies on the presence of anti-cancer immune response and an inflamed tumor microenvironment (TME) in patients (Ji et al., 2012; Chen and Mellman, 2017). The TME contains a diverse combination of cells, comprising both tumor cells and non-tumor cells. The two major constituents among the non-tumor cells are immune cells and stromal cells (Eruslanov et al., 2012; Müller et al., 2012; Said and Theodorescu, 2012). The levels and spatial arrangement of tumor infiltrating lymphocytes (TILs) have the potential to indicate tumor inflammation stages, subtypes, and patient survival rates. Elevated levels of TILs are indicative of an inflamed subtype, which is associated with a disease-specific 5-year survival rate of 80%, while the absence of immune infiltration is considered a non-inflamed subtype with the survival rate of below 25% (Pfannstiel et al., 2019). Therefore, we need biomarkers to define TME subtypes in order to predict the effectiveness of immunotherapy.

The antigen processing and presentation by tumor cells and immune cells plays a pivotal role in the activation of T cells and the generation of a long-lasting clinical response to ICIs. Integration of the antigen presentation machinery (APM), molecular and clinical data have demonstrated the ability to predict the efficacy of immunotherapy (Li et al., 2021; Yang et al., 2023). Cytotoxic T lymphocytes (CTL) kill cancer cells by releasing granules or inducing FasL-mediated apoptosis. However, due to immunosuppressive interactions between tumor cells and stromal cells, the function of CTL is suppressed. Increasing research had shown that the infiltration levels of CTL influence the efficacy of immune checkpoint blockade (ICB) therapy (SNYDER et al., 2014; Farhood et al., 2019). Additionally, IFN-γ is a key cytokine for activated T cells as well as natural killer (NK) and NK T cell production in the tumor microenvironment (Ikeda et al., 2002). And IFN-γ signaling enables the PD-1 signaling axis to become activated to downregulate the cytotoxic response (Abiko et al., 2015; Bellucci et al., 2015; Ayers et al., 2017). These are considered be potential biomarkers to predict clinical response to immunotherapy. In addition to, various biomarkers are also used to employe for the prediction of effectiveness, which encompass PD-L1 mRNA levels, tumor mutation burden (TMB), microsatellite instability (MSI), and BLCA molecular subtypes (McLaughlin et al., 2016; Bonneville et al., 2017; Kamoun et al., 2020; Sha et al., 2020). However, they also have limitations. Various factors can affect the accuracy of PD-L1 expression prediction, while the complex, slow, and expensive nature of identifying TMB, MSI, and molecular subtypes limits their clinical usability (McLaughlin et al., 2016; Bonneville et al., 2017; Nishino et al., 2017; Kamoun et al., 2020; Sha et al., 2020). Therefore, there is an immediate requirement to investigate novel biomarkers that are stable, convenient, and cost-effective.

IL4I1, a gene induced by Interleukin-4 (IL-4), was first discovered in B spleen cells of mice after being stimulated by IL-4 (Chu and Paul, 1997). IL4I1 exhibits L-amino acid oxidase activity and predominantly metabolizes L-phenylalanine, with a minor metabolic involvement in L-arginine, at the physiologically optimal pH (Boulland et al., 2007). IL4I1 has been described to be expressed primarily within the human immune system, central nervous system, and sperm, where it regulates immune cell differentiation and activation, affects sperm function, or promotes central nervous system development (Chavan et al., 2002; Houston et al., 2015; Pluchino and Peruzzotti-Jametti, 2016). Moreover, IL4I1 is closely linked to tumor progression. It is considered a metabolic immune checkpoint, and IL4I1-mediated catabolism of tryptophan (Trp) produces indoles and kynurenic acid, which activate aromatic receptors (AHR), thereby promoting cancer cell movement and inhibiting adaptive immunity (Sadik et al., 2020; Castellano et al., 2021). Excessive expression of IL4I1 has been detected in primary mediastinal B cell lymphoma, where it functions as a regulator of immune response by suppressing the proliferation of T lymphocytes (Boulland et al., 2007). A vitro experiments showed that the suppression IL4I1 led to the hindrance of ovarian cancer cell growth, movement, and infiltration (Zhao et al., 2021). IL4I1 has the ability to decrease the activity of $CD8^+$ T cells, enhance the development of inducible regulatory (iTreg) cells, and limit the expansion of T helper 17 (Th17) cells. In addition to promoting tumor evasion, it also minimizes the potentially detrimental impact of adaptive immune responses in chronic inflammatory conditions (Romagnani, 2016). These studies indicate the close association of IL4I1 with immune regulation and its ability to modulate the TME, thereby influencing tumor occurrence and progression. However, the complete understanding of IL4I1's role in BLCA remains to be fully clarified.

We extensively investigated the immunological characteristics of IL4I1 in BLCA through the multiple cohort analysis in our research. The study findings emphasize the robust correlation between the IL4I1 expression level and TME in BLCA, showcasing its accurate prognostic potential for BLCA molecular subtypes, inflamed TME, and response to immunotherapy. The results offer crucial hints for a more profound understanding of the immunological traits of BLCA and provide valuable perspectives for the development of personalized immunotherapeutic strategies.

Materials and methods

The flowchart of this study is demonstrated in Figure 1.

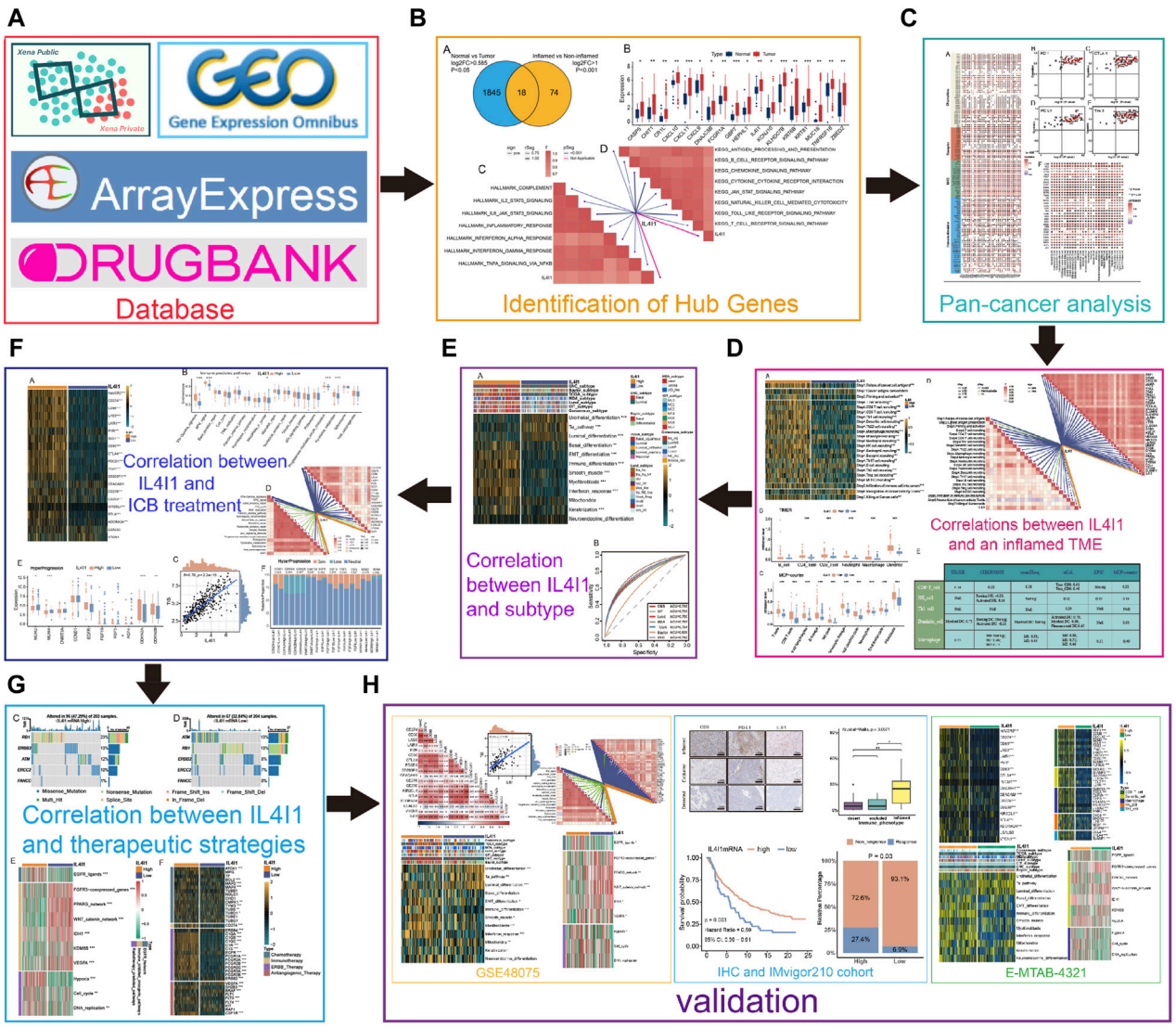

FIGURE 1
An overview of designation in our study. **(A)** The database used in this study. **(B)** Identifying differential expressed genes (DEGs) for inflamed and non-inflamed phenotypes. **(C)** Correlations between IL4I1 and pan-cancer immunological features. **(D)** Correlations between IL4I1 and an inflamed TME. **(E)** The predictive value of IL4I1 for the molecular subtypes in BLCA. **(F)** The predictive value of IL4I1 for clinical response of ICB treatment. **(G)** Correlation between IL4I1 and therapeutic strategies. **(H)** Validation by external cohorts and immunohistochemistry.

Data acquisition and preprocessing

The RNA sequencing data (FPKM value), somatic mutation data, and clinicopathological features for various cancer types of The Cancer Genome Atlas (TCGA) were obtained from the UCSC Xena (https://xenabrowser.net/datapages/) data portal (Goldman et al., 2020). FPKM values were converted into TPM values using the following formula:

$$TPM_i = \frac{FPKM_i}{\Sigma_j FPKM_j} \times 10^6$$

Following that, we applied a $\log2^{(TPM+1)}$ transformation to the TPM value for further investigation. The somatic mutation data were processes via Varscan (https://varscan.sourceforge.net/) (Koboldt et al., 2013). The data on copy number variation (CNV) of the genes that indicate hyperprogression were obtained from a previous research (Hu et al., 2021). Additionally, for external validation purposes, we downloaded three independent cohorts namely GSE48075,E-MTAB-4321 and IMvigor210 (http://research-pub.gene.com/IMvigor210CoreBiologies/) (Choi et al., 2014; Hedegaard et al., 2016; Mariathasan et al., 2018). And we collected six immunotherapy cohorts in melanoma. These datasets were also converted from FPKM to TPM values for subsequent analysis.

Exploration of the immunological characteristics of the TME in BLCA

The immunological features of TME in BLCA comprise the presence of immunomodulators, the functioning of the cancer immunity cycle, the degree of infiltration by tumor infiltrating

immune cells (TIICs), and the presence of inhibitory immune checkpoints. Initially, data on 121 immunomodulators, encompassing major histocompatibility complex (MHC), receptors, chemokines, and immunostimulators, were gathered from Charoentong et al.'s research (Charoentong et al., 2017). The cancer immunity cycle represents the immune response against cancer and comprises of seven stages: release of cancer cell antigens (step 1), cancer antigen presentation (step 2), priming and activation (step 3), trafficking of T cells to tumors (step 4), infiltration of T cells into tumors (step 5), recognition of cancer cells by T cells (step 6), and killing of cancer cells (step 7) (Chen and Mellman, 2013). Investigation of these steps' activity was conducted through the utilization of a single sample gene set enrichment analysis (ssGSEA).

Using the R package "GSVA," we performed ssGSEA to assess the extent of TIIC infiltration in the BLCA, utilizing signatures from the TISIDB database (Ru et al., 2019). Then, to avoid bias, six independent algorithms were used to determine the level of TIIC infiltration in BLCA, namely, TIMER (Li et al., 2017), MCP-counter (Becht et al., 2016), CIBERSORT (Newman et al., 2015), quanTIseq (Finotello et al., 2019), xCell (Aran et al., 2017), and EPIC (Racle et al., 2017). From previous studies, we adopted effector genes of TIICs as well (Hu et al., 2021). Next, we gathered several inhibitory immune checkpoints with promising therapeutic potential as reported in Auslander's research (Auslander et al., 2018).

T cell inflammation score (TIS), was employed for assessing the inflammation level within the TME in BLCA. TIS serves as a previously developed predictive factor for assessing the effectiveness of cancer immunotherapy and anti-PD-1 therapy (Ayers et al., 2017). Calculating the TIS, which includes 18 IFN-γ-responsive genes, helps to reflect pre-existing anti-cancer immunity and predict the clinical response to ICB. Genes collected in this study were identified by Ayers et al. (Ayers et al., 2017).

$$TIS = \Sigma_{\gamma=1}^{18} \beta_\gamma X_\gamma$$

where βγ represents the coefficient of a gene predefined in a previous study, and Xγ is the expression level of this gene.

Hyperprogression is considered to be an adverse event of abnormally accelerated tumor growth when ICB is performed. We identified several predictors used to predict hyperprogression from previous studies (Kato et al., 2017; Singavi et al., 2017; Giusti et al., 2019). Kato et al. reported in Clinical Cancer Research on a study investigating the association between genomic variants and hyperprogression. Among 155 patients with tumors treated with anti-PD-1/PD-L1 monotherapy, the study revealed that six patients with MDM2/MDM4 and DNMT3A amplification experienced TTF of less than 2 months. Singavi found that patients with chromosome 11 region 13 amplification variants (CCND1, FGF3, FGF4, and FGF19 amplification) were prone to hyperprogression on immunotherapy by examining the occurrence of somatic mutations in 696 patients with solid tumors. Giusti et al. collected clinical data on 20 patients with advanced NSCLC treated with pembrolizumab immunotherapy, in which five hyperprogressing patients were identified, and NGS revealed CDKN2A/B deletion in 4/5 hyperprogressing patients.

Immunohistochemistry staining of bladder cancer microarray

CD8 and PD-L1 staining was conducted using the BLCA tumor tissue microarray (HBlaU050CS01), which included 40 bladder cancer tissue samples and 10 adjacent peritumoral tissues, offered by Shanghai Outdo Biotech Company located in Shanghai, China. The positive ratio of $CD8^+$ T cells were defined based on a comparison of the infiltration ratio of $CD8^+$ cells within each nest to the number of total cells within each nest. Only the proportion of strongly positive cells were recorded, while the proportion of weakly positive cells was disregarded. The ethics committee of Shanghai Outdo Biotech Company granted approval for this study. Immunohistochemistry of the tumor tissue microarray was performed by Biossci Company in Hubei, China. An antibody against IL4I1 (ab222102) was purchased from Abcam company. For IL4I1 and PD-L1, we performed a semi-quantitative evaluation for staining intensity, categorizing it as negative (0), weakly positive (1^+), moderately positive (2^+), or strongly positive (3^+), and determining the percentage of positive cells present. To determine the histochemistry score (H-score) for each observed tissue component (cytoplasm and nucleus), we multiplied the intensity score (ranging from 0 to 3) and the percentage of positive cells (ranging from 0 to 100).

Anticipation of the BLCA molecular subtypes

To analyze the molecular subtypes in the samples and establish the correlation between IL4I1 expression and molecular subtypes, we utilized a range of subtype systems such as CIT, Lund, MDA, TCGA, Baylor, UNC, and Consensus subtypes and determined each sample's subtype using consensusMIBC and BLCAsubtyping R packages (Damrauer et al., 2014; Rebouissou et al., 2014; Robertson et al., 2017; Marzouka et al., 2018; Mo et al., 2018; Kamoun et al., 2020). The molecular subtype of BLCA can be classified into binary subtype, including basal subtype and luminal subtype (Kamoun et al., 2020). The Basal subtype, which is considered more aggressive, also shows an increased response to certain treatments such as immunotherapy and anti-EGFR therapy. We also have gathered a total of 12 specific bladder cancer gene signatures (Kamoun et al., 2020). To assess the predictive precision of IL4I1 in identifying BLCA molecular subtypes, we created receiver operating characteristic (ROC) curves.

Evaluating the correlation between IL4I1 and different treatment effectiveness

A set of gene signatures positively correlated with clinical response to anti-PD-L1 (atezolizumab) in BLCA from Mariathasan's study (Mariathasan et al., 2018). Significantly, the determining factors for neoadjuvant chemotherapy in BLCA encompass the genetic mutation status of various pivotal genes like RB1, ATM, ERBB2, ERCC2, and FANCC (van Allen et al., 2014; Groenendijk et al., 2016; Pietzak et al., 2019; Singla et al., 2019). Additionally, we gathered additional

10.3389/fphar.2024.1365683

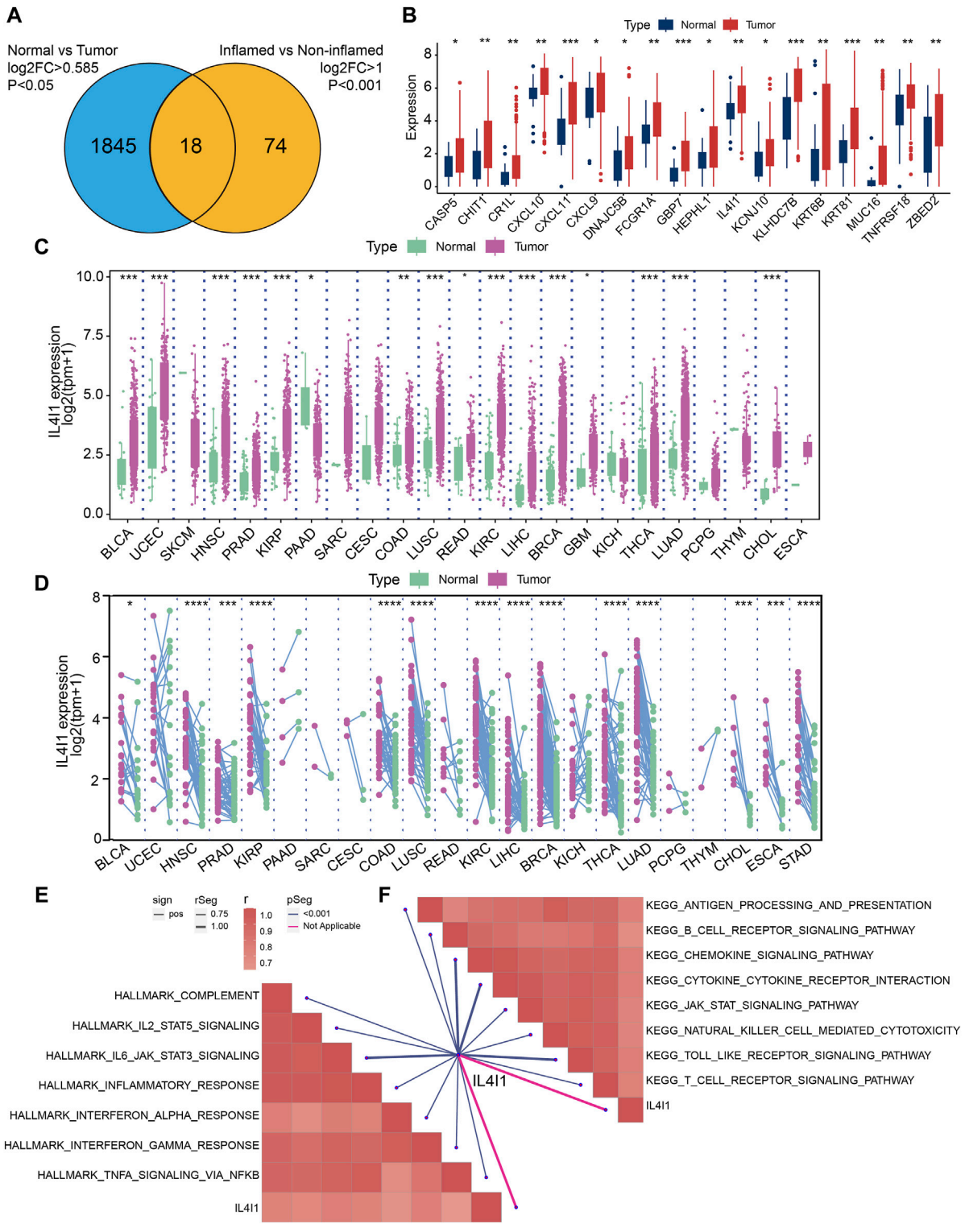

FIGURE 2
Identifying differential expressed genes (DEGs) for inflamed and non-inflamed phenotypes. **(A)** Common upregulated DEGs of TCGA-BLCA cohort and IMvigor210 cohort. **(B)** The expression of 18 DEGs in normal and tumor tissues of BLCA. **(C,D)** Pan-cancer expression pattern of IL4I1. GSEA for IL4I1 in Hallmark gene sets **(E)** or in KEGG gene sets **(F)** based on the TCGA-BLCA cohort.

therapeutic signatures, such as oncogenic pathways that could contribute to a non-inflamed TME, the EGFR ligands and radiotherapy predicted pathways. We used the 'GSVA' R package to calculate the enrichment scores for these signatures (Hänzelmann et al., 2013). Lastly, we acquired target genes of drugs employed in various therapeutic approaches by Drugbank

(Wishart et al., 2018) database (https://www.drugbank.com/) and examined their association with IL4I1.

Statistical analysis

To evaluate differences among continuous variables, either the Wilcoxon ranking test or Kruskal Wallis test was utilized, depending on the quantity of groups, whereas the chi-square test was employed to examine distinctions among categorical variables. The Pearson correlation analysis was utilized to quantify correlation. The survival cruve were generated using the Kaplan-Meier method and the prognostic value were obtained via univariate Cox regression. Statistical analyses were all conducted using R project (version 4.2.3). A significance level of 0.05 was used, and *p*-values less than this threshold were considered statistically significant.

Results

Identifying differential expressed genes (DEGs) for inflamed and non-inflamed phenotypes

Firstly, 1863 differential expressed genes between normal and tumor samples in the TCGA cohort were identified, followed by 92 DEGs between inflamed tumor samples and non-inflamed tumor samples in the IMvigor210 cohort. After crossing the DEGs from the two cohorts, we finally identified 18 common DEGs (Figure 2A). Figure 2B demonstrated the relative expression of these 18 DEGs. For these genes, IL4I1, CXCL9, CXCL10, CXCL11, KLHDC7B, and TNFRSF18 had a relative high expression in tumor samples. Here, we focused on the role of IL4I1 expression in bladder cancer. Then, we explored the pan-cancer expression pattern of IL4I1 by analyzing the different expression between normal and tumor tissues in 23 tumor types. It was found that the expression of IL4I1 was significantly higher in tumor tissues than normal tissues in most tumor types such as BLCA, HNSC, PRAD, KIRP, and so on (Figure 2C). The paired analysis showed the same trend (Figure 2D). Subsequently, we performed GSEA for IL4I1 in terms of Hallmark gene sets or KEGG gene sets based on the TCGA-BLCA cohort. As demonstrated, IL4I1 was significantly positively correlated with immune-related pathways, including IL-2-STAT5 signaling, IL4-JAK-STAT3 signaling and antigen processing and presentation (Figures 2E, F).

Pan-cancer expression patterning and immunological function of IL4I1

We have demonstrated that IL4I1 is highly expressed in a variety of tumor tissues, prompting us to explore the prognostic value of IL4I1. We assessed the prognostic value of IL4I1 through univariate cox analysis and survival curves. Although IL4I1 has no prognostic value in bladder cancer, its overexpression was observed as a significant risk factor for ACC, GBM, KIRC, KIRP, LAML, LGG, LIHC, THYM, and UVM in terms of overall survival (OS), while a protective effect was observed only in SKCM (Supplementary Figure S1). The analysis of progression-free survival (PFS) revealed that high expression of IL4I1 was also found to be a contributing factor for GBM, KIRCK, IRPK, and LGG. In addition to SKCM, IL4I1 overexpression also had a significant protective effect on CESC, CHOL, and HNSC (Supplementary Figure S2). However, in the disease-free survival (DFS) analysis, only KIRP and THCA had a significant risk effect and were protective factors for OV (Supplementary Figure S3). Considering the results of GSEA suggests that IL4I1 is closely related to immune-related pathways, a comprehensive analysis was performed to identify the correlation between IL4I1 and immunological characteristics across various types of tumors. It was found that the expression of IL4I1 showed positive correlation with the vast majority of immunomodulators in almost all tumors, especially BLCA, HNSC, and KICH (Figure 3A). However, in certain tumors, such as THCT and UCEC, it is negatively correlated with some immunomodulators. In multiple types of cancers, we discovered a positive correlation between IL4I1 expression and various immune checkpoints, including PD-1, CTLA-4, PD-L1, and Tim-3 (Figures 3B–E). Next, the ssGSEA algorithm was utilized to analyze the infiltration level of TIICs. In contrast, except for DLBC and CHOL, IL4I1 showed a positive association with various types of TIICs in different tumors (Figure 3F). These findings suggested that the expression of IL4I1 holds immunological relevance and prognostic value across various types of tumors, suggesting that IL4I1 can serve as a target for immunotherapy.

IL4I1 suggests an inflamed TME in BLCA

Subsequently, we proceeded to analyze the immunological properties of IL4I1 in BLCA. Given that the immune system is a complex and interconnected network involving numerous molecules and pathways. To further evaluate the immunological functions of IL4I1, we assessed its impact on the cancer immune cycle. Our findings indicated that the enrichment score of most steps in the cancer immune cycle is upregulated in the high IL4I1 group (Figure 4A). The process involved release of cancer cell antigens (step 1), priming and activation (step 3), as well as trafficking of T cells to tumors (step 4) (except for B cell recruitment, all other steps including $CD8^+$ T cell, DC, macrophage, Th1 cell, NK cell, MDSC, and Th17 cell recruitment showed increased activity). The connection between these processes and the infiltration of immune cells in the TME is evident through the heightened T cell infiltration into tumors (step 5) observed in the high-IL4I1 group. Furthermore, there was an upregulation in the activity of eliminating cancer cells (step 7) within the high-IL4I1 group. Significantly, the T cells' ability to identify cancer cells (step 6) was observed to be reduced in the high IL4I1 group, possibly because of the increased inhibitory immune checkpoints expression in this specific group.

Furthermore, we employed the TIMER and MCP-counter algorithms to quantify the infiltration levels of immune cells and analyzed their relationship with IL4I1. The results displayed a favorable association between IL4I1 manifestation and the levels of infiltration by $CD8^+$T cells, macrophages, and dendritic cells

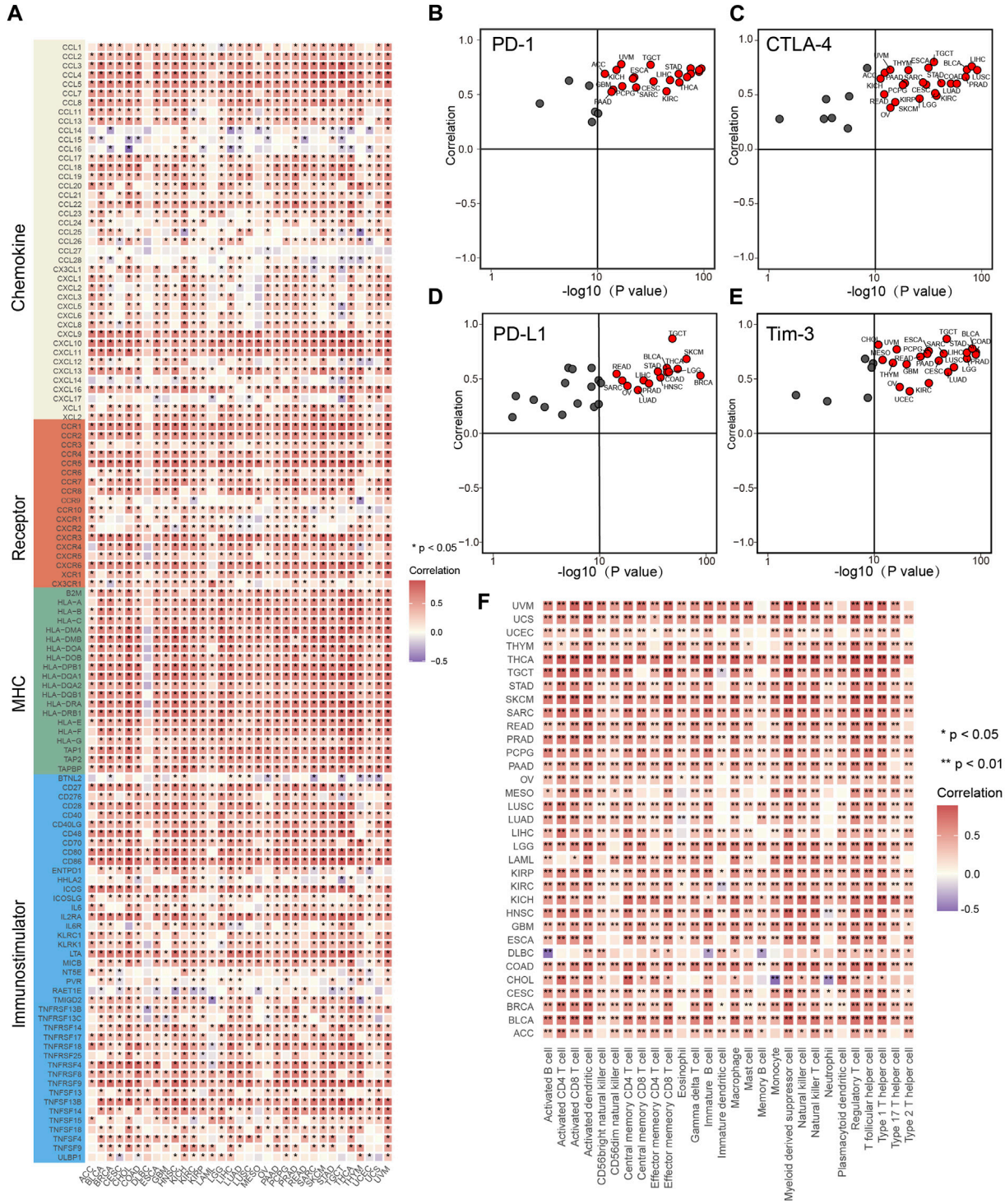

FIGURE 3
The effect of IL4I1 on immunological status in pan-cancers. **(A)** The heat map shows the relationship between IL4I1 and 121 immunomodulators (chemokines, receptors, MHC and immunomodulators). **(B–E)** The relationship between IL4I1 and four immune checkpoints, PD-1, CTLA-4, PD-L1, and Tim-3. These dots represent types of cancer. The vertical axis means the Pearson correlation, while the horizontal axis means -log10 (*p*-value). **(F)** The relationship between IL4I1 and 28 tumor-associated immune cells calculated by the ssGSEA algorithm. The color represents the correlation coefficient. (*$p < 0.05$; **$p < 0.01$).

(Figures 4B, C). Additionally, the expression of IL4I1 exhibited a positive relationship with the effector genes of TIICs (Figure 4D). Furthermore, we utilized six different algorithms to further investigate the relationship between IL4I1 and TIICs (including $CD8^+$ T cells, NK cells, Th1 cells, dendritic cells, and macrophages) (Figure 4E).

10.3389/fphar.2024.1365683

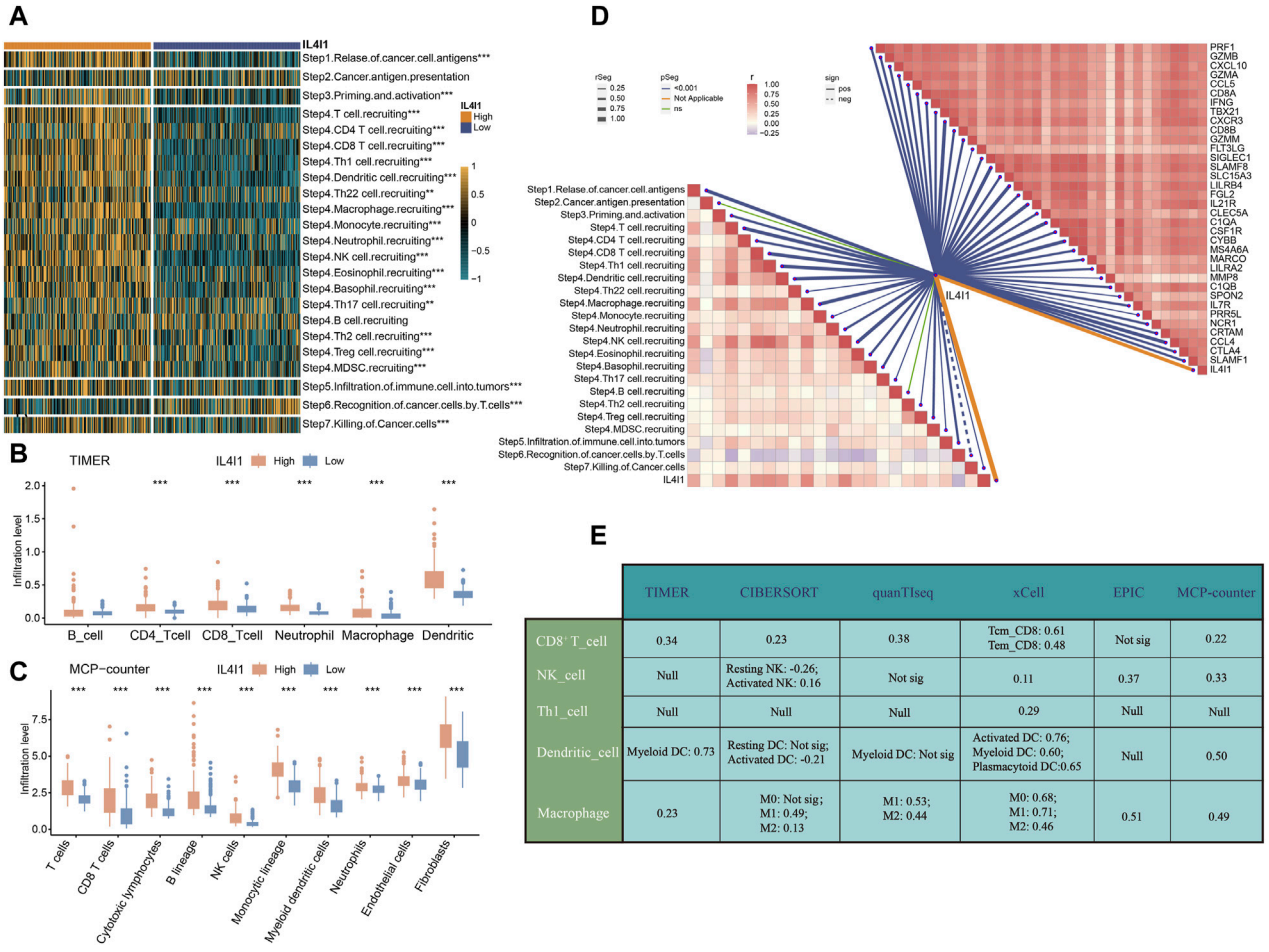

	TIMER	CIBERSORT	quanTIseq	xCell	EPIC	MCP-counter
CD8$^+$ T_cell	0.34	0.23	0.38	Tcm_CD8: 0.61 Tem_CD8: 0.48	Not sig	0.22
NK_cell	Null	Resting NK: -0.26; Activated NK: 0.16	Not sig	0.11	0.37	0.33
Th1_cell	Null	Null	Null	0.29	Null	Null
Dendritic_cell	Myeloid DC: 0.73	Resting DC: Not sig; Activated DC: -0.21	Myeloid DC: Not sig	Activated DC: 0.76; Myeloid DC: 0.60; Plasmacytoid DC:0.65	Null	0.50
Macrophage	0.23	M0: Not sig; M1: 0.49; M2: 0.13	M1: 0.53; M2: 0.44	M0: 0.68; M1: 0.71; M2: 0.46	0.51	0.49

FIGURE 4
IL4I1 develops an inflamed TME in bladder cancer. **(A)** Correlation between IL4I1 and the activities of cancer immunity cycle. **(B)** Differences in the infiltration levels of five types of TIICs in the high- and low-IL4I1 groups using TIMER algorithm in bladder cancer. **(C)** Differences in the infiltration levels of five types of TIICs in the high- and low-IL4I1 groups using MCP-counter algorithm in bladder cancer. **(D)** Correlation between IL4I1 and the activities of cancer immunity cycle, effector genes of Tumor-associated immune cells mentioned above. **(E)** Correlation between IL4I1 and five types of TIICs using different algorithms. (*$p < 0.05$, **$p < 0.01$, ***$p < 0.001$, Not sig refers to not significant, Null means no data for analysis, T cm refers to central memory T cell, and T em refers to effector memory T cell).

To summarize, these findings indicated a notable correlation between the excessive expression of IL4I1 and the inflamed TME within BLCA.

IL4I1 predicts clinical response and hyperprogression of ICB in BLCA

Based on the previous description, we proposed that IL4I1 suggested an inflamed TME, thereby suggesting that high expression of IL4I1 may confer increased sensitivity to ICB therapy. Consequently, we embarked on an analysis to explore the association between IL4I1 and 20 inhibitory immune checkpoints. With the exception of LGALS3 and VTCN1, the expression levels of immune checkpoints exhibited significant upregulation. Correlation analysis further indicated a positive association between IL4I1 expression and these immune checkpoints (Figures 5A, D). Furthermore, IL4I1 exhibited positive correlations with certain pathway enrichment scores that are known to be favorable for immunotherapy (Figure 5B). Furthermore, there is a significant and positive association between IL4I1 and TIS (Figure 5C). The above results suggested that IL4I1 has the capacity to serve as a promising indicator for the effectiveness of ICB. Conversely, the high-IL4I1 group exhibited a lower incidence of hyperprogression. The correlation between IL4I1 and hyperprogression related genes was examined, and our results showed a notable decrease in the expression of genes that exhibited a positive correlation with the occurrence of hyperprogression in the high IL4I1 group. This reduction was observed in genes such as MDM2, MDM4, as well as a significant decrease in the rate of copy number amplification, including CCND1, FGF19, FGF3, and FGF4 (Figures 5E, F). Conversely, two predictors that exhibited a negative correlation with hyperprogression, namely CDKN2A and CDKN2B, exhibited significantly higher expression levels in the high-IL4I1 group compared to the low-IL4I1 group, along with a higher copy number amplification rate. These findings suggested that patients exhibiting high IL4I1 expression are less prone to experiencing hyperprogression associated with ICB treatment, thus making them more appropriate candidates for ICB therapy.

10.3389/fphar.2024.1365683

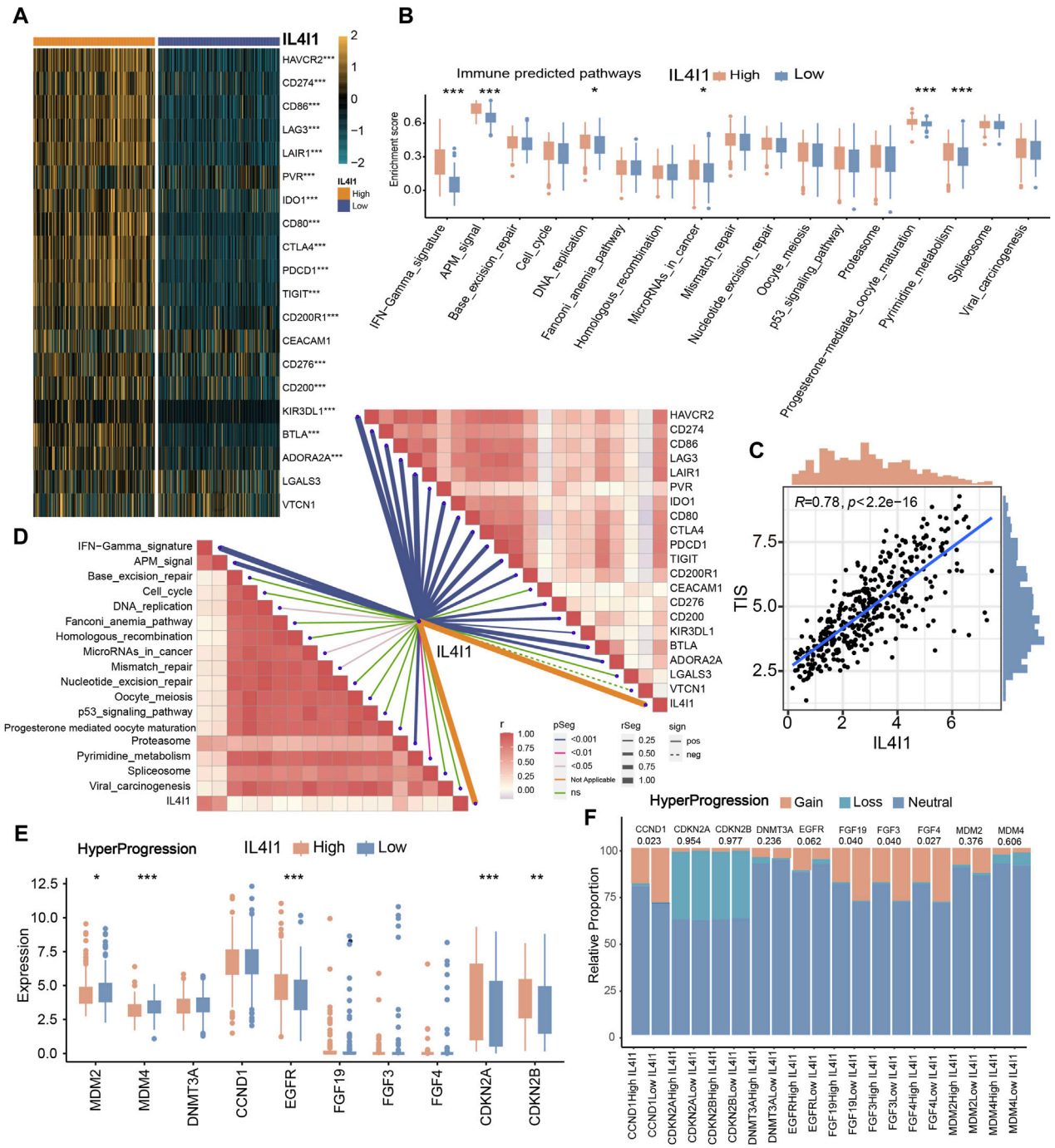

FIGURE 5
The role of IL4I1 in predicting the response to immunotherapy. **(A)** Correlation between IL4I1 and 20 immune checkpoints. **(B)** Differences in the enrichment scores of immunotherapy-predicted pathways in the high- and low-IL4I1 groups. **(C)** Correlation between IL4I1 and pan-cancer T cell inflamed score. **(D)** Correlation between IL4I1 and immunotherapy-predicted pathways, 20 immune checkpoints. **(E,F)** Differences in the expression and mutation status of hyperprogression-related biomarker in the high- and low-IL4I1 groups. (*$p < 0.05$, **$p < 0.01$, ***$p < 0.001$, ns means not significant, pos means positive correlation, and neg mean negative correlation).

IL4I1 expression could precisely predict the molecular subtypes and possible therapeutic strategies in BLCA

The different molecular subtypes of BLCA affect the prognosis and treatment effect of patients. Hence, an analysis was conducted to examine the correlation between the IL4I1 expression and molecular subtypes across various classification systems. Figure 6A demonstrated that the high-IL4I1 group displayed a stronger preference for the basal subtype of BLCA in the findings. Furthermore, the low-IL4I1 group exhibited elevated enrichment scores for urothelial differentiation, the Ta pathway, and luminal

10.3389/fphar.2024.1365683

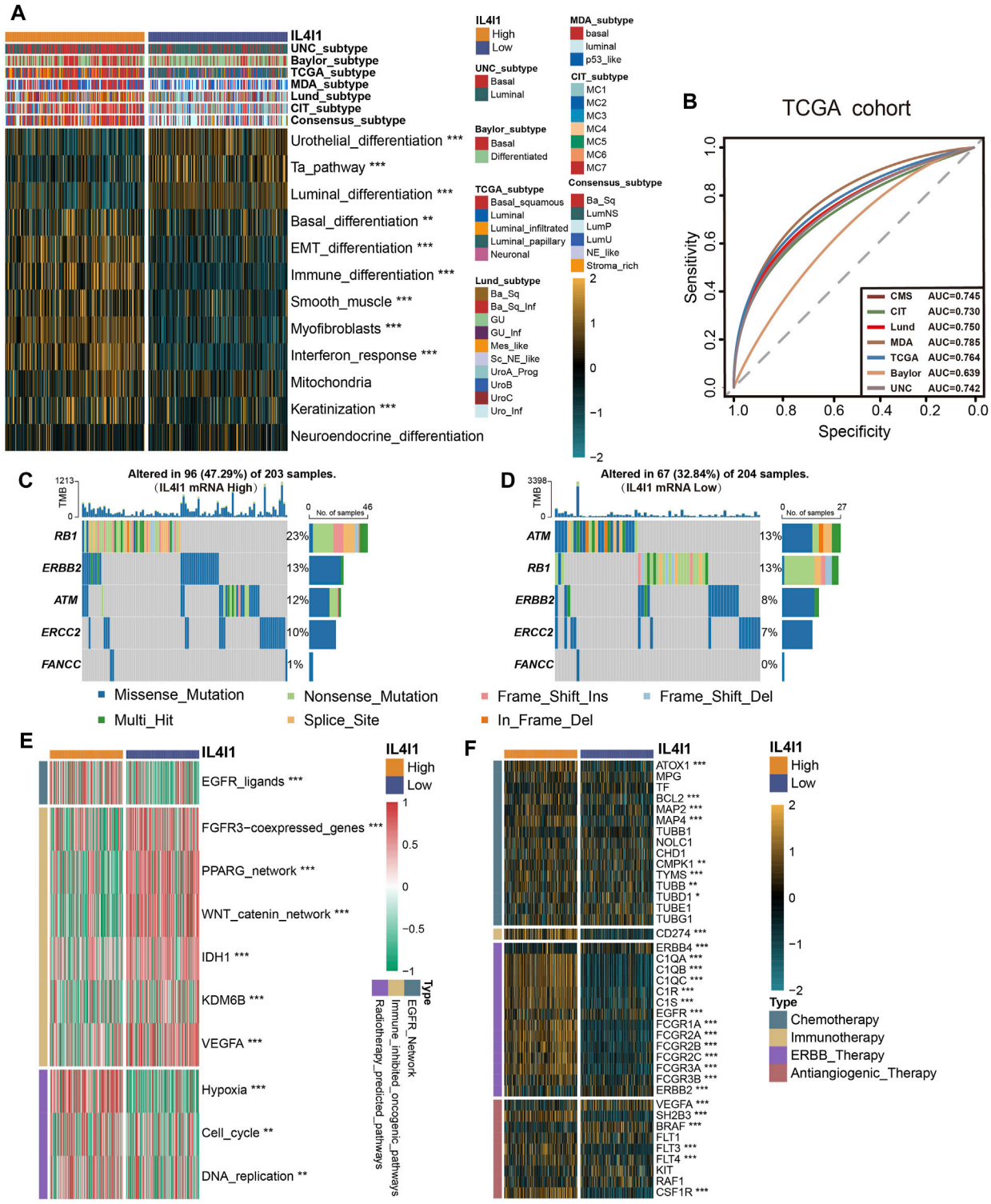

FIGURE 6
L4I1 can predict the molecular subtype and the curative effect of several treatments in bladder cancer. **(A)** Differences in the seven different subtype systems and bladder cancer signatures between high- and low- IL4I1 groups. **(B)** ROC curves measuring the predictive value about molecular subtypes using seven algorithms. **(C,D)** Differences in mutations of neoadjuvant chemotherapy-related genes in high- and low- IL4I1 groups. **(E)** Correlation between IL4I1 and the enrichment scores of several therapeutic-related signaling pathways such as targeted therapy. **(F)** Correlation between IL4I1 and drug-target genes of different therapy extracted from the Drugbank database. (*$p < 0.05$, **$p < 0.01$, ***$p < 0.001$).

differentiation (Figure 6A). The high-IL4I1 group exhibited elevated enrichment scores in basal differentiation, EMT differentiation, immune differentiation, smooth muscle, myofibroblast, interferon response, and keratinization. Moreover, apart from the Baylor system, all molecular subtypes exhibited an AUC value exceeding 0.7 (Figure 6B), signifying that IL4I1 has the ability to accurately

10.3389/fphar.2024.1365683

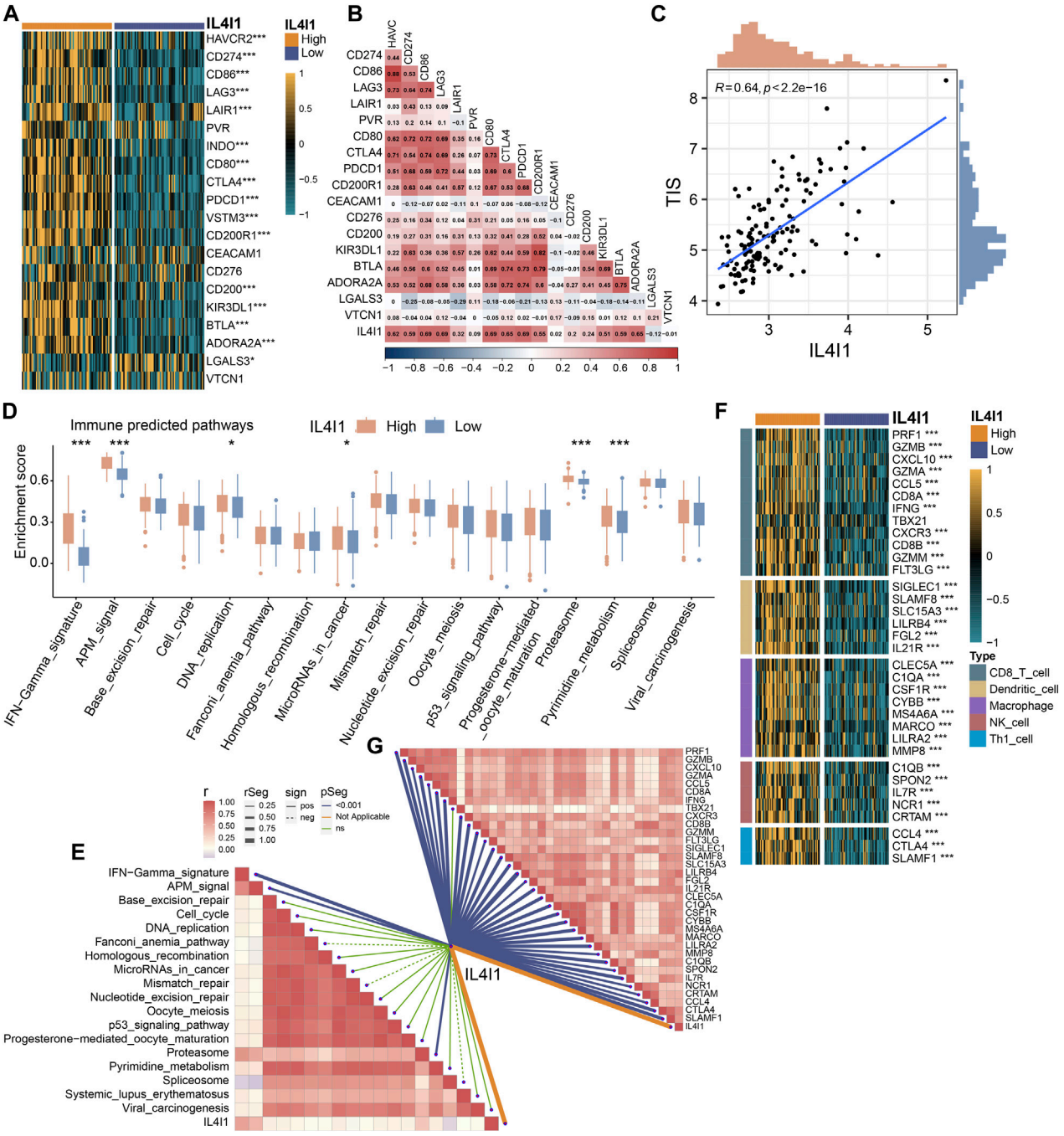

FIGURE 7
Validating the predictive ability of IL4I1 expression for immune therapy response in the GSE48075 cohort. **(A)** Differences in the expression of immune checkpoint in the high- and low-IL4I1 groups. **(B)** The correlation between IL4I1 expression and immune checkpoints by Pearson's correlation analysis. **(C)** Correlation between IL4I1 expression and T cell-inflamed scores in the GSE48075 cohort. **(D)** Differences in the enrichment scores of immune predicted pathways between the high- and low-IL4I1 groups. **(E)** The correlation analysis between IL4I1 expression and enrichment scores of immune predicted pathways. **(F)** Comparison for expression of effector genes in the high- and low-IL4I1-expression groups. **(G)** The correlation analysis between IL4I1 expression and expression of effector genes (*$p < 0.05$, **$p < 0.01$, ***$p < 0.001$, ns means not significant, pos means positive correlation, and neg mean negative correlation).

anticipate the molecular subtype of BLCA, thus providing precise treatment guidance.

In addition to immunotherapy, IL4I1 can predict the efficacy of other therapeutic strategies, like neoadjuvant chemotherapy, radiotherapy, and various targeted therapies. We collected mutation data for molecules associated with neoadjuvant chemotherapy, various therapeutic signatures, and gene expression related to targeted drugs. In the high-IL4I1 group, the mutation frequency of specific genes (RB1, ERBB2, ERCC2) linked to neoadjuvant chemotherapy exhibited a higher rate (Figures 6C, D). Furthermore, the group with high

IL4I1 levels demonstrated increased enrichment scores for pathways linked to EGFR ligands and radiotherapy. On the contrary, the group exhibiting low IL4I1 levels demonstrated an enrichment of oncogenic pathways, as depicted in Figure 6E. The activation of these pathways was found to be connected with a non-inflamed TME and resistance to immunotherapy (Peng et al., 2015; Sweis et al., 2016; Spranger and Gajewski, 2018). By utilizing the Drugbank database, we discovered an observation indicating significantly higher expression levels of numerous drug target genes in the high-IL4I1 group (Figure 6F). In particular, the high IL4I1 group exhibited a significant increase in nearly all aspects related to chemotherapy, immunotherapy, and ERBB target gene expression. And some target genes of anti-angiogenesis (including SH2B3, FTL3, FTL4, and CDF1R) were also significantly increased, while the expression levels of BRAF and RAF1 were low.

In general, these results suggested that BLCA patients with high IL4I1 expression may benefit more from neoadjuvant and adjuvant chemotherapy, radiotherapy, immunotherapy, and ERBB therapy.

Validating the role of IL4I1 in GSE48075 and E-MTAB-4321 cohort

To provide more robust results, we performed a validation analysis in the GSE48075 cohort and E-MTAB-4321 cohort. There was a significant increase in the expression of the majority of immune checkpoints in patients with high IL4I1 expression levels (Figure 7A; Supplementary Figure S4A), and correlation analysis also showed a positive correlation (Figure 7B). Similarly, the expression of IL4I1 was positively correlated with TIS (Figure 7C). Several immunotherapy positive predictable pathways also significantly enriched in high-IL4I1 group (Figure 7D, Supplementary Figure S4B) and are positively associated with IL4I1 (Figure 7E). Furthermore, the majority of effector genes in TIICs exhibited a positive correlation with IL4I1, as depicted in Figures 7F, G; Supplementary Figure S4C. Two external cohort revealed a significant correlation between elevated IL4I1 expression and the basal molecular subtypes of BLCA, thereby validating IL4I1's potential as a predictive indicator for BLCA molecular subtypes (Figures 8A, B; Supplementary Figures S4D, E). For several therapeutic strategies, IL4I1 also showed its predictive value. The high-IL4I1 group showed significant enrichment of EGFR and radiotherapy predictive pathways (Figure 8C; Supplementary Figure S4F), and IL4I1 was positively correlated with the expression of drug target for chemotherapy, immunotherapy, ERBB and anti-angiogenic therapy (Figure 8D). The validation of the GSE48075 and E-MTAB-4321 cohort further confirmed IL4I1 suggested an inflamed TME and the potential of IL4I1 to predict molecular subtypes and several therapeutic strategies for BLCA.

Validating of IL4I1′role from immunohistochemistry and the IMvigor210 cohort

Next, we performed immunohistochemical staining of BLCA and classified the tumor tissue microarray cohort into inflamed, excluded, and desert subtypes (Ott et al., 2019) derived from the spatial distribution pattern of $CD8^+$ T cells (Figure 9A). In the inflamed subtype, the H-score of IL4I1 and PD-L1 were found to be higher comparison to the other two subtypes (Figures 9B, C). Figures 9D–F showed that there was a positive association between the H-score of PD-L1 and the rate of CD8 positivity, while the H-score of IL4I1 was positively linked to the H-score of PD-L1 and the positive rate of CD8. In the IMvigor210 cohort (a BLCA immunotherapy cohort), according to the clinical efficacy of the patients, the cohort was divided into PR/CR group and PD/SD group, and the correlation of IL4I1 with immunological characteristics and its predictive value for molecular subtypes and therapy were explored respectively. And we also arrived a similar conclusion. (Supplementary Figures S6, S7). Additionally, we conducted investigations into the involvement of IL4I1 in immunotherapy. As anticipated, the high-IL4I1 group displayed notably elevated percentages of IC2 (immune cells with the utmost PD-L1 level) and TC2 (tumor cells with the utmost PD-L1 level) (Figure 9G), aligning with our expectations for patients who received anti-PD-1 therapy. In addition, the high-IL4I1 group had a higher survival rate and response rate to anti-PD-L1 therapy, and IL4I1 expression was higher in the complete response group (Figures 9H–J). These findings collectively suggested that IL4I1 was closely related to the formation of inflamed TME and has a certain value in predicting the response to immunotherapy in bladder cancer. Additionally, we collected six immunotherapy cohorts, including five melanoma ICB treatment cohorts and one adoptive T cell therapy cohort to investigate the predictive role of IL4I1 in immunotherapy response. Although not reaching statistical significance, it is noteworthy that in cohorts such as Gide 2019, Nathanson2017 post, and GSE78220, the high IL4I1 group exhibited higher response rates and thus a more favorable prognosis, consistent with our findings in bladder cancer. In contrast, in cohort Nathanson2017 pre, the high IL4I1 group displayed a lower response rate compared to the low IL4I1 group, resulting in a poorer prognosis (Supplementary Figures S8A–F).

Discussion

Secreted L-amino acid oxidase IL4I1 is primarily produced by inflammatory antigen presenting cells, such as monocytes, macrophages, and dendritic cells (Marquet et al., 2010; Park et al., 2017). By decomposing phenylalanine, IL4I1 can change the biochemical environment of immune cells (Molinier-Frenkel et al., 2019), thereby regulating the immune response. According to recent research, IL4I1 has the ability to control the immune response by impacting the growth of immune cells (Chavan et al., 2002; Boulland et al., 2007; Houston et al., 2015; Pluchino and Peruzzotti-Jametti, 2016; Romagnani, 2016; Bod et al., 2018; Sadik et al., 2020; Castellano et al., 2021). In this study, we elucidated the expression pattern of IL4I1 in pan cancer and its association with poor prognosis in various tumors. Furthermore, we observed a positive correlation between IL4I1 and immunological characteristics in BLCA, suggesting that IL4I1 may serve as a representative marker for an inflamed tumor microenvironment. Building

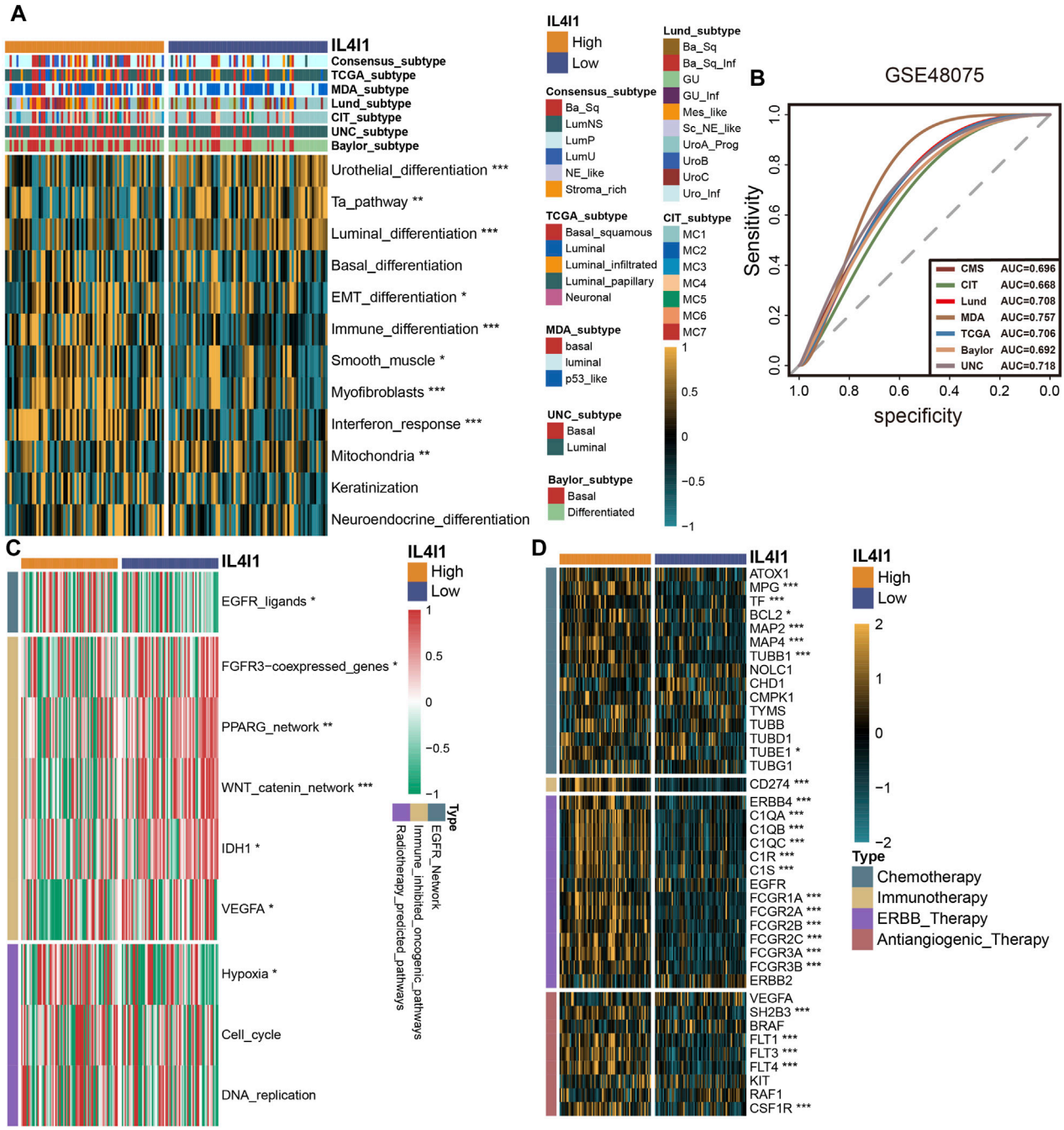

FIGURE 8
Validating the predictive ability of IL4I1 expression for the molecular subtype and response for various treatment strategies of bladder cancer in the GSE48075 cohort. **(A)** Difference of bladder cancer molecular subtypes in patients with different IL4I1 expression levels calculated via multiple algorithms. **(B)** Receiver operating characteristics (ROC) curve and area under curve (AUC) for IL4I1 in molecular subtype prediction in the GSE48075 cohort. **(C)** Difference for enrichment scores of various therapeutic signatures in the high- and low-IL4I1 groups. **(D)** Difference for expression of various drug-targeted genes in the high- and low-IL4I1 groups. (*$p < 0.05$, **$p < 0.01$, ***$p < 0.001$).

upon this foundation, we further demonstrated that IL4I1 can accurately predict immunotherapy response and BLCA molecular subtypes.

In this study, we revealed that IL4I1 was a prognostic factor in various cancer types. For instance, the survival curve indicates that patients with high IL4I1 expression obtained an unfavorable prognosis in LGG and GBM which was in consist with research of Feng Ye et al. IL4I1 was predominantly expressed on tumor associated macrophages (TAMs) in glioma. IL4I1-induced polarization of M2 macrophages can promote tumor invasion and metastasis (Ye et al., 2023). Similarly, IL4I1 was also found to be oncogenic effects in clear cell renal cell carcinoma through polarization of M2-like macrophages via JAK1/STAT3 signaling (Lin et al.,

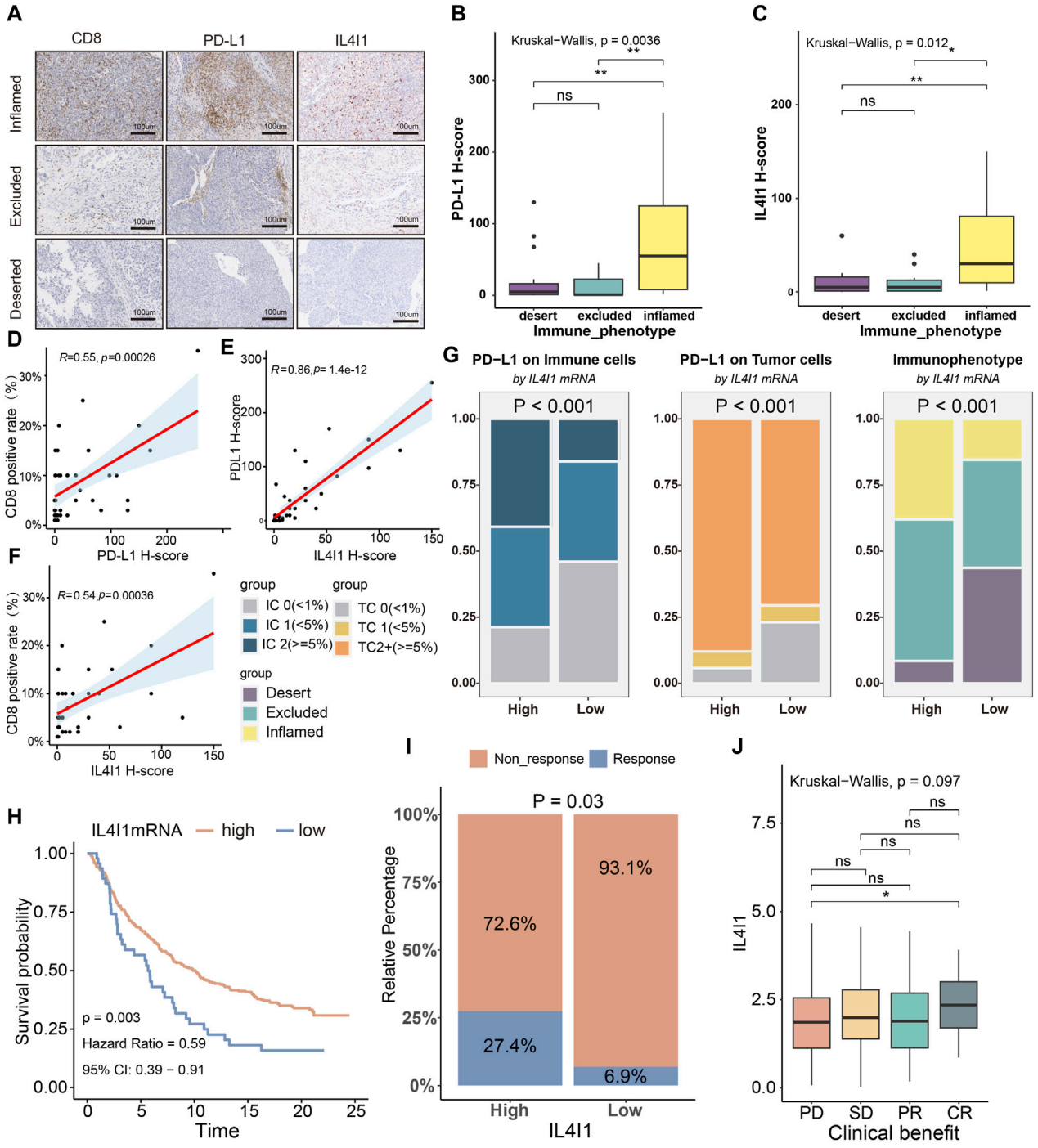

FIGURE 9
Correlation between IL4I1, the immune phenotype and the clinical response of immunotherapy in BLCA. **(A)** Expression of IL4I1, CD8, and PD-L1 in the BLCA TMA cohort was measured using immunohistochemistry. Representative images of CD8, PD-L1, and IL4I1 in three immune phenotypes were displayed. The scale bars correspond to 200 μm. **(B,C)** PD-L1 H score and IL4I1 positive rate (detected using immunohistochemistry) in the three phenotypes of the TMA cohort. **(D,E)** Correlation between PD-L1 H score, IL4I1 positive rate and CD8 positive rate. **(F)** Correlation between IL4I1 positive rate and PD-L1 H score. **(G)** Differences in the expression of PD-L1 on the immune cells and tumor cells, and immunophenotype in the high- and low-IL4I1 groups. **(H)** Kaplan-Meier analysis for overall survival of bladder cancer patients with ICB therapy based on IL4I1. **(I)** Differences in the response to immunotherapy in the high- and low-IL4I1 groups. **(J)** Correlation between Siglec15 and the clinical response of cancer immunotherapy in the IMvigor210 cohort. (*$p < 0.05$, **$p < 0.01$, ns refers to not significant, TC refers to tumor cells, IC refers to immune cells; PD: Progressed disease; SD: Stable disease; PR: Partial response; CR: Complete response).

2023). Regretfully, the prognostic value of IL4I1 in bladder cancer was not observed in terms of both OS, PFS and DFS. Considering that IL4I1 is mainly expressed by TAMs, it is necessary to identify specific markers of IL4I1$^+$ TAMs via scRNA-seq in the future, and further clarify whether it could serve as prognostic value in bladder cancer.

IL4I1 was positively correlated with the expression of multiple immunomodulators and immune checkpoints in most tumor types, thus validating its regulatory function in the immune system. Notably, immune cell infiltration analysis highlights a positive association between IL4I1 and immune cell infiltration across nearly all tumor types, particularly in BLCA, LGG, SKCM, THCA, and UVM. However, it's worth noting that in SKCM, there are indications that IL4I1 inhibits $CD8^+$ T cell infiltration, potentially mediating resistance to immunosuppressive agents (Bod et al., 2017). Given the complicated TME, the immunological characteristics of IL4I1 exhibit varying outcomes across distinct tumor types, and further validation through *in vitro* and *in vivo* experiments is warranted.

Specific chemokines play a dual role in modulating the migration of immune cells into the tumor microenvironment and directly targeting non-immune cells, such as tumor cells and vascular endothelial cells. For instance, CXC-chemokine ligand 9 (CXCL9) and CXCL10 bind to CXC-chemokine receptor 3 (CXCR3) expressed on effector $CD8^+$ T cells, TH1 cells, and NK cells, facilitating their migration into the tumor site (Nagarsheth et al., 2017). Studies have demonstrated that the upregulation of CXCL9 and CXCL10 expression enhances $CD8^+$ T cell infiltration in tumors, leading to improved prognosis in ovarian and colon cancers (Zhang et al., 2003; Pagès et al., 2005; Sato et al., 2005; Galon et al., 2006). Our study revealed a positive correlation between IL4I1 expression and various immunomodulators associated with T cell activation and expansion in bladder cancer, including CXCL9 and CXCL10. And the cancer immunity cycle encompasses seven steps ranging from release of cancer cells antigen to the killing of cancer cells. Disruption or diminished activity in any of these steps can impede the maximization of anti-cancer immune responses. For instance, impaired recognition and presentation of tumor antigens, as well as ineffective recruitment and infiltration of tumor infiltrating immune cells into the tumor microenvironment, ultimately lead to the inadequate killing of cancer cells (Chen and Mellman, 2013; Motz and Coukos, 2013). In this study, we identified a significant positive correlation between IL4I1 expression and several steps of the cancer immunity cycle, including T-cell recruitment and immune cell infiltration into tumor tissues. The inflamed TME in bladder cancer is characterized by the presence of $CD4^+$ and $CD8^+$ T cells localized in proximity to tumor cells (Spranger et al., 2013; Gajewski, 2015; Fehrenbacher et al., 2016). Since IL4I1 is positively correlated with the expression of immunomodulators and the activity of most steps of the cancer immunity cycle was significantly upregulated in the high IL4I1 group, these implied that IL4I1 is strongly associated with the inflamed tumor microenvironment. Consequently, T cells, NK cells, and macrophages, collectively termed tumor infiltrating immune cells (TIICs), exhibited increased infiltration in the high IL4I1 expression group, a phenomenon validated through immunohistochemical. Moreover, the impact of IL4I1 on the TME appears to vary across different tumor types. For instance, in melanoma, IL4I1 overexpression was associated with a reduction in CD8 mRNA levels and $CD8^+$ T cell infiltration (Bod et al., 2017). Tong Li et al. discovered that inhibition of IL4I1 via Thymol could enhance $CD8^+$ T cell infiltration and reshape the inflamed TME. This approach had the potential to improve the efficacy of anti-PD-1 antibody treatment in lung adenocarcinoma (Li et al., 2020). This variability may be attributed to tumor heterogeneity and histological differences, which reminds us that immunological functions of IL4I1 in different tumors need to be further explored. In summary, our findings indicate that IL4I1 delineates an inflamed TME in bladder cancer, highlighting its potential as a key regulator of immune responses in the context of tumor progression.

Another feature of the inflamed TME is the elevated expression of suppressive immune checkpoints, which is induced by pre-existing tumor infiltrating immune cells (Spranger et al., 2013). Under physiological conditions, immune checkpoint molecules regulate the immune system by stimulating and suppressing the immune response; however, in tumors, their interaction suppresses pre-existing anticancer immunity, leading to immune escape. The clinical efficacy of immune checkpoint blockade (ICB) depends on the pre-existing anticancer immunity (Pardoll, 2012; Wykes and Lewin, 2018; Anandappa et al., 2020). Our results demonstrated that the high IL4I1 group exhibited upregulated expression of most immune checkpoints. This suggests that this group of patients has pre-existing anticancer immunity and is more likely to achieve better clinical efficacy of ICB. Additionally, the enrichment scores of immune predictive pathways were higher in the high IL4I1 group, and IL4I1 demonstrated a positive correlation with Tumor Inflammation Signature (TIS), which is used to predict ICB efficacy (St Paul and Ohashi, 2020). In the IMvigor210 cohort, the high IL4I1 group exhibited superior prognoses and higher response rates to immunotherapy. Collectively, these findings indicate that high IL4I1 expression may be more conducive to improved response to ICB in BLCA. Additionally, the correlation of IL4I1 with TME and immunotherapy varies across other tumor types. For instance, Tong Li et al. demonstrated that IL4I1 silencing in LUAD leads to increased infiltration of $CD8^+$ T cells. Targeting IL4I1 with Thymol can reshape TME and enhance sensitivity to immunotherapy (Li et al., 2020). Hirose et al. found that IL4I1 overexpression defined an immunosuppressive TME in melanoma leading to resistance to anti-PD-L1 therapy (Hirose et al., 2024), which was not entirely consistent with the results of six melanoma immunotherapy cohorts in our study. It is worth mentioning that Matusiak's study revealed the $IL4I1^+$ TAM were involved in phagocytosis of tumor cells within the colon cancer TME and were associated with favorable clinical outcomes (Matusiak et al., 2024), which provided ideas for targeting specific TAM. Therefore, further investigation is required to explore the impact of IL4I1 on the inflamed TME in various types of tumors, as well as its potential as a predictive marker for the efficacy of immunotherapy.

We explored the association between IL4I1 and molecular subtypes of BLCA, considering that basal subtypes of BLCA are more prone to chemotherapy, ICB therapy, and EGFR-based targeted therapy. (Sjödahl et al., 2012; Choi et al., 2014; Damrauer et al., 2014; Rebouissou et al., 2014; Robertson et al., 2017; Mo et al., 2018; Kamoun et al., 2020). Our findings revealed that BLCA patients with elevated IL4I1 expression had a higher likelihood of displaying the basal subtype. Additionally, there was a notable enrichment of the associated pathways. The findings indicated that IL4I1 can be utilized for predicting molecular subtypes of BLCA, and the AUC value serves to validate the precision of the findings. On the other hand, an increased mutation rate of neoadjuvant chemotherapy-related genes and a

greater enrichment score of EGFR ligand and chemotherapy predictive pathway were observed in association with elevated levels of IL4I1. And the expression of most drug target genes was higher in the high IL4I1 group according to results from the Drugbank database. Through these results, we believe that IL4I1 has predictive value in the selection of multiple therapeutic approaches targeting BLCA.

The study also has some limitations. Our results are mainly based on bioinformatics analysis of public databases. Although we integrate multiple data sources and different types of data for validation, the generation of data is usually based on statistical methods and models, and the interpretation of the results needs to consider the biological context and functional annotation. Nevertheless, there remain unexplored aspects of the functionalities of genes and pathways, presenting specific obstacles for data analysis that necessitate conducting experimental validation to elucidate the immunological function of IL4I1. Additionally, due to the absence of follow-up information and immunotherapy efficacy data for the patient sample from Shanghai Outdo Biotech Company, the effectiveness data for ICB treatment in the IMvigor210 cohort might be influenced by random effects and biases, and have not undergone independent validation.

In conclusion, this study shows that IL4I1 represents an inflamed TME in BLCA, and can also predict the molecular subtypes of BLCA and the clinical response to immunotherapy, providing guidance for clinical treatment options.

Data availability statement

The original contributions presented in the study are included in the article/Supplementary Materials, further inquiries can be directed to the corresponding author.

Ethics statement

The studies involving humans were approved by the ethics Committee of Biobank of Shanghai Outdo Biotech Company. The studies were conducted in accordance with the local legislation and institutional requirements. The participants provided their written informed consent to participate in this study.

Author contributions

XP: Writing–original draft, Writing–review and editing, Data curation, Formal Analysis, Software, Validation, Investigation, Visualization. CL: Data curation, Validation, Writing–review and editing, Software. LZh: Formal Analysis, Software, Writing–review and editing, Data curation, Validation. YC: Validation, Visualization, Writing–review and editing. LM: Visualization, Writing–review and editing. SG: Conceptualization, Funding acquisition, Methodology, Project administration, Supervision, Writing–review and editing. XS: Conceptualization, Data curation, Formal Analysis, Funding acquisition, Methodology, Project administration, Supervision, Writing–review and editing. LZu: Conceptualization, Funding acquisition, Investigation, Methodology, Project administration, Resources, Supervision, Writing–review and editing.

Funding

The author(s) declare that financial support was received for the research, authorship, and/or publication of this article. This work was supported by Changzhou Sci & Tech Program. Grant number: CJ20220146. Science Development Fund of Nanjing Medical University, Grant number: NMUB20220197, Top Talent of Changzhou "The 14th Five-Year Plan" High-Level Health Talents Training Project. Grant number: 2022CZBJ058. Top Talent of Changzhou "The 14th Five-Year Plan" High-Level Health Talents Training Project. Grant number: 2022CZBJ057. Leading Talent of Changzhou "The 14th Five-Year Plan" High-Level Health Talents Training Project. Grant number: 2022CZLJ015. Youth Science and Technology Project of Changzhou Health Commission. Grant number: QN202315. Qinghai Province basic research project,Grant number: 2024-ZJ-743.

Conflict of interest

The authors declare that the research was conducted in the absence of any commercial or financial relationships that could be construed as a potential conflict of interest.

Publisher's note

Supplementary material

The Supplementary Material for this article can be found online at: https://www.frontiersin.org/articles/10.3389/fphar.2024.1365683/full#supplementary-material

SUPPLEMENTARY FIGURE S1
The prognostic value of IL4I1 in pan-cancers in terms of overall survival (OS). **(A)** Forest map of univariate cox analysis for IL4I1 in cancers in terms of OS. **(B–I)** Kaplan-Meier survival curve for IL4I1 in various cancer types in terms of OS.

SUPPLEMENTARY FIGURE S2
The prognostic value of IL4I1 in pan-cancers in terms of progression-free survival (PFS). **(A)** Forest map of univariate cox analysis for IL4I1 in pan-cancers in terms of PFS. **(B–I)** Kaplan-Meier survival curve for IL4I1 in various cancer types in terms of PFS.

SUPPLEMENTARY FIGURE S3
The prognostic value of IL4I1 in pan-cancers in terms of Disease-free survival (DFS). **(A)** Forest map of univariate cox analysis for IL4I1 in pan-cancers in terms of DFS. **(B–I)** Kaplan-Meier survival curve for IL4I1 in various cancer types in terms of DFS.

SUPPLEMENTARY FIGURE S4
Validation in the E-MTAB-4321 cohort. **(A)** Correlations between IL4I1 and immune checkpoint. **(B)** Correlation between IL4I1 and immunotherapy predicted pathway. **(C)** Correlation between IL4I1 and effector genes associated with five types of TIIC. **(D)** Correlations between IL4I1 and molecular subtypes of BLCA. **(F)** Correlations between IL4I1 and several therapeutic signatures.

SUPPLEMENTARY FIGURE S5
Validation in IMvigor210 cohort. **(A)** Differences in the expression of immunomodulators between high and low IL4I1 groups. **(B)** Differences in the expression of effector genes associated with five types of TIIC between high and low IL4I1 groups. **(C)** Differences in the expression of immune checkpoint between high and low IL4I1 groups. **(D)** Correlation between IL4I1 and immunotherapy predicted pathway. **(E)** Correlations between IL4I1 and molecular subtypes of BLCA. **(F)** ROC curve and AUC for IL4I1 in molecular subtype prediction in the IMvigor210 cohort. **(G)** Correlations between IL4I1 and several therapeutic signatures.

SUPPLEMENTARY FIGURE S6
Validation in PR/CR group of IMvigor210 cohort. **(A)** Differences in the expression of immunomodulators between high and low IL4I1 groups. **(B)** Differences in the expression of effector genes associated with five types of TIIC between high and low IL4I1 groups. **(C)** Differences in the expression of immune checkpoint between high and low IL4I1 groups. **(D)** Correlation between IL4I1 and immunotherapy predicted pathway. **(E)** Correlations between IL4I1 and molecular subtypes of BLCA. **(F)** Correlations between IL4I1 and several therapeutic signatures.

SUPPLEMENTARY FIGURE S7
Validation in PD/SD group of IMvigor210 cohort. **(A)** Differences in the expression of immunomodulators between high and low IL4I1 groups. **(B)** Differences in the expression of effector genes associated with five types of TIIC between high and low IL4I1 groups. **(C)** Differences in the expression of immune checkpoint between high and low IL4I1 groups. **(D)** Correlation between IL4I1 and immunotherapy predicted pathway. **(E)** Correlations between IL4I1 and molecular subtypes of BLCA. **(F)** Correlations between IL4I1 and several therapeutic signatures.

SUPPLEMENTARY FIGURE S8
IL4I1 predicted the response to immunotherapy in several immunotherapy cohorts. **(A-F)** Five ICB cohorts (VanAllen 2015, Gide 2019, Nathanson 2017 pre, Nathanson 2017 post, GSE78220) and one adoptive T cell therapy cohort (Lauss 2017 cohorts) in Melanoma: In each graph, the upper half depicted the survival analysis within the IL4I group, while the lower half illustrated the proportion of immunotherapy responses in the high and low IL4I1 groups.

References

Abiko, K., Matsumura, N., Hamanishi, J., Horikawa, N., Murakami, R., Yamaguchi, K., et al. (2015). IFN-γ from lymphocytes induces PD-L1 expression and promotes progression of ovarian cancer. *Br. J. Cancer* 112, 1501–1509. doi:10.1038/bjc.2015.101

Anandappa, A. J., Wu, C. J., and Ott, P. A. (2020). Directing traffic: how to effectively drive T cells into tumors. *Cancer Discov.* 10, 185–197. doi:10.1158/2159-8290.CD-19-0790

Aran, D., Hu, Z., and Butte, A. J. (2017). xCell: digitally portraying the tissue cellular heterogeneity landscape. *Genome Biol.* 18, 220. doi:10.1186/s13059-017-1349-1

Auslander, N., Zhang, G., Lee, J. S., Frederick, D. T., Miao, B., Moll, T., et al. (2018). Robust prediction of response to immune checkpoint blockade therapy in metastatic melanoma. *Nat. Med.* 24, 1545–1549. doi:10.1038/s41591-018-0157-9

Ayers, M., Lunceford, J., Nebozhyn, M., Murphy, E., Loboda, A., Kaufman, D. R., et al. (2017). IFN-γ-related mRNA profile predicts clinical response to PD-1 blockade. *J. Clin. Invest.* 127, 2930–2940. doi:10.1172/JCI91190

Becht, E., Giraldo, N. A., Lacroix, L., Buttard, B., Elarouci, N., Petitprez, F., et al. (2016). Estimating the population abundance of tissue-infiltrating immune and stromal cell populations using gene expression. *Genome Biol.* 17, 218. doi:10.1186/s13059-016-1070-5

Bellucci, R., Martin, A., Bommarito, D., Wang, K., Hansen, S. H., Freeman, G. J., et al. (2015). Interferon-γ-induced activation of JAK1 and JAK2 suppresses tumor cell susceptibility to NK cells through upregulation of PD-L1 expression. *Oncoimmunology* 4, e1008824. doi:10.1080/2162402X.2015.1008824

Bod, L., Douguet, L., Auffray, C., Lengagne, R., Bekkat, F., Rondeau, E., et al. (2018). IL-4-Induced gene 1: a negative immune checkpoint controlling B cell differentiation and activation. *J. Immunol.* 200, 1027–1038. doi:10.4049/jimmunol.1601609

Bod, L., Lengagne, R., Wrobel, L., Ramspott, J. P., Kato, M., Avril, M.-F., et al. (2017). IL4-induced gene 1 promotes tumor growth by shaping the immune microenvironment in melanoma. *Oncoimmunology* 6, e1278331. doi:10.1080/2162402X.2016.1278331

Bonneville, R., Krook, M. A., Kautto, E. A., Miya, J., Wing, M. R., Chen, H.-Zi, et al. (2017). Landscape of microsatellite instability across 39 cancer types. *JCO Precis. Oncol.* 2017, 1–15. doi:10.1200/PO.17.00073

Boulland, M.-L., Marquet, J., Molinier-Frenkel, V., Möller, P., Guiter, C., Lasoudris, F., et al. (2007). Human IL4I1 is a secreted L-phenylalanine oxidase expressed by mature dendritic cells that inhibits T-lymphocyte proliferation. *Blood* 110, 220–227. doi:10.1182/blood-2006-07-036210

Castellano, F., Prevost-Blondel, A., Cohen, J. L., and Molinier-Frenkel, V. (2021). What role for AHR activation in IL4I1-mediated immunosuppression. *Oncoimmunology* 10, 1924500. doi:10.1080/2162402X.2021.1924500

Charoentong, P., Finotello, F., Angelova, M., Mayer, C., Efremova, M., Rieder, D., et al. (2017). Pan-cancer immunogenomic analyses reveal genotype-immunophenotype relationships and predictors of response to checkpoint blockade. *Cell Rep.* 18, 248–262. doi:10.1016/j.celrep.2016.12.019

Chavan, S. S., Tian, W., Hsueh, K., Jawaheer, D., Gregersen, P. K., and Chu, C. C. (2002). Characterization of the human homolog of the IL-4 induced gene-1 (Fig1). *Biochim. Biophys. Acta* 1576, 70–80. doi:10.1016/s0167-4781(02)00295-6

Chen, D. S., and Mellman, I. (2013). Oncology meets immunology: the cancer-immunity cycle. *Immunity* 39, 1–10. doi:10.1016/j.immuni.2013.07.012

Chen, D. S., and Mellman, I. (2017). Elements of cancer immunity and the cancer-immune set point. *Nature* 541, 321–330. doi:10.1038/nature21349

Choi, W., Porten, S., Kim, S., Willis, D., Plimack, E. R., Hoffman-Censits, J., et al. (2014). Identification of distinct basal and luminal subtypes of muscle-invasive bladder cancer with different sensitivities to frontline chemotherapy. *Cancer Cell* 25, 152–165. doi:10.1016/j.ccr.2014.01.009

Chu, C. C., and Paul, W. E. (1997). Fig1, an interleukin 4-induced mouse B cell gene isolated by cDNA representational difference analysis. *Proc. Natl. Acad. Sci. U. S. A.* 94, 2507–2512. doi:10.1073/pnas.94.6.2507

Damrauer, J. S., Hoadley, K. A., Chism, D. D., Fan, C., Tiganelli, C. J., Wobker, S. E., et al. (2014). Intrinsic subtypes of high-grade bladder cancer reflect the hallmarks of breast cancer biology. *Proc. Natl. Acad. Sci. U. S. A.* 111, 3110–3115. doi:10.1073/pnas.1318376111

Eruslanov, E., Neuberger, M., Daurkin, I., Perrin, G. Q., Algood, C., Dahm, P., et al. (2012). Circulating and tumor-infiltrating myeloid cell subsets in patients with bladder cancer. *Int. J. Cancer* 130, 1109–1119. doi:10.1002/ijc.26123

Farhood, B., Najafi, M., and Mortezaee, K. (2019). CD8+ cytotoxic T lymphocytes in cancer immunotherapy: a review. *J. Cell. Physiol.* 234, 8509–8521. doi:10.1002/jcp.27782

Fehrenbacher, L., Spira, A., Marcus, B., Kowanetz, M., Vansteenkiste, J., Mazieres, J., et al. (2016). Atezolizumab versus docetaxel for patients with previously treated non-small-cell lung cancer (POPLAR): a multicentre, open-label, phase 2 randomised controlled trial. *Lancet* 387, 1837–1846. doi:10.1016/S0140-6736(16)00587-0

Finotello, F., Mayer, C., Plattner, C., Laschober, G., Rieder, D., Hackl, H., et al. (2019). Molecular and pharmacological modulators of the tumor immune contexture revealed by deconvolution of RNA-seq data. *Genome Med.* 11, 34. doi:10.1186/s13073-019-0638-6

Gajewski, T. F. (2015). The next hurdle in cancer immunotherapy: overcoming the non–T-cell–inflamed tumor microenvironment. *Seminars Oncol.* 42, 663–671. doi:10.1053/j.seminoncol.2015.05.011

Galon, J., Costes, A., Sanchez-Cabo, F., Kirilovsky, A., Mlecnik, B., Lagorce-Pagès, C., et al. (2006). Type, density, and location of immune cells within human colorectal tumors predict clinical outcome. *Sci. (New York, N.Y.)* 313, 1960–1964. doi:10.1126/science.1129139

Giusti, R., Mazzotta, M., Filetti, M., Marinelli, D., Di Napoli, A., Scarpino, S., et al. (2019). CDKN2A/B gene loss and MDM2 alteration as a potential molecular signature for hyperprogressive disease in advanced NSCLC: a next-generation-sequencing approach. *JCO* 37, e20628. doi:10.1200/JCO.2019.37.15_suppl.e20628

Goldman, M. J., Craft, B., Hastie, M., Repečka, K., McDade, F., Kamath, A., et al. (2020). Visualizing and interpreting cancer genomics data via the Xena platform. *Nat. Biotechnol.* 38, 675–678. doi:10.1038/s41587-020-0546-8

Groenendijk, F. H., Jong, J. de, van de Fransen Putte, E. E., Michaut, M., Schlicker, A., Peters, D., et al. (2016). ERBB2 mutations characterize a subgroup of muscle-invasive bladder cancers with excellent response to neoadjuvant chemotherapy. *Eur. Urol.* 69, 384–388. doi:10.1016/j.eururo.2015.01.014

Hänzelmann, S., Castelo, R., and Guinney, J. (2013). GSVA: gene set variation analysis for microarray and RNA-seq data. *BMC Bioinforma.* 14, 7. doi:10.1186/1471-2105-14-7

Hedegaard, J., Lamy, P., Nordentoft, I., Algaba, F., Høyer, S., Ulhøi, B. P., et al. (2016). Comprehensive transcriptional analysis of early-stage urothelial carcinoma. *Cancer Cell* 30, 27–42. doi:10.1016/j.ccell.2016.05.004

Hirose, S., Mashima, T., Yuan, X., Yamashita, M., Kitano, S., Torii, S., et al. (2024). Interleukin-4 induced 1-mediated resistance to an immune checkpoint inhibitor through suppression of CD8+ T cell infiltration in melanoma. *Cancer Sci.* 115, 791–803. doi:10.1111/cas.16073

Houston, B., Curry, B., and Aitken, R. J. (2015). Human spermatozoa possess an IL4I1 l-amino acid oxidase with a potential role in sperm function. *Reproduction* 149, 587–596. doi:10.1530/REP-14-0621

Hu, J., Yu, A., Othmane, B., Qiu, D., Li, H., Li, C., et al. (2021). Siglec15 shapes a non-inflamed tumor microenvironment and predicts the molecular subtype in bladder cancer. *Theranostics* 11, 3089–3108. doi:10.7150/thno.53649

Ikeda, H., Old, L. J., and Schreiber, R. D. (2002). The roles of IFNγ in protection against tumor development and cancer immunoediting. *Cytokine & Growth Factor Rev.* 13, 95–109. doi:10.1016/S1359-6101(01)00038-7

Ji, R.-R., Chasalow, S. D., Wang, L., Hamid, O., Schmidt, H., Cogswell, J., et al. (2012). An immune-active tumor microenvironment favors clinical response to ipilimumab. *Cancer Immunol. Immunother.* 61, 1019–1031. doi:10.1007/s00262-011-1172-6

Kamoun, A., Reyniès, A., Allory, Y., Sjödahl, G., Robertson, A. G., Seiler, R., et al. (2020). A Consensus molecular classification of muscle-invasive bladder cancer. *Eur. Urol.* 77, 420–433. doi:10.1016/j.eururo.2019.09.006

Kato, S., Goodman, A., Walavalkar, V., Barkauskas, D. A., Sharabi, A., and Kurzrock, R. (2017). Hyperprogressors after immunotherapy: analysis of genomic alterations associated with accelerated growth rate. *Clin. Cancer Res.* 23, 4242–4250. doi:10.1158/1078-0432.CCR-16-3133

Koboldt, D. C., Larson, D. E., and Wilson, R. K. (2013). Using VarScan 2 for germline variant calling and somatic mutation detection. *Curr. Protoc. Bioinforma.* 44 (15.4), 1–17. doi:10.1002/0471250953.bi1504s44

Li, F., Li, C., Cai, X., Xie, Z., Zhou, L., Cheng, B., et al. (2021). The association between CD8+ tumor-infiltrating lymphocytes and the clinical outcome of cancer immunotherapy: a systematic review and meta-analysis. *eClinicalMedicine* 41, 101134. doi:10.1016/j.eclinm.2021.101134

Li, T., Fan, J., Wang, B., Traugh, N., Chen, Q., Liu, J. S., et al. (2017). TIMER: a web server for comprehensive analysis of tumor-infiltrating immune cells. *Cancer Res.* 77, e108–e110. doi:10.1158/0008-5472.CAN-17-0307

Li, T., Shi, J., Wang, L., Qin, X., Zhou, R., Dong, M., et al. (2020). Thymol targeting interleukin 4 induced 1 expression reshapes the immune microenvironment to sensitize the immunotherapy in lung adenocarcinoma. *MedComm* 2023, e355. doi:10.1002/mco2.355

Lin, H., Fu, L., Li, P., Zhu, J., Xu, Q., Wang, Y., et al. (2023). Fatty acids metabolism affects the therapeutic effect of anti-PD-1/PD-L1 in tumor immune microenvironment in clear cell renal cell carcinoma. *J. Transl. Med.* 21, 343. doi:10.1186/s12967-023-04161-z

Mariathasan, S., Turley, S. J., Nickles, D., Castiglioni, A., Yuen, K., Wang, Y., et al. (2018). TGFβ attenuates tumour response to PD-L1 blockade by contributing to exclusion of T cells. *Nature* 554, 544–548. doi:10.1038/nature25501

Marquet, J., Lasoudris, F., Cousin, C., Puiffe, M.-L., Martin-Garcia, N., Baud, V., et al. (2010). Dichotomy between factors inducing the immunosuppressive enzyme IL-4-induced gene 1 (IL4I1) in B lymphocytes and mononuclear phagocytes. *Eur. J. Immunol.* 40, 2557–2568. doi:10.1002/eji.201040428

Marzouka, N.-a.-d., Eriksson, P., Rovira, C., Liedberg, F., Sjödahl, G., and Höglund, M. (2018). A validation and extended description of the Lund taxonomy for urothelial carcinoma using the TCGA cohort. *Sci. Rep.* 8, 3737. doi:10.1038/s41598-018-22126-x

Matusiak, M., Hickey, J. W., van Ijzendoorn, D. G. P., Lu, G., Kidzinski, L., Zhu, S., et al. (2024). Spatially segregated macrophage populations predict distinct outcomes in colon cancer. *Cancer Discov*. doi:10.1158/2159-8290.CD-23-1300

McLaughlin, J., Han, G., Schalper, K. A., Carvajal-Hausdorf, D., Pelekanou, V., Rehman, J., et al. (2016). Quantitative assessment of the heterogeneity of PD-L1 expression in non-small-cell lung cancer. *JAMA Oncol.* 2, 46–54. doi:10.1001/jamaoncol.2015.3638

Mo, Q., Nikolos, F., Chen, F., Tramel, Z., Lee, Y.-C., Hayashi, K., et al. (2018). Prognostic power of a tumor differentiation gene signature for bladder urothelial carcinomas. *J. Natl. Cancer Inst.* 110, 448–459. doi:10.1093/jnci/djx243

Molinier-Frenkel, V., Prévost-Blondel, A., and Castellano, F. (2019). The IL4I1 enzyme: a new player in the immunosuppressive tumor microenvironment. *Cells* 8, 757. doi:10.3390/cells8070757

Motz, G. T., and Coukos, G. (2013). Deciphering and reversing tumor immune suppression. *Immunity* 39, 61–73. doi:10.1016/j.immuni.2013.07.005

Müller, K., Ellenberger, C., Hoppen, H.-O., and Schoon, H.-A. (2012). Immunohistochemical study of angiogenesis and angiogenic factors in equine granulosa cell tumours. *Res. Vet. Sci.* 92, 471–477. doi:10.1016/j.rvsc.2011.02.016

Nagarsheth, N., Wicha, M. S., and Zou, W. (2017). Chemokines in the cancer microenvironment and their relevance in cancer immunotherapy. *Nat. Rev. Immunol.* 17, 559–572. doi:10.1038/nri.2017.49

Necchi, A., Joseph, R. W., Loriot, Y., Hoffman-Censits, J., Perez-Gracia, J. L., Petrylak, D. P., et al. (2017). Atezolizumab in platinum-treated locally advanced or metastatic urothelial carcinoma: post-progression outcomes from the phase II IMvigor210 study. *Ann. Oncol.* 28, 3044–3050. doi:10.1093/annonc/mdx518

Newman, A. M., Liu, C. L., Green, M. R., Gentles, A. J., Feng, W., Xu, Y., et al. (2015). Robust enumeration of cell subsets from tissue expression profiles. *Nat. Methods* 12, 453–457. doi:10.1038/nmeth.3337

Nishino, M., Ramaiya, N. H., Hatabu, H., and Hodi, F. S. (2017). Monitoring immune-checkpoint blockade: response evaluation and biomarker development. *Nat. Rev. Clin. Oncol.* 14, 655–668. doi:10.1038/nrclinonc.2017.88

Ott, P. A., Bang, Y.-J., Piha-Paul, S. A., Razak, A. R. A., Bennouna, J., Soria, J.-C., et al. (2019). T-Cell-Inflamed gene-expression profile, programmed death ligand 1 expression, and tumor mutational burden predict efficacy in patients treated with pembrolizumab across 20 cancers: KEYNOTE-028. *JCO* 37, 318–327. doi:10.1200/JCO.2018.78.2276

Pagès, F., Berger, A., Camus, M., Sanchez-Cabo, F., Costes, A., Molidor, R., et al. (2005). Effector memory T cells, early metastasis, and survival in colorectal cancer. *N. Engl. J. Med.* 353, 2654–2666. doi:10.1056/NEJMoa051424

Pardoll, D. M. (2012). The blockade of immune checkpoints in cancer immunotherapy. *Nat. Rev. Cancer* 12, 252–264. doi:10.1038/nrc3239

Park, S. H., Kang, K., Giannopoulou, E., Qiao, Y., Kang, K., Kim, G., et al. (2017). Type I interferons and the cytokine TNF cooperatively reprogram the macrophage epigenome to promote inflammatory activation. *Nat. Immunol.* 18, 1104–1116. doi:10.1038/ni.3818

Peng, D., Kryczek, I., Nagarsheth, N., Zhao, L., Wei, S., Wang, W., et al. (2015). Epigenetic silencing of TH1-type chemokines shapes tumour immunity and immunotherapy. *Nature* 527, 249–253. doi:10.1038/nature15520

Pfannstiel, C., Strissel, P. L., Chiappinelli, K. B., Sikic, D., Wach, S., Wirtz, R. M., et al. (2019). The tumor immune microenvironment drives a prognostic relevance that correlates with bladder cancer subtypes. *Cancer Immunol. Res.* 7, 923–938. doi:10.1158/2326-6066.CIR-18-0758

Pietzak, E. J., Zabor, E. C., Bagrodia, A., Armenia, J., Hu, W., Zehir, A., et al. (2019). Genomic differences between "primary" and "secondary" muscle-invasive bladder cancer as a basis for disparate outcomes to cisplatin-based neoadjuvant chemotherapy. *Eur. Urol.* 75, 231–239. doi:10.1016/j.eururo.2018.09.002

Pluchino, S., and Peruzzotti-Jametti, L. (2016). Interleukin-4 induced 1 (IL4I1) promotes central nervous system remyelination. *Brain* 139, 3052–3054. doi:10.1093/brain/aww266

Powles, T., Durán, I., van der Heijden, M. S., Loriot, Y., Vogelzang, N. J., Giorgi, U. de, et al. (2018). Atezolizumab versus chemotherapy in patients with platinum-treated locally advanced or metastatic urothelial carcinoma (IMvigor211): a multicentre, open-label, phase 3 randomised controlled trial. *Lancet* 391, 748–757. doi:10.1016/S0140-6736(17)33297-X

Racle, J., de Jonge, K., Baumgaertner, P., Speiser, D. E., and Gfeller, D. (2017). Simultaneous enumeration of cancer and immune cell types from bulk tumor gene expression data. *eLife* 6, e26476. doi:10.7554/eLife.26476

Rebouissou, S., Bernard-Pierrot, I., Reyniès, A., Lepage, M. L., Krucker, C., Chapeaublanc, E., et al. (2014). EGFR as a potential therapeutic target for a subset of muscle-invasive bladder cancers presenting a basal-like phenotype. *Sci. Transl. Med.* 6, 244ra91. doi:10.1126/scitranslmed.3008970

Robertson, A. G., Kim, J., Al-Ahmadie, H., Bellmunt, J., Guo, G., Cherniack, A. D., et al. (2017). Comprehensive molecular characterization of muscle-invasive bladder cancer. *Cell* 171, 540–556.e25. doi:10.1016/j.cell.2017.09.007

Romagnani, S. (2016). IL4I1: key immunoregulator at a crossroads of divergent T-cell functions. *Eur. J. Immunol.* 46, 2302–2305. doi:10.1002/eji.201646617

Rosenberg, J. E., Hoffman-Censits, J., Powles, T., van der Heijden, M. S., Balar, A. V., Necchi, A., et al. (2016). Atezolizumab in patients with locally advanced and metastatic urothelial carcinoma who have progressed following treatment with platinum-based chemotherapy: a single-arm, multicentre, phase 2 trial. *Lancet* 387, 1909–1920. doi:10.1016/S0140-6736(16)00561-4

Ru, B., Wong, C. N., Tong, Y., Zhong, J. Y., Zhong, S. S. W., Wu, W. C., et al. (2019). TISIDB: an integrated repository portal for tumor-immune system interactions. *Bioinformatics* 35, 4200–4202. doi:10.1093/bioinformatics/btz210

Sadik, A., Somarribas Patterson, L. F., Öztürk, S., Mohapatra, S. R., Panitz, V., Secker, P. F., et al. (2020). IL4I1 is a metabolic immune checkpoint that activates the AHR and promotes tumor progression. *Cell* 182, 1252–1270. doi:10.1016/j.cell.2020.07.038

Said, N., and Theodorescu, D. (2012). RhoGDI2 suppresses bladder cancer metastasis via reduction of inflammation in the tumor microenvironment. *Oncoimmunology* 1, 1175–1177. doi:10.4161/onci.20594

Sato, E., Olson, S. H., Ahn, J., Bundy, B., Nishikawa, H., Qian, F., et al. (2005). Intraepithelial CD8+ tumor-infiltrating lymphocytes and a high CD8+/regulatory T cell ratio are associated with favorable prognosis in ovarian cancer. *Proc. Natl. Acad. Sci. U. S. A.* 102, 18538–18543. doi:10.1073/pnas.0509182102

Sha, D., Jin, Z., Budczies, J., Kluck, K., Stenzinger, A., and Sinicrope, F. A. (2020). Tumor mutational burden as a predictive biomarker in solid tumors. *Cancer Discov.* 10, 1808–1825. doi:10.1158/2159-8290.CD-20-0522

Sharma, P., Retz, M., Siefker-Radtke, A., Baron, A., Necchi, A., Bedke, J., et al. (2017). Nivolumab in metastatic urothelial carcinoma after platinum therapy (CheckMate 275): a multicentre, single-arm, phase 2 trial. *Lancet Oncol.* 18, 312–322. doi:10.1016/S1470-2045(17)30065-7

Siegel, R. L., Miller, K. D., Wagle, N. S., and Jemal, A. (2023). Cancer statistics, 2023. *CA Cancer J. Clin.* 73, 17–48. doi:10.3322/caac.21763

Singavi, A. K., Menon, S., Kilari, D., Alqwasmi, A., Ritch, P. S., Thomas, J. P., et al. (2017). Predictive biomarkers for hyper-progression (HP) in response to immune checkpoint inhibitors (ICI) – analysis of somatic alterations (SAs). *Ann. Oncol.* 28, v405. doi:10.1093/annonc/mdx376.006

Singla, N., Ghandour, R. A., and Raj, G. V. (2019). Biomarkers for platinum sensitivity in bladder cancer: are we there yet? *Transl. Androl. Urology* 8, S236–S239. doi:10.21037/tau.2019.01.10

Sjödahl, G., Lauss, M., Lövgren, K., Chebil, G., Gudjonsson, S., Veerla, S., et al. (2012). A molecular taxonomy for urothelial carcinoma. *Clin. Cancer Res.* 18, 3377–3386. doi:10.1158/1078-0432.CCR-12-0077-T

Snyder, A., Makarov, V., Merghoub, T., Yuan, J., Zaretsky, J. M., Desrichard, A., et al. (2014). Genetic basis for clinical response to CTLA-4 blockade in melanoma. *N. Engl. J. Med.* 371, 2189–2199. doi:10.1056/NEJMoa1406498

Spranger, S., and Gajewski, T. F. (2018). Impact of oncogenic pathways on evasion of antitumour immune responses. *Nat. Rev. Cancer* 18, 139–147. doi:10.1038/nrc.2017.117

Spranger, S., Spaapen, R. M., Zha, Y., Williams, J., Meng, Y., Ha, T. T., et al. (2013). Up-regulation of PD-L1, Ido, and T(regs) in the melanoma tumor microenvironment is driven by CD8(+) T cells. *Sci. Transl. Med.* 5, 200ra116. doi:10.1126/scitranslmed.3006504

St Paul, M., and Ohashi, P. S. (2020). The roles of CD8+ T cell subsets in antitumor immunity. *Trends Cell Biol.* 30, 695–704. doi:10.1016/j.tcb.2020.06.003

Sweis, R. F., Spranger, S., Bao, R., Paner, G. P., Stadler, W. M., Steinberg, G., et al. (2016). Molecular drivers of the non-T-cell-inflamed tumor microenvironment in urothelial bladder cancer. *Cancer Immunol. Res.* 4, 563–568. doi:10.1158/2326-6066.CIR-15-0274

van Allen, E. M., Mouw, K. W., Kim, P., Iyer, G., Wagle, N., Al-Ahmadie, H., et al. (2014). Somatic ERCC2 mutations correlate with cisplatin sensitivity in muscle-invasive urothelial carcinoma. *Cancer Discov.* 4, 1140–1153. doi:10.1158/2159-8290.CD-14-0623

Wishart, D. S., Feunang, Y. D., Guo, A. C., Lo, E. J., Marcu, A., Grant, J. R., et al. (2018). DrugBank 5.0: a major update to the DrugBank database for 2018. *Nucleic Acids Res.* 46, D1074–D1082. doi:10.1093/nar/gkx1037

Witjes, J. A., Bruins, H. M., Cathomas, R., Compérat, E. M., Cowan, N. C., Gakis, G., et al. (2021). European association of urology guidelines on muscle-invasive and metastatic bladder cancer: summary of the 2020 guidelines. *Eur. Urol.* 79, 82–104. doi:10.1016/j.eururo.2020.03.055

Wykes, M. N., and Lewin, S. R. (2018). Immune checkpoint blockade in infectious diseases. *Nat. Rev. Immunol.* 18, 91–104. doi:10.1038/nri.2017.112

Yang, K., Halima, A., and Chan, T. A. (2023). Antigen presentation in cancer - mechanisms and clinical implications for immunotherapy. *Nat. Rev. Clin. Oncol.* 20, 604–623. doi:10.1038/s41571-023-00789-4

Ye, F., Wang, L., Li, Y., Dong, C., Zhou, L., and Xu, J. (2023). IL4I1 in M2-like macrophage promotes glioma progression and is a promising target for immunotherapy. *Front. Immunol.* 14, 1338244. doi:10.3389/fimmu.2023.1338244

Zhang, L., Conejo-Garcia, J. R., Katsaros, D., Gimotty, P. A., Massobrio, M., Regnani, G., et al. (2003). Intratumoral T cells, recurrence, and survival in epithelial ovarian cancer. *N. Engl. J. Med.* 348, 203–213. doi:10.1056/NEJMoa020177

Zhao, H., Teng, Y., Hao, W., Li, J., Li, Z., Chen, Q., et al. (2021). Single-cell analysis revealed that IL4I1 promoted ovarian cancer progression. *J. Transl. Med.* 19, 454. doi:10.1186/s12967-021-03123-7

frontiers | Frontiers in Pharmacology

TYPE Original Research
PUBLISHED 05 June 2024
DOI 10.3389/fphar.2024.1388613

OPEN ACCESS

EDITED BY
Huan Yang,
Huazhong University of Science and Technology, China

REVIEWED BY
Jianjun Zhou,
Tongji University, China
S. Aidan Quinn,
Dana–Farber Cancer Institute, United States

*CORRESPONDENCE
Yuan Gao,
yuan_gao@fudan.edu.cn
Zhuo Wang,
wztgyx223@163.com
Jiyuan Chen,
hobartchanjy@163.com

†These authors have contributed equally to this work

RECEIVED 20 February 2024
ACCEPTED 09 May 2024
PUBLISHED 05 June 2024

CITATION
Chen X, Gong L, Wang Y, Ye C, Guo H, Gao S, Chen J, Wang Z and Gao Y (2024), IL-23 inhibitor enhances the effects of PTEN DNA-loaded lipid nanoparticles for metastatic CRPC therapy.
Front. Pharmacol. 15:1388613.
doi: 10.3389/fphar.2024.1388613

IL-23 inhibitor enhances the effects of PTEN DNA-loaded lipid nanoparticles for metastatic CRPC therapy

Xinlu Chen[1,2†], Luyao Gong[1†], Yuanyuan Wang[1], Chen Ye[2], Huanhuan Guo[2], Shen Gao[2], Jiyuan Chen[3]*, Zhuo Wang[1]* and Yuan Gao[1,2]*

[1]School of Pharmacy, Fudan University, Shanghai, China, [2]Department of Pharmacy, Changhai Hospital, Naval Medical University, Shanghai, China, [3]Department of Pharmacy, Shanghai Ninth People's Hospital, Shanghai Jiao Tong University School of Medicine, Shanghai, China

Introduction: Metastatic castration-resistant prostate cancer (mCRPC) patients face challenges due to limited treatment options. About 50% of patients with mCRPC have a functional loss of phosphatase and tensin homology deleted on chromosome 10 (PTEN), leading to tumor progression, metastasis, and immune suppression. Moreover, elevated IL-23 produced by myeloid-derived suppressor cells (MDSCs) is found in CRPC patients, driving tumor progression. Therefore, a combination strategy based on PTEN restoration and IL-23 inhibition may block CRPC progression and metastasis.

Methods: The antitumor effect of restoring PTEN expression combined with the IL-23 inhibitor Apilimod was studied in a mouse model of bone metastasis CRPC and mouse prostate cancer RM-1 cells. To verify the targeting ability of PTEN DNA coated with lipid nanoparticles (LNP@PTEN) *in vitro* and *in vivo*. In addition, RT-qPCR and flow cytometry were used to investigate the related mechanisms of the antitumor effect of LNP@PTEN combined with Apilimod.

Results: LNPs exhibited significant tumor-targeting and tumor accumulation capabilities both *in vitro* and *in vivo*, enhancing PTEN expression and therapeutic efficacy. Additionally, the combination of LNP@PTEN with the IL-23 inhibitor Apilimod demonstrated enhanced inhibition of tumor growth, invasion, and metastasis (particularly secondary organ metastasis) compared to other groups, and extended the survival of mice to 41 days, providing a degree of bone protection. These effects may be attributed to the PTEN function restoration combined with IL-23 inhibition, which help reverse immune suppression in the tumor microenvironment by reducing MDSCs recruitment and increasing the $CD8^+/CD4^+$ T cell ratio.

Discussion: In summary, these findings highlight the potential of LNPs for delivering gene therapeutic agents. And the combination of LNP@PTEN with Apilimod could achieve anti-tumor effects and improve tumor microenvironment. This combinational strategy opens new avenues for the treatment of mCRPC.

KEYWORDS

prostate cancer, bone metastases, lipid nanoparticles, nucleic acid delivery, immune microenvironment

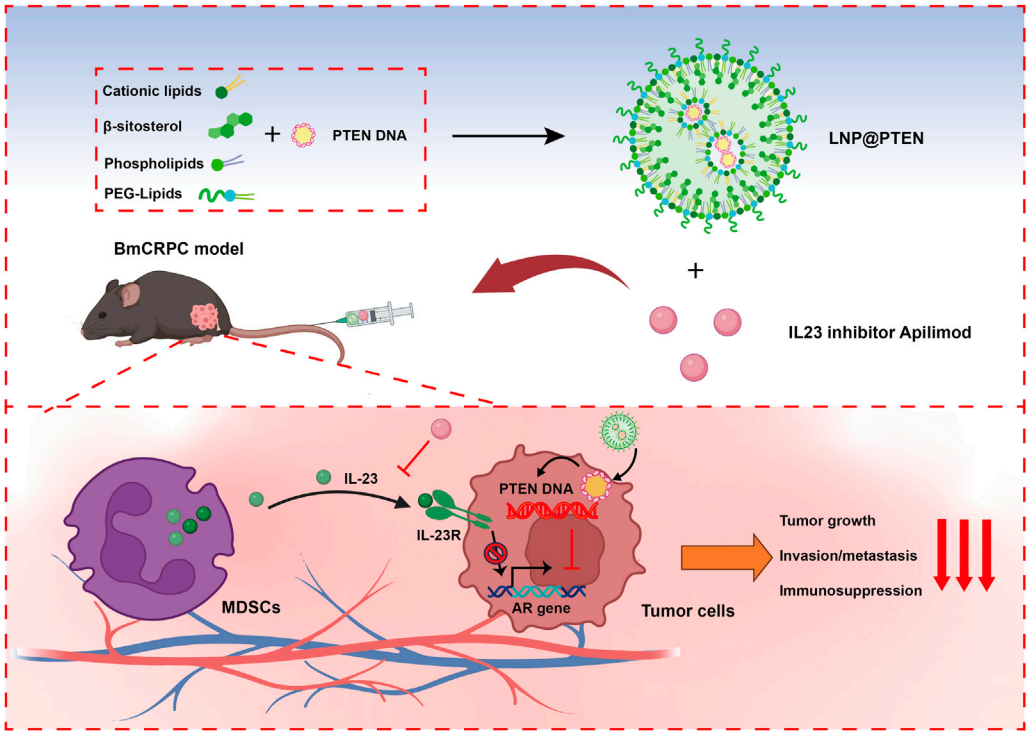

GRAPHICAL ABSTRACT
Cationic lipids, β-sitosterol, phospholipids and PEG-lipids self-assemble in aqueous solution to form cationic lipid nanoparticles (LNPs), which could encapsulate PTEN DNA through electrostatic adsorption to generate LNP@PTEN. This formulation could be delivered to prostate cancer bone metastatic sites. LNP@PTEN combined with the IL-23 inhibitor Apilimod showed enhanced anti-tumor effects by inhibiting tumor proliferation and metastasis, and reactivating anti-tumor immunity with good safety (Created with BioRender.com).

1 Introduction

Prostate cancer (PCa) is the second most frequent cancer among men worldwide (Sung et al., 2021; Siegel et al., 2023). The emergence of castration-resistant prostate cancer (CRPC) following 18–24 months of androgen deprivation therapy is one of the main clinical challenges in managing PCa (Harris et al., 2009; Jiang et al., 2020). Moreover, a substantial proportion of these CRPC patients progress to a more aggressive stage known as metastatic CRPC (mCRPC), with nearly 90% of cases metastasizing to the bone, leading to the development of bone metastasis CRPC (BmCRPC) with a limited survival period of less than 2 years (Garcia, 2011; Halabi et al., 2016; Chen et al., 2020).

Phosphatase and tensin homology deleted on chromosome 10 (PTEN) loss frequently occurs during human PCa progression. Functional loss of the PTEN tumor suppressor gene is estimated to occur in more than 40% of patients with mCRPC, with up to 70% of advanced-stage samples showing loss of PTEN function (Taylor et al., 2010; Mulholland et al., 2011; Jamaspishvili et al., 2018). The loss of PTEN results in enhanced tumor cell proliferation, viability, and migration, as well as castration-resistant growth (Mulholland et al., 2011). In addition, the loss of PTEN can also promote immune suppression by escalating the population of myeloid-derived suppressor cells (MDSCs) and the secretion of immune-inhibitory cytokines, leading to reduced T-cell infiltration and enhanced infiltration of regulatory T-cells (Treg) within the tumor (Rizvi and Chan, 2016; Bezzi et al., 2018). Therefore, restoring the PTEN function may inhibit the CRPC progression as well as enhance immune function.

Currently, various therapeutic strategies are under exploration to target PTEN-deficient tumors, including conventional inhibition of the PI3K-AKT-mTOR signaling network as well as innovative approaches to restore PTEN function (Mukherjee et al., 2021; Bergholz et al., 2023). *In vitro* experiments have shown that transfecting tumor cells with plasmid DNA can restore PTEN function; however, the use of plasmid DNA still faces challenges related to tumor targeting, transfection efficacy, and maintaining nucleic acid stability (Yin and Anderson, 2017; Islam et al., 2018). Presently, lipid nanoparticles (LNPs) are being used for *in vivo* delivery of nucleic acid drugs (Zhang et al., 2021), which can protect DNA plasmids from enzymatic degradation, prevent unwanted clearance, and promote cellular uptake. Therefore, LNPs could be developed for PTEN DNA delivery, providing an effective therapeutic approach for mCRPC.

In addition, it was reported that patients with CRPC had elevated mRNA levels of IL-23 in the tumor microenvironment, which is released by MDSCs and could activate phoshpo-STAT3–RORγ signaling to drive AR transcription. Therefore, treatments that block IL-23 with its inhibitors may effectively reverse MDSC-mediated resistance to CRPC and synergize with other therapies (Duvallet et al., 2011; Calcinotto et al., 2018).

Due to the high frequency of PTEN loss and high expression of IL-23 in CRPC, the combination of the IL-23 inhibitor Apilimod with PTEN DNA may achieved enhanced effects for cancer

therapy. For this purpose, we developed an ionizable cationic lipid, which could self-assemble into LNPs with β-sitosterol, phospholipids, and PEG-lipids for PTEN DNA delivery. We hypothesized that PTEN loaded in LNPs (LNP@PTEN) could effectively reach tumor sites, restoring the anti-tumor function of PTEN. Moreover, the combination of LNP@PTEN with Apilimod could enhance the anticancer effect and immune function for the treatment of CRPC progression.

2 Materials and methods

2.1 Materials

Commercial suppliers provided all reagents and solvents, which were utilized without additional purification. 1,4-bis (3-aminopropyl) piperazine, 1,2-epoxydodecane, dichloromethane, agarose and crystal violet were acquired from Aladdin (Shanghai, China). 1,2-distearoyl-sn-glycero-3-phosphocholine (DSPC), and 1,2-dimyristoyl-rac-glycero-3-methoxypolyethylene glycol-2000 (PEG_{2K}-DMG) were obtained from AVT (Shanghai, China). β-sitosterol was purchased from BIDE (Shanghai, China). Matrigel was obtained from Corning (United States). PTEN plasmid DNA (PTEN), enhanced green fluorescent protein plasmid DNA (pEGFP) and FAM-labeled siRNA (siFAM) were purchased from GenePharma (Shanghai, China). TAE electrophoresis buffer, 4% Paraformaldehyde fix solution, the TUNEL kit, Anti -Ki67 Mouse mAb, and Alexa Fluor® 488-conjugated Goat Anti-Mouse IgG (H + L) were acquired from Servicebio (Wuhan, China). Cell Counting Kit-8 (CCK-8), Propidium iodide (PI), 4′,6-diamidino-2-phenylindole (DAPI) were obtained from Beyotime (Shanghai, China). Apilimod mesylate was purchased from MedChemExpress (United States). Isoflurane was acquired from RWD (Shenzhen, Guangdong). Deoxyribonuclease I (DNase I), Collagenase IV and Hyaluronidase (HAase) were purchased from Biofroxx (Germany). 1,1-dioctadecyl-3,3,3,3-tetramethylindotricarbocyanine iodide (DIR iodide) was obtained from Maokang (Shanghai, China). Distilled water was used throughout the process.

2.2 Cell lines and animals

Human embryonic kidney 293T cells (HEK-293T cells), mouse prostate cancer cells (RM-1), mouse embryonic fibroblast cells (NIH-3T3) and mouse embryo osteoblast precursor cells (MC3T3-E1) were provided from Cell Bank of Shanghai, Chinese Academy of Sciences (CAS, Shanghai, China). HEK-293T cells NIH-3T3 cells were cultured in DMEM (Gibco, United States). RM-1 cells were cultured in RPMI-1640 medium (Gibco, United States). MC3T3-E1 cells were cultured in α-MEM medium (Gibco, United States). All cell media were added with 10% fetal bovine serum (FBS) (Gibco, United States) and 100 U/mL penicillin/streptomycin (P/S) (Gibco, United States). The cell culture incubator was used to perform cell culture at a temperature of 37°C and under 5% CO_2 conditions.

Six-week-old C57BL/6J male normal mice (18–22 g) were ordered from the Clinical Experimental Center, Changhai Hospital, Naval Medical University (Shanghai, China). All experiments were carried out in accordance with the relevant regulations of Committee on Ethics of Medicine, Naval Medical University, PLA. To establish the RM-1 BmCRPC mouse model, RM-1 cells were injected into marrow cavity at 1×10^6 cells per mouse. Tumor formation occurred about 10 d later (Hoang et al., 2017).

2.3 Synthesis and identification of cationic lipid 246C10

The 246C10 was synthesized according to the reference (Kim et al., 2021). In detail, in a 5-mL vial, 1 mL of 1,4-Bis (3-aminopropyl) piperazine (4.65 mmol, 4.8 equivalents) was added, and 200 μL of 1,2-Epoxydodecane (0.97 mmol, 1 equivalent) was added dropwise. The reaction mixture was stirred at 90°C with 300 rpm for 3 d, yielding light yellow oil. The product was purified by dichloromethane/methanol column chromatography to obtain high-quality products. The structural identification was performed using hydrogen nuclear magnetic resonance (NMR) and tandem mass spectrometry (MS) spectra.

2.4 Preparation and characterization of LNPs

The formulation of LNPs was prepared utilizing the thin-film rehydration methodology. Briefly, 246C10, DSPC, β-sitosterol, and PEG_{2K}-DMG were weighed in a molar ratio of 50: 10: 38.5: 1.5 and then were dissolved in anhydrous ethanol, stirring at room temperature (RT) at 100 rpm for 8 h. Subsequently, a thin film was generated through an evaporation process conducted under reduced pressure and then dispersed in pure water using a sonication probe (YM-650Y, Yuming, China) at 400 W for 5 min, resulting in the formation of blank LNPs (LNP-Blank). LNP-Blank was further mixed with PTEN DNA and allowed to incubate at RT for 30 min, ultimately producing PTEN-DNA-loaded LNPs (LNP@PTEN).

The ability of LNPs to transport DNA was assessed via agarose gel electrophoresis. Initially, agarose was dissolved in TAE electrophoresis buffer (0.8% w/v) and heated until completely dissolved. Gel-red (Biosharp, China) was subsequently added to the solution, thoroughly mixed, and then poured into a pre-prepared electrophoresis chamber equipped with a comb. A mixture containing 10 μL of the sample and 1 μL of loading buffer (6×) was prepared and carefully loaded into the wells of the gel after it solidified. Electrophoresis was conducted at RT with 110V for 40 min, and then the gel block was visualized using a UV gel imaging system to capture images.

The morphology of LNP-Blank and LNP@PTEN was assessed using transmission electron microscopy (TEM, TECNAI G2 S-TWIN, United States) after applying negative staining with saturated uranyl acetate solution. Additionally, dynamic light scattering (DLS) analysis was conducted using a Nano ZS90 instrument (Malvern, England) to determine nanoparticles size distribution and zeta potential values. Moreover, to assess their stability in simulated physiological fluids, nanoparticles were stored in PBS (pH 7.4) at 4°C for a period of 20 d.

2.5 Gene transfection assays

To evaluate the transfection efficiency of LNPs, HEK-293T cells were seeded in 48-well plates. Subsequently, pEGFP were co-incubated with LNPs at different mass ratios (LNPs: pEGFP = 3, 5, 7, 10), with Lipo8000@pEGFP as the control group (mass ratios is 2). And, pEGFP was 0.5 μg/well. After 24 h of co-culturing with cells, the fluorescence intensity of each group was observed by a fluorescence microscope (CKX53, OLYMPUS, Japan) and quantified by ImageJ software.

2.6 *In vitro* cellular toxicity assessment

RM-1 cells and NIH-3T3 cells were cultured in a 96-well plate at a density of 5×10^4 cells/mL. Following this, the cells were co-incubated for 24 h with formulations at varying concentrations (Lipo8000-Blank: 0–50 μg/mL, LNP-Blank: 0–50 μg/mL, PTEN: 1–0.5 μg/mL, Apilomod: 0–10 nM). PBS and NC (PTEN negative control, non-coding random DNA) were used as controls. Cell viability was assessed using CCK-8, and absorbance was measured at 450 nm (OD) by a microplate reader (MULTISKAN MK3, Thermo, United States).

RM-1 cells were seeded in a 48-well plate and cultured overnight. Subsequently, the cells were treated with LNP@pEGFP, with Lipo8000@pEGFP as the control group. After 24 h, RM-1 cells were co-incubated with PI and DAPI (100 μg/mL, 10 μL) in darkness for 30 min and then fixed with paraformaldehyde. Fluorescence expressions within the cells were observed by a fluorescence microscope, and the quantification of fluorescence intensity in each group was conducted using ImageJ software.

2.7 *In vitro* cellular uptake and intracellular colocalization assay

To assess cellular uptake efficiency, RM-1 cells were seeded in 24-well plates, then incubated overnight. Subsequently, FAM-labeled siRNA (siFAM) was encapsulated in LNPs and Lipo8000 for 30 min (siFAM, 20 ng/mL). LNP@siFAM was added for co-incubation for 24 h, while an equal volume of PBS, free siFAM and Lipo8000@siFAM served as the controls. Cellular uptake in each group was evaluated via the FACS Calibur flow cytometer (BD Biosciences, United States), with subsequent data analysis employing FlowJo software.

Cover the bottom of the 24-well plate with sterilized coverslips. Following 24 h co-incubation with siFAM, Lipo8000@siFAM and LNP@siFAM, RM-1 cells were fixed with paraformaldehyde, and then a sealing solution containing DAPI was applied to the coverslip. The intracellular distribution of LNP@siFAM was observed by confocal laser scanning microscope (CLSM, SpinSR10, Olympus, Japan).

2.8 Lysosome escape assay

To investigate the lysosomal escape capability, RM-1 cells were seeded in 24-well plates, then incubated overnight. Subsequently, LNP@siFAM and Lipo8000@siFAM (siFAM, 20 ng/mL) were co-incubated with RM-1 cells for 1 and 4 h. RM-1 cells were labeled with LysoTracker Red (50 ng/mL) to mark lysosomes, and DAPI was used for cell nucleus staining. Images were acquired by CLSM.

2.9 Quantitative real-time PCR

Total RNA was extracted from cellular samples in RNase-free tubes using Trizol (Vazyme, China). Subsequently, reverse transcription into cDNA was carried out with HiScript III All-in-one RT SuperMix Perfect (Vazyme, China). The primer sequences are provided in Supplementary Table S1. Real-time PCR was conducted using Taq Pro universal SYBR qPCR Master Mix (Vazyme, China) following a three-step PCR reaction procedure. Gene expression levels were normalized to GAPDH expression and analyzed using the $2^{-\Delta\Delta Ct}$ method.

2.10 *In vitro* cell migration and invasion assays

The *in vitro* inhibitory effects on tumor cell migration and invasion were assessed via Transwell assays. RM-1 cells were cultured in medium without FBS for 24 h. Subsequently, the cells were seeded into the upper chambers of Transwell plates (8-μm, Corning). In the bottom of the chambers, DMEM containing 20% FBS (800 μL) served as chemokines. Matrigel was inserted into the upper chambers of Transwell plates for the anti-migration experiment. Subsequently, RM-1 cells were co-incubated with different treatment groups (PTEN DNA: 0.5 μg/well, Apilimod: 10 nM) for 24 h (anti-migration experiment) and 48 h (anti-invasion experiment). After being fixed in methanol for 30 min, the cells were stained for 20 min with 0.1% crystal violet and then washed three times in PBS (pH 7.2). Bright-field fluorescence microscopy was used to capture images of nine randomly selected fields for each group. Quantitative analysis of cell counts was performed using ImageJ software.

2.11 Penetration of LNPs in three-dimensional (3D) multicellular tumor spheroids

The preparation of RM-1 and MC3T3-E1 multicellular spheroids was accomplished through the liquid overlay method. In brief, sterile agarose (50 μL per well) was added to 96-well plates. Subsequently, DiO-stained RM-1 cells and DiD-stained MC3T3-E1 cells (1×10^4 cells each) were proportionally distributed in the 96-well plate at the ratio of 1:1 and then subjected to centrifugation at 1,500 rpm for 12 min at 4°C. During the spheroid formation process, the culture medium (DMEM) was refreshed every 3 d. The image of the tumor spheroids was monitored by CLSM.

Then, 3D multicellular tumor spheroids were prepared without the addition of any dye. LNPs were stained with DiO for 20 min at RT, and then loaded with Cy7-DNA (LNP-DiO@Cy7-DNA, DiO: 20 μg/mL, Cy7-DNA: 0.5 μg/mL), which were

co-cultured with the tumor spheroids for 8 h. After fixing with 4% paraformaldehyde, DAPI was employed for nuclei staining. These spheroids were then transferred to a confocal dish, and images were captured by CLSM. Image processing was performed using ImageJ software.

2.12 *In vivo* biodistribution study

A mouse model of BmCRPC was established to investigate the *in vivo* distribution of LNPs with DIR serving as a model drug. This was achieved by intravenously injecting free DIR and DIR-loaded LNPs (LNP@DIR, 1 mg/kg). *In vivo* imaging system (IVIS Lumina III *In Vivo* Imaging System, Perkin Elmer) was applied to the *in vivo* fluorescence of each group of mice at 0, 2, 4, 8, 12, and 24 h, as well as fluorescence measurements of all hearts, livers, spleens, lungs, kidneys, and tumor tissues collected from each group of mice euthanized at 24 h. Subsequently, all data were analyzed employing the Quick View 3,000 software.

2.13 *In vivo* antitumor effects of LNPs

A mouse model of bone metastasis CRPC was established as previously described. The mice were randomly divided into five groups (n = 5): (a) PBS; (b) Apilimod; (c) LNP-Blank; (d) LNP@PTEN; (e) Apilimod + LNP@PTEN (PTEN DNA: 700 μg/kg, Apilimod: 10 mg/kg) (Wada et al., 2006; Wada et al., 2012; Islam et al., 2018). When the tumor size reached approximately 100 mm^3, the mice received treatment with tail vein injections every 3 days for 2 weeks. Tumor volume and body weight were monitored every other day, with the first dose being reported on the first day. The formula used to compute the tumor volume was $V = L \times W^2/2$, in which 'L' stood for the tumor's longest axis and 'W' for the axis length that was perpendicular to the longest axis. Sixteen days following the first injection, all animals were anesthetized to obtain blood samples from the retro-orbital venous plexus to assess biochemical indicators (ALT, AST, BUN, and CREAT), and tumor tissues were harvested and weighed. Both tumors and organs were collected to be fixed with 4% paraformaldehyde, embedded in paraffin, and sectioned into tissue slices for subsequent hematoxylin and eosin (H&E) staining examination.

Moreover, five groups of mice (n = 5) were randomly divided and treated according to the above protocol for the survival study. According to animal ethical standards, the mice were euthanized when the tumor volume reached 2000 mm^3.

2.14 *In vivo* effects on inhibiting cell proliferation and inducing apoptosis

In the TUNEL staining process, paraffin-embedded sections were deparaffinized in water. Following proteinase K repair, the sections were permeabilized for 10 min at RT. After applying the reaction solution, the sections were incubated for 2 h at 37°C. Lastly, cell nuclei were stained with DAPI by incubating them in the dark at RT for 10 min. Tumor tissue sections were stained by anti-Ki67 mouse mAb (1:200 dilution), followed by an Alexa Fluor 488-labeled goat anti-rabbit IgG (H + L) secondary antibody (1:400 dilution) to assess the proliferation of tumor cells. The cell nuclei were stained with DAPI. The sections were then observed under a fluorescent microscope to capture images. DAPI emits blue light at with an 330–380 nm excitation and 420 nm emission; while TMR emits red light at 520–560 nm excitation and 570–620 nm emission. Alexa Fluor 488 emits green light at 488 nm excitation and 519 nm emission. The ImageJ software was employed to analyze the TUNEL and Ki67 signals in the captured images.

2.15 Characterization of the tumor immune microenvironment

The single-cell suspensions of spleens and tumors were prepared as described (Calcinotto et al., 2018; Lin et al., 2021). In brief, tumor tissues underwent mechanical disaggregation followed by enzymatic digestion using collagenase D and DNase for a 30-min incubation at 37°C to achieve a homogeneous single-cell suspension. Each group took three samples and prepared single-cell suspensions in 1.5 mL EP tubes, ensuring a cell count of 10^6/100 μL PBS per tube using a cell counter. Add 2 uL of Fc Receptor Blocking solution (biolegend, lot no. 422302) to each EP tube, mixed by vortexing, and then placed in the dark for 20 min. Subsequently, single-cell suspensions were labeled with specific monoclonal antibodies, which were primary antibodies directly conjugated. The antibodies used for labeling $CD4^+$/$CD8^+$ T cells included APC anti-mouse CD45 recombinant antibody (biolegend, clone QA17A26, lot no. 157605), PerCP-Cyanine 5.5 anti-mouse CD4 antibody (biolegend, clone GK1.5, lot no. 100539), and Alexa Fluor 488 anti-mouse CD8a antibody (biolegend, clone 53–6.7, lot no. 100726). The antibodies for labeling MDSCs included FITC anti-mouse CD45 antibody (biolegend, clone I3/2.3, lot no. 147709), APC anti-Ly-6G/Ly-6C (Gr-1) antibody (biolegend, clone RB6-8C5, lot no. 108411), and PE anti-mouse/human CD11b antibody (biolegend, clone M1/70, lot no. 101207). The specific steps were processed in accordance with the manufacturer's instructions. Then, the samples were incubated in the dark at 4°C for 20 min, centrifuged at 1,000 r/min for 3 min, and the cells were washed with PBS and resuspended in 500 μL PBS. Stained cells were finally evaluated by FACS Calibur flow cytometer (BD Biosciences, United States) and analyzed using FlowJo software.

2.16 MicroCT imaging and bone loss analysis

The right hind limb tibia was collected with the normal left hind limb serving as the control (n = 3). Bone images were obtained using microCT (μCT-100, SCANCO Medical AG, Switzerland) under 70 kV conditions. The Evaluation V6.5-3 software was utilized for the measurement and analysis of parameters, including bone surface area (BS), total tissue volume (TV), and bone volume (BV).

2.17 Statistical analysis

The statistical analysis was carried out with the software Graphpad Prism® 7. In cases where there were just two sample

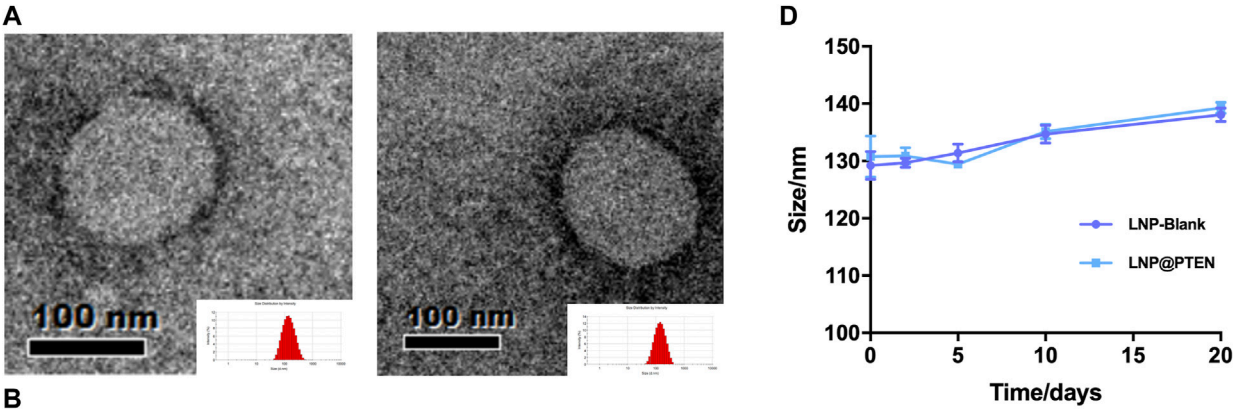

B

	Size/nm	PDI	Zeta/mV
LNP-Blank	129.5 ± 2.3	0.188 ± 0.013	29.7 ± 1.4
LNP@PTEN	131.8 ± 3.1	0.170 ± 0.015	-2.35 ± 0.75

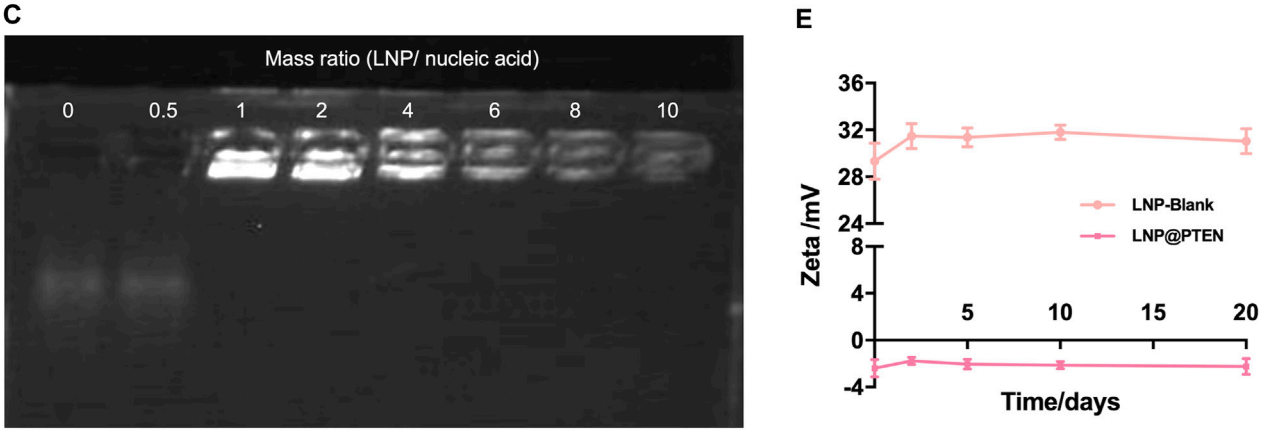

FIGURE 1
Characterization of LNPs. **(A)** TEM images of LNP-Blank and LNP@PTEN; scale bars = 100 nm. **(B)** The particles size distribution and ζ potential values of LNP-Blank and LNP@PTEN by DLS analysis. **(C)** The agarose gel electrophoresis results of different mass ratios of LNP@PTEN. **(D, E)** The stability of LNP-Blank and LNP@PTEN in PBS (pH 7.4) at 4°C for 20 d (n = 3, mean ± SD).

groups, the two-tailed Student's t-test was utilized. The mean ± SD is used to present the results. When comparing two groups, the Student's t-test was used; when comparing several groups, one-way analysis of variances (ANOVA) was used. Statistical differences were significant at $^{*}p < 0.05$ and very significant at $^{**}p < 0.01$, $^{***}p < 0.001$.

3 Results

3.1 Synthesis and characterization of LNPs

The cationic lipid 246C10, a crucial component of LNPs, was successfully synthesized through the Michael addition reaction, achieving effective gene therapeutic delivery via electrostatic interactions with negatively charged nucleic acids. Detailed synthesis process and characterization of 246C10 are available in the supporting information (Supplementary Figures S1–S3). The formulation of LNPs was composed of 246C10, DSPC, β-sitosterol, and PEG_{2K}-DMG. Both LNP-Blank and LNP@PTEN were prepared for characterization. Transmission electron microscopy (TEM) revealed that both LNP-Blank and LNP@PTEN were nanoscale spherical particles with an approximate diameter of 130 nm (Figure 1A, Supplementary Figure S4). The dynamic light scattering (DLS) analysis indicated that the z-average diameter of LNP-Blank was 129.55 ± 2.35 nm, with a polydispersity index (PDI) of 0.188 ± 0.013 (Figure 1B). After co-incubation with the PTEN DNA, the z-average diameter of

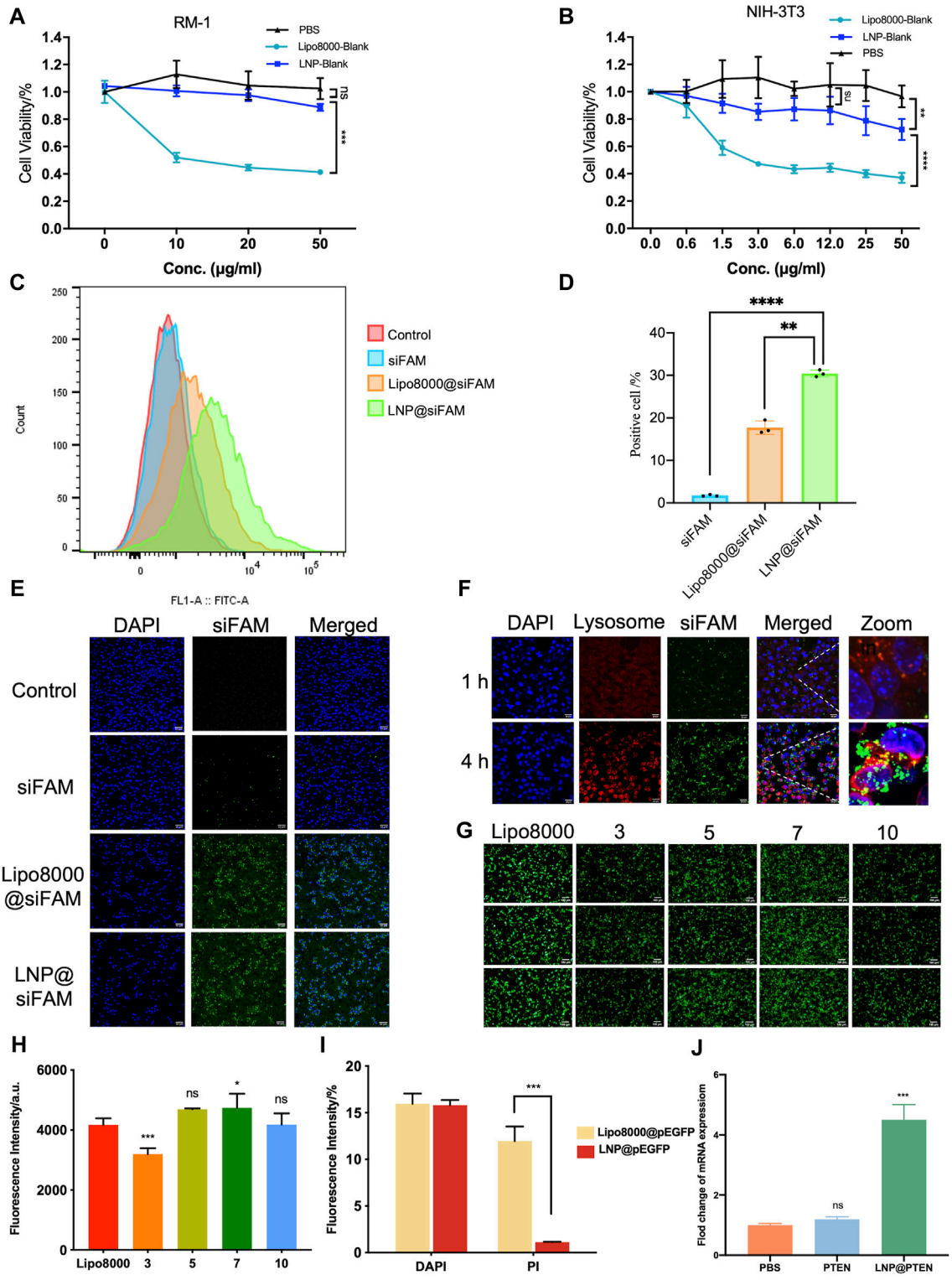

FIGURE 2
Evaluations of LNPs *in vitro*. **(A, B)** Cytotoxicity of LNPs at different concentrations on RM-1 cells and NIH-3T3 cells for 24 h (n = 6, mean ± SD), 2way ANOVA, *p < 0.05, **p < 0.01, ***p < 0.001, ns: no significance. **(C, D)** Statistic results of flow cytometry, RM-1 cells were co-incubated with siFAM, Lipo8000@siFAM, and LNP@siFAM (n = 3, mean ± SD), **p < 0.01, ***p < 0.001, one-way ANOVA. **(E, F)** Investigation of intracellular transfection ability in LNPs. CLSM images of **(E, F)** lysosome escape of LNP@siFAM in RM-1 cells for 1 and 4 h scale bars = 20 μm. **(G)** Transfection assessments of LNP@pEGFP complexes on RM-1 cells (n = 3). scale bars = 50 μm. **(H)** Fluorescence intensity at different mass ratios in RM-1 cells for 24 h, Lipo8000 was used as control (n = 5, mean ± SD), *p < 0.05, **p < 0.01, ***p < 0.001, ns: no significance, one-way ANOVA. **(I)** The fluorescence intensity of DAPI and PI for 24 h after treatment of LNP@pEGFP and Lipo8000@pEGFP (n = 3, mean ± SD), ***p < 0.001, ns: no significance, t-test. **(J)** RT-qPCR results of the expression of PTEN in RM-1 cells (n = 3, mean ± SD), ***p < 0.001, ns: no significance, one-way ANOVA.

LNP@PTEN was 131.8 ± 3.1 nm, with a PDI of 0.170 ± 0.015 (Figure 1B). The particle size of the LNPs changed minimally, consistent with that of TEM results. Furthermore, LNP-Blank exhibited positive surface charges, which transitioned to neutral surface charges upon the formation of LNP@PTEN. The ζ-potential values were recorded as (29.7 ± 1.4) mV and (−2.35 ± 0.75) mV, respectively (Figure 1B). When they were incubated in the mimicked physiological fluids of phosphate buffered saline (PBS, pH 7.4) for 20 d, the average diameters and ζ-potential of LNP-Blank and LNP-PTEN were rarely changed (Figures 1D, E). These results confirmed the stability of LNP-Blank and LNP@PTEN in simulated physiological fluids.

Given the enzymatic activity prevalent in the bloodstream, nucleic acids are susceptible to enzymatic degradation, leading to their inactivation. To ensure the effectiveness of gene therapy, LNPs play a pivotal role by encapsulating PTEN DNA, thereby shielding them from enzymatic degradation. We evaluated the encapsulation of PTEN DNA within LNPs using agarose gel electrophoresis (Figure 1C). These findings indicated that when the mass ratio >6, PTEN DNA could be entirely absorbed into the LNPs.

3.2 LNPs enhanced cellular uptake and transfection effeciency with lower toxicity *in vitro*

The cytotoxicity of LNP-Blank on RM-1 and NIH-3T3 cells for 24 h was investigated using Lipo8000-Blank as a control (Figures 2A, B). Our findings indicated that LNP-Blank has lower cytotoxicity than Lipo8000-Blank on NIH-3T3 cells ($p < 0.001$), with a safety concentration up to 12.5 μg/mL (vs. NC group, $p < 0.05$). Similarly, LNP-Blank showed much lower cytotoxicity on RM-1 cells as compared to Lipo8000-Blank ($p < 0.001$), maintains cell viability at approximately 80% at a concentration of 50 μg/mL. These results demonstrated that LNP-Blank had less acute and cell-intrinsic toxicity than Lipo8000-Blank *in vitro*.

Moreover, we investigated the cellular uptake of LNPs in RM-1 cells with siFAM serving as the model drug. Flow cytometry quantification results showed that the cellular uptake of siFAM loaded LNPs (LNP@siFAM) was 1.84 times higher than that of the Lipo8000@siFAM group (Figures 2C, D). The CLSM results showed that green fluorescence (siFAM) was mainly distributed around the cell nucleus (DAPI blue staining). Notably, RM-1 cells exhibited pronounced green fluorescence in LNP@siFAM group, compare to those in free siFAM group (Figure 2E), which was similar to that in the Lipo8000@siFAM group. These results indicated that the LNPs could be effectively internalized by cells, and accurately delivered gene drugs to tumor cells, thus establishing a robust foundation for subsequent drug delivery therapies.

In order to investigate the intracellular transport of LNPs, the lysosomes of RM-1 cells were labeled with LysoTracker Red. After 1 h of incubation, CLSM images illustrated that the red lysosome fluorescence and the green fluorescence (siFAM) overlapped. After 4 h, the green and red fluorescence became clearly separated, indicating that the LNPs had the remarkable lysosomal escape capacity (Figure 2F). Compared with Lipo8000@siFAM (Supplementary Figure S5), both LNPs and Lipo8000 had lysosome escape effect. Consequently, these findings indicated that LNPs can effectively traverse the lysosomal barrier and enhance targeted drug delivery efficiency by efficiently delivering encapsulated drugs to the cytoplasm.

Moreover, we assessed the efficiency of gene transfection in HEK-293T cells *in vitro*. The results demonstrated that a notably higher transfection efficiency was achieved at a mass ratio of 7, surpassing that of Lipo8000 ($p < 0.05$), which indicated that the LNPs had good gene transfection ability and provided the best mass ratio of drug for subsequent assays (Figures 2G, H). In addition, we investigated cell viability post-transfection with LNP@pEGFP and Lipo8000@pEGFP in RM-1 cells with the most optimal transfection efficiency (Figure 2I). PI and DAPI staining were performed on the dead cells and cell nuclei of the two groups, respectively, to assess the proportion of cell death. The findings revealed that the LNP@pEGFP group exhibited superior transfection efficiency compared to that of the Lipo8000@pEGFP group, along with a lower cell death rate ($p < 0.001$), thus underscoring the less acute and cell-intrinsic toxicity of this LNPs *in vitro*.

We further evaluated the impact of LNP@PTEN on PTEN-mRNA levels in RM-1 cells using RT-qPCR (Figure 2J). The results clearly indicated that PTEN-mRNA levels in the LNP@PTEN group were significantly higher than those in both the PBS group and the free PTEN group ($p < 0.001$), affirming the successful delivery of PTEN by LNP@PTEN into tumor cells. These experiments collectively verified the nucleic acid delivery and transfection capabilities of the LNPs *in vitro*.

3.3 LNP@PTEN suppressed cell growth, cell invasion and metastasis *in vitro*

Figure 3A showed the results of *in vitro* cytotoxicity of different groups. As shown in Figure 3A, the LNP@PTEN (IC_{50} = 0.4827 μg/mL) group as well as the IL-23 inhibitor Apilimod + LNP@PTEN group (Apilimod/PTEN: IC_{50} = 8.32 nM/0.416 μg/mL) exhibited dose-dependent cytotoxic effects on the RM-1 cells. There was no significant difference between these two groups ($p < 0.05$). Moreover, the Apilimod group showed no significantly higher cytotoxicity than the negative control (NC) group ($p < 0.05$) (Supplementary Figure S6). Our results indicated that there was no obviously exhibition effect of Apilimod on the RM-1 cells *in vitro*. This may due to that the IL-23 was primarily released by MDSCs (Calcinotto A et al., 2018); and the effect of Apilimod might be shown in CRPC microenvironment.

Next, the anti-invasive and anti-metastatic potential of Apilimod + LNP@PTEN was further evaluated by Transwell assay. Microscopic examination of cell migration was conducted. The effects of the combined treatment were subsequently confirmed through quantification of anti-migration and anti-invasion cells (Figures 3B–D). Given the instability of nucleic acids, the cell numbers in the free PTEN DNA group closely resembled those in the PBS group, signifying the absence of any anti-invasive or anti-metastatic influence. In contrast, the LNP@PTEN group and the Apilimod group showed noticeable abilities to inhibit invasion and metastasis in comparison to the PBS

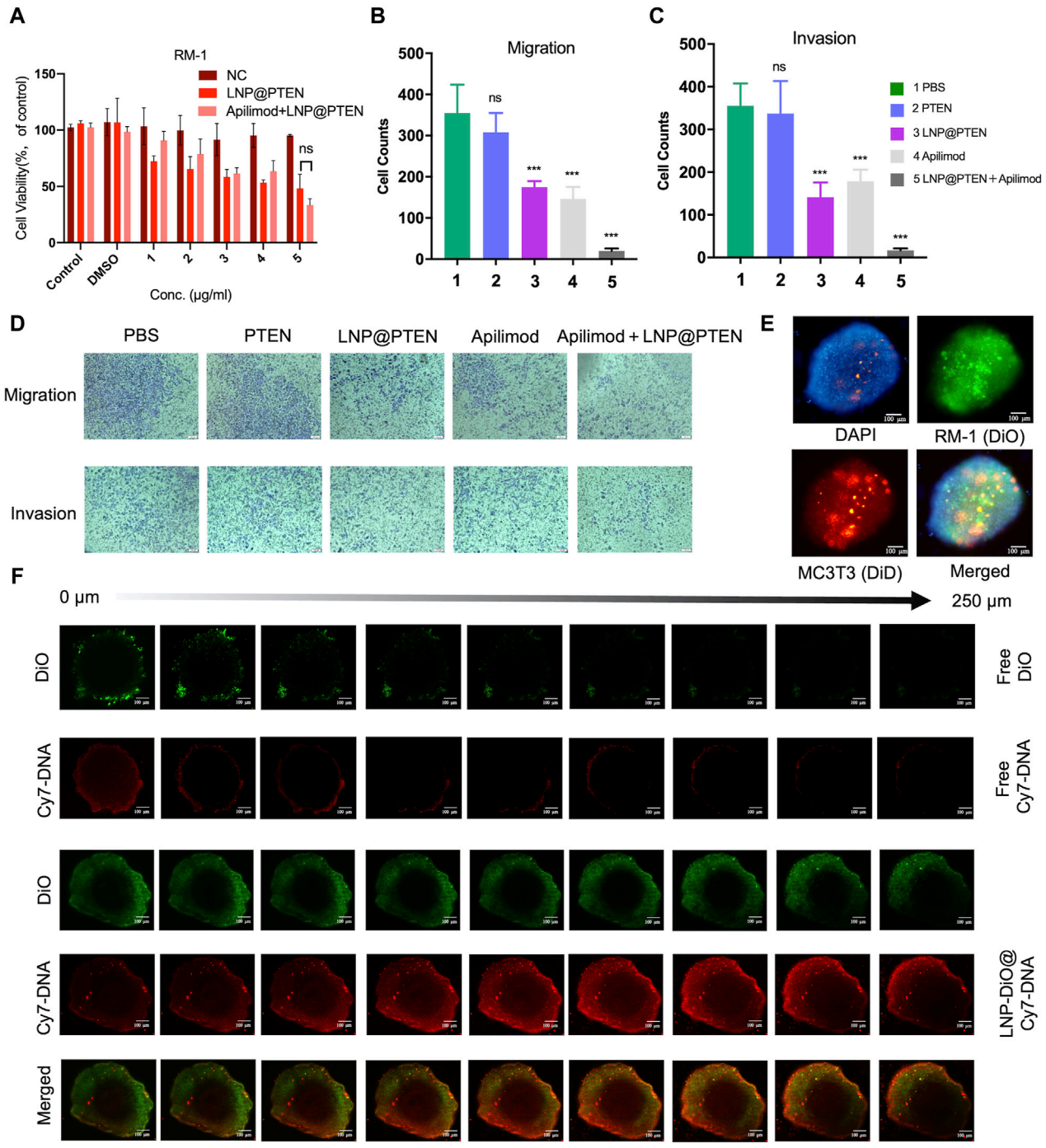

FIGURE 3
Antitumor assays *in vitro*. **(A)** Cell viability of RM-1 cells after treatment with LNP@PTEN and Apilimod + LNP@PTEN for 24 h (n = 3, means ± SD). ns: no significance, 2way ANOVA. **(B, C)** The statistical analysis of cells in nine fields of view of **(B)** anti-migration effects and **(C)** anti-invasion effects, respectively (n = 9, mean ± SD), *p < 0.05, **p < 0.01, ***p < 0.001, ns: no significance, one-way ANOVA. **(D)** Microscope images of anti-migration effects and anti-invasion effects in each group (Apilimod: 10 nM, PTEN: 0.5 μg/mL), scale bars = 50 μm. **(E)** 3D tumor spheroid model. DiO-stained RM-1 cells and DiD-stained MC3T3-E1 cells. Blue fluorescence: DAPI, green fluorescence: DiO, red fluorescence: DiD, Scale bars = 100 μm. **(F)** The images of *in vitro* tumor spheroids penetration of each group were acquired by CLSM. DiO-stained LNPs (DiO: 20 μg/mL, Cy7-DNA: 0.5 μg/mL). Scale bars = 100 μm.

group. Furthermore, the combination of LNP@PTEN with the IL-23 inhibitor Apilimod displayed a more pronounced anti-invasive and anti-metastatic ability compared to the monotherapy groups (p < 0.001). These results suggested an enhanced effect of the combined treatment in curtailing the invasion and metastasis of RM-1 cells.

3.4 LNPs improved penetration in a 3D tumor model

In order to more accurately simulate the *in vitro* bone metastatic microenvironment, we established a 3D tumor spheroid model using MC3T3-E1 and RM-1 cells (Figure 3E).

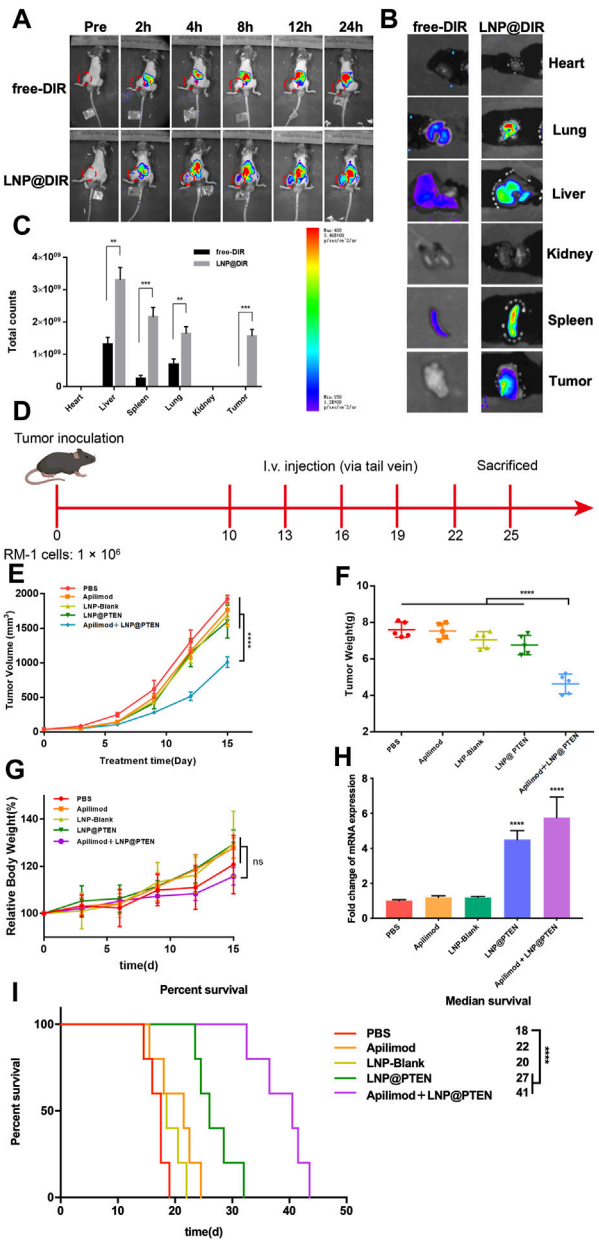

FIGURE 4
In vivo study of LNPs. **(A)** Representative images of BmCRPC-bearing mice from each group were taken at 0–24 h after injection, with the tumor area marked by a red circle. **(B)** Fluorescence imaging of tumors and major organs. **(C)** The semiquantitative fluorescence intensity in major organs of each group (n = 3, mean ± SD), *p < 0.05, **p < 0.01, ***p < 0.001, multiple t-test. **(D)** The *in vivo* study protocol of Apilimod + LNP@PTEN (PTEN DNA: 700 μg/kg, Apilimod: 10 mg/kg). **(E)** The five groups' tumor volume curves (n = 5, mean ± SD). **(F)** The five groups' weight curves (n = 5, mean ± SD). **(G)** Mice growth curves for body weight among the five groups (n = 5, mean ± SD). **(H)** RT-qPCR results of the expression of PTEN in different treatment groups (n = 3, mean ± SD), ***p < 0.001, ****p < 0.0001, one-way ANOVA. **(I)** Survival curve of mice in different treatment groups (n = 5, mean ± SD). ****p < 0.0001, ns: no significance, one-way ANOVA.

To assess whether LNPs can enhance drug penetration within these spheroids, we loaded Cy7-DNA (red) into LNPs to mimic PTEN DNA, and LNPs labeled with DiO (LNP@DiO, green). Various formulations were applied to treat the 3D tumor spheroids, and the penetration process was visualized using CLSM. Free DiO and free Cy7-DNA were predominantly localized around the spheroids. Importantly, DiO and Cy7-DNA in the LNP-DiO@Cy7-DNA group penetrated the spheroids deeply with the fluorescence intensity much higher than those in the free group at a depth of 250 μm (Figure 3F, Supplementary Figure S7), indicating the superior tumor penetration capability of LNPs.

3.5 LNPs efficiently targeted tumor sites

Metastasis is a fatal factor in CRPC progression, and once cancer spreads to the bone, it gives rise to skeletal-related events (SREs), leading to reduced treatment efficacy (Weilbaecher and McCauley, 2011; Steega, 2016). Therefore, we established a mouse model of mCRPC and LNP was labeled with a near-infrared dye (DIR) to investigate the *in vivo* biodistribution of LNPs.

The *in vivo* biodistribution study results were shown in Figure 4A. As shown in Figure 4A, the fluorescence signal could be monitored at the tumor site in the LNP@DIR group at 2 h early, followed by a gradual increase in the fluorescence signal over the next 16 h, with a peak signal intensity obtained at 24 h in the bone metastasis model. Furthermore, within 24 h, minimal fluorescence was observed at the tumor site in the free DIR group, while substantial DIR accumulated in the liver. The mice were sacrificed after being observed for 24 h in order to measure the biodistribution of fluorescence in different organs. Notably, compared to the free group, the LNP@DIR group exhibited significantly higher fluorescence intensity at the site of the bone metastatic tumor (p < 0.001), whereas the fluorescence signal was nearly not detectable in the free DIR group at the primary tumor site (Figures 4B, C). These results substantiated that DIR could be efficiently transported *in vivo*, accumulating at tumor sites via LNPs and achieving targeted delivery to the tumor site through the enhanced permeability and retention (EPR) effect.

3.6 LNP@PTEN cooperated with IL-23 inhibitor to inhibit tumor growth and metastasis *in vivo*

We further used BmCRPC models to study the therapeutic effects of combination therapy *in vivo* (Figure 4D). The results showed that the combination of Apilimod + LNP@PTEN group had the strongest antitumor effect among all the groups (Figure 4E). Post-treatment, tumors were subjected to weight measurement (Figure 4F), revealing a significantly reduced tumor weight in the Apilimod + LNP@PTEN group compared to the other treatment groups (p < 0.001). This outcome concurred with the tumor volume measurements taken during the course of tumor growth. Furthermore, no substantial variation in mice weight was observed between the Apilimod + LNP@PTEN group and the other treatment groups (p > 0.05) (Figure 4G). Remarkably,

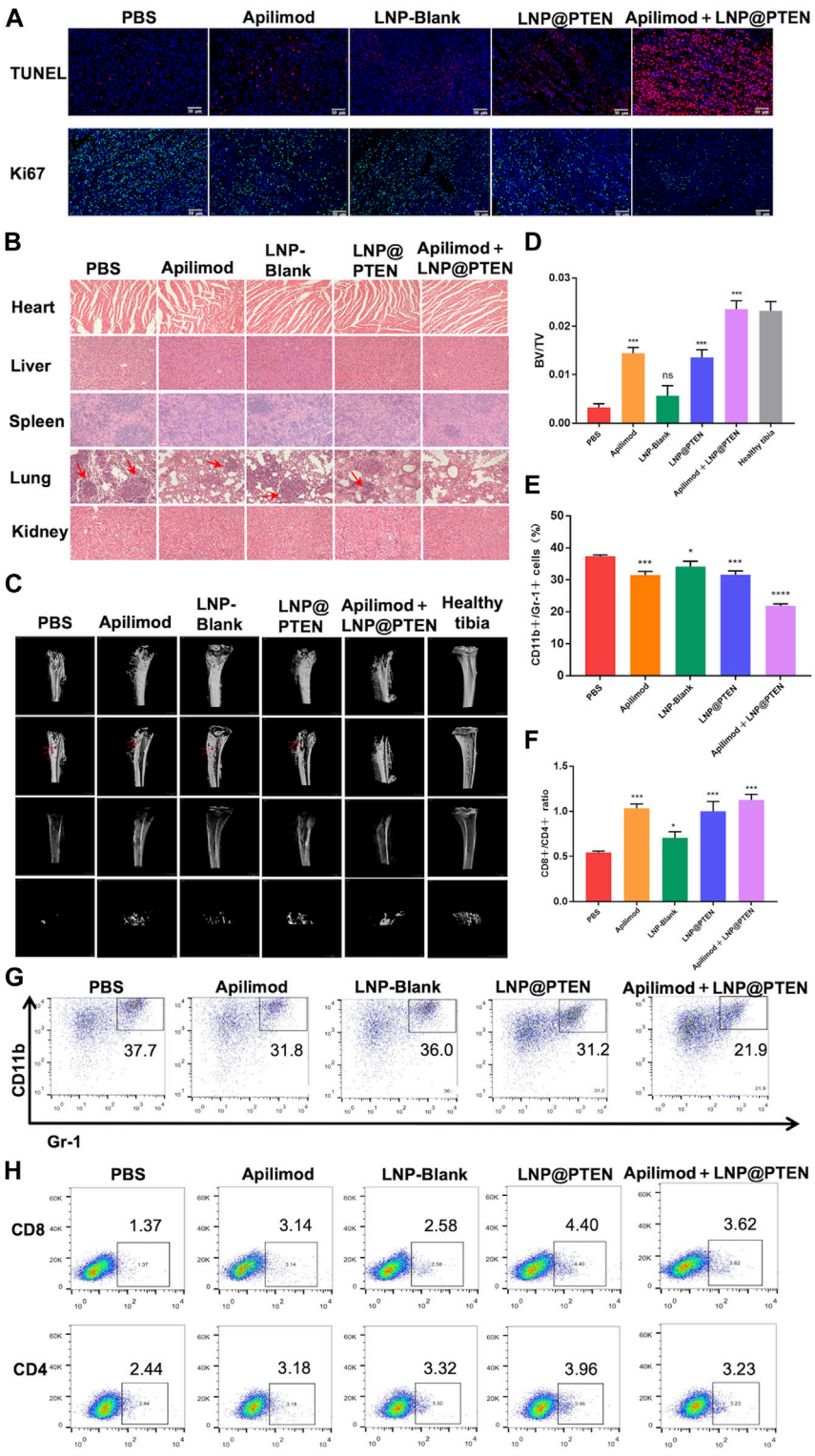

FIGURE 5
The safety and mechanism of LNPs and immune regulation mechanism. **(A)** TUNEL staining (red) and Ki67 staining (green) of tumor tissues in each group. Scale bars = 50 μm. **(B)** The 200 × HE images of the heart, liver, spleen, lung, kidney of each group (red arrow: Lung metastasis). **(C)** MicroCT images of tibia bearing tumor in each administration group, tibia of normal left hind limb as control (red arrow: Bone erosion and bone damage). **(D)** Tibia BV/TV detection results at different treatment group (n = 3, mean ± SD). **(E)** and **(G)** The proportional representative images and statistical images of MDSCs in tumor from various treatment groups (n = 3, mean ± SD). **(F, H)** Representative and statistical images of $CD8^+$ T cells and $CD4^+$ T cells mouse tumor from different treatment groups (n = 3, mean ± SD). *p < 0.05, **p < 0.01, ***p < 0.001, ****p < 0.0001, one-way ANOVA.

during the treatment period, mice treated with the five groups displayed analogous and steady weight growth. Moreover, mice treated with Apilimod + LNP@PTEN exhibited a longer median survival time, reaching 40 d in the BmCRPC mouse model (Figure 4I). The q-PCR results showed a significant increase in PTEN mRNA in both the LNP@PTEN group and the combined therapy group (Figure 4H), which indicated that PTEN restoration might contribute to the therapeutic efficacy.

TUNEL staining was used to detect tumor cell apoptosis. The Apilimod + LNP@PTEN group displayed an elevated number of red fluorescent cells in comparison to the Apilimod and LNP@PTEN groups, signifying a significant induction of cell apoptosis. Notably, no TUNEL-positive cells were observed in the other groups (Figure 5A). Tumor sections were subjected to Ki67 staining, revealing that the Apilimod + LNP@PTEN group exhibited a markedly diminished green fluorescent signal compared to the other groups. These showed the lowest proliferation level of Ki67-positive tumor cells in the combination treatment group, which was consistent with the trends observed in the TUNEL staining (Figure 5A). Collectively, these results provided further compelling evidence of the inhibitory effect of combination therapy on tumor growth.

Additionally, there was no discernible histological damage in all groups when major organs such as the heart, liver, spleen, lung, and kidney were stained with H&E, suggesting that this therapy demonstrated strong tissue tolerance and biocompatibility. (Figure 5B). In line with the previously mentioned findings, the biochemical indicators from mouse blood samples, including serum aspartate aminotransferase (AST), alanine aminotransferase (ALT), blood urea nitrogen (BUN), and creatinine (CR), were demonstrated to be all within the normal range in BmCRPC models after treatment with PBS, Apilimod, LNP-Blank, LNP@PTEN, and Apilimod + LNP@PTEN groups (Supplementary Table S2). These data collectively substantiate the safety profile of the Apilimod + LNP@PTEN combination therapy system. Notably, it is essential to highlight that while tumor metastatic lesions were apparent within the lungs of mice from the PBS group, Apilimod group, LNP-Blank group, and LNP@PTEN group in the bone metastasis model, no secondary organ metastases were discernible in the Apilimod + LNP@PTEN group (Figure 5B).

Subsequently, to assess the potential of Apilimod + LNP@PTEN in SREs associated with BmCRPC, we conducted a comprehensive bone analysis employing microCT (Figure 5C). As a baseline, the left hind limb's normal tibia in mice served as the control group. In the tumor-bearing tibia of mice from the PBS, Apilimod, LNP-Blank, and LNP@PTEN groups, varying degrees of bone damage and bone resorption were observed, while in the Apilimod + LNP@PTEN group, there was a remarkable mitigation of these effects. Moreover, the bone volume fraction (BV/TV) serves as a widely-used parameter for evaluating cortical and trabecular bone mass. An increase in BV/TV suggests that bone synthesis metabolism surpasses degradation metabolism, leading to an augmented bone mass. This parameter indirectly reflects bone metabolism. Compared to the other treatment groups, the BV/TV ratio in the Apilimod + LNP@PTEN group most closely resembled that of a healthy tibia (Figure 5D). These showed the protective effect of combination therapy on bone metabolism, leading to a reduction in bone damage. These findings substantiated that Apilimod + LNP@PTEN treatment had a significant bone-protective effect. It effectively impeded the growth of BmCRPC tumors, alleviated bone damage and loss in the tumor-bearing tibia, improved SRE outcomes in BmCRPC mice, and proficiently suppressed secondary organ metastasis of BmCRPC.

3.7 LNP@PTEN cooperated with IL-23 inhibitor to improve immunosuppressive microenvironment

Bone marrow cell differentiation and functional anomalies represent critical hallmarks of cancer (Croucher et al., 2016). MDSCs, which originate in the bone marrow, play a role in immune suppression and impact T cell activation during the course of cancer development (Kumar et al., 2016). To corroborate the potential of combination therapy in enhancing the tumor immune microenvironment, we employed flow cytometry for the detection of MDSCs ($CD11b^+$ $Gr\text{-}1^+$) infiltration within tumor tissues after 2 weeks treatment (Figures 5E, G, Supplementary Figure S8). The findings revealed that the Apilimod + LNP@PTEN group exhibited the lowest proportion of MDSCs, with a marked reduction compared to the PBS group ($p < 0.001$).

Furthermore, $CD4^+$ T cells fulfill a regulatory role in immune responses, while $CD8^+$ T cells serve as vital effector cells in the context of anti-tumor responses, and an elevated $CD8^+$ ratio is indicative of a more potent anti-tumor effect (Shi et al., 1995). The outcomes demonstrated that the Apilimod + LNP@PTEN group attained the highest $CD8^+/CD4^+$ ratio (Figures 5F, H, Supplementary Figure S9), implying a more robust anti-tumor immune response relative to the other treatment groups. This heightened immune response played as a pivotal contributor to the effective inhibition of CRPC development in the combination therapy group.

4 Discussion

The loss of the tumor suppressor PTEN is a common occurrence in CRPC. Up to 40% of patients with mCRPC face the challenge of PTEN deficiency. In addition, PTEN insufficiency can also promote immune suppression by escalating the population of MDSCs and the secretion of the immune-inhibitory cytokines IL-23 (Calcinotto et al., 2018). Therefore, restoration of PTEN function as well as inhibiting IL-23 to reverse MDSC-mediated resistance to CRPC may bring potential therapies for mCRPC treatment.

Promising therapeutic strategies have been developed to restore PTEN function alone or combine with PI3K-AKT-mTOR inhibition, chemotherapy, androgen receptor-directed agents, DNA damage response (DDR) -targeting agents, immune oncology agents, or additional PI3K-AKT-mTOR-targeted therapies (Turnham et al., 2020). Among these approaches, gene therapy is most effective in restoring PTEN function. However, these strategies face challenges such as low delivery efficiency, poor transfection efficiency, insufficient expression, and the potential

for insertional mutations (Islam et al., 2018). Therefore, novel gene vectors with high efficiency and low toxicity still need to be further explored.

Here, in our study, we successfully developed an ionizable cationic lipid 246C10 that could self-assemble into LNPs with β-sitosterol, phospholipids, and PEG-lipids for PTEN DNA delivery. The characterization results indicated that LNP-Blank possesses a positive charge of 29.7 mV and maintains a particle size of approximately 130 nm. Following the loading of PTEN DNA, the particle size increased slightly, and the charge became neutral (Figures 1A, B). The *in vitro* and *in vivo* results demonstrated the high transfection efficiency of LNPs and low toxicity of the LNP-Blank (Figures 2A, B, and Supplementary Table S2), which are suitable as carriers for PTEN DNA delivery.

Previous study reported that elevated levels of MDSCs and IL-23 were found in the blood and tumor samples of CRPC mice and patients, compared to those in hormone-sensitive PCa patients (Calcinotto et al., 2018). Our results showed that IL-23 inhibitor Apilimod alone had no obvious effect on RM-1 cells *in vitro* (Supplementary Figure S6; Figure 3A) and *in vivo* (Figure 4E), while significantly improved the anticancer effect of LNP@PTEN *in vivo* ($p < 0.001$) (Figure 4E). This demonstrated that the IL-23 was mainly released by MDSCs, which was in line with the result reported (Calcinotto et al., 2018). Moreover, the combination of LNP@PTEN with IL-23 inhibitor Apilimod showed a significantly anticancer effect (Figure 4E). All these results indicated that for PTEN-deficient CRPC patients, only restoration of PTEN function may be not enough to inhibit the CRPC progression, and the combination therapies with other strategies are needed. Furthermore, the MDSCs in tumor microenvironment play a critical role for CRPC progress, and blocking MDSCs recruiting is one of the choices for combinational therapies. Therefore, the combination of LNP@PTEN and Apilimod may provide a potential strategy for CRPC clinical treatment, especially for PTEN-deficient CRPC patients.

Since 90% of patients with CRPC will eventually develop metastasis to bone. Once cancer spreads to the bone, it gives rise to SREs, such as severe pain and abnormal bone remodeling, leading to poor prognosis and reduced treatment efficacy (Weilbaecher and McCauley, 2011; Steega, 2016). We established a CRPC bone metastasis animal model and conducted an intra-tumoral distribution study using LNPs in these model mice. The *in vivo* distribution experiments indicated the successful accumulation of LNPs (LNP@DIR) in the tumor sites of tumor-bearing mice, which may be associated with the nanoparticle's EPR effect (Figures 4A–C). Moreover, our research demonstrated the highest effectiveness of the Apilimod + LNP@PTEN among all groups, showing superior anti-tumor growth, anti-invasive and anti-metastatic properties as compared to those of monotherapy *in vivo* (Figures 4E–I). In addition, we also found that the combination therapy of LNP@PTEN and Apilimod also significantly inhibited bone metastasis CRPC distant organ secondary metastasis with excellent safety (Figures 4G, 5B; Supplementary Table S2).

Furthermore, we investigated the immunomodulatory effects of the combination therapy by assessing immune cells in tumor tissues, thereby alleviating immune suppression, enhancing the immune response, and inhibiting tumor progression to some extent (Figures 5E–H). The PTEN/PI3K/AKT pathway had been shown to be a crucial route for MDSCs activation, and MDSCs indirectly promote the development of CRPC through the secretion of IL-23. LNP@PTEN compensated for PTEN deficiency, blocking the activation of this pathway in MDSCs, thereby reducing the proportion of immunosuppressive cells. Additionally, the reduction in MDSC activation and interference with IL-23's regulatory role in tumor development, due to the application of the IL-23 inhibitor, relieved immune suppression from two different aspects. This is probably a key reason for the inhibition of tumor growth in the Apilimod + LNP@PTEN group. Finally, we also investigated the bone-protective effects of the treatment. The combined intervention of LNP@PTEN + Apilimod could maximize the preservation of normal bone metabolism, reducing bone injury and resorption (Figures 5C, D).

5 Conclusion

In summary, a combinational therapeutic strategy based on LNP@PTEN and the IL-23 inhibitor Apilimod was established, which could significantly inhibit tumor growth and metastasis for CRPC. The prepared LNPs exhibit excellent stability and high transfection efficiency, allowing for efficient drug delivery to tumor sites. Furthermore, the combination of LNP@PTEN and Apilimod inhibited tumor progression, distant organ secondary metastases, and extended the survival period of tumor-bearing mice, by the restoration of PTEN function and reversing the immunosuppressive tumor environment. This work provides a new strategy for CRPC treatment.

Data availability statement

The original contributions presented in the study are included in the article/supplementary material, further inquiries can be directed to the corresponding authors.

Ethics statement

The animal study was approved by the Committee on Ethics of Medicine, Naval Medical University, PLA. The study was conducted in accordance with the local legislation and institutional requirements.

Author contributions

XC: Conceptualization, Writing–original draft, Methodology, Software, Validation, Visualization. LG: Methodology, Writing–original draft, Formal Analysis. YW: Software, Validation, Writing–review and editing. CY: Software, Writing–review and editing. HG: Writing–review and editing, Formal Analysis. SG: Supervision, Writing–review and editing. JC: Writing–review and editing, Conceptualization, Supervision. ZW: Supervision, Writing–review and editing, Conceptualization. YG: Conceptualization, Supervision, Writing–review and editing, Funding acquisition, Project administration.

Funding

The author(s) declare that financial support was received for the research, authorship, and/or publication of this article. This work was supported by the National Natural Science Foundation of China (Nos. 81972392, 82272769, 82102902 and 82203168).

Conflict of interest

The authors declare that the research was conducted in the absence of any commercial or financial relationships that could be construed as a potential conflict of interest.

Publisher's note

All claims expressed in this article are solely those of the authors and do not necessarily represent those of their affiliated organizations, or those of the publisher, the editors and the reviewers. Any product that may be evaluated in this article, or claim that may be made by its manufacturer, is not guaranteed or endorsed by the publisher.

Supplementary material

The Supplementary Material for this article can be found online at: https://www.frontiersin.org/articles/10.3389/fphar.2024.1388613/full#supplementary-material

References

Bergholz Js, W. Q., Wang, Q., Ramseier, M., Prakadan, S., Wang, W., Fang, R., et al. (2023). PI3Kβ controls immune evasion in PTEN-deficient breast tumours. *Nature* 617 (7959), 139–146. doi:10.1038/s41586-023-05940-w

Bezzi, M., Seitzer, N., Ishikawa, T., Reschke, M., Chen, M., Wang, G., et al. (2018). Diverse genetic-driven immune landscapes dictate tumor progression through distinct mechanisms. *Nat. Med.* 24 (2), 165–175. doi:10.1038/nm.4463

Calcinotto, A., Spataro, C., Zagato, E., Di Mitri, D., Gil, V., Crespo, M., et al. (2018). IL-23 secreted by myeloid cells drives castration-resistant prostate cancer. *Nature* 559 (7714), 363–369. doi:10.1038/s41586-018-0266-0

Calcinotto A, S. C., Zagato, E., Di Mitri, D., Gil, V., Crespo, M., De Bernardis, G., et al. (2018). IL-23 secreted by myeloid cells drives castration-resistant prostate cancer. *Nature* 559 (7714), 363–369. doi:10.1038/s41586-018-0266-0

Chen, J. W. Z., Ding, W., Xiao, C., Zhang, Y., Gao, S., Gao, Y., et al. (2020). SREBP1 siRNA enhance the docetaxel effect based on a bone-cancer dual-targeting biomimetic nanosystem against bone metastatic castration-resistant prostate cancer. *Theranostics* 10 (4), 1619–1632. doi:10.7150/thno.40489

Croucher, P. I., McDonald, M. M., and Martin, T. J. (2016). Bone metastasis: the importance of the neighbourhood. *Nat. Rev. Cancer.* 16 (6), 373–386. doi:10.1038/nrc.2016.44

Duvallet E, S. L., Assier, E., Falgarone, G., and Boissier, M. C. (2011). Interleukin-23: a key cytokine in inflammatory diseases. *Ann. Med.* 43 (7), 503–511. doi:10.3109/07853890.2011.577093

Garcia, J. A. R. B. I., and Rini, B. I. (2011). Castration-resistant prostate cancer: many treatments, many options, many challenges ahead. *Cancer* 118 (10), 2583–2593. doi:10.1002/cncr.26582

Halabi, S., Kelly, W. K., Ma, H., Zhou, H., Solomon, N. C., Fizazi, K., et al. (2016). Meta-analysis evaluating the impact of site of metastasis on overall survival in men with castration-resistant prostate cancer. *J. Clin. Oncol.* 34 (14), 1652–1659. doi:10.1200/JCO.2015.65.7270

Harris, M. E., Nelson, P. S., and Montgomery, B. (2009). Androgen deprivation therapy: progress in understanding mechanisms of resistance and optimizing androgen depletion. *Nat. Clin. Pract. Urol.* 6 (2), 76–85. doi:10.1038/ncpuro1296

Hoang, B. E. M., Tang, W. S., Bteich, J., Undzys, E., Kiyota, T., Li, S. D., et al. (2017). Cabazitaxel-conjugated nanoparticles for docetaxel-resistant and bone metastatic prostate cancer. *Cancer Lett.* 410, 169–179. doi:10.1016/j.canlet.2017.09.029

Islam, M. A., Xu, Y., Tao, W., Ubellacker, J. M., Lim, M., Aum, D., et al. (2018). Restoration of tumour-growth suppression *in vivo* via systemic nanoparticle-mediated delivery of PTEN mRNA. *Nat. Biomed. Eng.* 2 (11), 850–864. doi:10.1038/s41551-018-0284-0

Jamaspishvili, T., Berman, D. M., Ross, A. E., Scher, H. I., De Marzo, A. M., Squire, J. A., et al. (2018). Clinical implications of PTEN loss in prostate cancer. *Nat. Rev. Urol.* 15 (4), 222–234. doi:10.1038/nrurol.2018.9

Jiang, W. C. J., Gong, C., Wang, Y., Gao, Y., and Yuan, Y. (2020). Intravenous delivery of enzalutamide based on high drug loading multifunctional graphene oxide nanoparticles for castration-resistant prostate cancer therapy. *J. Nanobiotechnology* 18 (1), 50. doi:10.1186/s12951-020-00607-4

Kim, M., Hur, S., Cho, Y., Park, J., Jung, H., Seo, Y., et al. (2021). Engineered ionizable lipid nanoparticles for targeted delivery of RNA therapeutics into different types of cells in the liver. *Sci. Adv.* 7 (9), eabf4398. doi:10.1126/sciadv.abf4398

Kumar V, P. S., Tcyganov, E., and Gabrilovich, D. I. (2016). The nature of myeloid-derived suppressor cells in the tumor microenvironment. *Trends Immunol.* 37 (3), 208–220. doi:10.1016/j.it.2016.01.004

Lin, Y.-X., Wang, Y., Ding, J., Jiang, A., Wang, J., Yu, M., et al. (2021). Reactivation of the tumor suppressor PTEN by mRNA nanoparticles enhances antitumor immunity in preclinical models. *Sci. Transl. Med.* 13 (599), eaba9772. doi:10.1126/scitranslmed.aba9772

Mukherjee, R., Boyer, J. A., Gadal, S., Solomon, H., Chandarlapaty, S., Levchenko, A., et al. (2021). Regulation of PTEN translation by PI3K signaling maintains pathway homeostasis. *Mol. Cell* 81 (4), 708–723.e5. doi:10.1016/j.molcel.2021.01.033

Mulholland, D. J., Tran, L. M., Li, Y., Cai, H., Morim, A., Wang, S., et al. (2011). Cell autonomous role of PTEN in regulating castration-resistant prostate cancer growth. *Cancer Cell* 19 (6), 792–804. doi:10.1016/j.ccr.2011.05.006

Rizvi, N. A. C., and Chan, T. A. (2016). Immunotherapy and oncogenic pathways: the PTEN connection. *Cancer Discov.* 6 (2), 128–129. doi:10.1158/2159-8290.CD-15-1501

Shi, Y., Radvanyi, L. G., Sharma, A., Shaw, P., Green, D. R., Miller, R. G., et al. (1995). CD28-mediated signaling *in vivo* prevents activation-induced apoptosis in the thymus and alters peripheral lymphocyte homeostasis. *J. Immunol.* 155 (4), 1829–1837. doi:10.4049/jimmunol.155.4.1829

Siegel, R. L., Miller, K. D., Wagle, N. S., and Jemal, A. (2023). Cancer statistics, 2023. *CA A Cancer J. Clin.* 73 (1), 17–48. doi:10.3322/caac.21763

Steega, S. (2016). Targeting metastasis. *Nat. Rev. Cancer* 16 (4), 201–218. doi:10.1038/nrc.2016.25

Sung, H., Siegel, R. L., Laversanne, M., Soerjomataram, I., Jemal, A., Bray, F., et al. (2021). Global cancer statistics 2020: GLOBOCAN estimates of incidence and mortality worldwide for 36 cancers in 185 countries. *CA Cancer J. Clin.* 71 (3), 209–249. doi:10.3322/caac.21660

Taylor, B. S., Schultz, N., Hieronymus, H., Gopalan, A., Xiao, Y., Carver, B. S., et al. (2010). Integrative genomic profiling of human prostate cancer. *Cancer Cell* 18 (1), 11–22. doi:10.1016/j.ccr.2010.05.026

Turnham, D. J., Bullock, N., Dass, M. S., Staffurth, J. N., and Pearson, H. B. (2020). The PTEN conundrum: how to target PTEN-deficient prostate cancer. *Cells* 9 (11), 2342. doi:10.3390/cells9112342

Wada, Y., Cardinale, I., Khatcherian, A., Chu, J., Kantor, A. B., Gottlieb, A. B., et al. (2012). Apilimod inhibits the production of IL-12 and IL-23 and reduces dendritic cell infiltration in psoriasis. *PLoS One* 7 (4), e35069. doi:10.1371/journal.pone.0035069

Wada, Y., Lu, R., Zhou, D., Chu, J., Przewloka, T., Zhang, S., et al. (2006). Selective abrogation of Th1 response by STA-5326, a potent IL-12/IL-23 inhibitor. *Blood* 109 (3), 1156–1164. doi:10.1182/blood-2006-04-019398

Weilbaecher Kn, G. T., and McCauley, L. K. (2011). Cancer to bone: a fatal attraction. *Nat. Rev. Cancer* 11 (6), 411–425. doi:10.1038/nrc3055

Yin, H. K. K., and Anderson, D. G. (2017). Delivery technologies for genome editing. *Nat. Rev. Drug Discov.* 16 (6), 387–399. doi:10.1038/nrd.2016.280

Zhang, Y. S. C., Wang, C., Jankovic, K. E., and Dong, Y. (2021). Lipids and lipid derivatives for RNA delivery. *Chem. Rev.* 121 (20), 12181–12277. doi:10.1021/acs.chemrev.1c00244

frontiers | Frontiers in Pharmacology

TYPE Original Research
PUBLISHED 19 July 2024
DOI 10.3389/fphar.2024.1427318

OPEN ACCESS

EDITED BY
Lei Yin,
Shanghai Jiaotong University School of Medicine, China

REVIEWED BY
Hengping Li,
Gansu Provincial Hospital, China
Leli Zeng,
Sun Yat-sen University, China

*CORRESPONDENCE
Guangzhi Li,
guangzhili@email.szu.edu.cn
Song Wu,
songwu_lzu@126.com

†These authors have contributed equally to this work

RECEIVED 03 May 2024
ACCEPTED 02 July 2024
PUBLISHED 19 July 2024

CITATION
Li R, Huang G, Li Y, Huang M, Huang Y, Li Y, Li G and Wu S (2024), Assessing the role of statin therapy in bladder cancer: evidence from a Mendelian Randomization study.
Front. Pharmacol. 15:1427318.
doi: 10.3389/fphar.2024.1427318

Assessing the role of statin therapy in bladder cancer: evidence from a Mendelian Randomization study

Rongkang Li[1,2,3†], Guixiao Huang[2†], Yunfei Li[2], Mou Huang[2], Ying Huang[2], Yingrui Li[2], Guangzhi Li[2]* and Song Wu[1,3]*

[1]Institute of Urology, Lanzhou University Second Hospital, Lanzhou University, Lanzhou, China, [2]Institute of Urology, The Affiliated Luohu Hospital of Shenzhen University, Shenzhen University, Shenzhen, China, [3]Institute of Urology, South China Hospital, Health Science Center, Shenzhen University, Shenzhen, China

Background: Statins, which are medications that lower lipid levels, are extensively used to decrease cardiovascular disease risk. Recently, the use of statins in cancer prevention has attracted considerable interest. However, it is still unclear whether the use of statins has a causal effect on bladder cancer.

Methods: The two-sample Mendelian Randomization (MR) was performed to infer the causal relationship between statin therapy (atorvastatin, simvastatin, and rosuvastatin) and bladder cancer. Single-nucleotide polymorphisms (SNP)-based genome-wide association studies (GWAS) of statins (atorvastatin, simvastatin, and rosuvastatin) were gathered from the UK Biobank, involving 462,933 participants. We acquired summary-level genetic data on bladder cancer from a European cohort of 175,121 individuals. The inverse variance weighted (IVW) method was the main analytical technique used, supplemented by MR-Egger, weighted median, weighted mode, and simple mode to estimate causal effects. Additionally, sensitivity analyses were conducted to verify the robustness and reliability of our findings.

Results: Based on the IVW analysis, we identified a significant causal association between rosuvastatin use and a decreased risk of bladder cancer, with genetic analysis inferring the substantial reduction in odds (OR = 3.52E-19, 95% CI: 5.48E-32–2.26E-06, p = 0.005). In contrast, the IVW results did not reveal a statistically significant relationship between the genetically estimated use of atorvastatin (OR = 7.42E-03, 95% CI: 6.80E-06–8.084, p = 0.169) or simvastatin (OR = 0.135, 95% CI: 0.008–2.330, p = 0.168) and bladder cancer risk.

Conclusion: We investigated the causal link between statin therapy (atorvastatin, simvastatin, and rosuvastatin) and bladder cancer using a two-sample Mendelian Randomization analysis among the European population. Our findings indicated that genetically predicted use of rosuvastatin was associated with a decreased risk of bladder cancer, whereas no significant genetically predicted causal effects were observed for atorvastatin and simvastatin use.

KEYWORDS

Mendelian Randomization, statin, bladder cancer, causal analysis, GWAS

1 Introduction

Bladder cancer (BCa), frequently diagnosed as a malignant urological tumor, originates mainly from malignant transitional epithelial cells (Dyrskjot et al., 2023). In 2022, this cancer accounted for 84,825 new cases in the United States and 91,893 in China, while Europe reported 204,000 new cases in 2020 (Dyba et al., 2021; Xia et al., 2022). Known as the costliest malignancy to manage, bladder cancer poses a significant healthcare challenge due to its tendency for frequent relapses and the static nature of treatment advancements, necessitating expensive ongoing monitoring and multiple interventions (Leal et al., 2016; Richters et al., 2020). In the United States, the annual total cost of cancer was $183 billion in 2015, and it is projected to increase to $246 billion by 2030. Among these costs, the annual medical burden of bladder cancer was approximately $7.93 billion, with an expected increase to $11.6 billion by 2030 (Mariotto et al., 2020). Similarly, in the European Union member states, the total cost of cancer was €152.8 billion in 2012, with the medical burden of bladder cancer accounting for approximately €5.24 billion (Leal et al., 2016). Effective early prevention, screening, and accurate diagnosis are pivotal in lessening the burden of this disease on society (Lenis et al., 2020). In the realm of cancer prevention, particularly through chemoprevention, medications commonly used for metabolic and cardiovascular conditions have been noticed for their beneficial impacts on the anticancer process (Gronich and Rennert, 2013; Morales and Morris, 2015).

Statins, which are 3-Hydroxy-3-methylglutaryl-coenzyme A reductase (HMGCoAR) inhibitors, effectively reduce lipids and are the primary treatment for hypercholesterolemia by blocking liver-based endogenous cholesterol production (Igel et al., 2002; Ziaeian and Fonarow, 2017). These medications might also serve a chemopreventive function against cancer, as a decrease in cholesterol could restrict the cell proliferation necessary for cancer development and spread (Rosch and McCully, 2013). As the critical enzyme in the mevalonate pathway, HMGCoAR supports essential cellular growth and survival processes (Mullen et al., 2016). Furthermore, statins are known to obstruct Ras/Rho pathways, thereby curtailing various cancer-promoting signaling routes (Ahmadi et al., 2017; Patel and Kashfi, 2022). A nested case-control study within the UK Clinical Practice Research Datalink (CPRD) found that current statins use correlates with a 12% reduction in the risk of biliary tract cancers compared to non-use (Liu et al., 2019). However, few randomized controlled trials (RCTs) have been conducted to evaluate the effect of statins on bladder cancer (Symvoulidis et al., 2023).

Mendelian randomization (MR) is an analytical method increasingly employed to determine causal relationships between exposures and outcomes (Davies et al., 2018). This technique uses genetic variations as instrumental variables (IV) to firmly establish causality between exposures and outcomes (Davey Smith and Hemani, 2014; Burgess et al., 2015). By leveraging the random distribution of these genetic variations, MR effectively minimizes the impact of confounding factors and reverse causality. This approach emulates the randomization seen in RCTs, thereby circumventing the confounding effects and potential biases associated with traditional RCTs (Lawlor et al., 2008). Utilizing data from Genome-wide association studies (GWAS), MR has been extensively applied in various public health sectors (Sekula et al., 2016; Hemani et al., 2018). Accordingly, a two-sample MR method was used to investigate the causal link between statin usage and bladder cancer, thus providing a more robust basis for clinical decision-making through GWAS data insights.

2 Methods

2.1 Study design and ethics statement

In this study, MR analysis was utilized to explore the causal relationship between statin use and bladder cancer (Figure 1). MR analysis is based on public GWAS data, and we utilized publicly available GWAS datasets for atorvastatin, simvastatin, and rosuvastatin usage in this MR analysis. The use of atorvastatin, simvastatin, and rosuvastatin served as the exposure variables in our study. The study design and reporting conformed to using STROBE-MR (Skrivankova et al., 2021a; Skrivankova et al., 2021b). MR analysis employs instrumental variables (IVs) to evaluate causal links between exposures and outcomes. This method hinges on three critical assumptions (Lawlor et al., 2008). The first assumption requires that the genetic variants (single-nucleotide polymorphisms, SNPs) used as IVs must have a strong association with the exposure (statins). The second assumption states that these genetic variants should not be linked with any confounders affecting the relationship between the exposure and outcomes. Finally, the third assumption mandates that the genetic variants should influence the outcome solely through their effect on the exposure, excluding any other indirect pathways. Since our data were sourced from previously conducted research and publicly available databases, obtaining further ethical approval from an ethics committee was not necessary.

2.2 Data source

We obtained summary statistics for statin use and bladder cancer from the International Oncology Unit (IEU) Open GWAS project (https://gwas.mrcieu.ac.uk/datasets/). The data for atorvastatin, simvastatin, and rosuvastatin came from the MRC-IEU consortium (Bycroft et al., 2018; Hemani et al., 2018). Specifically, the atorvastatin dataset (ukb-b-10008) included 13,851 cases and 449,082 controls; the simvastatin dataset (ukb-b-11268) included 52,427 cases and 410,506 controls; and the rosuvastatin dataset (ukb-b-13664) included 2,870 cases and 460,063 controls. To avoid population overlap in the exposure and outcome assessments, we sourced GWAS summary-level data linked to BCa from a FinnGen biobank cohort of European descent (1,115 cases and 174,006 controls) via the IEU Open GWAS database (Kurki et al., 2023). We exclusively used datasets of European ancestry to mitigate bias due to population stratification. Detailed information about these four GWAS datasets is available in Table 1.

2.3 Selection of instrumental variables

Drawing from the GWAS summary data mentioned earlier, a rigorous procedure was followed to select suitable SNPs as IVs.

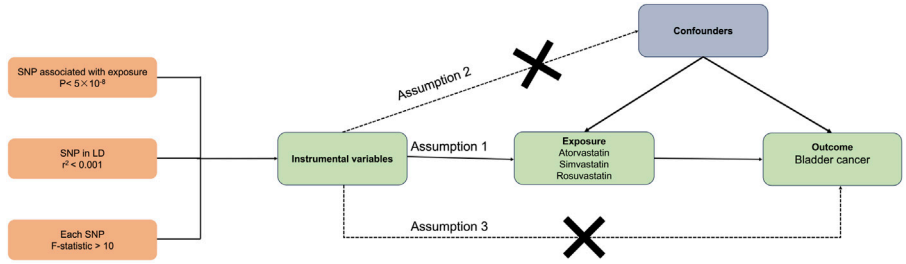

FIGURE 1
Overall design of this MR analyses.

TABLE 1 Characteristics of statin (atorvastatin, simvastatin, and rosuvastatin) use and bladder cancer GWAS cohorts in this study.

Exposure/ outcome	IEU GWAS id	Cases	Controls	Sample size	Number of SNPs	Population	Consortium	Year
Atorvastatin use	ukb-b-10008	13,851	449,082	462,933	9,851,867	European	MRC-IEU	2018
Simvastatin use	ukb-b-11268	52,427	410,506	462,933	9,851,867	European	MRC-IEU	2018
Rosuvastatin use	ukb-b-13664	2,870	460,063	462,933	9,851,867	European	MRC-IEU	2018
Bladder cancer	finn-b-C3_BLADDER_EXALLC	1,115	174,006	175,121	16,380,305	European	FinnGen study	2021

Initially, SNPs had to demonstrate a strong association with the exposure, achieving a genome-wide significance with a p-value $< 5 \times 10^{-8}$. Secondly, to prevent results skewed by linkage disequilibrium (LD), a clumping process was implemented with an R^2 cutoff of 0.001 and a window size of 10,000 kb. Thirdly, the Phenoscanner database (http://www.phenoscanner.medschl.cam.ac.uk/) was employed to identify genetic variants linked to potential confounders. SNPs closely related to the potential confounders, including smoking, body mass index, waist-to-hip ratio, and type 2 diabetes mellitus were excluded (p-value $< 5 \times 10^{-8}$). The remaining SNPs were correspondingly chosen as IVs for exposes (Cheng et al., 2023). Fourthly, if these specific SNPs were absent in the outcome GWAS dataset, proxy SNPs (with a high LD, $R^2 > 0.8$, with the target SNPs) were sought as alternatives. Finally, to ensure the consistency of effect alleles between the exposure and outcome datasets, harmonization was carried out to exclude palindromic and ambiguous SNPs with non-matching alleles. Additionally, to robustly adhere to the first key assumption, the F-statistic for each SNP was calculated individually; SNPs with F statistics < 10 were deemed weak IVs and excluded from further analysis (Burgess et al., 2011; Li et al., 2023; 2024). Following these stringent filters, the selected SNPs were utilized as the definitive IVs for the ensuing two-sample MR study.

2.4 Statistical analysis

In our research, we utilized a range of methods to analyze the causal connections and effects between exposure and outcome, including inverse-variance weighted (IVW) (Burgess et al., 2016), MR-Egger (Bowden et al., 2015), weighted median (Bowden et al., 2016), weighted mode (Hartwig et al., 2017), and simple mode (Zhang et al., 2023). Each method is suited to different scenarios. The IVW method uses SNPs' Wald estimators to determine the influence of exposure on outcome. We primarily rely on the IVW approach when there is no pleiotropy, or when pleiotropy is balanced, to derive reliable causal estimates. If significant heterogeneity among the IVs was detected ($p < 0.05$), a random effects model was applied; otherwise, a fixed effects model was employed (Burgess et al., 2016). The MR-Egger regression provides credible estimates under conditions of IV pleiotropy (Bowden et al., 2015). The Weighted Median method, not requiring the Instrument Strength Independent of Direct Effect (InSIDE) assumption, offers significant improvements over MR-Egger by achieving unbiased effect estimates and lower type I error through evaluation of the weighted median of instrumental variable ratio estimate (Bowden et al., 2016). The weighted mode method is effective for MR causal inference assuming most IVs are valid (Hartwig et al., 2017), while the simple mode method generally yields less robust results compared to IVW(Zhang et al., 2023). All these methods were executed and visually presented using R version 4.3.1 with the "MRPRESSO" and "TwoSampleMR" packages, considering a p-value under 0.05 as statistically significant.

2.5 Sensitivity analysis

We conducted MR-Egger regression to evaluate pleiotropy in the instrumental variables, considering pleiotropy confirmed when the p-value fell below 0.05. We also implemented the MR-PRESSO test to further assess pleiotropy and identify outliers. In instances where the MR-PRESSO test revealed significant horizontal pleiotropy, we removed the implicated outlier variants and repeated the MR analysis. To quantify heterogeneities uncovered

TABLE 2 MR analysis of the causality of statin (atorvastatin, simvastatin, and rosuvastatin) use on Bladder cancer.

Exposure	Outcome	MR method	Number of SNPs	β	SE	OR (95% CI)	*p*-value
Atorvastatin use	Bladder cancer	MR Egger	22	−13.291	8.704	1.69E-06 (6.59E-14–41.313)	0.142
		Weighted median	22	−8.413	4.535	2.22E-04 (3.06E-08–1.608)	0.064
		Inverse variance weighted	22	−4.904	3.568	7.42E-03 (6.80E-06–8.084)	0.169
		Simple mode	22	−13.347	9.318	1.60E-06 (1.87E-14–136.345)	0.167
		Weighted mode	22	−11.072	6.166	1.55E-05 (8.77E-11–2.754)	0.087
Simvastatin use	Bladder cancer	MR Egger	39	1.400	2.795	4.055 (0.017–970.731)	0.619
		Weighted median	39	0.209	2.134	1.232 (0.019–80.700)	0.922
		Inverse variance weighted	39	−2.002	1.453	0.135 (0.008–2.330)	0.168
		Simple mode	39	−8.037	5.378	3.23E-04 (8.54E-09–12.231)	0.143
		Weighted mode	39	2.464	4.407	11.756 (0.002–6.63E+04)	0.579
Rosuvastatin use	Bladder cancer	MR Egger	6	−30.950	88.525	3.61E-14 (1.60E-89–8.18E+61)	0.744
		Weighted median	6	−41.864	19.141	6.59E-19 (3.36E-35–0.013)	0.029
		Inverse variance weighted	6	−42.490	15.047	3.52E-19 (5.48E-32–2.26E-06)	0.005
		Simple mode	6	−45.048	27.191	2.73E-20 (1.95E-43–3,810.426)	0.158
		Weighted mode	6	−42.213	24.370	4.65E-19 (8.73E-40–257.729)	0.144

SNPs, single-nucleotide polymorphisms; SE, standard error; OR, odds ratio; CI, confidence interval

by both the IVW and MR-Egger regression methods, we calculated Cochran's Q statistic, with a *p*-value of less than 0.05 indicating significant heterogeneity. Additionally, we executed a "leave-one-out" sensitivity analysis to ascertain whether any single SNP could significantly skew the overall causal inference.

3 Results

3.1 Selection of instrumental variables

Adhering to strict criteria for instrumental SNP selection, we identified appropriate SNPs as IVs that met three key assumptions. We identified 22 SNPs highly correlated with atorvastatin use, 39 SNPs highly correlated with simvastatin use, and 6 SNPs highly correlated with rosuvastatin use. These SNPs served as IVs for exposure, with each SNP displaying an F-statistic greater than 10, indicating a minimal likelihood of weak IV bias. Detailed descriptions of the included SNPs are provided in the Supplementary Tables S1-S3.

3.2 Causal effects of atorvastatin use on bladder cancer

Table 2 displayed the outcomes of the MR analysis on the causal effects of atorvastatin use on bladder cancer. The inverse variance weighted (IVW) method revealed no causal connection between atorvastatin use and bladder cancer (OR = 7.42E-03, 95% CI: 6.80E-06–8.084, p = 0.169), a finding supported by additional methods including MR-Egger, Weighted Median, Weighted Mode, and Simple Mode. These results were graphically represented in the forest plot (Figure 2) and the scatter plot (Figure 3). The forest plot delineated the effect estimates and their confidence intervals for each SNP, while the scatter plot illustrated the relationship between atorvastatin use and bladder cancer using the instrumental variables. Thus, our analysis indicated that there was no significant causal effect of atorvastatin use on bladder cancer.

Additionally, the MR-Egger regression intercept analysis (p = 0.304) and the MR-PRESSO global test (p = 0.121) did not show significant pleiotropy (Table 3). The Cochran Q-test results from both the MR-Egger (p = 0.137) and IVW (p = 0.128) methods also demonstrated no heterogeneity in our findings. The funnel plots, presented in Supplementary Figure S1. Furthermore, the leave-one-out analysis verified that excluding any single SNP did not significantly influence the estimated causal relationship (Supplementary Figure S2).

3.3 Causal effects of simvastatin use on bladder cancer

The results from the MR analysis investigating the causal effects of simvastatin on bladder cancer were presented in Table 2. The IVW method indicated that simvastatin use had no causal impact on bladder cancer (OR = 0.135, 95% CI: 0.008–2.330, p = 0.168), a conclusion corroborated by the MR-Egger, Weighted Median, Weighted Mode, and Simple Mode analyses. Figures 2, 3 respectively illustrated these findings through a forest plot and a scatter plot, reinforcing the lack of a significant causal relationship between simvastatin use and bladder cancer.

Further evaluations using the MR-Egger regression intercept analysis for assessing pleiotropy among the instrumental

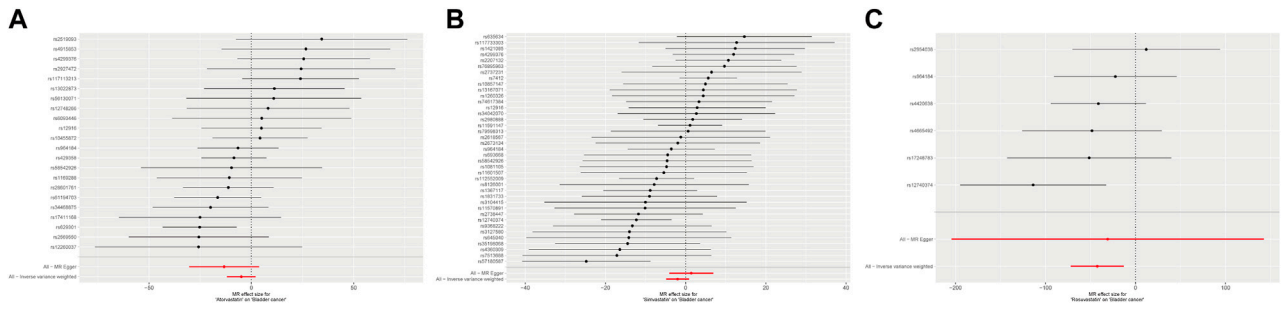

FIGURE 2
Forest plot of the causal effects of atorvastatin **(A)**, simvastatin **(B)**, and rosuvastatin **(C)** use associated SNPs on bladder cancer.

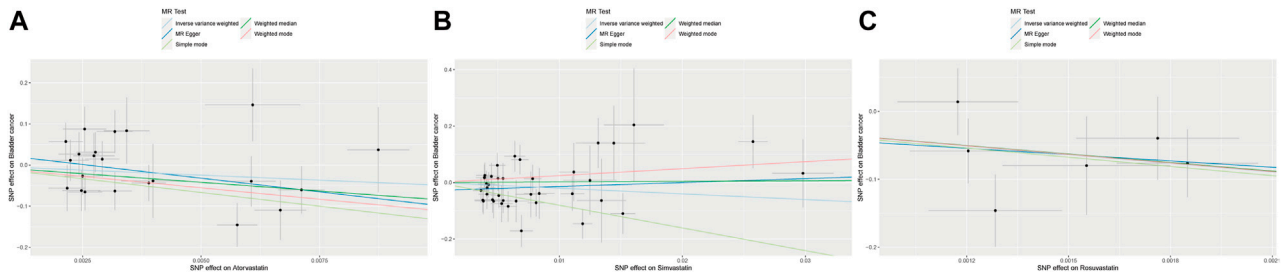

FIGURE 3
Scatter plot of the causal relationships between atorvastatin **(A)**, simvastatin **(B)**, and rosuvastatin **(C)** use on bladder cancer. The regression slopes of the lines represent the magnitude of the causal effect.

TABLE 3 Sensitivity analyses of MR.

Exposure	Pleiotropy					Heterogeneity			
	MR-PRESSO global outlier test			MR-egger regression		MR-egger		Inverse variance weighted (IVW)	
	p-value	Outlier	*p*-value after outlier	Intercept	*p*-value	Q statistic	*p*-value	Q statistic	*p*-value
Atorvastatin use	0.121	—	—	0.035	0.304	26.927	0.137	28.428	0.128
Simvastatin use	0.039	No significant outliers	NA	−0.028	0.164	48.641	0.095	51.285	0.074
Rosuvastatin use	0.487	—	—	−0.017	0.901	5.026	0.285	5.048	0.410

variables showed no significant pleiotropic effects (p = 0.164) (Table 3). Although the p-value of MR-PRESSO global test was less than 0.05, MR-PRESSO global test showed that no significant outliers. The outlier-corrected causal estimate showed the NA. Heterogeneity assessments conducted through the MR-Egger (p = 0.095) and IVW (p = 0.074) methods also indicated no significant heterogeneity among the instrumental variables. The funnel plots depicted in Supplementary Figure S1. Additionally, the leave-one-out analysis verified the stability of the causal association estimate, demonstrating that it was unaffected by the exclusion of any individual SNP (Supplementary Figure S2).

3.4 Causal effects of rosuvastatin use on bladder cancer

The outcomes of the MR analysis of the causality of rosuvastatin use on bladder cancer were encapsulated in Table 2. IVW revealed a statistically significant negative causal impact of A rosuvastatin use on bladder cancer (OR = 3.52E-19, 95% CI: 5.48E-32–2.26E-06, p = 0.005). Simultaneously, a relationship following the same trend was discerned through the weighted median method (OR = 6.59E-19, 95% CI = 3.36E-35–0.013, p = 0.029). These results were graphically represented in both the forest plot (Figure 2) and the scatter plot (Figure 3). Given that IVW and weighted median method hold an

edge in preserving superior estimation precision over the MR-Egger method in MR analysis, the outcomes from the MR analysis provide support for a potential causal association between rosuvastatin use on bladder cancer.

Additionally, the MR-Egger regression intercept analysis (p = 0.901) and the MR-PRESSO global test (p = 0.487) did not show significant pleiotropy (Table 3). The Cochran Q-test results from both the MR-Egger (p = 0.285) and IVW (p = 0.410) methods also demonstrated no heterogeneity in our findings. The funnel plots were shown in Supplementary Figure S1. Furthermore, the leave-one-out analysis demonstrated that the causal association estimate was not influenced by the exclusion of any individual SNP (Supplementary Figure S2). These outcomes provide confidence in the validity and robustness of the causal inference derived from the MR analysis.

4 Discussion

In this research, we utilized a two-sample MR analysis based on GWAS summary-level data to assess the causal impact of statin therapy (atorvastatin, simvastatin, and rosuvastatin) on bladder cancer. The MR analysis indicated that rosuvastatin usage had a genetically determined causal effect on reducing bladder cancer risk. However, there were no causal effects on bladder cancer risk from the use of atorvastatin or simvastatin.

In the present epidemiological research, the influence of statins on cancer risk remains uncertain. A population-based, nested, case-control study with 3,129 patients and 16,976 controls from the PHARMO database was conducted to investigate the potential protective effect of statin therapy on cancer risk. This study reported a 20% reduction in cancer risk associated with statin use (adjusted odds ratio [OR], 0.80; 95% CI, 0.66–0.96) (Graaf et al., 2004). Additionally, a multi-regional observational study from the BioBank Japan cohort indicated that statin monotherapy was effective in reducing all-cause and cancer mortality (Yokomichi et al., 2017). In contrast, a matched case-control study using the General Practice Research Database observed no significant relationship between current statin use and the risk of 13 types of cancer (Kaye and Jick, 2004). Another investigation involving 4,913 cancer patients and 3,900 controls found no evidence to support a positive or negative association between statin use and 10 cancer types (Coogan et al., 2007).

Further research by Jun-Jun Yeh et al., utilizing Taiwan's National Health Insurance Research Database, assessed the effects of statins on cancer risk among patients with interstitial lung disease (ILD) and pulmonary fibrosis. Their findings suggested a lower risk of bladder cancer associated with statin use in this population (Yeh et al., 2021). A multicenter study on patients with T1 high-grade non-muscle invasive urothelial bladder cancer showed that statin use was independently associated with a lower risk of recurrence (HR: 0.80, 95% CI: 0.67–0.95; p = 0.009), implying a beneficial effect on recurrence rates (Ferro et al., 2021). Additionally, a retrospective cohort study of individuals aged 66 and over, diagnosed with non-muscle invasive bladder cancer (NMIBC) between 1992 and 2012, demonstrated that statin users had better overall survival compared to nonusers (Richard et al., 2017). However, a population-based case-control study in Taiwan, including 325 bladder cancer cases and 1,300 controls, did not provide evidence supporting any beneficial or detrimental associations between statin use and bladder cancer risk (Kuo et al., 2012). A retrospective analysis of 1,117 patients treated with transurethral resection of the bladder (TURB) for NMIBC at three institutions from 1996 to 2007 assessed the impact of statin use on patient outcomes and the efficacy of intravesical BCG therapy. The findings indicated that statin use did not affect outcomes differently compared to non-use, nor did it impact the efficacy of BCG immunotherapy (Crivelli et al., 2013). And a meta-analysis including 10 studies found a non-significant increase in bladder cancer risk among statin users compared with non-users, and no association between statin use and BCa local control, recurrence, survival or mortality (Symvoulidis et al., 2023). Another meta-analysis including 13 studies also suggested that there was no association between statin use and risk of BCa(Zhang et al., 2013). It is noteworthy that these studies did not differentiate the effects based on specific statins.

Atorvastatin demonstrated notable antiproliferative and pro-apoptotic effects in human bladder cancer cells (Kamat and Nelkin, 2005). It also induced autophagy in these cells *in vitro*. Additionally, when used with autophagy inhibitors, atorvastatin's cytotoxicity was enhanced, further promoting apoptotic cell death (Kang et al., 2014). In animal studies, Belmiro Parada et al. explored the chemopreventive efficacy of atorvastatin against nitrosamine-induced rat bladder cancer and observed a significant inhibitory impact on cancer development, likely due to its antioxidant, anti-proliferative, and anti-inflammatory actions (Parada et al., 2012). Despite these findings, no clinical trials have confirmed atorvastatin's protective effect in bladder cancer patients. Similarly, our findings did not support a causal link between atorvastatin use and reduced bladder cancer risk.

Simvastatin inhibited bladder cancer cell metastasis by blocking epithelial-mesenchymal transition (EMT) and disrupting AKT/GSK3β pathways, while also suppressing cell proliferation and causing G1/G0 phase cell cycle arrest through the Peroxisome Proliferator-Activated Receptor (PPAR)γ signaling pathway (Wang et al., 2016). Additionally, the combination of simvastatin with romidepsin synergistically killed bladder cancer cells, with mechanisms involving ER stress induction, AMPK activation, histone acetylation, and enhanced PPARγ expression (Okubo et al., 2021). Moreover, Pleomorphic adenoma gene like-2 (PLAGL2) facilitated bladder cancer progression via RACGAP1/RhoA GTPase/YAP1 signaling, and its proproliferative and prometastatic effects were negated by the RhoA inhibitor simvastatin (Chen et al., 2023). Contrarily, a 10-year multicentric retrospective study in Lebanon established a duration-response relationship between simvastatin use and bladder cancer risk (OR = 1.189), revealing a detrimental link with the increased duration of simvastatin intake (Chalhoub et al., 2023). Our findings showed that there was no causal link between simvastatin use and bladder cancer risk among the European population.

Rosuvastatin triggered autophagic responses in human papillary thyroid cancer B-CPAP cells at lower doses, with a transition to apoptosis observed as rosuvastatin concentrations increased (Zeybek et al., 2011). When used alone or in a combined strategy with difluoromethylornithine, rosuvastatin significantly inhibited colon adenocarcinomas in male F344 rats induced by azoxymethane

(AOM) and enhanced the functionality of natural killer (NK) cells (Janakiram et al., 2016). Furthermore, rosuvastatin prevented spheroid formation and epithelial-mesenchymal transition (EMT) in the prostate cancer PC-3 cell line (Deezagi and Safari, 2020) and exhibited antiangiogenic and antitumor properties that curtailed prostate cancer growth (Wang et al., 2010). A population-based cohort study from the Database of Clalit Health Services indicated that extended use of rosuvastatin was linked to a lower risk of prostate cancer (HR 0.22, 95% CI 0.08–0.75) (Lustman et al., 2014). In this study, MR analysis suggested that rosuvastatin use has a genetically determined causal effect in reducing bladder cancer risk.

Our research has several noteworthy strengths. Initially, we assessed the impact of three specific statins on bladder cancer risk using a two-sample MR analysis, potentially offering more profound insights for subsequent research. Given statins' known benefits in lowering cardiovascular risk through their antidyslipidemic properties, their potential protective effects against bladder cancer could translate into significant medical and socioeconomic advantages for patients with common risk factors. Furthermore, Mendelian Randomization, which utilizes extensive data from Genome-Wide Association Studies (GWAS) to simulate a randomized controlled trial, offers a cost-effective alternative to observational studies and minimizes the risk of reverse causation. Additionally, the selection of our instrumental variable SNP, which occurs randomly at conception, helps eliminate confounding bias. Lastly, by choosing participants from the European demographic, we aimed to decrease potential biases stemming from population stratification.

This study is subject to several limitations that must be considered when interpreting and generalizing the results. Initially, while the study population addressed racial discrepancies, it remains uncertain if these findings can be extended to different racial groups and geographic areas. Additional GWAS studies across diverse regions might yield stronger evidence concerning the relationship between statin use and bladder cancer risk. Additionally, our reliance on summary-level data precluded the possibility of analyzing non-linear relationships or effects that vary across subgroups. Moreover, we accessed only the GWAS summary-level data for atorvastatin, simvastatin, and rosuvastatin, which limits our understanding of how other statins might affect bladder cancer risk. Then, the funnel plot for the instrumental variables is asymmetric, indicating bias and confounding in the findings. Lastly, the MR method used was restricted to establishing causal connections and did not allow for the investigation of the mechanisms underlying these associations, which would require more comprehensive studies.

5 Conclusion

In this study, we presented evidence supporting a potential genetically determined causal link between rosuvastatin use and a decreased risk of bladder cancer in the European population, using two-sample Mendelian Randomization analysis. The results indicated that rosuvastatin usage was linked to a lower risk of bladder cancer, while no significant genetically predicted causal effects were observed for atorvastatin or simvastatin. The results of this study were not sufficient to support the conclusion that statins were associated with low incidence of bladder cancer. Additional research into the mechanisms is required to elucidate the intricate relationship between statin treatment and bladder cancer risk.

Data availability statement

The original contributions presented in the study are included in the article/Supplementary Material, further inquiries can be directed to the corresponding authors.

Author contributions

RL: Conceptualization, Data curation, Formal Analysis, Investigation, Software, Writing–original draft. GH: Conceptualization, Data curation, Formal Analysis, Investigation, Software, Writing–original draft. YFL: Formal Analysis, Software, Writing–original draft. MH: Formal Analysis, Software, Writing–original draft. YH: Formal Analysis, Software, Writing–original draft. YGL: Formal Analysis, Software, Writing–original draft. GL: Funding acquisition, Methodology, Project administration, Resources, Supervision, Writing–review and editing. SW: Funding acquisition, Methodology, Project administration, Resources, Supervision, Writing–review and editing.

Funding

The author(s) declare that financial support was received for the research, authorship, and/or publication of this article. This work was partially supported by the Shenzhen Key Medical Discipline (No. SZXK021) and the Sanming Project of Medicine in Shenzhen (No. SASM202201024).

Conflict of interest

The authors declare that the research was conducted in the absence of any commercial or financial relationships that could be construed as a potential conflict of interest.

Publisher's note

Supplementary material

The Supplementary Material for this article can be found online at: https://www.frontiersin.org/articles/10.3389/fphar.2024.1427318/full#supplementary-material

References

Ahmadi, Y., Ghorbanihaghjo, A., and Argani, H. (2017). The balance between induction and inhibition of mevalonate pathway regulates cancer suppression by statins: a review of molecular mechanisms. *Chem. Biol. Interact.* 273, 273–285. doi:10.1016/j.cbi.2017.06.026

Bowden, J., Davey Smith, G., and Burgess, S. (2015). Mendelian randomization with invalid instruments: effect estimation and bias detection through Egger regression. *Int. J. Epidemiol.* 44 (2), 512–525. doi:10.1093/ije/dyv080

Bowden, J., Davey Smith, G., Haycock, P. C., and Burgess, S. (2016). Consistent estimation in mendelian randomization with some invalid instruments using a weighted median estimator. *Genet. Epidemiol.* 40 (4), 304–314. doi:10.1002/gepi.21965

Burgess, S., Daniel, R. M., Butterworth, A. S., Thompson, S. G., and Consortium, E.P.-I. (2015). Network Mendelian randomization: using genetic variants as instrumental variables to investigate mediation in causal pathways. *Int. J. Epidemiol.* 44 (2), 484–495. doi:10.1093/ije/dyu176

Burgess, S., Dudbridge, F., and Thompson, S. G. (2016). Combining information on multiple instrumental variables in Mendelian randomization: comparison of allele score and summarized data methods. *Stat. Med.* 35 (11), 1880–1906. doi:10.1002/sim.6835

Burgess, S., Thompson, S. G., and Collaboration, C. C. G. (2011). Avoiding bias from weak instruments in Mendelian randomization studies. *Int. J. Epidemiol.* 40 (3), 755–764. doi:10.1093/ije/dyr036

Bycroft, C., Freeman, C., Petkova, D., Band, G., Elliott, L. T., Sharp, K., et al. (2018). The UK Biobank resource with deep phenotyping and genomic data. *Nature* 562 (7726), 203–209. doi:10.1038/s41586-018-0579-z

Chalhoub, I. G., Boulos, R. T., Dagher, Y. G., El Helou, S., Haifa, K. G., Atallah, B., et al. (2023). Statins, commonly coprescribed drugs, and concomitant risk factors: a protective, neutral, or harmful association with common cancer types development: a 10-year multicentric retrospective lebanese study. *Med. Baltim.* 102 (39), e34562. doi:10.1097/MD.0000000000034562

Chen, H., Yang, W., Li, Y., and Ji, Z. (2023). PLAGL2 promotes bladder cancer progression via RACGAP1/RhoA GTPase/YAP1 signaling. *Cell Death Dis.* 14 (7), 433. doi:10.1038/s41419-023-05970-2

Cheng, Z., Ye, F., Liang, Y., Xu, C., Zhang, Z., Ou, Y., et al. (2023). Blood lipids, lipid-regulatory medications, and risk of bladder cancer: a Mendelian randomization study. *Front. Nutr.* 10, 992608. doi:10.3389/fnut.2023.992608

Coogan, P. F., Rosenberg, L., and Strom, B. L. (2007). Statin use and the risk of 10 cancers. *Epidemiology* 18 (2), 213–219. doi:10.1097/01.ede.0000254694.03027.a1

Crivelli, J. J., Xylinas, E., Kluth, L. A., da Silva, R. D., Chrystal, J., Novara, G., et al. (2013). Effect of statin use on outcomes of non-muscle-invasive bladder cancer. *BJU Int.* 112 (2), E4–E12. doi:10.1111/bju.12150

Davey Smith, G., and Hemani, G. (2014). Mendelian randomization: genetic anchors for causal inference in epidemiological studies. *Hum. Mol. Genet.* 23 (R1), R89–R98. doi:10.1093/hmg/ddu328

Davies, N. M., Holmes, M. V., and Davey Smith, G. (2018). Reading Mendelian randomisation studies: a guide, glossary, and checklist for clinicians. *BMJ* 362, k601. doi:10.1136/bmj.k601

Deezagi, A., and Safari, N. (2020). Rosuvastatin inhibit spheroid formation and epithelial-mesenchymal transition (EMT) in prostate cancer PC-3 cell line. *Mol. Biol. Rep.* 47 (11), 8727–8737. doi:10.1007/s11033-020-05918-1

Dyba, T., Randi, G., Bray, F., Martos, C., Giusti, F., Nicholson, N., et al. (2021). The European cancer burden in 2020: incidence and mortality estimates for 40 countries and 25 major cancers. *Eur. J. Cancer* 157, 308–347. doi:10.1016/j.ejca.2021.07.039

Dyrskjot, L., Hansel, D. E., Efstathiou, J. A., Knowles, M. A., Galsky, M. D., Teoh, J., et al. (2023). Bladder cancer. *Nat. Rev. Dis. Prim.* 9 (1), 58. doi:10.1038/s41572-023-00468-9

Ferro, M., Marchioni, M., Lucarelli, G., Vartolomei, M. D., Soria, F., Terracciano, D., et al. (2021). Association of statin use and oncological outcomes in patients with first diagnosis of T1 high grade non-muscle invasive urothelial bladder cancer: results from a multicenter study. *Minerva Urol. Nephrol.* 73 (6), 796–802. doi:10.23736/S2724-6051.20.04076-X

Graaf, M. R., Beiderbeck, A. B., Egberts, A. C., Richel, D. J., and Guchelaar, H. J. (2004). The risk of cancer in users of statins. *J. Clin. Oncol.* 22 (12), 2388–2394. doi:10.1200/JCO.2004.02.027

Gronich, N., and Rennert, G. (2013). Beyond aspirin-cancer prevention with statins, metformin and bisphosphonates. *Nat. Rev. Clin. Oncol.* 10 (11), 625–642. doi:10.1038/nrclinonc.2013.169

Hartwig, F. P., Davey Smith, G., and Bowden, J. (2017). Robust inference in summary data Mendelian randomization via the zero modal pleiotropy assumption. *Int. J. Epidemiol.* 46 (6), 1985–1998. doi:10.1093/ije/dyx102

Hemani, G., Zheng, J., Elsworth, B., Wade, K. H., Haberland, V., Baird, D., et al. (2018). The MR-Base platform supports systematic causal inference across the human phenome. *Elife* 7, e34408. doi:10.7554/eLife.34408

Igel, M., Sudhop, T., and von Bergmann, K. (2002). Pharmacology of 3-hydroxy-3-methylglutaryl-coenzyme A reductase inhibitors (statins), including rosuvastatin and pitavastatin. *J. Clin. Pharmacol.* 42 (8), 835–845. doi:10.1177/009127002401102731

Janakiram, N. B., Mohammed, A., Bryant, T., Zhang, Y., Brewer, M., Duff, A., et al. (2016). Potentiating NK cell activity by combination of Rosuvastatin and Difluoromethylornithine for effective chemopreventive efficacy against Colon Cancer. *Sci. Rep.* 6, 37046. doi:10.1038/srep37046

Kamat, A. M., and Nelkin, G. M. (2005). Atorvastatin: a potential chemopreventive agent in bladder cancer. *Urology* 66 (6), 1209–1212. doi:10.1016/j.urology.2005.06.075

Kang, M., Jeong, C. W., Ku, J. H., Kwak, C., and Kim, H. H. (2014). Inhibition of autophagy potentiates atorvastatin-induced apoptotic cell death in human bladder cancer cells *in vitro*. *Int. J. Mol. Sci.* 15 (5), 8106–8121. doi:10.3390/ijms15058106

Kaye, J. A., and Jick, H. (2004). Statin use and cancer risk in the general Practice research database. *Br. J. Cancer* 90 (3), 635–637. doi:10.1038/sj.bjc.6601566

Kuo, C. C., Chiu, H. F., Lee, I. M., Kuo, H. W., Lee, C. T., and Yang, C. Y. (2012). Statin use and the risk of bladder cancer: a population-based case-control study. *Expert Opin. Drug Saf.* 11 (5), 733–738. doi:10.1517/14740338.2012.712960

Kurki, M. I., Karjalainen, J., Palta, P., Sipila, T. P., Kristiansson, K., Donner, K. M., et al. (2023). FinnGen provides genetic insights from a well-phenotyped isolated population. *Nature* 613 (7944), 508–518. doi:10.1038/s41586-022-05473-8

Lawlor, D. A., Harbord, R. M., Sterne, J. A., Timpson, N., and Davey Smith, G. (2008). Mendelian randomization: using genes as instruments for making causal inferences in epidemiology. *Stat. Med.* 27 (8), 1133–1163. doi:10.1002/sim.3034

Leal, J., Luengo-Fernandez, R., Sullivan, R., and Witjes, J. A. (2016). Economic burden of bladder cancer across the European union. *Eur. Urol.* 69 (3), 438–447. doi:10.1016/j.eururo.2015.10.024

Lenis, A. T., Lec, P. M., Chamie, K., and Mshs, M. D. (2020). Bladder cancer: a review. *JAMA* 324 (19), 1980–1991. doi:10.1001/jama.2020.17598

Li, R., Peng, L., Deng, D., Li, G., and Wu, S. (2023). Potential causal association between aspirin use and erectile dysfunction in European population: a Mendelian randomization study. *Front. Endocrinol. (Lausanne)* 14, 1329847. doi:10.3389/fendo.2023.1329847

Li, R., Peng, L., Deng, D., Li, G., and Wu, S. (2024). Causal relationship between Alzheimer's disease and prostate cancer: a bidirectional Mendelian randomization analysis. *Front. Endocrinol. (Lausanne)* 15, 1354528. doi:10.3389/fendo.2024.1354528

Liu, Z., Alsaggaf, R., McGlynn, K. A., Anderson, L. A., Tsai, H. T., Zhu, B., et al. (2019). Statin use and reduced risk of biliary tract cancers in the UK Clinical Practice Research Datalink. *Gut* 68 (8), 1458–1464. doi:10.1136/gutjnl-2018-317504

Lustman, A., Nakar, S., Cohen, A. D., and Vinker, S. (2014). Statin use and incident prostate cancer risk: does the statin brand matter? A population-based cohort study. *Prostate Cancer Prostatic Dis.* 17 (1), 6–9. doi:10.1038/pcan.2013.34

Mariotto, A. B., Enewold, L., Zhao, J., Zeruto, C. A., and Yabroff, K. R. (2020). Medical care costs associated with cancer survivorship in the United States. *Cancer Epidemiol. Biomarkers Prev.* 29 (7), 1304–1312. doi:10.1158/1055-9965.EPI-19-1534

Morales, D. R., and Morris, A. D. (2015). Metformin in cancer treatment and prevention. *Annu. Rev. Med.* 66, 17–29. doi:10.1146/annurev-med-062613-093128

Mullen, P. J., Yu, R., Longo, J., Archer, M. C., and Penn, L. Z. (2016). The interplay between cell signalling and the mevalonate pathway in cancer. *Nat. Rev. Cancer* 16 (11), 718–731. doi:10.1038/nrc.2016.76

Okubo, K., Miyai, K., Kato, K., Asano, T., and Sato, A. (2021). Simvastatin-romidepsin combination kills bladder cancer cells synergistically. *Transl. Oncol.* 14 (9), 101154. doi:10.1016/j.tranon.2021.101154

Parada, B., Reis, F., Pinto, A., Sereno, J., Xavier-Cunha, M., Neto, P., et al. (2012). Chemopreventive efficacy of Atorvastatin against nitrosamine-induced rat bladder cancer: antioxidant, anti-proliferative and anti-inflammatory properties. *Int. J. Mol. Sci.* 13 (7), 8482–8499. doi:10.3390/ijms13078482

Patel, K. K., and Kashfi, K. (2022). Lipoproteins and cancer: the role of HDL-C, LDL-C, and cholesterol-lowering drugs. *Biochem. Pharmacol.* 196, 114654. doi:10.1016/j.bcp.2021.114654

Richard, P. O., Ahmad, A. E., Bashir, S., Hamilton, R. J., Nam, R. K., Leao, R., et al. (2017). Effect of statins as a secondary chemopreventive agent among individuals with non-muscle-invasive bladder cancer: a population-based analysis. *Urol. Oncol.* 35 (6), 342–348. doi:10.1016/j.urolonc.2016.12.009

Richters, A., Aben, K. K. H., and Kiemeney, L. (2020). The global burden of urinary bladder cancer: an update. *World J. Urol.* 38 (8), 1895–1904. doi:10.1007/s00345-019-02984-4

Rosch, P. J., and McCully, K. (2013). Statin use and reduced cancer-related mortality. *N. Engl. J. Med.* 368 (6), 576. doi:10.1056/NEJMc1214827

Sekula, P., Del Greco, M. F., Pattaro, C., and Kottgen, A. (2016). Mendelian randomization as an approach to assess causality using observational data. *J. Am. Soc. Nephrol.* 27 (11), 3253–3265. doi:10.1681/ASN.2016010098

Skrivankova, V. W., Richmond, R. C., Woolf, B. A. R., Davies, N. M., Swanson, S. A., VanderWeele, T. J., et al. (2021a). Strengthening the reporting of observational studies in epidemiology using mendelian randomisation (STROBE-MR): explanation and elaboration. *BMJ* 375, n2233. doi:10.1136/bmj.n2233

Skrivankova, V. W., Richmond, R. C., Woolf, B. A. R., Yarmolinsky, J., Davies, N. M., Swanson, S. A., et al. (2021b). Strengthening the reporting of observational studies in epidemiology using mendelian randomization: the STROBE-MR statement. *JAMA* 326 (16), 1614–1621. doi:10.1001/jama.2021.18236

Symvoulidis, P., Tsioutis, C., Zamboglou, C., and Agouridis, A. P. (2023). The effect of statins on the incidence and prognosis of bladder cancer: a systematic review and meta-analysis. *Curr. Oncol.* 30 (7), 6648–6665. doi:10.3390/curroncol30070488

Wang, C., Tao, W., Wang, Y., Bikow, J., Lu, B., Keating, A., et al. (2010). Rosuvastatin, identified from a zebrafish chemical genetic screen for antiangiogenic compounds, suppresses the growth of prostate cancer. *Eur. Urol.* 58 (3), 418–426. doi:10.1016/j.eururo.2010.05.024

Wang, G., Cao, R., Wang, Y., Qian, G., Dan, H. C., Jiang, W., et al. (2016). Simvastatin induces cell cycle arrest and inhibits proliferation of bladder cancer cells via PPARγ signalling pathway. *Sci. Rep.* 6, 35783. doi:10.1038/srep35783

Xia, C., Dong, X., Li, H., Cao, M., Sun, D., He, S., et al. (2022). Cancer statistics in China and United States, 2022: profiles, trends, and determinants. *Chin. Med. J. Engl.* 135 (5), 584–590. doi:10.1097/CM9.0000000000002108

Yeh, J. J., Lai, J. N., Lin, C. L., Hsu, C. Y., and Kao, C. H. (2021). Time-dependent propensity-matched general population study of the effects of statin use on cancer risk in an interstitial lung disease and pulmonary fibrosis cohort. *BMJ Open* 11 (10), e047039. doi:10.1136/bmjopen-2020-047039

Yokomichi, H., Nagai, A., Hirata, M., Tamakoshi, A., Kiyohara, Y., Kamatani, Y., et al. (2017). Statin use and all-cause and cancer mortality: BioBank Japan cohort. *J. Epidemiol.* 27 (3S), S84–S91. doi:10.1016/j.je.2016.12.011

Zeybek, N. D., Gulcelik, N. E., Kaymaz, F. F., Sarisozen, C., Vural, I., Bodur, E., et al. (2011). Rosuvastatin induces apoptosis in cultured human papillary thyroid cancer cells. *J. Endocrinol.* 210 (1), 105–115. doi:10.1530/JOE-10-0411

Zhang, K., Li, A., Zhou, J., Zhang, C., and Chen, M. (2023). Genetic association of circulating C-reactive protein levels with idiopathic pulmonary fibrosis: a two-sample Mendelian randomization study. *Respir. Res.* 24 (1), 7. doi:10.1186/s12931-022-02309-x

Zhang, X. L., Geng, J., Zhang, X. P., Peng, B., Che, J. P., Yan, Y., et al. (2013). Statin use and risk of bladder cancer: a meta-analysis. *Cancer Causes Control* 24 (4), 769–776. doi:10.1007/s10552-013-0159-3

Ziaeian, B., and Fonarow, G. C. (2017). Statins and the prevention of heart disease. *JAMA Cardiol.* 2 (4), 464. doi:10.1001/jamacardio.2016.4320

frontiers | Frontiers in Pharmacology

TYPE Original Research
PUBLISHED 06 August 2024
DOI 10.3389/fphar.2024.1443045

OPEN ACCESS

EDITED BY
Lei Yin,
Shanghai Jiaotong University School of Medicine, China

REVIEWED BY
Cuncai Guo,
Washington University in St. Louis, United States
Jiahao Cai,
Guangzhou Medical University, China

*CORRESPONDENCE
Yilong Lin,
linyilong0925@163.com
Liyi Zhang,
zhanglh0923@outlook.com
Qingmo Yang,
yqm8383@163.com

†These authors have contributed equally to this work

RECEIVED 03 June 2024
ACCEPTED 19 July 2024
PUBLISHED 06 August 2024

CITATION
Lin Y, Zhang Y, Wang S, Cao L, Zhao R, Ma X, Yang Q, Zhang L and Yang Q (2024), Pharmacological targets of SGLT2 inhibition on prostate cancer mediated by circulating metabolites: a drug-target Mendelian randomization study.
Front. Pharmacol. 15:1443045.
doi: 10.3389/fphar.2024.1443045

Pharmacological targets of SGLT2 inhibition on prostate cancer mediated by circulating metabolites: a drug-target Mendelian randomization study

Yilong Lin[1,2*†], Yue Zhang[3†], Songsong Wang[2†], Lin Cao[4], Ruidan Zhao[1], Xilai Ma[2], Qiaolu Yang[1], Liyi Zhang[1*] and Qingmo Yang[1,5*]

[1]Department of Breast Surgery, The First Affiliated Hospital of Xiamen University, School of Medicine, Xiamen University, Xiamen, China, [2]School of Medicine, Xiamen University, Xiamen, China, [3]Department of Hematology, Xiangya Hospital, Xiangya School of Medicine, Central South University, Changsha, China, [4]The First Clinical College of Guangzhou Medical University, Guangzhou Medical University, Guangzhou, China, [5]The School of Clinical Medicine, Fujian Medical University, Fuzhou, China

Background: The relationship between sodium-glucose cotransporter 2 (SGLT2) inhibitors and prostate cancer is still unknown. Although these inhibitors can influence tumor glycolysis, the underlying mechanism requires further exploration.

Methods: A two-sample two-step MR was used to determine 1) causal effects of SGLT2 inhibition on prostate cancer; 2) causal effects of 1,400 circulating metabolites or metabolite ratios on prostate cancer; and 3) mediation effects of these circulating metabolites. Genetic proxies for SGLT2 inhibition were identified as variants in the SLC5A2 gene and glycated hemoglobin level (HbA1c). Additionally, positive control analysis on type 2 diabetes mellitus (T2DM) was conducted to test the selection of genetic proxies. Phenome Wide Association Study (PheWAS) and MR-PheWAS analysis were used to explore potential treatable diseases and adverse outcomes of SGLT2 inhibitors.

Results: Genetically predicted SGLT2 inhibition (per 1 SD decrement in HbA1c) was associated with reduced risk of T2DM [odds ratio (OR) = 0.66 (95% CI 0.53, 0.82), $P = 1.57 \times 10^{-4}$]; prostate cancer [0.34 (0.23, 0.49), $P = 2.21 \times 10^{-8}$] and prostate-specific antigen [0.26 (0.08, 0.81), $P = 2.07 \times 10^{-2}$]. The effect of SGLT2 inhibition on prostate cancer was mediated by uridine level, with a

Abbreviations: AMPK, AMP-activated kinase; CLSA, Canadian Longitudinal Study on Aging; DIAGRAM, DIAbetes Genetics Replication and Meta-analysis; eQTLs, expression quantitative trait loci; GTEx, Genotype-Tissue Expression; GWAS, genome-wide association study; INTERVEL, Efficiency and safety of varying the frequency of whole blood donation; LD, linkage disequilibrium; MR, Mendelian randomization; MR-PRESSO, Mendelian Randomization Pleiotropy RESidual Sum and Outlier; MVMR, multivariable MR; PRACTICAL, Prostate Cancer Association Group to Investigate Cancer-Associated Alterations in the Genom; PRISM, Profiling Relative Inhibition Simultaneously in Mixtures; PSA, Prostate-Specific Antigen; RNA, Ribonucleic acid; SGLT2, sodium-glucose cotransporter 2; SNPs, single nucleotide polymorphisms; STROBE-MR, Strengthening the Reporting of Observational Studies in Epidemiology Using Mendelian Randomization; T2DM, type 2 diabetes mellitus; TCA, tricarboxylic acid; UTP, uridine 5′-triphosphate; UVMR, univariable Mendelian randomization.

mediated proportion of 9.34% of the total effect. In MR-PheWAS, 65 traits were found to be associated with SLGT2 inhibitors ($P < 1.78 \times 10^{-5}$), and among them, 13 were related to diabetes.

Conclusion: Our study suggested that SGLT2 inhibition could lower prostate cancer risk through uridine mediation. More mechanistic and clinical research is necessary to explore how uridine mediates the link between SGLT2 inhibition and prostate cancer.

KEYWORDS

SGLT2 inhibitor, prostate cancer, uridine, Mendelian randomization, PheWAS

Introduction

Sodium-glucose cotransporter 2 (SGLT2) inhibitors are a type of oral antidiabetic medication that directly removes glucose of the systemic circulation (Heerspink et al., 2016; Brown et al., 2021). Extensive clinical trials have offered strong evidence supporting the positive impact of these interventions on reducing glucose levels, as well as enhancing cardiovascular, heart failure, and renal outcomes (Neal et al., 2017; Wiviott et al., 2019; Cannon et al., 2020; Bhatt et al., 2021). Additionally, emerging evidence indicated their potential of reducing the risk of cancers. A meta-analysis revealed that SGLT2 inhibitors provided a protective effect against cancers compared to a placebo group, with a notable effectiveness observed for dapaglifozin and ertuglifozin (Benedetti et al., 2022). SGLT2 inhibitors were considered as potential anticancer drugs that could slow down the tumor growth of carcinoma expressing SGLT2 (Koepsell, 2017). The expression of SGLT2 has been confirmed at the mRNA level and by immunohistochemistry in prostate cancer (Scafoglio et al., 2015). However, the associations between SGLT2 inhibitors and prostate cancer are controversial and the underlying metabolic mechanism still need further exploring.

Uridine, a pyrimidine nucleoside, is characterized by its high abundance and solubility in the bloodstream. The bioavailability of uridine is crucial for the synthesis of RNA and cell metabolism. For RNA synthesis, uridine 5′-triphosphate (UTP) participates in the process, which is produced by adding a third phosphate group to uridine. For cell metabolism, uracil and beta-alanine engage in the tricarboxylic acid (TCA) cycle, which are the products of the catabolism of uridine (Connolly and Duley, 1999). A study employed nutrient-sensitized genome-wide genetic screens and the Profiling Relative Inhibition Simultaneously in Mixtures (PRISM) growth assay on 482 cancer cell lines, to identify cells capable of tolerating complete glucose deprivation and to elucidate the underlying mechanisms (Skinner et al., 2023). The research revealed a significant upsurge in uridine levels at various stages of prostate cancer, particularly in tissue samples. These findings suggested that cancer cells can harness uridine and its metabolic byproducts for glycolysis, thereby bolstering their growth metabolism, and this capability appears to be widespread. It also suggested that uridine may play a role in the pathogenesis of prostate cancer. As a SGLT2 inhibitor, empagliflozin has been reported to have the potential to upregulate uridine, thereby potentially protecting the kidney (Bangarbale et al., 2022). However, the influence of SGLT2 inhibitors on uridine metabolism remains controversial.

Mendelian randomization (MR) is a relatively vigorous and widely used approach, which uses single nucleotide polymorphisms (SNPs) as genetic instruments to examine the causal association. In this study, genetic colocalization was employed to selected MR instrumental variables that were correlated with drug target mRNA expression (Chen J. et al., 2023; Bakker et al., 2023). The method can be applied to investigate the biological mechanisms of how SGLT2 inhibition affects type 2 diabetes mellitus (T2DM) and prostate cancer (Bouras et al., 2022; Lin et al., 2022). In earlier studies on cardiovascular-related diseases, similar methods have been employed to obtain instrumental variables for exposure and use metabolites as mediators (Xu et al., 2022; Li et al., 2023). Although previous studies have examined the casual association between inflammation factors, lipids, amino acid alterations and prostate cancer, these studies were limited in sample size and the range of metabolites investigated. Therefore, more comprehensive research is needed to explore the relationship between the metabolome and prostate cancer.

In order to investigate the causal link between SGLT2 inhibitors and prostate cancer risk via circulating metabolites or metabolite ratios, we conducted a two-sample, two-step MR study to delve into the hypothetical metabolic pathways that might interconnect the pharmacological action of SGLT2 inhibitors with the development of prostate cancer. The finding would provide insights into the uridine metabolism linking the effect of SGLT2 inhibitors with prostate cancer.

Materials and methods

Study design

The research aims to ascertain if metabolites or metabolite ratios (mediators) play a causal function in facilitating the impact of SGLT2 inhibition on prostate cancer. In this study, we performed a two-sample two-step MR design (Figure 1): Initially, genetic variants representing the effects of SGLT2 inhibition were chosen, followed by the estimation of the causal effects of SGLT2 inhibition on T2DM. Based on that, we further selected prostate cancer as our outcome, and investigating the association between SGLT2 inhibitors and prostate cancer. Then we explored changes in metabolites associated with prostate cancer. In final, we investigated the casual impact of SGLT2 inhibition on prostate cancer related metabolites and calculated mediation effect (Figure 1). The MR analyses fulfilled three core assumptions. First, genetic variants are strongly linked to the outcome. Second,

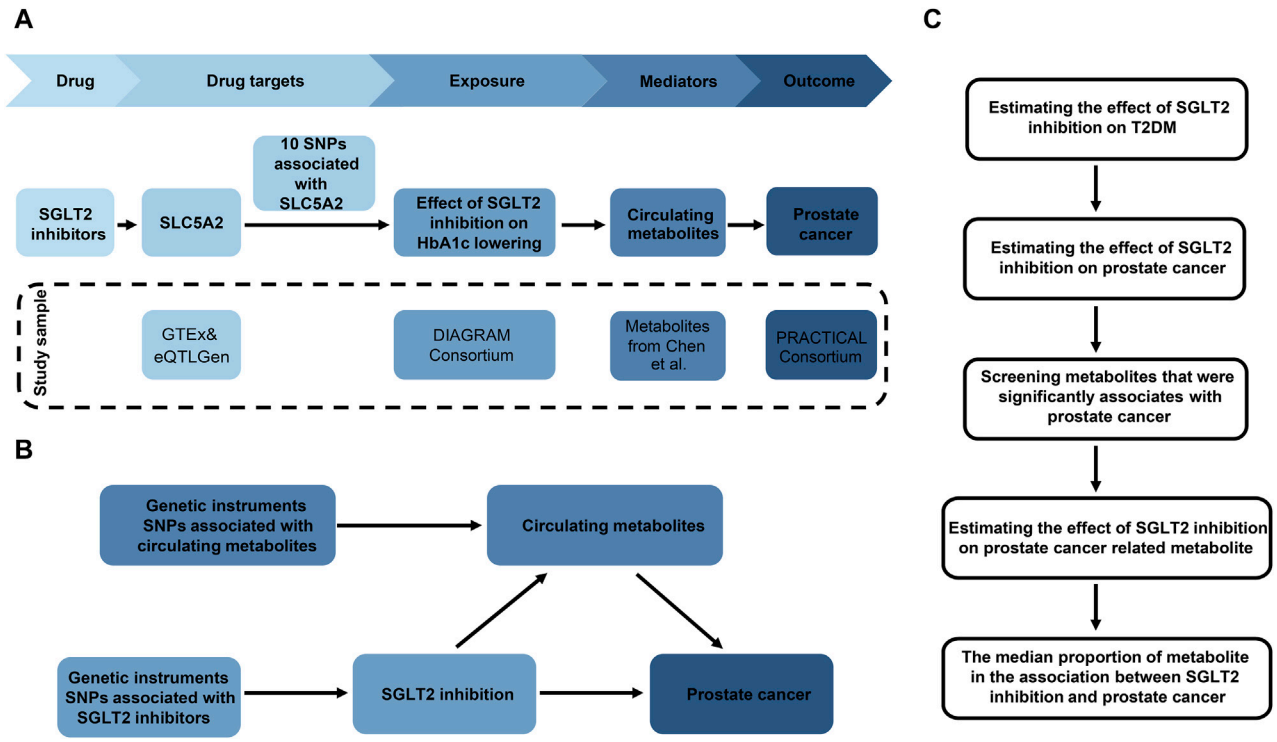

FIGURE 1
Overview of the study design. **(A)** The flowchart of evaluating the effects of circulating metabolites in mediating the effect of SGLT2 inhibition on prostate cancer. **(B)** The framework of the two-step MR. **(C)** Diagram of the two steps of MR models. HbA1c, glycated hemoglobin; SNP, single nucleotide polymorphism.

genetic variants are not influenced by other confounding factors. Third, the impact of genetic variants on the outcome is solely driven by exposure. Our study was conducted following the Strengthening the Reporting of Observational Studies in Epidemiology Using Mendelian Randomization (STROBE-MR) guidelines (Skrivankova et al., 2021).

Data source and genetic instruments for SGLT2 inhibition

The selection of genetic variants serving as proxies for SGLT2 inhibition involved four steps (Figure 1A). 1) Gather GWAS data from the Genotype-Tissue Expression (GTEx) (GTEx Consortium, 2020) and eQTLGen Consortium (Võsa et al., 2021) to identify genetic variants linked to the mRNA expression of SLC5A2 (Supplementary Table S1). 2) Determine the correlation between each SLC5A2 variant and HbA1c levels, which reflect the glucose-lowering impact through SGLT2 inhibition, and identify variants strongly linked to HbA1c ($P < 1 \times 10^{-4}$). The GWAS data for HbA1c level was obtained from UK Biobank (n = 344,182) (Supplementary Table S1). 3) Investigate if SLC5A2 gene and HbA1c level share the same causal variant through colocalization analysis. Colocalization aims to estimate the posterior probability that SLC5A2 expression and circulating HbA1c levels share the same causal variant in specific region (Zuber et al., 2022). Evidence for colocalization (a posterior probability >70%) was defined as significant (Lin et al., 2023). 4) Conduct a standard clumping process, using the 1,000 Genomes European reference panel to select genetic variants in linkage disequilibrium (LD) with an $r^2 < 0.8$ within 1,000 kb. 5) Extract the instrumental variables from the GWAS of HbA1c and obtain the inverse beta values to represent the SGLT2 inhibition.

Data source and genetic instruments for circulating metabolites

In this study, we systematically obtained GWAS data of 1,091 metabolites and 309 metabolite ratios from 8,299 individuals from the Canadian Longitudinal Study on Aging (CLSA) cohort, and uridine was available, named as Uridine (1) (Supplementary Table S1). The GWAS summary statistics of the 1,400 metabolites or metabolite ratios were publicly available through the GWAS Catalog study (https://www.ebi.ac.uk/gwas/) and the accession numbers for European GWASs: GCST90199621-90201020 (Chen Y. et al., 2023). We also gathered another data through the IEU Open-GWAS Project (ID: ebi-a-GCST90026036) (Panyard et al., 2021) (Uridine2) (Supplementary Table S1). Given the limited number of metabolite-associated SNPs, we select SNPs related to metabolites using a relaxed threshold ($P < 1 \times 10^{-5}$, $r^2 < 0.1$, and a 500 kb distance) at first. To mitigate the effect of weak IV bias and sensitivity analysis, we replicated the MR analysis with a strict threshold. We selected SNPs at conventional GWAS thresholds

($P < 5 \times 10^{-8}$), and we excluded SNPs in LD, with an R^2 value greater than or equal to 0.001 and within a 10 mb distance.

Study outcomes

To ascertain the significance of the selected SGLT2 inhibitor, a positive control analysis was conducted using T2DM. We utilized the latest 2024 meta-analyses data on T2DM, from the DIAbetes Genetics Replication and Meta-analysis (DIAGRAM) Consortium. The data conclude all ancestry and we choose European individuals (36 GWAS, 242,283 T2DM cases and 1,569,734 controls) (Suzuki et al., 2023) (Supplementary Table S1). We obtained publicly available GWAS summary data for prostate cancer from the Prostate Cancer Association Group to Investigate Cancer-Associated Alterations in the Genome (PRACTICAL) Consortium (Schumacher et al., 2018) (79,148 prostate cancer cases and 61,106 disease-free controls, European ancestry) (Supplementary Table S1). Prostate-specific antigen (PSA) data were from INTERVAL study (Sun et al., 2018) (2,994 plasma proteins in 3,301 healthy participants) (Supplementary Table S1).

Statistical analyses

MR estimates of SGLT2 inhibition on T2DM and prostate cancer

Two-sample univariable MR (UVMR) was used to assess the influence of SGLT2 inhibition on T2DM, prostate cancer, and PSA. The MR results demonstrated the impact of SGLT2 inhibition on outcomes. An odds ratio (OR) > 1 indicated an increased risk of outcome, while an OR < 1 signified a reduced risk of outcome occurrence. Mendelian Randomization Pleiotropy RESidual Sum and Outlier (MR-PRESSO) was employed to detect and correct potential horizontal pleiotropy and heterogeneity, with the objective of identifying and address outlier genetic variants (Bowden et al., 2018; Verbanck et al., 2018). Firstly, we employed the inverse variance-weighted (IVW) approach as the main analytical method, as it can provide the most accurate and robust estimates, given the assurance that all genetic variants are valid after screening (Bowden et al., 2016; Bowden et al., 2019). Then we utilized the weighted median and MR-PRESSO method to estimate the MR effects, improving numerical performance and stability.

Mediation MR analysis through metabolites or metabolite ratios

Two-step MR was performed to assess how metabolites or metabolite ratios mediated the association between SGLT2 inhibitor use and prostate cancer (Figures 1B, C). We first used UVMR to screen for metabolites significantly correlated with prostate cancer among 1,091 human circulating metabolites and 309 metabolite ratios (β2). Significant MR outputs (0.05/1,400 = 3.57×10^{-5}) were regarded based on a *P*-value <0.05 Bonferroni-corrected for the number of metabolites and metabolite ratios. Metabolite that remained significant after *P*-value adjustment under both lenient and strict criteria was considered as prostate cancer related metabolite. Then, we utilized UVMR to assess the impact of SGLT2 inhibition on prostate cancer related metabolites (β1). The mediation proportion of significant metabolite in the association between SGLT2 inhibition and prostate cancer was calculated as the product of β1 and β2 divided by the total effect of SGLT2 inhibition on prostate cancer (β3). Then, we further performed multivariable MR (MVMR) to evaluate the effect of uridine on prostate cancer after adjusting for the genetic effect of SGLT2 inhibition (β2′). The mediation proportion was calculated as the product of β1and β2′ divided by β3.

Sensitivity analysis

The MR- PRESSO method detects potential outliers and removing these outliers, thus quantifying the presence of pleiotropy during analysis process (Verbanck et al., 2018). The weighted median approach can reliably estimate when over 50% of genetic instruments are valid (Bowden et al., 2016). In MR analysis, we used weighted median and MR-PRESSO approaches to confirm the robustness and reliability of the IVW MR estimates. The effectiveness of the instrument variables was measured using F statistics, with instruments being considered weak if the F statistics were less than 10. The MR-Egger intercept test was used to detect horizontal pleiotropy for MR estimates (Bowden et al., 2015). To assess the heterogeneity between the instruments, Cochrane's Q test and the global test for MR-PRESSO were computed. The MR analysis and sensitivity analysis were performed utilizing the "TwoSampleMR" and "MRPRESSO" packages in R software (version 4.2.1). Meta-analysis was performed through the Reviewer Manager software (Version 5.3). To account for multiple testing, we considered a two-sided *P*-value that met the Bonferroni corrected *P* threshold as statistically significant. For the impact of SGLT2 inhibition on T2DM and prostate cancer-related outcomes, a *P*-value <0.05 was considered statistically significant.

PheWAS analysis

GeneATLAS (http://geneatlas.roslin.ed.ac.uk/) is a comprehensive database utilizing the UK Biobank cohort, encompassing hundreds of traits and millions of variant associations (Canela-Xandri et al., 2018). These associations were computed using 452,264 UK Biobank British white individuals. GeneATLAS includes information on 778 traits (118 quantitative traits and 660 binary traits) and the database allows for querying of GWAS results for 9,113,133 genetic variants and downloading GWAS summary statistics for over 30 million imputed genetic variants, which corresponds to more than 23 billion phenotype-genotype pairs (Canela-Xandri et al., 2018). We searched the GeneATLAS for trait associated with SGLT2 inhibition SNPs. *p* values of traits for each SNP were corrected using the Bonferroni method, setting the threshold for *P* values at 6.43×10^{-6} (0.05/7,780), where 7,780 represented the product of the SNP counts (10) and number of traits (778) queried for each SNP. In addition, we performed MR-PheWAS to explore the potential causal relationship between SGLT2 inhibitors and other diseases. The 2,803 outcomes were obtained from FinnGen consortium R5 release data, including 218,792 individuals and 16,962,023 variants (Kurki et al., 2023). The FinnGen project is a large public-private collaboration that combines genome and health data from 500,000 Finnish biobank participants with digital health records from the Finnish National Health Registers (https://www.finngen.fi/en). IVW was used as the main analytical method and we

Exposure	Outcome	Method	P value	OR (95%CI)	P (Cochran Q)	P (MR-Egger)
SGLT2 inhibition	Type 2 diabetes	Inverse variance weighted	1.57E−04	0.66 (0.53 to 0.82)	0.653	0.261
SGLT2 inhibition	Type 2 diabetes	Weighted median	2.99E−02	0.73 (0.55 to 0.97)		
SGLT2 inhibition	Type 2 diabetes	MR−PRESSO	2.98E−03	0.66 (0.55 to 0.79)		
SGLT2 inhibition	Prostate cancer	Inverse variance weighted	2.21E−08	0.34 (0.23 to 0.49)	0.844	0.384
SGLT2 inhibition	Prostate cancer	Weighted median	4.05E−04	0.39 (0.23 to 0.66)		
SGLT2 inhibition	Prostate cancer	MR−PRESSO	3.35E−05	0.34 (0.23 to 0.49)		
SGLT2 inhibition	Prostate−specific antigen	Inverse variance weighted	2.07E−02	0.26 (0.08 to 0.81)	0.386	0.109
SGLT2 inhibition	Prostate−specific antigen	Weighted median	1.52E−02	0.13 (0.03 to 0.68)		
SGLT2 inhibition	Prostate−specific antigen	MR−PRESSO	4.60E−02	0.26 (0.08 to 0.81)		

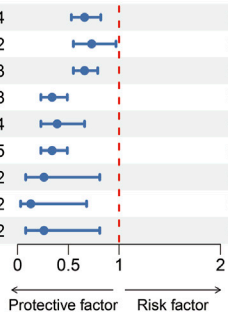

FIGURE 2
MR estimates of the effect of SGLT2 inhibition on T2DM, prostate cancer and prostate specific antigen. OR, odds ratio; SGLT2, sodium-glucose cotransporter 2.

Exposure	Outcome	P value	OR (95%CI)	P (Cochran Q)	P (MR−Egger)
X−17690	Prostate cancer	6.10E−09	0.89 (0.85 to 0.92)	1.34E−04	0.967
X−12798	Prostate cancer	7.14E−09	0.94 (0.92 to 0.96)	1.12E−06	0.136
Cysteinylglycine disulfide	Prostate cancer	4.41E−07	0.94 (0.92 to 0.96)	3.35E−01	0.780
X−21312	Prostate cancer	2.35E−06	0.94 (0.85 to 0.94)	9.95E−06	0.206
Uridine	Prostate cancer	4.12E−06	1.12 (1.07 to 1.18)	2.70E−01	0.843
X−07765	Prostate cancer	5.57E−06	0.89 (0.84 to 0.93)	2.93E−04	0.614
Cys−gly, oxidized	Prostate cancer	1.44E−05	0.96 (0.94 to 0.98)	3.59E−02	0.568
Glucose−to−mannose ratio	Prostate cancer	8.05E−07	1.08 (1.05 to 1.12)	7.81E−02	0.396

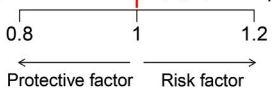

FIGURE 3
MR estimates of the effects of blood metabolites or metabolite ratios on prostate cancer. OR, odds ratio.

also performed MR analysis by MR-Egger and weighted median method. Significant MR-PheWAS outputs were regarded based on a p-value <0.05 Bonferroni-corrected for the number of traits (0.05/2,803 = 1.78×10^{-5}). For Sensitivity analysis, the MR-Egger intercept test and Cochran's Q test was employed to identify horizontal pleiotropy and heterogeneity.

Results

Causal effects of SGLT2 inhibition on T2DM and prostate cancer

Altogether, 10 distinct SNPs were chosen as instrumental variables of SGLT2 inhibition. The F-statistics ranged from 15.897 to 97.893, which indicated sufficient instrument strength for univariable analyses (Supplementary Table S2). Through two-sample MR analysis, we observed an association between SGLT2 inhibition and a reduced risk of T2DM [OR = 0.66 (95% CI 0.53, 0.82), $P = 1.57 \times 10^{-4}$], prostate cancer [0.34 (0.23, 0.49), $P = 2.21 \times 10^{-8}$] and PSA [0.26 (0.08, 0.81), $P = 2.07 \times 10^{-2}$], for per 1 SD lowering of HbA1c via SGLT2 inhibition (Figure 2). The weighted median and MR-PRESSO supported these results. No heterogeneity was detected for the impact of SGLT2 inhibition on T2DM, prostate cancer and PSA ($P = 0.653$; $P = 0.844$; $P = 0.386$), and no evidence of horizontal pleiotropy was found ($P = 0.261$; $P = 0.384$; $P = 0.109$) (Figure 2).

Causal effects of metabolites or metabolite ratios on prostate cancer

We explored the influences of 1,091 metabolites and 309 metabolite ratios on the risk for prostate cancer under the relaxed threshold ($P < 1 \times 10^{-5}$) of instrument variables selection, and results demonstrated that total seven metabolites and one metabolite ratios were significantly linked to prostate cancer (Bonferroni-corrected p-value threshold = 0.05/1,400 = 3.57×10^{-5}) (Figure 3). X-17690, X-12798, X-21312, and X-07765 were currently unidentified metabolites. The result revealed that cysteinylglycine disulfide [OR = 0.94 (95% CI 0.92, 0.96), $P = 4.41 \times 10^{-7}$, Figure 3] and cys-gly, oxidized [0.96 (0.94, 0.98), $P = 1.44 \times 10^{-5}$, Figure 3] could reduce the risk of prostate cancer. Uridine [1.12 (1.07, 1.18), $P = 4.12 \times 10^{-6}$, Figure 3] was identified as the only risk metabolite for prostate cancer that remains significant even after adjustment. Then, the strict threshold was used to choose instrument variables. Interestingly, only the uridine levels remained significant after Bonferroni

TABLE 1 MR estimates of the effect of SGLT2 inhibition on uridine level.

Exposure	Outcome	Method	β (95%CI)	*P*	Q	P_h	Intercept	P_{Int}
SGLT2 inhibition	Uridine (1)	IVW	−0.84 (−1.54, −0.14)	0.018	7	0.601	−0.042	0.987
		WM	−1.02 (−2.00, −0.03)	0.043				
		MR-PRESSO	−0.84 (−1.48, −0.21)	0.031				
	Uridine (2)	IVW	−0.40 (−0.88, 0.08)	0.104	3	0.929	0.008	0.614
		WM	−0.90 (−2.82, 1.02)	0.159				
		MR-PRESSO	−0.40 (−0.70, −0.10)	0.031				

IVW, inverse-variance weighted; *P*h, the *P*-value of Cochrane's Q test; *P*Int, the *P*-value of MR-Egger intercept test; SGLT2, sodium-glucose cotransporter 2; WM, weighted median.

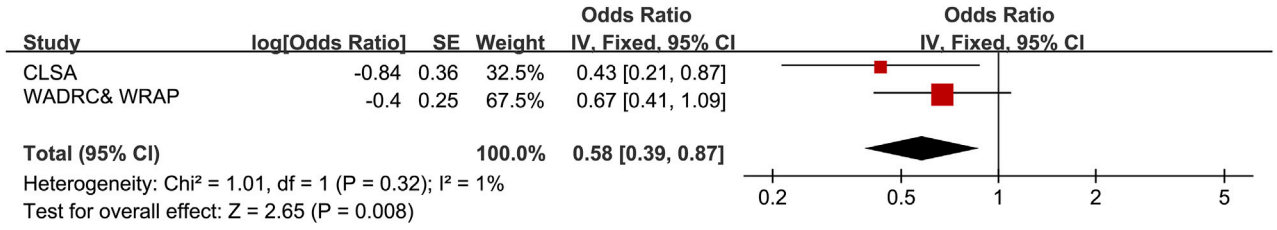

FIGURE 4
Meta-analysis result of the causal associations between SGLT2 inhibition and uridine levels. CLSA, Canadian Longitudinal Study on Aging; WADRC, Wisconsin Alzheimer's Disease Research Center; WRAP, Wisconsin Registry for Alzheimer's Prevention.

corrected and it was considered prostate cancer related metabolite for further analysis.

Causal effects of SGLT2 inhibition on prostate cancer related metabolite

The MR results revealed that SGLT2 inhibition decreased the total concentration of uridine (1) [P = 0.018, β = −0.84 (95% CI −1.54, −0.14), Table 1]. Cochrane's Q test implied no evidence of heterogeneity (Q = 7.352, P = 0.60, Table 1). To further validate the causal association between SGLT2 inhibition and uridine, we included another GWAS dataset of uridine level and conducted a meta-analysis of the MR results. The meta-analysis indicated that SGLT2 inhibition could decrease uridine levels significantly [OR = 0.58 (95% CI 0.39, 0.87), Figure 4]. Based on previous findings, we discovered that uridine level mediated the reduction in prostate cancer risk associated with SGLT2 inhibition, with the mediating effect accounting for 9.07% of the total effect. In MVMR analysis, SGLT2 inhibitor and uridine were still associated with prostate cancer [$OR_{SGLT2\ inhibitor}$ = 0.43 (95% CI 0.24, 0.77), $P_{SGLT2\ inhibitor}$ = 0.005, $OR_{uridine}$ = 1.13 (95% CI 1.08, 1.18), $P_{uridine}$ < 0.001]. And the uridine level had a mediated proportion of 9.34% of the total effect.

PheWAS analysis

We obtained trait associations with prioritized druggable target genes from GeneATLAS, and then we set the threshold for P values at 6.43×10^{-6} (0.05/7, 780). The top 15 traits with the highest number of SNPs associated with them were listed in Supplementary Table S3. The traits most closely related to SGLT2 inhibitors included platelet count, volume, red blood cell distribution width, reticulocyte count, and systemic impedance. These traits can also serve as potential therapeutic indications and targets for SGLT2 inhibitors. In MR-PheWAS, 65 traits associated with SLGT2 inhibitor ($P < 1.78 \times 10^{-5}$, Supplementary Table S4) were identified, with 13 of these traits being linked to diabetes. The use of SGLT2 inhibitors was associated with a reduced risk of benign neoplasms of the meninges, pediculosis, acariasis, scabies, strabismus, and venous thromboembolism. On the other hand, the administration of SGLT2 inhibitors might result in various drug side effects, including endometriosis, psoriasis vulgaris, alcoholic gastritis, and other alcohol-related diseases.

Discussion

In this study, we focused on evaluating the causal associations between SGLT2 inhibition and two main outcomes: T2DM and prostate cancer. Additionally, we explored the metabolites or metabolite ratios related to prostate cancer risk. Our study revealed that genetic variation in SGLT2 inhibition targets was linked to a reduced risk of prostate cancer [0.34 (0.23, 0.49), $P = 2.21 \times 10^{-8}$] and PSA [0.26 (0.08, 0.81), $P = 2.07 \times 10^{-2}$]. The circulating uridine level might mediate 9.07% of the impact of SGLT2 inhibition on prostate cancer.

As a part of another glucose import system for cancer cells, SGLT2 is functionally expressed in several cancer types

(Scafoglio et al., 2015). Large random clinical trials and meta-analysis have indicated that the medicine which can silence or inhibit SGLT2, such like SGLT2 inhibitors, has the potential ability to suppress cancer cell growth. Research has demonstrated that SGLT2 inhibitors exhibit anti-proliferative effects on liver cancer, breast cancer (Shiba et al., 2018; Komatsu et al., 2020). The mechanisms underlying the inhibition of SGLT2 in prostate cancer remain controversial. Glucose is an indispensable metabolic required for cancer cell survival and growth. SGLT2 inhibitors can block the uptake of glucose by cancer cells, thus whether their anti-proliferative effects on tumor cells are mediated through the reduction of glucose concentration requires further evidence for support. Besides, emerging evidence indicate that SGLT2 inhibitors effect the progression and metastasis of prostate cancer cells through metabolic dysregulation, especially mitochondria function. AMP-activated kinase (AMPK), a master regulator of metabolism, its activation led to reduced cancer cell proliferation (Penfold et al., 2023). A random clinical trial indicated that, Canagliflozin, a kind of SGLT inhibitors, can leads to the activation of AMPK (Hawley et al., 2016; Villani et al., 2016). Act as an attractive strategy based on targeting mitochondrial metabolism, Canagliflozin has expressed potential anti-cancer activity for prostate cancer (Ali et al., 2023). Further research is needed to determine whether SGLT2 affects mitochondrial metabolism through the activation of the AMPK pathway, and more research to investigate whether SGLT2 has other potential effects on metabolic pathways that contribute to its anti-cancer effects.

Our study confirmed that SGLT2 inhibitors reduced the total content of uridine in the serum. This finding highlights the lack of research on the impact of SGLT2 inhibitors on pyrimidine metabolism, particularly regarding uridine levels. One study found no significant difference in uridine levels before and after treatment with canagliflozin on the metabolome of liver cancer cells (P = 0.5648) (Nakano et al., 2020). Other studies have mainly discussed the relationship between SGLT2 inhibitors and pyrimidine metabolism, and conclusion remains controversial. An *in vitro* study analyzed the effects of different SGLT2 inhibitors on pyrimidine metabolism (Zügner et al., 2022). The results suggested that treatment with canagliflozin led to an increase in metabolites in the pyrimidine pathway, while the trend was opposite for dapagliflozin and ertugliflozin. An *in vivo* experiment selected 40 type 2 diabetes patients and measured the plasma and urine metabolites after 8 weeks of treatment with a 25 mg dose of the SGLT2 inhibitor empagliflozin. The study results showed that SGLT2 treatment influences pyrimidine metabolism, but changes in UTP levels were not detected (Lu et al., 2022). Further experimental research is needed to investigate whether SGLT2 affects pyrimidine levels in prostate cancer cells and in the plasma metabolites of patients, particularly the influence of uridine.

Given our research findings that SGLT2 inhibitors could reduce uridine levels, and considering that uridine has a positive association with prostate cancer, we hypothesize that the anti-cancer ability of SGLT2 inhibitors may be mediated through uridine. Previous studies have described the characteristics of plasma metabolomics in prostate cancer patients, suggesting a correlation between uridine and PSA metabolism (Markin et al., 2020). Research at the tissue level has confirmed that uridine levels are elevated in prostate tumor tissues compared to adjacent normal control tissues (Ren et al., 2016). The above studies have supported our hypothesis to some extent.

The investigation of whether SGLT2 is worthwhile as a novel anti-pancreatic cancer drug is a promising area for further research. The methods of metabolomics have become more prominent focus for understanding the mechanisms of anti-pancreatic cancer drugs. Proxalutamide is a novel androgen receptor inhibitor currently used in the castration-resistant prostate cancer patients, and it has entered Phase III clinical trials. Research has been conducted to analyze the metabolomics of prostate cancer cells to elucidate the anti-tumor efficacy of Proxalutamide, and results demonstrated that it significantly decreased the intracellular levels of uridine (Qu et al., 2020). Although the study observed significant differences in other metabolites of prostate cancer cells, such as glutamine (a kind of TCA cycle markers), after treatment with Proxalutamide, the results suggest that one of the potential mechanisms of anti-tumor activity of Proxalutamide is the inhibition of pyrimidine synthesis. The study provided support for the potential key role of uridine in the anti-tumor mechanism of SGLT2 inhibitors in prostate cancer. Our study proposes a novel perspective on the potential anti-prostate cancer mechanism of SGLT2 inhibitors, focus on the uridine, providing a theoretical basis for their potential clinical applications in oncology.

Given the potential of SGLT2 inhibitors in preventing prostate cancer, we should not ignore their side effects. A retrospective cohort study found that SGLT2 inhibitors was associated with an approximately three-fold increased risk of genital infections when compared to the use of Dipeptidyl peptidase-4 inhibitors and Glucagon-like peptide-1 receptor agonists (Dave et al., 2019). In addition, SGLT2 inhibitors may lead to other concerns, including cardiovascular safety, acute renal failure, hypoglycemia, volume depletion, volume depletion, euglycemic ketoacidosis, and bone fractures (Scheen, 2019). In our MR-PheWAS analysis, we found SGLT2 inhibitors may lead to some side effects, which provided cautionary notes for the use of SGLT2 inhibitors in the future.

Although previous studies have investigated the impact of SGLT2 inhibitors on prostate cancer using MR, these studies were incomplete and published as research letters. Interestingly, the two studies reported contradictory results: Lin et al. (2024) study suggested a protective effect of SGLT2 inhibitors on prostate cancer, whereas Han et al. (2024) study indicated an increased risk. The reason for the different results obtained from two studies is that the study by Han et al. did not further analyze the instrumental variables' beta values by taking its opposite into consideration, or convert the OR into its reciprocal as the final outcome. Therefore, the conclusion drawn in Han et al. (2024) study is actually the association between SGLT2 activator and prostate cancer. In comparison to previous research, we used T2DM as a positive control, demonstrating the effectiveness of the obtained SGLT2 inhibitor instrumental variables. The T2DM and prostate cancer GWAS data were sourced from the largest genetic studies to date. What's more, our study has the novel findings that SGLT2 was associated with prostate cancer mediated by uridine levels. In our investigation of the relationship between circulating metabolites and prostate cancer, we applied the Bonferroni method to correct P values, ensuring statistical robustness and the reliability of our research findings. Based on SGLT2 inhibitor's instrument variables, we also conducted PheWAS analysis to explore the potential causal relationship between SGLT2 inhibitors and other diseases. What's more, we employed colocalization analysis, a powerful tool in uncovering the pleiotropic effects of certain loci on multiple traits (Zuber et al., 2022).

This approach aids in a better understanding of the genetic architecture underlying complex traits. We have provided evidence for the potential anti-cancer mechanism of SGLT2 inhibitors, indicating that the overall concentration of uridine exerts anti-cancer effects on prostate cancer.

Nevertheless, our study is subject to certain limitations. Firstly, the genetic variations emulating SGLT2 inhibition demonstrate the long-term effects of SGLT2 inhibitors, whereas the SGLT2 inhibitors in prior studies are mainly intended for short-term use (Li et al., 2023). Therefore, whether short-term use of SGLT2 inhibitors actually leads to the same results as lifelong effects needs further exploration in experimental and clinical trials. Although the variety of circulating metabolites data we used is comprehensive, due to the lack of available GWAS of pyrimidines in the cohort, limits our ability to further validate the results of our study (Julkunen et al., 2023). Finally, further research is needed to generalize the results of this study to populations other than individuals of European descent.

Conclusion

In conclusion, this study suggested the causal associations between genetically predicted SGLT2 inhibition, uridine level and prostate cancer. Our findings provide novel insights into the mechanism by which SGLT2 inhibitors reduce the risk of cancer, particularly prostate cancer, and supports further basic and clinical trials of SGLT2 inhibitors in cancer therapy.

Data availability statement

The GWAS Summary statistics used in this study were publicly accessed from the IEU OpenGWAS project (https://gwas.mrcieu.ac.uk/), the GWAS Catalog (https://www.ebi.ac.uk/gwas/), the GTEx Portal (https://www.gtexportal.org/), the eQTLGen Consortium (https://eqtlgen.org/), DIAGRAM consortium (https://diagram-consortium.org/) and PRACTICAL Consortium (http://practical.icr.ac.uk/blog/). Further inquiries can be directed to the corresponding authors.

Author contributions

YL: Conceptualization, Data curation, Formal Analysis, Validation, Visualization, Writing–original draft, Writing–review and editing. YZ: Data curation, Writing–original draft. SW: Data curation, Formal Analysis, Investigation, Visualization, Writing–original draft. LC: Data curation, Writing–review and editing. RZ: Data curation, Writing–review and editing. XM: Data curation, Writing–review and editing. QLY: Data curation, Writing–review and editing. LZ: Conceptualization, Data curation, Writing–review and editing. QMY: Conceptualization, Data curation, Funding acquisition, Writing–review and editing.

Funding

The author(s) declare that financial support was received for the research, authorship, and/or publication of this article. This study received funding from the National Natural Science Foundation of China (grant no. 82303078) and the Beijing Medical Award Foundation (grant no. YXJL-2020-0941-0746).

Acknowledgments

We thank the participants in all the GWASs used in this study and the investigators who made these GWAS data publicly available. We thank the contribution of the PRACTICAL consortium and DIAGRAM consortium for this study.

Conflict of interest

The authors declare that the research was conducted in the absence of any commercial or financial relationships that could be construed as a potential conflict of interest.

Publisher's note

Supplementary material

The Supplementary Material for this article can be found online at: https://www.frontiersin.org/articles/10.3389/fphar.2024.1443045/full#supplementary-material

References

Ali, A., Mekhaeil, B., Biziotis, O. D., Tsakiridis, E. E., Ahmadi, E., Wu, J., et al. (2023). The SGLT2 inhibitor canagliflozin suppresses growth and enhances prostate cancer response to radiotherapy. *Commun. Biol.* 6 (1), 919. doi:10.1038/s42003-023-05289-w

Bakker, M. K., van Straten, T., Chong, M., Paré, G., Gill, D., and Ruigrok, Y. M. (2023). Anti-epileptic drug target perturbation and intracranial aneurysm risk: mendelian randomization and colocalization study. *Stroke* 54 (1), 208–216. doi:10.1161/STROKEAHA.122.040598

Bangarbale, S., Shepard, B. D., Bansal, S., Jayatilake, M. M., Kurtz, R., Levi, M., et al. (2022). Renal metabolome in obese mice treated with empagliflozin suggests a reduction in cellular respiration. *Biomolecules* 12 (9), 1176. doi:10.3390/biom12091176

Benedetti, R., Benincasa, G., Glass, K., Chianese, U., Vietri, M. T., Congi, R., et al. (2022). Effects of novel SGLT2 inhibitors on cancer incidence in hyperglycemic patients: a meta-analysis of randomized clinical trials. *Pharmacol. Res.* 175, 106039. doi:10.1016/j.phrs.2021.106039

Bhatt, D. L., Szarek, M., Pitt, B., Cannon, C. P., Leiter, L. A., McGuire, D. K., et al. (2021). Sotagliflozin in patients with diabetes and chronic kidney disease. *N. Engl. J. Med.* 384 (2), 129–139. doi:10.1056/NEJMoa2030186

Bouras, E., Karhunen, V., Gill, D., Huang, J., Haycock, P. C., Gunter, M. J., et al. (2022). Circulating inflammatory cytokines and risk of five cancers: a Mendelian randomization analysis. *BMC Med.* 20 (1), 3. doi:10.1186/s12916-021-02193-0

Bowden, J., Davey Smith, G., and Burgess, S. (2015). Mendelian randomization with invalid instruments: effect estimation and bias detection through Egger regression. *Int. J. Epidemiol.* 44 (2), 512–525. doi:10.1093/ije/dyv080

Bowden, J., Del Greco, F. M., Minelli, C., Zhao, Q., Lawlor, D. A., Sheehan, N. A., et al. (2019). Improving the accuracy of two-sample summary-data Mendelian randomization: moving beyond the NOME assumption. *Int. J. Epidemiol.* 48 (3), 728–742. doi:10.1093/ije/dyy258

Bowden, J., Smith, G. D., Haycock, P. C., and Burgess, S. (2016). Consistent estimation in mendelian randomization with some invalid instruments using a weighted median estimator. *Genet. Epidemiol.* 40 (4), 304–314. doi:10.1002/gepi.21965

Bowden, J., Spiller, W., Del Greco, M. F., Sheehan, N., Thompson, J., Minelli, C., et al. (2018). Improving the visualization, interpretation and analysis of two-sample summary data Mendelian randomization via the Radial plot and Radial regression. *Int. J. Epidemiol.* 47 (4), 1264–1278. doi:10.1093/ije/dyy101

Brown, E., Heerspink, H. J. L., Cuthbertson, D. J., and Wilding, J. P. H. (2021). SGLT2 inhibitors and GLP-1 receptor agonists: established and emerging indications. *Lancet* 398 (10296), 262–276. doi:10.1016/S0140-6736(21)00536-5

Canela-Xandri, O., Rawlik, K., and Tenesa, A. (2018). An atlas of genetic associations in UK Biobank. *Nat. Genet.* 50 (11), 1593–1599. doi:10.1038/s41588-018-0248-z

Cannon, C. P., Pratley, R., Dagogo-Jack, S., Mancuso, J., Huyck, S., Masiukiewicz, U., et al. (2020). Cardiovascular outcomes with ertugliflozin in type 2 diabetes. *N. Engl. J. Med.* 383 (15), 1425–1435. doi:10.1056/NEJMoa2004967

Chen, J., Xu, F., Ruan, X., Sun, J., Zhang, Y., Zhang, H., et al. (2023a). Therapeutic targets for inflammatory bowel disease: proteome-wide Mendelian randomization and colocalization analyses. *EBioMedicine* 89, 104494. doi:10.1016/j.ebiom.2023.104494

Chen, Y., Lu, T., Pettersson-Kymmer, U., Stewart, I. D., Butler-Laporte, G., Nakanishi, T., et al. (2023b). Genomic atlas of the plasma metabolome prioritizes metabolites implicated in human diseases. *Nat. Genet.* 55 (1), 44–53. doi:10.1038/s41588-022-01270-1

Connolly, G. P., and Duley, J. A. (1999). Uridine and its nucleotides: biological actions, therapeutic potentials. *Trends Pharmacol. Sci.* 20 (5), 218–225. doi:10.1016/s0165-6147(99)01298-5

Dave, C. V., Schneeweiss, S., and Patorno, E. (2019). Comparative risk of genital infections associated with sodium-glucose co-transporter-2 inhibitors. *Diabetes Obes. Metab.* 21 (2), 434–438. doi:10.1111/dom.13531

GTEx Consortium (2020). The GTEx Consortium atlas of genetic regulatory effects across human tissues. *Science* 369 (6509), 1318–1330. doi:10.1126/science.aaz1776

Han, Z., He, Y., Li, X., Li, S., and Ai, J. (2024). Insights into the impact of sodium-glucose cotransporter 2 inhibition on urinary tract malignancy: a two-sample Mendelian randomization. *Diabetes Obes. Metab.* 26 (5), 1986–1989. doi:10.1111/dom.15490

Hawley, S. A., Ford, R. J., Smith, B. K., Gowans, G. J., Mancini, S. J., Pitt, R. D., et al. (2016). The Na+/Glucose cotransporter inhibitor canagliflozin activates AMPK by inhibiting mitochondrial function and increasing cellular AMP levels. *Diabetes* 65 (9), 2784–2794. doi:10.2337/db16-0058

Heerspink, H. J., Perkins, B. A., Fitchett, D. H., Husain, M., and Cherney, D. Z. (2016). Sodium glucose cotransporter 2 inhibitors in the treatment of diabetes mellitus: cardiovascular and kidney effects, potential mechanisms, and clinical applications. *Circulation* 134 (10), 752–772. doi:10.1161/CIRCULATIONAHA.116.021887

Julkunen, H., Cichońska, A., Tiainen, M., Koskela, H., Nybo, K., Mäkelä, V., et al. (2023). Atlas of plasma NMR biomarkers for health and disease in 118,461 individuals from the UK Biobank. *Nat. Commun.* 14 (1), 604. doi:10.1038/s41467-023-36231-7

Koepsell, H. (2017). The Na+-D-glucose cotransporters SGLT1 and SGLT2 are targets for the treatment of diabetes and cancer. *Pharmacol. Ther.* 170, 148–165. doi:10.1016/j.pharmthera.2016.10.017

Komatsu, S., Nomiyama, T., Numata, T., Kawanami, T., Hamaguchi, Y., Iwaya, C., et al. (2020). SGLT2 inhibitor ipragliflozin attenuates breast cancer cell proliferation. *Endocr. J.* 67 (1), 99–106. doi:10.1507/endocrj.EJ19-0428

Kurki, M. I., Karjalainen, J., Palta, P., Sipilä, T. P., Kristiansson, K., Donner, K. M., et al. (2023). FinnGen provides genetic insights from a well-phenotyped isolated population. *Nature* 613 (7944), 508–518. doi:10.1038/s41586-022-05473-8

Li, J., Yu, Y., Sun, Y., Yu, B., Tan, X., Wang, B., et al. (2023). SGLT2 inhibition, circulating metabolites, and atrial fibrillation: a Mendelian randomization study. *Cardiovasc. Diabetol.* 22 (1), 278. doi:10.1186/s12933-023-02019-8

Lin, J., Zhou, J., and Xu, Y. (2023). Potential drug targets for multiple sclerosis identified through Mendelian randomization analysis. *Brain* 146 (8), 3364–3372. doi:10.1093/brain/awad070

Lin, L., Ning, K., Xiang, L., Peng, L., and Li, X. (2024). SGLT2 inhibition and three urological cancers: up-to-date results. *Diabetes Metab. Res. Rev.* 40 (3), e3797. doi:10.1002/dmrr.3797

Lin, Y., Yang, Z., Li, J., Sun, Y., Zhang, X., Qu, Z., et al. (2022). Effects of glutamate and aspartate on prostate cancer and breast cancer: a Mendelian randomization study. *BMC Genomics* 23 (1), 213. doi:10.1186/s12864-022-08442-7

Lu, Y. P., Zhang, Z. Y., Wu, H. W., Fang, L. J., Hu, B., Tang, C., et al. (2022). SGLT2 inhibitors improve kidney function and morphology by regulating renal metabolic reprogramming in mice with diabetic kidney disease. *J. Transl. Med.* 20 (1), 420. doi:10.1186/s12967-022-03629-8

Markin, P. A., Brito, A., Moskaleva, N., Lartsova, E. V., Shpot, Y. V., Lerner, Y. V., et al. (2020). Plasma metabolomic profile in prostatic intraepithelial neoplasia and prostate cancer and associations with the prostate-specific antigen and the Gleason score. *Metabolomics* 16 (7), 74. doi:10.1007/s11306-020-01694-y

Nakano, D., Kawaguchi, T., Iwamoto, H., Hayakawa, M., Koga, H., and Torimura, T. (2020). Effects of canagliflozin on growth and metabolic reprograming in hepatocellular carcinoma cells: multi-omics analysis of metabolomics and absolute quantification proteomics (iMPAQT). *PLoS One* 15 (4), e0232283. doi:10.1371/journal.pone.0232283

Neal, B., Perkovic, V., Mahaffey, K. W., de Zeeuw, D., Fulcher, G., Erondu, N., et al. (2017). Canagliflozin and cardiovascular and renal events in type 2 diabetes. *N. Engl. J. Med.* 377 (7), 644–657. doi:10.1056/NEJMoa1611925

Panyard, D. J., Kim, K. M., Darst, B. F., Deming, Y. K., Zhong, X., Wu, Y., et al. (2021). Cerebrospinal fluid metabolomics identifies 19 brain-related phenotype associations. *Commun. Biol.* 4 (1), 63. doi:10.1038/s42003-020-01583-z

Penfold, L., Woods, A., Pollard, A. E., Arizanova, J., Pascual-Navarro, E., Muckett, P. J., et al. (2023). AMPK activation protects against prostate cancer by inducing a catabolic cellular state. *Cell Rep.* 42 (4), 112396. doi:10.1016/j.celrep.2023.112396

Qu, F., Gu, Y., Wang, Q., He, M., Zhou, F., Sun, J., et al. (2020). Metabolomic profiling to evaluate the efficacy of proxalutamide, a novel androgen receptor antagonist, in prostate cancer cells. *Invest. New Drugs* 38 (5), 1292–1302. doi:10.1007/s10637-020-00901-w

Ren, S., Shao, Y., Zhao, X., Hong, C. S., Wang, F., Lu, X., et al. (2016). Integration of metabolomics and transcriptomics reveals major metabolic pathways and potential biomarker involved in prostate cancer. *Mol. Cell Proteomics* 15 (1), 154–163. doi:10.1074/mcp.M115.052381

Scafoglio, C., Hirayama, B. A., Kepe, V., Liu, J., Ghezzi, C., Satyamurthy, N., et al. (2015). Functional expression of sodium-glucose transporters in cancer. *Proc. Natl. Acad. Sci. U. S. A.* 112 (30), E4111–E4119. doi:10.1073/pnas.1511698112

Scheen, A. J. (2019). An update on the safety of SGLT2 inhibitors. *Expert Opin. Drug Saf.* 18 (4), 295–311. doi:10.1080/14740338.2019.1602116

Schumacher, F. R., Al Olama, A. A., Berndt, S. I., Benlloch, S., Ahmed, M., Saunders, E. J., et al. (2018). Association analyses of more than 140,000 men identify 63 new prostate cancer susceptibility loci. *Nat. Genet.* 50 (7), 928–936. doi:10.1038/s41588-018-0142-8

Shiba, K., Tsuchiya, K., Komiya, C., Miyachi, Y., Mori, K., Shimazu, N., et al. (2018). Canagliflozin, an SGLT2 inhibitor, attenuates the development of hepatocellular carcinoma in a mouse model of human NASH. *Sci. Rep.* 8 (1), 2362. doi:10.1038/s41598-018-19658-7

Skinner, O. S., Blanco-Fernández, J., Goodman, R. P., Kawakami, A., Shen, H., Kemény, L. V., et al. (2023). Salvage of ribose from uridine or RNA supports glycolysis in nutrient-limited conditions. *Nat. Metab.* 5 (5), 765–776. doi:10.1038/s42255-023-00774-2

Skrivankova, V. W., Richmond, R. C., Woolf, B. A. R., Yarmolinsky, J., Davies, N. M., Swanson, S. A., et al. (2021). Strengthening the reporting of observational studies in Epidemiology using mendelian randomization: the STROBE-MR statement. *Jama* 326 (16), 1614–1621. doi:10.1001/jama.2021.18236

Sun, B. B., Maranville, J. C., Peters, J. E., Stacey, D., Staley, J. R., Blackshaw, J., et al. (2018). Genomic atlas of the human plasma proteome. *Nature* 558 (7708), 73–79. doi:10.1038/s41586-018-0175-2

Suzuki, K., Hatzikotoulas, K., Southam, L., Taylor, H. J., Yin, X., Lorenz, K. M., et al. (2023). Multi-ancestry genome-wide study in >2.5 million individuals reveals heterogeneity in mechanistic pathways of type 2 diabetes and complications. medRxiv.

Verbanck, M., Chen, C. Y., Neale, B., and Do, R. (2018). Detection of widespread horizontal pleiotropy in causal relationships inferred from Mendelian randomization between complex traits and diseases. *Nat. Genet.* 50 (5), 693–698. doi:10.1038/s41588-018-0099-7

Villani, L. A., Smith, B. K., Marcinko, K., Ford, R. J., Broadfield, L. A., Green, A. E., et al. (2016). The diabetes medication Canagliflozin reduces cancer cell proliferation by inhibiting mitochondrial complex-I supported respiration. *Mol. Metab.* 5 (10), 1048–1056. doi:10.1016/j.molmet.2016.08.014

Võsa, U., Claringbould, A., Westra, H. J., Bonder, M. J., Deelen, P., Zeng, B., et al. (2021). Large-scale cis- and trans-eQTL analyses identify thousands of genetic loci and polygenic scores that regulate blood gene expression. *Nat. Genet.* 53 (9), 1300–1310. doi:10.1038/s41588-021-00913-z

Wiviott, S. D., Raz, I., Bonaca, M. P., Mosenzon, O., Kato, E. T., Cahn, A., et al. (2019). Dapagliflozin and cardiovascular outcomes in type 2 diabetes. *N. Engl. J. Med.* 380 (4), 347–357. doi:10.1056/NEJMoa1812389

Xu, M., Zheng, J., Hou, T., Lin, H., Wang, T., Wang, S., et al. (2022). SGLT2 inhibition, choline metabolites, and cardiometabolic diseases: a mediation mendelian randomization study. *Diabetes Care* 45 (11), 2718–2728. doi:10.2337/dc22-0323

Zuber, V., Grinberg, N. F., Gill, D., Manipur, I., Slob, E. A. W., Patel, A., et al. (2022). Combining evidence from Mendelian randomization and colocalization: review and comparison of approaches. *Am. J. Hum. Genet.* 109 (5), 767–782. doi:10.1016/j.ajhg.2022.04.001

Zügner, E., Yang, H. C., Kotzbeck, P., Boulgaropoulos, B., Sourij, H., Hagvall, S., et al. (2022). Differential *in vitro* effects of SGLT2 inhibitors on mitochondrial oxidative phosphorylation, glucose uptake and cell metabolism. *Int. J. Mol. Sci.* 23 (14), 7966. doi:10.3390/ijms23147966

frontiers | Frontiers in Pharmacology

TYPE Review
PUBLISHED 29 August 2024
DOI 10.3389/fphar.2024.1448872

OPEN ACCESS

EDITED BY
Lei Yin,
Shanghai Jiaotong University School of Medicine, China

REVIEWED BY
Wei-jia Wang,
Xiamen University, China
Zhengyan Chang,
Tongji University, China

*CORRESPONDENCE
Ronghao Wang,
gmack@163.com
Bo Cheng,
cb1949@swmu.edu.cn

RECEIVED 14 June 2024
ACCEPTED 14 August 2024
PUBLISHED 29 August 2024

CITATION
Cao Y, Jia M, Duan C, Yang Z, Cheng B and Wang R (2024) The m^{6}A regulators in prostate cancer: molecular basis and clinical perspective.
Front. Pharmacol. 15:1448872.
doi: 10.3389/fphar.2024.1448872

The m^{6}A regulators in prostate cancer: molecular basis and clinical perspective

Yu Cao[1], Man Jia[1], Chunyan Duan[1], Zhihui Yang[2], Bo Cheng[3]* and Ronghao Wang[1]*

[1]Department of Biochemistry and Molecular Biology, School of Basic Medical Sciences, Southwest Medical University, Luzhou, China, [2]Department of Pathology, The Affiliated Hospital of Southwest Medical University, Luzhou, Sichuan, China, [3]Department of Urology, The Affiliated Hospital of Southwest Medical University, Luzhou, Sichuan, China

Prostate cancer (PCa) is the second leading cause of cancer-related death among men in western countries. Evidence has indicated the significant role of the androgen receptor (AR) as the main driving factor in controlling the development of PCa, making androgen receptor inhibition (ARI) therapy a pivotal management approach. In addition, AR independent signaling pathways also contribute to PCa progression. One such signaling pathway that has garnered our attention is N6-Methyladenosine (m^{6}A) signaling, which refers to a chemical modification on RNA with crucial roles in RNA metabolism and disease progression, including PCa. It is important to comprehensively summarize the role of each individual m^{6}A regulator in PCa development and understand its interaction with AR signaling. This review aims to provide a thorough summary of the involvement of m^{6}A regulators in PCa development, shedding light on their upstream and downstream signaling pathways. This summary sets the stage for a comprehensive review that would benefit the scientific community and clinical practice by enhancing our understanding of the biology of m^{6}A regulators in the context of PCa.

KEYWORDS

PCa, N6-Methyladenosine, androgen deprivation therapy (ADT), androgen recepter, signaling pathway

1 Introduction

Prostate cancer (PCa), a malignancy originating from epithelial cells in the peripheral zone of prostate (Zhou et al., 2023), remains the second commonly diagnosed adenocarcinoma and the leading cause of cancer related deaths among men worldwide. The World Cancer Research Fund International survey estimated that 1,467,854 new cases of PCa were reported globally in 2022, resulting in approximately 397,430 deaths (Bray et al., 2024). Epidemiological studies have established that age (Godtman et al., 2022; Choi et al., 2018), race (Akaza et al., 2011; Jeong et al., 2016) and genetic factors (Bratt, 2002; Rebbeck, 2017; Thalgott et al., 2018) as the significant risk factors for PCa. PCa progresses through four stages, as determined by digital rectal examination (DRE) (Mottet et al., 2017), serum prostate specific antigen (PSA) level (Mottet et al., 2017) and pathological examination of biopsy samples (Kwon et al., 2020). Generally, low-grade and early localized PCa patients (PSA ≤10, Gleason score ≤6, or clinical stage T1-2a) are often managed by either radiotherapy or surgery. However, approximately 8% of PCa patients are viewed as advanced

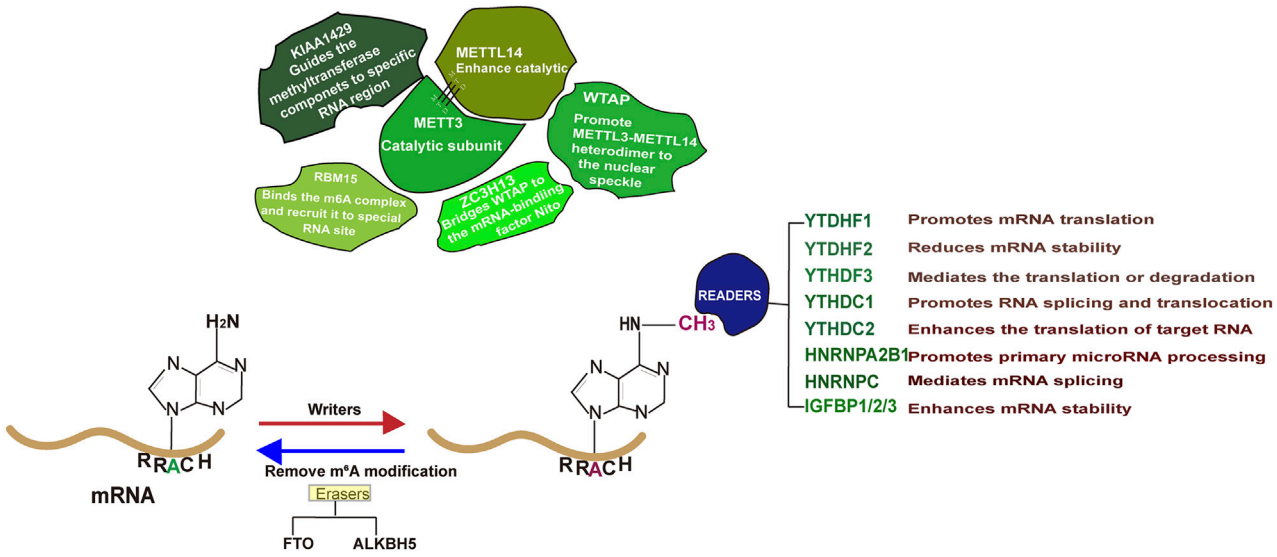

FIGURE 1
The general role of each individual m^{6}A regulator in RNA metabolism.

disease at their first diagnosis (Siegel et al., 2022). The cancer cells may spread from the prostate to other parts of the body, particularly the bones (Peng et al., 2017) and lymph nodes (Cai et al., 2011). In advanced stage, it may lead to urinary difficulty, hematuria, or pelvic pain. Targeting the androgen receptor (AR) signaling axis with androgen deprivation therapy (ADT) has been a primary treatment approach, showing favorable outcome (Dai et al., 2017; Davies et al., 2021; Guan et al., 2022; Jeon et al., 2023). Unfortunately, ADT is not curative and most patients will relapse within 2 years despite the low castrated level of serum testosterone. These patients are then considered to acquire castration-resistant PCa (CRPC), a highly lethal disease that accounts for the main mortality (Shigeta et al., 2019; Cai et al., 2023; Cheng et al., 2022; Wang et al., 2023a). Increasing evidence suggest that the reactivation of AR signaling plays a critical role in CRPC development, leading to the clinical approval of the second-generation AR antagonists such as enzalutamide (Enz) for managing this disease (de Bono et al., 2011; Agarwal et al., 2023; Powles et al., 2022; Wenzel et al., 2022). Despite the initial responses to this therapy, patients will eventually become Enz resistance owing to various mechanisms (Bennett et al., 2024; Liu et al., 2019; Zhang et al., 2020; Zheng et al., 2022). Additionally, approximately 30% of patients exhibit primary resistance to Enz treatment. These clinical findings collectively indicate limitations in the application of Enz.

Although AR is the main driving force for PCa progression, other signaling pathways, such as m^{6}A signaling, are also involved in the regulation of PCa carcinogenesis and therapy resistance (He et al., 2022; Han et al., 2023). This review aims to comprehensively summarize the current understanding of the roles of RNA m^{6}A regulators in PCa development and offer insights for further scientific research and clinical strategies.

2 Epitranscriptome and RNA m^{6}A modification

Epitranscriptome, a biochemical modification on RNA, has received significant attention from scientists due to its critical roles in determining RNA metabolism as well as disease progression (Murakami and Jaffrey, 2022; Wang Y. et al., 2014; He et al., 2018; Bokar et al., 1997; Clancy et al., 2002; Sommer et al., 1978; Zhong et al., 2008). It is estimated that over 170 types of biochemical modifications occur in RNAs, with m^{6}A as the major form (Wiener and Schwartz, 2021). Early identified in 1970s, m^{6}A, the methyl-nitrogen at the position six of adenylate (Figure 1), has been reported to be functional (Wei et al., 1976; Desrosiers et al., 1974). The enzyme responsible for catalyzing RNA m^{6}A modification, known as "Writer," includes methyltransferase-like protein 3 (METTL3), METTL16, METTL5 and zinc finger CCHC type containing 4 (ZCCHC4) (Jiang et al., 2021). Among them, METTL3 methyltransferase complex, consisting of METTL3, METT14, WTAP (Wilms tumor 1 associated protein), Zinc finger CCCH-type containing 13 (ZC3H13), RNA-binding motif protein 15 (RBM15) and VIRMA (Vir Like M6A Methyltransferase Associated), is mainly responsible for the RNA m^{6}A modification on the consensus sequence DRACH (D = A/G/U, R = A/G, H = A/C/U) (Linder et al., 2015; Zaccara et al., 2019; Huang et al., 2022; Raj et al., 2022; Wei et al., 2022; Ma et al., 2019). It is noting that the m^{6}A modification is a reversible process and the methyl group can be removed by demetyltransferase (Eraser) such as obesity-associated protein (FTO) and Human AlkB homolog H5 (ALKBH5) (He et al., 2019). Once an RNA molecule is m^{6}A modified, it becomes prone to recognition by a variety of proteins (Readers) and undergoes distinct fate (Zaccara et al., 2019). In general, m^{6}A modification on mRNA enables to influence its splicing, stability or translation. Recent advances in this area suggest that m^{6}A regulators play vital roles in various human cancers, including PCa (Zhu W. et al., 2023).

TABLE 1 The m^{6}A targets in PCa.

Regulators	Target	m^{6}A site	Reader	Biological consequence
METTLE3	c-Myc	NA	NA	Increase c-Myc mRNA transcription
	USP4	3′-UTR	YTHDF2	Increase USP4 mRNA degradation
	LEF1	NA	IGF2BP2	Increase LEF1 protein level
	Gli	NA	NA	Increase Gli protein level
	KIF3C	NA	IGF2BP1	Increase KIF3C mRNA stability
	ITGB1	NA	NA	Increase ITGB1 mRNA stability
	CTNNB1	3′-UTR	NA	Decrease CTNNB1 mRNA stability
	NAP1L2	NA	HNRNPC	Increase NAP1L2 mRNA stability
	HRAS	3′-UTR	IGF2BP2	Increase mRNA stability
	MEK2	5′-UTR	IGF2BP2	Promote protein transcription
	AR	3′-UTR	YTHDF3	Regulate AR spling
	CLIC4	3′-UTR	NA	Increase CLIC4 mRNA stability
	ERG2	NA	NA	Increase ERG2 mRNA stability
	PLK1	3′-URT	YTHDF1	Increase PLK1 mRNA transcripotion
	LHPP	NA	YTHDF2	Increase LHPP mRNA degradation
	NKX3-1	NA	YTHDF2	Increase NKX3-1 mRNA degradation
	PRMT6	NA	NA	Stability
	SIAH1	NA	NA	Increase SIAH1 mRNA degradation
	ARHGDIA	NA	NA	Increase ARHGDIA mRNA stability by regulating ELAVL1 expression
	PCAT6	NA	IGF2BP2	Increase PCAT6 mRNA stability
	lncRNA SNHG7	NA	NA	Increase SNHG7 RNA stability
	lncRNA NEAT1	5′-UTR 3′UTR	NA	Increase NEAT1 RNA stability
	lncR MALAT1	NA	NA	Increase MALATI RNA stability
	lncR PVT1	NA	NA	Increase PVT1 RNA stability
	miR-139-5p	NA	NA	Increase miR-139-5p RNA stability
	pre-miR-25	NA	HNRNPA2B1	Promote pre-miR-25 maturation
	pre-miR-93	NA	HNRNPA2B1	Promote pre-miR-93 maturation
	miR-148-3p	NA	NA	Promote pre-miR-148-3p maturation
	circDDIT4	3′-UTR 5′-UTR	NA	Promote circDDIT4 circularization
	circABCC4	NA	IG2BP2	Increae circABCC4 RNA stability
	circRBM33	NA	NA	NA
METTL14	THBS1	NA	YTHDF2	Increase THBS1 mRNA degradatiom
FTO	CLIC4	3′-UTR	NA	Increase CLIC4 mRNA stability
	MC4R	3′-UTR	NA	Increase MC4R mRNA degradation
	ERG2	NA	NA	Increase ERG2 mRNA stability
	miR-139-5p	NA	NA	Increase miR-139-5p stability
	DDIT4	3′-UTR	IGFBP2/3	Increase DDIT4 mRNA stability
	ZFHX3	NA	—	Increase the stability of ZFHX3 transcripts

(Continued on following page)

TABLE 1 (*Continued*) The m^{6}A targets in PCa.

Regulators	Target	m^{6}A site	Reader	Biological consequence
ALKBH5	SIAH1	NA	NA	Increase SIAH1 mRNA degradation
	PRMT6	NA	NA	Suppress PRMT6 level
IGF2BP1/2/3	LEF1	NA	—	Increase LEF1 protein level
	LDHA	3′-UTR	—	Increase LDHA mRNA stability
	IGF1R	NA	—	Icrease IGF1R mRNA stability via PCAT6/IGF2BP2 complex
	HMGCS1	NA	—	Increase HMGCS1 mRNA stability
	HDAC4	NA	—	Increase HDAC4 mRNA stability
YTHDF1	PLK1	3′-UTR	—	Increase PLK1 mRNA transcripotion
	TRIM44	NA	—	Increase TRIM44 level
YTHDF2	USP4	3′-UTR	—	Increase USP4 mRNA degradation
	MOB3B	NA	—	Increase MOB3B mRNA degradation
	LHPP	NA	—	Increase LHPP mRNA degradation
	NKX3-1	NA	—	Increase NKX3-1 mRNA degradation
	PRSS8	NA	—	Increase PSRR8 mRNA degradation
YTHDC1	CD44	NA	—	Increase CD44 splicing
	HOBX13	NA	—	Increase HOBX13 mRNA stability
HNRNPA2B1	miR-93-5p	NA	—	Promote pre-miR-93 maturation
	miR-25-3p	NA	—	Promote pre-miR-25 maturation

Studies have demonstrated that m^{6}A level in PCa is disease stage dependent and m^{6}A regulators are causally related to PCa growth, metastasis and targeted therapy resistance (Lothion-Roy et al., 2022). Therefore, there is a need to comprehensively summarize the molecular basis of m^{6}A regulator mediated PCa carcinogenesis, which will definitely provide valuable insights for future scientific investigations and clinical applications.

2.1 METTL3/METTL14 m^{6}A writer in PCa

METTL3/METTL14 methyltransferase complex is primarily responsible for the m^{6}A modification of RNAs (Wang P. et al., 2016; Wang X. et al., 2016; Śledź and Jinek, 2016; Choe et al., 2018; Geula et al., 2015; Lin et al., 2016). Several studies have demonstrated that the expression levels of METTL3 and METTL14 are elevated in PCa as compared to normal tissues, acting as tumor promoting driver (Xu and Ge, 2022). Additionally, castration resistance perpetuates the increased expression levels of these two proteins (Wu et al., 2021). Supported by *in vitro and in vivo* evidence, METT3 complex promotes PCa growth and metastasis via catalyzing m^{6}A modification of various mRNAs and non-coding RNAs (ncRNAs).

2.1.1 The targets and biological functions of METTL3 in PCa

Advance in this field has led to the identification of a wide range of m^{6}A targets. To date, mRNAs including c-Myc (Liu et al., 2022), USP4 (Chen et al., 2021a), LEF1 (Ma et al., 2020), DDIT4 (Zhao Y. et al., 2024), PRSS8 (Zhao X. et al., 2024), ZFHX3 (Hu et al., 2024) and others have been viewed as m^{6}A targets in PCa (Table 1). In addition, ncRNAs, a class of RNAs without protein coding potential but proven to be physiologically and pathologically functional in a variety of disease models, are also potential targets of METTL3 complex in PCa. Specifically, lncRNAs (NEAT1 (Wen et al., 2020), MALAT1 (Mao et al., 2022), SNHG7 (Liu et al., 2022), PVT1 (Chen B. et al., 2023)), miRNAs (miR-139-5p (Azhati et al., 2023), pre-miR-25 (Qi et al., 2023), pre-miR-93 (Qi et al., 2023), miR-148-3p (Li G. et al., 2023)) and circRNAs (circDDIT4 (Kong et al., 2023), circABCC4 (Huang C. et al., 2023), circRBM33 (Zhong et al., 2023) and hsa_circ_0003258 (Yu et al., 2022)) have been reported as the substrates of METTL3. The m^{6}A modification site, the RNA fate, the specific reader and the biological consequence of each individual RNA molecule are summarized and listed in Table 1. The literature illustrate a high expression level of METTL3 in PCa, implying it may contribute to PCa development. Indeed, by catalyzing m^{6}A modifications of RNAs, METTL3 promotes PCa survival, metastasis and therapy resistance. For example, ubiquitin-specific protease 4 (USP4) was identified by Chen et al. as one target of METTL3 by the m^{6}A-RIP (RNA immunoprecipitation) qPCR. Upon being m^{6}A modified at the A2696, USP4 mRNA is recognized by YTH N (6)-Methyladenosine RNA Binding Protein 2 (YTHDF2) and undergoes degradation, subsequently leading to the protein degradation of ELAV like RNA-binding protein 1 (ELAV1). As a consequence, METTL3 mediated ELAV1 degradation increases ARHGDIA expression and promotes PCa growth and metastasis.

Thus, targeting METTL3 by shRNAs powerfully attenuated PCa development *in vitro and in vivo* (Chen et al., 2021a).

METTL3 has also been implicated in the regulation of glycolysis in PCa by adding methyl groups to lncRNA SNHG7, thereby enhancing its stability. Consequently, SNHG7 interacts with SRSF1 to promote the expression of c-Myc, a transcription factor related to glycolysis by regulating the expression of various genes (Liu et al., 2022). Furthermore, Li et al. observed an increased level of METTL3 in enzalutamide resistant PCa cells, implying it may be a causal factor determining enzalutamide resistance. Indeed, METTL3 could activate MAPK signaling via catalyzing the m^{6}A modifications of HRAS and MEK2 mRNAs to bypass AR inhibition therapy (Li Y. et al., 2023). Based on this, we can envision a potential combined therapy involving enzalutamide and a specific METTL3 inhibitor for the treatment of CRPC patients.

To summarize, METTL3 plays a tumor promoting role in PCa progression and targeted therapy resistance at least by catalyzing some oncogenes (c-Myc) (Liu et al., 2022) and core component of multiple signaling pathways including WNT signaling (CTNNB1) (Zhang S. et al., 2023), Hedgehog signaling (Gli) (Cai et al., 2019), MAPK signaling (HRAS, MEK2) (Li Y. et al., 2023). Whether METTL3 has an impact on other signaling pathways that influence PCa remains to be further explored through the continuous identification of its targets.

2.1.2 The role of METTL14 in PCa

As a critical component of METTL3 complex (Liu et al., 2014), METTL14 is also clinically correlated to PCa prognosis. Functionally, METT14 increases PCa proliferation *in vitro and in vivo*, largely through its regulation of thrombospondin 1 (THBS1) mRNA based on the analysis of RNA-seq and MeRIP (Methylated RNA Immunoprecipitation)-seq. Mechanistically, the m^{6}A mark of THBS1 mRNA in the presence of METTL14 is recognized by YTHDF2, predisposing THBS1 mRNA to degrade (Wang Y. et al., 2022). However, in our opinion, the observed phenotype caused by METTL14 knockdown may be METTL3 complex dependent since the main role of METTL14 is to enhance METTL3 activity. It is anticipated that METTL14 deficiency severely impairs the enzymatic activity of METTL3 complex, leading to abnormal m^{6}A modifications and impeding PCa growth. Nevertheless, it is plausible that METTL14 may have a METTL3 complex independent role in PCa, and this hypothesis can be tested by proposing experiments in METTL13-KO cells.

2.1.3 Other m^{6}A writers in PCa

METTL16, another methyltransferase responsible for the m^{6}A modifications of snRNAs and some lncRNAs (Pendleton et al., 2017; Shima et al., 2017; Warda et al., 2017), has not been investigated in PCa yet. It is noteworthy that the splicing events in PCa, especially CRPC, are highly active, leading to the generation of splicing products such as androgen receptor variant 7 (ARv7). Given the facts that 1) METTL16 is a m^{6}A writer of *MALAT1* (Ruszkowska et al., 2018); 2) *MALAT1* mediated ARv7 signaling contribute to enzalutamide resistance (Wang et al., 2017), it would be interesting enough to explore the potential connections of METTL16 with anti-androgen resistance. Besides, whether METTL5 and ZCCHC4, the enzymes adding methyl group to ribosome RNAs (rRNAs), play contributing roles in PCa development is worthy of future investigations (van Tran et al., 2019).

2.2 M^{6}A eraser

As mentioned above, it is important to note that m^{6}A modification is a reversible process. FTO and ALKBH5 are the two well-known demethylases responsible for the removal of m^{6}A in RNA molecule.

2.2.1 FTO in PCa

FTO was initially viewed as a demethylase of methylated DNAs (Gerken et al., 2007). However, subsequent studies have unraveled its preference for selecting RNAs, especially snRNAs (small nuclear RNAs), as substrates. Specifically, FTO recognizes m^{6}A$_m$ (N6,2′-O-dimethyladenosine) in snRNAs and removes the methyl base (Wei et al., 2018; Mauer et al., 2017; Mauer et al., 2019) (Figure 2). Nevertheless, upcoming evidence suggests that FTO also holds a weak activity towards m^{6}A, indicating its abnormal expression may impair the mRNAs metabolism (Li Y. et al., 2022).

FTO is expressed at a lower level in PCa as compared to normal prostate tissues (Zhu et al., 2021). Moreover, PCa patients with low FTO expression often experience advanced disease and poor survival, suggesting that it acts as a tumor suppressor during PCa development (Wang Z. et al., 2022). Indeed, FTO depletion remarkably facilitates PCa malignancy *in vitro and in vivo* by increasing the total m^{6}A level. Mechanistically, the loss of FTO increases the m^{6}A levels of chloride intracellular channel 4(CLIC4) and ERG2, which are two tumor suppressors in PCa, accelerating their degradation (Zou et al., 2022). Moreover, melanocortin 4 receptor (MC4R), identified as another substrate of FTO in PCa, exhibits a high expression level owing to its abundant m^{6}A mark resulting from FTO loss (Li and Cao, 2022). A recent literature has also demonstrated that FTO enables to decrease Zinc Finger Protein (ZNF217) expression by stabilizing miR-139-5p level via an m^{6}A dependent manner. Consequently, FTO mediated ZNF217 reduction inactivates PI3K/AKT/mTOR signaling, impeding PCa progression. Collectively, these results suggest that FTO exerts a tumor-suppressing role in PCa progression via altering the m^{6}A level of a specific RNA population (Figure 2). Intriguingly, the biological function of FTO is cancer context dependent. For instance, in renal cell carcinoma (Zhang et al., 2022), bladder cancer (Tao et al., 2021), breast cancer (Xu et al., 2020) and leukemia (Li et al., 2017), FTO functions as a tumor promoting factor. We postulate that the targets of FTO in different cancer models vary and determine the its functional identity. Therefore, it will be necessary to devote more efforts to identify the substrates of FTO in order to fully understand its biology in PCa.

2.2.2 ALKBH5 in PCa

ALKBH5, a member of the ALKB Family, specifically catalyzes the removal of the m^{6}A modification on small nuclear RNAs (Figure 2). In contrast to FTO, ALKBH5 does not exhibit activity towards m^{6}A$_m$ (Mauer et al., 2017; Mauer et al., 2019; Koh et al., 2019). Despite appearing to be an oncogene in cancer development due to its reported induction by hypoxia (Dong et al., 2021; Thalhammer et al., 2011), ALKBH5 actually functions to

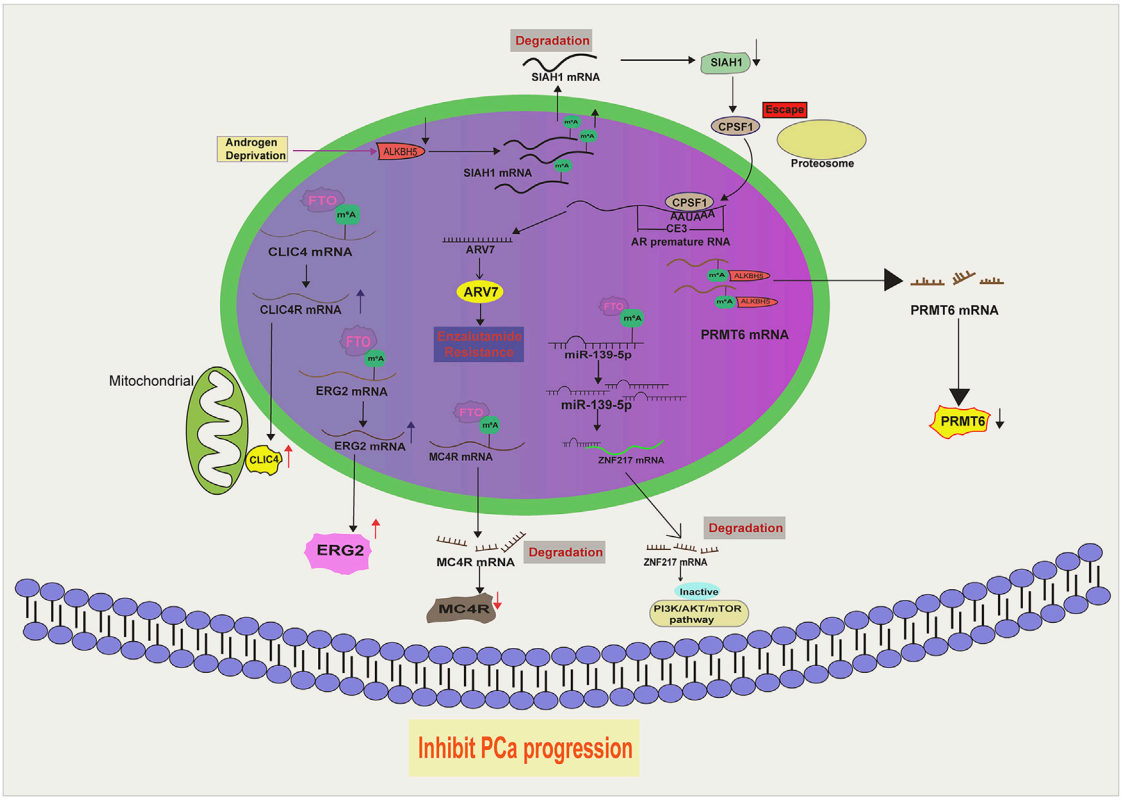

FIGURE 2
The molecular basis of FTO and ALKB5 in PCa.

attenuate PCa growth. A study by Li et al. revealed that ALKBH5 has a marginal expression in PCa tissues and its overexpression apparently suppresses PCa cell growth and cell invasion via reducing the expression level of protein arginine methyltransferase 6 (PRMT6) via an m^{6}A dependent manner (Li X. et al., 2023) (Figure 2). Similarly, Xia et al. (2022) observed a reduction of ALKBH5 in PCa cells with androgen deprivation. Consequently, SIAH1 mRNA is degraded due to the elevated m^{6}A level resulted from the reduction of ALKBH5. Being a target of SIAH1, cleavage and polyadenylation specificity factor 1 (CPSF1) evades the proteosomal degradation and binds to the enriched AAUAAA sequence in the CE3 (cryptic exon 3) region of the AR premature mRNA, thereby facilitating its splicing to ARv7, a potent AR variant playing a critical role in castration resistance (Figure 2). These evidence suggest that ALKBH5 is a tumor suppressor in PCa. Again, the identification of ALKBH5 targets should be pursued if we want to fully understand its PCa associated biology. Potentially, an ALKBH5 agonist, if available in the future, may offer clinical benefits for PCa patients.

2.3 M^{6}A readers

2.3.1 YTHDF family proteins

The YTHDF family consists of YTHDF1, YTHDF2 and YTHDF3 (Patil et al., 2018). Although sharing similar identity at the amino acid sequence, they have distinct biological effects on their targets (Patil et al., 2018; Chen L. et al., 2023). An early study has demonstrated that YTHDF1 binds to the m^{6}A modified 3′-UTR of mRNAs, enhancing their translation (Wang et al., 2015; Wang X. et al., 2014). In contrast, YTHDF2 binds to its targets, leading to their instability and degradation (Li et al., 2020). While YTHDF3 has the capacity to influence both translation and stability of its bound targets (Shi et al., 2017).

Li et al. (2021) demonstrated that YTHDF1 exhibits high expressionin in PCa and its level is correlated with disease prognosis. Knockdown of YTHDF1 significantly represses PCa survival, migration and invasion by regulating tripartite motif containing 44 (TRIM44) (Figure 3). Agreeably, another literature also suggested that YTHDF1, which is transcriptionally controlled by ELK1, facilitates PCa development *in vitro* and *in vivo* by activating polo-like kinase1 (PLK1) mediated PI3K-AKT signaling. Mechanistically, YTHDF1 binds to the m^{6}A modified 3′-UTR of PLK1 mRNA and enhances its translation (Li P. et al., 2022) (Figure 3). YTHDF2 is also increased in PCa and its high expression indicates a poor overall survival. YTHDF2 exerts its oncogenic effect at least by mediating the instability and degradation of Phospholysine Phosphohistidine Inorganic Pyrophosphate Phosphatase (LHPP) and Homeobox Protein NK-3 Homolog A (NKX3–1) mRNAs, leading to the activation of AKT signaling and PCa progression (Li et al., 2020) (Figure 3). Therefore, upregulation of YTHDF2 via Lysine Demethylase 5A (KDM5A) mediated miR-495 reduction could drive PCa progression *in vitro and in vivo* (Du et al., 2020) (Figure 3). As another YTHDF family protein,

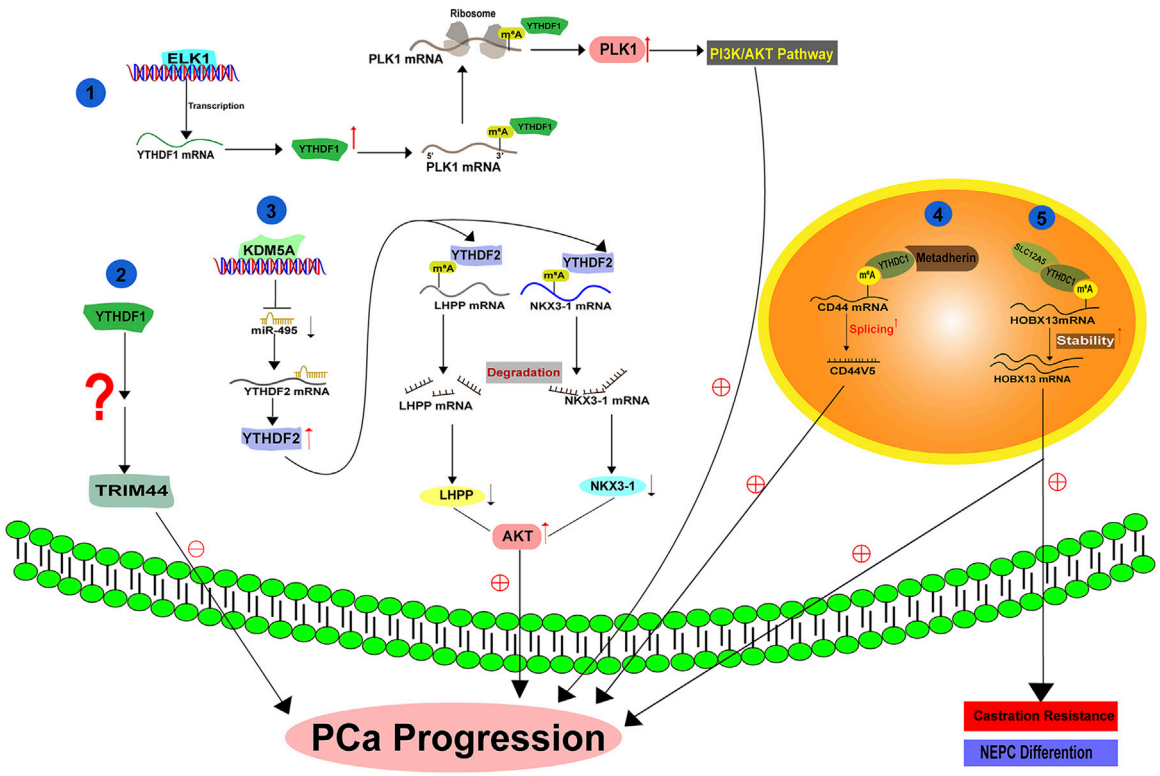

FIGURE 3
The molecular basis of YTH family protein in PCa.

YTHDF3 has not been functionally characterized in PCa. A recent literature has illustrated that YTHDF3 can bind the m^{6}A modified AR mRNA and increase its translation in PCa cells (Somasekharan et al., 2022) (Figure 3). Given the significance of AR in PCa, it is tempting to hypothesize that YTHDF3 may act as an oncogenic protein to facilitate PCa growth, although this hypothesis requires experimental supports.

2.3.2 YTHDC1 and YTHDC2 in PCa

Primarily localized in the nucleus (Hartmann et al., 1999), YTHDC1 has been reported to regulate the splicing and nuclear export of the targets with m^{6}A modification (Widagdo et al., 2022; Roundtree et al., 2017). The splicing activity of YTHDC1 is attributed to its association with serine and arginine-rich splicing factor 3 (SRSF3), an important splicing factor that regulates exon inclusion (Xiao et al., 2016). A recent study by Cheng et al. (2021) reported that YTHDC1 undergoes phase separation to control gene expression via various means, suggesting its diverse biological functions. In PCa, YTHDC1 interacts with the oncogene protein MTDH (Metadherin), facilitating the generation of splicing product CD44v5 and promoting PCa malignancy (Luxton et al., 2019) (Figure 3). In addition, YTHDC1 can also complex with SLC12A5 (a neuron-specific potassium-chloride co-transporter) and enhance its oncogenic function. As a result, YTHDC1-SLC12A5 complex promotes PCa progression, castration resistance and neuroendocrine differentiation by recognizing and stabilizing m^{6}A modified Homeobox B13 (HOXB13) mRNA (Yuan et al., 2023) (Figure 3). Considering the highly active splicing process during the progression of PCa to an advanced stage, we surmise that YTHDC1 may hold a fundamental role in the development of PCa by regulating the amount of various splicing products in an m^{6}A dependent manner.

Although YTHDC2 is not ubiquitously expressed and its high abundance is observed in testes (Bailey et al., 2017; Hsu et al., 2017; Jain et al., 2018), it does not exclude the possible causal involvement of YTHDC2 into the development of other diseases. Notably, a high expression of YTHDC2 is observed in PCa as compared to BPH (Benign prostatic hyperplasia) and normal prostate tissues. Experimental results have shown that YTHDC2 induction substantially promotes PCa cell growth and invasion (Song et al., 2023). Nevertheless, the underlying mechanism by which YTHDC2 drives PCa progression has not been investigated, and the exploration of the downstream targets of YTHDC2 in PCa remains an open area. Since the early claim suggested that YTHDC2 exhibits a very weak affinity towards m^{6}A motif (Wojtas et al., 2017), it is reasonable to speculate that YTHDC2 may have non-m^{6}A targets.

2.3.3 IGF2BP family proteins

IGF2BP proteins enable to recognize m^{6}A targets or non m^{6}A targets and to increase their stabilities (Jiang et al., 2021; Huang et al., 2018; Lan et al., 2021), thus having a great impact on PCa development. A literature has demonstrated an increase of IGF2BP1 expression in prostate cancer stem cells (PCSCs), contributing to cabazitaxel resistance. Thus targeting CXCR4 (C-X-C chemokine receptor type 4)/let-7 mediated

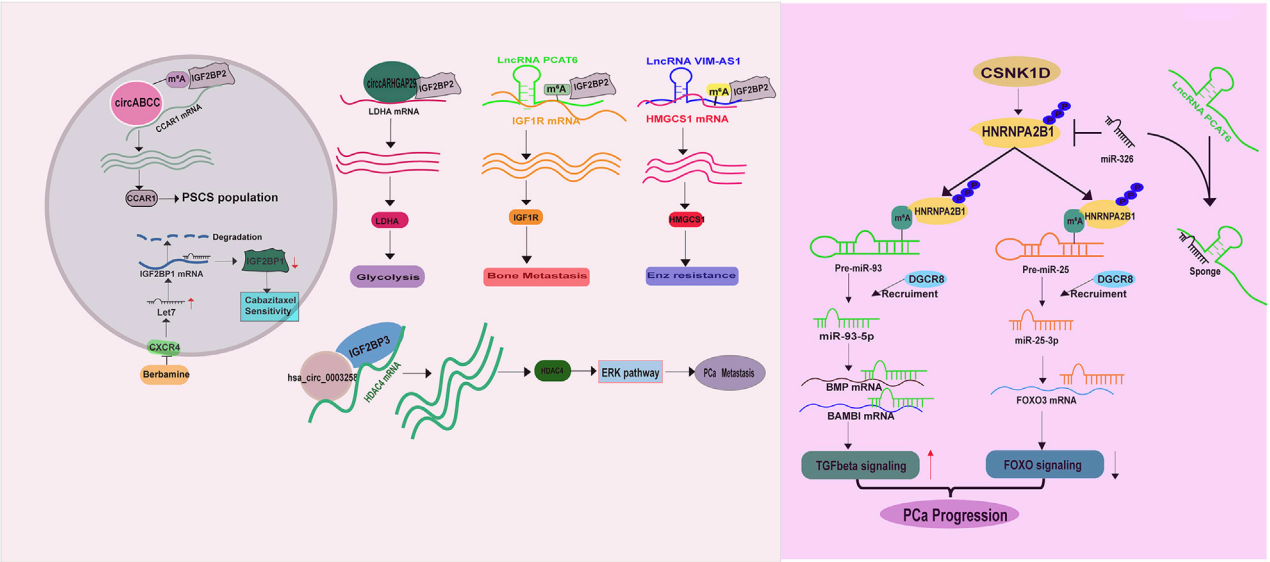

FIGURE 4
The molecular basis of IGF2BP and HnRNP family proteins in PCa.

IGF2BP1 induction in PCSCs by Berbamine could restore PCa response to cabazitaxel treatment (Wang et al., 2024). Similarly, IGF2BP2 has been reported to recognize m^{6}A labeled circABCC (circular ATP Binding Cassette Subfamily C Member), a prerequisite for stabilizing Cell Division Cycle And Apoptosis Regulator 1 (CCAR1) mRNA, expanding PCSCs population (Huang C. et al., 2023) (Figure 4). Besides, IGF2BP2 exerts a tumor promoting role in altering PCa metabolism, bone metastasis and targeted therapy resistance. A study from Jiang et al. unraveled that IGF2BP2 increases its binding affinity to Lactate dehydrogenase A (LDHA) mRNA in the presence of circARHGAP29 (circular Rho GTPase Activating Protein 29), thereby enhancing glycolytic metabolism (Jiang et al., 2022) (Figure 4). Another study demonstrated that IGF2BP2 is recruited by m^{6}A modified lncRNA PCAT6 (Prostate Cancer Associated Transcript 6) to interact with IGF1R (Insulin-Like Growth Factor I Receptor) mRNA, resulting in its stabilization and the promotion of PCa bone metastasis (Lang et al., 2021) (Figure 4). Moreover, IGF2BP2 can confer enzalutamide resistance via binding to and stabilizing 3-Hydroxy-3-Methylglutaryl-CoA Synthase 1 (HMGCS1) mRNA in the presence of lncRNA VIM-AS1 (VIM Antisense RNA 1) (Shi et al., 2023) (Figure 4). IGF2BP3 also serves as an oncogene in PCa, as a study illustrated its ability to combine with hsa_circ_0003258 to directly enhance the stability of histone deacetylase 4 (HDAC4) mRNA, consequently activating ERK signaling pathway to drive PCa metastasis (Yu et al., 2022) (Figure 4).

Together, these evidences suggest that IGF2BP proteins support PCa survival and hasten its malignancy via stabilizing a wide range of mRNAs. Furthermore, it is evident that the impact of IGF2BP proteins on mRNA stabilization is m^{6}A and non-m^{6}A dependent, suggesting that classifying and identifying the targets of IGF2BP proteins based on the m^{6}A status may aid in comprehending their biologies in PCa.

2.3.4 HnRNP family proteins

Accumulating evidence have demonstrated that the heterogeneous nuclear ribonucleoproteins (HnRNP) such as HnRNPC, HnRNPG and HNRNPA2B1 are direct or indirect readers of m^{6}A labeled RNAs, especially miRNAs (Wang et al., 2020; Liu et al., 2015; Spitale et al., 2015; Liu et al., 2017; Wu et al., 2018). In PCa, elevated HnRNPC expression is closely correlated with tumor stage, tumor grade and the overall survival (Wang et al., 2021). Functionally, HnRNPC promotes PCa proliferation and metastasis (Cheng et al., 2023). Moreover, a high level of HNRNPA2B1 is also examined in PCa. HNRNPA2B1 binds to the m^{6}A marks in several miRNA precursors (miR-93-5p (Qi et al., 2023; Sun et al., 2023), miR-25-3p (Qi et al., 2023)) and facilitates their processing and maturation via recruiting DGCR8 (DiGeorge syndrome critical region gene 8) (Sun et al., 2023), driving PCa development (Figure 4). For this point of view, molecules enabling to regulate HNRNPA2B1 expression is supposed to have a considerable impact on PCa survival and metastasis. As expected, casein kinase 1 delta (CSNK1D) phosphorylates and stabilizes HNRNPA2B1 protein, exacerbating PCa malignancy (Qi et al., 2023) (Figure 4). The lncRNA PCAT6 also has capacity to increase HNRNPA2B1 expression via acting as sponge of miR-326 to facilitate PCa neuroendocrine differentiation (Liu B. et al., 2021) (Figure 4). However, the role of another m^{6}A reader, HnRNPG, has not been investigated in PCa.

3 The upstream signaling pathways regulating m^{6}A regulators

A literature suggest that the total m^{6}A levels are gradually increased as PCa progresses from the localized mass to the metastatic disease (Wan et al., 2022), indicating the existence of a molecular network upstream of m^{6}A regulators in PCa.

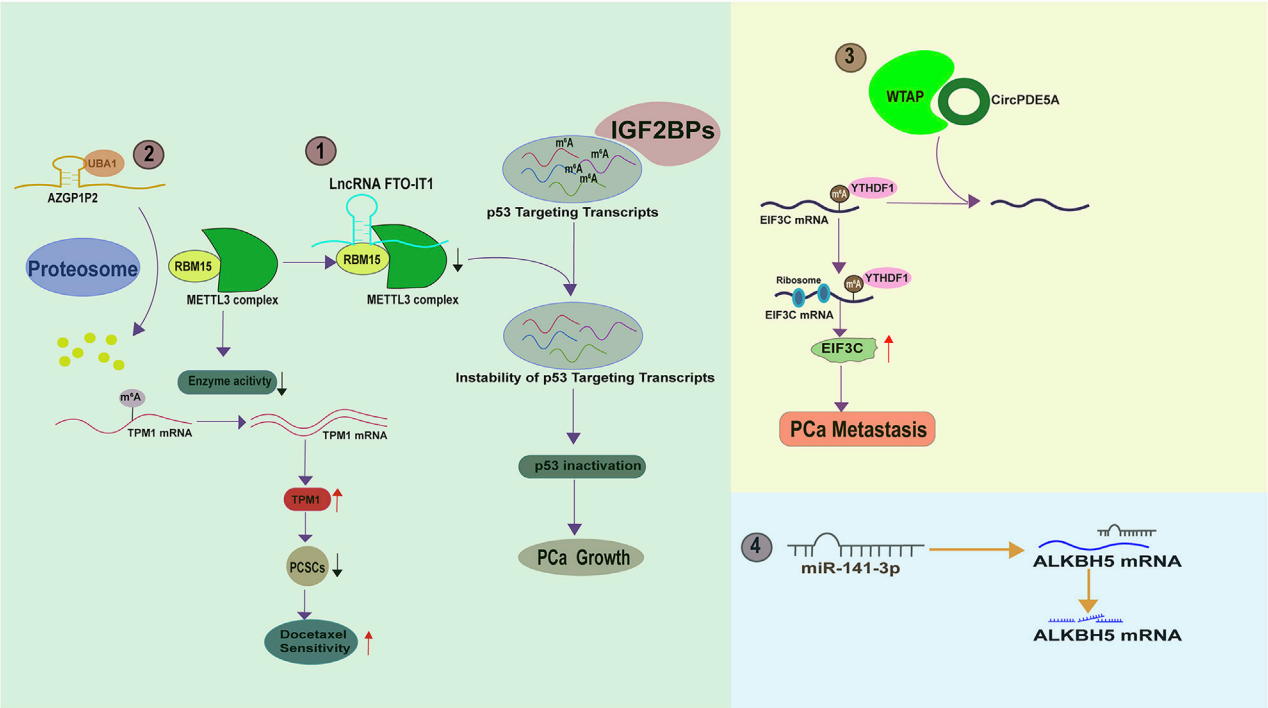

FIGURE 5
The upstream signaling molecules regulating m^{6}A regulator in PCa.

Understanding this network may provide insight into novel strategies to improve the efficacy of current therapies. A fascinating study by Zhang et al. demonstrated that FTO-IT1 (FTO intronic transcript 1), a lncRNA transcribed from the intron 8 of *FTO* gene focus, downregulates the transcript levels of several p53 targeting genes such as FAS (Fas Cell Surface Death Receptor), TP53INP1 (Tumor protein p53-inducible nuclear protein 1), SESN2 (Sestrin2), and MDM2 (Mouse double minute 2 homolog), thereby recapitulating p53 inactivation. Results from RNA pull down and subsequent mass spectrum analysis illustrated that FTO-IT1 directly interacts with RBM15 but not other m^{6}A regulator to inhibit the methyltransferase activity of METTL3 complex. As a sequence specific RNA binding protein, RBM15 fails to bind p53 targeting transcripts for m^{6}A modification in the presence of FTO-IT1, leading to their failure to be recognized by IGF2BP proteins. Thus, FTO-IT1 knock-out specifically boosts the m^{6}A levels of p53 targeting transcripts by releasing RBM15 mediated m^{6}A "writer" activity and caused PCa cell growth arrest (Zhang J. et al., 2023) (Figure 5). Another study by Wang et al. also documented that RBM15 can be regulated by AZGP1P2, a pseudogene of AZGP2. According to the data, AZGP1P2 binds and recruits UBA1 (Ubiquitin Like Modifier Activating Enzyme 1) as a E1 conjugating enzyme for RBM15 degradation. As a result, the m^{6}A of RBM15 recognized TPM1 mRNA (tropomyosin 1) at its coding region is erased and TPM1 mRNA is stabilized. TPM1 induction by AZGP1P2 functions as a tumor suppressor to sensitize PCa cells to docetaxel therapy via eradicating the population of prostate cancer stem cells (PCSCs) (Wang et al., 2023b) (Figure 5).

WTAP, a known m^{6}A regulator, is reportedly regulated by circPDE5A, a circular form of exon 2 and exon 3 of PDE5A (Phosphodiesterase 5A). CircPDE5A binds WTAP and disrupts its mediated m^{6}A modification of eukaryotic translation initiation factor 3c (EIF3C) (Figure 5). Therefore, circPDE5A inactivation in CRPC leads to an m^{6}A increase of EIF3C mRNA, which is subsequently recognized by YTHDF1 and has an enhanced translation efficiency, eventually promoting PCa metastasis (Ding et al., 2022). Moreover, it has been documented that the m^{6}A "eraser" ALKBH5 is a direct target of miR-141-3p (Li X. et al., 2023) (Figure 5). In the future, we can anticipate the identification of more upstream molecules that affect m^{6}A regulators. Armed with this knowledge, we can effectively silence m^{6}A signaling by targeting these upstream molecules.

4 The cross-talk between RNA m^{6}A modification and AR signaling

Androgen receptor (AR), a member of steroid hormone receptors, has been acknowledged as the key driving factor determining PCa development for decades (Tang et al., 2021). Structurally consisting of N-terminal, DNA binding domain, Hinge region and Ligand binding domain, AR responds to dihydrotestosterone (DHT) and translocates into nucleus as dimer to regulate the transcription of numerous genes (Tan et al., 2015). Owing to the significant role of AR in PCa development, for a long time, AR signaling inhibition has been the main strategy for PCa management.

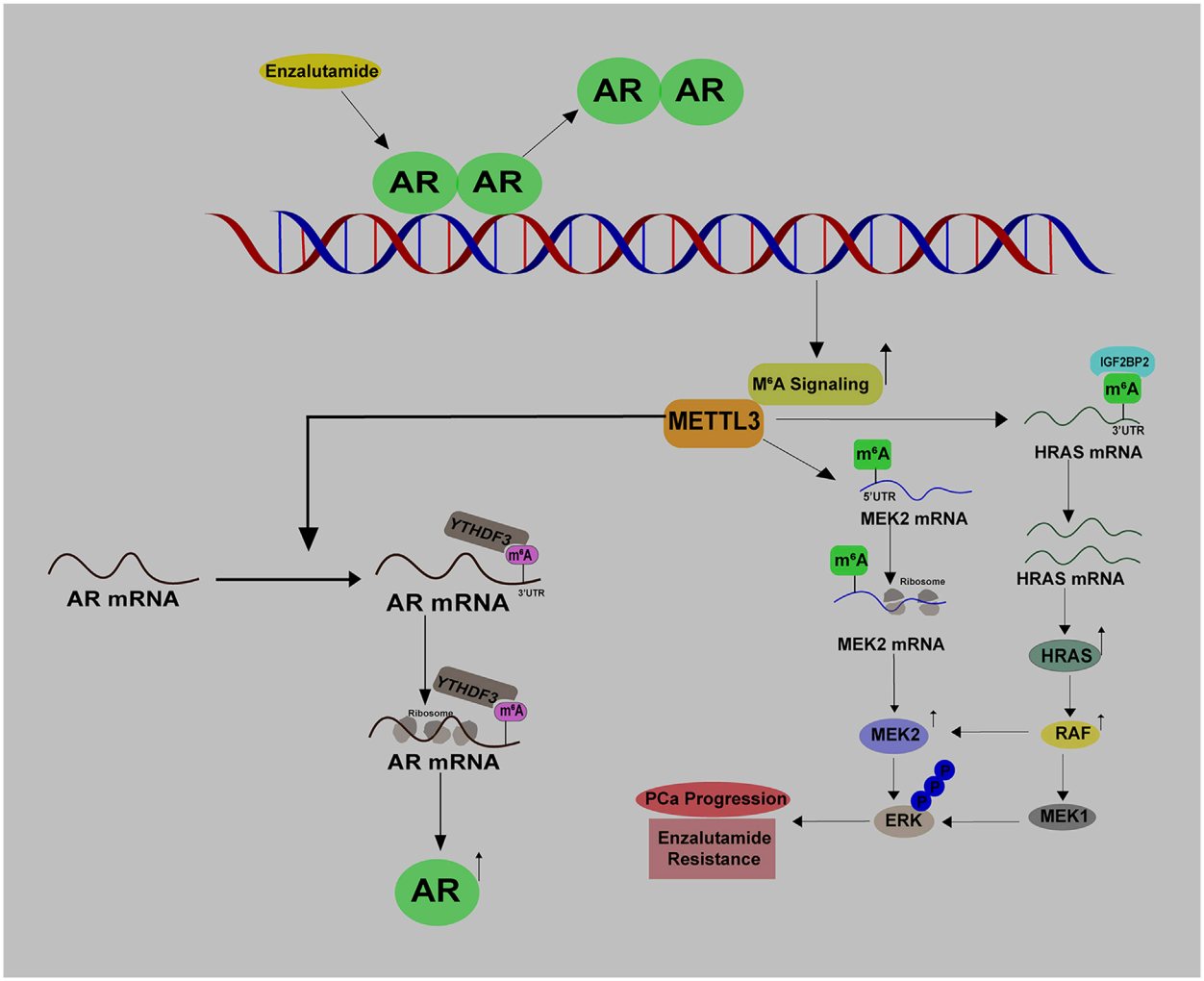

FIGURE 6
The crosstalk between m^{6}A signaling and AR signaling in PCa.

Androgen deprivation therapy (ADT) has been utilized as the golden mean to treat PCa for many decades, with promising clinical outcomes. Li et al. have uncovered a direct link between RNA m^{6}A modification and androgen receptor (AR) signaling. Their research showed that ADT with enzalutamide treatment leads to an increase in METTL3 expression and the total m^{6}A levels, suggesting METTL3 mediated m^{6}A modification may contribute to the acquired Enz resistance (Figure 6). By performing MeRIP-seq and RNA-seq, the authors identified that METTL3 directly mediates m^{6}A modifications of HRAS and MEK2 mRNAs. Mechanistically, HRAS mRNA with m^{6}A at its 3′-UTR is much more stable, and MEK2 mRNA with m^{6}A at 5′-UTR has a higher translation potential as compared to the corresponding non-modified controls. As a result, MAPK signaling is activated and bypasses AR signaling inhibition to promote PCa growth (Li Y. et al., 2023) (Figure 6). Therefore, activation of m^{6}A signaling serves as a self-protective mechanism in response to AR inhibition, providing a non-AR survival source for PCa growth. Given the fact that enzalutamide is an anti-androgen drug specifically preventing the transcription activity of AR, it will be intriguing to explore whether AR enables to control the expression of m^{6}A regulators at the chromatin level, thus affecting the m^{6}A signaling.

Reciprocally, m^{6}A signaling also has a great impact on AR signaling. Evidence from Haigh et al. suggested that METTL3 inhibition by siRNAs could substantially impair androgen regulated transcriptome in PCa (Haigh et al., 2022). Additionally, in early 2022, Somasekharan et al. (2022) discovered that AR mRNA is a direct target of METTL3 and its translation is potentiated with the m^{6}A modification at 8953A (Figure 6). By connecting these two findings, we speculate that METTL3 may affect androgen regulated transcriptome via directly methylating AR mRNA. Given that CRPC expresses more abundant AR protein than primary PCa, it is hypothesized that METTL3-mediated AR mRNA translation at least partially accounts for this phenomenon (Wu et al., 2021). Therefore, targeting METTL3 may alleviate the reactivation of AR signaling and aid in overcoming CRPC progression. In summary, there exists a reciprocal regulation between AR signaling and m^{6}A signaling in PCa.

TABLE 2 The clinical value of each individual m^{6}A regulator in PCa.

Name	PCa/N	CRPC/PCa	Means	Prognosis	References
METTL3	High	High	MeRIP-qPCR RT-qPCR Western Bloting, IHC	Poor	Cai et al. (2019), Yuan et al. (2020), Chen et al. (2021a), Ma et al. (2020), Li et al. (2020), Haigh et al. (2022), Mao et al. (2022), Li et al. (2023a), Cotter et al. (2021), Li et al. (2023b), Lothion-Roy et al. (2023)
METTL14	High	High	IHC	Poor	Wang et al. (2022a), Li et al. (2023b), Lothion-Roy et al. (2023)
FTO	Low	NA	IHC,RT-qPCR Western Bloting	Good	Wang et al. (2022b), Zou et al. (2022), Li et al. (2022b), Azhati et al. (2023) Zhu et al. (2021)
ALKBH5	Low	NA	RT-qPCR, Western Bloting	Good	Li et al. (2023c)
YTHDF1	High	NA	IHC,Western Bloting,RT-qPCR	Poor	Li et al. (2021), Li et al. (2022b), Nie et al. (2023)
YTHDF2	High	NA	Western Bloting,RT-qPCR,IHC	Poor	Du et al. (2020) Li et al. (2020)
YTHDC1	NA	NA	NA	NA	NA
YTHDC2	High	NA	IHC,Western Bloting	Poor	Song et al. (2023), Ding et al. (2022)
IGF2BP1/2/3	NA	NA	NA	NA	NA
WTAP	High	NA	IHC,Western Bloting	NA	Lothion-Roy et al. (2023), Zhao et al. (2024)
HnRNP	High	NA	RT-qPCR, IHC	Poor	Wang et al. (2021), Cheng et al. (2023), Qi et al. (2023), Quan et al. (2023), Cheng et al. (2023)

5 Clinical implications of RNA m^{6}A modification in PCa and future perspectives

The clinical significance of RNA m^{6}A modification should be acknowledged owing to its close relationship with PCa initiation, progression and therapy resistance. METTL3 and METTL14, the main components of m^{6}A "writer," elevate their expression when prostate epithelial cells become malignant (Xu and Ge, 2022) (Table 2). A continual rise in METTL3 and METTL14 expression is observed in CRPC disease (Wu et al., 2021). Conversely, the expression levels of m^{6}A "eraser," FTO and ALKBH5, display an opposite trend (Fang et al., 2022). In line with this, Lu et al. found that m^{6}A modification levels are elevated in metastatic PCa as compared to the primary control, as evidenced by MeRIP-seq and RNA-seq on 4 metastatic PCa, 4 primary PCa tumors and 4 benign prostate hyperplasia (BPH). Importantly, they also reported that PCa patients with high m^{6}A-modified mRNA (MMM) score experience shorter biochemical recurrence free survival and have a poor response to androgen signaling inhibition therapy as compared to the patients with a low MMM score, suggesting m^{6}A modification status is a poor prognostic factor for predicting disease development and therapy resistance. However, their findings also exhibited that the primary PCa harbors a paucity of m^{6}A modified mRNAs as compared to the BPH, implying hypo m^{6}A modification of mRNAs contributes to PCa initiation In this context, a discrepancy is found between the expression pattern of m^{6}A regulators and the m^{6}A levels when the comparison was made between BPH and primary PCa (Lu et al., 2023). We hypothesize that the activities of m^{6}A regulators are inhibited by some proteins so that a hypo m^{6}A levels are observed in PCa.

According to this information, total m^{6}A levels may serve as a diagnostic biomarker to predict disease status of PCa, and the elimination of m^{6}A levels by METTL3/METTL14 inhibitor or others holds promise as a therapeutic strategy to prevent PCa progression. In 2021, Yankova et al identified a small molecule STM2457 as a potent METTL3 inhibitor to suppress acute myeloid leukaemia (AML), opening a new avenue of METTL3 targeted therapy. Additionally, Storm Therapeutics Company has screened another METTL3 inhibitor STC-15, which displays anti-tumor activity across different AML models and is currently being investigated in a clinical trail (NCT05584111) (Yankova et al., 2021). Although currently not available, it would be promising to test the efficacy of METTL3 inhibitors in PCa models and PCa patients. It is noting that some small molecules including curcumin (Chen et al., 2021b), quercetin (Zhu J. et al., 2023), epigallocatechin gallate (EGCG) (Wu et al., 2005) and simvastatin (Chen et al., 2020), have been reported to influence m^{6}A signaling. However, in our opinion, they are not specific for interrupting m^{6}A levels and their contributions to cancer prevention may not be solely due to the m^{6}A alteration. Therefore, the continuous screening of METTL3-specific and potent inhibitors remains a priority for scientists and pharmacologists.

6 Conclusion

PCa is a male carcinoma and its mortality is continuously rising. Despite of the initial response, ADT treatment will lead to the emergence of recurrent tumor, suggesting other signaling pathways

actively respond in order to bypass AR inhibition. As a type of epitranscriptomal modifications, m^{6}A is now received much attention and it is indeed implicated into a variety of biological processes including tumorigenesis. Particularly in PCa, abnormal expression levels of m^{6}A regulators are frequently observed by many researchers. The experimental evidence suggest that m^{6}A writers, m^{6}A erasers and m^{6}A readers all contribute to PCa survival and malignancy. Additional evidence also suggest that the total m^{6}A levels and METTL3 are closely related to enzalutamide resistance. These findings provide a strong rationale to propose a therapy using m^{6}A inhibitor, alone or with anti-androgen, to treat CRPC patients.

Although numerous RNAs has been identified to be m^{6}A modified, the blueprint of m^{6}A signaling remains incomplete. In the clinical setting, a comprehensive understanding of m^{6}A targets and their related signaling pathways can guide the discovery of novel targeted therapies to overcome PCa development. To this end, scientists should exert significant efforts to identify functional m^{6}A targets during PCa evolution.

Although FTO inhibitors such as bisisantrene (Su et al., 2020), brequinar (Su et al., 2020), and Dac51 (Wu et al., 2023; Yang and Al-Hendy, 2023; Huang Y. et al., 2023; Liu Y. et al., 2021) have shown potency against several solid tumors, including renal carcinoma, bladder cancer, they may not be the ideal choice for the treatment of PCa model as researchers have confirmed the tumor suppressing role of FTO in PCa models. Alternatively, researchers should consider screening specific inhibitors of m^{6}A readers, as they are positively implicated in PCa development. YTH family proteins, IGF2BP proteins, and other m^{6}A readers have been proven to be oncogenic factors driving PCa progression. From our perspective, m^{6}A reader inhibitors may be more specific than METTL3 inhibitors in suppressing a small population of RNA. While METTL3 has a variety of targets, each m^{6}A reader has its uniquely recognized RNA population. Indeed, IGF2BP1 inhibitors (AVJ16 (Singh et al., 2024), BTYNB (Müller et al., 2020; Mahapatra et al., 2017; Jamal et al., 2023; Hagemann et al., 2023; Xiao et al., 2023; Wang JJ. et al., 2023), and 7773 (Singh et al., 2024)), IGF2BP2 inhibitor CWI1-2 (Weng et al., 2022), and YTHDF proteins inhibitor ebselen (Micaelli et al., 2022) all show promising anti-cancer activity in preclinical models. However, the identification of m^{6}A reader inhibitors is still in the preliminary stage and requires intensive dedication.

Author contributions

YC: Writing–original draft, Writing–review and editing. MJ: Writing–original draft, Writing–review and editing. CD: Writing–original draft, Writing–review and editing. ZY: Writing–original draft. BC: Conceptualization, Funding acquisition, Writing–original draft, Writing–review and editing. RW: Conceptualization, Funding acquisition, Writing–original draft, Writing–review and editing.

Funding

The author(s) declare that financial support was received for the research, authorship, and/or publication of this article. This study was kindly supported by the Sichuan Science and Technology Program (2022YFS0636) and the Science and Technology Program of Luzhou (2020LZXNYDJ43).

Conflict of interest

The authors declare that the research was conducted in the absence of any commercial or financial relationships that could be construed as a potential conflict of interest.

Publisher's note

References

Agarwal, N., Azad, A. A., Carles, J., Fay, A. P., Matsubara, N., Heinrich, D., et al. (2023). Talazoparib plus enzalutamide in men with first-line metastatic castration-resistant prostate cancer (TALAPRO-2): a randomised, placebo-controlled, phase 3 trial. *Lancet London, Engl.* 402, 291–303. doi:10.1016/S0140-6736(23)01055-3

Akaza, H., Kanetake, H., Tsukamoto, T., Miyanaga, N., Sakai, H., Masumori, N., et al. (2011). Efficacy and safety of dutasteride on prostate cancer risk reduction in Asian men: the results from the REDUCE study. *Jpn. J. Clin. Oncol.* 41, 417–423. doi:10.1093/jjco/hyq221

Azhati, B., Reheman, A., Dilixiati, D., and Rexiati, M. (2023). FTO-stabilized miR-139-5p targets ZNF217 to suppress prostate cancer cell malignancies by inactivating the PI3K/Akt/mTOR signal pathway. *Archives Biochem. biophysics* 741, 109604. doi:10.1016/j.abb.2023.109604

Bailey, A. S., Batista, P. J., Gold, R. S., Chen, Y. G., de Rooij, D. G., Chang, H. Y., et al. (2017). The conserved RNA helicase YTHDC2 regulates the transition from proliferation to differentiation in the germline. *eLife* 6, e26116. doi:10.7554/eLife.26116

Bennett, L., Jaiswal, P. K., Harkless, R. V., Long, T. M., Gao, N., Vandenburg, B., et al. (2024). Glucocorticoid receptor (GR) activation is associated with increased cAMP/PKA signaling in castration-resistant prostate cancer. *Mol. cancer Ther.* 23, 552–563. doi:10.1158/1535-7163.MCT-22-0479

Bokar, J. A., Shambaugh, M. E., Polayes, D., Matera, A. G., and Rottman, F. M. (1997). Purification and cDNA cloning of the AdoMet-binding subunit of the human mRNA (N6-adenosine)-methyltransferase. *RNA (New York, NY)* 3, 1233–1247.

Bratt, O. (2002). Hereditary prostate cancer: clinical aspects. *J. urology* 168, 906–913. doi:10.1097/01.ju.0000024402.67529.ca

Bray, F., Laversanne, M., Sung, H., Ferlay, J., Siegel, R. L., Soerjomataram, I., et al. (2024). Global cancer statistics 2022: GLOBOCAN estimates of incidence and mortality worldwide for 36 cancers in 185 countries. *CA a cancer J. Clin.* 74, 229–263. doi:10.3322/caac.21834

Cai, J., Yang, F., Zhan, H., Situ, J., Li, W., Mao, Y., et al. (2019). RNA m(6)A methyltransferase METTL3 promotes the growth of prostate cancer by regulating Hedgehog pathway. *OncoTargets Ther.* 12, 9143–9152. doi:10.2147/OTT.S226796

Cai, M., Song, X. L., Li, X. A., Chen, M., Guo, J., Yang, D. H., et al. (2023). Current therapy and drug resistance in metastatic castration-resistant prostate cancer. *Drug Resist. Updat. Rev. Comment. Antimicrob. anticancer Chemother.* 68, 100962. doi:10.1016/j.drup.2023.100962

Cai, T., Nesi, G., Tinacci, G., Giubilei, G., Gavazzi, A., Mondaini, N., et al. (2011). Clinical importance of lymph node density in predicting outcome of prostate cancer patients. *J. Surg. Res.* 167, 267–272. doi:10.1016/j.jss.2009.05.004

Chen, B., Liu, C., Long, H., Bai, G., Zhu, Y., and Xu, H. (2023a). N(6)-methyladenosine-induced long non-coding RNA PVT1 regulates the miR-27b-3p/BLM axis to promote prostate cancer progression. *Int. J. Oncol.* 62, 16. doi:10.3892/ijo.2022.5464

Chen, L., Gao, Y., Xu, S., Yuan, J., Wang, M., Li, T., et al. (2023b). N6-methyladenosine reader YTHDF family in biological processes: structures, roles, and mechanisms. *Front. Immunol.* 14, 1162607. doi:10.3389/fimmu.2023.1162607

Chen, W. W., Qi, J. W., Hang, Y., Wu, J. X., Zhou, X. X., Chen, J. Z., et al. (2020). Simvastatin is beneficial to lung cancer progression by inducing METTL3-induced m6A modification on EZH2 mRNA. *Eur. Rev. Med. Pharmacol. Sci.* 24, 4263–4270. doi:10.26355/eurrev_202004_21006

Chen, Y., Pan, C., Wang, X., Xu, D., Ma, Y., Hu, J., et al. (2021a). Silencing of METTL3 effectively hinders invasion and metastasis of prostate cancer cells. *Theranostics* 11, 7640–7657. doi:10.7150/thno.61178

Chen, Y., Wu, R., Chen, W., Liu, Y., Liao, X., Zeng, B., et al. (2021b). Curcumin prevents obesity by targeting TRAF4-induced ubiquitylation in m(6) A-dependent manner. *EMBO Rep.* 22, e52146. doi:10.15252/embr.202052146

Cheng, Q., Butler, W., Zhou, Y., Zhang, H., Tang, L., Perkinson, K., et al. (2022). Pre-existing castration-resistant prostate cancer-like cells in primary prostate cancer promote resistance to hormonal therapy. *Eur. Urol.* 81, 446–455. doi:10.1016/j.eururo.2021.12.039

Cheng, Y., Li, L., Wei, X., Xu, F., Huang, X., Qi, F., et al. (2023). HNRNPC suppresses tumor immune microenvironment by activating Treg cells promoting the progression of prostate cancer. *Cancer Sci.* 114, 1830–1845. doi:10.1111/cas.15745

Cheng, Y., Xie, W., Pickering, B. F., Chu, K. L., Savino, A. M., Yang, X., et al. (2021). N(6)-Methyladenosine on mRNA facilitates a phase-separated nuclear body that suppresses myeloid leukemic differentiation. *Cancer cell* 39, 958–972.e8. doi:10.1016/j.ccell.2021.04.017

Choe, J., Lin, S., Zhang, W., Liu, Q., Wang, L., Ramirez-Moya, J., et al. (2018). mRNA circularization by METTL3-eIF3h enhances translation and promotes oncogenesis. *Nature* 561, 556–560. doi:10.1038/s41586-018-0538-8

Choi, J. B., Kim, J. H., Hong, S. H., Han, K. D., and Ha, U. S. (2018). Difference in prostate cancer incidence around sixty years: effects of age and metabolic diseases. *Cancer Med.* 7, 2736–2743. doi:10.1002/cam4.1462

Clancy, M. J., Shambaugh, M. E., Timpte, C. S., and Bokar, J. A. (2002). Induction of sporulation in *Saccharomyces cerevisiae* leads to the formation of N6-methyladenosine in mRNA: a potential mechanism for the activity of the IME4 gene. *Nucleic acids Res.* 30, 4509–4518. doi:10.1093/nar/gkf573

Cotter, K. A., Gallon, J., Uebersax, N., Rubin, P., Meyer, K. D., Piscuoglio, S., et al. (2021). Mapping of m(6)A and its regulatory targets in prostate cancer reveals a METTL3-low induction of therapy resistance. *Mol. cancer Res.: MCR* 19, 1398–1411.

Dai, C., Heemers, H., and Sharifi, N. (2017). Androgen signaling in prostate cancer. *Cold Spring Harb. Perspect. Med.* 7, a030452. doi:10.1101/cshperspect.a030452

Davies, A., Nouruzi, S., Ganguli, D., Namekawa, T., Thaper, D., Linder, S., et al. (2021). An androgen receptor switch underlies lineage infidelity in treatment-resistant prostate cancer. *Nat. cell Biol.* 23, 1023–1034. doi:10.1038/s41556-021-00743-5

de Bono, J. S., Logothetis, C. J., Molina, A., Fizazi, K., North, S., Chu, L., et al. (2011). Abiraterone and increased survival in metastatic prostate cancer. *N. Engl. J. Med.* 364, 1995–2005. doi:10.1056/NEJMoa1014618

Desrosiers, R., Friderici, K., and Rottman, F. (1974). Identification of methylated nucleosides in messenger RNA from Novikoff hepatoma cells. *Proc. Natl. Acad. Sci. U. S. A.* 71, 3971–3975. doi:10.1073/pnas.71.10.3971

Ding, L., Wang, R., Zheng, Q., Shen, D., Wang, H., Lu, Z., et al. (2022). circPDE5A regulates prostate cancer metastasis via controlling WTAP-dependent N6-methyladenisine methylation of EIF3C mRNA. *J. Exp. and Clin. cancer Res. CR* 41, 187. doi:10.1186/s13046-022-02391-5

Dong, F., Qin, X., Wang, B., Li, Q., Hu, J., Cheng, X., et al. (2021). ALKBH5 facilitates hypoxia-induced paraspeckle assembly and IL8 secretion to generate an immunosuppressive tumor microenvironment. *Cancer Res.* 81, 5876–5888. doi:10.1158/0008-5472.CAN-21-1456

Du, C., Lv, C., Feng, Y., and Yu, S. (2020). Activation of the KDM5A/miRNA-495/YTHDF2/m6A-MOB3B axis facilitates prostate cancer progression. *J. Exp. and Clin. cancer Res. CR* 39, 223. doi:10.1186/s13046-020-01735-3

Fang, Z., Mei, W., Qu, C., Lu, J., Shang, L., Cao, F., et al. (2022). Role of m6A writers, erasers and readers in cancer. *Exp. Hematol. and Oncol.* 11, 45. doi:10.1186/s40164-022-00298-7

Gerken, T., Girard, C. A., Tung, Y. C., Webby, C. J., Saudek, V., Hewitson, K. S., et al. (2007). The obesity-associated FTO gene encodes a 2-oxoglutarate-dependent nucleic acid demethylase. *Sci. (New York, NY)* 318, 1469–1472. doi:10.1126/science.1151710

Geula, S., Moshitch-Moshkovitz, S., Dominissini, D., Mansour, A. A., Kol, N., Salmon-Divon, M., et al. (2015). Stem cells. m6A mRNA methylation facilitates resolution of naïve pluripotency toward differentiation. *Sci. (New York, NY)* 347, 1002–1006. doi:10.1126/science.1261417

Godtman, R. A., Kollberg, K. S., Pihl, C. G., Månsson, M., and Hugosson, J. (2022). The association between age, prostate cancer risk, and higher Gleason score in a long-term screening Program: results from the göteborg-1 prostate cancer screening trial. *Eur. Urol.* 82, 311–317. doi:10.1016/j.eururo.2022.01.018

Guan, X., Polesso, F., Wang, C., Sehrawat, A., Hawkins, R. M., Murray, S. E., et al. (2022). Androgen receptor activity in T cells limits checkpoint blockade efficacy. *Nature* 606, 791–796. doi:10.1038/s41586-022-04522-6

Hagemann, S., Misiak, D., Bell, J. L., Fuchs, T., Lederer, M. I., Bley, N., et al. (2023). IGF2BP1 induces neuroblastoma via a druggable feedforward loop with MYCN promoting 17q oncogene expression. *Mol. cancer* 22, 88. doi:10.1186/s12943-023-01792-0

Haigh, D. B., Woodcock, C. L., Lothion-Roy, J., Harris, A. E., Metzler, V. M., Persson, J. L., et al. (2022). The METTL3 RNA methyltransferase regulates transcriptional networks in prostate cancer. *Cancers* 14, 5148. doi:10.3390/cancers14205148

Han, Z., Yi, X., Li, J., Zhang, T., Liao, D., You, J., et al. (2023). RNA m(6)A modification in prostate cancer: a new weapon for its diagnosis and therapy. *Biochimica biophysica acta Rev. cancer* 1878, 188961. doi:10.1016/j.bbcan.2023.188961

Hartmann, A. M., Nayler, O., Schwaiger, F. W., Obermeier, A., and Stamm, S. (1999). The interaction and colocalization of Sam68 with the splicing-associated factor YT521-B in nuclear dots is regulated by the Src family kinase p59(fyn). *Mol. Biol. cell* 10, 3909–3926. doi:10.1091/mbc.10.11.3909

He, L., Li, H., Wu, A., Peng, Y., Shu, G., and Yin, G. (2019). Functions of N6-methyladenosine and its role in cancer. *Mol. cancer* 18, 176. doi:10.1186/s12943-019-1109-9

He, L., Li, J., Wang, X., Ying, Y., Xie, H., Yan, H., et al. (2018). The dual role of N6-methyladenosine modification of RNAs is involved in human cancers. *J. Cell. Mol. Med.* 22, 4630–4639. doi:10.1111/jcmm.13804

He, Y., Xu, W., Xiao, Y. T., Huang, H., Gu, D., and Ren, S. (2022). Targeting signaling pathways in prostate cancer: mechanisms and clinical trials. *Signal Transduct. Target. Ther.* 7, 198. doi:10.1038/s41392-022-01042-7

Hsu, P. J., Zhu, Y., Ma, H., Guo, Y., Shi, X., Liu, Y., et al. (2017). Ythdc2 is an N(6)-methyladenosine binding protein that regulates mammalian spermatogenesis. *Cell Res.* 27, 1115–1127. doi:10.1038/cr.2017.99

Hu, Q., Yin, J., Zhao, S., Wang, Y., Shi, R., Yan, K., et al. (2024). ZFHX3 acts as a tumor suppressor in prostate cancer by targeting FTO-mediated m(6)A demethylation. *Cell death Discov.* 10, 284. doi:10.1038/s41420-024-02060-w

Huang, C., Xu, R., Zhu, X., and Jiang, H. (2023a). m6A-modified circABCC4 promotes stemness and metastasis of prostate cancer by recruiting IGF2BP2 to increase stability of CCAR1. *Cancer gene Ther.* 30, 1426–1440. doi:10.1038/s41417-023-00650-x

Huang, H., Weng, H., Sun, W., Qin, X., Shi, H., Wu, H., et al. (2018). Recognition of RNA N(6)-methyladenosine by IGF2BP proteins enhances mRNA stability and translation. *Nat. cell Biol.* 20, 285–295. doi:10.1038/s41556-018-0045-z

Huang, Q., Mo, J., Liao, Z., Chen, X., and Zhang, B. (2022). The RNA m(6)A writer WTAP in diseases: structure, roles, and mechanisms. *Cell death and Dis.* 13, 852. doi:10.1038/s41419-022-05268-9

Huang, Y., Xia, W., Dong, Z., and Yang, C. G. (2023b). Chemical inhibitors targeting the oncogenic m(6)A modifying proteins. *Accounts Chem. Res.* 56, 3010–3022. doi:10.1021/acs.accounts.3c00451

Jain, D., Puno, M. R., Meydan, C., Lailler, N., Mason, C. E., Lima, C. D., et al. (2018). Ketu mutant mice uncover an essential meiotic function for the ancient RNA helicase YTHDC2. *eLife* 7, e30919. doi:10.7554/eLife.30919

Jamal, A., Hassan Dalhat, M., Jahan, S., Choudhry, H., and Imran Khan, M. (2023). BTYNB, an inhibitor of RNA binding protein IGF2BP1 reduces proliferation and induces differentiation of leukemic cancer cells. *Saudi J. Biol. Sci.* 30, 103569. doi:10.1016/j.sjbs.2023.103569

Jeon, H. Y., Pornour, M., Ryu, H., Khadka, S., Xu, R., Jang, J., et al. (2023). SMAD3 promotes expression and activity of the androgen receptor in prostate cancer. *Nucleic acids Res.* 51, 2655–2670. doi:10.1093/nar/gkad043

Jeong, I. G., Dajani, D., Verghese, M., Hwang, J., Cho, Y. M., Hong, J. H., et al. (2016). Differences in the aggressiveness of prostate cancer among Korean, Caucasian, and African American men: a retrospective cohort study of radical prostatectomy. *Urol. Oncol.* 34 (3), e9–e14. doi:10.1016/j.urolonc.2015.08.004

Jiang, X., Guo, S., Wang, S., Zhang, Y., Chen, H., Wang, Y., et al. (2022). EIF4A3-Induced circARHGAP29 promotes aerobic glycolysis in docetaxel-resistant prostate cancer through IGF2BP2/c-Myc/LDHA signaling. *Cancer Res.* 82, 831–845. doi:10.1158/0008-5472.CAN-21-2988

Jiang, X., Liu, B., Nie, Z., Duan, L., Xiong, Q., Jin, Z., et al. (2021). The role of m6A modification in the biological functions and diseases. *Signal Transduct. Target. Ther.* 6, 74. doi:10.1038/s41392-020-00450-x

Koh, C. W. Q., Goh, Y. T., and Goh, W. S. S. (2019). Atlas of quantitative single-base-resolution N(6)-methyl-adenine methylomes. *Nat. Commun.* 10, 5636. doi:10.1038/s41467-019-13561-z

Kong, Z., Lu, Y., Yang, Y., Chang, K., Lin, Y., Huang, Y., et al. (2023). m6A-Mediated biogenesis of circDDIT4 inhibits prostate cancer progression by sequestrating ELAVL1/HuR. *Mol. cancer Res. MCR* 21, 1342–1355. doi:10.1158/1541-7786.MCR-22-0271

Kwon, D. H., Borno, H. T., Cheng, H. H., Zhou, A. Y., and Small, E. J. (2020). Ethnic disparities among men with prostate cancer undergoing germline testing. *Urol. Oncol.* 38, 80.e81–80. doi:10.1016/j.urolonc.2019.09.010

Lan, Q., Liu, P. Y., Bell, J. L., Wang, J. Y., Hüttelmaier, S., Zhang, X. D., et al. (2021). The emerging roles of RNA m(6)A methylation and demethylation as critical regulators of tumorigenesis, drug sensitivity, and resistance. *Cancer Res.* 81, 3431–3440. doi:10.1158/0008-5472.CAN-20-4107

Lang, C., Yin, C., Lin, K., Li, Y., Yang, Q., Wu, Z., et al. (2021). m(6) A modification of lncRNA PCAT6 promotes bone metastasis in prostate cancer through IGF2BP2-mediated IGF1R mRNA stabilization. *Clin. Transl. Med.* 11, e426. doi:10.1002/ctm2.426

Li, G., Liu, J., Wang, Y., Liu, H., Fu, J., Zhao, Y., et al. (2023a). METTL3-mediated m6A modification of pri-miR-148a-3p affects prostate cancer progression by regulating TXNIP. *Environ. Toxicol.* 38, 2377–2390. doi:10.1002/tox.23874

Li, J., Xie, H., Ying, Y., Chen, H., Yan, H., He, L., et al. (2020). YTHDF2 mediates the mRNA degradation of the tumor suppressors to induce AKT phosphorylation in N6-methyladenosine-dependent way in prostate cancer. *Mol. cancer* 19, 152. doi:10.1186/s12943-020-01267-6

Li, P., Shi, Y., Gao, D., Xu, H., Zou, Y., Wang, Z., et al. (2022b). ELK1-mediated YTHDF1 drives prostate cancer progression by facilitating the translation of Polo-like kinase 1 in an m6A dependent manner. *Int. J. Biol. Sci.* 18, 6145–6162. doi:10.7150/ijbs.75063

Li, S., and Cao, L. (2022). Demethyltransferase FTO alpha-ketoglutarate dependent dioxygenase (FTO) regulates the proliferation, migration, invasion and tumor growth of prostate cancer by modulating the expression of melanocortin 4 receptor (MC4R). *Bioengineered* 13, 5598–5612. doi:10.1080/21655979.2021.2001936

Li, W., Chen, G., Feng, Z., Zhu, B., Zhou, L., Zhang, Y., et al. (2021). YTHDF1 promotes the proliferation, migration, and invasion of prostate cancer cells by regulating TRIM44. *Genes and genomics.* 43, 1413–1421. doi:10.1007/s13258-021-01175-z

Li, X., Liu, B., Wang, S., Li, J., and Ge, X. (2023c). MiR-141-3p promotes malignant progression in prostate cancer through AlkB homolog 5-mediated m(6)A modification of protein arginine methyltransferase 6. *Chin. J. physiology* 66, 43–51. doi:10.4103/cjop.CJOP-D-22-00071

Li, Y., Su, R., Deng, X., Chen, Y., and Chen, J. (2022a). FTO in cancer: functions, molecular mechanisms, and therapeutic implications. *Trends cancer* 8, 598–614. doi:10.1016/j.trecan.2022.02.010

Li, Y., Zhu, S., Chen, Y., Ma, Q., Kan, D., Yu, W., et al. (2023b). Post-transcriptional modification of m(6)A methylase METTL3 regulates ERK-induced androgen-deprived treatment resistance prostate cancer. *Cell death and Dis.* 14, 289. doi:10.1038/s41419-023-05773-5

Li, Z., Weng, H., Su, R., Weng, X., Zuo, Z., Li, C., et al. (2017). FTO plays an oncogenic role in acute myeloid leukemia as a N(6)-methyladenosine RNA demethylase. *Cancer cell* 31, 127–141. doi:10.1016/j.ccell.2016.11.017

Lin, S., Choe, J., Du, P., Triboulet, R., and Gregory, R. I. (2016). The m(6)A methyltransferase METTL3 promotes translation in human cancer cells. *Mol. cell* 62, 335–345. doi:10.1016/j.molcel.2016.03.021

Linder, B., Grozhik, A. V., Olarerin-George, A. O., Meydan, C., Mason, C. E., and Jaffrey, S. R. (2015). Single-nucleotide-resolution mapping of m6A and m6Am throughout the transcriptome. *Nat. methods* 12, 767–772. doi:10.1038/nmeth.3453

Liu, B., Jiang, H. Y., Yuan, T., Luo, J., Zhou, W. D., Jiang, Q. Q., et al. (2021a). Enzalutamide-Induced upregulation of PCAT6 promotes prostate cancer neuroendocrine differentiation by regulating miR-326/HNRNPA2B1 Axis. *Front. Oncol.* 11, 650054. doi:10.3389/fonc.2021.650054

Liu, B., Li, L., Yang, G., Geng, C., Luo, Y., Wu, W., et al. (2019). PARP inhibition suppresses GR-MYCN-CDK5-RB1-E2F1 signaling and neuroendocrine differentiation in castration-resistant prostate cancer. *Clin. cancer Res. official J. Am. Assoc. Cancer Res.* 25, 6839–6851. doi:10.1158/1078-0432.CCR-19-0317

Liu, J., Yuan, J. F., and Wang, Y. Z. (2022). METTL3-stabilized lncRNA SNHG7 accelerates glycolysis in prostate cancer via SRSF1/c-Myc axis. *Exp. cell Res.* 416, 113149. doi:10.1016/j.yexcr.2022.113149

Liu, J., Yue, Y., Han, D., Wang, X., Fu, Y., Zhang, L., et al. (2014). A METTL3-METTL14 complex mediates mammalian nuclear RNA N6-adenosine methylation. *Nat. Chem. Biol.* 10, 93–95. doi:10.1038/nchembio.1432

Liu, N., Dai, Q., Zheng, G., He, C., Parisien, M., and Pan, T. (2015). N(6)-methyladenosine-dependent RNA structural switches regulate RNA-protein interactions. *Nature* 518, 560–564. doi:10.1038/nature14234

Liu, N., Zhou, K. I., Parisien, M., Dai, Q., Diatchenko, L., and Pan, T. (2017). N6-methyladenosine alters RNA structure to regulate binding of a low-complexity protein. *Nucleic acids Res.* 45, 6051–6063. doi:10.1093/nar/gkx141

Liu, Y., Liang, G., Xu, H., Dong, W., Dong, Z., Qiu, Z., et al. (2021b). Tumors exploit FTO-mediated regulation of glycolytic metabolism to evade immune surveillance. *Cell metab.* 33, 1221–1233.e11. doi:10.1016/j.cmet.2021.04.001

Lothion-Roy, J., Haigh, D. B., Harris, A. E., Metzler, V. M., Alsaleem, M., Toss, M. S., et al. (2022). Clinical and molecular significance of the RNA m(6)A methyltransferase complex in prostate cancer. *Front. Genet.* 13, 1096071. doi:10.3389/fgene.2022.1096071

Lu, J., Chen, J., Lin, Z., Liu, Q., Zhong, C., Cai, Z., et al. (2023). A prognostic signature consisting of N6-methyladenosine modified mRNAs demonstrates clinical potential in prediction of biochemical recurrence and guidance on precision therapy in prostate cancer. *Transl. Oncol.* 33, 101670. doi:10.1016/j.tranon.2023.101670

Luxton, H. J., Simpson, B. S., Mills, I. G., Brindle, N. R., Ahmed, Z., Stavrinides, V., et al. (2019). The oncogene metadherin interacts with the known splicing proteins YTHDC1, Sam68 and T-STAR and plays a novel role in alternative mRNA splicing. *Cancers.* 11, 1233. doi:10.3390/cancers11091233

Ma, H., Wang, X., Cai, J., Dai, Q., Natchiar, S. K., Lv, R., et al. (2019). N(6-)Methyladenosine methyltransferase ZCCHC4 mediates ribosomal RNA methylation. *Nat. Chem. Biol.* 15, 88–94. doi:10.1038/s41589-018-0184-3

Ma, X. X., Cao, Z. G., and Zhao, S. L. (2020). m6A methyltransferase METTL3 promotes the progression of prostate cancer via m6A-modified LEF1. *Eur. Rev. Med. Pharmacol. Sci.* 24, 3565–3571. doi:10.26355/eurrev_202004_20817

Mahapatra, L., Andruska, N., Mao, C., Le, J., and Shapiro, D. J. (2017). A novel IMP1 inhibitor, BTYNB, targets c-myc and inhibits melanoma and ovarian cancer cell proliferation. *Transl. Oncol.* 10, 818–827. doi:10.1016/j.tranon.2017.07.008

Mao, Y., Li, W., Weng, Y., Hua, B., Gu, X., Lu, C., et al. (2022). METTL3-Mediated m(6)A modification of lncRNA MALAT1 facilitates prostate cancer growth by activation of PI3K/AKT signaling. *Cell Transplant.* 31, 9636897221122997. doi:10.1177/09636897221122997

Mauer, J., Luo, X., Blanjoie, A., Jiao, X., Grozhik, A. V., Patil, D. P., et al. (2017). Reversible methylation of m(6)A(m) in the 5' cap controls mRNA stability. *Nature* 541, 371–375. doi:10.1038/nature21022

Mauer, J., Sindelar, M., Despic, V., Guez, T., Hawley, B. R., Vasseur, J. J., et al. (2019). FTO controls reversible m(6)Am RNA methylation during snRNA biogenesis. *Nat. Chem. Biol.* 15, 340–347. doi:10.1038/s41589-019-0231-8

Micaelli, M., Dalle Vedove, A., Cerofolini, L., Vigna, J., Sighel, D., Zaccara, S., et al. (2022). Small-molecule ebselen binds to YTHDF proteins interfering with the recognition of N (6)-methyladenosine-modified RNAs. *ACS Pharmacol. and Transl. Sci.* 5, 872–891. doi:10.1021/acsptsci.2c00008

Mottet, N., Bellmunt, J., Bolla, M., Briers, E., Cumberbatch, M. G., De Santis, M., et al. (2017). EAU-ESTRO-SIOG guidelines on prostate cancer. Part 1: screening, diagnosis, and local treatment with curative intent. *Eur. Urol.* 71, 618–629. doi:10.1016/j.eururo.2016.08.003

Müller, S., Bley, N., Busch, B., Glaß, M., Lederer, M., Misiak, C., et al. (2020). The oncofetal RNA-binding protein IGF2BP1 is a druggable, post-transcriptional super-enhancer of E2F-driven gene expression in cancer. *Nucleic acids Res.* 48, 8576–8590. doi:10.1093/nar/gkaa653

Murakami, S., and Jaffrey, S. R. (2022). Hidden codes in mRNA: control of gene expression by m(6)A. *Mol. cell* 82, 2236–2251. doi:10.1016/j.molcel.2022.05.029

Nie, Q., Wu, X., Huang, Y., Guo, T., Kuang, J., and Du, C. (2023). RNA N6-methyladenosine-modified-binding protein YTHDF1 promotes prostate cancer progression by regulating androgen function-related gene TRIM68. *Eur. J. Med. Res.*

Patil, D. P., Pickering, B. F., and Jaffrey, S. R. (2018). Reading m(6)A in the transcriptome: m(6)a-binding proteins. *Trends cell Biol.* 28, 113–127. doi:10.1016/j.tcb.2017.10.001

Pendleton, K. E., Chen, B., Liu, K., Hunter, O. V., Xie, Y., Tu, B. P., et al. (2017). The U6 snRNA m(6)A methyltransferase METTL16 regulates SAM synthetase intron retention. *Cell* 169, 824–835. doi:10.1016/j.cell.2017.05.003

Peng, S., Yi, Z., and Liu, M. (2017). Ailanthone: a new potential drug for castration-resistant prostate cancer. *Chin. J. cancer* 36, 25. doi:10.1186/s40880-017-0194-7

Powles, T., Yuen, K. C., Gillessen, S., Kadel, E. E., 3rd, Rathkopf, D., Matsubara, N., et al. (2022). Atezolizumab with enzalutamide versus enzalutamide alone in metastatic castration-resistant prostate cancer: a randomized phase 3 trial. *Nat. Med.* 28, 144–153. doi:10.1038/s41591-021-01600-6

Qi, F., Shen, W., Wei, X., Cheng, Y., Xu, F., Zheng, Y., et al. (2023). CSNK1D-mediated phosphorylation of HNRNPA2B1 induces miR-25-3p/miR-93-5p maturation to promote prostate cancer cell proliferation and migration through m(6)A-dependent manner. *Cell. Mol. life Sci. CMLS* 80, 156. doi:10.1007/s00018-023-04798-5

Quan, Y., Ping, H., Wang, M., and Zhang, X. (2023). RNA-sequencing analysis indicates that N-cadherin promotes prostate cancer progression by the epigenetic modification of key genes. *DNA cell biol.* 42, 563–577.

Raj, N., Wang, M., Seoane, J. A., Zhao, R. L., Kaiser, A. M., Moonie, N. A., et al. (2022). The Mettl3 epitranscriptomic writer amplifies p53 stress responses. *Mol. cell* 82, 2370–2384.e10. doi:10.1016/j.molcel.2022.04.010

Rebbeck, T. R. (2017). Prostate cancer genetics: variation by race, ethnicity, and geography. *Seminars Radiat. Oncol.* 27, 3–10. doi:10.1016/j.semradonc.2016.08.002

Roundtree, I. A., Luo, G. Z., Zhang, Z., Wang, X., Zhou, T., Cui, Y., et al. (2017). YTHDC1 mediates nuclear export of N(6)-methyladenosine methylated mRNAs. *eLife* 6, e31311. doi:10.7554/eLife.31311

Ruszkowska, A., Ruszkowski, M., Dauter, Z., and Brown, J. A. (2018). Structural insights into the RNA methyltransferase domain of METTL16. *Sci. Rep.* 8, 5311. doi:10.1038/s41598-018-23608-8

Shi, H., Wang, X., Lu, Z., Zhao, B. S., Ma, H., Hsu, P. J., et al. (2017). YTHDF3 facilitates translation and decay of N(6)-methyladenosine-modified RNA. *Cell Res.* 27, 315–328. doi:10.1038/cr.2017.15

Shi, S. J., Han, D. H., Zhang, J. L., Li, Y., Yang, A. G., and Zhang, R. (2023). VIM-AS1 promotes proliferation and drives enzalutamide resistance in prostate cancer via IGF2BP2-mediated HMGCS1 mRNA stabilization. *Int. J. Oncol.* 62, 34. doi:10.3892/ijo.2023.5482

Shigeta, K., Kosaka, T., Hongo, H., Yanai, Y., Matsumoto, K., Morita, S., et al. (2019). Castration-resistant prostate cancer patients who had poor response on first androgen deprivation therapy would obtain certain clinical benefit from early docetaxel administration. *Int. J. Clin. Oncol.* 24, 546–553. doi:10.1007/s10147-018-01388-5

Shima, H., Matsumoto, M., Ishigami, Y., Ebina, M., Muto, A., Sato, Y., et al. (2017). S-adenosylmethionine synthesis is regulated by selective N(6)-adenosine methylation and mRNA degradation involving METTL16 and YTHDC1. *Cell Rep.* 21, 3354–3363. doi:10.1016/j.celrep.2017.11.092

Siegel, R. L., Miller, K. D., Fuchs, H. E., and Jemal, A. (2022). Cancer statistics. *CA a cancer J. Clin.* 72, 7–30. doi:10.3322/caac.21332

Singh, A., Singh, V., Wallis, N., Abis, G., Oberman, F., Wood, T., et al. (2024). Development of a specific and potent IGF2BP1 inhibitor: a promising therapeutic agent for IGF2BP1-expressing cancers. *Eur. J. Med. Chem.* 263, 115940. doi:10.1016/j.ejmech.2023.115940

Śledź, P., and Jinek, M. (2016). Structural insights into the molecular mechanism of the m(6)A writer complex. *eLife.* 5, e18434. doi:10.7554/eLife.18434

Somasekharan, S. P., Saxena, N., Zhang, F., Beraldi, E., Huang, J. N., Gentle, C., et al. (2022). Regulation of AR mRNA translation in response to acute AR pathway inhibition. *Nucleic acids Res.* 50, 1069–1091. doi:10.1093/nar/gkab1247

Sommer, S., Lavi, U., and Darnell, J. E. (1978). The absolute frequency of labeled N-6-methyladenosine in HeLa cell messenger RNA decreases with label time. *J. Mol. Biol.* 124, 487–499. doi:10.1016/0022-2836(78)90183-3

Song, J., You, G., Yin, X., Zhu, G., Wang, W., Yu, Y., et al. (2023). Overexpression of YTHDC2 contributes to the progression of prostate cancer and predicts poor outcomes in patients with prostate cancer. *J. Biochem. Mol. Toxicol.* 37, e23308. doi:10.1002/jbt.23308

Spitale, R. C., Flynn, R. A., Zhang, Q. C., Crisalli, P., Lee, B., Jung, J. W., et al. (2015). Structural imprints *in vivo* decode RNA regulatory mechanisms. *Nature* 519, 486–490. doi:10.1038/nature14263

Su, R., Dong, L., Li, Y., Gao, M., Han, L., Wunderlich, M., et al. (2020). Targeting FTO suppresses cancer stem cell maintenance and immune evasion. *Cancer cell* 38, 79–96. doi:10.1016/j.ccell.2020.04.017

Sun, M., Shen, Y., Jia, G., Deng, Z., Shi, F., Jing, Y., et al. (2023). Activation of the HNRNPA2B1/miR-93-5p/FRMD6 axis facilitates prostate cancer progression in an m6A-dependent manner. *J. Cancer* 14, 1242–1256. doi:10.7150/jca.83863

Tan, M. H., Li, J., Xu, H. E., Melcher, K., and Yong, E. L. (2015). Androgen receptor: structure, role in prostate cancer and drug discovery. *Acta Pharmacol. Sin.* 36, 3–23. doi:10.1038/aps.2014.18

Tang, Q., Cheng, B., Dai, R., and Wang, R. (2021). The role of androgen receptor in cross talk between stromal cells and prostate cancer epithelial cells. *Front. cell Dev. Biol.* 9, 729498. doi:10.3389/fcell.2021.729498

Tao, L., Mu, X., Chen, H., Jin, D., Zhang, R., Zhao, Y., et al. (2021). FTO modifies the m6A level of MALAT and promotes bladder cancer progression. *Clin. Transl. Med.* 11, e310. doi:10.1002/ctm2.310

Thalgott, M., Kron, M., Brath, J. M., Ankerst, D. P., Thompson, I. M., Gschwend, J. E., et al. (2018). Men with family history of prostate cancer have a higher risk of disease recurrence after radical prostatectomy. *World J. urology* 36, 177–185. doi:10.1007/s00345-017-2122-5

Thalhammer, A., Bencokova, Z., Poole, R., Loenarz, C., Adam, J., O'Flaherty, L., et al. (2011). Human AlkB homologue 5 is a nuclear 2-oxoglutarate dependent oxygenase and a direct target of hypoxia-inducible factor 1α (HIF-1α). *PloS one* 6, e16210. doi:10.1371/journal.pone.0016210

van Tran, N., Ernst, F. G. M., Hawley, B. R., Zorbas, C., Ulryck, N., Hackert, P., et al. (2019). The human 18S rRNA m6A methyltransferase METTL5 is stabilized by TRMT112. *Nucleic acids Res.* 47, 7719–7733. doi:10.1093/nar/gkz619

Wan, H., Feng, Y., Wu, J., Zhu, L., and Mi, Y. (2022). Functions and mechanisms of N6-methyladenosine in prostate cancer (Review). *Mol. Med. Rep.* 26, 280. doi:10.3892/mmr.2022.12796

Wang, H., Li, N., Liu, Q., Guo, J., Pan, Q., Cheng, B., et al. (2023a). Antiandrogen treatment induces stromal cell reprogramming to promote castration resistance in prostate cancer. *Cancer cell* 41, 1345–1362.e9. doi:10.1016/j.ccell.2023.05.016

Wang, H., Liu, J., Zhu, X., Yang, B., He, Z., and Yao, X. (2023b). AZGP1P2/UBA1/RBM15 cascade mediates the fate determinations of prostate cancer stem cells and promotes therapeutic effect of docetaxel in castration-resistant prostate cancer via TPM1 m6A modification. *Res. Wash. DC* 6, 0252. doi:10.34133/research.0252

Wang, J. J., Chen, D. X., Zhang, Y., Xu, X., Cai, Y., Wei, W. Q., et al. (2023c). Elevated expression of the RNA-binding protein IGF2BP1 enhances the mRNA stability of INHBA to promote the invasion and migration of esophageal squamous cancer cells. *Exp. Hematol. and Oncol.* 12, 75. doi:10.1186/s40164-023-00429-8

Wang, L., Lyu, C., Stadlbauer, B., Buchner, A., Nößner, E., and Pohla, H. (2024). Berbamine targets cancer stem cells and reverses cabazitaxel resistance via inhibiting IGF2BP1 and p-STAT3 in prostate cancer. *Prostate* 84, 131–147. doi:10.1002/pros.24632

Wang, P., Doxtader, K. A., and Nam, Y. (2016a). Structural basis for cooperative function of Mettl3 and Mettl14 methyltransferases. *Mol. cell* 63, 306–317. doi:10.1016/j.molcel.2016.05.041

Wang, R., Sun, Y., Li, L., Niu, Y., Lin, W., Lin, C., et al. (2017). Preclinical study using Malat1 small interfering RNA or androgen receptor splicing variant 7 degradation enhancer ASC-j9® to suppress enzalutamide-resistant prostate cancer progression. *Eur. Urol.* 72, 835–844. doi:10.1016/j.eururo.2017.04.005

Wang, S., Xu, G., Chao, F., Zhang, C., Han, D., and Chen, G. (2021). HNRNPC promotes proliferation, metastasis and predicts prognosis in prostate cancer. *Cancer Manag. Res.* 13, 7263–7276. doi:10.2147/CMAR.S330713

Wang, T., Kong, S., Tao, M., and Ju, S. (2020). The potential role of RNA N6-methyladenosine in Cancer progression. *Mol. cancer* 19, 88. doi:10.1186/s12943-020-01204-7

Wang, X., Feng, J., Xue, Y., Guan, Z., Zhang, D., Liu, Z., et al. (2016b). Structural basis of N(6)-adenosine methylation by the METTL3-METTL14 complex. *Nature* 534, 575–578. doi:10.1038/nature18298

Wang, X., Lu, Z., Gomez, A., Hon, G. C., Yue, Y., Han, D., et al. (2014b). N6-methyladenosine-dependent regulation of messenger RNA stability. *Nature* 505, 117–120. doi:10.1038/nature12730

Wang, X., Zhao, B. S., Roundtree, I. A., Lu, Z., Han, D., Ma, H., et al. (2015). N(6)-methyladenosine modulates messenger RNA translation efficiency. *Cell* 161, 1388–1399. doi:10.1016/j.cell.2015.05.014

Wang, Y., Chen, J., Gao, W. Q., and Yang, R. (2022a). METTL14 promotes prostate tumorigenesis by inhibiting THBS1 via an m6A-YTHDF2-dependent mechanism. *Cell death Discov.* 8, 143. doi:10.1038/s41420-022-00939-0

Wang, Y., Li, Y., Toth, J. I., Petroski, M. D., Zhang, Z., and Zhao, J. C. (2014a). N6-methyladenosine modification destabilizes developmental regulators in embryonic stem cells. *Nat. cell Biol.* 16, 191–198. doi:10.1038/ncb2902

Wang, Z., Sun, H., Zhu, H., Gu, D., Chen, X., Pan, Y., et al. (2022b). Demethylase FTO inhibits the development of prostate cancer by upregulating EGR2 expression in an m6A manner. *Turkish J. Biol. = Turk biyoloji dergisi* 46, 426–438. doi:10.55730/1300-0152.2629

Warda, A. S., Kretschmer, J., Hackert, P., Lenz, C., Urlaub, H., Höbartner, C., et al. (2017). Human METTL16 is a N(6)-methyladenosine (m(6)A) methyltransferase that targets pre-mRNAs and various non-coding RNAs. *EMBO Rep.* 18, 2004–2014. doi:10.15252/embr.201744940

Wei, C. M., Gershowitz, A., and Moss, B. (1976). 5'-Terminal and internal methylated nucleotide sequences in HeLa cell mRNA. *Biochemistry* 15, 397–401. doi:10.1021/bi00647a024

Wei, J., Liu, F., Lu, Z., Fei, Q., Ai, Y., He, P. C., et al. (2018). Differential m(6)A, m(6)A(m), and m(1)A demethylation mediated by FTO in the cell nucleus and cytoplasm. *Mol. cell* 71, 973–985. doi:10.1016/j.molcel.2018.08.011

Wei, X., Huo, Y., Pi, J., Gao, Y., Rao, S., He, M., et al. (2022). METTL3 preferentially enhances non-m(6)A translation of epigenetic factors and promotes tumourigenesis. *Nat. cell Biol.* 24, 1278–1290. doi:10.1038/s41556-022-00968-y

Wen, S., Wei, Y., Zen, C., Xiong, W., Niu, Y., and Zhao, Y. (2020). Long non-coding RNA NEAT1 promotes bone metastasis of prostate cancer through N6-methyladenosine. *Mol. cancer* 19, 171. doi:10.1186/s12943-020-01293-4

Weng, H., Huang, F., Yu, Z., Chen, Z., Prince, E., Kang, Y., et al. (2022). The m(6)A reader IGF2BP2 regulates glutamine metabolism and represents a therapeutic target in acute myeloid leukemia. *Cancer cell* 40, 1566–1582.e10. doi:10.1016/j.ccell.2022.10.004

Wenzel, M., Nocera, L., Collà Ruvolo, C., Würnschimmel, C., Tian, Z., Shariat, S. F., et al. (2022). Overall survival and adverse events after treatment with darolutamide vs. apalutamide vs. enzalutamide for high-risk non-metastatic castration-resistant prostate cancer: a systematic review and network meta-analysis. *Prostate cancer prostatic Dis.* 25, 139–148. doi:10.1038/s41391-021-00395-4

Widagdo, J., Anggono, V., and Wong, J. J. (2022). The multifaceted effects of YTHDC1-mediated nuclear m(6)A recognition. *Trends Genet. TIG* 38, 325–332. doi:10.1016/j.tig.2021.11.005

Wiener, D., and Schwartz, S. (2021). The epitranscriptome beyond m(6)A. *Nat. Rev. Genet.* 22, 119–131. doi:10.1038/s41576-020-00295-8

Wojtas, M. N., Pandey, R. R., Mendel, M., Homolka, D., Sachidanandam, R., and Pillai, R. S. (2017). Regulation of m(6)A transcripts by the 3'→5' RNA helicase YTHDC2 is essential for a successful meiotic Program in the mammalian germline. *Mol. cell* 68, 374–387. doi:10.1016/j.molcel.2017.09.021

Wu, B., Su, S., Patil, D. P., Liu, H., Gan, J., Jaffrey, S. R., et al. (2018). Molecular basis for the specific and multivariant recognitions of RNA substrates by human hnRNP A2/B1. *Nat. Commun.* 9, 420. doi:10.1038/s41467-017-02770-z

Wu, Q., Xie, X., Huang, Y., Meng, S., Li, Y., Wang, H., et al. (2021). N6-methyladenosine RNA methylation regulators contribute to the progression of prostate cancer. *J. Cancer* 12, 682–692. doi:10.7150/jca.46379

Wu, R., Yao, Y., Jiang, Q., Cai, M., Liu, Q., Wang, Y., et al. (2005)2018). Epigallocatechin gallate targets FTO and inhibits adipogenesis in an mRNA m(6)A-YTHDF2-dependent manner. *Int. J. Obes.* 42, 1378–1388. doi:10.1038/s41366-018-0082-5

Wu, T., Shao, Y., Li, X., Wu, T., Yu, L., Liang, J., et al. (2023). NR3C1/Glucocorticoid receptor activation promotes pancreatic β-cell autophagy overload in response to glucolipotoxicity. *Autophagy* 19, 2538–2557. doi:10.1080/15548627.2023.2200625

Xia, L., Han, Q., Duan, X., Zhu, Y., Pan, J., Dong, B., et al. (2022). m(6)A-induced repression of SIAH1 facilitates alternative splicing of androgen receptor variant 7 by regulating CPSF1. *Mol. Ther. Nucleic acids* 28, 219–230. doi:10.1016/j.omtn.2022.03.008

Xiao, P., Meng, Q., Liu, Q., Lang, Q., Yin, Z., Li, G., et al. (2023). IGF2BP1-mediated N6-methyladenosine modification promotes intrahepatic cholangiocarcinoma progression. *Cancer Lett.* 557, 216075. doi:10.1016/j.canlet.2023.216075

Xiao, W., Adhikari, S., Dahal, U., Chen, Y. S., Hao, Y. J., Sun, B. F., et al. (2016). Nuclear m(6)A reader YTHDC1 regulates mRNA splicing. *Mol. cell* 61, 507–519. doi:10.1016/j.molcel.2016.01.012

Xu, P., and Ge, R. (2022). Roles and drug development of METTL3 (methyltransferase-like 3) in anti-tumor therapy. *Eur. J. Med. Chem.* 230, 114118. doi:10.1016/j.ejmech.2022.114118

Xu, Y., Ye, S., Zhang, N., Zheng, S., Liu, H., Zhou, K., et al. (2020). The FTO/miR-181b-3p/ARL5B signaling pathway regulates cell migration and invasion in breast cancer. *Cancer Commun. Lond. Engl.* 40, 484–500. doi:10.1002/cac2.12075

Yang, Q., and Al-Hendy, A. (2023). The functional role and regulatory mechanism of FTO m(6)A RNA demethylase in human uterine leiomyosarcoma. *Int. J. Mol. Sci.* 24, 7957. doi:10.3390/ijms24097957

Yankova, E., Blackaby, W., Albertella, M., Rak, J., De Braekeleer, E., Tsagkogeorga, G., et al. (2021). Small-molecule inhibition of METTL3 as a strategy against myeloid leukaemia. *Nature* 593, 597–601. doi:10.1038/s41586-021-03536-w

Yu, Y. Z., Lv, D. J., Wang, C., Song, X. L., Xie, T., Wang, T., et al. (2022). Hsa_circ_0003258 promotes prostate cancer metastasis by complexing with IGF2BP3 and sponging miR-653-5p. *Mol. cancer* 21, 12. doi:10.1186/s12943-021-01480-x

Yuan, S., He, S. H., Li, L. Y., Xi, S., Weng, H., Zhang, J. H., et al. (2023). A potassium-chloride co-transporter promotes tumor progression and castration resistance of prostate cancer through m(6)A reader YTHDC1. *Cell death and Dis.* 14, 7. doi:10.1038/s41419-022-05544-8

Yuan, Y., Du, Y., Wang, L., and Liu, X. (2020). The M6A methyltransferase METTL3 promotes the development and progression of prostate carcinoma via mediating MYC methylation. *J. Cancer* 11, 3588–3595.

Zaccara, S., Ries, R. J., and Jaffrey, S. R. (2019). Reading, writing and erasing mRNA methylation. *Nat. Rev. Mol. cell Biol.* 20, 608–624. doi:10.1038/s41580-019-0168-5

Zhang, D., Wornow, S., Peehl, D. M., Rankin, E. B., and Brooks, J. D. (2022). The controversial role and therapeutic development of the m6A demethylase FTO in renal cell carcinoma. *Transl. Oncol.* 25, 101518. doi:10.1016/j.tranon.2022.101518

Zhang, J., Wei, J., Sun, R., Sheng, H., Yin, K., Pan, Y., et al. (2023b). A lncRNA from the FTO locus acts as a suppressor of the m(6)A writer complex and p53 tumor suppression signaling. *Mol. cell* 83, 2692–2708.e7. doi:10.1016/j.molcel.2023.06.024

Zhang, S., Lv, C., Niu, Y., Li, C., Li, X., Shang, Y., et al. (2023a). RBM3 suppresses stemness remodeling of prostate cancer in bone microenvironment by modulating N6-methyladenosine on CTNNB1 mRNA. *Cell death and Dis.* 14, 91. doi:10.1038/s41419-023-05627-0

Zhang, Z., Zhou, C., Li, X., Barnes, S. D., Deng, S., Hoover, E., et al. (2020). Loss of CHD1 promotes heterogeneous mechanisms of resistance to AR-targeted therapy via chromatin dysregulation. *Cancer cell* 37, 584–598. doi:10.1016/j.ccell.2020.03.001

Zhao, P., Han, P., Ma, Y., Tian, P., and Li, J. (2024c). Circ_0082878 contributes to prostate cancer progression via the miR-455-3p/WTAP axis. *Environ. Toxicol.* 39, 979–990.

Zhao, X., Lv, S., Li, N., Zou, Q., Sun, L., and Song, T. (2024b). YTHDF2 protein stabilization by the deubiquitinase OTUB1 promotes prostate cancer cell proliferation via PRSS8 mRNA degradation. *J. Biol. Chem.* 300, 107152. doi:10.1016/j.jbc.2024.107152

Zhao, Y., Hu, X., Yu, H., Sun, H., Zhang, L., and Shao, C. (2024a). The FTO mediated N6-methyladenosine modification of DDIT4 regulation with tumorigenesis and metastasis in prostate cancer. *Res. Wash. DC* 7, 0313. doi:10.34133/research.0313

Zheng, Z., Li, J., Liu, Y., Shi, Z., Xuan, Z., Yang, K., et al. (2022). The crucial role of AR-V7 in enzalutamide-resistance of castration-resistant prostate cancer. *Cancers* 14, 4877. doi:10.3390/cancers14194877

Zhong, C., Long, Z., Yang, T., Wang, S., Zhong, W., Hu, F., et al. (2023). M6A-modified circRBM33 promotes prostate cancer progression via PDHA1-mediated mitochondrial respiration regulation and presents a potential target for ARSI therapy. *Int. J. Biol. Sci.* 19, 1543–1563. doi:10.7150/ijbs.77133

Zhong, S., Li, H., Bodi, Z., Button, J., Vespa, L., Herzog, M., et al. (2008). MTA is an Arabidopsis messenger RNA adenosine methylase and interacts with a homolog of a sex-specific splicing factor. *Plant cell* 20, 1278–1288. doi:10.1105/tpc.108.058883

Zhou, Y., Li, T., Jia, M., Dai, R., and Wang, R. (2023). The molecular biology of prostate cancer stem cells: from the past to the future. *Int. J. Mol. Sci.* 24, 7482. doi:10.3390/ijms24087482

Zhu, J., Cheng, X., Naumovski, N., Hu, L., and Wang, K. (2023b). Epigenetic regulation by quercetin: a comprehensive review focused on its biological mechanisms. *Crit. Rev. food Sci. Nutr.*, 1–20. doi:10.1080/10408398.2023.2278760

Zhu, K., Li, Y., and Xu, Y. (2021). The FTO m(6)A demethylase inhibits the invasion and migration of prostate cancer cells by regulating total m(6)A levels. *Life Sci.* 271, 119180. doi:10.1016/j.lfs.2021.119180

Zhu, W., Zhao, R., Guan, X., and Wang, X. (2023a). The emerging roles and mechanism of N6-methyladenosine (m(6)A) modifications in urologic tumours progression. *Front. Pharmacol.* 14, 1192495. doi:10.3389/fphar.2023.1192495

Zou, L., Chen, W., Zhou, X., Yang, T., Luo, J., Long, Z., et al. (2022). N6-methyladenosine demethylase FTO suppressed prostate cancer progression by maintaining CLIC4 mRNA stability. *Cell death Discov.* 8, 184. doi:10.1038/s41420-022-01003-7

Glossary

ARv7	Androgen receptor variant 7
EGR-2	Early growth response protein 2
MeRIP	Methylated RNA Immunoprecipitation
ADT	Androgen deprivation therapy
FTO	Fat mass and obesity-associated
ALKBH5	Human Alk B homolog 5
c-MYC	c-Myelocytomatosis
USP4	Ubiquitin specific protease 4
LEF1	Lymphoid Enhancer Binding Factor 1
PRSS8	Serine protease 8
ZFHX3	Zinc-Finger Homeobox 3
NEAT1	Nuclear paraspeckle assembly transcript 1
MALAT1	Metastasis Associated Lung Adenocarcinoma Transcript 1
PVT1	Plasmacytoma variant translocation 1
DDIT4	DNA damage-inducible transcript 4
ABCC4	ATP binding cassette subfamily C member 4
RBM33	RNA Binding Motif Protein 33
YTHDF2	YTH N6-Methyladenosine RNA Binding Protein F2
ARHGDIA	Rho GDP Dissociation Inhibitor Alpha
SNHG7	Small nucleolar RNA hostgene 7
SRSF1	Serine And Arginine Rich Splicing Factor 1
MAPK	Mitogen activated protein kinase
MEK2	MAP kinase kinase 2
MALAT1	Metastasis associated in lung denocarcinoma transcript 1
ZNF217	Zinc Finger Protein 217
SIAH1	Siah E3 Ubiquitin Protein Ligase 1
TRIM44	Tripartite motif-containing 44
ELK1	ETS Transcription Factor 1
PLK1	Polo-like Kinase 1
NKX3-1	Neurokinin-3 Homeobox 1
KDM5A	Lysine-specific demethylase 5A
YTHDC1	YTH N6-Methyladenosine RNA Binding Protein C1
CD44v5	CD44 Vriant 5
SLC12A5	Solute Carrier Family 12 Member 5
HOXBI3	Homeobox B 13
IGF2BPs	Insulin-like growth factor 2 mRNA-binding proteins
CXCR4	Chemokine receptor type 4
CCAR1	Cell-cycle and apoptosis regulator 1
LDHA	Lactate Dehydrogenase A
ARHGAP29	Rho GTPase activating protein 29
PCAT6	Prostate cancer associated transcript 6
IGF1R	Insulin-like growth factor 1 receptor
VIM-AS1	Vimentin antisense RNA 1
HDAC4	Histone deacetylase 4
ERK	Extracellular regulated protein kinases
FAS	Fas cell surface death receptor
TP53INP1	Tumor Protein P53 Inducible Nuclear Protein 1
SESN2	Sestrin2
MDM2	Murine double minute2
RBM15	RNA Binding Motif Protein 15
AZGP1P2	Zinc-alpha 2-glycoprotein pseudogene 2
PDE5A	Phosphodiesterase 5A
MeRIP-seq	Methylated RNA Immunoprecipitation sequencing

frontiers | Frontiers in Oncology

TYPE Original Research
PUBLISHED 26 September 2024
DOI 10.3389/fonc.2024.1446894

OPEN ACCESS

EDITED BY
Jialin Meng,
University of Science and Technology of China, China

REVIEWED BY
Yingkun Xu,
Shandong University, China
Jamal Deen,
AMA Education System, Philippines

*CORRESPONDENCE
Ruohui Huang
huangruohui@gmu.edu.cn

†These authors share first authorship

RECEIVED 10 June 2024
ACCEPTED 09 September 2024
PUBLISHED 26 September 2024

CITATION
Xia W, Ye M, Jiang B, Xu G, Xiao G, Zeng Q and Huang R (2024) Anoikis in prostate cancer bone metastasis gene signatures and therapeutic implications.
Front. Oncol. 14:1446894.
doi: 10.3389/fonc.2024.1446894

Anoikis in prostate cancer bone metastasis gene signatures and therapeutic implications

Wei Xia[1†], Miao Ye[2†], Bo Jiang[1], Gang Xu[1], Guancheng Xiao[1], Qingming Zeng[1] and Ruohui Huang[1*]

[1]Department of Urology, First Affiliated Hospital of Gannan Medical University, Ganzhou, Jiangxi, China, [2]Breast Diagnosis and Treatment Center, First Affiliated Hospital of Gannan Medical University, Ganzhou, Jiangxi, China

Background: Bone metastasis from prostate cancer severely impacts patient outcomes and quality of life. Anoikis, a form of programmed cell death triggered by the loss of cell-matrix interactions, plays a critical role in cancer progression. However, its precise relationship with prostate cancer-induced bone metastasis remains unclear. This study aims to elucidate this relationship, focusing on anoikis-related gene signatures, molecular pathways, and therapeutic implications.

Methods: We used the TCGA-PRAD dataset for training, with MSKCC and GSE70769 as validation cohorts. To evaluate immunotherapy efficacy, we examined IMvigor 210 and GSE91016 datasets, and GSE137829 provided single-cell insights into prostate cancer. Specific anoikis-related genes (ARGs) were identified, and Random Survival Forest analysis and multivariate Cox regression were employed to develop anoikis-linked features. The 'clustanoikisProfilanoikis' and 'GSEA' packages were used to explore potential ARG-related pathways.

Results: Analyzing 553 samples from TCGA, 231 from MSKCC, 94 from GSE70769, and single-cell data from 6 prostate cancer patients (GSE137829), we constructed a prognostic model based on 9 ARGs. GSVA revealed upregulation of carcinogenic pathways, including epithelial-mesenchymal transition, E2F targets, and angiogenesis, with downregulation of metabolic pathways. Significant differences in somatic mutations were observed between cohorts, with a positive correlation between anoikis scores and tumor mutational burden (TMB). Immune landscape analysis suggested high-risk patients might benefit more from chemotherapy than immunotherapy based on their risk score. Single-cell analysis indicated overactivation of carcinogenic pathways in the high anoikis score group.

Conclusion: This study elucidates the complex interplay between anoikis and bone metastasis in prostate cancer. Our findings highlight the critical role of anoikis in metastatic progression, enhancing the understanding of key biomarkers and molecular dynamics. The identified anoikis-related gene signatures and disrupted pathways offer promising avenues for predictive and therapeutic strategies in prostate cancer management.

KEYWORDS

prostate cancer, anoikis, model, bioinformatics, metastasis

1 Introduction

Prostate cancer (PCa) represents one of the most prevalent malignancies and the second leading cause of cancer-related mortality among men in Western countries (1). Since the 1990s, prostate-specific antigen (PSA) has been used as a standard test for prostate cancer (2). However, multiple studies have shown that PSA testing does not confer a significant reduction in mortality (3). PSA levels also have limited value in predicting PCa prognosis, with 27-53% of patients experiencing biochemical recurrence (BCR) after radical prostatectomy or radiation therapy (4). BCR often precedes progression to advanced castration-resistant PCa (CRPC), which carries increased risks of distant metastasis, cancer-specific mortality, and overall mortality (5). Therefore, there is an unmet need for novel prognostic biomarkers in PCa to improve risk stratification and clinical decision-making.

Anoikis occurs when tumor cells are detached from the extracellular matrix (ECM) during metastasis, which has been documented in many studies in recent years (6). Detachment from ECM causes anoikis, a specific type of apoptosis. Epithelial and endothelial cells are responsible for anoikis, which is believed to contribute to tissue homeostasis in development (7). Apoptosis prevents isolated cells from attaching to other substrates for aberrant proliferation to protect organisms (8). In the absence of anoikis, adherent cells may suspend or proliferate in an environment other than their original ECM (9). Several cancers, including breast cancer, lung cancer, gastric cancer, and esophageal cancer, have been associated with ARGs (10–13). According to the study, FAIM2 overexpression in lung cancer leads to adverse clinical outcomes, while silencing FAIM2 may decrease tumor cell viability and resistance to anoikis (14). A novel predictor of the prognosis of colorectal cancer has been identified in KLF5, a protein that regulates cell proliferation and anoikis resistance (15). Activating cancer-initiating cells in HEC-1A cells promotes esophageal cancer epithelial-mesenchymal transition (EMT), thereby inhibiting apoptosis and negatively affecting patient outcomes (16). Lee et al. demonstrated that TMPRSS4 promotes prostate cancer cells to resist anoikis, thereby improving the survival of circulating tumor cells and promoting early metastasis, and demonstrated that TMPRSS4 promotes CSC characteristics of prostate cancer by upregulating SLUG and TWIST1-induced stem cell factor SOX2 (17).

Anoikis-related genes-based prognostic indicators are rarely analyzed in prostate cancer, despite being associated with prognosis for multiple tumors. Thus, we examined the clinical outcomes of prostate cancer patients who had combined anoikis-related genes. In our study, we identified a powerful feature and validated it in two other independent databases. In addition, we integrated single-cell data to confirm that several carcinogenic pathways in the high anoikis score group were significantly overactivated.

2 Results

2.1 Consensus clustering of anoikis-related genes

Figure 1 describes the flowchart of this study. First, the mutations of anoikis related genes were analyzed. PIK3CA mutation frequency was the highest (2%), followed by TSC2, TLE1, AKT1, MTOR (Figure 2A). The location of anoikis-related genes in the chromosome is shown in Figure 2B. Accordingly, two subgroups of PRAD patients were defined based on their expression profiles of anoikis-related genes (Figure 2C; Supplementary Figure S1). K-M analysis showed that BCRF survival was significantly better in cluster 2 than in cluster 1 (Figure 2D). GSVA enrichment analysis showed that cluster 1 was mainly related to metabolism, mismatch repair, and cell cycle, such as NEGATIVE REGULATION OF METAPHASE ANAPHASE TRANSITION OF CELL CYCLE, BASE EXCISION REPAIR, MISMATCH REPAIR, DNA REPLICATION, GLYOXYLATE, and DICARBOXYLATE METABOLISM. PYRIMIDINE METABOLISM. On the contrary, cluster 2 is mainly related to stem cell proliferation, angiogenesis, and other pathways (Figures 2E–F). However, cluster 2 shows a better survival outcome, so the analysis content needs to be further explored. Taken together, our findings suggest that the two anoikis-associated subgroups are well separated in terms of prognostic outcome and biological function.

2.2 Anoikis-based model construction

As a first step, WGCNA identified the gene modules closely related to the anoikis subtype (647 genes, Figure 3A). The TCGA cohort was analyzed with univariate Cox regression and 83 prognostic genes were identified (Figure 3B). RSF analysis further identified 27 candidate genes for model construction based on the minimum depth method (Figure 3C). Using multivariate Cox regression, eight important genes were selected to form an anoikis score, namely THSD4, PIK3R1, SULF1, B4GALT1, CDC20, COL1A2, S100A10, B4GALNT4, NUAK1.

Patients were stratified into high-risk and low-risk groups based on the median risk score derived from the anoikis gene signature. Kaplan-Meier analysis revealed a significant difference in biochemical recurrence-free (BCRF) survival times between the high-risk and low-risk cohorts (Figure 3D). The distribution of risk scores, survival status, and risk level of each patient are visualized in Figure 3E. The anoikis gene signature demonstrated consistent prognostic power for 1-year (AUC = 0.74), 3-year (AUC = 0.768), and 5-year (AUC = 0.781) BCRF survival (Figure 3F). Additionally, we validated the risk model in two external datasets, MSKCC and GSE70769, where it maintained strong prognostic performance (Figures 3G–L). Further analysis illuminated correlations between higher anoikis scores and more advanced tumor (T) staging, higher Gleason scores (GS), and increased likelihood of BCR, implicating this gene signature as a marker of aggressive disease (Figure 4A). High-risk patients were also more likely to originate from the poor prognosis cluster 1 identified in our previous work (Figure 4B). Univariate Cox regression indicated the anoikis score and clinical variables were significantly associated with BCRF survival. Moreover, the anoikis score retained independent prognostic value in multivariate analysis after adjusting for other clinical factors (Figure 4C). ROC curve

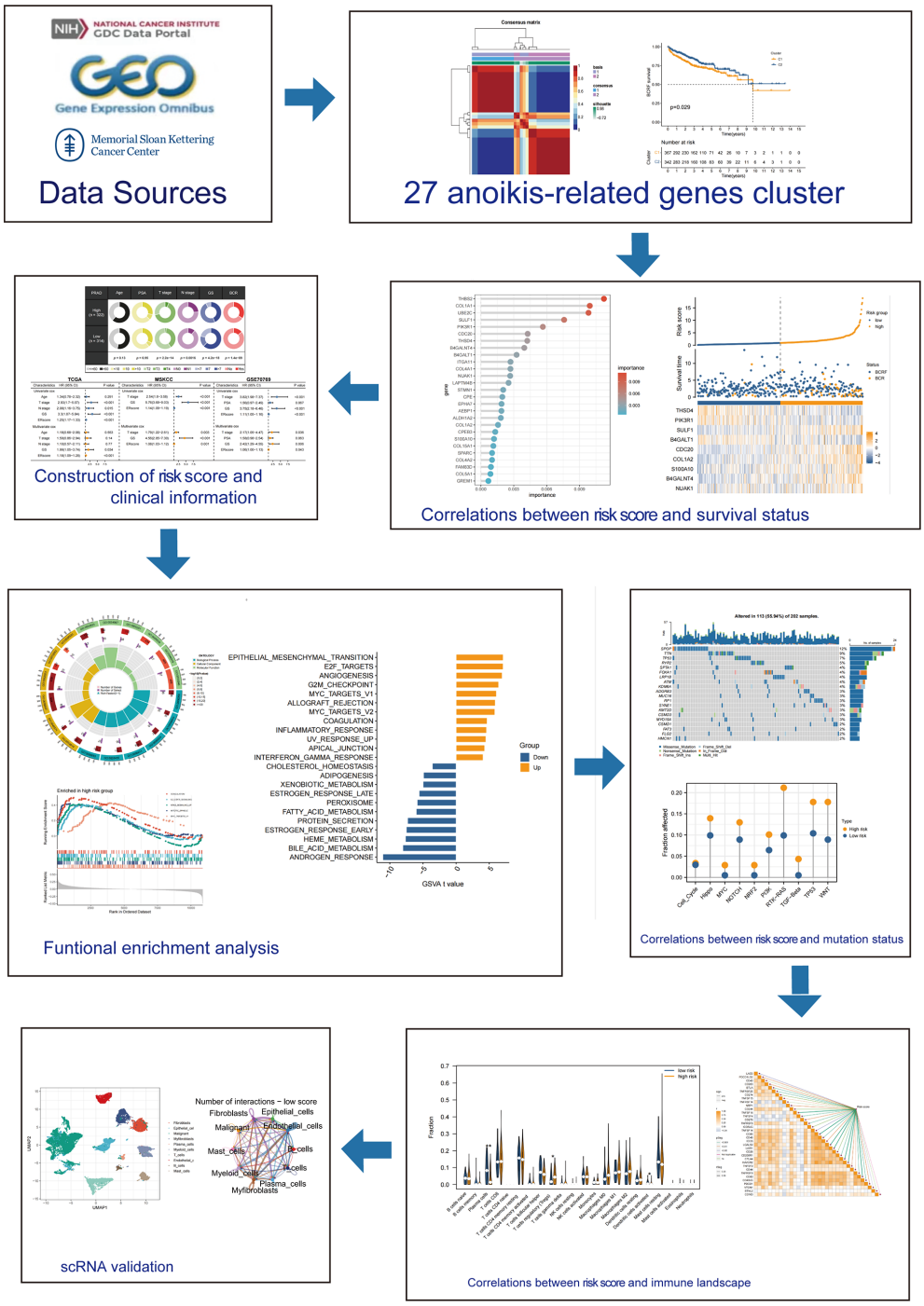

FIGURE 1
Flow chart of the main steps of this study.

analysis verified the superior predictive accuracy of the risk model over individual clinical variables. External validation in the MSKCC and GSE70769 cohorts confirmed the reproducible prognostic utility of the anoikis gene signature for BCRF prediction (Figures 4D–F). Taken together, these findings strongly endorse the anoikis gene signature as a robust and reliable prognostic indicator for prostate cancer. Further investigation is warranted to determine the biological mechanisms underlying this model and assess its clinical value in guiding management and therapeutic decisions.

2.3 Functional enrichment analysis

To examine the potential mechanisms of risk score, GO and KEGG analyses were conducted. According to Figure 5A, GO analysis shows

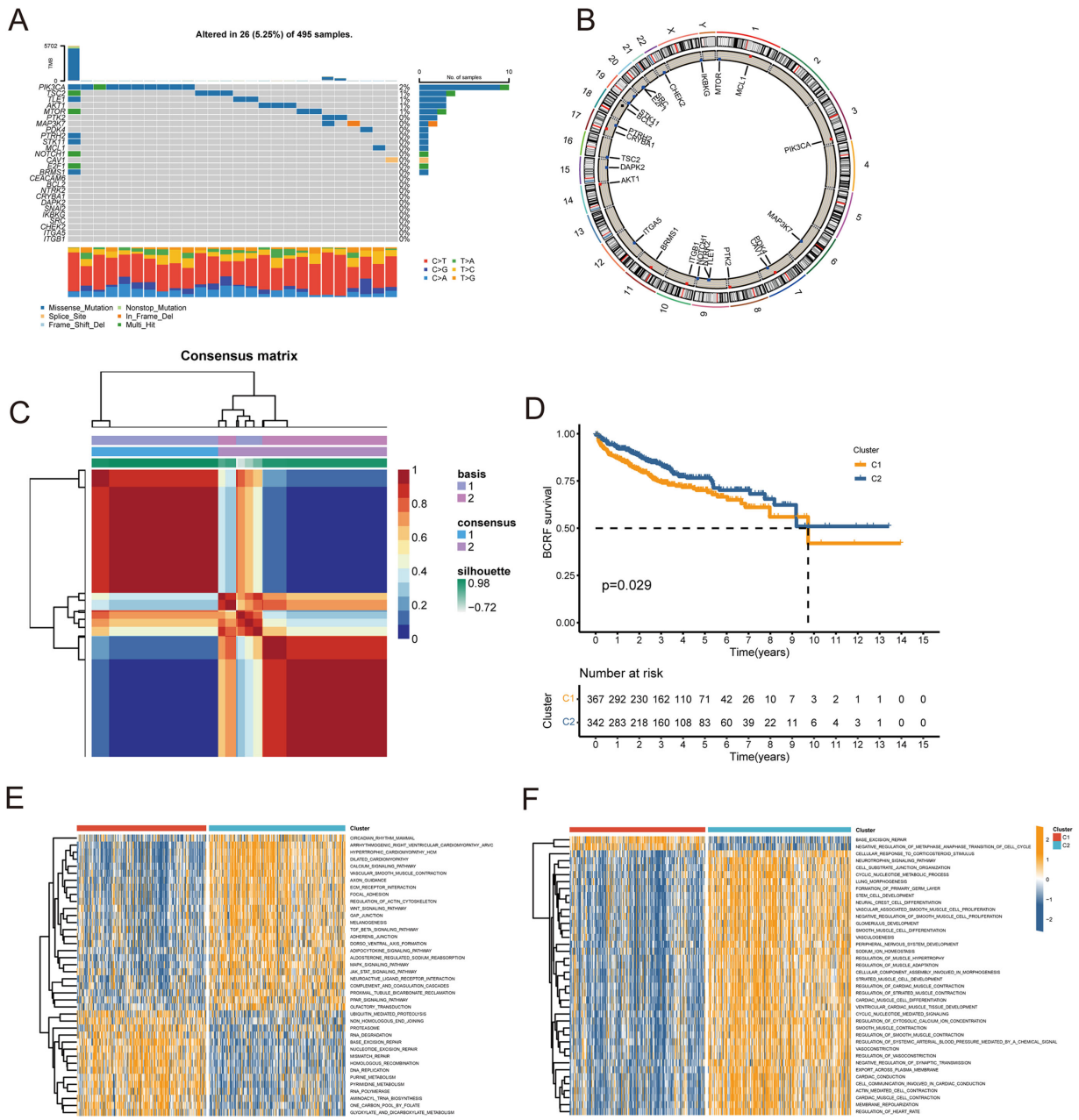

FIGURE 2
Consensus clustering of anoikis-related genes. **(A)** Waterfall plot for mutation analysis of anoikis-related genes. **(B)** Circle plot showing the location of anoikis-related genes in chromosomes. **(C)** Heatmap of NMF cluster analysis. **(D)** Survival analysis of C1 and C2 subtypes. **(E, F)** GSVA enrichment analysis of C1 and C2 Isoforms.

that there are mainly pathways associated with GO: 0003823, 0005201, and 0009897. According to KEGG analysis, differentially expressed genes were enriched in hsa04512, hsa05144, and other pathways (Figure 5B). Subsequently, 50 carcinogenic marker pathways were included in the GSVA, and the results showed that carcinogenic pathways such as EPI-THELIAL MESENCHYMAL TRANSITION, E2F TARGETS, and ANGIOGENESIS were up-regulated, while metabolic-related pathways were down-regulated (Figure 5C). Significant enrichment of 15 pathways was found in high-risk cohorts, whereas a significant enrichment of 5 pathways was found in low-risk cohorts, as shown in Figure 5D. Kaplan-Meier method was used to analyze the pathways obtained through cross-over, and different BCRF survival probabilities of several known carcinogenic path-ways (ANDROGEN RESPONSE, E2F TARGETS, G2M CHECKPOINT, MYC TARGETS V1) were observed (Figure 5E). Overall, the risk score is involved in a variety of biological functions, especially the carcinogenic pathways in PRAD.

2.4 Analysis of somatic mutations

As you can see in the waterfall diagram, gene mutations differ between high-risk and low-risk populations (Figures 6A, B). High-risk cohorts exhibited the most mutations at TP53, while low-risk

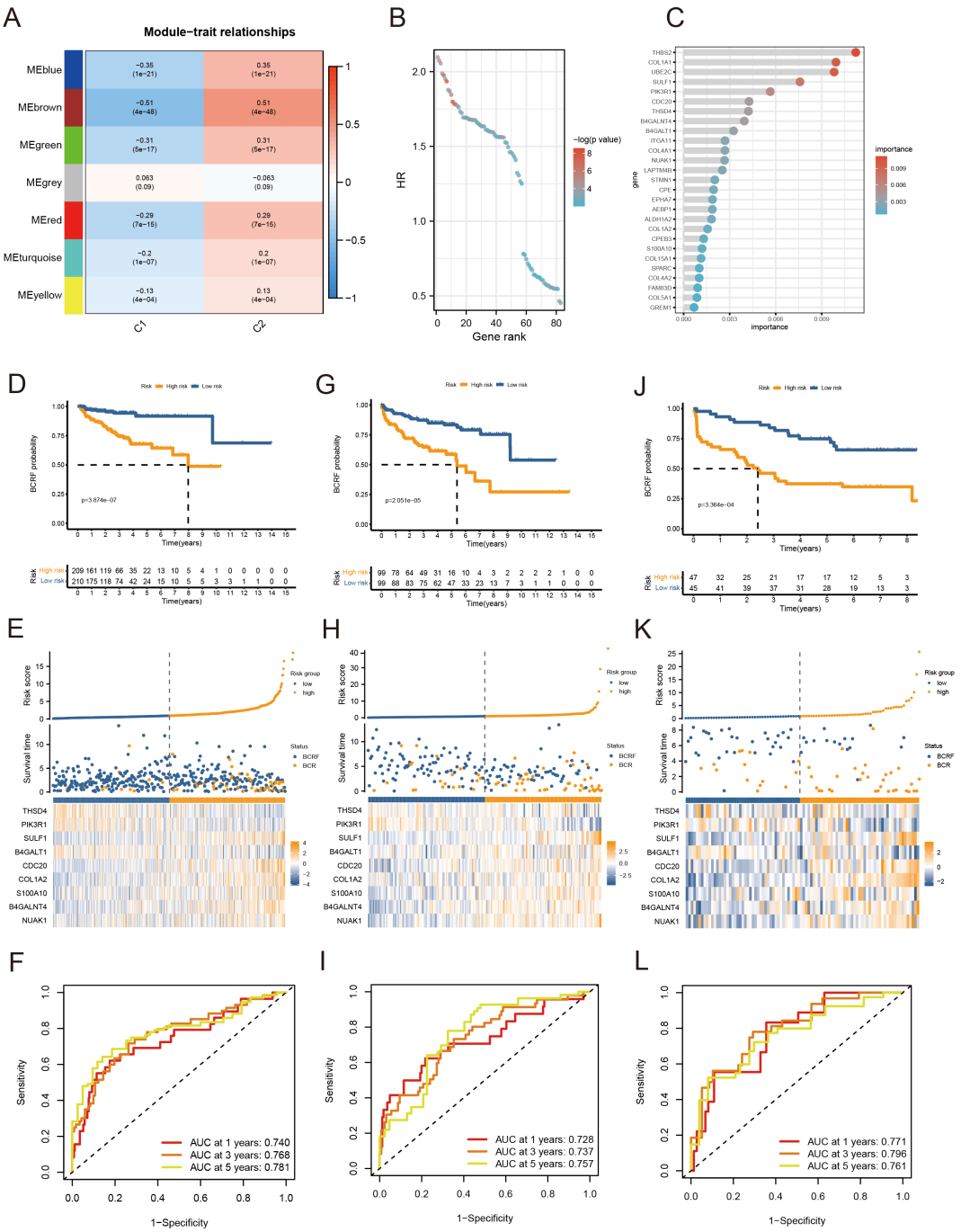

FIGURE 3
Anoikis-based model construction. **(A)** Heat map showing gene modules analyzed by WGCNA. **(B)** Dot plot for univariate Cox regression. **(C)** Screening modeling genes based on random forest analysis. **(D–F)** Kaplan – Meier curves, heat maps, and ROC curves for survival analysis of the training set cohort. **(G–I)** Kaplan – Meier curves, heat maps, and ROC curves for survival analysis of the MSKCC cohort. **(J–L)** Kaplan – Meier curves, heat maps, and ROC curves for survival analysis of the GSE70769 cohort.

cohorts showed the most mutations at SPOP. In addition, the first 25 mutant genes between the two cohorts also showed co-occurrence or exclusive mutations (Figure 6C). Mutation enrichment of known carcinogenic pathways showed that the Hippo, RTK-RAS, TP53, and WNT signaling pathways were significantly increased in the high-risk group, while the MYC, NRF2, and TGF-beta signaling pathways were significantly reduced (Figure 6D). Further analysis also confirmed a positive correlation between TMB and anoikis score, with higher TMB and poorer BCRF survival (Figures 6F, G). The worst prognosis was associated with high TMB and anoikis scores (Figure 6E). In summary, the comprehensive analysis revealed the mutational differences between high-risk and low-risk cohorts, and multiple significant genes and pathways showed significant mutation abnormalities between cohorts.

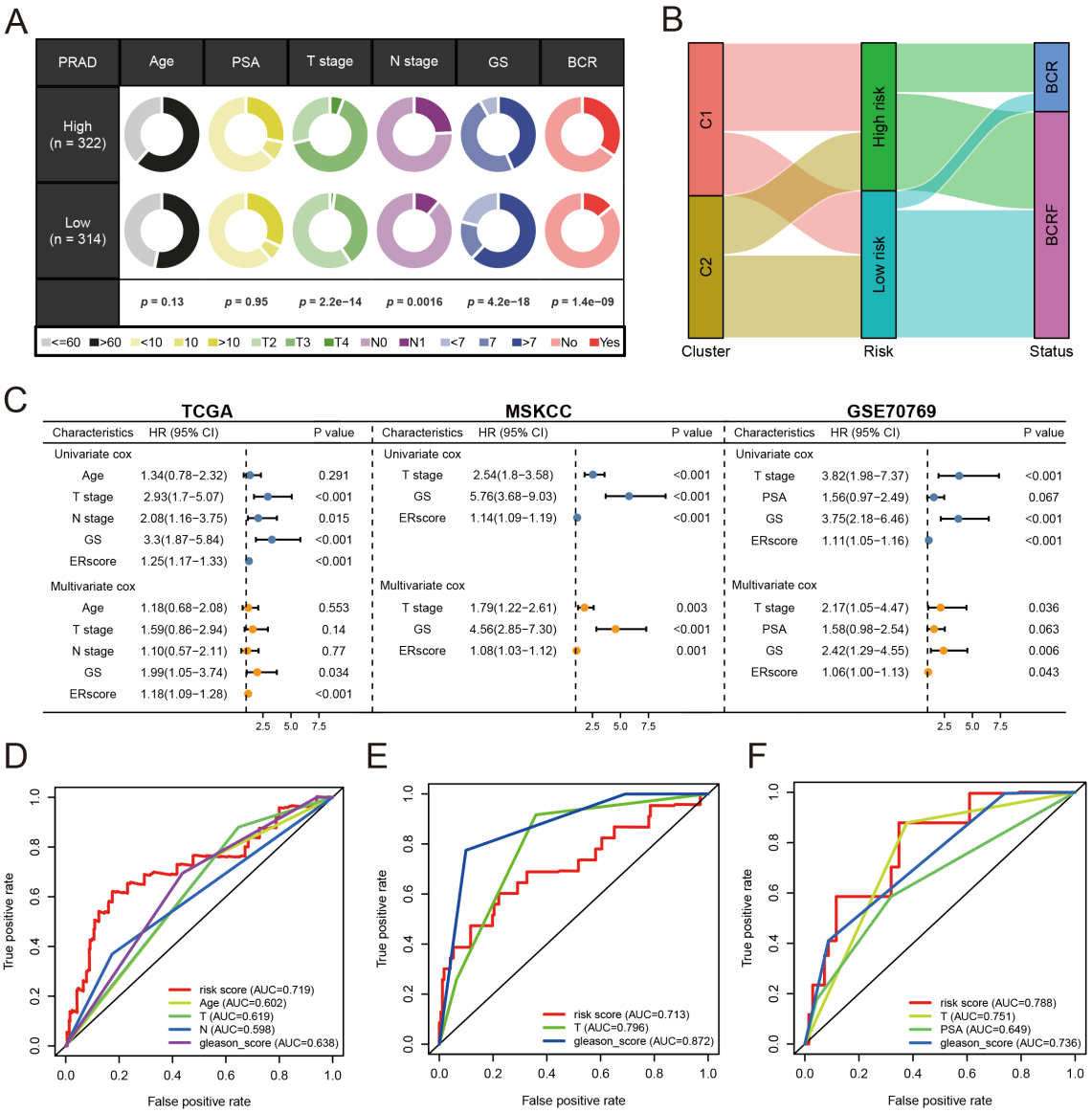

FIGURE 4
Analysis of anoikis score. **(A)** Pie chart for anoikis score versus clinical traits analysis. **(B)** Sanky chart for prognostic survival in patients at risk. **(C)** Forest plot for multivariate Cox regression analysis of risk scores in the three cohorts. **(D)** ROC analysis of anoikis score in the training set cohort. **(E)** ROC analysis of anoikis score in the MSKCC cohort. **(F)** ROC analysis of anoikis score in the GSE70769 cohort.

2.5 Immune landscape and treatment response prediction

High-risk groups had a higher number of T cell regulatory (Treg) cells than low-risk groups based on immune landscape analysis (Figure 7A). Most immune functions increased relatively in the high-risk group (Figure 7B). The expression of immunosuppressive receptors and immunosuppressive ligands was also higher in high-risk patients (Figure 7C). Additionally, the TIDE algorithm determined that there were no significant differences in immunotherapy response between high-risk and low-risk patients (Figure 7D). The prediction results of the IMvigor210 cohort and the GSE91061 cohort showed no difference in the effect of immunotherapy (Figure 7E). To evaluate chemotherapy response in PRAD patients with different Anoikis scores, the oncopredict R package was used. Our results showed that the IC50 values of high-risk patients in several chemotherapy molecules were significantly lower, including WIKI4, WEHI−539, MIM1, AZD7762, JQ1, Tozasertib, Axitinib (Figure 7F). Overall, immune landscape analysis showed that risk score was associated with different immune responses, and chemotherapy may be more effective than immunotherapy for high-risk patients.

2.6 scRNA-seq data analysis

After sample pretreatment, the cells were aggregated and annotated into 10 major clusters of fibroblasts, epithelial cells, malignant cells,

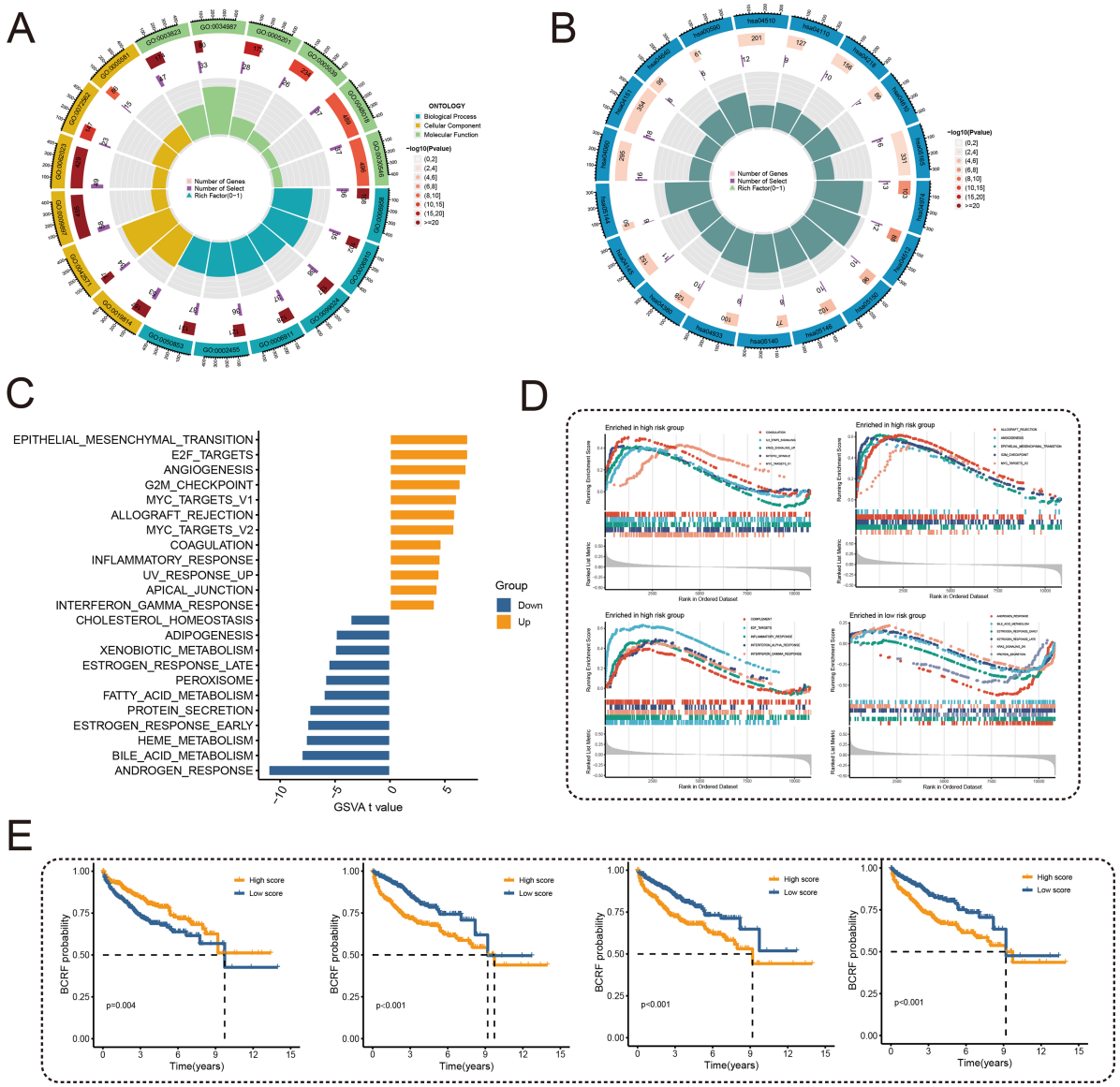

FIGURE 5
Functional enrichment analysis. **(A)** Circle plot for GO enrichment analysis. **(B)** Circle plot for KEGG enrichment analysis. **(C)** Bar graph of GSVA analysis of 50 oncogenic marker pathways. **(D)** GSEA enriched pathway analysis. **(E)** Survival curves for different BCRFs in four pathways: androgen response, E2F target, G2M check-point, MYC target V1.

myofibroblasts, plasma cells, myeloid cells, T cells, endothelial cells, B cells and mast cells (Figure 8A). The expression of signature genes in cell subsets suggests that our clustering was successful (Supplementary Figure S2A). The distribution of cell types in each sample is shown in Supplementary Figure S2B. Subsequently, we divided all cells into high and low groups according to anoikis-related AUC scores (Figure 8B). The high anoikis score group showed an increased number and intensity of intercellular interactions based on ligand-receptor signals (Figures 8C, D). In comparison with the low anoikis score group, the VEGF signaling pathway network and CCL signaling pathway networks were enhanced in the high anoikis scores group (Figures 8E, F). Overall, patients in the high anoikis score group and the low anoikis score group showed differences in intercellular communication, whereas several carcinogenic pathways were significantly overactivated in the high anoikis score group.

2.7 Validating the ARG-based signature model genes

To further demonstrate the accuracy of the, we used three prostate cancer cell lines (PC3 (RRID: CVCL_0035), DU145 (RRID: CVCL_0105), and LNCaP (RRID: CVCL_0395)) and a normal prostate epithelial cell line, RWPE-1 (RRID: CVCL_3791). B4GALNT4 and NUAK1 were validated in the model, respectively. the mRNA of B4GALNT4 was sequentially highly

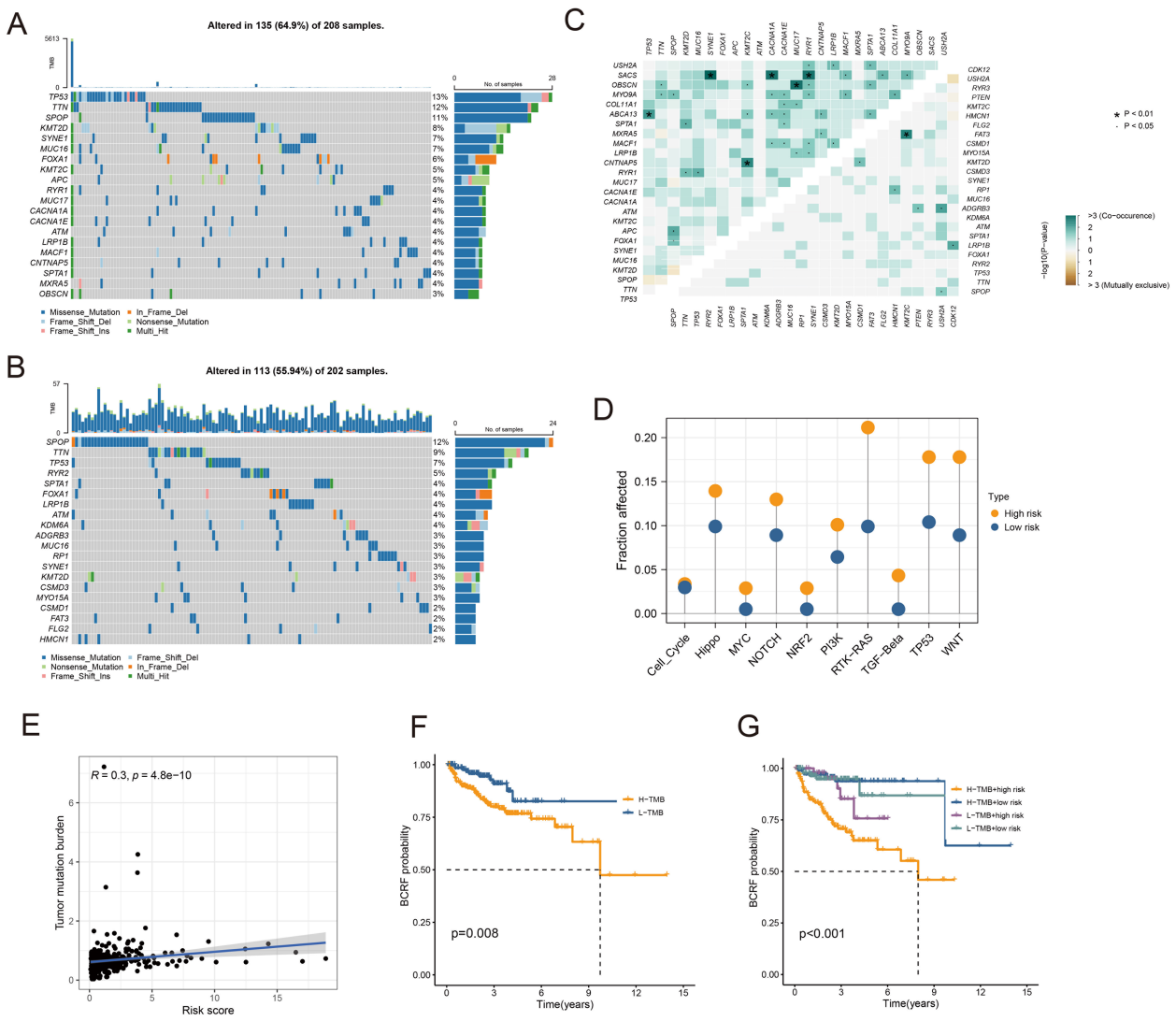

FIGURE 6
Analysis of somatic mutations. **(A)** Waterfall plot of gene mutation frequency in high-risk patients. **(B)** Waterfall plot of gene mutation frequency in low-risk patients. **(C)** Heatmap for correlation analysis between mutated genes. **(D)** Mutant gene pathway analysis between high and low-risk groups. **(E)** Scatter plot for correlation analysis between TMB and risk score. **(F)** Survival analysis between patients in high and low TMB groups. **(G)** Survival analysis between high and low TMB patients and high and low-risk patients.

expressed in LNCaP, PC3 and DU145, and lowly expressed in RWPE-1 (Figure 9A). In addition, the mRNA of NUAK1 was similarly highly expressed in the prostate cancer cell lines (sequentially PC3, DU145, and LNCaP) (Figure 9B).

3 Discussion

Prostate cancer poses a major threat to men's health worldwide (18). While prostate-specific antigen (PSA) is widely used for diagnosis and prognostication, it has limitations in accuracy and timeliness. Thus, there is an urgent need for robust biomarkers to improve prediction of prostate cancer prognosis. Recent evidence indicates that apoptosis, a form of programmed cell death, critically regulates the biological behaviors of various cancers (19, 20). For instance, CPT1A which controls fatty acid oxidation can confer anoikis resistance and promote colorectal cancer metastasis (21). IQGAP1 has also been shown to enhance viability and inhibit anoikis by activating Src/FAK signaling in hepatocellular carcinoma, suggesting its potential as a marker for metastasis and prognosis (22). Additionally, CCN2 suppresses lung cancer progression through anoikis pathways involving DAPK (23). Hence, targeting anoikis-related genes may provide promising therapeutic and prognostic opportunities in cancer.

In the present study, we identified a total of 27 anoikis-related genes (ARGs) and developed a robust ARG-based signature model with significant prognostic utility in prostate cancer. This 9-gene model comprised THSD4, PIK3R1, SULF1, B4GALT1, CDC20, COL1A2, S100A10, B4GALNT4 and NUAK1, all of which have established functional relevance in cancer. For instance, THSD4 is downregulated in prostate cancer and cooperates with other genes to drive malignant transformation (24). Clinical sequencing by

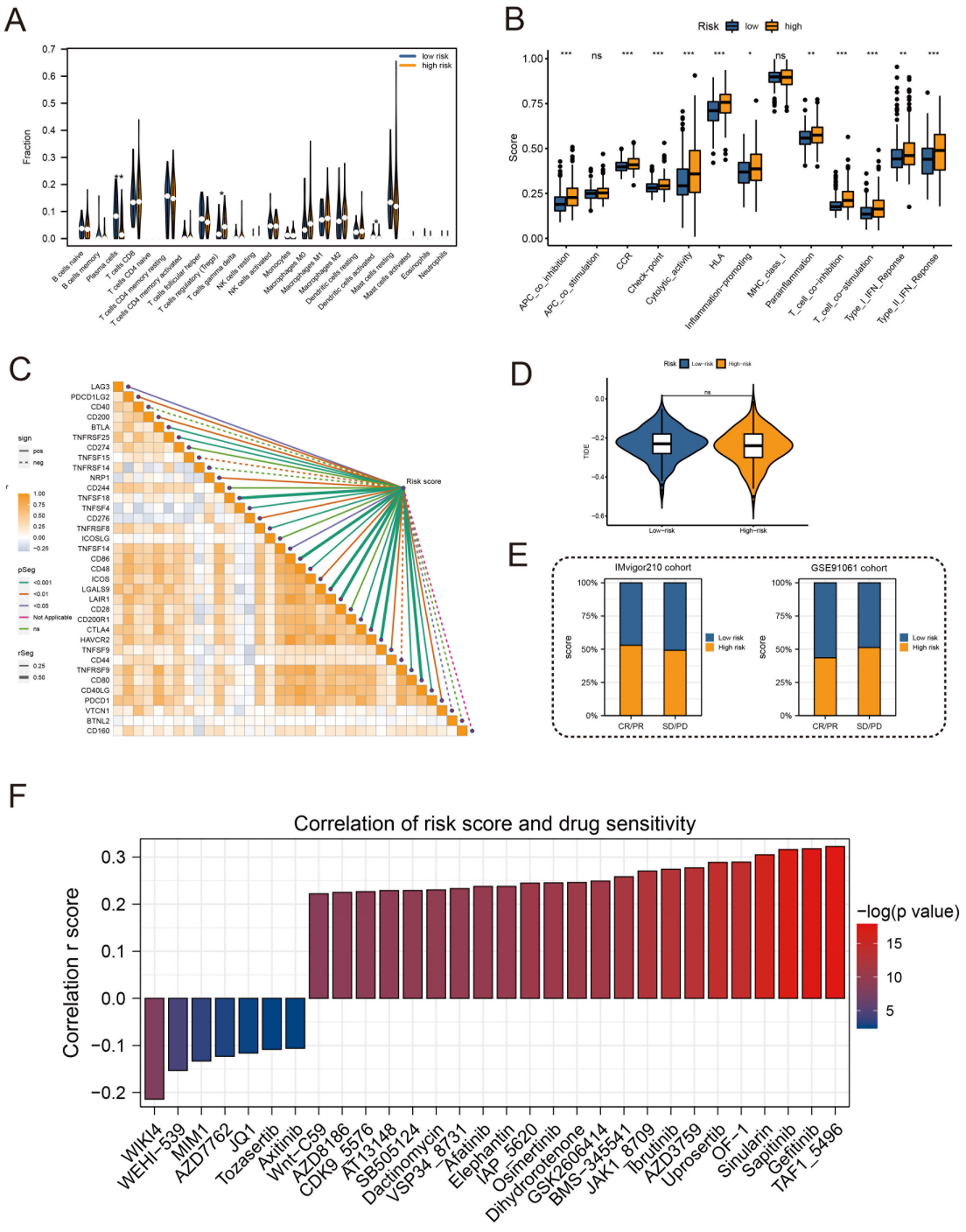

FIGURE 7
Immune profile and prediction of response to treatment. **(A)** Violin plot for immune cell infiltration analysis. **(B)** Boxplots for immunologic function assays. **(C)** Heatmap of correlation analysis between immunosuppressive receptors and immunosuppressive ligands and risk scores. **(D)** Violin plot for immunotherapy response analysis in high-risk and low-risk groups. **(E)** Bar plots of immunotherapy response analysis for the IMvigor210 cohort and GSE91061 cohort. **(F)** Drug sensitivity analysis between patients in high and low-risk groups. (*:p<0.05, **:p<0.01, ***:p<0.001).

Chakraborty et al. revealed alterations in PIK3R1 as a potential key regulator of the insulin-PI3K-glycolysis pathway in prostate cancer (25). SULF1 was demonstrated to antagonize Wnt3A-induced growth and disrupt cellular architecture in prostate cancer models (26). B4GALT1 was identified as a unique tumor suppressor silenced by AKR1C3 activation, thereby facilitating castration-resistant prostate cancer progression (27). Additionally, while CDC20, COL1A2 and S100A10 possess recognized pro-oncogenic activities, the precise roles of B4GALNT4 and NUAK1 in prostate cancer warrant elucidation. Functional characterization of these ARGs could unveil novel mechanisms driving disease progression and metastasis. Critically evaluating their clinical utility as

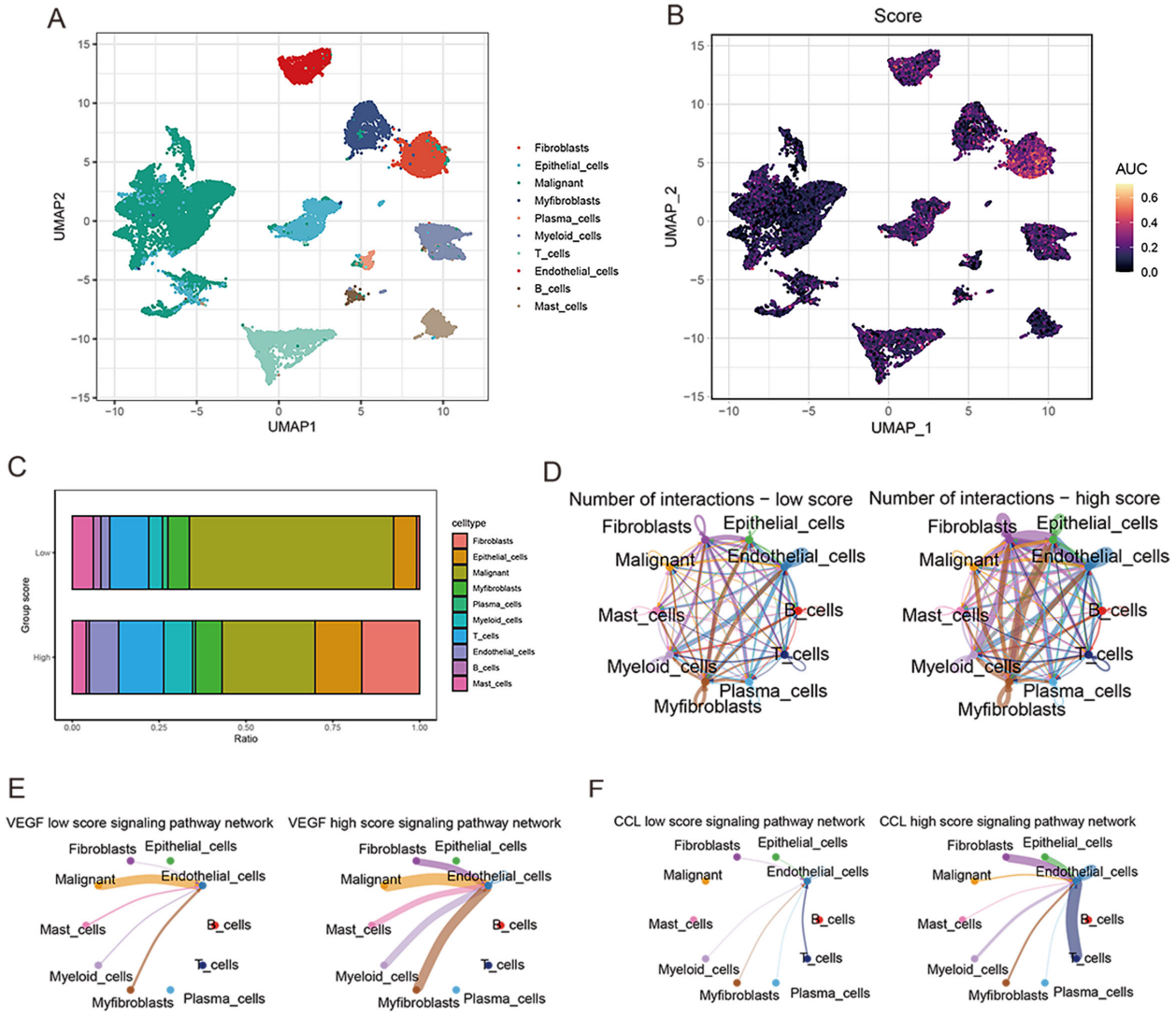

FIGURE 8
ScRNA-seq data analysis. **(A)** UMAP plot for single-cell dimensional cluster analysis. **(B)** Expression of anoikis score in single cell subsets. **(C)** Bar graph of cell content for samples from the high and low anoikis score groups. **(D)** Network diagram for cellular communication analysis. **(E)** The difference in VEGF signal between high and low anoikis scores. **(F)** The difference in CCL signal between high and low anoikis scores.

prognostic biomarkers and therapeutic targets will enable personalized management. Our findings provide a compelling rationale for investigating this anoikis gene signature, given the predictive power of these 9 ARGs for improving prostate cancer risk assessment, prognostication, and informing clinical decision-making. Future studies validating this signature in independent cohorts and delineating the molecular pathways are warranted to realize its full translational potential.

Through an unbiased gene set variation analysis (GSVA), we identified biological pathways associated with the anoikis gene signature in prostate cancer. Enrichment of established oncogenic pathways including epithelial-mesenchymal transition (EMT), E2F targets, and angiogenesis was observed in the high-risk group, whereas metabolic pathways were downregulated. These pathways have known roles in driving prostate cancer progression. For example, EMT and DNA repair pathway activation can increase therapeutic resistance and invasiveness (27), while E2F inhibition triggers replication stress representing a potential treatment approach (28). Moreover, angiogenesis is a recognized key factor enabling irreversible tumor growth (29, 30). Intriguingly, our GSVA screen also revealed involvement of cholesterol/lipid metabolism and extracellular matrix organization pathways, which have emerging links to prostate cancer through dysregulated lipid metabolism and matrix remodeling (31–33). By systematically delineating the functional interactions between anoikis-related genes and impacted pathways, our findings provide a foundation to uncover novel mechanisms of treatment resistance in prostate cancer. Elucidating how this gene signature influences oncogenic signaling and metabolic programs could illuminate new therapeutic targets and strategies to overcome resistance. Future experimental validation is warranted to realize the full translational potential of these biological insights.

Recently, novel immunotherapeutic approaches have emerged for prostate cancer management (31). The tumor

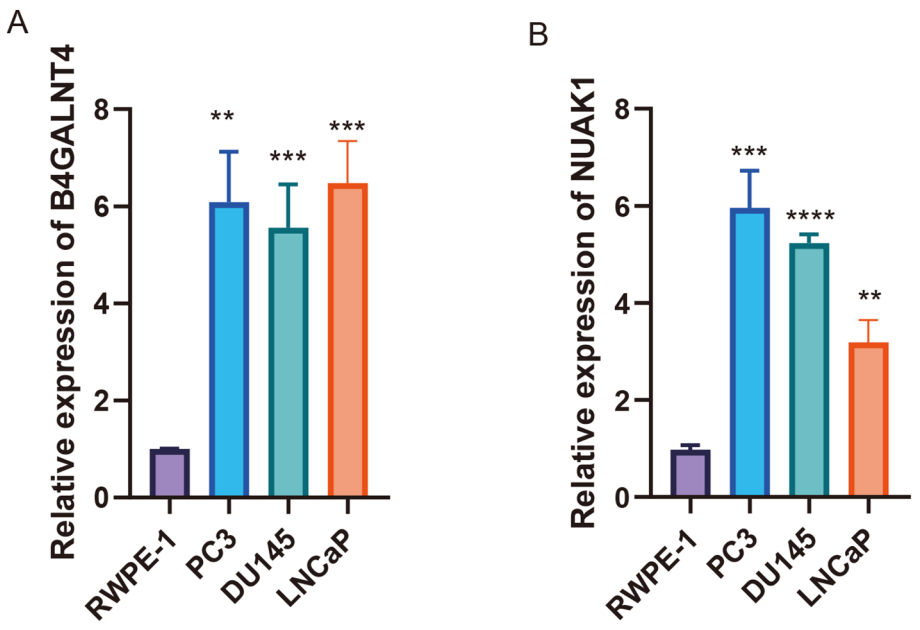

FIGURE 9
Validating the ARG-based signature model genes. **(A, B)** The expression of B4GALNT4 and NUAK1 in RWPE-1, LNCaP, PC3 and DU145 (**:p<0.01, ***:p<0.001).

microenvironment comprising stromal cells, vasculature and immune infiltrates plays a crucial role in cancer progression and metastasis (32). Multiple studies have demonstrated that immunosuppressive cells can promote tumor growth and metastasis within the microenvironment (33–35). However, the lack of understanding of the prostate cancer microenvironment and immune landscape has resulted in suboptimal responses to immunotherapy in patients. Additionally, numerous immunotherapies effective in preclinical studies have failed in clinical trials, underscoring the limitations of current prostate cancer models (36). To evaluate the utility of our risk signature in predicting immunotherapy response, we analyzed immune-associated cell infiltration in tumors with high versus low risk scores (37, 38). Our findings suggest this approach of stratifying immunotherapy response holds promise, pending experimental validation. Future research is warranted to systematically characterize the immuno-phenotypes associated with anoikis gene expression, which could guide more precise immunotherapeutic strategies and improve outcomes for prostate cancer patients. Large scale validation studies, especially those incorporating assessments before and after immunotherapy, are essential to firmly establish the clinical utility of this gene signature in immune response prediction.

Although our proposed model demonstrates promising results in predicting prostate cancer prognosis, there remain several limitations that need to be addressed before it can be widely applied in clinical practice (39). Firstly, as the current study utilizes public databases for analysis, the model has not been verified on real-world patient data. Further validation on clinical samples is required to confirm its prognostic power. Secondly, while gene expression profiling can identify potential prognostic biomarkers, additional experiments such as immunohistochemistry, immunofluorescence and analysis of clinical variables are necessary to elucidate the underlying mechanisms and interactions between the identified genes and prostate cancer progression. Thirdly, the potential biological pathways and downstream effects of the prognostic gene signature remain to be fully characterized through *in vitro* and *in vivo* functional studies (40). In addition, we also note the role of epigenetic modifications in prostate cancer, where histone methylation modifications promote epithelial cell migration, proliferation, etc., as well as play a role in the expression of anti-apoptotic genes to enhance the viability of prostate cancer cells. We will consider the more comprehensive role of Anoikis in relation to prostate cancer in future studies (41). Finally, as prostate cancer is a highly heterogeneous disease, the model may need to be optimized and tailored to specific molecular subtypes (42). Extensive analysis on large cohorts reflecting diverse patient populations will help improve its generalizability and clinical utility. In summary, though promising, the current prognostic model requires more rigorous validation and mechanistic investigation before its effects on guiding patient management and improving prostate cancer survival outcomes can be realized. We propose several follow-up studies to address these limitations and bring the model closer to clinical application.

4 Materials and methods

4.1 Data preprocessing

We downloaded RNA transcriptome data from 501 PRAD tumors and 52 normal tissues in the TCGA database, along with corresponding clinical data. Download standardized RNA expression data and complete clinical data for 231 PRAD patients from the MSKCC database, and 94 PRAD patients from the GEO

database. Adjust the batch effect through the 'sva 'R package. The IMvigor 210 cohort of bladder cancer patients receiving anti-PD-L1 treatment was obtained through the ' IMvigor210 Core Biologies ' R package, and the GSE91016 data set receiving anti-PD-1 and anti-CTLA4 treatment was also obtained to predict the efficiency of immunotherapy. In addition, we registered the single-cell RNA sequencing (scRNA-seq) dataset (GSE137829) for six PRAD patients and performed quality control, cell clustering, and annotation using the 'Seurat 'R package.

4.2 Consensus clustering analysis

From the MSigDB database, 27 anoikis-related genes were identified (Supplementary Table S1). The PRAD samples were subdivided according to these genes using the non-negative matrix factorization (NMF) method in the R package ' NMF '. We used the K-M survival curve to compare biochemical recurrence-free (BCRF) survival between sub-groups. Two gene sets were extracted from the MsigDB database to estimate the difference in biological function and immune activity between subgroups using gene set variation analysis (GSVA) with the ' GSVA 'R package. The statistically significant cut-off for GSVA is p.adjust < 0.05.

4.3 Generation of anoikis-related signatures

To establish anoikis-related features, we used WGCNA to find gene modules significantly associated with anoikis-related subgroups and extract corresponding genes. We used the TCGA cohort as the training set, while the MSKCC and GSE70769 datasets were the validation sets. A univariate Cox analysis was performed to examine prognostic genes ($p<0.05$). Using the ' randomForestSRC ' R package, the prognostic genome was further reduced using Random Survival Forests (RSF). A smaller value indicates greater predictability when variables were sorted by minimum depth in RSF analysis. Using multivariate Cox regression analysis, the best features associated with anoikis were identified based on their respective coefficients (β) and gene expression levels (Exp). The formula is used to calculate each patient's anoikis-related risk score. Using the median of their anoikis scores, we further categorize the patients into two groups. Kaplan-Meanoikis was used to determine prognostic differences between the two groups. In addition, we examined the correlation between anoikis score and clinical features, including age, PSA level, TN stage, and Gleason score (GS). Cox analyses were performed univariately and multivariate to evaluate the prognostic significance of Anoikis scores. Similarly, we collected the MSKCC and GSE70769 cohorts to check the risk score's predictive ability.

4.4 Functional enrichment analysis

Genes that are differentially expressed between low-risk and high-risk cohorts have been identified as potential mechanisms behind anoikis. Gene Ontology (GO) enrichment and Kyoto Encyclopedia of Genes and Genomes (KEGG) pathway analysis were performed using the R package clustanoikisProfilanoikis. The R package ' loop ' shows GO and KEGG terms with p 0.05. The MSigDB was analyzed using GSVA to determine the differences in the carcinogenic marker pathways (h.all v7.1.symbols) between the two cohorts. For the same signature pathway, gene set enrichment analysis (GSEA) was conducted using the 'GSEA 'R package (FDR < 0.25, NES > 1, p.adjust < 0.05). The prognostic significance of GSVA and GSEA overlapping marker pathways was determined using the K-M method.

4.5 Somatic mutation analysis

Somatic mutations in PRAD patients were extracted from the TCGA database. The ' maftools ' R package explored specific somatic mutation variants in different risk score groups. Next, we studied the coexistence or exclusion of mutations, oncogenes, and enrichment of known carcinogenic pathways between the two cohorts. The tumor mutation burden (TMB) reflecting the total mutation count of each PRAD patient was calculated and its correlation with the anoikis score was tested. In addition, we analyzed the predictive value of TMB and Anoikis score for survival outcomes in the Anoikis score risk cohort.

4.6 Immune landscape and treatment response prediction

In high-risk and low-risk groups, we compared immune cell abundance, immune function, and immune checkpoints. On the basis of RNA expression profiles of PRAD patients, the tumor immune dysfunction and rejection algorithm (TIDE) predicts potential immunotherapy responses. The IMvigor210 and GSE91061 datasets were also used to determine the correlation between the Anoikis score and the efficacy of potential immunotherapy. In addition, we investigated the chemotherapy responses of the two groups of patients, and the ' oncopredict ' R package predicted the sensitivity of each patient to chemotherapy.

4.7 scRNA-seq data analysis

Next, we use the GSE137829 dataset to study the single-cell characteristics of PRAD. The software Seurat (version 4.3.0) were then used to process and evaluate the gene expression matrix. Based on the number of identified genes per cell (500–7000) and the percentage of mitochondrial genes expressed (10%), we performed Seurat-based filtering of the cells. Additionally, the ribosomal and mitochondrial genes were taken out of the gene expression matrix. After quality inspection, 21,292 high-quality cells with an average of 2419 genes per cell were kept. Then, we calculated the activity of risk score-related gene sets at the single cell level through the ' AUCell 'R package. After dividing all cells according to AUC, we classified them into two groups: high and low. By using the R software package CellChat, signaling pathways were analyzed between participants with high anoikis scores and those with low anoikis scores.

4.8 qRT-PCR

Prostate cancer cell lines (PC3 (RRID: CVCL_0035), DU145 (RRID: CVCL_0105) and LNCaP (RRID: CVCL_0395)) and normal prostate epithelial cell line RWPE-1 (RRID: CVCL_3791) were purchased from Shanghai Zhongqiao Xinzhou Biotech Co. and cultured in DMEM medium containing 10% FBS and 1% penicillin-streptomycin (Solarbio, Beijing, China). FBS and 1% penicillin-streptomycin in DMEM medium (Solarbio, Beijing, China). For isolation of total RNA, TRIzol reagent (from Invitrogen, Carlsbad, CA, USA) was used and RNA was reverse transcribed to cDNA using ReverTra Ace qPCR RT premix and gDNA Remover kit. cDNA was extracted from the RNA by SYBR Premix Ex Taq II on a Mx3005P Real-Time Fluorescence Quantitative PCR System (from Stratagene, San Diego, CA, USA). qRT-PCR was performed and GAPDH was selected as an endogenous control for mRNA. The reaction conditions were pre-denaturation at 95°C for 10 min, denaturation at 95°C for 5 s, and annealing at 60°C for 30 s, for a total of 45 cycles. Amplification of target and internal endogenous reference genes was performed separately for each sample. Each set of samples contained 3 replicate wells. Data were analyzed using the 2^(-ΔΔCt) method. The primer sequences are detailed in Supplementary File 1.

5 Conclusions

This comprehensive study unravels the intricate relationship between anoikis and bone metastasis in prostate cancer. Our findings shed light on the critical role of anoikis in driving metastatic progression, contributing to our understanding of the underlying biomarkers and molecular mechanisms. The identified anoikis-related gene signatures and dysregulated molecular pathways hold promise as potential targets for prognostication and therapeutic interventions in the management of prostate cancer.

Data availability statement

The original contributions presented in the study are included in the article/Supplementary Material. Further inquiries can be directed to the corresponding author.

Author contributions

WX: Data curation, Writing – original draft, Writing – review & editing. MY: Investigation, Methodology, Writing – review & editing. BJ: Data curation, Methodology, Software, Writing – review & editing. GX: Conceptualization, Investigation, Writing – review & editing. GCX: Methodology, Writing – review & editing. QZ: Data curation, Writing – review & editing. RH: Writing – original draft, Writing – review & editing.

Funding

The author(s) declare financial support was received for the research, authorship, and/or publication of this article. This research was funded by the Science and Technology research project of The Education Department of Jiangxi Province (No. GJJ211550 and GJJ2201413), and the Science and Technology Project of Jiangxi Provincial Health Commission (No. 202310780 and No. 202310840).

Conflict of interest

The authors declare that the research was conducted in the absence of any commercial or financial relationships that could be construed as a potential conflict of interest.

Publisher's note

Supplementary material

The Supplementary Material for this article can be found online at: https://www.frontiersin.org/articles/10.3389/fonc.2024.1446894/full#supplementary-material

SUPPLEMENTARY FIGURE 1
The optimal number of clusters was determined by co-occurrence, dispersion, and contour indices, and the optimal number of clusters selected was 2.

SUPPLEMENTARY FIGURE 2
Single cell dimension reduction cluster analysis. **(A)** Bubble plots showing expression of signature genes in cell subsets. **(B)** Distribution of cell types in each sample.

References

1. Kimura T, Egawa S. Epidemiology of prostate cancer in Asian countries. *Int J Urol*. (2018) 25:524–31. doi: 10.1111/iju.2018.25.issue-6

2. Dijkstra S, Mulders PF, Schalken JA. Clinical use of novel urine and blood based prostate cancer biomarkers: a review. *Clin Biochem*. (2014) 47:889–96. doi: 10.1016/j.clinbiochem.2013.10.023

3. Negoita S, Feuer EJ, Mariotto A, Cronin KA, Petkov VI, Hussey SK, et al. Annual Report to the Nation on the Status of Cancer, part II: Recent changes in prostate cancer trends and disease characteristics. *Cancer*. (2018) 124:2801–14. doi: 10.1002/cncr.v124.13

4. Miyake H, Muramaki M, Kurahashi T, Takenaka A, Fujisawa M. Expression of potential molecular markers in prostate cancer: correlation with clinicopathological

outcomes in patients undergoing radical prostatectomy. *Urol Oncol.* (2010) 28:145–51. doi: 10.1016/j.urolonc.2008.08.001

5. Cornford P, Bellmunt J, Bolla M, Briers E, De Santis M, Gross T, et al. EAU-ESTRO-SIOG guidelines on prostate cancer. Part II: treatment of relapsing, metastatic, and castration-resistant prostate cancer. *Eur Urol.* (2017) 71:630–42. doi: 10.1016/j.eururo.2016.08.002

6. Mason JA, Hagel KR, Hawk MA, Schafer ZT. Metabolism during ECM detachment: achilles heel of cancer cells? *Trends Cancer.* (2017) 3:475–81. doi: 10.1016/j.trecan.2017.04.009

7. Henson PM, Vandivier RW, Douglas IS. Cell death, remodeling, and repair in chronic obstructive pulmonary disease? *Proc Am Thorac Soc.* (2006) 3:713–7. doi: 10.1513/pats.200605-104SF

8. Song L, Rape M. Reverse the curse–the role of deubiquitination in cell cycle control. *Curr Opin Cell Biol.* (2008) 20:156–63. doi: 10.1016/j.ceb.2008.01.012

9. Paoli P, Giannoni E, Chiarugi P. Anoikis molecular pathways and its role in cancer progression. *Biochim Biophys Acta.* (2013) 1833:3481–98. doi: 10.1016/j.bbamcr.2013.06.026

10. Eckert LB, Repasky GA, Ulku AS, McFall A, Zhou H, Sartor CI, et al. Involvement of Ras activation in human breast cancer cell signaling, invasion, and anoikis. *Cancer Res.* (2004) 64:4585–92. doi: 10.1158/0008-5472.CAN-04-0396

11. Aixinjueluo W, Furukawa K, Zhang Q, Hamamura K, Tokuda N, Yoshida S, et al. Mechanisms for the apoptosis of small cell lung cancer cells induced by anti-GD2 monoclonal antibodies: roles of anoikis. *J Biol Chem.* (2005) 280:29828–36. doi: 10.1074/jbc.M414041200

12. Ye G, Yang Q, Lei X, Zhu X, Li F, He J, et al. Nuclear MYH9-induced CTNNB1 transcription, targeted by staurosporin, promotes gastric cancer cell anoikis resistance and metastasis. *Theranostics.* (2020) 10:7545–60. doi: 10.7150/thno.46001

13. Yue GG, Lee JK, Li L, Chan KM, Wong EC, Chan JY, et al. Andrographis paniculata elicits anti-invasion activities by suppressing TM4SF3 gene expression and by anoikis-sensitization in esophageal cancer cells. *Am J Cancer Res.* (2015) 5:3570–87.

14. Wang J, Luo Z, Lin L, Sui X, Yu L, Xu C, et al. Anoikis-associated lung cancer metastasis: mechanisms and therapies. *Cancers (Basel).* (2022) 14. doi: 10.3390/cancers14194791

15. Liao Q, Chen L, Zhang N, Xi Y, Hu S, Ng DM, et al. Network analysis of KLF5 targets showing the potential oncogenic role of SNHG12 in colorectal cancer. *Cancer Cell Int.* (2020) 20:439. doi: 10.1186/s12935-020-01527-x

16. Guo JC, Xie YM, Ran LQ, Cao HH, Sun C, Wu JY, et al. L1CAM drives oncogenicity in esophageal squamous cell carcinoma by stimu-lation of ezrin transcription. *J Mol Med (Berl).* (2017) 95:1355–68. doi: 10.1007/s00109-017-1595-4

17. Lee Y, Yoon J, Ko D, Yu M, Lee S, Kim S. TMPRSS4 promotes cancer stem-like properties in prostate cancer cells through upregulation of SOX2 by SLUG and TWIST1. *J Exp Clin Cancer Res.* (2021) 40:372. doi: 10.1186/s13046-021-02147-7

18. Rawla P. Epidemiology of prostate cancer. *World J Oncol.* (2019) 10:63–89. doi: 10.14740/wjon1191

19. Meier P, Finch A, Evan G. Apoptosis in development. *Nature.* (2000) 407:796–801. doi: 10.1038/35037734

20. Lowe SW, Lin AW. Apoptosis in cancer. *Carcinogenesis.* (2000) 21:485–95. doi: 10.1093/carcin/21.3.485

21. Wang YN, Zeng ZL, Lu J, Wang Y, Liu ZX, He MM, et al. CPT1A-mediated fatty acid oxidation promotes colorectal cancer cell metastasis by inhibiting anoikis. *Oncogene.* (2018) 37:6025–40. doi: 10.1038/s41388-018-0384-z

22. Mo CF, Li J, Yang SX, Guo HJ, Liu Y, Luo XY, et al. IQGAP1 pro-motes anoikis resistance and metastasis through Rac1-dependent ROS accumulation and activation of Src/FAK signalling in hepatocellular carcinoma. *Br J Cancer.* (2020) 123:1154–63. doi: 10.1038/s41416-020-0970-z

23. Chang CC, Yang MH, Lin BR, Chen ST, Pan SH, Hsiao M, et al. CCN2 inhibits lung cancer metastasis through promoting DAPK-dependent anoikis and inducing EGFR degradation. *Cell Death Differ.* (2013) 20:443–55. doi: 10.1038/cdd.2012.136

24. Wu J, Li X, Luo F, Yan J, Yang K. Screening key miRNAs and genes in prostate cancer by microarray analysis. *Transl Cancer Res.* (2020) 9:856–68. doi: 10.21037/tcr.2019.12.30

25. Chakraborty G, Nandakumar S, Hirani R, Nguyen B, Stopsack KH, Kreitzer C, et al. The impact of PIK3R1 mutations and insulin-PI3K-glycolytic pathway regulation in prostate cancer. *Clin Cancer Res.* (2022) 28:3603–17. doi: 10.1158/1078-0432.CCR-21-4272

26. Brasil da Costa FH, Lewis MS, Truong A, Carson DD, Farach-Carson MC. SULF1 suppresses Wnt3A-driven growth of bone metastatic prostate cancer in perlecan-modified 3D cancer-stroma-macrophage triculture models. *PloS One.* (2020) 15:e0230354. doi: 10.1101/2020.02.28.969485

27. Wang B, Wu S, Fang Y, Sun G, He D, Hsieh JT, et al. The AKR1C3/AR-V7 complex maintains CRPC tumour growth by repressing B4GALT1 expression. *J Cell Mol Med.* (2020) 24:12032–43. doi: 10.1111/jcmm.v24.20

28. Kim YR, Oh KJ, Park RY, Xuan NT, Kang TW, Kwon DD, et al. HOXB13 promotes androgen independent growth of LNCaP prostate cancer cells by the activation of E2F signaling. *Mol Cancer.* (2010) 9:124. doi: 10.1186/1476-4598-9-124

29. Yarden Y, Baselga J, Miles D. Molecular approach to breast cancer treatment. *Semin Oncol.* (2004) 31:6–13. doi: 10.1053/j.seminoncol.2004.07.016

30. Zhao Y, Cai C, Zhang M, Shi L, Wang J, Zhang H, et al. Ephrin-A2 promotes prostate cancer me-tastasis by enhancing angiogenesis and promoting EMT. *J Cancer Res Clin Oncol.* (2021) 147:2013–23. doi: 10.1007/s00432-021-03618-2

31. Sridhar SS, Freedland SJ, Gleave ME, Higano C, Mulders P, Parker C, et al. Castra-tion-resistant prostate cancer: from new pathophysiology to new treatment. *Eur Urol.* (2014) 65:289–99. doi: 10.1016/j.eururo.2013.08.008

32. Anderson NM, Simon MC. The tumor microenvironment. *Curr Biol.* (2020) 30:R921–5. doi: 10.1016/j.cub.2020.06.081

33. Kuo CL, Chou HY, Chiu YC, Cheng AN, Fan CC, Chang YN, et al. Mitochondrial oxidative stress by Lon-PYCR1 maintains an immunosuppressive tumor microenvironment that promotes cancer progression and metastasis. *Cancer Lett.* (2020) 474:138–50. doi: 10.1016/j.canlet.2020.01.019

34. Goubran HA, Kotb RR, Stakiw J, Emara ME, Burnouf T. Regulation of tumor growth and metastasis: the role of tumor microenvironment. *Cancer Growth Metastasis.* (2014) 7:9–18. doi: 10.4137/CGM.S11285

35. Kahlert C, Kalluri R. Exosomes in tumor microenvironment influence cancer progression and metastasis. *J Mol Med (Berl).* (2013) 91:431–7. doi: 10.1007/s00109-013-1020-6

36. Kaczanowska S, Joseph AM, Davila E. TLR agonists: our best frenemy in cancer immunotherapy. *J Leukoc Biol.* (2013) 93:847–63. doi: 10.1189/jlb.1012501

37. Liu Z, Zhong J, Zeng J, Duan X, Lu J, Sun X, et al. Characterization of the m6A-associated tumor immune microenvironment in prostate cancer to aid immunotherapy. *Front Immunol.* (2021) 12:735170. doi: 10.3389/fimmu.2021.735170

38. Tang S, Zhuge Y. An immune-related pseudogene signature to improve prognosis prediction of endometrial carcinoma patients. *BioMed Eng Online.* (2021) 20:64. doi: 10.1186/s12938-021-00902-7

39. Huntley C, Torr B, Sud A, Rowlands CF, Way R, Snape K, et al. Utility of polygenic risk scores in UK cancer screening: a modelling analysis. *Lancet Oncol.* (2023) 24:658–68. doi: 10.1016/S1470-2045(23)00156-0

40. Spratt DE, Yousefi K, Deheshi S, Ross AE, Den RB, Schaeffer EM, et al. Individual patient-level meta-analysis of the performance of the decipher genomic classifier in high-risk men after prostatectomy to predict development of metastatic disease. *J Clin Oncol.* (2017) 35:1991–8. doi: 10.1200/JCO.2016.70.2811

41. Luo H, Li Y, Song H, Zhao K, Li W, Hong H, et al. Role of EZH2-mediated epigenetic modification on vascular smooth muscle in cardiovascular diseases: A mini-review. *Front Pharmacol.* (2024) 15:1416992. doi: 10.3389/fphar.2024.1416992

42. Hwang C, Heath EI. Angiogenesis inhibitors in the treatment of prostate cancer. *J Hematol Oncol.* (2010) 3:26. doi: 10.1186/1756-8722-3-26

frontiers | Frontiers in Pharmacology

TYPE Original Research
PUBLISHED 08 October 2024
DOI 10.3389/fphar.2024.1446920

OPEN ACCESS

EDITED BY
Jialin Meng,
University of Science and Technology of China, China

REVIEWED BY
Jungshan Chang,
Taipei Medical University, Taiwan
Lian Zeng,
Huazhong University of Science and Technology, China

*CORRESPONDENCE
Tianyuan Xu,
xvtianyuan@126.com
Zonglin Wu,
cnurol@126.com
Keyi Wang,
wangkeyi0910@163.com

†These authors have contributed equally to this work

RECEIVED 10 June 2024
ACCEPTED 23 September 2024
PUBLISHED 08 October 2024

CITATION
Song W, Zhang H, Lu Y, Zhang H, Ni J, Chang L, Gu Y, Wang G, Xu T, Wu Z and Wang K (2024) KHSRP knockdown inhibits papillary renal cell carcinoma progression and sensitizes to gemcitabine.
Front. Pharmacol. 15:1446920.
doi: 10.3389/fphar.2024.1446920

KHSRP knockdown inhibits papillary renal cell carcinoma progression and sensitizes to gemcitabine

Wei Song[1,2,3†], Heng Zhang[4†], Yi Lu[1†], Houliang Zhang[5], Jinliang Ni[5], Lan Chang[5], Yongzhe Gu[6], Guangchun Wang[3], Tianyuan Xu[3*], Zonglin Wu[1*] and Keyi Wang[1,3*]

[1]Department of Urology, Shanghai Shidong Hospital of Yangpu District, Shanghai, China, [2]Department of Urology, Shanghai Putuo District People's Hospital, Tongji University, Shanghai, China, [3]Department of Urology, Shanghai 10th People's Hospital, School of Medicine, Tongji University, Shanghai, China, [4]Guiqian International General Hospital, Guiyang, China, [5]Shanghai Putuo District Health Affairs Management Center, Hospital Operation Department, Shanghai, China, [6]Department of Neurology, Shanghai 10th People's Hospital, School of Medicine, Tongji University, Shanghai, China

Patients diagnosed with papillary renal cell carcinoma (pRCC) exhibit a high rate of clinical metastasis; however, the underlying molecular mechanism is unclear. In this study, KH-type splicing regulatory protein (KHSRP) participated in pRCC progression and was associated with metastasis. It was positively correlated with the hallmark of epithelial-mesenchymal transition. KHSRP inhibition effectively alleviated the cellular function of migration and invasion. Additionally, KHSRP knockdown inhibited the proliferative ability of pRCC cells. A pharmaceutical screening was based on the KHSRP protein structure. Gemcitabine (Gem) decreased KHSRP expression. UIO-66@Gem@si-KHSRP (UGS) nanoparticles (NPs) were prepared for targeted delivery and applied in both *in vitro* and *in vivo* experiments to explore the clinical transition of KHSRP. UGS NPs exhibited better performance in inhibiting cellular proliferation, migration, and invasion than Gem. Additionally, the *in vivo* experiment results confirmed their therapeutic effects in inhibiting tumor metastasis with excellent biosafety. The silico analysis indicated that KHSRP knockdown increased cytotoxic cell infiltration in the tumor microenvironment to potentiate anti-tumor effects. Thus, KHSRP can promote pRCC progression as an oncogene and serve as a target in clinical transition through UGS NP-based therapy.

KEYWORDS

papillary renal cell carcinoma, metastasis, KHSRP, gemcitabine, target therapy

Introduction

Renal cell carcinoma (RCC) is a common tumor of the urinary system. RCC incidence is associated with the region and sex, with a higher incidence in men than in women and in urban than in rural areas. The age of onset ranges between 50 and 70 years (Mao et al., 2022). Papillary renal cell carcinoma (pRCC) is the most common pathological type of RCC apart from clear cell renal cell carcinoma (ccRCC). It accounts for 10%–15% of all RCC cases (Patard et al., 2005). pRCC is of two types, namely, types 1 and 2. Type 1 is more common and develops gradually. Type 2 is more malignant and develops rapidly (Peruzzi and Bottaro, 2006). p pRCC can invade, compress, and destroy the renal calyx and pelvis.

Simultaneously, it can break through the outer renal peritoneum to form a vascular thrombus or metastasize to the lymph nodes (LN) and other organs. LN is the most common site of pRCC metastasis (Dudani et al., 2021; Karaman and Detmar, 2014). However, the biological characteristics of pRCC are unclear.

KH-type splicing regulatory protein (KHSRP) is a multifunctional RNA-binding protein involved in the transcriptional and post-transcriptional regulation of gene expression (Palzer et al., 2022; Trabucchi et al., 2009). KHSRP is central to numerous biological processes, including innate and adaptive immune responses, DNA damage response, inflammatory diseases, tissue remodeling, and lipid metabolism (Gherzi et al., 2014). It may play opposing roles at different stages of cancer development. For example, KHSRP inhibits motility in brain tumors and non-small cell lung cancer (NSCLC); furthermore, it is associated with a good prognosis (Yang et al., 2013; Fujita et al., 2017). In NSCLC, the anti-metastatic effects of KHSRP have been associated with inducing microRNA (miR)-23a maturation, which mediates early growth response gene 3 (EGR3) mRNA degradation. However, KHSRP can promote the growth or invasion of oesophageal squamous cell carcinoma and melanoma by enhancing miRNA maturation, such as miR-21, miR-130b, and miR-301, and by inducing Killin mRNA destabilization (Liu et al., 2019). Despite its roles in different cancers, the association between KHSRP and pRCC, including its function, molecular mechanism, and clinical potential, remains unclear.

In this study, we identified a positive correlation between KHSRP and epithelial-mesenchymal transition markers through a bioinformatics analysis. Subsequent cell function experiments demonstrated that KHSRP inhibition effectively alleviated the proliferation, migration, and invasion functions of pRCC cells. Drug screening results indicated that gemcitabine (Gem) targeted KHSRP and reduced its expression. Additionally, UIO-66@Gem@si-KHSRP (UGS) nanoparticles (NPs) were prepared for targeted delivery and applied in *ex vivo* experiments. UGS NPs exhibited superior efficacy in inhibiting cell proliferation, migration, and invasion, compared with Gem. Thus, KHSRP, an oncogene, is central to pRCC progression and can be considered a promising target for clinical translation by UGS NP-based therapies.

Methods and materials

Data collection and bioinformatics analysis

pRCC clinical data were obtained from The Cancer Genome Atlas (TCGA) database (https://genome-cancer.ucsc.edu/). A total of 291 pRCC and 32 normal tissue transcriptome data with the RNA-seq count type were analyzed to compare the clinical features. All normalized data were analyzed through the R software. The associations between KHSRP expression and clinical features, including the tumor (T), nodes (N), metastases (M) and pathological stages, were determined. Additionally, the predictive performances of KHSRP expression towards patient survival were evaluated through the Kaplan–Meier curves. Moreover, the Kyoto Encyclopedia of Genes and Genomes (KEGG), Gene Ontology (GO), and Gene Set Enrichment Analysis data were analyzed using the clusterProfiler package (R software).

Cell culture and transfection

CAKI-2 and ACHN pRCC cell lines were brought from the Cell Bank of the Chinese Academy of Sciences (Shanghai, China). These cell lines were cultured in Minimum Essential Medium and McCoy's 5A media (Gibco, United States) added with 10% fetal bovine serum (FBS, Hyclone, United States) and 1% penicillin/streptomycin (P/S, YEASEN, China), respectively, at 37°C in 5% CO_2. Small interfering KHSRP RNAs (si-KHSRP) were obtained from RIBOBIO (China) and transfected in the cells through jetPRIME (YEASEN, China). The si-KHSRP sequence was GCGTGCGGATACAGTTCAA. For inducible gene silencing, cells were cultured in 6-wells palate for 24 h with the confluence around 60%. Next, the cells were treated with si-KHSRP (5 μL per well) for 24–48 h in the presence of Lipofectamine 3000 Reagent. The cells were collected for the next experiments after the confirmation of KHSRP knockdown with the results of WB and qPCR.

RNA extraction and quantitative real-time PCR

Total RNA was extracted using the Trizol reagent (Invitrogen, United States), with the RNA concentration measured using a Nanodrop 2000 spectrophotometer (Thermo Scientific, United States). After complementary DNA synthesis, KHSRP expression was detected by reverse transcription-quantitative polymerase chain reaction with KHSRP-specific primers (Sangon Biotech, Shanghai, China). Glyceraldehyde-3-phosphate dehydrogenase (GAPDH) was considered as a control to calculate the relative RNA expression. Supplementary Material enlists the primer sequences (Supplementary Table S1).

Western blotting

The tissues or cells were lysed on ice for 30 min using a lysis buffer (PC102, Epizyme, Shanghai, China). The protein concentration was determined using a bicinchoninic acid protein assay kit (ZJ101, Epizyme, Shanghai, China). The proteins (20 μg) were separated by sodium dodecyl sulfate-polyacrylamide gel electrophoresis on 10% polyacrylamide gels and transferred onto nitrocellulose membranes (WJ004, EpiZyme, Shanghai, China). These membranes were blocked with 5% skim milk at room temperature for 1 h, followed by overnight incubation with primary antibodies at 4°C. After thorough washing, they were incubated with horseradish peroxidase-conjugated secondary antibodies at room temperature for 1 h, followed by membrane blotting using enhanced chemiluminescence detection reagents (NCM, Suzhou, China). Chemiluminescence signals were detected using an imaging system (AI600, GE, United States). Individual protein band intensities were measured using ImageJ software (NIH, Rasband, WS, United States). KHSRP and GAPDH antibodies were obtained from Abcam.

Wound healing

Wound healing experiments were conducted to assess the migration ability of cells. First, the cells underwent different treatments. Second, after 12 h of transfection, they were digested into cell suspension and seeded into six-well plates. The cell fusion rate reached 90%; subsequently, the tip of the pipette gun was used to scratch the cell layer. The tip was maintained vertically. Third, after scratching, the cells were washed with phosphate-buffered saline (PBS) three times to remove the shed cells and added to the 1640 culture medium. Finally, a similar field of view was selected for photography at 0 h and 24 h time points. The wound healing rate was determined through the ImageJ software.

Transwell assay

The invasion and migration abilities were measured through a transwell assay. First, the cells underwent different treatments. Second, after 12 h of transfection, they were digested into a cell suspension and numbered for the ensuing step. For the transwell assay, 5104 cells in 200 μL of serum-free medium were cultured in the upper chambers, with (invasion) or without (migration) Matrigel. Additionally, 500 μL of medium with 10% FBS was loaded in the lower chambers. Third, the cells were incubated in 5% CO_2 and 37°C for 24 h. After incubation, the chamber was removed and the remaining cells were extracted. Finally, the upper surface of the upper chamber was gently rubbed with a cotton swab. The lower surface of the lower chamber was washed with PBS and fixed and stained for photography.

5-ethynyl-2 deoxyuridine analysis for cell proliferation

The cells were cultured in 24-well plates after treatment and exposed to 10 μM 5-ethynyl-2 deoxyuridine (EdU) (EpiZyme, China) for 2 h at 37°C in 5% CO_2. Pre-treated cells were fixed with 4% paraformaldehyde for the ensuing stage. After washing with PBS/0.3% bovine serum albumin, they were incubated with Alexa Fluor 555 and DAPI in the dark. The EdU results were visualized through the Leica DM6 B upright microscope system (Leica, Germany).

Colony formation

A colony formation assay was performed to evaluate cell proliferation. First, the cells underwent different treatments. Second, after 12 h of transfection, they were digested into a cell suspension and numbered for the subsequent step. According to a density gradient of 1,000 cells per well, they were inoculated into a six-well plate. Third, each well was filled with the complete culture medium up to 2,000 μL. The cells were incubated in 5% CO_2 and 37°C for 14 days. Fourth, the culture was terminated upon observing visible clones in the culture dish. The culture medium was discarded and carefully soaked twice in PBS. Finally, the colonies were fixed and stained for photography after air drying. The number of clones was directly quantified.

Pharmaceutical screening for KHSRP

A pharmaceutical screening was based on the KHSRP protein crystal structure. KHSRP protein structure was obtained from the Protein Data Bank database. The structure was processed using UCSF Chimera, and the SiteMap database was used to predict the optimal binding sites. The screening library comprised the drug molecules approved for marketing by the U.S. Food and Drug Administration. It was derived from the ZINC20 database, a specialized screening molecule library consisting of 1,766 drug molecules.

USG NPs preparation and characterization

UIO-66 NPs were prepared for targeted delivery (Zhou et al., 2023; Jarai et al., 2020). Briefly, 90.0 mg (0.386 mmol) of ZrCl4 and terephthalic acid were separately added to N, N-dimethylformamide (DMF) in a 20 mL vial and sonicated for dissolution. Upon obtaining a clear solution, the samples were heated at 110°C for 24 h. After heating, they were diluted in DMF for 72 h and washed in methanol. Finally, they were dissolved in diethylpyrocarbonate (DEPC)-treated water. The size of UIO-66 NPs was measured through digital light synthesis. UGS NPs (20 μL) were dissolved in distilled water (1 mL). And the size of the UGS NPs were measured through a particle size potentiometer (Nano ZS90, Worcestershire, United Kingdom). Gem (100 μg/mL) was added to the water-diluted UIO-66 NPs and stirred for 24 h to obtain the UIO-66@Gem NPs. Then, UIO-66@Gem NPs were collected after centrifugation and washed three times. Varying concentrations of UIO-66@Gem NPs and si-KHSRP were dissolved in DEPC-treated water to prepare the UGS NPs through electrostatic interaction. Gem release was assessed through absorbance changes at 280 nm using the ultraviolet-visible-near infrared spectrometer. The experiments were measured through a UV-vis spectrophotometer. Gel electrophoresis was conducted to detect si-KHSRP encapsulation through UGS NPs. The gels were prepared and the procedures were conducted according to the previously reports (Mao et al., 2022). Using the empty plasmid as a control, UIO-66@Gem NPs with the different concentration were examined to evaluate the RNA encapsulation capability. To examine the cellular internalization of UGS NPs, the tumor cells were treated with UGS NPs for 12 h. Then, the cells were digested for the bio-TEM. The cells were collected through glutaraldehyde fixative (2.5%) overnight under 4°C. Next, the prepared cells were washed and dehydrated for the polymerization in spurr's low-viscosity solution at 60°C. Finally, the cells visualized through bio-TEM.

Animal models

A lung metastasis model was established in 4-week-old female BALB/c nude mice (Charles River, China). Briefly, 1 × 105 cells were injected into the bloodstream via the tail vein. After 3 weeks, the mice were intraperitoneally injected with D-luciferin (Goldbio, United States) (100 mg/kg), and images were captured using the AniView100 imaging system (Guangzhou, China). In the UGS NP treatment model, the mice were intravenously injected with PBS and NPs every 3 days (200 μL).

10.3389/fphar.2024.1446920

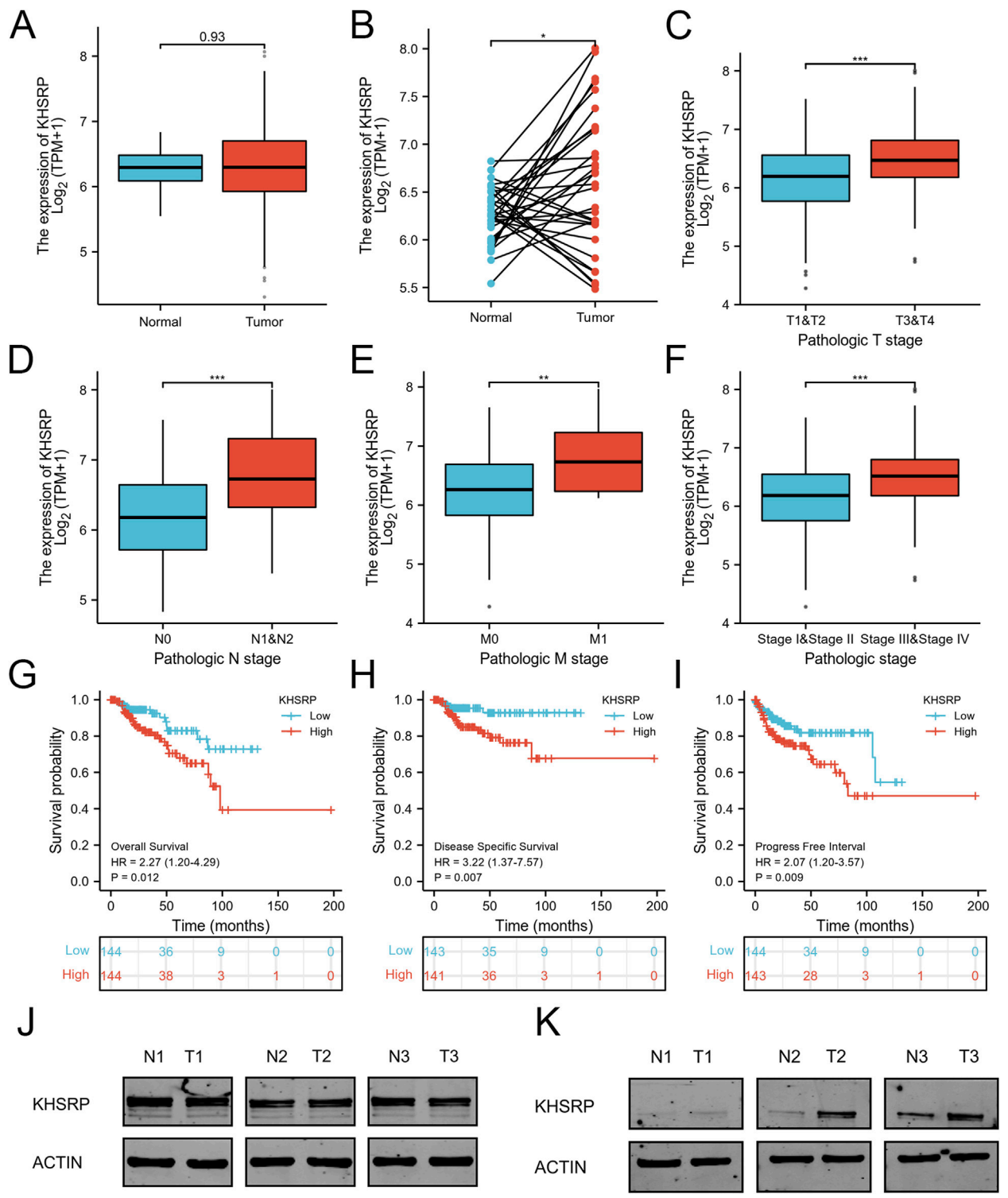

FIGURE 1
Expression analysis of KHSRP in pRCC. **(A)** Expression differences of KHSRP in the matched analysis. **(B)** Expression of KHSRP in ccRCC tissues and adjacent normal tissues. **(C–F)** Relationship between the expression of KHSPR and clinicopathological features in pRCC. **(G–I)** Kaplan-Meier curves analysis of KHSRP expression in predicting overall survival, disease-specific survival, and progress free interval. **(J)** KHSRP protein expression in ccRCC paired samples. **(K)** KHSRP protein expression in pRCC paired samples.

TABLE 1 The detailed information of clinical samples.

Characteristics	Low expression of KHSRP	High expression of KHSRP	P value
n	145	146	
Pathologic T stage, n (%)			< 0.001
T1&T2	125 (43.3%)	102 (35.3%)	
T3&T4	19 (6.6%)	43 (14.9%)	
Pathologic N stage, n (%)			0.005
N0	27 (34.6%)	23 (29.5%)	
N2&N1	6 (7.7%)	22 (28.2%)	
Pathologic M stage, n (%)			0.736
M0	43 (41.3%)	52 (50%)	
M1	3 (2.9%)	6 (5.8%)	
Pathologic stage, n (%)			0.001
Stage I&Stage II	106 (40.6%)	88 (33.7%)	
Stage III&Stage IV	21 (8%)	46 (17.6%)	
OS event, n (%)			0.010
Alive	131 (45%)	116 (39.9%)	
Dead	14 (4.8%)	30 (10.3%)	
DSS event, n (%)			0.005
No	137 (47.7%)	122 (42.5%)	
Yes	7 (2.4%)	21 (7.3%)	
PFI event, n (%)			0.031
No	123 (42.3%)	109 (37.5%)	
Yes	22 (7.6%)	37 (12.7%)	

Statistical analysis

All analyses were performed using R (v.3.6.3). A Wilcoxon test or Student's t-test was conducted to investigate the association between clinical features and KHSRP expression. Kaplan-Meier analysis was conducted to evaluate the TCGA patient survival rates. A p-value <0.05 indicated statistical significance. All data are presented as mean ± SD, and significant differences were determined based on the t-test results.

Results

KHSRP expression is negatively associated with pRCC clinical features

KHSRP participated in tumor progression as an oncogene. KHSRP expression was elevated in the tumor tissues based on the matched analysis ($p < 0.05$; Figure 1B), but not the comparative analysis (Figure 1A). Meanwhile, the relationship between KHSRP expression and T-stage ($p < 0.05$; Figure 1C), N-stage ($p < 0.05$; Figure 1D), M-stage ($p < 0.05$; Figure 1E), and pathological stage ($p < 0.05$; Figure 1F). The detailed information of all samples was exhibited in Table 1. Additionally, the receiver operating characteristic curve analysis evaluated the predictive performances of KHSRP expression in determining the higher TNM and pathological stages (Supplementary Figure S1A). Results of the Kaplan-Meier analysis confirmed that high KHSRP expression was associated with poor overall survival ($p = 0.012$; Figure 1G), disease specific survival ($p = 0.007$; Figure 1H), and progression free interval ($p = 0.009$; Figure 1I). All the results confirmed that KHSRP as the oncogene, participated in the pRCC tumor progression. Finally, protein levels in ccRCC and pRCC clinical samples were examined, and it was demonstrated that KHSRP was not differentially expressed in paired ccRCC samples (Figure 1J) and was highly expressed in pRCC (Figure 1K).

Inhibition of KHSRP alleviate the progression of pRCC

To explore the potential function of KHSRP, the correlated functional genes were screened and analyzed. GO and KEGG analyses were based on the screened functional genes. KHSRP was associated with the negative regulation of the execution phase of apoptosis according to the biological process analysis (Figure 2A). The correlated functional genes were divided into

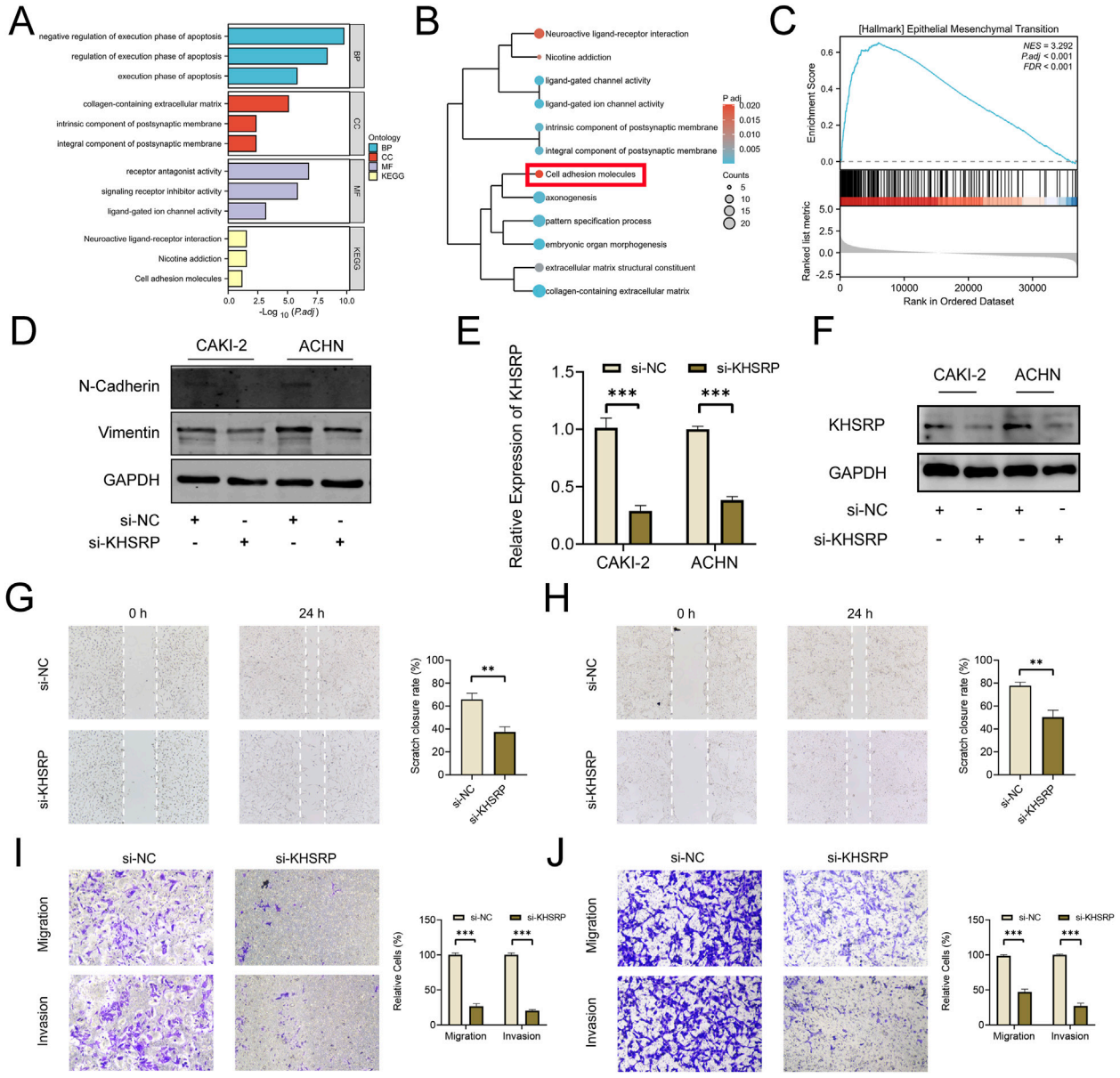

FIGURE 2
KHSRP knockdown inhibits cell migration and invasion *in vitro*. **(A)** GO and KEGG analysis of KHSRP related functional genes in pRCC. **(B)** GO and KEGG analysis of KHSRP positively related functional genes in pRCC. **(C)** GSEA analysis of KHSRP related functional genes in pRCC. **(D)** Western blotting analysis of EMT marker expression in 2 cell lines after transfection. **(E, F)** qPCR and Western blot analysis of KHSRP expression in 2 cell lines after transfection. **(G, H)** Wound-healing assay results after KHSRP knockdown in 2 cell lines for migration measurements. **(I, J)** Transwell assay results for cell migration and invasion after KHSRP knockdown in 2 cell lines.

positive and negative related subgroups, with separate GO and KEGG analyses (Figure 2B; Supplementary Figure 1B). The KEGG analysis confirmed that KHSRP was positively correlated with the cell adhesion molecules (Figure 2B). Meanwhile, the GESA analysis confirmed that KHSRP was positively associated with the hallmark of epithelial-mesenchymal transition (Figure 2C). Additionally, Western blot analysis demonstrated that KHRSP knockdown reduced the expression of epithelial-mesenchymal transition markers (Figure 2D). Based on the silico results, the function of KHSRP in promoting pRCC progression was explored *in vitro*. CAKI-2 and ACHN exhibited higher KHSRP expression than HK-2 (Supplementary Figures S1C, S2A). si-KHSRP treatment effectively inhibited KHSRP mRNA and protein expressions (Figures 2E,F). Wound healing and transwell assays were conducted with si-KHSRP treatment to assess KHSRP function in promoting pRCC progression. KHSRP knockdown alleviated the cellular migration and invasion in both cell lines (Figures 2G–J). Moreover, pRCC cell line proliferation was evaluated before/after si-KHSRP treatment. KHSRP inhibition suppressed the proliferative ability of pRCC cells (Figures 3A–C).

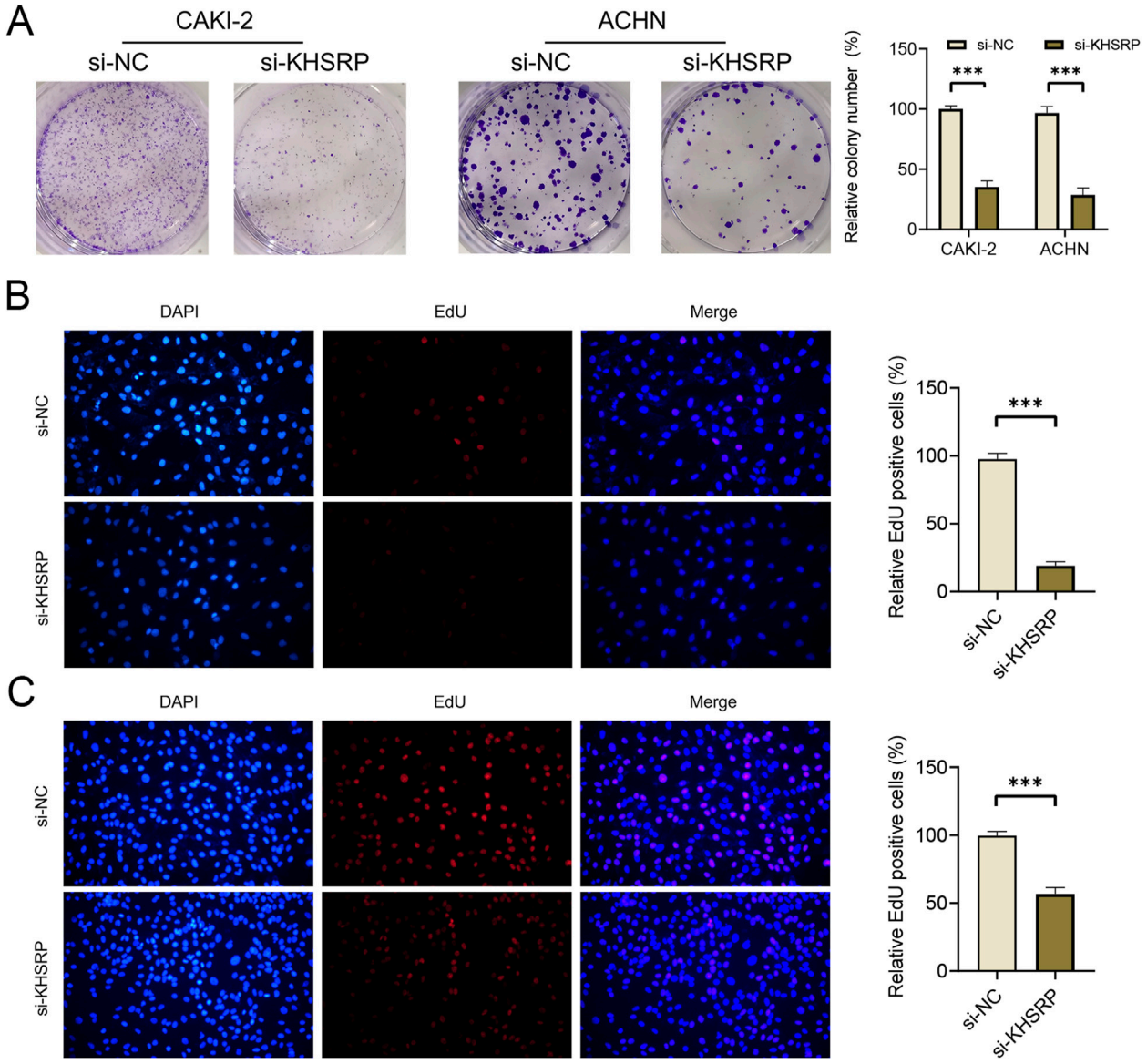

FIGURE 3
KHSRP knockdown inhibits cell proliferation *in vitro*. **(A)** Results of KHSRP knockdown in 2 cell lines evaluated through the colony assay. **(B, C)** EdU results of KHSRP knockdown in cell proliferation with the quantitative analysis in the right.

Pharmaceutical screening targets KHSRP

To explore the potential clinical therapy based on KHSRP, pharmaceutical screening was conducted to investigate the targeted drugs. Gem could bind to the KHSRP protein structure as a chemotherapy drug (Figure 4A). Gem and KHSRP formed seven hydrogen bonds, with a docking fraction of −5.769 kcal/mol (Figure 4B; Supplementary Figure S1D). Additionally, Gem treatments effectively decreased KHSRP expression in a time-dependent manner (Figure 4C), indicating Gem inhibited KHSRP expression. Furthermore, we investigated the impact of KHSRP knockdown on the IC50 of cells to Gem. Our findings revealed a notable decline in IC50 following KHSRP knockdown (Figure 4D), suggesting that KHSRP depletion enhanced the sensitivity of cells to Gem. UIO-66 NPs were prepared for the targeting delivery of Gem. It was reported that UIO-66 NPs were in an advantageous range for cellular uptake, and contained the advantage for drug delivery (Jarai et al., 2020). Both transmission electron microscopy and scanning electron microscopy confirmed the successful preparation of UIO66 NPs with uniform size and morphology (Figures 4E,G). The size of UIO66 NPs was measured through the digital light synthesis, which was around 50 nm (Supplementary Figure S2B). The energy dispersive x-ray spectroscopy mapping results affirmed that UIO-66 NPs comprised C, O, and Zr elements (Figure 4F). Meanwhile, the X-ray diffraction results suggested that the prepared UIO-66 NPs possessed the identical (111) crystal plane of 7.48o and (002) 8.62o as reported previously (Zhou et al., 2023) (Figure 4H). UIO-66@Gem NPs were synthesized (Wu et al., 2019). Fourier transform infrared spectroscopy results

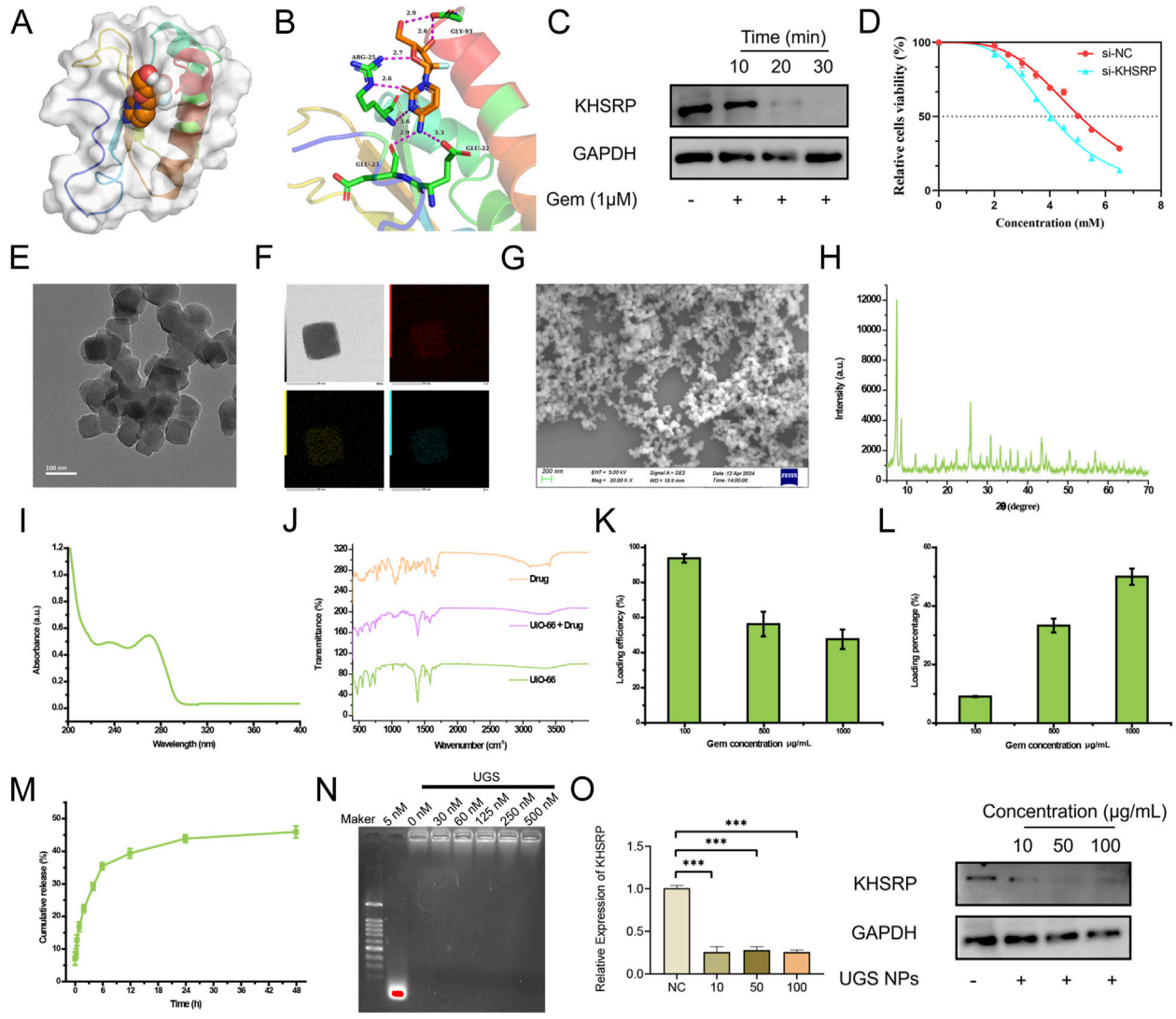

FIGURE 4
Pharmaceutical screening for KHSRP. **(A, B)** Gem could bind to the protein structure of KHSRP with 7 hydrogen bonds formed. **(C)** Western blot analysis of KHSRP expression in ACHN after Gem treatments. **(D)** IC50 for Gem in normal and low expression groups. **(E)** TEM image of UIO-66. **(F)** EDS mapping image of UIO-66. **(G)** SEM image of UIO-66. **(H)** XRD results of UIO-66. **(I)** FTIR results of UIO-66, Gem, and UIO-66@Gem. **(J)** UV-absorbance of Gem. **(K, L)** Gem loading efficiency and percentage through UIO-66. **(M)** UIO-66 could release Gem. **(N)** si-KHSRP could be loaded through UGS. **(O)** qPCR and Western blot analysis of KHSRP expression in ACHN after the treatment of UGS.

indicated that the UiO-66 NPs were loaded with Gem, matching both characteristic peaks (Figure 4I). Additionally, the Gem loading and releasing assays were based on their absorbance (Figure 4J). UIO-66 NPs effectively loaded and subsequently released Gem (Figures 4K–M). Considering the anti-tumor function of si-KHSRP, UGS NPs were prepared to achieve the combination therapy effect. UGS NPs effectively loaded the si-KHSRP at a concentration of 500 nM (Figure 4N). *In vitro* experiments were conducted to examine their anti-tumor performances. It was confirmed that UGS NPs could been effectively uptake by the tumor cells (Supplementary Figure S2C). UGS effectively inhibited KHSRP expression in both pRCC cell lines (Supplementary Figure S2D). Meanwhile, these inhibiting performances were exhibited in a concentration-dependent manner under UGS NP treatment (Figure 4O).

UGS NPs inhibit tumor progression for potential clinical therapy

To measure the anti-tumor function of UGS NPs, wound healing, and transwell assays were conducted. UGS NP treatments strongly alleviated the cellular migration and invasion in both cell lines, compared with Gem (Figures 5A–D and Supplementary Figures 2E, F). Furthermore, better pRCC cell line proliferation was observed before/after UGS NP treatment, compared with Gem treatment. The experimental evidence confirmed that UGS NP treatment suppressed the proliferative ability of pRCC cells (Figures 5E–G and Supplementary Figures 2G, H). All *in vitro* experiment results confirmed the anti-tumor function of UGS NPs. UGS NP function was explored *in vivo* using a lung metastasis model (Figure 6A). The *in vivo* imaging system

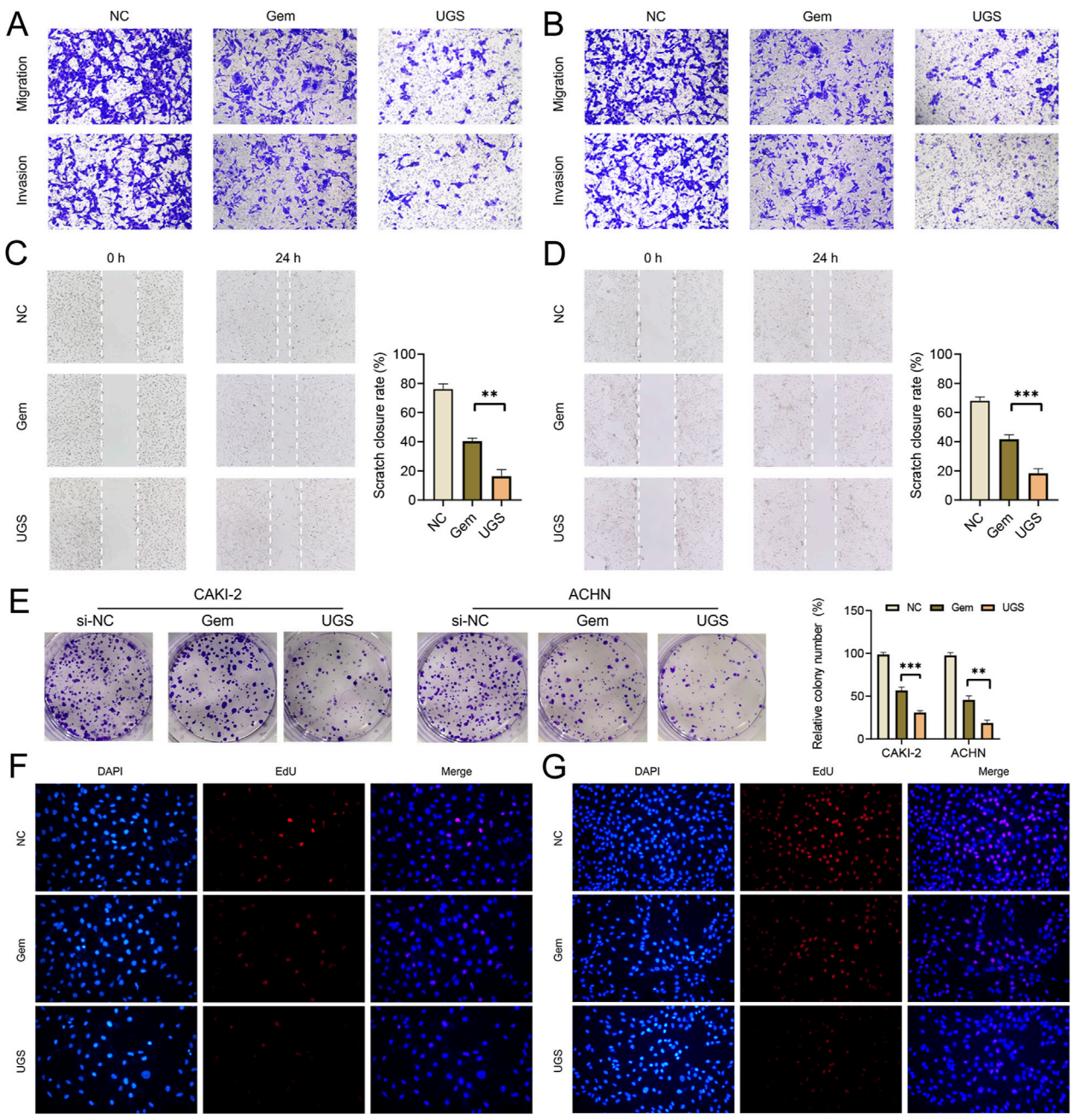

FIGURE 5
UGS treatment inhibits cell proliferation, migration, and invasion *in vitro*. **(A, B)** Transwell assay results for cell migration and invasion after different treatments in 2 cell lines. **(C, D)** Wound-healing assay results after different treatments in 2 cell lines for migration measurements. **(E)** Results of different treatments towards proliferation in 2 cell lines evaluated through the colony assay. **(F, G)** EdU results of different treatments in cell proliferation.

confirmed that UGS NPs significantly inhibited lung metastasis in nude mice, compared with the negative control (Figure 6B). Additionally, histogram equalization results of the primary organs of UGS-treated mice affirmed that UGS NPs possessed excellent biosafety, causing no noticeable damage (Figure 6C). Meanwhile, the blood tests were conducted to evaluate the biosafety of UGS NPs, which indicting that UGS treatments caused no obviously damages to the red blood cells, hemoglobin, platelets, and white blood cells (Supplementary Figures S2I–K). We finally constructed an *in situ* model of pRCC to explore the potential of UGS NPs to inhibit primary tumour growth. The findings demonstrated that UGS NPs markedly suppressed the proliferation of subcutaneous tumours in comparison to the control group (Figures 6D–G). Additionally, the KHSRP protein level in subcutaneous tumours in the UGS NPs group was also found to be significantly reduced (Figure 6H).

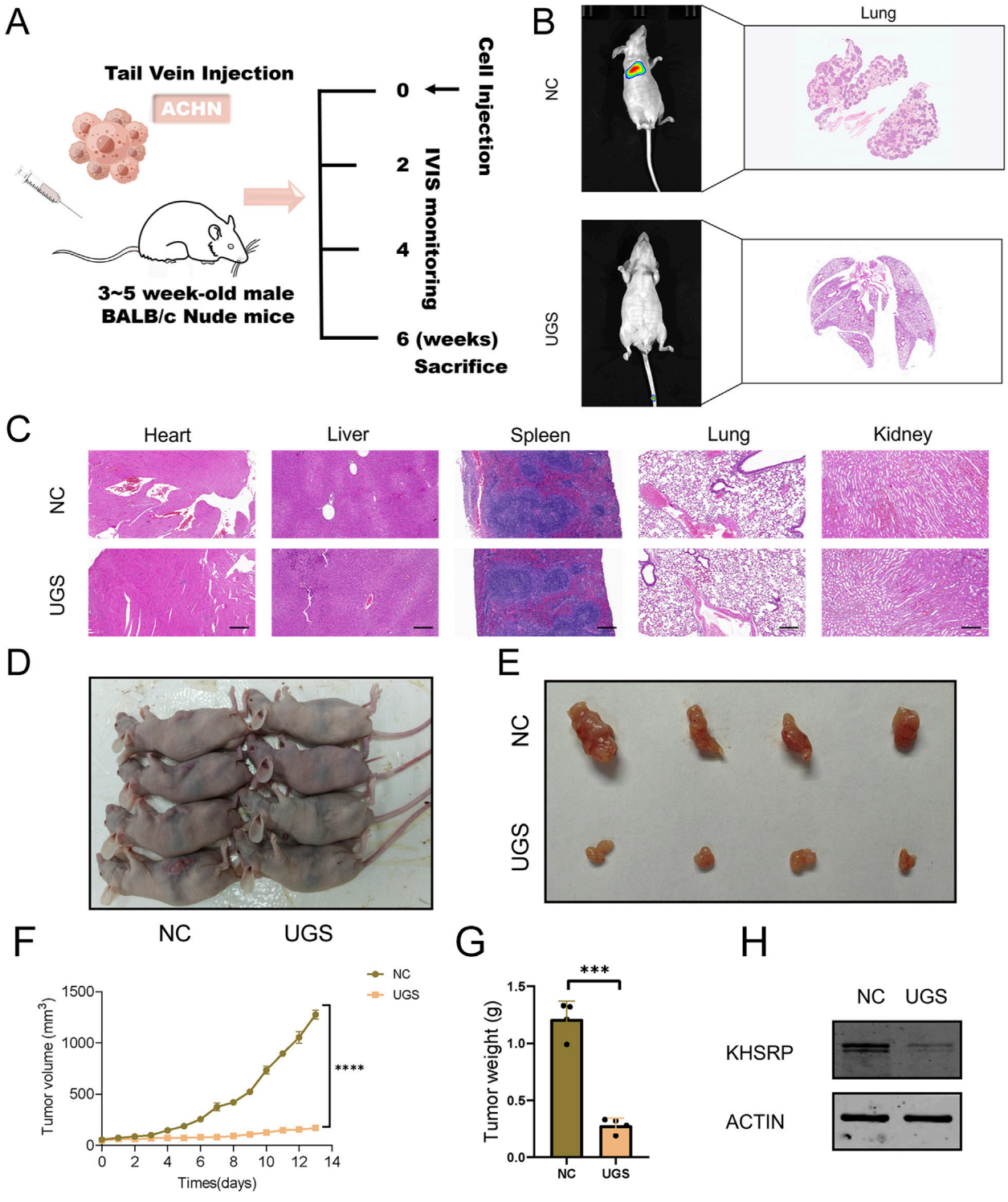

FIGURE 6
UGS treatment suppresses tumor metastasis *in vivo*. **(A)** Schematic diagram of animal experiment process. **(B)** IVIS and HE images of tumors in the two subgroups. **(C)** HE images of main organs in the two subgroups. **(D–E)** Primary tumour images of two subgroups. **(F)** Subcutaneous tumour growth curve. **(G)** Weight statistics of subcutaneous tumours. **(H)** KHSRP protein expression in subcutaneous tumours.

Discussion

pRCC prognosis is more favorable than ccRCC prognosis, which is confined to the organs. However, the histological prognosis of pRCC in metastatic disease is less favorable than that of ccRCC (Steffens et al., 2012). Researchers have made advances in pRCC treatment, including combination strategies with targeted therapies and immune checkpoint inhibitors. However, its overall progress

lags behind that of ccRCC, partly because of the heterogeneity of different pRCC subtypes (Chawla et al., 2023). In this study, *ex vivo* and *in vivo* experiments demonstrated that UGS NPs effectively inhibited the proliferation, migration, and invasion of pRCC cells. *In vivo* experiments demonstrated the outstanding therapeutic effects of UGS NPs in suppressing lung metastasis. Furthermore, KHSRP knockdown increased the infiltration of cytotoxic cells within the tumor microenvironment, thereby enhancing the anti-tumor effect.

KHSRP is a multifunctional nucleic acid-binding protein comprising 711 amino acids. It comprises a terminal structural domain of amino acids, a central structural domain of four KH motifs, and a terminal structural domain of carboxyl groups (Nicastro et al., 2012). The KH1 and KH4 domains of the central structure can interact with other proteins to form a β-folded structure, whereas the KH2 and KH3 domains comprise negative regulatory binding sites (Yan et al., 2019). Furthermore, KHSRP can interact with other proteins (Diaz-Moreno et al., 2009) and bind to not only ribonucleic acids but also other proteins. Additionally, it plays regulatory roles (Gherzi et al., 2010). Furthermore, KHSRP is involved in the pathophysiological regulation of neuromuscular disorders (Amirouche et al., 2013), obesity (Lin et al., 2014), type II diabetes mellitus (Briata et al., 2016), and cancer (Yuan et al., 2017).

To date, most studies have focused on the function and potential mechanisms underlying KHSRP in tumorigenesis and development. However, KHSRP plays distinct roles in different tumors. Chien et al. (Chien et al., 2017) demonstrated that KHSRP is associated with favorable survival and prognosis in patients with non-small cell lung cancer. KHSRP inhibits the invasion and migration of non-small cell lung cancer through the miR-23a/EGR3 axis. However, Bikkavilli et al. (Bikkavilli et al., 2017) reported that KHSRP silencing attenuates the malignant biological behavior of cell proliferation, migration, and invasion, suggesting its oncogenic role in lung cancer. Furthermore, Wang et al. (2016) demonstrated that KHSRP facilitates the cell cycle and enhances chemoresistance to adriamycin in breast cancer. In conclusion, the diverse functions of KHSRP in different tumors indicate that its role in cancer progression and drug sensitivity is highly dependent on the tumor cell type. To the best of our knowledge, this is the first study to elucidate the role of KHSRP in pRCC cells. KHSRP knockdown inhibits the malignant biological behavior of pRCC during clinical treatment.

Cancer treatment has witnessed substantial advances in the long-term evolution of medicine. In addition to the advancement and development of surgical approaches, neoadjuvant therapy has promoted longevity, based on drug development and innovation. For instance, preoperative and postoperative radiotherapy and chemotherapy have become the mainstay of cancer treatments, relying on the high drug toxicity to cancer cells as well as high killing efficiency. However, conventional chemotherapeutic agents have certain limitations, including non-targeted distribution and poor solubility *in vivo*, poor bioavailability, and rapid blood clearance (Cho et al., 2008; Han et al., 2013). The development of nanomaterials has led to their use in tumor diagnosis and treatment. This can be attributed to their good biocompatibility, high drug-carrying efficacy, controllable drug-release ability, and enhanced tumor penetration (Qin et al., 2017; Zhu et al., 2023). Adjuvant nanocarriers are used to address these issues, such as inorganic nano frames for drug delivery (Zhang et al., 2013; Tarn et al., 2013). These nanocarriers protect the drug from rapid metabolism or clearance by the blood, liver, and kidneys. Additionally, they facilitate long-term drug accumulation within solid tumors through enhanced permeability and retention effects (Kobayashi et al., 2013; Maeda, 2015). UiO-66 is a zirconium-based metal-organic framework (MOF) consisting of a biocompatible and water-stable terephthalic acid ligand, rendering it an optimal material for drug delivery applications (Orellana-Tavra et al., 2015). UiO-66 has been utilized in numerous drug delivery applications, including oral, dermal, and intravenous drug delivery (Javanbakht et al., 2019). Despite the extensive range of delivery methods utilizing UiO-66 and other MOFs, few studies have used formulated UiO-66 to deliver Gem for pRCC treatment.

KHSRP knockdown inhibits the malignant biological behavior of pRCC, and Gem can reduce KHSRP expression. UGS NPs were constructed for the targeted delivery of Gem and applied in *ex vivo* experiments. UGS NPs exhibited superior efficacy in inhibiting pRCC proliferation, migration, and invasion. Additionally, they exhibited a favorable biosafety profile for pRCC treatment, compared with Gem alone. Thus, KHSRP is central to pRCC progression and can be considered a potential target for clinical translation through UGS NP-based therapies.

Data availability statement

The original contributions presented in the study are included in the article/Supplementary Material, further inquiries can be directed to the corresponding authors.

Ethics statement

The study was approved by the Ethics Committee of Shanghai Tenth People's Hospital (2020tjdx050). This animal experiment was conducted in compliance with the regulations set forth by the Animal Care and Use Committee of Shanghai Tenth People's Hospital (SHDSYY-2020-1726).

Author contributions

WS: Data curation, Formal Analysis, Investigation, Methodology, Project administration, Resources, Software, Supervision, Validation, Visualization, Writing–original draft, Writing–review and editing. HeZ: Conceptualization, Project administration, Software, Supervision, Validation, Visualization, Writing–original draft, Writing–review and editing. YL: Conceptualization, Investigation, Methodology, Project administration, Supervision, Writing–original draft, Writing–review and editing. HoZ: Formal Analysis, Investigation, Methodology, Project administration, Visualization, Writing–original draft, Writing–review and editing. JN: Conceptualization, Investigation, Methodology, Project administration, Validation, Writing–original draft, Writing–review and editing. LC: Conceptualization, Data curation, Investigation, Methodology, Project administration,

Resources, Supervision, Writing–original draft, Writing–review and editing. YG: Conceptualization, Formal Analysis, Methodology, Project administration, Writing–original draft, Writing–review and editing. GW: Funding acquisition, Investigation, Validation, Methodology, Writing–original draft, Writing–review and editing. TX: Project administration, Resources, Software, Funding acquisition, Investigation, Methodology, Writing–original draft, Writing–review and editing. ZW: Project administration, Resources, Writing–original draft, Writing–review and editing, Conceptualization, Data curation, Validation, Methodology. KW: Data curation, Methodology, Resources, Validation, Writing–original draft, Writing–review and editing, Funding acquisition, Investigation, Software, Supervision, Visualization, Conceptualization.

Funding

The author(s) declare that financial support was received for the research, authorship, and/or publication of this article. This work was supported by the National Natural Science Foundation of China (Grant No. 82270809 and 32070646); Climbing Talent Projects of Shanghai 10th People's Hospital (No. 2018SYPDRC046) and the Fundamental Research Funds for the Central Universities (No. 22120180586). Science and Technology Innovation Project of Shanghai Putuo District Health and Wellness System (ptkwws202213).

Acknowledgments

The authors are grateful for the invaluable support and useful discussions with other members of the Urological Department.

Conflict of interest

The authors declare that the research was conducted in the absence of any commercial or financial relationships that could be construed as a potential conflict of interest.

Publisher's note

Supplementary material

The Supplementary Material for this article can be found online at: https://www.frontiersin.org/articles/10.3389/fphar.2024.1446920/full#supplementary-material

SUPPLEMENTARY FIGURE S1
Clinical and silico analysis of KHSRP. **(A)** ROC curves of KHSRP expression in predicting TNM-stage and pathological stage. **(B)** GO and KEGG analysis of KHSRP negatively related functional genes in pRCC. **(C)** KHSRP expression in pRCC cell lines. **(D)** Gem could bind to the protein structure of KHSRP with 7 hydrogen bonds formed.

SUPPLEMENTARY FIGURE S2
UGS NPs inhibit KHSRP expression. **(A)** KHSRP expression in different cell lines. **(B)** Particle size distribution of UGS NPs. **(C)** Bio-TEM images for cell phagocytosis of UGS NPs. **(D)** Western blot analysis of KHSRP expression in 2 cell lines after the treatment of UGS. **(E, F)** Quantitative analysis of transwell assay results in the 2 cell lines. **(G, H)** Quantitative analysis of EdU assay results in the 2 cell lines. **(I–K)** Blood tests for red blood cells, hemoglobin, platelets, and white blood cells after UGS NPs treatments.

References

Amirouche, A., Tadesse, H., Lunde, J. A., Belanger, G., Cote, J., and Jasmin, B. J. (2013). Activation of p38 signaling increases utrophin A expression in skeletal muscle via the RNA-binding protein KSRP and inhibition of AU-rich element-mediated mRNA decay: implications for novel DMD therapeutics. *Hum. Mol. Genet.* 22, 3093–3111. doi:10.1093/hmg/ddt165

Bikkavilli, R. K., Zerayesus, S. A., Van Scoyk, M., Wilson, L., Wu, P. Y., Baskaran, A., et al. (2017). K-homology splicing regulatory protein (KSRP) promotes post-transcriptional destabilization of Spry4 transcripts in non-small cell lung cancer. *J. Biol. Chem.* 292, 7423–7434. doi:10.1074/jbc.M116.757906

Briata, P., Bordo, D., Puppo, M., Gorlero, F., Rossi, M., Perrone-Bizzozero, N., et al. (2016). Diverse roles of the nucleic acid-binding protein KHSRP in cell differentiation and disease. *Wiley Interdiscip. Rev. RNA* 7, 227–240. doi:10.1002/wrna.1327

Chawla, N. S., Sayegh, N., Prajapati, S., Chan, E., Pal, S. K., and Chehrazi-Raffle, A. (2023). An update on the treatment of papillary renal cell carcinoma. *Cancers (Basel)* 15, 565. doi:10.3390/cancers15030565

Chien, M. H., Lee, W. J., Yang, Y. C., Li, Y. L., Chen, B. R., Cheng, T. Y., et al. (2017). KSRP suppresses cell invasion and metastasis through miR-23a-mediated EGR3 mRNA degradation in non-small cell lung cancer. *Biochim. Biophys. Acta Gene Regul. Mech.* 1860, 1013–1024. doi:10.1016/j.bbagrm.2017.08.005

Cho, K., Wang, X., Nie, S., Chen, Z. G., and Shin, D. M. (2008). Therapeutic nanoparticles for drug delivery in cancer. *Clin. Cancer Res.* 14, 1310–1316. doi:10.1158/1078-0432.CCR-07-1441

Diaz-Moreno, I., Hollingworth, D., Frenkiel, T. A., Kelly, G., Martin, S., Howell, S., et al. (2009). Phosphorylation-mediated unfolding of a KH domain regulates KSRP localization via 14-3-3 binding. *Nat. Struct. Mol. Biol.* 16, 238–246. doi:10.1038/nsmb.1558

Dudani, S., de Velasco, G., Wells, J. C., Gan, C. L., Donskov, F., Porta, C., et al. (2021). Evaluation of clear cell, papillary, and chromophobe renal cell carcinoma metastasis sites and association with survival. *JAMA Netw. Open* 4, e2021869. doi:10.1001/jamanetworkopen.2020.21869

Fujita, Y., Masuda, K., Hamada, J., Shoda, K., Naruto, T., Hamada, S., et al. (2017). KH-type splicing regulatory protein is involved in esophageal squamous cell carcinoma progression. *Oncotarget* 8, 101130–101145. doi:10.18632/oncotarget.20926

Gherzi, R., Chen, C. Y., Ramos, A., and Briata, P. (2014). KSRP controls pleiotropic cellular functions. *Semin. Cell. Dev. Biol.* 34, 2–8. doi:10.1016/j.semcdb.2014.05.004

Gherzi, R., Chen, C. Y., Trabucchi, M., Ramos, A., and Briata, P. (2010). The role of KSRP in mRNA decay and microRNA precursor maturation. *Wiley Interdiscip. Rev. RNA* 1, 230–239. doi:10.1002/wrna.2

Han, K., Chen, S., Chen, W. H., Lei, Q., Liu, Y., Zhuo, R. X., et al. (2013). Synergistic gene and drug tumor therapy using a chimeric peptide. *Biomaterials* 34, 4680–4689. doi:10.1016/j.biomaterials.2013.03.010

Jarai, B. M., Stillman, Z., Attia, L., Decker, G. E., Bloch, E. D., and Fromen, C. A. (2020). Evaluating UiO-66 metal-organic framework nanoparticles as acid-sensitive carriers for pulmonary drug delivery applications. *ACS Appl. Mater Interfaces* 12, 38989–39004. doi:10.1021/acsami.0c10900

Javanbakht, S., Shadi, M., Mohammadian, R., Shaabani, A., Amini, M. M., Pooresmaeil, M., et al. (2019). Facile preparation of pH-responsive k-Carrageenan/tramadol loaded UiO-66 bio-nanocomposite hydrogel beads as a nontoxic oral delivery vehicle. *J. Drug Deliv. Sci. Technol.* 54, 101311. doi:10.1016/j.jddst.2019.101311

Karaman, S., and Detmar, M. (2014). Mechanisms of lymphatic metastasis. *J. Clin. Investig.* 124, 922–928. doi:10.1172/JCI71606

Kobayashi, H., Watanabe, R., and Choyke, P. L. (2013). Improving conventional enhanced permeability and retention (EPR) effects; what is the appropriate target? *Theranostics* 4, 81–89. doi:10.7150/thno.7193

Lin, Y. Y., Chou, C. F., Giovarelli, M., Briata, P., Gherzi, R., and Chen, C. Y. (2014). KSRP and MicroRNA 145 are negative regulators of lipolysis in white adipose tissue. *Mol. Cell. Biol.* 34, 2339–2349. doi:10.1128/MCB.00042-14

Liu, W., Chou, C. F., Liu, S., Crossman, D., Yusuf, N., Wu, Y., et al. (2019). KSRP modulates melanoma growth and efficacy of vemurafenib. *Biochim. Biophys. Acta Gene Regul. Mech.* 1862, 759–770. doi:10.1016/j.bbagrm.2019.06.005

Maeda, H. (2015). Toward a full understanding of the EPR effect in primary and metastatic tumors as well as issues related to its heterogeneity. *Adv. Drug Deliv. Rev.* 91, 3–6. doi:10.1016/j.addr.2015.01.002

Mao, W., Wang, K., Zhang, W., Chen, S., Xie, J., Zheng, Z., et al. (2022). Transfection with Plasmid-Encoding lncRNA-SLERCC nanoparticle-mediated delivery suppressed tumor progression in renal cell carcinoma. *J. Exp. Clin. Cancer Res.* 41, 252. doi:10.1186/s13046-022-02467-2

Nicastro, G., Garcia-Mayoral, M. F., Hollingworth, D., Kelly, G., Martin, S. R., Briata, P., et al. (2012). Noncanonical G recognition mediates KSRP regulation of let-7 biogenesis. *Nat. Struct. Mol. Biol.* 19, 1282–1286. doi:10.1038/nsmb.2427

Orellana-Tavra, C., Baxter, E. F., Tian, T., Bennett, T. D., Slater, N. K., Cheetham, A. K., et al. (2015). Amorphous metal-organic frameworks for drug delivery. *Chem. Commun. (Camb)* 51, 13878–13881. doi:10.1039/c5cc05237h

Palzer, K. A., Bolduan, V., Käfer, R., Kleinert, H., Bros, M., and Pautz, A. (2022). The role of KH-type splicing regulatory protein (KSRP) for immune functions and tumorigenesis. *Cells* 11, 1482. doi:10.3390/cells11091482

Patard, J. J., Leray, E., Rioux-Leclercq, N., Cindolo, L., Ficarra, V., Zisman, A., et al. (2005). Prognostic value of histologic subtypes in renal cell carcinoma: a multicenter experience. *J. Clin. Oncol.* 23, 2763–2771. doi:10.1200/JCO.2005.07.055

Peruzzi, B., and Bottaro, D. P. (2006). Targeting the c-Met signaling pathway in cancer. *Clin. Cancer Res.* 12, 3657–3660. doi:10.1158/1078-0432.CCR-06-0818

Qin, S. Y., Zhang, A. Q., Cheng, S. X., Rong, L., and Zhang, X. Z. (2017). Drug self-delivery systems for cancer therapy. *Biomaterials* 112, 234–247. doi:10.1016/j.biomaterials.2016.10.016

Steffens, S., Janssen, M., Roos, F. C., Becker, F., Schumacher, S., Seidel, C., et al. (2012). Incidence and long-term prognosis of papillary compared to clear cell renal cell carcinoma--a multicentre study. *Eur. J. Cancer* 48, 2347–2352. doi:10.1016/j.ejca.2012.05.002

Tarn, D., Ashley, C. E., Xue, M., Carnes, E. C., Zink, J. I., and Brinker, C. J. (2013). Mesoporous silica nanoparticle nanocarriers: biofunctionality and biocompatibility. *Acc. Chem. Res.* 46, 792–801. doi:10.1021/ar3000986

Trabucchi, M., Briata, P., Garcia-Mayoral, M., Haase, A. D., Filipowicz, W., Ramos, A., et al. (2009). The RNA-binding protein KSRP promotes the biogenesis of a subset of microRNAs. *Nature* 459, 1010–1014. doi:10.1038/nature08025

Wang, Y. Y., Gu, X. L., Wang, C., Wang, H., Ni, Q. C., Zhang, C. H., et al. (2016). The far-upstream element-binding protein 2 is correlated with proliferation and doxorubicin resistance in human breast cancer cell lines. *Tumour Biol.* 37, 9755–9769. doi:10.1007/s13277-016-4819-2

Wu, C., Wang, S., Zhao, J., Liu, Y., Zheng, Y., Luo, Y., et al. (2019). Biodegradable Fe (III)@ WS2-PVP nanocapsules for redox reaction and TME-enhanced nanocatalytic, photothermal, and chemotherapy. *Adv. Funct. Mater.* 29, 1901722. doi:10.1002/adfm.201901722

Yan, M., Sun, L., Li, J., Yu, H., Lin, H., Yu, T., et al. (2019). RNA-binding protein KHSRP promotes tumor growth and metastasis in non-small cell lung cancer. *J. Exp. Clin. Cancer Res.* 38, 478. doi:10.1186/s13046-019-1479-2

Yang, J., Fan, J., Li, Y., Li, F., Chen, P., Fan, Y., et al. (2013). Genome-wide RNAi screening identifies genes inhibiting the migration of glioblastoma cells. *PLoS One* 8, e61915. doi:10.1371/journal.pone.0061915

Yuan, H., Deng, R., Zhao, X., Chen, R., Hou, G., Zhang, H., et al. (2017). SUMO1 modification of KHSRP regulates tumorigenesis by preventing the TL-G-Rich miRNA biogenesis. *Mol. Cancer* 16, 157. doi:10.1186/s12943-017-0724-6

Zhang, J., Yuan, Z. F., Wang, Y., Chen, W. H., Luo, G. F., Cheng, S. X., et al. (2013). Multifunctional envelope-type mesoporous silica nanoparticles for tumor-triggered targeting drug delivery. *J. Am. Chem. Soc.* 135, 5068–5073. doi:10.1021/ja312004m

Zhou, F., Huang, L., Li, S., Yang, W., Chen, F., Cai, Z., et al. (2023). From structural design to delivery: mRNA therapeutics for cancer immunotherapy. *Exploration* 4, 20210146. doi:10.1002/EXP.20210146

Zhu, Y. X., Jia, H. R., Jiang, Y. W., Guo, Y., Duan, Q. Y., Xu, K. F., et al. (2023). A red blood cell-derived bionic microrobot capable of hierarchically adapting to five critical stages in systemic drug delivery. *Exploration* 4, 20230105. doi:10.1002/EXP.20230105

Frontiers in Pharmacology

Explores the interactions between chemicals and living beings

The most cited journal in its field, which advances access to pharmacological discoveries to prevent and treat human disease.

Discover the latest Research Topics

See more →

Frontiers

Avenue du Tribunal-Fédéral 34
1005 Lausanne, Switzerland
frontiersin.org

Contact us

+41 (0)21 510 17 00
frontiersin.org/about/contact